

# Geologic Studies in Alaska by the U.S. Geological Survey, 1992

CYNTHIA DUSEL-BACON *and* ALISON B. TILL, *Editors*

---

U.S. GEOLOGICAL SURVEY BULLETIN 2068



UNITED STATES GOVERNMENT PRINTING OFFICE, WASHINGTON : 1993

U.S. DEPARTMENT OF THE INTERIOR

BRUCE BABBITT, Secretary

U.S. GEOLOGICAL SURVEY

Robert M. Hirsch, Acting Director

For sale by Book and Open-File Report Sales  
U.S. Geological Survey  
Federal Center, Box 25286  
Denver, CO 80225

Any use of trade, product, or firm names in this publication is for descriptive purposes only  
and does not imply endorsement by the U.S. Government.

**COVER:** Geologist Julie Dumoulin examines Cambrian carbonate rocks exposed in the Baird Mountains quadrangle, western Brooks Range. Proterozoic(?) and lower Paleozoic carbonate rocks are exposed in the background. Two papers by Dumoulin and others included in this volume discuss younger Paleozoic rocks exposed in the west-central Brooks Range. Photograph by Alison B. Till.

## CONTENTS

Introduction	
Cynthia Dusel-Bacon and Alison B. Till .....	1
NORTHERN ALASKA	
Late Holocene Longitudinal and Parabolic Dunes in Northern Alaska: Preliminary Interpretations of Age and Paleoclimatic Significance	
John P. Galloway and L. David Carter .....	3
Deep-Water Lithofacies and Conodont Faunas of the Lisburne Group, West- Central Brooks Range, Alaska	
Julie A. Dumoulin, Anita G. Harris, and Jeanine M. Schmidt .....	12
Lithofacies and Conodonts of Carboniferous Strata in the Ivotuk Hills, Western Brooks Range, Alaska	
Julie A. Dumoulin and Anita G. Harris .....	31
Depositional Sequences in Lower Cretaceous Rocks, Atigun Syncline and Slope Mountain Areas, Alaskan North Slope	
Christopher J. Schenk and Kenneth J. Bird .....	48
U-Pb Ages of Zircon, Monazite, and Sphene from Devonian Metagranites and Metafelsites, Central Brooks Range, Alaska	
John N. Aleinikoff, Thomas E. Moore, Marianne Walter, and Warren J. Nokleberg .....	59
Appeal for Nonproliferation of Escalating Terrane Nomenclature	
Susan M. Karl and Charles G. Mull .....	71
SOUTHWESTERN ALASKA	
Favorable Areas for Metallic Mineral Resources in and near the Horn Mountains, Sleetmute Quadrangle, Southwestern Alaska	
John E. Gray, Peter M. Theodorakos, Leon A. Bradley, and John H. Bullock, Jr. ....	79
Gold and Cinnabar in Heavy-Mineral Concentrates from Stream-Sediment Samples Collected from the Western Half of the Lime Hills 1° x 3° Quadrangle, Alaska	
Robert G. Eppinger .....	91
SOUTH-CENTRAL ALASKA	
Early Cenozoic Depositional Systems, Wishbone Hill District, Matanuska Coal Field, Alaska	
Romeo M. Flores and Gary D. Stricker .....	101
Reservoir Framework Architecture in the Clamgulchian Type Section (Pliocene) of the Sterling Formation, Kenai Peninsula, Alaska	
Romeo M. Flores and Gary D. Stricker .....	118
Geochemistry of Ophiolitic Rocks from Knight Island, Prince William Sound, Alaska	
Steven W. Nelson and Matthew S. Nelson .....	130
Structural Evolution of the Chugach-Prince William Terrane at the Hinge of the Orocline in Prince William Sound, and Implications for Ore Deposits	
Peter J. Haeussler and Steven W. Nelson .....	143

Timing of Early Tertiary Ridge Subduction in Southern Alaska Dwight C. Bradley, Peter J. Haeussler, and Timothy M. Kusky .....	163
Geochemical Evaluation of Stream-Sediment Data from the Bering Glacier and Icy Bay Quadrangles, South-Central Alaska Richard J. Goldfarb and J. Carter Borden .....	178

## SOUTHEASTERN ALASKA

Newly Discovered Molybdenite Occurrences at Dora Bay, Prince of Wales Island, Southeast Alaska, and Preliminary Scanning Electron Microscope Studies John Philpotts, Cliff Taylor, John Evans, and Poul Emsbo .....	187
Geochemical Character of Upper Paleozoic and Triassic Greenstone and Related Metavolcanic Rocks of the Wrangellia Terrane in Northern Southeastern Alaska Arthur B. Ford and David A. Brew .....	197
Reconnaissance Geochemistry of Permian and Triassic Basalts of the Taku and Wrangellia Terranes, Southeastern Alaska George E. Gehrels and Fred Barker .....	218

## GEOLOGIC NOTES

Ostracode Assemblages from Modern Bottom Sediments of Vitus Lake, Bering Piedmont Glacier, Southeast Alaska Elisabeth M. Brouwers and Richard M. Forester .....	228
Rubidium-Strontium Isotopic Systematics of Vein Minerals in the Juneau Gold Belt, Alaska Ronald W. Kistler, Rainer J. Newberry, and David A. Brew .....	236

## BIBLIOGRAPHIES

U.S. Geological Survey Reports on Alaska Released in 1992 Compiled by Ellen R. White .....	241
Reports About Alaska in Non-USGS Publications Released in 1992 that Include USGS Authors Compiled by Ellen R. White .....	246



## CONTRIBUTORS TO THIS BULLETIN

## Anchorage

U.S. Geological Survey  
4200 University Drive  
Anchorage, Alaska 99508-4667

*Bradley, Dwight C.*  
*Carter, L. David*  
*Dumoulin, Julie A.*  
*Haeussler, Peter J.*  
*Karl, Susan M.*  
*Nelson, Steven W.*

## Denver

U.S. Geological Survey MS-  
Box 25046 Denver Federal Center  
Lakewood, Colorado 80225-0046

*Aleinikoff, John MS 963*  
*Barker, Fred MS 913*  
*Borden, J. Carter MS 973*  
*Bradley, Leon A. MS 973*  
*Brouwers, Elisabeth M. MS 919*  
*Bullock, John H., Jr. MS 973*  
*Emsbo, Poul MS 973*  
*Eppinger, Robert G. MS 973*  
*Flores, Romeo M. MS 972*  
*Forester, Richard M. MS 919*  
*Goldfarb, Richard J. MS 973*  
*Gray, John E. MS 973*  
*Schenk, Christopher J. MS 971*  
*Stricker, Gary D. MS 972*  
*Taylor, Cliff MS 973*  
*Theodorakos, Peter M. MS 973*  
*Walter, Marianne MS 963*

## Menlo Park

U.S. Geological Survey  
345 Middlefield Rd. MS-  
Menlo Park, California 94025-3591

*Bird, Kenneth J. MS 999*  
*Brew, David A. MS 904*  
*Ford, Arthur B. MS 904*  
*Galloway, John P. MS 904*  
*Kistler, Ronald W. MS 937*  
*Moore, Thomas E. MS 904*  
*Nokleberg, Warren MS 904*  
*White, Ellen R. MS 955*

## CONTENTS

**Reston**

U.S. Geological Survey  
National Center, MS-  
12201 Sunrise Valley Drive  
Reston, Virginia 22092-0001

*Evans, John MS 957*  
*Harris, Anita G. MS 970*  
*Philpotts, John MS 923*

**Others**

*Gehrels, George E.*  
Department of Geosciences  
University of Arizona  
Tucson, Arizona 85721

*Kusky, Timothy M.*  
Department of Geology  
675 Commonwealth Avenue  
Boston University  
Boston, Massachusetts 02215

*Mull, Charles G.*  
Alaska State Division of Geologic and Geophysical Surveys  
794 University Avenue Suite 200  
Fairbanks, Alaska 99709

*Nelson, Matthew S.*  
2515 Cottonwood Street  
Anchorage, Alaska 99508

*Newberry, Rainer J.*  
Department of Geology and Geophysics  
University of Alaska  
Fairbanks, Alaska 99709

# GEOLOGIC STUDIES IN ALASKA BY THE U.S. GEOLOGICAL SURVEY, 1992

Cynthia Dusel-Bacon and Alison B. Till, *Editors*

## INTRODUCTION

This collection of 19 papers continues the annual series of U.S. Geological Survey reports on the geology of Alaska. The contributions, which include full-length Articles and shorter Geologic Notes, cover a broad range of topics including dune formation, stratigraphy, paleontology, isotopic dating, mineral resources, and tectonics. Articles, grouped under four regional headings, span nearly the entire State from the North Slope to southwestern, south-central, and southeastern Alaska (fig. 1).

In the section on northern Alaska, Galloway and Carter use new data on dune morphology and radiocarbon ages from the western Arctic Coastal Plain to develop a late Holocene chronology of multiple episodes of dune stabilization and reactivation for the region. Their study has important implications for climatic changes in northern Alaska during the past 4,000 years. In two papers, Dumoulin and her coauthors describe lithofacies and conodont faunas of Carboniferous strata in the western Brooks Range, discuss depositional environments, and propose possible correlations and source areas for some of the strata. Schenk and Bird propose a preliminary division of the Lower Cretaceous stratigraphic section in the central part of the North Slope into depositional sequences. Aleinikoff and others present new U-Pb data for zircons from metagneous rocks from the central Brooks Range. Karl and Mull, reacting to a proposal regarding terrane nomenclature for northern Alaska that was published in last year's *Alaskan Studies Bulletin*, provide a historical perspective of the evolution of terminology for tectonic units in the Brooks Range and present their own recommendations.

Under the heading of southwestern Alaska, Gray and his coworkers present geochemical data from stream-sediment and heavy-mineral-concentrate samples, which they interpret to indicate two areas that are favorable for the presence of polymetallic vein deposits and eight that are favorable for epithermal mercury-rich vein deposits. Eppinger reports on a newly discovered occurrence of fine-grained gold and cinnabar in heavy-mineral-concentrate samples collected from streams in the western half of the Lime Hills quadrangle.

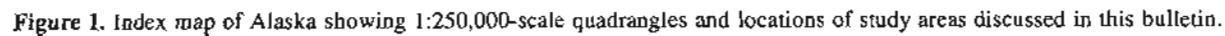
Two papers by Flores and Stricker begin the section on south-central Alaska. In the first, they report on facies

investigations of early Cenozoic depositional systems exposed in the Matanuska coal field, and in the second they describe reservoir and source rock characteristics of the Pliocene upper part of a coal-bearing and gas-producing unit within the Kenai Group on the Kenai Peninsula. The next three papers focus on the accretionary complex that arcs around the Gulf of Alaska. Nelson and Nelson present major- and trace-element data for the basaltic rocks of an ophiolitic suite that forms part of the complex in Prince William Sound and, using various discriminant diagrams, propose several possible tectonic environments of ophiolite formation. Haeussler and Nelson describe the structural evolution of rocks in the hinge of the accretionary orocline and speculate as to the origin of ore-forming fluids within the hinge zone. Bradley and others speculate, on the basis of a new compilation of isotopic ages, about the origin of a belt of eastward-younging early Tertiary near-trench plutons that intrude the accretionary complex. Finally, Goldfarb and Borden evaluate stream-sediment geochemical data from the Bering Glacier quadrangle and report on its usefulness to delineate various bedrock sources and to identify two previously unrecognized areas that are favorable for the presence of metallic mineral resources.

In the section on southeastern Alaska, Philpotts and others describe the occurrence of newly discovered molybdenite at two sites on Prince of Wales Island and discuss the relations between alkali metasomatism and molybdenite crystallization. Major- and minor-element geochemical fingerprinting of upper Paleozoic and Triassic basaltic rocks in northern southeastern Alaska is the topic of papers by Ford and Brew and by Gehrels and Barker. These two papers arrive at similar conclusions and provide important constraints for terrane evolution in southeastern Alaska.

Two geologic notes follow the above articles. Bouwers and her coworkers discuss the response of biota in a large proglacial lake on the southern margin of the Bering Glacier to an increase in salinity during the last few years. Kistler and others present rubidium-strontium isotopic data for vein minerals in the Juneau gold belt and discuss the implications of their data for the origin of the ore-bearing fluids at three mines within the belt.

Two bibliographies at the end of the volume list (1) reports about Alaska in USGS publications released in 1992 and (2) reports about Alaska by USGS authors in publications outside the USGS in 1992.



# LATE HOLOCENE LONGITUDINAL AND PARABOLIC DUNES IN NORTHERN ALASKA: PRELIMINARY INTERPRETATIONS OF AGE AND PALEOCLIMATIC SIGNIFICANCE

By John P. Galloway and L. David Carter

## ABSTRACT

Climatic changes during the late Holocene have caused repeated stabilization and reactivation of parabolic and longitudinal dunes and sand sheets over a major portion of the landscape on the western Arctic Coastal Plain. The dunes are currently stabilized, and their density varies throughout the region from a few dunes to over 275 dunes for a 100-square-kilometer area. Dune length ranges from 320 to 2,500 m and most dunes are about 15 to 40 m wide. Field observations suggest that most dunes are 1 to 3 m thick. Modern blowouts indicate a bimodal wind regime of ENE-WSW, with the majority of the blowouts produced by easterly winds. Most stabilized parabolic and longitudinal dunes are parallel to this trend, and the parabolic dunes indicate westerly sand transport. This suggests that these late Holocene dunes formed in a wind regime similar to the present one. Twelve radiocarbon ages on peat and humic sand (paleosols) from nine locations suggest that three episodes of dune stabilization separated four periods of late Holocene sand movement and dune building. The episodes of stabilization are dated at about 4.3 to 3.9, 2.7 to 2.0, and 1.1 to 0.7 ka. Each of the four dune building episodes (1) before 4.3, (2) 3.9 to 2.7, (3) 2.0 to 1.1, and (4) 0.7 ka to near the present, broadly correlates with one or more Neoglacial expansions of cirque glaciers in the Brooks Range. Reactivation of small longitudinal and parabolic dunes on the western Arctic Coastal Plain apparently occurred as a result of cooler and drier surface conditions than those that exist today.

## INTRODUCTION

Late Holocene stabilized longitudinal and parabolic dunes and thin sand sheets occur over a major portion of the landscape on the western Arctic Coastal Plain between the Colville and Meade Rivers (fig. 1). The dunes were first described by Black (1951), but he presented little information about their age or paleoclimatic significance.

More recent investigations indicated that these small dunes and sand sheets overlie an older sand sheet that in turn covers large stabilized dunes of a Pleistocene sand sea (Carter, 1981). Also, it is now known that the dunes described by Black have formed during the late Holocene, following a middle Holocene period of landscape stability and the formation of organic soils (Carter, 1992, and in press).

A parabolic dune forms when a disruption of stabilizing vegetation exposes underlying sand to erosion. The dune accumulates downwind from the local sand source and does not migrate (Pye and Tsoar, 1990). The widespread occurrence of the parabolic dunes and associated longitudinal dunes on the western Arctic Coastal Plain indicates that the disruption of vegetation was regional. Such a regional decrease in ground cover indicates drier surface conditions, which were almost certainly caused by climatic change. This paper describes the geomorphic setting of the dunes, provides preliminary information on the age of dune formation, and presents a discussion of the possible significance of the dunes for regional interpretations of late Holocene climatic change.

## DESCRIPTION OF THE DUNES

Stabilized longitudinal and parabolic dunes occur across much of the western Arctic Coastal Plain except for river floodplains and terraces. Measurements from aerial photographs in areas subjectively judged as regionally representative show that the density of dunes varies throughout the study area from a few dunes per 100 km<sup>2</sup> to a maximum of over 275 dunes for a 100-km<sup>2</sup> area 12 km south-southwest of Teshekpuk Lake. Just west of the Ikpikuk River, there is an average of 135 dunes per 100 km<sup>2</sup>, and from there eastward to the Meade River, dune density decreases to 10 to 40 per 100 km<sup>2</sup>.

The dunes vary in length locally and regionally. Dune length in the 100-km<sup>2</sup> areas chosen as regionally representative increases from the range 320 to 960 m

(average 600 m) southeast of Teshekpuk Lake to the range 370 to 1,300 m (average 835 m) just west of the Ikpikpuk River. Eastward to the Meade River the average dune length decreases to 470 m. The longest dune observed in the entire region is 2,500 m long. Most dunes are 15 to 40 m wide. Field observations suggest that most dunes are 1 to 3 m thick. The dunes commonly merge into the tundra, and are generally marked by a change in color of the vegetation (fig. 2).

U.S. Weather Bureau records show east-northeast (ENE) as the dominant wind direction at Barrow and west-southwest (WSW) as the secondary maximum; Black

(1951, p. 93) stated that "numerous oriented lakes and dunes throughout the coastal plain show that these maximum winds are just as consistent and effective inland and that slightly more erosion is produced by the easterly ( $65^{\circ}$  to  $80^{\circ}$ ) than by the westerly winds ( $245^{\circ}$  to  $260^{\circ}$ )." Modern blowouts (deflation hollows on pre-existing dunes) in the region also indicate a bimodal wind regime of ENE-WSW, with the majority of the blowouts produced by easterly winds. Most stabilized parabolic and longitudinal dunes are parallel to this trend and the parabolic dunes indicate a westerly sand transport. This suggests that these late Holocene dunes formed in a wind regime similar to the present one.

Buried organic horizons (paleosols) in the dunes and thin sand sheets temporally equivalent to the dunes are common throughout the study area. Rickert and Tedrow's (1967) study of several buried soils near the Meade River showed that dune profiles usually contained several buried organic horizons, with each horizon representing a period of surface stability. However, except for one radiocarbon age discussed below for a buried organic horizon immediately beneath a stabilized dune near the Ikpikpuk River, Rickert and Tedrow presented no information about the age or paleoclimatic significance of the soils in the Meade River area.

## AGE OF EOLIAN SAND MOVEMENT

Stabilization and subsequent reactivation of eolian sand on the Arctic Coastal Plain is recorded by thin, discontinuous paleosols. Twelve radiocarbon ages on peat and humic sand (paleosols) from nine locations suggest that three periods of late Holocene landscape stability separate four episodes of dune activity (table 1). Three sites are described here to illustrate the stratigraphy of humic paleosols and eolian sand. Minimal modern soil development at each of these sites indicates that the dunes have been stabilized only recently.

Site 1 is a thaw lake bluff about 50 m high composed entirely of eolian sand. An amphitheater at the top of the bluff cuts into a small longitudinal dune that is parallel to the main bluff face (fig. 3). The dune is about 30 m wide and 480 m long, and its top is about 1.8 m above the adjacent ground surface. The long axis of the dune trends N.  $60^{\circ}$  E. A paleosol composed of cryoturbated sandy humus 25 cm thick occurs about 2.8 m below the top of the dune (fig. 4). A sample of humus from the lower 15 cm of this paleosol yielded a radiocarbon age of  $2,290 \pm 80$  yr B.P. (table 1).

At site 2, a 10-m-high thaw lake bluff truncates a small longitudinal dune (fig. 5). The dune rises 60 to 80 cm above the adjacent ground surface and its long axis trends N.  $65^{\circ}$  E. The dune is approximately 920 m long and 30 m wide. A sandy paleosol 25 cm thick occurs about 80 cm below the surface of the dune.

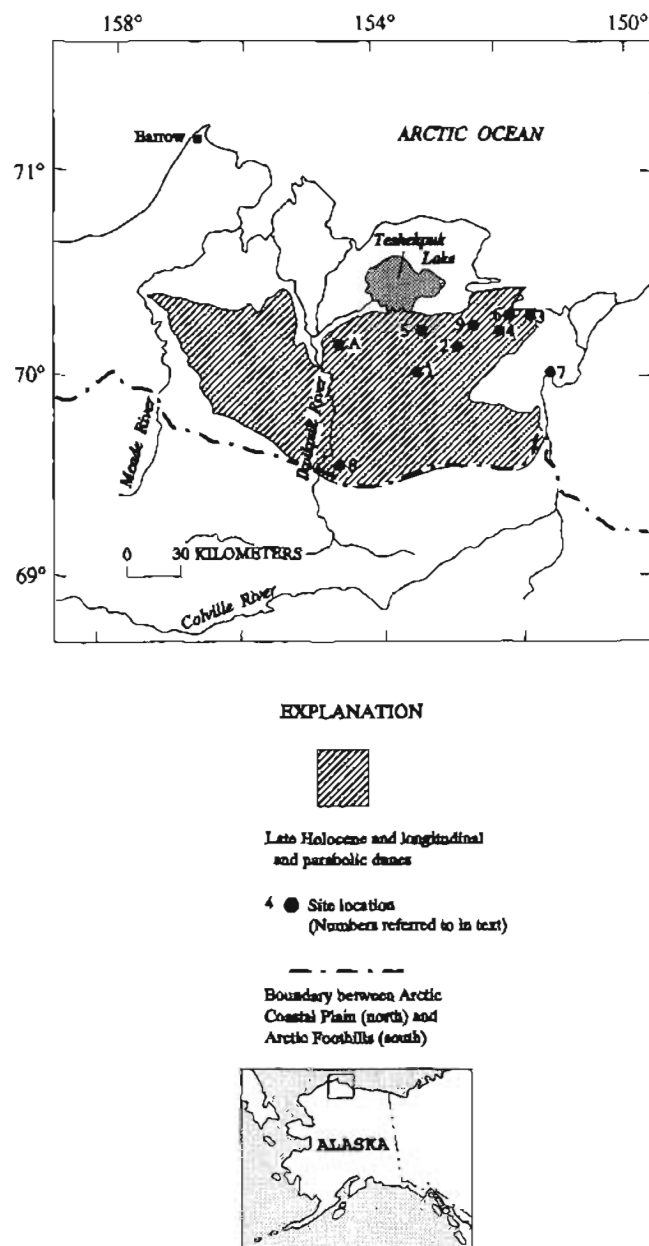


**Figure 1.** Distribution of stabilized and longitudinal and parabolic dunes and sites mentioned in text.

Sand is cryoturbated to a depth of about 40 cm below this paleosol. An upper paleosol lies 25 cm above the lower paleosol (fig. 6). Both paleosols consist of very fine-grained humic sand to sandy humus with small

roots. Fine-grained organic material and roots are more abundant between the two paleosols than between the upper paleosol and the thin (2.5 to 5 cm) tundra mat at the surface. A sample of humus from the lower half of

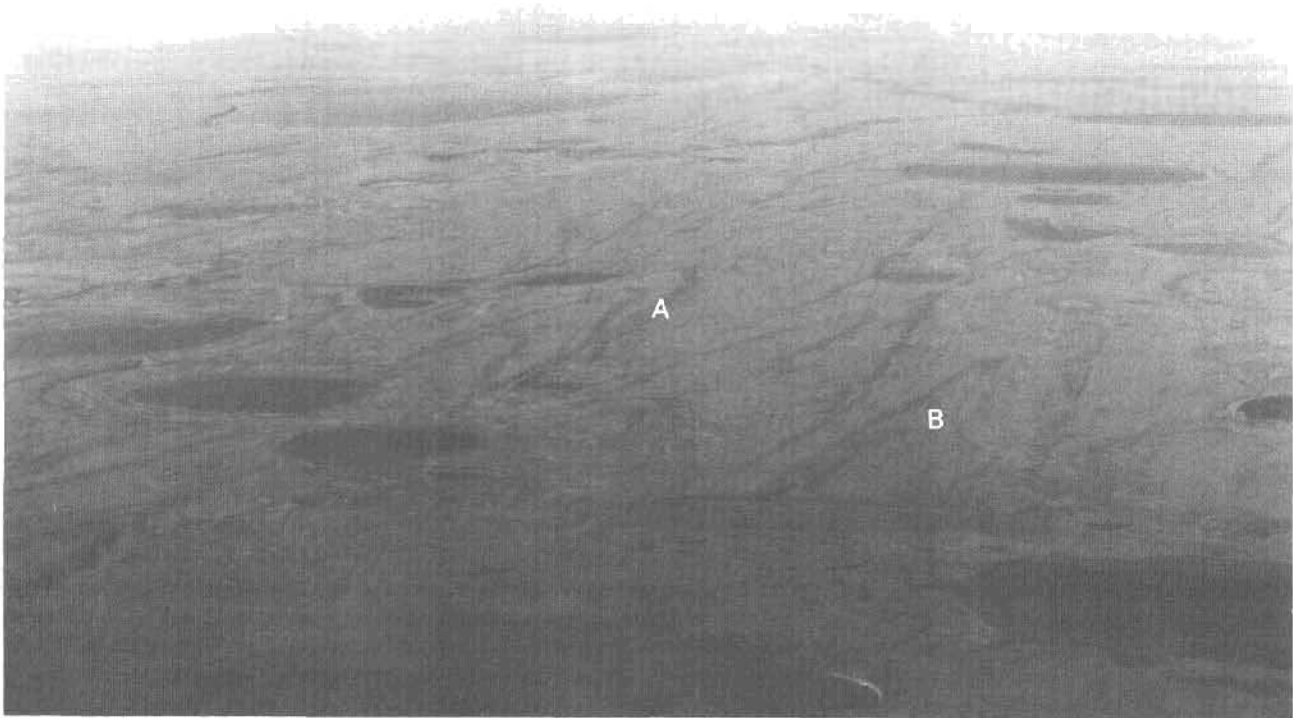


Figure 2. Oblique aerial photograph, looking west-southwest, showing longitudinal (A) and parabolic (B) dunes.



Figure 3. Oblique aerial photograph, looking east-northeast, showing longitudinal dune truncated by lake bluff at site 1.

Table 1. Radiocarbon ages of late Holocene paleosols and other organic material in eolian sand

Site (fig. 1)	Latitude	Longitude	Sample	Material	Laboratory number <sup>1</sup>	Age (yr B.P.) <sup>2</sup>	Description
Paleosols related to longitudinal and parabolic dunes							
1	70° 03.9'	153° 31.6'	78ACrII-099D	Humus	I-10,891	2,290±80	Lower half of 25 cm thick humic horizon beneath longitudinal dune (fig. 4).
2	70° 16.8'	152° 55.2'	82ACr-224A	Humus	I-13,041	2,420±80	Lower half of 25 cm thick humic horizon beneath longitudinal dune (fig. 6).
3	70° 26.2'	151° 45.5'	78ACrII-045F	Humus	I-10,890	1,100±80	Humic horizon 10 cm thick 50 cm below top of parabolic dune (fig. 8).
3			79ACr-106	Herbaceous plant debris	I-11,602	3,690±90	Collapsed nest of burrowing rodent 30 cm below base of parabolic dune (fig. 8).
Older radiocarbon ages for site 3							
3	70° 26.2'	151° 45.5'	78ACrII-045D	Humus	I-10,889	5,745±115	Humic horizon 10 to 20 cm thick developed on eolian sand. Overlain and truncated by sand of a parabolic dune.
3			78ACrII-045B1	Wood	I-10,716	10,220±150	Wood from eolian sand 1.5 m above base of a 7.5 m coastal bluff.
Late Holocene paleosols in eolian sand							
4	70° 22.65'	152° 09.2'	78ACrII-046D	Peat	I-11,489	890±75	Thin interbeds of peat and sand in zone 20 cm thick within eolian sand. Occurs 3 m below top of a 16 m river bluff.
5	70° 22.4'	153° 12.2'	77ACrII-002D	Peat	USGS-380	940±110	Thin interbeds of peat and sand in zone 25 cm thick within eolian sand. Occurs 2 m below the top of a 27 m river bluff.
6	70° 26.8'	152° 09.0'	81ACr-006	Peat	I-12,179	2,130±90	Base of 30 cm thick peat within eolian sand. Occurs 1 m below the top of a 6.4 m river bluff.
6			81ACr-006	Peat	USGS-1381	2,210±50	As above.
7	70° 04.4'	151° 22.9'	82ACr-074G	Peat	I-13,075	2,200±80	Peat 7 to 15 cm thick within eolian sand. Occurs 0.5 m below the top of a 25 m river bluff.
7			75ACr-022	Peat	USGS-185	2,280±50	As above.
8	69° 41.8'	154° 27.2'	79ACr-074T	Peat	I-11,920	2,480±80	Peat 20 to 30 cm thick within eolian sand. Occurs 1 m below the top of a 23 m river bluff.
9	70° 25.7'	152° 34.2'	81ACr-005B	Peat	I-12,178	2,500±80	Peat about 5 cm thick within eolian sand. Occurs 1 m below the top of a 3 m lake bluff.
From Rickert and Tedrow (1967)							
A	70° 17.0'	154° 43.0'		Buried soil	I-1004	3,840±140	A buried organic horizon beneath a stabilized dune (p. 258-259).

<sup>1</sup> I., Teledyne Isotopes, Inc., Westwood, N.J.

USGS-, U.S. Geological Survey Radiocarbon Laboratory, Menlo Park, Calif.

<sup>2</sup> Uncalibrated.



the lower paleosol yielded a radiocarbon age of  $2,420 \pm 80$  yr B.P. (table 1).

At site 3, a 7.6-m-high coastal bluff along Harrison Bay truncates a compound parabolic dune (fig. 7) that opens to the northeast and has a long axis that trends N.  $78^\circ$  E. The parabolic dune is 273 m long and 137 m in

maximum width, and the top of the dune is about 2 m above the adjacent land surface. The north arm of the parabolic dune is as much as 3 m thick and the sand is underlain by a paleosol 10 to 20 cm thick (fig. 8) composed of sandy humus that has yielded a radiocarbon age of  $5,745 \pm 115$  yr B.P. (table 1). A better maximum

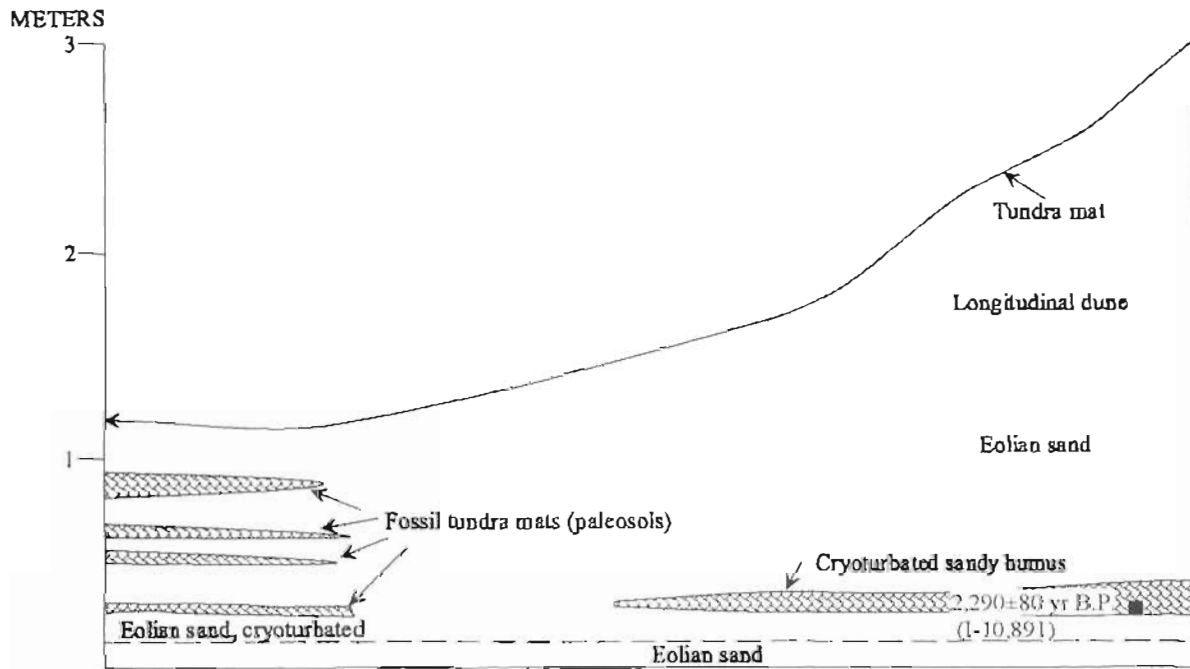


Figure 4. Diagrammatic cross section showing location of dated paleosol, site 1 (fig. 3).



Figure 5. Oblique aerial photograph, looking east-northeast, showing longitudinal dune truncated by lake bluff at site 2.

limiting radiocarbon age for the dune, however, is provided by a collapsed rodent nest that underlies an unconformity that truncates the paleosol and forms the base of the south arm of the dune. The unconformity was most likely produced by deflation as the dune began to form, and the nest was probably collapsed by the weight of the accumulating dune. A radiocarbon age of  $3,690 \pm 90$  yr B.P. was determined for herbaceous plant material from the nest (table 1). A pause in dune activity is marked by a paleosol 10 cm thick composed of sandy humus that occurs 50 cm below the top of the dune. This paleosol has a radiocarbon age of  $1,100 \pm 80$  yr B.P.

Correlative paleosols in eolian sand are found at sites 4 through 9 (fig. 1). Five of these paleosols consist of peat 10 to 30 cm thick within eolian sand and the sixth of sandy humus. Radiocarbon ages on the paleosols range from 890 to 2,500 yr B.P. (table 1).

### CALIBRATION OF RADIOCARBON AGES

Radiocarbon yr B.P. do not correspond to calendar yr B.P., because the rate of production of  $^{14}\text{C}$  in the atmosphere and other reservoirs has not been constant over geologic time.

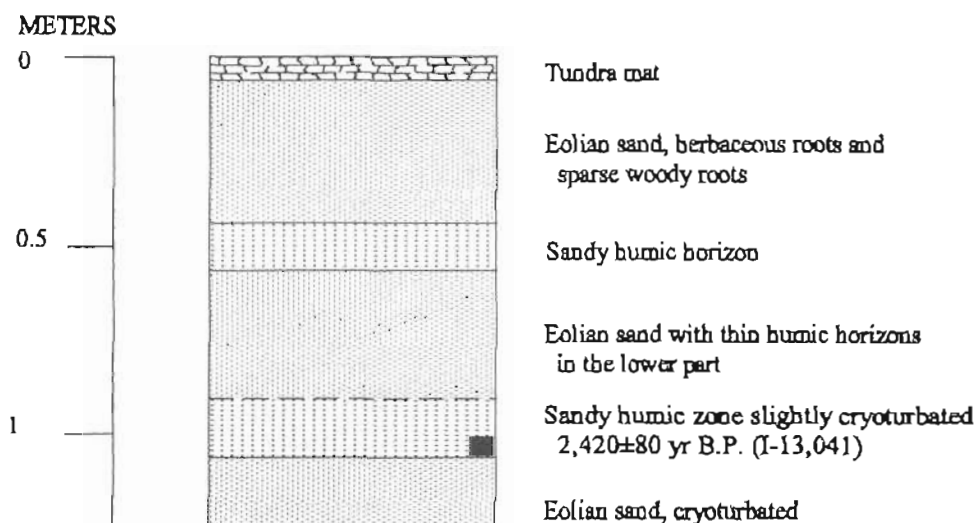


Figure 6. Measured section at site 2 (fig. 5) showing location of dated paleosol.



Figure 7. Oblique aerial photograph, looking west-southwest, showing parabolic dune truncated by coastal bluff at site 3.

Ages in radiocarbon years (table 1) were converted to calendar yr B.P. (table 2) using the calibration curve of Stuiver and Reimer (1986). From one to several calibrated ages are possible for each radiocarbon age, because the measured radiocarbon activity of the sample may intersect the calibration curve in one or more places. Values shown in parentheses in table 2 are the calibration curve intersections, and the limiting values shown without parentheses represent intersections of the radiocarbon analytical error with the calibration curve and its analytical error.

## PALEOCLIMATIC SIGNIFICANCE

Eolian sand on the Arctic Coastal Plain is highly susceptible to wind erosion if the stabilizing tundra vegetation is absent or disturbed by natural or anthropogenic processes. Over the past 20,000 years, climatic change has caused repeated stabilization of the dunes and sand sheets (Carter and others, 1984; Carter, in press). Stabilization of the eolian surfaces occurred when climatic conditions were relatively moist and allowed the growth of stabilizing vegetation, whereas reactivation of eolian activity occurred when surface conditions were relatively dry. Alternating periods of eolian sand transport and soil formation thus record changes in surface-moisture conditions, and dating these periods provides information that can be integrated with other proxy climatic information to produce a more complete record of climatic change.

The time of late Holocene dune reactivation following middle Holocene development of organic soils is not precisely known. Two radiocarbon ages for the uppermost parts of the middle Holocene paleosols are calibrated to 5.9 and 5.1 ka (Carter, in press). The thin, discontinuous paleosols associated with the late Holocene eolian sand indicate that during most of the late Holocene, dry surface

conditions promoted eolian sand transport and dune formation. The calibrated radiocarbon ages reported here for these paleosols (fig. 9) suggest that these generally dry surface conditions were interrupted by at least three relatively moist intervals of soil formation and relative landscape stability.

The maximum limiting age for the parabolic dune at site 3 suggests a possible period of soil formation at about 4 ka (table 2). This possibility is strengthened by a calibrated age of 4,264 yr B.P. (table 2) determined for a buried organic horizon beneath a stabilized dune near the Ikpikuk River (fig. 1, site A) described by Rickert and Tedrow (1967).

At least two longitudinal dunes formed after the development of paleosols that have calibrated basal dates of about 2.7 to 2.4 ka (fig. 9). Paleosols in eolian sand at four other localities (sites 6 through 9, figs. 1 and 2 and tables 1 and 2) are about the same age as the paleosols beneath the two longitudinal dunes, which suggests the possibility that the period 2.7 to 2 ka may have been a time of regional soil formation and dune stabilization on the Arctic Coastal Plain. At site 3, however, no evidence for soil development during the period 2.7 to 2 ka is present. It is possible that the soil was removed by erosion, or that soil development was patchy during this interval. Renewed eolian transport evidently occurred after about 2 ka.

A third episode of soil formation and stabilization is suggested by paleosols at several sites. The age of the paleosol near the top of the parabolic dune (site 3, fig. 1) is similar to ages for the youngest paleosol in eolian sand at two other localities (sites 4 and 5, figs. 1 and 2 and tables 1 and 2). The calibrated ages range from about 1.15 to 0.72 ka (fig. 9), which is roughly contemporaneous with the Medieval Warm Period in temperate northern latitudes (Williams and Wigley, 1983). Graybill and Shiyatov

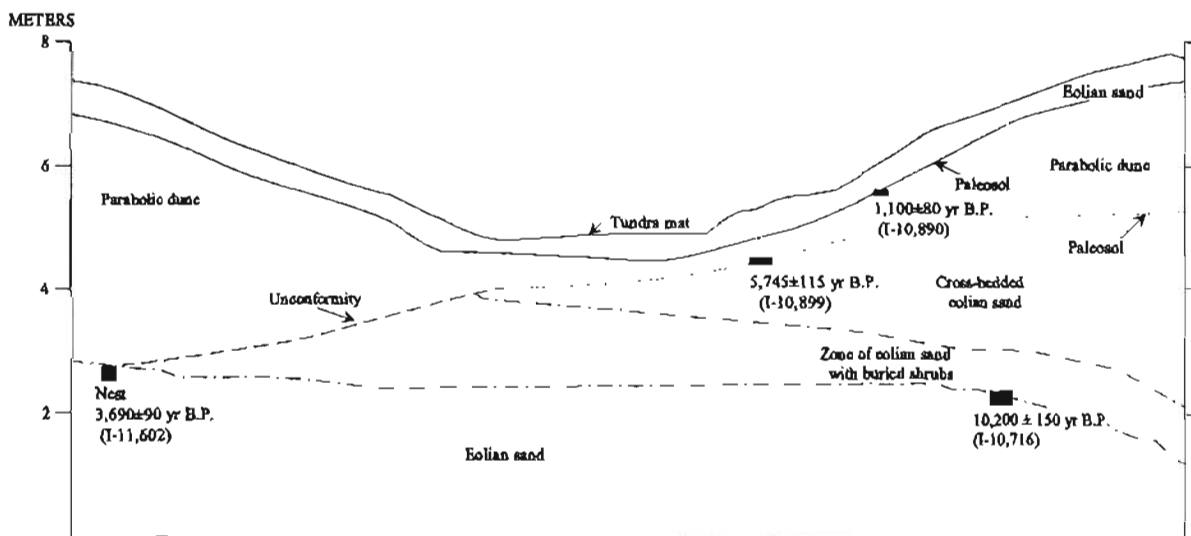


Figure 8. Diagrammatic cross section showing location of dated paleosols, site 3 (fig. 7).

**Table 2.** Calibrated radiocarbon ages

[Calibrations follow curve of Stuiver and Reimer (1986). Refer to text for explanations of ages in parentheses]

Site (fig. 1)	Laboratory number	Radiocarbon age (yr B.P.)	Calibrated age (yr B.P.)
1	I-10,891	2,290 ± 80	2,355 (2,340) 2,162
2	I-13,041	2,420 ± 80	2,713 (2,455, 2,434, 2,419, 2,379, 2,367, 2,364) 2,349
3	I-10,890	1,100 ± 80	1,168 (1,040, 1,035, 973) 950
3	I-11,602	3,690 ± 90	4,219 (4,082, 4,030, 4,020, 4,009, 3,989) 3,907
4	I-11,489	890 ± 75	925 (792) 727
5	USGS-380	940 ± 110	960 (913, 808, 801) 730
6	I-12,179	2,130 ± 90	2,306 (2,145, 2,144, 2,121, 2,084) 2,000
6	USGS-1381	2,210 ± 50	2,334 (2,303, 2,241, 2,206, 2,202, 2,181, 2,166, 2,163) 2,152
7	I-13,075	2,200 ± 80	2,338 (2,301, 2,244, 2,179, 2,168, 2,162) 2,078
7	USGS-185	2,280 ± 50	2,348 (2,338) 2,183
8	I-11,920	2,480 ± 80	2,740 (2,708, 2,635, 2,606, 2,587, 2,565, 2,564, 2,541, 2,521, 2,507, 2,405, 2,404) 2,359
9	I-12,178	2,500 ± 80	2,743 (2,712, 2,629, 2,609, 2,578, 2,572, 2,558, 2,545) 2,363
A	I-1004	3,840 ± 140	4,503 (4,264) 3,996

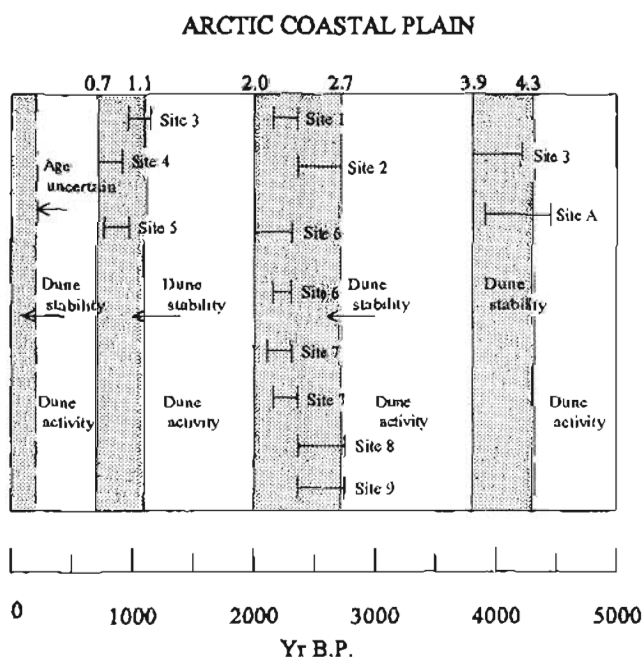
(1992) present dendroclimatic evidence for warming to above-long-term means during the Medieval Warm Period in the Soviet sub-arctic. On the Alaskan Arctic Coastal Plain, climatic conditions at about 1 ka may have been both wetter and warmer than conditions before and after that time. As the landscape became drier after 0.7 ka, renewed eolian sand accumulation occurred.

Our evidence suggests that there have been at least four late Holocene episodes of eolian sediment transport and dune formation on this part of the western Arctic Coastal Plain: (1) the oldest episode, which terminated

**Table 3.** Mean ages of middle to late Holocene moraine-building events in Brooks Range based on lichen data compared with episodes of dune formation and episodes of paleosol development on Arctic Coastal Plain based on radiocarbon data

Brooks Range		Episodes on Arctic Coastal Plain (yr B.P.)
Lichen age (L) (yr B.P.) <sup>1</sup>	Number of moraines	
4400	8	Dune activity prior to 4300
		Paleosol development 4300 to 3900
3500	9	Dune activity 3900 to 2700
2800	8	
2300	4?	Paleosol development 2700 to 2000
1800	22	
1400	19	Dune activity 2000 to 1100
1100	31	
		Paleosol development 1100 to 700
800	45	
380	85	Dune activity 700 to near present day
90	42	

<sup>1</sup>Modified from Calkin (1988, table 2, p. 163).

**Figure 9.** Range of calibrated radiocarbon ages for middle to late Holocene paleosols and other organic material in eolian sand. See table 2 for list of possible ages yr B.P.

prior to 4.5 ka, (2) between about 3.9 and 2.7 ka, (3) from sometime after 2 to about 1.1 ka, and (4) from about 0.7 ka to near the present. Each of these episodes broadly correlates with one or more Neoglacial expansions of cirque glaciers in the Brooks Range (table 3; Calkin, 1988), which suggests that the dunes were active when climate was cooler and drier than today as was the case when the Pleistocene sand sea was active during the last glacial maximum (Carter, 1983). The episode of landscape stability and soil development on the Arctic Coastal Plain that began at about 2.7 ka, and separates the second and third

episodes of dune formation, appears to correspond with the early part of a period of alluviation identified by Hamilton (1981, 1986) in the headward regions of some Brooks Range valleys. Hamilton attributed this alluviation to cirque glacier advances, which agreed with chronologies of Brooks Range Neoglacial expansion presented by Calkin and others (1983) and Ellis and Calkin (1984). The most recent compilation of Brooks Range Neoglacial advances, however, shows little evidence for cirque glacier expansion between 2.8 and 1.8 ka (Calkin, 1988).

## REFERENCES CITED

- Black, R.F., 1951, Eolian deposits of Alaska: *Arctic*, v. 4, no. 2, p. 89-111.
- Calkin, P.E., 1988, Holocene glaciation in Alaska (and adjoining Yukon Territory, Canada): *Quaternary Science Reviews*, v. 7, no. 2, p. 159-184.
- Calkin, P.E., Haworth, L.A., and Ellis, J.M., 1983, Holocene glacier fluctuations in the Brooks Range, Alaska, in Thorson, R.M., and Hamilton, T.D., eds., *Glaciation in Alaska—Extended abstracts from a workshop*: Fairbanks, University of Alaska Museum Occasional Paper No. 2, p. 11-16.
- Carter, L.D., 1981, A Pleistocene sand sea on the Alaskan Arctic Coastal Plain: *Science*, v. 211, p. 381-383.
- , 1983, Fossil sand wedges on the Alaskan Arctic Coastal Plain and their paleoenvironmental significance, in *Permafrost, Fourth International Conference Proceedings*: Washington, D.C., National Academy Press, p. 109-114.
- , 1992, A chronostratigraphic framework for interpretation of Late Quaternary climatic change on the Alaskan Arctic Coastal Plain [abs.]: *International Conference on Arctic Margins*, Anchorage, Alaska, Sept. 2-4, 1992, *Proceedings*, p. 9.
- , in press, Late Pleistocene stabilization and reactivation of eolian sand in northern Alaska: Implications for the effects of future climatic warming on an eolian landscape in continuous permafrost: Beijing, Permafrost, Sixth International Conference Proceedings.
- Carter, L.D., Forester, R.M., and Nelson, R.E., 1984, Mid-Wisconsin through early Holocene changes in seasonal climate, northern Alaska: Boulder, Colo., American Quaternary Association Eighth Biennial Meeting, Program and Abstracts, p. 20-22.
- Ellis, J.M., and Calkin, P.E., 1984, Chronology of Holocene glaciation, central Brooks Range, Alaska: *Geological Society of America Bulletin*, v. 95, no. 8, p. 897-912.
- Graybill, D.A., and Shiyatov, S.G., 1992, Dendroclimatic evidence from the northern Soviet Union, in Bradley, R.S., and Jones, P.D., eds., *Climate since A.D. 1500*: New York, Routledge, p. 393-414.
- Hamilton, T.D., 1981, Episodic Holocene alluviation in the central Brooks Range: chronology, correlations, and climatic implications, in Albert, N.R.D., and Hudson, Travis, eds., *The United States Geological Survey in Alaska: Accomplishments during 1979*: U.S. Geological Survey Circular 823-B, p. 21-24.
- , 1986, Late Cenozoic glaciation of the central Brooks Range, in Hamilton, T.D., Reed, K.M., and Thorson, R.M., eds., *Glaciation in Alaska: The geologic record*: Anchorage, Alaska Geological Society, p. 9-50.
- Pye, Kenneth, and Tsoar, Haim, 1990, *Aeolian sand and sand dunes*: London, Unwin Hyman, 396 p.
- Rickert, D.A., and Tedrow, J.C.F., 1967, Pedologic investigations on some aeolian deposits of northern Alaska: *Soil Science*, v. 104, no. 4, p. 250-262.
- Stuiver, Minze, and Reimer, P.J., 1986, A computer program for radiocarbon age calibration: *Radiocarbon*, v. 28, no. 2B, p. 1022-1030.
- Williams, L.D., and Wigley, T.M.L., 1983, A comparison of evidence for Late Holocene summer temperature variations in the northern hemisphere: *Quaternary Research*, v. 20, no. 3, p. 286-307.

Reviewers: George Plafker and Warren Yocum

# DEEP-WATER LITHOFACIES AND CONODONT FAUNAS OF THE LISBURNE GROUP, WEST-CENTRAL BROOKS RANGE, ALASKA

By Julie A. Dumoulin, Anita G. Harris, and Jeanine M. Schmidt

## ABSTRACT

Deep-water lithofacies of the Lisburne Group occur in thrust sheets in the western part of the foreland fold and thrust belt of the Brooks Range and represent at least three discrete units. The Kuna Formation (Brooks Range allochthon) consists mostly of spiculitic mudstone and lesser shale; subordinate carbonate layers are chiefly diagenetic dolomite. Predominantly shale sections of the Kuna that contain few sponge spicules occur in the western part of the study area. The Akmalik Chert (Picnic Creek allochthon) is mostly radiolarian-spiculitic chert; rare limy beds are calcitized radiolarite. The Rim Butte unit (Ipsnavik River allochthon) consists chiefly of calcareous turbidites, derived from both shallow- and deep-water sources, interbedded with spiculitic mudstone. Much of the material in the turbidites came from a contemporaneous carbonate platform and margin, but some fossils and lithic clasts were eroded from older, already lithified carbonate-platform rocks. All three units appear to be roughly coeval and are chiefly Osagean (late Early Mississippian) in age in the study area.

Shallow-water lithofacies of the Lisburne Group exposed in the Howard Pass area (Brooks Range allochthon) are mostly of Meramecian (early Late Mississippian) age. Thus, these carbonate-platform rocks were not the source of the calcareous turbidites in the Rim Butte unit. Rim Butte turbidites could have been derived from older platform carbonate rocks such as those of the Utukok Formation (Kelly River allochthon) exposed mainly to the west of the Howard Pass quadrangle.

## INTRODUCTION

The chiefly Carboniferous Lisburne Group is a dominantly platform carbonate sequence exposed throughout northern Alaska in the foreland fold and thrust belt of the Brooks Range (fig. 1). Deeper water facies (used here to mean sediments deposited below the photic zone, probably at depths of 100 m or greater) occur within this group,

particularly in the western Brooks Range, but have been little studied. In this paper we describe deep-water Lisburne lithofacies found in the Howard Pass and western Killik River quadrangles (fig. 2). Previous workers (for example, Mayfield and others, 1988) considered these facies to be largely younger than nearby outcrops of the platform facies, but our work suggests that, in the Howard Pass area, the deeper water facies are chiefly older than nearby platform facies.

The deep-water carbonate rocks considered here belong to three units: the Kuna Formation, the Akmalik Chert, and the Rim Butte unit. In the structural framework of Mayfield and others (1988), these units were assigned to three discrete structural sequences or allochthons. The allochthons are distinguished on the basis of inferred structural level and differences in lithologic succession; differences are most pronounced in the Carboniferous facies. The distribution of these allochthons in the study area is shown in figure 2. Platform facies of the Lisburne Group, as well as deeper water facies of the Kuna Formation, were assigned to the Brooks Range allochthon (equivalent to Endicott Mountains allochthon; Mull, 1989). Chert and limestone equivalent to the Akmalik Chert is part of the Picnic Creek allochthon, and the Rim Butte unit is part of the Ipsnavik River allochthon.

The findings described here are based on measured sections and outcrop studies at localities shown in figure 2; petrographic descriptions are based on field observations and examination of about 200 thin sections. Identification of calcite and dolomite was made using the Alizarin Red-S and potassium ferricyanide staining technique of Dickson (1966); the presence of dolomite was confirmed in some samples by X-ray diffraction analysis (Elizabeth Bailey, U.S. Geological Survey, written commun., 1992).

## KUNA FORMATION

The Kuna Formation was examined across the study area (fig. 2); outcrops investigated include the type section (fig. 2, loc. 9) and one of the reference sections (fig. 2, loc.

13) established by Mull and others (1982). In the study area, the Kuna is at most 70 m thick; it depositionally overlies the Kayak Shale and generally underlies fine-grained sedimentary rocks of the Etivluk Group. Locally, particularly in the eastern part of the study area, the upper contact of the Kuna is a fault.

As originally defined by Mull and others (1982), the Kuna Formation consists of black carbonaceous shale, black chert, fine-grained limestone, and dolostone. In the study area, some Kuna sections consist chiefly of black, carbonaceous, noncalcareous shale; such sections are generally poorly exposed and include only minor amounts of carbonate rocks and (or) chert (fig. 3A). These shale-rich outcrops are commonest in the western half of the Howard Pass quadrangle (fig. 2).

Most sections of the Kuna Formation examined in this study, however, consist primarily of siliceous mudstone with subordinate (5–20 percent) shaly beds or partings (fig. 3B). Mudstone beds are even to irregular and 2–20 cm thick; shale intervals are generally a few centimeters or less, but may be as much as 10 cm thick. The thicker beds, called chert by some previous workers (for example, Mull and others, 1982), are siliceous mudstone, not true chert; they have an earthy rather than vitreous luster and do not fracture conchoidally. In thin section, they contain abundant biosiliceous material, chiefly sponge spicules but also subordinate radiolarians, in a matrix of organic-rich mud (fig. 3C). Some mudstone layers have been locally

silicified; silica for this process may have come, at least in part, from dissolution and remobilization of the bio-siliceous component of these rocks.

Fine lamination is the only sedimentary structure visible in most outcrops of the Kuna Formation (fig. 3D). Laminae consist of local concentrations of sand- to silt-sized clasts, mostly of mudstone, or alternating concentrations of sponge spicules and mud (fig. 3E). Most laminated intervals probably represent distal turbidites, or lags left by bottom currents. But cyclic changes in productivity and (or) detrital influx into the Kuna basin(s) could also have played a role in forming some laminae.

Preservation of these laminae, as well as the apparently high organic content of much of the Kuna Formation, suggest that anoxic or dysaerobic bottom-water conditions prevailed during its deposition. Some intervals within the Kuna are burrowed, however, so oxygen levels at the sediment-water interface were locally or periodically high enough to support a bottom fauna. Bioturbated intervals (fig. 3F) are most common in the easternmost exposures of the Kuna in the study area. Burrows are round to ovoid in cross section, about 0.5–1 cm in diameter, and generally richer in siliceous bioclasts than the surrounding mudstone.

Carbonate forms 30 percent or less of most outcrops of the Kuna Formation that we studied. Carbonate occurs as concretions, 4–85 cm in diameter (fig. 4A), or more continuous layers a few millimeters to 30 cm thick (fig. 4B). Primary calcareous material, such as obvious

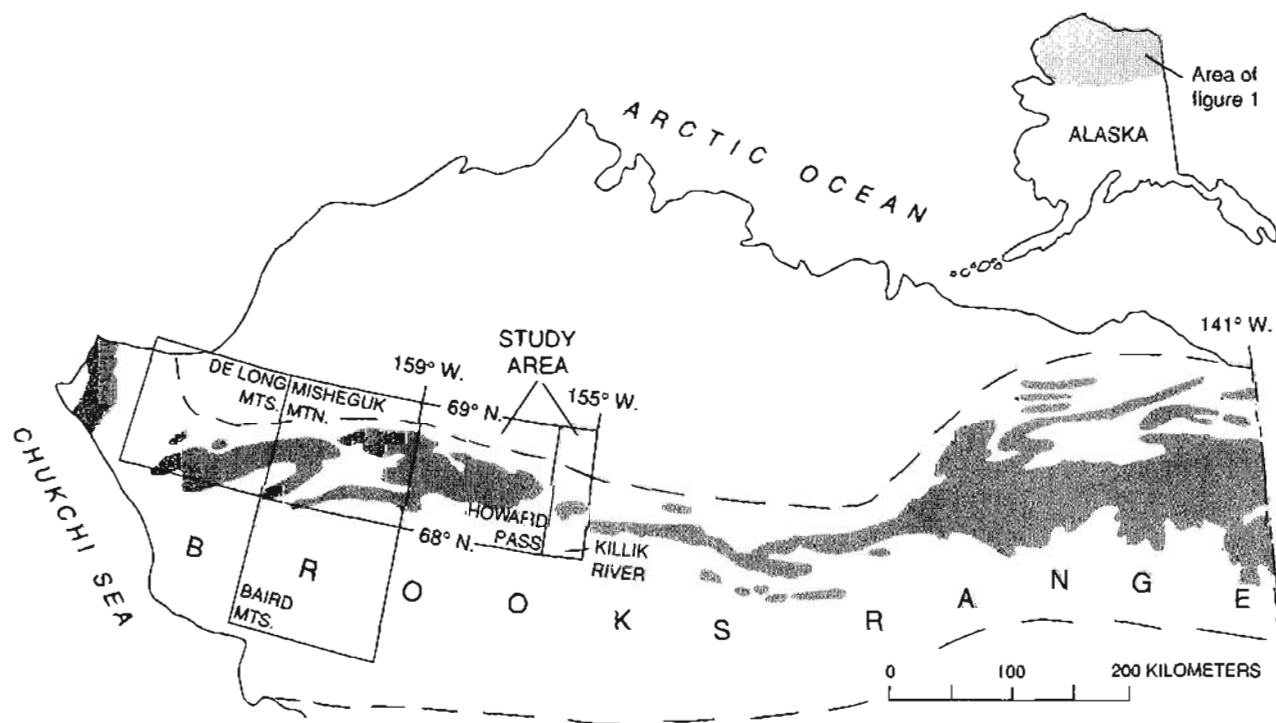


Figure 1. Distribution of Lisburne Group (pattern) in northern Alaska (generalized from Armstrong and Mamet, 1978) and location of quadrangles mentioned in text.



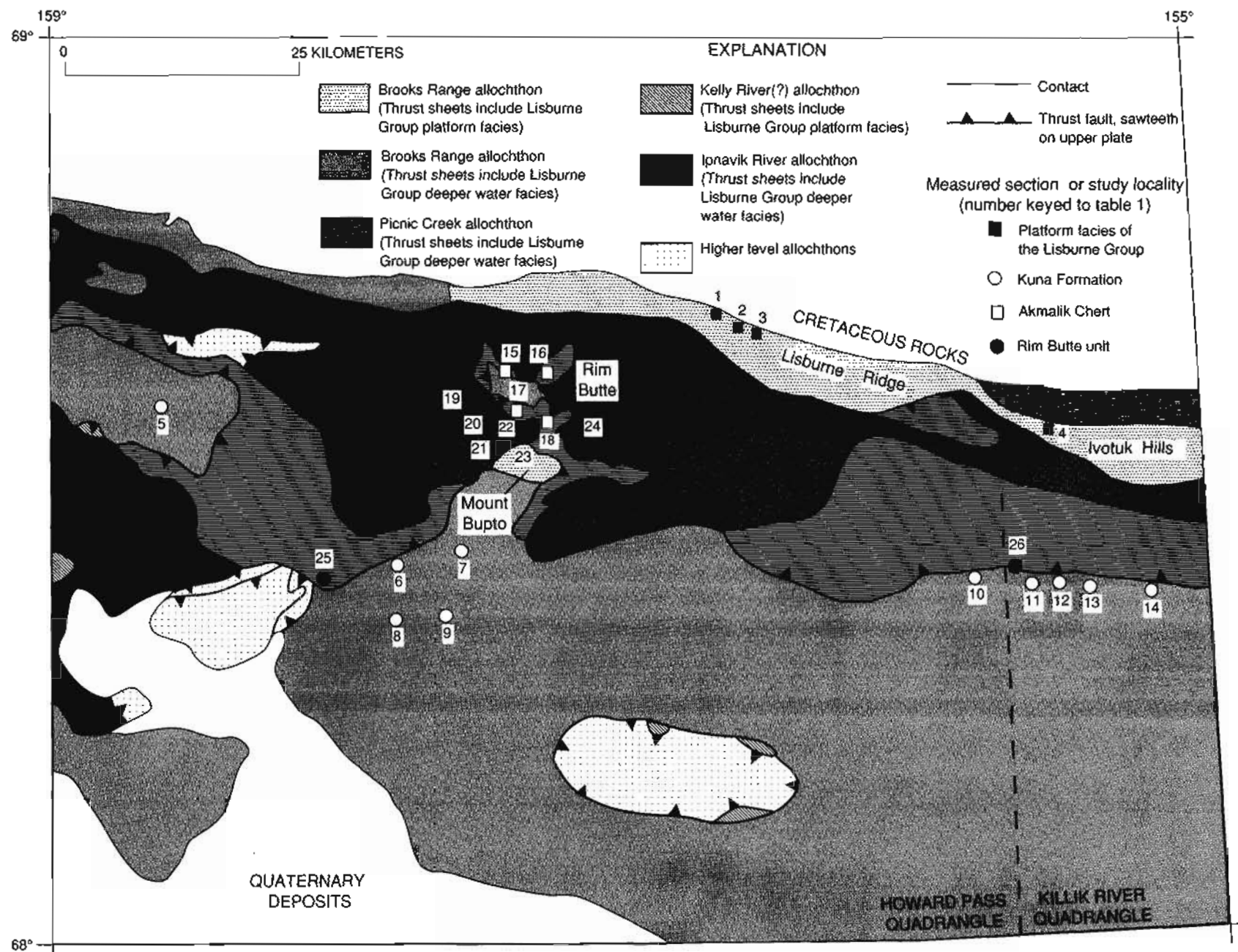


Figure 2. Distribution of allochthons, slightly modified from Mayfield and others (1988), and location of measured sections and lithologic and fossil collections in Howard Pass and western Killik River quadrangles. Allochthons may include thrust sheets of other allochthons too small to show at scale of map. See table 1 for geographic coordinates, key faunal components, and lithologies for numbered localities.



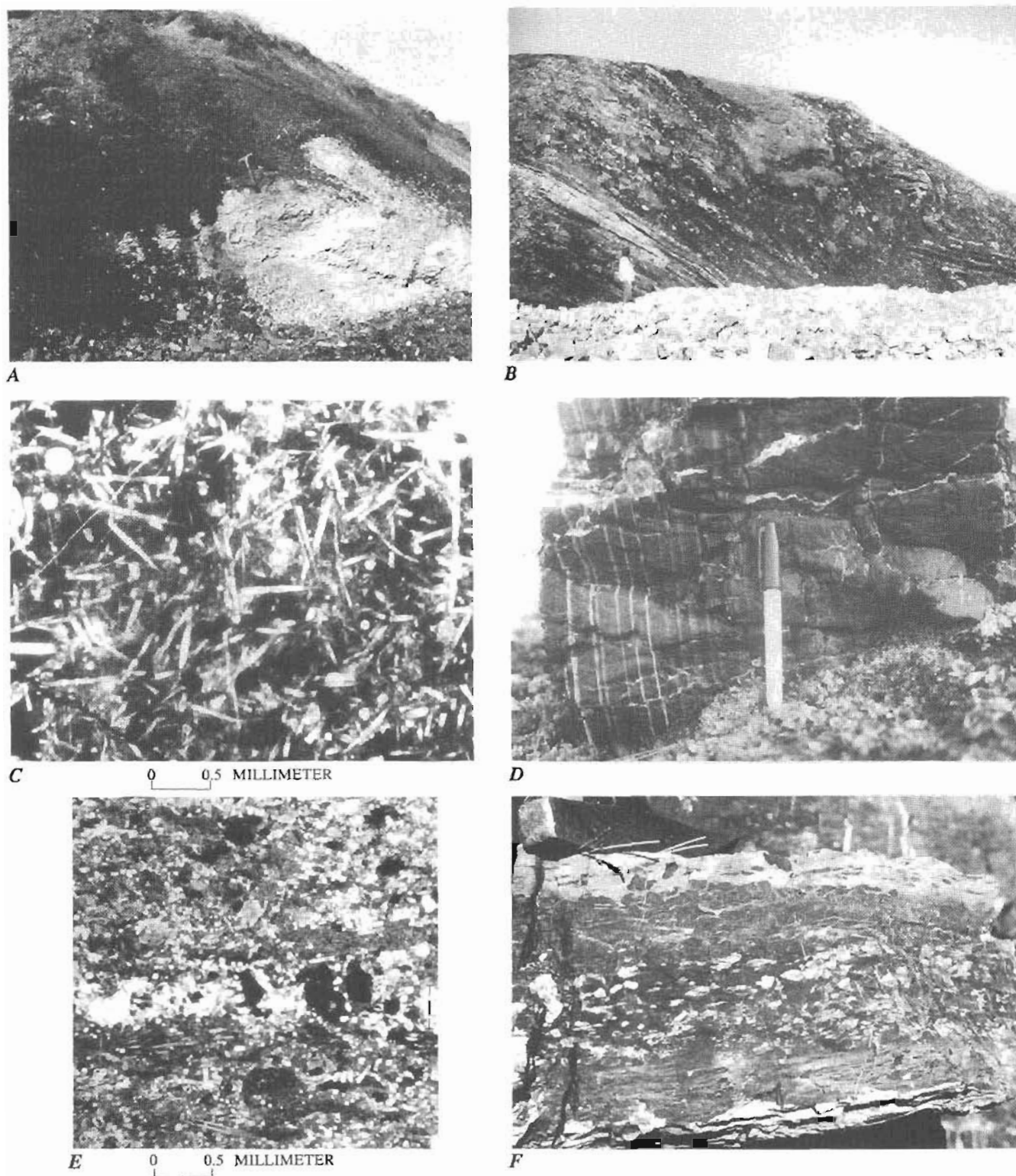
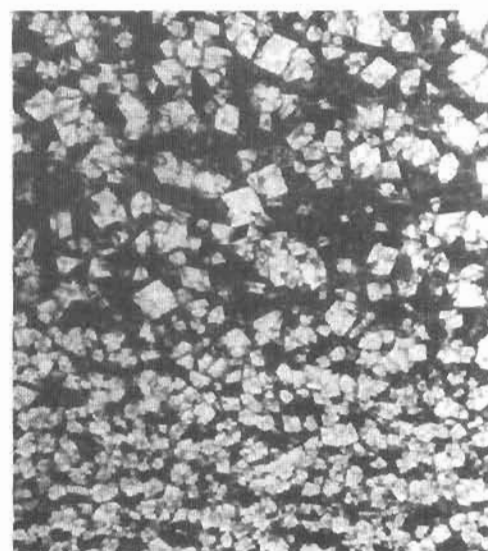
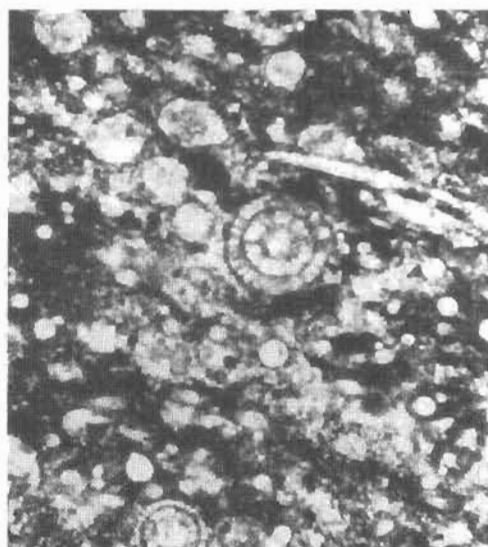


Figure 3. Sedimentary features of Kuna Formation. *A*, Section consisting chiefly of black carbonaceous shale and subordinate siliceous tuff; Drenchwater Creek (fig. 2, loc. 5). *B*, Section consisting chiefly of siliceous mudstone and subordinate shale (fig. 2, loc. 14). *C*, Photomicrograph of siliceous mudstone from section shown in *B*; note abundant siliceous bioclasts, chiefly sponge spicules and rare radiolarians, in mudstone matrix. *D*,

Fine laminae in siliceous mudstone (fig. 2, loc. 5). *E*, Photomicrograph of lamina (I) in siliceous mudstone made of abundant sponge spicules and lesser dark mudstone clasts (fig. 2, loc. 14); such laminae may have been produced by distal turbidites, bottom currents, and (or) cyclic changes in basin chemistry. *F*, Bioturbated interval in siliceous mudstone; burrows are richer in siliceous bioclasts than surrounding matrix (fig. 2, loc. 14).

*A**B**C* 0 0.5 MILLIMETER*D**E* 0 0.3 MILLIMETER*F* 0 0.5 MILLIMETER

bioclasts (foraminifers or crinoid columnals) were not observed in the samples we examined; brachiopod shells occur locally (see below) but have been completely replaced by silica. Thin-section observations indicate that almost all carbonate now present in the Kuna is of diagenetic origin.

Most carbonate layers in the Kuna Formation consist of euhedral crystals of dolomite in a mudstone matrix; crystals are 16–200  $\mu\text{m}$  in diameter and make up 80 percent or more of most samples from these layers (fig. 4C). Dolomite is an important component of many organic-rich marine sediments, because microbial activity in these sediments reduces sulfate and allows dolomite to form (Baker and Kastner, 1981). Such marine dolomite typically replaces calcite; in the Kuna samples, dolomite crystals may have replaced fine-grained calcitic bioclasts and bioclast fragments deposited by turbidity currents. Thin layers rich in calcareous skeletal fragments occur in the Kuna further to the west (for example, in the De Long Mountains quadrangle). Textural relationships observed in outcrop and thin-section indicate that dolomite formed prior to silicification in most Kuna samples; dolomite concentrations are locally cross-cut or partly replaced by quartz (fig. 4D).

Other carbonate occurrences in the Kuna Formation include calcitized radiolarite (fig. 4E). Radiolarians range from 80 to 320  $\mu\text{m}$  in diameter and generally make up 30–80 percent of these samples. Tests occur in a calcite matrix; most tests have been completely replaced by calcite, but concentrations of organic matter and (or) pyrite preserve details of the original test structure. Samples richest in radiolarians are generally graded and laminated and were probably deposited by turbidity currents.

Fossils are rare in the Kuna Formation, and include no forms restricted to shallow-water carbonate-platform environments. Concentrations of productid brachiopods occur locally, and probably represent storm deposits (fig. 4F).

Conodonts have been obtained from some carbonate layers. Some samples produce very few conodonts partly because the high organic and biosiliceous content of the rock inhibits disaggregation. Other samples, however, are rich in conodonts (table 1, loc. 14, USGS colln. no. 31738-PC), primarily representatives of *Bispathodus utahensis* Sandberg and Gutschick (fig. 5A–E). This

pelagic species probably lived in the more oxygenated upper part of the water column above the dysaerobic to anoxic basin floor. Sandberg and Gutschick (1984) reported that *B. utahensis* is most abundant and generally the only conodont in the deep basinal part of the Deseret basin, western Utah, during the middle Osagean *anchoralis-latus* Zone, but that the species also occurs in significant numbers in most other environments. They attributed this distribution to a pelagic life style. The distribution of *B. utahensis* in the Kuna Formation supports their model.

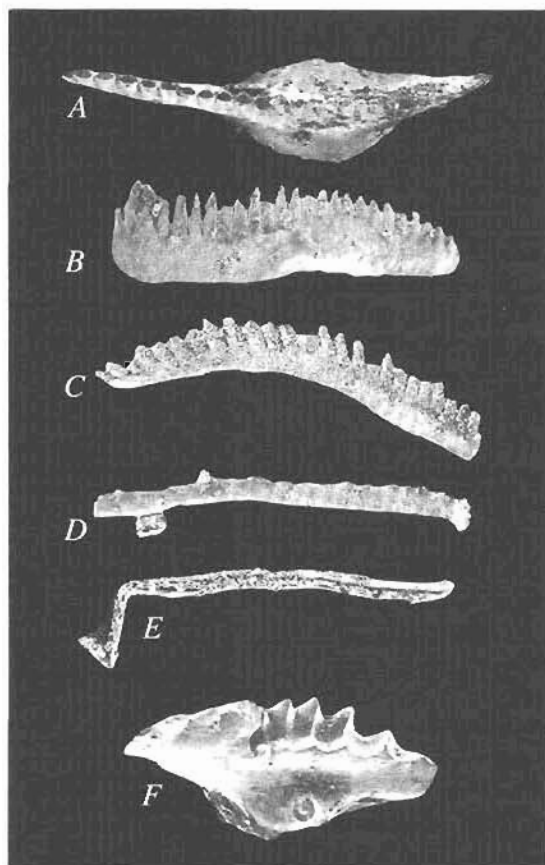


**Figure 5.** Scanning electron micrographs of Early Mississippian conodonts from Kuna Formation and Kayak Shale. A–E, Conodonts from Kuna Formation (fig. 2, loc. 14; table 1, USGS colln. 31738-PC), *Bispathodus utahensis* Sandberg and Gutschick: A, B, Pa elements, upper and outer lateral views,  $\times 40$  and  $\times 30$ , USNM 473769 and 473770, respectively. C, Pb element, inner lateral view,  $\times 30$ , USNM 473771. D, Sc element, inner lateral view,  $\times 20$ , USNM 473772. E, Sd element, upper view,  $\times 30$ , USNM 473773. F, Conodont from the Kayak Shale (fig. 2, loc. 7; table 1, USGS colln. 31743-PC), *Bispathodus? plumulus nodosus* (Rhodes, Austin, and Druce), Pa element, upper view,  $\times 50$ , USNM 473774. Specimens illustrated in this paper are repositied in type collections of the Paleobiology Department, U.S. National Museum, Washington, D.C. (USNM).

**Figure 4.** Sedimentary features of Kuna Formation. A, Carbonate concretions made up chiefly of calcitized radiolarite; type section, Kuna Formation (fig. 2, loc. 9). B, Laterally continuous carbonate layer made mostly of dolostone; reference section, Kuna Formation (fig. 2, loc. 13). C, Photomicrograph of carbonate layer shown in B; dolomite crystals in mudstone matrix. D, Carbonate concretion partly replaced by chert (arrows); reference section, Kuna Formation (fig. 2, loc. 13). E, Photomicrograph of calcitized radiolarite. Matrix and radiolarians replaced by calcite; details of original test structure outlined by organic matter (fig. 2, loc. 14). F, Photomicrograph of silicified productid brachiopods in storm bed (fig. 2, loc. 14).

Table 1. Locality register for key conodonts and lithologic features

[Map number indicates measured section or study locality shown on figure 2. Units are keyed to figure 2: LGP, Lisburne Group, platform facies; K, Kuna Formation; A, Akmalik Chert; RB, Rim Butte unit. Letters in field numbers refer to collector: AD, J.A. Dumoulin; AMu, C.G. Mulk; JS, J.M. Schmidt; ASi, J.P. Siok; and TR, I.L. Tailleux. CAI, color alteration index]

MAP NO. (UNIT)	FIELD NO. (USGS COLLN. NO.)	LATITUDE N/ LONGITUDE W.	KEY CONODONT SPECIES AND LITHOLOGIES	FOSSIL AGE AND CAI	REMARKS
1 (LGP)	92AD31G (31768-PC)	68°37'58"/ 156°43'45"	Thin-bedded dolostone interbedded with chert, shale, and pisolitic phosphate layers <i>Cavusgnathus unicornis</i> <i>Gnathodus homopunctatus</i> <i>Gnathodus semiglaber</i> <i>Syncladognathus geminus</i>	middle Late Mississippian (late Meramecian to early Chesterian?); CAI=1-1.5	Near top of Lisburne Group, no more than 20 m below top.
2 (LGP)	92AD7K (31769-PC)	68°37'25"/ 156°40'35"	Thin-bedded dolostone interbedded with chert <i>Bispathodus utahensis</i> <i>Cavusgnathus unicornis</i> <i>Hindeodus</i> sp. indet.	early Late Mississippian (late Meramecian); CAI=1-1.5	Five meters below exposed top (probably actual top) of Lisburne Group and 5 m below 92AD7I; base of overlying Siksikuk Formation concealed.
	92AD7I (31770-PC)		Thin-bedded dolostone interbedded with chert <i>Bispathodus utahensis</i> <i>Cavusgnathus unicornis</i> <i>Syncladognathus geminus</i>	early Late Mississippian (late Meramecian); CAI=1-1.5	At exposed top (probably actual top) of Lisburne Group; base of overlying Siksikuk Formation concealed.
3 (LGP)	92AD16-227 (31771-PC)	68°37'24" to 37°00"/ 156°37'05" to 50"	Crinoidal dolostone <i>Bispathodus utahensis</i> <i>Cavusgnathus unicornis</i>	early Late Mississippian (late Meramecian); CAI=1-1.5	Measured section of the Lisburne Group (305 m)
4 (LGP)	90AD59C and 85ASi14-18 (31734-37-PC and 29892-PC)	68°28'45"/ 155°42'48" and 68°28'42"/ 155°42'20"		Mississippian (Osagean to Chesterian)	Measured section of the Lisburne Group (~220 m); see Dumoulin and Harris (this volume) for description of section and conodont faunas. Contact between Lisburne Group and Siksikuk Formation concealed.
5 (K)	90AD62	68°34'43"/ 158°42'50"	Chiefly carbonaceous shale, lesser spiculitic mudstone and carbonate rocks		
6 (K)	91AD14	68°24'45"/ 157°54'00"	Chiefly spiculitic mudstone and notable calcitized radiolarite		
7 (K—Kuna Formation overlying Kayak Shale)	91AD9E, F (31743-PC)	68°23'30"/ 157°39'15"	Kuna Formation is predominantly carbonaceous shale and lesser spiculitic mudstone and carbonate rocks 91AD9E—Kayak Shale; bryozoan wackestone indeterminate bar fragments  91AD9F—Kayak Shale, 13 m above 91AD9E; skeletal pack/grainstone <i>Bispathodus? plumulus nodosus</i> (fig. 5F)	latest Devonian to Early Mississippian (probably Kinderhookian but could be Osagean; bispathodids appear to be longer ranging in northern Alaska than elsewhere); CAI=2-2.5	Conodont samples from limestone interval in uppermost part of Kayak Shale; contact between Kayak Shale and Kuna Formation concealed.
8 (K—Kuna Formation overlying Kayak Shale)	91JS38B (31757-PC)	68°19'40"/ 157°52'38"	Kuna Formation: predominantly carbonaceous shale and lesser spiculitic mudstone and carbonate rocks <i>Bispathodus?</i> aff. <i>B. stabilis</i> <i>Pseudopolygnathus</i> sp. indet. fragments of Early Mississippian morphotype	Early Mississippian; CAI indeterminate--conodonts covered with amorphous organic matter	An interval of concretion-bearing shale forms the uppermost part of the Kayak Shale. The concretions contain a variety of mollusks, including ammonoids that have not yet been dated.
	91JS38A (31756-PC)		Kayak Shale: black, very fine grained limestone associated with black shale <i>Bispathodus</i> aff. <i>B. aculeatus plumulus</i> fragment <i>Polygnathus</i> sp. indet. fragment	latest Devonian to Early Mississippian (late Famennian to Osagean), probably Kinderhookian; CAI=3.5-4	

Table 1. Locality register for key conodonts and lithologic features—Continued

MAP NO. (UNIT)	FIELD NO. (USGS COLLN. NO.)	LATITUDE N/ LONGITUDE W.	KEY CONODONT SPECIES AND LITHOLOGIES	FOSSIL AGE AND CAI	REMARKS
9(K)	90AD41	68°20'00"/ 157°44'30"	Carbonaceous shale, spiculitic mudstone, and notable carbonate concretions.		Type section of the Kuna Formation
10(K)	91JS19	68°20'52"/ 156°04'20"	Chiefly spiculitic mudstone and lesser carbonate rocks and carbonaceous shale		
11 (K—Kuna Formation overlying Kayak Shale)	91JS25F (31752-PC)	68°20'08"/ 155°52'45"	Kuna Formation: chiefly spiculitic mudstone and lesser carbonate rocks <i>Bispathodus stabilis</i> or <i>B. utahensis</i>	latest Devonian to Mississippian (late Famennian to Meramecian), probably Mississippian CAI=2; conodonts covered with amorphous organic matter	
	91JS25C (31751-PC)	68°19'28"/ 155°52'55"	Kayak Shale: bioclastic quartz sandstone layer <i>Polygnathus?</i> sp. indet. fragment	Late Devonian to Early Mississippian (probably Kinderhookian) CAI=2 or 3	
12(K)	91JS27	68°20'00"/ 155°48'20"	Chiefly spiculitic mudstone and lesser carbonate rocks		
13 (K—Kuna Formation overlying Kayak Shale)	90AD65S (30941-PC)	68°19'45"/ 155°42'20"	Kuna Formation: chiefly spiculitic mudstone, lesser carbonate rocks, and minor shale bispathodid or hindeodid mid-platform fragment	latest Devonian to Mississippian (late Famennian to Meramecian), probably Mississippian; CAI=2.5-3	Reference section of the Kuna Formation: 90AD65S: 15 m above exposed base of formation. 90AD65O: 45 m above exposed base of formation. Most conodonts are partly to nearly completely coated with amorphous organic matter.
	90AD65O (30942-PC)		<i>Bispathodus utahensis</i>	Mississippian (Osagean to Meramecian); CAI=2.5-3	
14 (K—Kuna Formation overlying Kayak Shale)	91AD1Y (31738-PC)	68°19'48"/ 155°30'55"	Kuna Formation: chiefly spiculitic mudstone and lesser carbonate rocks and shale; rare bioturbated horizons and productid brachiopods (storm deposits) <i>Bispathodus utahensis</i> (fig. 5A-E) <i>Idioproniodus</i> sp. <i>Kladognathus</i> sp.	Mississippian (Osagean to Meramecian); CAI=3	Measured section about 23.5 m thick; Kuna Formation appears to overlie relatively continuous section of Kayak(?) Shale and Kanayut Conglomerate; top of Kuna not exposed. 91AD1Y: 12.25 m above base of measured section; 91AD1A: 21 m above base of measured section. Sample 91AD1Y is representative of the bispathodid biofacies and is probably a postmortem lag concentrate because most ramiform elements are missing and those that do occur are relatively complete. <i>Bispathodus utahensis</i> platform elements are extremely abundant and most are complete.
	91AD1A (31739-PC)		<i>Bispathodus utahensis</i>		
15 (A)	91TR17 (31721-PC)	68°37'05"/ 157°36'00"	Black limestone interbedded with chert 1 M and 1 Sc elements of Mississippian morphotype	Mississippian CAI=1.5-2	From Bion barite deposit. Conodont sample about 25 m below chert containing Late Mississippian or Early Pennsylvanian radiolarians.
	91Tr30C (31767-PC)	68°37'30"/ 157°33'10"	Calcitized radiolarite interbedded with chert <i>Bispathodus utahensis</i> (fig. 7A-G) <i>Gnathodus semiglaber</i> (fig. 7H-J) <i>Mestognathus praebeckmanni</i> (fig. 7K-M)	late Early Mississippian (Osagean, but not earliest) CAI=1.5	



Table 1. Locality register for key conodonts and lithologic features—Continued

MAP NO. (UNIT)	FIELD NO. (USGS COLLN. NO.)	LATITUDE N/ LONGITUDE W.	KEY CONODONT SPECIES AND LITHOLOGIES	FOSSIL AGE AND CAI	REMARKS
16 (A)	91TR23A (31720-PC)	68°36'10"/ 157°29'35"	Calcitized radiolarite, barite, and minor black chert <i>Bispathodus</i> aff. <i>B. utahensis</i> fragments cavusgnathid fragment (fig. 7T) <i>Geniculatus</i> ? n. sp. transitional to <i>Embsaygnathus</i> sp. (fig. 7U-W) <i>Geniculatus</i> aff. <i>G. glottoides</i> (fig. 7R, S)	middle Mississippian (latest Osagean to Meramecian, probably middle Meramecian) CAI=1.5-2	From the Stack barite deposit. The conodont faunule indicates postmortem hydraulic mixing of chiefly shallow-water biofacies with some deeper water biofacies. Nearly all conodonts are fragmentary and are probably part of a gravity-flow deposit. Representatives of <i>Geniculatus glottoides</i> and <i>Embsaygnathus</i> spp. are virtually unknown beyond England and Ireland.
17 (A)	90AD60	68°34'00"/ 157°32'50"	Radiolarian chert		
18 (A)	91TR39 (31722-PC)	68°33'32"/ 157°25'49"	Calcitized radiolarite with barite. " <i>Hindeodella</i> " <i>segaformis</i> s.f. (fig. 7O-Q) <i>Scalioognathus</i> sp. indet. fragments (fig. 7N)	late Early Mississippian (Osagean, Upper <i>typicus</i> Zone through most of <i>anchoralis-latus</i> Zone)	From 70-meter-thick measured section 0.8 km east of the Abby Creek barite deposit. Conodont faunule is from a baritic limestone bed 34 m above base of section.
19 (RB)	91AD11A (31745-PC)	68°35'55"/ 157°41'00"	Calcareous turbidites and lesser spiculitic mudstone <i>Gnathodus</i> aff. <i>G. typicus</i> " <i>Hindeodella</i> " <i>segaformis</i> s.f. <i>Polygnathus communis</i> <i>Vogelgnathus</i> ? sp. REDEPOSITED LATE KINDERHOOKIAN FORMS: <i>Siphonodella</i> aff. <i>S. crenulata</i> <i>Siphonodella</i> spp. indet.	No older than late Early Mississippian (no older than middle Osagean) CAI=2-2.5	From 80-meter-thick section of the Rim Butte unit. 91AD11A: 70 m above base of section; 22-centimeter graded carbonate bed. Conodonts are all small and represent a postmortem winnow. 91AD11G: 80 m above base of section; crinoid-rich, coarse-grained skeletal packstone in bed ~10 cm thick.
	91AD11G (31746-PC)		<i>Polygnathus communis</i> REDEPOSITED CONODONTS OF KINDERHOOKIAN AGE: <i>Siphonodella</i> sp. (fig. 9Z)		
20 (RB)	90AD61Z (30939-PC)	68°33'58"/ 157°35'10"	Spiculitic mudstone and lesser calcareous turbidites <i>Gnathodus cuneiformis</i> <i>Hindeodus crassidentatus</i> <i>Syncladognathus geminus</i> (fig. 9U) REDEPOSITED KINDERHOOKIAN FORMS: <i>Siphonodella</i> sp. (fig. 9Y)	No older than late Early Mississippian (no older than early Osagean) CAI=3-3.5	All specimens are small and many are incomplete bar fragments indicating a postmortem winnow. The sample is from a fine-grained, locally silicified limestone bed that is 20 cm thick and contains parallel laminae. A few specimens have a surficial gray patina suggesting rapid heating—the sample is from 5 m above a mafic sill.
21 (RB)	91AD2B (31740-PC)	68°32'03"/ 157°34'15"	Spiculitic mudstone and lesser calcareous turbidites <i>Dolymae hassi</i> (fig. 9V) <i>Gnathodus cuneiformis</i> <i>Kladognathus</i> sp.	late Early Mississippian (lower 2/3 of Osagean-- <i>typicus</i> Zone--most of <i>anchoralis-latus</i> Zone CAI=1.5	From top of the Rim Butte unit, about 0.25 m below contact with overlying Imnaitchiak Chert. Conodont sample from fine-grained bioclastic packstone turbidite. Conodonts represent postmortem transport within the gnathodid biofacies.
	91AD6F (31741-PC)	68°32'00"/ 157°34'55"	Spiculitic mudstone and lesser calcareous turbidites <i>Bispathodus utahensis</i> <i>Gnathodus</i> aff. <i>G. semiglaber</i> " <i>Hindeodella</i> " <i>segaformis</i> s.f. REDEPOSITED KINDERHOOKIAN FORMS: <i>Siphonodella</i> sp. (fig. 9N)	No older than late Early Mississippian (no older than middle Osagean) CAI=1.5-2	From section 67 m thick within the Rim Butte unit. 91AD6F: 5.5 m above base of section and about 0.5 m above mafic sill. From crossbedded silty limestone grading upward into micrite. 91AD6U: 61 m above base of section. From calcitized spiculite about 10 cm thick.
	91AD6U (31742-PC)		<i>Bispathodus utahensis</i> " <i>Hindeodella</i> " <i>segaformis</i> s.f. (fig. 9M)	late Early Mississippian (middle Osagean) CAI=1.5-2	

Table 1. Locality register for key conodonts and lithologic features—Continued

MAP NO. (UNIT)	FIELD NO. (USGS COLLN. NO.)	LATITUDE N/ LONGITUDE W.	KEY CONODONT SPECIES AND LITHOLOGIES	FOSSIL AGE AND CAI	REMARKS
22 (RB)	90AD64F (30940-PC)	68°32'58"/ 157°29'10"	Calcareous turbidites and lesser spiculitic mudstone <i>Bispathodus utahensis</i> (fig. 9H) <i>Clydograthus</i> aff. <i>C. cavusformis</i> (fig. 9G) <i>Gnathodus</i> aff. <i>G. pseudosemiglaber</i> "Hindeodella" <i>segaformis</i> s.f. (fig. 9I) REDEPOSITED LATE KINDERHOOKIAN FORMS: <i>Siphonodella</i> sp. (fig. 9L)	No older than late Early Mississippian (no older than middle Osagean, middle <i>anchoralis-latus</i> Zone) CAI=2.5-3	Conodont sample from partly silicified, fine-grained, bioclastic packstone 16.5 m below mafic sill. Conodonts represent a postmortem winnow--most specimens are small and incomplete.
	90AD66A (30943-PC)	68°33'00"/ 157°29'30"	Black shale and lesser calcareous turbidites with well-developed flute casts <i>Bispathodus utahensis</i> <i>Gnathodus punctatus</i> (fig. 9X) <i>Polygnathus communis</i> <i>Polygnathus inornatus</i> (fig. 9W) <i>Scaliognathus?</i> sp. indet. fragments	late Early Mississippian (early Osagean, <i>typicus</i> Zone CAI= 3 to 4; about 25% of the specimens have a surficial gray patina suggesting nearby hydrothermal and (or) igneous activity.	Conodont sample from fining upward bioclastic packstone interlayered with spiculite; bed 4 cm thick. Nearly all specimens are broken and have a broad size range indicating a graded deposit.
23 (RB)	90AD67G (30944-PC)	68°32'55"/ 157°30'20"	Calcareous turbidites and lesser spiculitic mudstone <i>Bispathodus utahensis</i> "Hindeodella" <i>segaformis</i> s.f. REDEPOSITED KINDERHOOKIAN FORMS: <i>Siphonodella</i> sp.	No older than late Early Mississippian (no older than middle Osagean) CAI=2	Conodont sample from fine-grained bioclastic packstone 15 cm thick. Conodonts represent a postmortem distal winnow composed of small, mostly broken delicate bar fragments and complete juvenile elements.
	90AD68	68°33'03"/ 157°30'09"	Spiculitic mudstone and lesser calcareous turbidites		
24 (RB)	90AD52	68°33'58"/ 157°18'35"	Calcareous turbidites and spiculitic mudstone		
25 (RB)	91JS35D (31753-PC)	68°21'35"/ 158°08'35"	Calcareous turbidites and lesser spiculitic mudstone <i>Bispathodus utahensis</i> <i>Cavusgnathus unicornis</i> (fig. 9A) <i>Gnathodus pseudosemiglaber</i> (fig. 9B) REDEPOSITED OSAGEAN FORMS: <i>Bactrognathus</i> sp. indet. <i>Doliognathus latus</i> (fig. 9C) "Hindeodella" <i>segaformis</i> s.f. <i>Polygnathus communis</i> <i>Pseudopolygnathus pinnatus</i> (fig. 9D) <i>Pseudopolygnathus oxypageus</i> REDEPOSITED LATE KINDERHOOKIAN FORMS: <i>Gnathodus punctatus</i> (fig. 9E) <i>Siphonodella crenulata</i> <i>S. isosticha</i> - <i>S. obsoleta</i> (fig. 9F)	No older than early Late Mississippian (no older than late Meramecian) and containing redeposited conodonts of late Kinderhookian and Osagean age CAI=3.5	Conodont sample from graded bioclastic packstone. Mafic sill at least 7 m thick occurs 5 m above collection site.
25 (A)	91AD13	68°22'40"/ 158°08'45"	Radiolarian chert		
26 (RB)	90AMu81 (31724-PC)	68°24'25"/ 155°58'09"	Calcareous turbidites and spiculitic limestone <i>Bispathodus utahensis</i> (fig. 9O) <i>Dolymae hassi</i> (fig. 9P) <i>Gnathodus cuneiformis</i> (fig. 9R) <i>Kladognathus</i> sp. <i>Polygnathus communis</i> <i>Pseudopolygnathus multistriatus</i> <i>Ps. oxypageus</i> (fig. 9Q) <i>Ps. triangulus</i> REDEPOSITED LATE KINDERHOOKIAN FORMS: <i>Gnathodus punctatus</i> (fig. 9S) <i>Siphonodella obsoleta</i> (fig. 9T)	No older than late Early Mississippian (middle Osagean, Upper <i>typicus</i> Subzone to lower <i>anchoralis-</i> <i>latus</i> Zone) CAI=1-1.5	Conodont sample from fine-grained bioclastic, peloidal grainstone containing minor detrital quartz and glauconite. Abundant, very well preserved conodonts of the pseudopolygnathid-polygnathid- gnathodid biofacies; some postmortem transport within or from this biofacies. Open-marine deep ramp or middle to deep slope depositional environment. Carbonate bed is probably a gravity-flow deposit from slightly shallower water with some cannibalization of older Kinderhookian deposits.

Conodonts suggest that the Kuna Formation in the Howard Pass area is chiefly late Early Mississippian (Osagean) in age. *Bispathodus utahensis* indicates an early Osagean to Meramecian age, but rare pseudopolygnathids indicate that at least part of the Kuna is of late Early Mississippian age (table 1, loc. 8, USGS colln. 31757-PC). The underlying Kayak Shale produces early Early Mississippian (Kinderhookian, probably late Kinderhookian) conodonts, chiefly the shallow-water form *Bispathodus? plumulus nodosus* (Rhodes, Austin and Druce) (fig. 5F and table 1, loc. 7, USGS colln. 31743-PC). Conodont faunas of Osagean age have also been reported from the Kuna Formation in the De Long Mountains quadrangle to the west (fig. 1; Curtis and others, 1990; Ellersieck and others, 1990). However, siliceous strata assigned to the uppermost part of the Kuna in the De Long Mountains may be slightly younger; these strata yield radiolarians of late Meramecian(?) to Morrowan (Late Mississippian to early Middle Pennsylvanian) age. Previously, this radiolarian assemblage was considered Early to Middle Pennsylvanian (Mull and others, 1982), but the age was subsequently extended into the Late Mississippian by Murchey and others (1988, table 32.3, field no. 79MD-164-51 m). No post-Mississippian faunas have been recovered from the Kuna Formation in the Howard Pass area.

### AKMALIK CHERT

The Akmalik Chert was defined by Mull and others (1987) in the Killik River quadrangle. The unit consists of bedded black chert containing minor beds of black mudstone, black shale, and dolomitic limestone; it overlies the Kayak Shale and underlies gray and green chert of the Etivluk Group. We studied this unit mainly in the central part of the Howard Pass quadrangle (fig. 2), where it is at most a few tens of meters thick. Much of the Akmalik that we examined does consist of true chert; samples are vitreous, not earthy, and contain little argillaceous matter (fig. 6A). Siliceous microfossils are abundant, and radiolarians are more common than sponge spicules in most samples (fig. 6B).

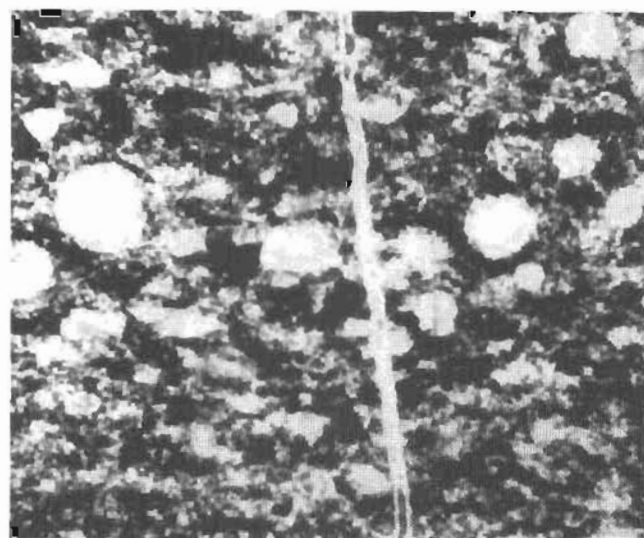
Carbonate beds are rare in the Akmalik Chert, and make up at most a few percent of the sections we studied. All the carbonate beds that we examined consist of calcitized radiolarite. The abundance of radiolarians relative to sponge spicules and the rarity of mud in the Akmalik suggest that it formed in deeper water than the Kuna Formation, in a position more distal and (or) restricted from clastic input.

The age of the Akmalik Chert in the central Howard Pass quadrangle is late Early to earliest Late Mississippian on the basis of its contained fossils. Conodonts from beds of calcitized radiolarite (fig. 2, locs. 15, 16, and 18),

collected by I.L. Tailleux and J.S. Kelley, U.S. Geological Survey, are of Osagean and Meramecian, probably middle Meramecian age. Conodonts are relatively rare in these beds and only a few specimens, such as representatives of *Bispathodus utahensis* Sandberg and Gutschick (fig. 7A-G) and *Gnathodus semiglaber* Bischoff (fig. 7H-J), are specifically identifiable. Most conodonts are indeterminate bar and blade fragments but, fortunately, even very small fragments of "*Hindeodella*" *segaformis* Bischoff s.f. (a middle Osagean index species) are specifically identifiable (fig. 7O-Q). The conodont species associations in the Akmalik Chert represent a mixture of shallow-water platform to slope biofacies as well as some pelagic elements such as *Bispathodus utahensis*. Mestognathids (fig. 7K-M),



A



B

Figure 6. Sedimentary features of Akmalik Chert. A, Typical view of Akmalik Chert beds which contain little argillaceous matter and lack shale partings; type locality, Akmalik Chert, central Killik River quadrangle. B, Photomicrograph of poorly preserved radiolarians filled with chalcedony in radiolarian chert.



cavusgnathids (fig. 7T), and possibly geniculatids (fig. 7S) and embaygnathids (fig. 7U–W) represent relatively shallow-water platform biofacies whereas scaliognathids (fig. 7N) and gnathodids (fig. 7H–J) are characteristic of deeper platform and slope biofacies. The preservation characteristics and species composition of the Akmalik conodonts indicate mixing of biofacies and breakage during basinward transport by turbidity currents.

Mull and others (1987) considered the Akmalik Chert in the central Killik River quadrangle to be Mississippian to Early Pennsylvanian in age; they reported Late Mississippian (Namurian) plant fossils, Late Mississippian to Early Pennsylvanian (Chesterian to Morrowan) radiolarians, and Early Pennsylvanian (Morrowan) conodonts from the Akmalik Chert. No fossils of late Late Mississippian or younger age have been found in the Akmalik Chert in the Howard Pass quadrangle.

## RIM BUTTE UNIT

The Rim Butte unit is an informal name used here to identify a previously unnamed unit of the Lisburne Group exposed mainly in thrust sheets of the Ignavik River allochthon (Mayfield and others, 1988). (Two apparent exceptions to this distribution are locs. 25 and 26, fig. 2.) The unit is well exposed at Rim Butte and in the cliffs to the south and west (area of loc. 24, fig. 2). In the Howard Pass area, this unit consists of 70 to 80 m of fine-grained calcareous and siliceous rocks which are abundantly intruded by 5- to 15-m-thick, locally vesicular, mafic igneous sills. Mayfield and others (1988) indicated that sedimentary rocks here referred to the Rim Butte unit overlie the Kayak Shale and underlie chert of the Etivluk Group. In the Howard Pass area, the base of the Rim Butte unit is generally faulted or not exposed, but a gradational upper contact with gray chert of the Etivluk Group was observed locally.

The Rim Butte unit is distinctively thin-bedded and rhythmically color-banded (fig. 8A). Lighter layers are limestone, and darker layers are siliceous mudstone. The darker layers contain abundant siliceous sponge spicules, and are lithologically identical to the siliceous mudstone that forms much of the Kuna Formation. We interpret these layers as the "background" sediment that was accumulating in the Rim Butte and Kuna basin(s).

The limy layers are carbonate turbidites (fig. 8B). They consist of complete or base-cut-out Bouma sequences, with sole-marked basal contacts. Lower parts of beds are typically graded and cross-laminated. Upper parts of beds are laminated, and bed-tops are generally bioturbated. The limestone-to-mudstone ratio varies from outcrop to outcrop and within a single section; limestone comprises 15–70 percent of the sections studied. Limestone beds range from 3 to 80 cm thick; siliceous mudstone beds are thinner, generally 20 cm or less.

Redeposited material in limestone beds consists chiefly of sand- to silt-sized calcareous and lesser siliceous bioclasts (figs. 8C–E). Bioclasts include forms derived from shallow-water depositional environments, such as foraminifers and echinoderm and bryozoan debris, as well as grains of deeper water provenance, such as radiolarians and siliceous sponge spicules. Abundance of specific bioclasts varies from bed to bed; grains of shallow-water provenance dominate some samples, but are rare in others. Carbonate turbidites of the Rim Butte unit also contain sedimentary lithic clasts (mainly limestone and noncalcareous mudstone) (figs. 8D–F) and some samples include as much as 10–15 percent detrital quartz.

Little paleontologic information has previously been reported from these rocks. Our conodont samples (table 1 and fig. 9) indicate that, in the Howard Pass quadrangle, the Rim Butte unit is no older than late Early and early Late Mississippian (Osagean and late Meramecian). In addition to Osagean conodonts, many Rim Butte turbidites contain a subordinate number of redeposited earliest Mississippian (Kinderhookian) conodonts, chiefly representatives of *Siphonodella* and *Gnathodus* (figs. 9E, F, L, N, S, T, X–Z). These redeposited conodonts indicate that the Rim Butte turbidites were derived, at least in part, from erosion of older carbonate strata.

One turbidite of the Rim Butte unit, the westernmost Rim Butte sample (which is somewhat geographically distant from other Rim Butte samples; fig. 2, loc. 25; table 1, USGS colln. 31753–PC), produced conodonts of no older than late Meramecian age (fig. 9A) together with abundant redeposited conodonts of Osagean (fig. 9C, D) and Kinderhookian age (fig. 9E, F). The Osagean conodonts in this younger Rim Butte sample could have been derived from older Rim Butte deposits. The presence of redeposited conodonts in Rim Butte turbidites raises the possibility that none of the conodonts are indigenous, and that they merely indicate a maximum possible age.

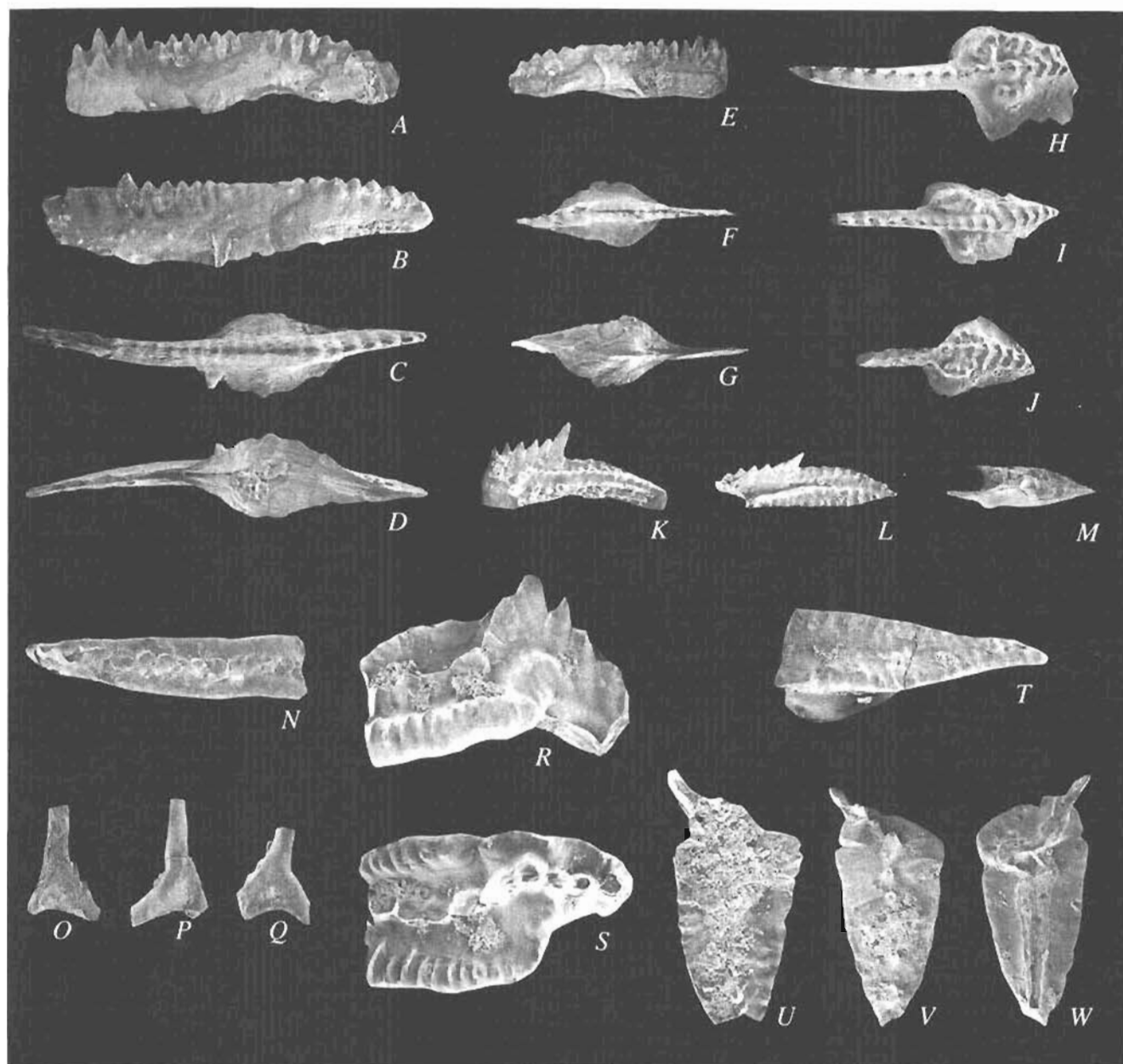
Conodont biofacies analysis supports the interpretations of depositional environment outlined above. The Osagean conodonts represent a mixture of forms characteristic of open-marine, moderate-depth, platform to slope biofacies, along with a few shallow-water forms. The species diversity and lack of dominance by one or two genera indicate postmortem hydraulic mixing of conodonts from several biofacies, and strongly support our interpretation of deposition by turbidity currents in a slope to basinal environment.

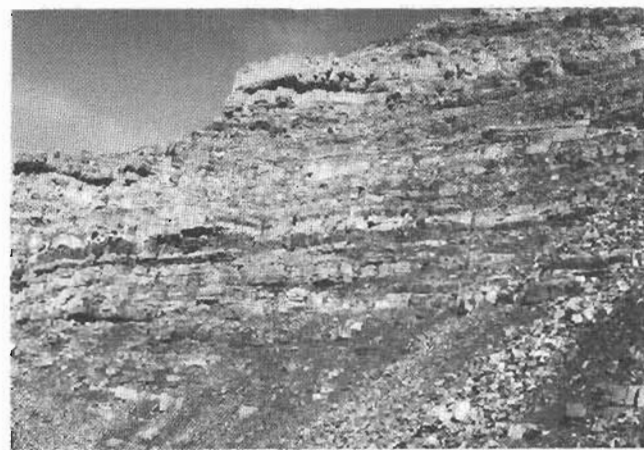
## DISCUSSION

The age and lithofacies of the deep-water units of the Lisburne Group discussed above offer new constraints for paleogeographic reconstructions of the western Brooks Range. Some previous workers (for example, Mayfield

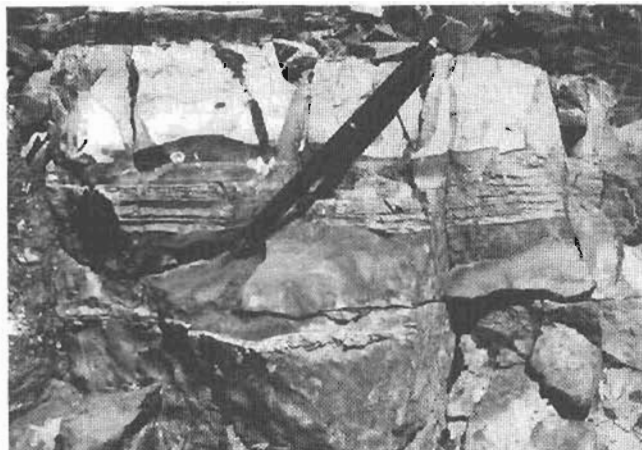
**Figure 7.** Mississippian conodonts from Akmalik Chert (scanning electron micrographs,  $\times 40$ ).

- A–M, Osagean conodonts from calcitized radiolarite interbedded with chert, USGS colln. 31767–PC (table 1 and fig. 2, loc. 15).
- A–G, *Bispathodus utahensis* Sandberg and Gutschick.
    - A, Pa element, inner lateral view, USNM 473775.
    - B–D, Pa element, outer lateral, upper, and lower views, USNM 473776.
    - E–G, Juvenile Pa element, inner lateral, upper, and lower views, USNM 473777.
  - H–J, *Gnathodus semiglaber* Bischoff, Pa elements, upper views, USNM 473778–80.
  - K–M, *Mestognathus praebeckmanni* Sandberg and others, Pa element, inner lateral, upper, and lower views, USNM 473781. This juvenile specimen displays diagnostic characteristics of the species.
- N–Q, Osagean conodonts from baritic limestone bed near Abby Creek barite deposit, USGS colln. 31722–PC (table 1 and fig. 2, loc. 18).
- N, *Scaliognathus* sp. indet., bar fragment, upper view, USNM 473782.
  - O–Q, "*Hindeodella*" *segaformis* Bischoff s.f. bar fragments, lateral view, USNM 473783–85.
- R–W, Latest Osagean to Meramecian (probably middle Meramecian) conodonts from Stack barite deposit, USGS colln. 31720–PC (table 1 and fig. 2, loc. 16).
- R, S, *Geniculatus* aff. *G. glottoides* Voges, incomplete Pa element, lateral and upper views, USNM 473786. This specimen has a wide platform with a serrated margin that curves upward and thus differs from *G. glottoides* which has a narrower, flatter, and smooth platform. Angle between anterolateral process and the platform is greater than in *G. glottoides*. Serrated arched margin may indicate relationship to *Embsaygnathus*.
  - T, Cavusgnathid, posterior Pa element fragment, upper view, USNM 473787. This specimen occurs with advanced forms of *Geniculatus* (fig. 7R, S) that suggest a probable middle Meramecian age for the collection.
  - U–W, *Geniculatus*? n. sp. transitional to *Embsaygnathus* sp., P elements, upper view and upper and lower views, USNM 473788 and 473789, respectively. Specimens are nearly complete and thus lack long anterolateral blade of *Embsaygnathus*. They may represent a transitional form between *Geniculatus* and *Embsaygnathus* or they may be the Pb element of *Embsaygnathus asymmetricus*. Two morphotypes are shown, one with corrugated margins and incipient transverse ridges (fig. 7U) and another with a smooth platform (7V, W). Similar morphotypes occur in *Doliognathus latus*.

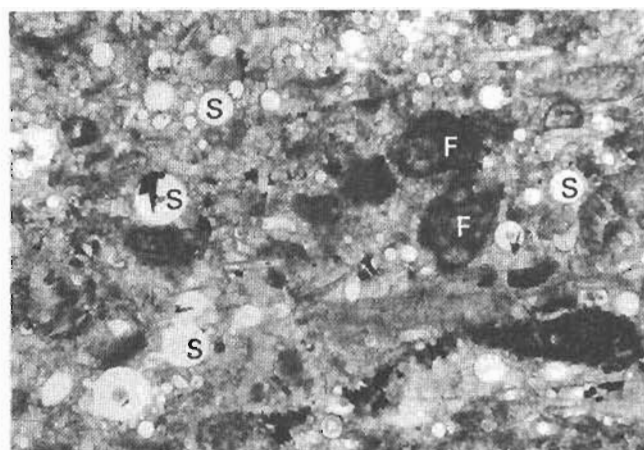




A

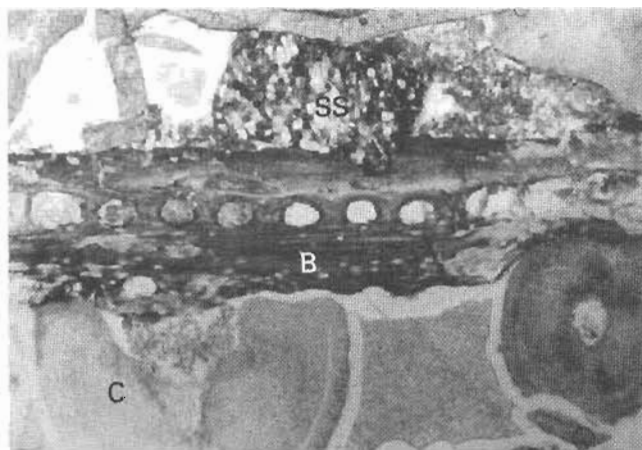


B



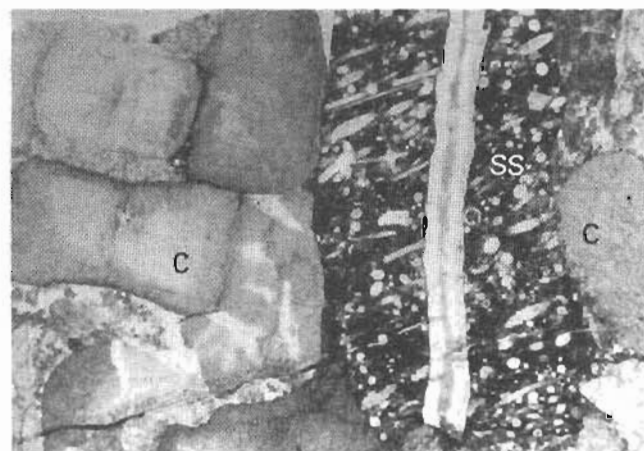
C

0 0.5 MILLIMETER



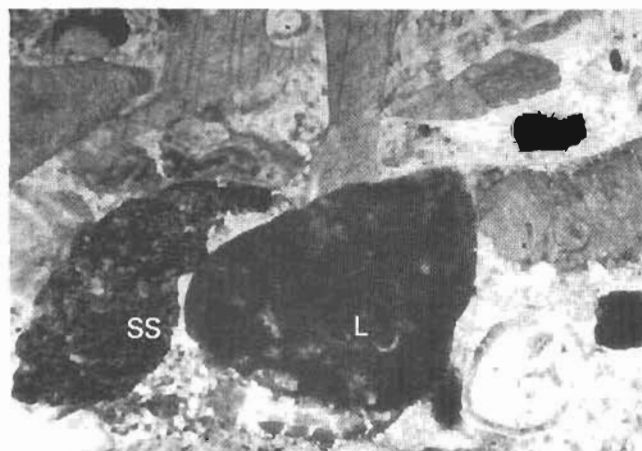
D

0 0.5 MILLIMETER



E

0 0.5 MILLIMETER



F

0 0.5 MILLIMETER

Figure 8. Sedimentary features of Rim Butte unit. A, Typical section, thin-bedded and color-banded (fig. 2, loc. 23); outcrop is 10 m high. B, Carbonate turbidite, with scoured base (just above pencil tip), graded, parallel-laminated lower part and burrowed upper part, overlain and underlain by spiculitic

mudstone (fig. 2, loc. 21). C-F, Photomicrographs of carbonate turbidites, made up of calcareous and siliceous bioclasts and lesser sedimentary lithic clasts (fig. 2, loc. 19). B, bryozoan fragment; C, crinoid ossicle; F, foraminifer; L, lime mudstone; S, sponge spicule; SS, spiculitic mudstone clast.

and others, 1988) interpreted deep-water Lisburne facies in the Howard Pass area as in part coeval with, but chiefly younger than, Lisburne carbonate-platform rocks exposed in the same area and inferred that most Carboniferous successions deepened upward.

Our data suggest a more complicated paleogeography and (or) geologic history for the Howard Pass region. In this area, carbonate-platform rocks of the Lisburne Group (included in the Brooks Range allochthon of Mayfield and others, 1988) are exposed at Mount Bupto, Lisburne Ridge, and in the Ivotuk Hills (fig. 2). Megafossil data from Mount Bupto and Lisburne Ridge (Armstrong, 1970) and conodonts from Lisburne Ridge (table 1) and the Ivotuk Hills (Dumoulin and Harris, this volume) indicate that these platform sequences are primarily early Late Mississippian (Meramecian) and locally as young as Chesterian in age. That is, they are chiefly younger than the deep-water Lisburne facies in the Howard Pass area discussed above. Thus, in at least some parts of the west-central Brooks Range, shallow-water Carboniferous carbonate strata may have been deposited above older, deeper-water deposits (see also Dumoulin and Harris, this volume).

Conodont age data reported above also indicate that these younger (Meramecian) carbonate-platform rocks could not have provided a source for the older (Kinderhookian and Osagean) carbonate material in the Rim Butte unit. Strata of the appropriate age, lithofacies, and biofacies to produce the carbonate turbidites of the Rim Butte unit are exposed in thrust sheets further west, such as those of the Kelly River allochthon. This allochthon includes a virtually continuous sequence of Middle Devonian through lower Upper Mississippian platform-carbonate rocks (Dumoulin and Harris, 1992), including the Utukok Formation of Early Mississippian (Kinderhookian and Osagean) age. Shallow-water, locally quartzose, carbonate shelf deposits of the Utukok Formation contain a diverse biota including foraminifers, bryozoans, echinoderms, and conodonts (Dumoulin and Harris, 1992). Both *Siphonodella* and *Gnathodus*, the Kinderhookian conodonts found in Rim Butte turbidites, occur in the Utukok Formation in the Baird and De Long Mountains quadrangles (fig. 1; Dumoulin and Harris, 1992; A.G. Harris, unpublished data).

Exposures of carbonate rocks assigned to the Kelly River allochthon are rare in the Howard Pass quadrangle (fig. 2), but are more widely distributed to the west and southwest, in the Misheguk Mountain and Baird Mountains quadrangles (fig. 1; Mayfield and others, 1988; Dumoulin and Harris, 1992). In the Paleozoic paleogeographic and tectonic reconstruction of the western Brooks Range proposed by Mayfield and others (1988), rocks of the Kelly River allochthon are restored to a position imme-

diately north of rocks of the Ipnarik River allochthon. Paleocurrent data and additional conodont collections over a wider geographic area are needed to test the proposed relationship between the Rim Butte unit and the Utukok Formation. However, the match in age, lithofacies, biofacies, and individual conodont genera between these two units suggests that the Utukok Formation is a likely source for at least some of the carbonate detritus in the turbidites of the Rim Butte unit.

*Acknowledgments.*—We are grateful to Nancy R. Stamm, who worked unconventional hours at breakneck speed to photograph and prepare conodont figures used in this report and who kept her sense of humor throughout.

## REFERENCES CITED

- Armstrong, A.K., 1970, Mississippian dolomites from Lisburne Group, Killik River, Mount Bupto region, Alaska: *American Association of Petroleum Geologists Bulletin*, v. 54, p. 251–264.
- Armstrong, A.K., and Mamet, B.L., 1978, Microfacies of the Carboniferous Lisburne Group, Endicott Mountains, Arctic Alaska, in Stelck, C.R., and Chatterton, B.D.E., eds., *Western and Arctic Canadian biostratigraphy: Geological Association of Canada Special Paper 18*, p. 333–394.
- Baker, P.A., and Kastner, Miriam, 1981, Constraints on the formation of sedimentary dolomite: *Science*, v. 213, p. 214–216.
- Curtis, S.M., Ellersieck, Inyo, Mayfield, C.F., and Tailleux, I.L., 1990, Reconnaissance geologic map of the De Long Mountains A1, B1, and part of the C1 quadrangles, Alaska: U.S. Geological Survey Miscellaneous Investigations Map I–1930, 2 sheets, scale 1:63,360.
- Dickson, J.A.D., 1966, Carbonate identification and genesis as revealed by staining: *Journal of Sedimentary Petrology*, v. 36, p. 491–505.
- Dumoulin, J.A., and Harris, A.G., 1992, Devonian-Mississippian carbonate sequence in the Maiyuncrak Mountains, western Brooks Range, Alaska: U.S. Geological Survey Open-File Report 92–3, 83 p.
- Ellersieck, Inyo, Curtis, S.M., Mayfield, C.F., and Tailleux, I.L., 1990, Reconnaissance geologic map of the De Long Mountains A2, B2, and part of the C2 quadrangles, Alaska: U.S. Geological Survey Miscellaneous Investigations Map I–1931, 2 sheets, scale 1:63,360.
- Lane, H.R., Sandberg, C.A., and Ziegler, Willi, 1980, Taxonomy and phylogeny of some Lower Carboniferous conodonts and preliminary standard post-*Siphonodella* zonation: *Geologica et Palaeontologica*, v. 14, p. 117–164.
- Mayfield, C.F., Tailleux, I.L., and Ellersieck, Inyo, 1988, Stratigraphy, structure, and palinspastic synthesis of the western Brooks Range, northwestern Alaska, in Gryc, George, ed., *Geology and exploration of the National Petroleum Reserve in Alaska, 1974–1982: U.S. Geological Survey Professional Paper 1399*, p. 143–186.
- Mull, C.G., 1989, Generalized stratigraphy and structure of the

Figure 9. Mississippian conodonts from the Rim Butte unit (scanning electron micrographs).

A–F, Late Meramecian and redeposited Kinderhookian and Osagean conodonts from graded bioclastic packstone turbidite, USGS colln. 31753–PC (table 1 and fig. 2, loc. 25).

A, *Cavusgnathus unicornis* Youngquist and Miller, Pa element, upper view,  $\times 60$ , USNM 473790. This species restricts age of this collection to late Meramecian.

B, *Gnathodus pseudosemiglaber* Thompson and Fellows, Pa element, upper view,  $\times 40$ , USNM 473791. Representatives of this relatively long-ranging species may be indigenous and (or) redeposited.

C, *Doliognathus latus* Branson and Mehl, morphotype 3 of Lane and others (1980), Pa element, upper view,  $\times 40$ , USNM 473792. A redeposited middle Osagean (*anchoralis-latus* Zone) index species.

D, *Pseudopolygnathus pinnatus* Voges, Pa element, upper view,  $\times 40$ , USNM 473793. Redeposited Osagean species.

E, *Gnathodus punctatus* (Cooper), Pa element, upper view,  $\times 50$ , USNM 473794. Redeposited late Kinderhookian or Osagean species.

F, *Siphonodella isosticha* (Cooper) transitional to *S. obsoleta* Hass, Pa element, upper view,  $\times 40$ , USNM 473795. Redeposited late Kinderhookian species.

G–L, Osagean and redeposited Kinderhookian conodonts from bioclastic packstone turbidite, USGS colln. 30940–PC (table 1 and fig. 2, loc. 22).

G, *Clydagnathus* aff. *C. cavusformis* Rhodes, Austin, and Druce, Pa element, upper view,  $\times 50$ , USNM 473796. Redeposited and (or) indigenous Kinderhookian or Osagean species.

H, *Bispathodus utahensis* Sandberg and Gutschick, Pa element, inner lateral view,  $\times 40$ , USNM 473797. Osagean or Meramecian species.

I, "*Hindeodella*" *segaformis* Bischoff s.f., bar fragment, lateral view,  $\times 50$ , USNM 473798. Chiefly middle Osagean (*anchoralis-latus* Zone) index species.

J, *Pseudopolygnathus nudus* Pierce and Langenheim, Pa element, upper view,  $\times 50$ , USNM 473799. Middle Osagean species.

K, *Polygnathus communis communis* Branson and Mehl, Pa element, upper view,  $\times 60$ , USNM 473800. Redeposited and (or) indigenous Kinderhookian or Osagean species.

L, *Siphonodella* sp., juvenile Pa element, upper view,  $\times 50$ , USNM 473801. Redeposited Kinderhookian species.

M, "*Hindeodella*" *segaformis* Bischoff s.f., bar fragment, lateral view,  $\times 50$ , USNM 473802. Chiefly middle Osagean (*anchoralis-latus* Zone) index species from calcitized spiculite, USGS colln. 31742–PC (table 1 and fig. 2, loc. 21).

N, *Siphonodella* sp., Sb element, lateral view,  $\times 50$ , USNM 473803. Redeposited Kinderhookian species from calcareous turbidite, USGS colln. 31741–PC (table 1 and fig. 2, loc. 21).

O–T, Middle Osagean and redeposited Kinderhookian conodonts from peloidal grainstone turbidite, USGS colln. 31724–PC (table 1 and fig. 2, loc. 26).

O, *Bispathodus utahensis* Sandberg and Gutschick, Pa element, inner later view,  $\times 40$ , USNM 473804. Osagean or Meramecian species.

P, *Dolymae hassi* Voges, Pa element, upper view,  $\times 60$ , USNM 473805. Osagean species.

Q, *Pseudopolygnathus oxypageus* Lane, Sandberg, and Ziegler, Pa element, upper view,  $\times 50$ , USNM 473806. Middle Osagean species.

R, *Gnathodus cuneiformis* Mehl and Thomas, Pa element, upper view,  $\times 50$ , USNM 473807. Osagean species.

S, *Gnathodus punctatus* (Cooper), Pa element, upper view,  $\times 50$ , USNM 473808. Indigenous and (or) redeposited late Kinderhookian or Osagean species.

T, *Siphonodella obsoleta* Hass, Pa element, upper view,  $\times 50$ , USNM 473809. Redeposited Kinderhookian species.

U, Y, Osagean to early Chesterian and redeposited Kinderhookian conodonts from USGS colln. 30939–PC (table 1 and fig. 2, loc. 20).

U, *Synclydograthus geminus* (Hinde), Sb? element, inner lateral view,  $\times 60$ , USNM 473810. Osagean to early Chesterian species.

Y, *Siphonodella* sp., juvenile Pa element, upper view,  $\times 50$ , USNM 473811. Redeposited Kinderhookian species.

V, *Dolymae hassi* Voges, Pa element fragment, upper view,  $\times 60$ , USNM 473812, USGS colln. 31740–PC (table 1 and fig. 2, loc. 21). Osagean species from fine-grained bioclastic packstone turbidite in uppermost part of Rim Butte unit.

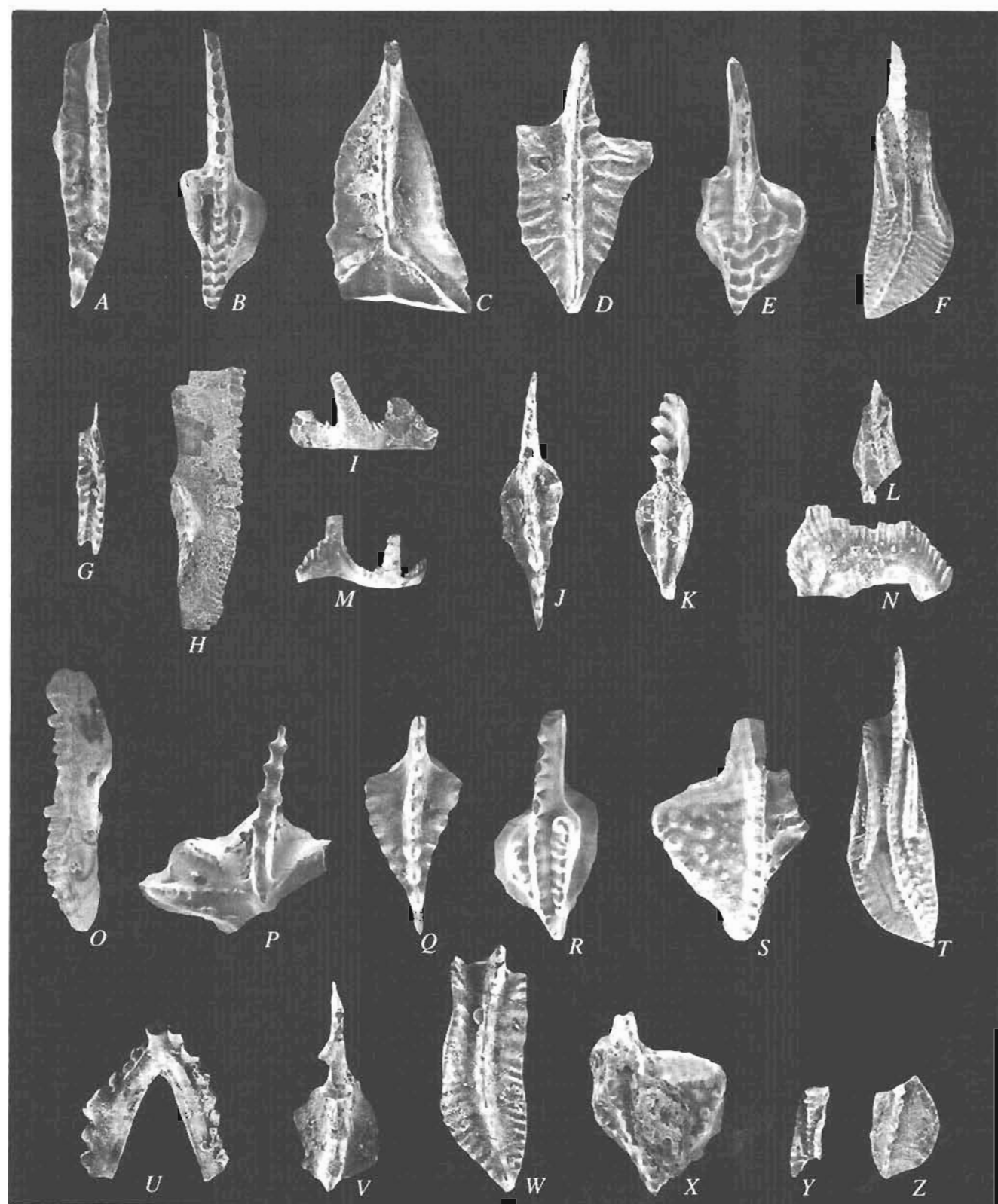
W, X, Early(?) Osagean conodonts from USGS colln. 30943–PC (table 1 and fig. 2, loc. 22).

W, *Polygnathus inornatus* E.R. Branson, Pa element, upper view,  $\times 40$ , USNM 473813. Kinderhookian and early Osagean species.

X, *Gnathodus punctatus* (Cooper), Pa element, upper view,  $\times 50$ , USNM 473814. Late Kinderhookian and early Osagean species.

Z, *Siphonodella* sp., juvenile Pa element fragment, upper view,  $\times 50$ , USNM 473815. Redeposited Kinderhookian species in Osagean carbonate turbidite, USGS colln. 31745–PC (table 1, fig. 2, loc. 19).





- Brooks Range and Arctic Slope, in Mull, C.G., and Adams, K.E., eds., Dalton Highway, Yukon River to Prudhoe Bay, Alaska: Alaska Division of Geological and Geophysical Surveys, Guidebook 7, v. 1, p. 31-46.
- Mull, C.G., Crowder, R.K., Adams, K.E., Siok, J.P., Bodnar, D.A., Harris, E.E., Alexander, R.A., and Solie, D.N., 1987, Stratigraphy and structural setting of the Picnic Creek Allochthon, Killik River quadrangle, central Brooks Range, Alaska: a summary, in Tailleux, I.L., and Weimer, Paul, eds., Alaskan North Slope Geology: Bakersfield, California, Pacific Section, Society of Economic Paleontologists and Mineralogists, Book 50, p. 649-662.
- Mull, C.G., Tailleux, I.L., Mayfield, C.F., Ellersieck, Inyo, and Curtis, S.M., 1982, New upper Paleozoic and lower Mesozoic stratigraphic units, central and western Brooks Range, Alaska: American Association of Petroleum Geologists Bulletin, v. 66, p. 348-362.
- Murchey, B.L., Jones, D.L., Holdsworth, B.K., and Wardlaw, B.R., 1988, Distribution patterns of facies, radiolarians, and conodonts in the Mississippian to Jurassic siliceous rocks of the northern Brooks Range, Alaska, in Gryc, George, ed., Geology and exploration of the National Petroleum Reserve in Alaska, 1974 to 1982: U.S. Geological Survey Professional Paper 1399, p. 697-724.
- Sandberg, C.A., and Gutschick, R.C., 1984, Distribution, microfauna, and source-rock potential of Mississippian Delle Phosphatic Member of Woodman Formation and equivalents, Utah and adjacent States, in Woodward, Jane, and others, eds., Hydrocarbon source rocks of the Greater Rocky Mountain region: Denver, Rocky Mountain Association of Geologists, p. 135-178.
- Reviewers: C. G. Mull and John E. Repetski



# LITHOFACIES AND CONODONTS OF CARBONIFEROUS STRATA IN THE IVOTUK HILLS, WESTERN BROOKS RANGE, ALASKA

By Julie A. Dumoulin and Anita G. Harris

## ABSTRACT

Carboniferous strata in the Ivotuk Hills, in the western Brooks Range fold and thrust belt, consist of about 45 m of dark-gray shale, mudstone, dolostone, and spiculitic chert (upper part of the Kayak Shale, Endicott Group) and at least 225 m of light- to dark-gray dolostone, chert, and minor shale (Lisburne Group). The Kayak Shale was deposited chiefly below wave base; subordinate beds of dolomitic bioclastic packstone probably formed as storm deposits. The Kayak contains conodonts of Early Mississippian (early Osagean) age. The Lisburne Group in the Ivotuk Hills can be divided into three subunits on the basis of bedding style and lithology. The lower and upper units are thin-bedded to laminated, consist chiefly of fine-grained dolostone and spiculite and subordinate dolomitized bioclastic packstone. The middle unit is massive and resistant and is made up mostly of crinoidal packstone and lesser bryozoan wackestone. The lower and middle units of the Lisburne Group yield conodonts of early Late Mississippian (late Meramecian) age; a sample from the upper unit produced latest Late Mississippian (late Chesterian) conodonts.

The Kayak Shale in the Ivotuk Hills is in general similar to the Kayak elsewhere in the Brooks Range, but also has some lithologic and faunal similarities to the Kuna Formation of the Lisburne Group. The Kayak was probably deposited in a middle to outer platform or shelf setting in somewhat deeper water than that in which most of the Kayak accumulated, but under more oxygenated conditions than those typical of Kuna environments.

Sedimentologic data and conodont biofacies indicate that the Lisburne Group in the Ivotuk Hills accumulated primarily in normal marine, middle to outer platform or shelf settings. The section correlates well in age and lithology with the Lisburne at Lisburne Ridge, about 40 km to the west. Repeated thrust panels of Carboniferous strata encountered in the Lisburne Test Well No. 1, drilled 1.5 km northeast of our study area in the Ivotuk Hills, correlate biostratigraphically and lithologically with rocks exposed at the surface, but appear to have formed, at least in

part, in somewhat shallower water and more restricted depositional environments.

## INTRODUCTION

Carboniferous carbonate rocks (Lisburne Group and carbonate layers in the underlying Kayak Shale) are widely exposed across northern Alaska in the Brooks Range fold and thrust belt. Lithofacies, biostratigraphy, and depositional environments of these units have been delineated at a reconnaissance scale in the eastern Brooks Range (Armstrong, 1974; Armstrong and Mamet, 1977), but are less well known to the west. Both shallow and deeper water Carboniferous facies occur in thrust sheets in the western Brooks Range; the structural, stratigraphic, and paleogeographic relationships of these facies remain controversial (Mayfield and others, 1988; Dumoulin and others, this volume).

This paper describes the lithofacies and conodont biostratigraphy of Carboniferous strata in the Ivotuk Hills, western Killik River B-5 quadrangle (fig. 1). Although these strata constitute the type section of the Ivotuk Hills structural sequence of Martin (1970) and Mayfield and others (1988), no detailed sedimentologic or paleontologic studies of these rocks have previously been published.

## PREVIOUS WORK

Carboniferous and younger rocks of the Ivotuk Hills area were first described by Martin (1970), who designated these strata, along with similar sections at Lisburne Ridge and Mount Bupto in the adjacent Howard Pass quadrangle (fig. 1), as the Ivotuk Hills structural sequence. The Carboniferous part of this sequence consists of about 300 m of dolomite and chert (Lisburne Group) overlying an indeterminate thickness of dark-gray shale with subordinate ironstone nodules and bioclastic limestone lenses (Kayak Shale) (Martin, 1970). In the tectonic reconstruction of Mayfield and others (1988), the Ivotuk Hills structural

sequence is included in the Brooks Range allochthon, which is the structurally lowest of seven formally named large-scale structural units. In the central Brooks Range this allochthon is also known as the Endicott Mountains allochthon (Mull, 1989).

Armstrong (1970) described lithologies and megafossils of the Lisburne Group at Lisburne Ridge and Mount Bupto, but did not describe the section in the Ivotuk Hills. The Lisburne No. 1 well, drilled in 1979–1980 on the northwest margin of the Ivotuk Hills during studies of the National Petroleum Reserve, encountered five repeated sections of Carboniferous and Permian rocks; this succession was interpreted as stacked thrust plates of the Ivotuk Hills sequence (Mayfield and others, 1988). Brief descriptions of lithologies and foraminifers from this well are given in Legg (1983).

## GEOLOGIC SETTING

Rocks of the western Brooks Range were folded and thrust-faulted during the Jurassic to Cretaceous Brooks Range orogeny (Mayfield and others, 1988). The Ivotuk Hills lie along the northern margin of the Brooks Range foothills; they consist chiefly of Carboniferous strata exposed as a steeply southward-dipping homocline (fig. 2), bounded on the north by a major thrust fault (fig. 1). The

Siksikpuk Formation (Permian) crops out along the south side of the hills in several small, discontinuous exposures and is presumed to depositionally overlie the Lisburne Group although the contact is generally concealed and was not observed during this study. Fault-bounded strata of the Otuk Formation (Triassic and Jurassic) and the Okpikruak Formation (Cretaceous) crop out north and south of the Ivotuk Hills (Mull and others, in press).

## IVOTUK HILLS MEASURED SECTION

The section described here (fig. 3) was measured with Jacob's staff and tape along the east side of Otuk Creek, at the western end of the Ivotuk Hills (Killik River B-5 quadrangle, T. 11 S., R. 16 W., western edge of sec. 20; fig. 1). The northern third of the section was measured at stream level; the rest was measured in cliffy outcrops several tens of meters above the creek. Through most of the section, beds strike N. 70–80° E. and dip 55–65° S. Color alteration indices (CAI's) of conodonts recovered from this section range from 1–1.5 to 1.5, indicating the host rocks reached at least 50–80°C (Epstein and others, 1977).

Petrographic descriptions are based on field observations and examination of 80 thin sections. Identification of calcite and dolomite was made using the Alizarin Red-S and potassium ferricyanide staining technique of Dickson (1966).

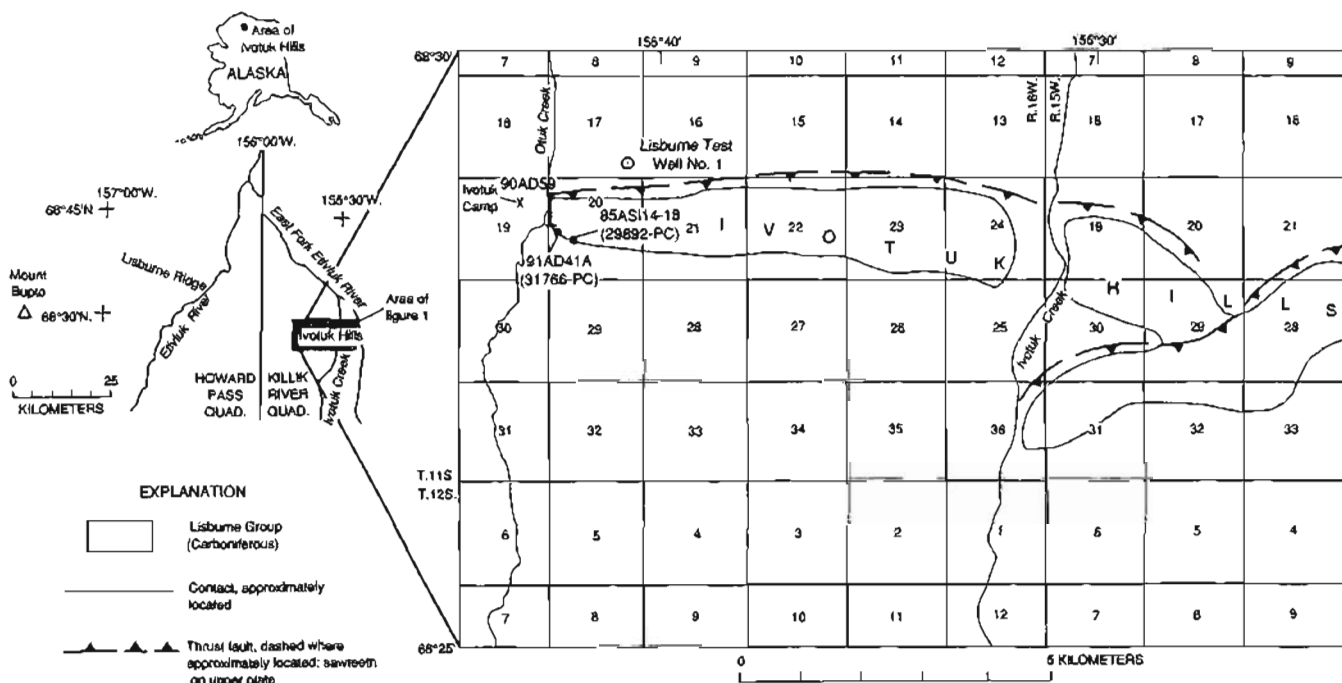


**Figure 1.** Distribution of Lisburne Group and location of section measured in Ivotuk Hills; geology from Mull and others (in press). Township and range grid from Killik River B-5 quadrangle. See table 1 for geographic coordinates, conodont faunules, and lithologies.

## LITHOFACIES

### KAYAK SHALE

About 45 m of shale, mudstone, silty shale, and dolostone assigned by Martin (1970) to the Kayak Shale is exposed beneath the Lisburne Group along Onuk Creek. The base of the section is concealed and is probably a thrust fault (C.G. Mull, written commun., 1992). The section consists chiefly of fissile, black shale and blocky mudstone, locally yellow- to red-weathering. Some samples, mainly in the lower third of the exposure, contain minor amounts of detrital quartz silt. Dark-gray, reddish-brown-weathering concretions, lenses, and layers of dolomitic mudstone to dolostone make up 10 to 20 percent of the lower half of the section (fig. 4A). Concretions reach 20 cm in diameter; lenses and layers range from 2 to 30 cm thick and display discontinuous, wispy laminae. In thin section, concretions consist of 25 to nearly 100 percent dolomite crystals, 6 to 60  $\mu\text{m}$  (rarely, to 200  $\mu\text{m}$ ) in diameter, in a noncalcareous mudstone matrix (fig. 4B).

Laminae reflect variations in the concentration of dolomite versus mud.

Spiculitic layers a few centimeters thick make up about 10 percent of the section. Some samples consist of calcareous spicules (fig. 4C), or a mixture of calcareous and siliceous spicules, in a mudstone matrix; other samples contain only siliceous spicules in a matrix of microcrystalline chert. Spicules are typically well aligned and may be concentrated into parallel or cross laminae; some spicules have been partly or completely replaced by pyrite.

Medium- to dark-gray, orange- to reddish-brown-weathering, dolomitic bioclastic packstone occurs near the base and middle of the section in beds and lenses 10 cm to 1.7 m thick (fig. 4D). Bedding surfaces are densely bioturbated; some beds are graded and display wispy parallel laminae. Clasts range from less than 1 mm to several centimeters in diameter; matrix consists of calcareous and noncalcareous mud. Most clasts are bioclasts, chiefly crinoid ossicles, brachiopods, and rare solitary corals (fig. 4D-F). Many bioclasts are broken and abraded, and some have bored and micritized rims. Five to 25 percent phosphatic

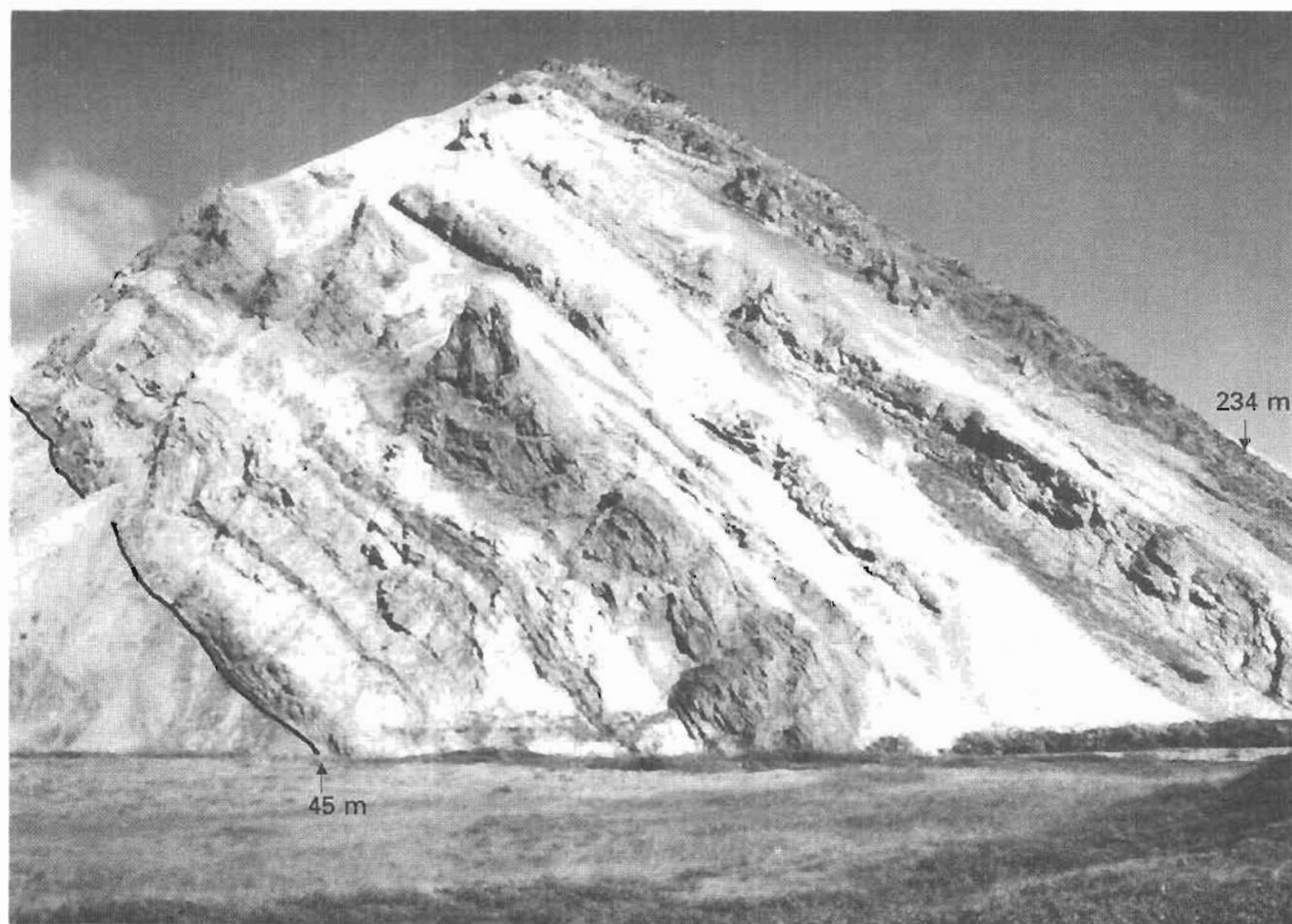
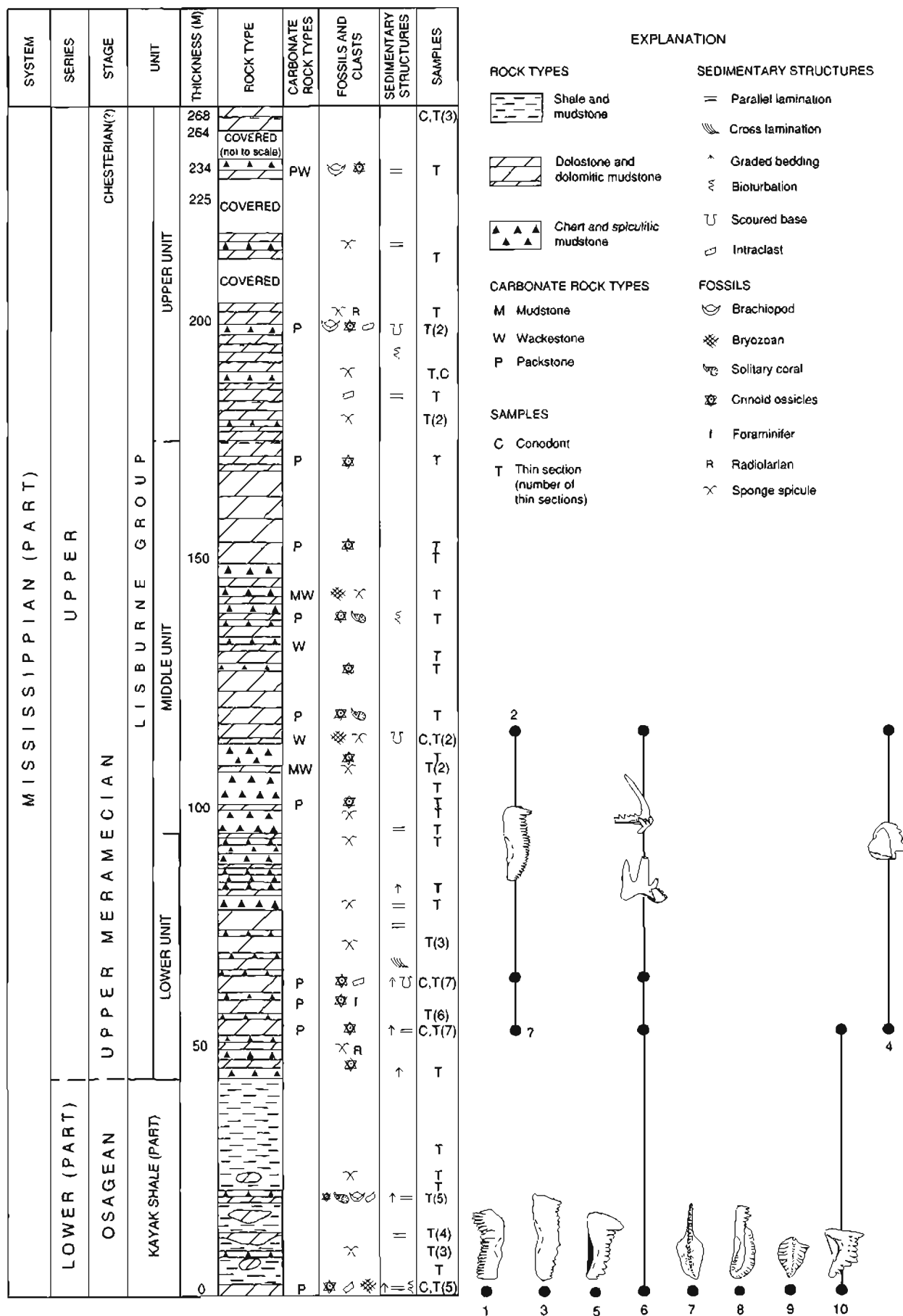


Figure 2. Carboniferous succession in Ivotuk Hills; view to east. Line marks contact between Kayak Shale below and Lisburne Group above. Meters correspond to thicknesses in figure 3.



grains, chiefly fish debris, and 10 to 20 percent intraclasts of black shale and spiculitic mudstone occur in some packstone layers (figs. 4E, F). Dolomite has replaced matrix and bioclasts in many samples (fig. 4F), although crinoid grains are generally still calcite; locally, bioclasts have been replaced by silica (fig. 4E) and (or) pyrite. Several samples grade from coarse, sand-sized bioclastic packstone into silt-sized siliceous spiculite.

The contact between the Kayak Shale and the overlying Lisburne Group is marked by an abrupt change from recessive, yellow-weathering, fissile shale to resistant, reddish-brown to black-weathering, thin-bedded spiculitic mudstone, dolostone, and chert (fig. 3).

### LISBURNE GROUP

At least 225 m of dolostone, chert, and minor shale makes up the Lisburne Group in the Ivotuk Hills. The section can be divided into three subunits on the basis of bedding style and lithology. The lower 50 m consists of chiefly dark-gray to black, thin-bedded chert, dolostone, and mudstone, and subordinate, lighter colored, thicker bedded dolomitic pack/grainstone containing abundant crinoid ossicles. The middle 80 m is more massive and resistant, white to medium-gray, dolomitized and (or) silicified skeletal packstone and lesser wackestone containing a variety of bioclasts. The upper 95 m is recessive, dark-gray to black, thin-bedded dolostone, chert, and shale.

#### LOWER UNIT

About 60 to 70 percent of the lower unit consists of thin-bedded to laminated spiculitic mudstone, spiculitic chert, dolomitic mudstone, and dolostone, interlayered on a scale of a few millimeters to 7 cm (fig. 5A). Sponge spicules are chiefly siliceous and 20 to 100  $\mu$ m in diameter (figs. 5B, C); some spiculitic chert samples also contain rare radiolarians. Dolomite crystals range from 50  $\mu$ m to 0.5 mm in size (fig. 5C).

Beds 7–40 cm thick of bioclastic pack/grainstone occur intercalated with these dark mudstones and are particularly abundant in the lower half of the unit. Some beds are clearly graded (fig. 5D) and display well-developed paral-

lel and local cross-lamination. Clasts range from 0.5 to 7 mm and are predominantly crinoid ossicles, although a few samples also contain foraminifers, bryozoan fragments, brachiopods, phosphatic grains, and (or) mudstone clasts. Most beds are pervasively dolomitized and (or) silicified, but the original supportstone texture can still be discerned (fig. 5E). Some bioclasts are outlined or partly replaced by pyrite (fig. 5F).

#### MIDDLE UNIT

The middle unit consists of subequal amounts of dolostone and chert, chiefly massive, but with subordinate intervals a few meters thick of irregular 3- to 20-cm-thick beds (fig. 6A). The base of this unit is the base of a distinctive, 20-m-thick interval of massive, white to pale bluish-gray-weathering chert with 10 to 20 percent dolostone; the dolostone fills irregular vugs, 0.5–1 cm long, and forms lenses 5 to 8 cm thick and as much as 30 cm long. Dolostone dominates the rest of the unit; some dolostone layers are vaguely parallel laminated and a few are obviously burrowed, but in general sedimentary structures are rare. A few intervals of massive dolostone contain vuggy porosity filled with solid hydrocarbons (fig. 6B).

Dolomitization has locally obscured or completely obliterated original textures in this unit. Where depositional textures can be discerned, massive strata consist of crinoidal pack/grainstone; thinner bedded zones comprise bryozoan wackestone (fig. 6C) and subordinate layers of bioclastic packstone. Bioclastic beds contain abundant crinoid ossicles and bryozoan fragments (fig. 6D–F), as well as rare solitary corals. Siliceous sponge spicules are abundant in mud-rich intervals, but are rare overall compared to overlying and underlying strata.

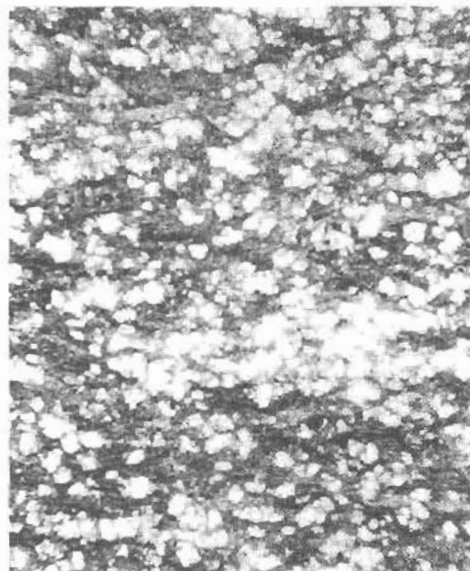
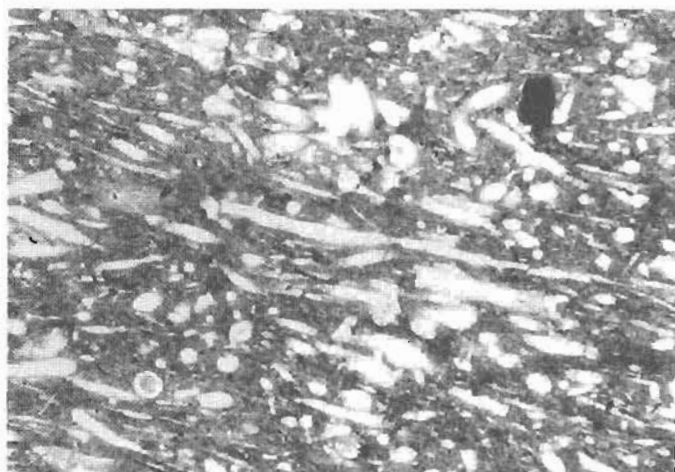
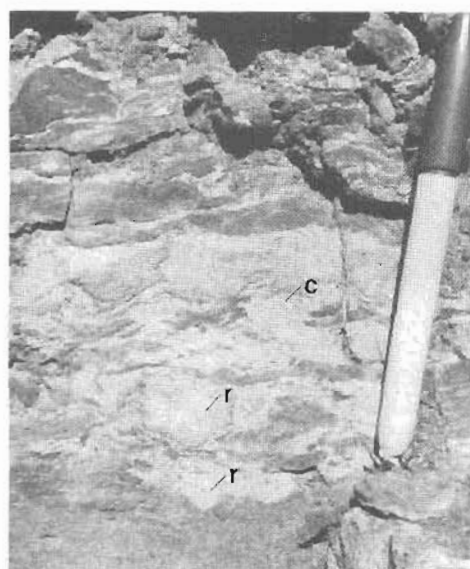
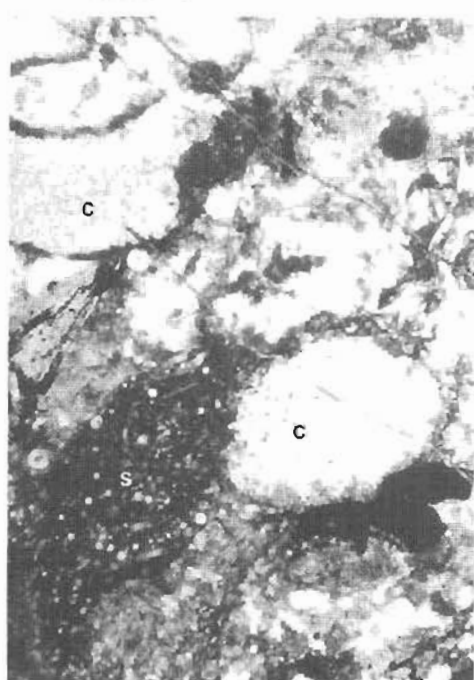
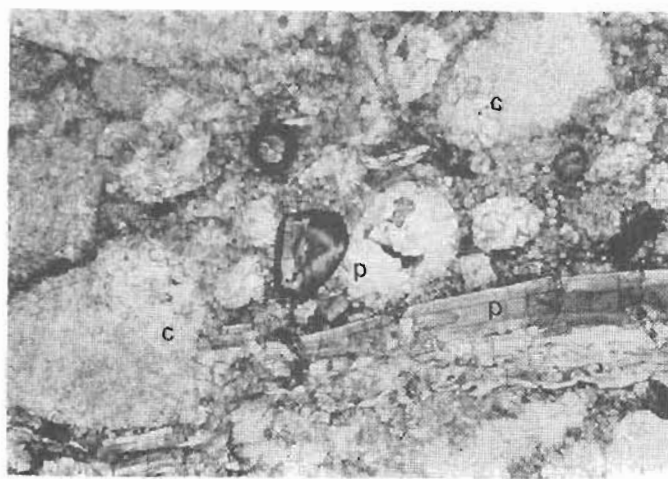
#### UPPER UNIT

The upper unit consists of dolostone, dolomitic and spiculitic mudstone, spiculitic chert, and black shale in even to slightly undulatory beds, 0.5 to 5 cm thick (figs. 7A, B). Only the lower third of the unit is well exposed. A distinctive zone of black shale, 10 to 50 cm thick, marks the basal part of the unit; the shale is fissile, slightly calcareous, and weathers into plates 1 to 3 cm thick.

Dolostone and dolomitic mudstone make up most of the unit; these rocks are medium gray to black, weather tan to pale yellow brown, and contain local wispy parallel laminae, starved ripples, and rip-up clasts. Some laminae have been partly disrupted by bioturbation. Samples consist of 50–99 percent euhedral dolomite in a mudstone matrix; dolomite crystals are 8–240  $\mu$ m (chiefly less than 80  $\mu$ m) in size.

Dolostone is interlayered on a scale of millimeters to centimeters with black spiculitic mudstone and spiculitic chert (fig. 7C); these lithologies contain abundant, chiefly siliceous, sponge spicules, minor clasts of mudstone, and (particularly in the upper part of the section) rare radiolarians. Chert constitutes only a few percent of the lower

Figure 3. Measured section, Kayak Shale and Lisburne Group, in Ivotuk Hills. Base of section is concealed and is probably a thrust fault (C.G. Mull, written commun., 1992); tundra covers top of section. Chesterian(?) age for uppermost part of section is based on a collection from an isolated outcrop nearby (see text). Conodont species numbered in figure are: 1, *Bispathodus aculeatus anteposicornis*; 2, *Bispathodus utahensis*; 3, *Bispathodus* sp. indet.; 4, *Cavusgnathus* sp. indet.; 5, *Hindeodus crassidentatus*; 6, *Kladognathus* sp.; 7, *Polygnathus communis*; 8, *Polygnathus lacinatus circaperipherus*; 9, *Pseudopolygnathus* sp. indet.; 10, *Syncladognathus geminus*.

**A****B** 0 0.25 MILLIMETER**C** 0 0.25 MILLIMETER**D****E** 0 0.5 MILLIMETER**F** 0 0.5 MILLIMETER



half of the unit, but 30 to 50 percent of the upper strata. Shale makes up 10 percent of the unit and occurs as partings between beds and rare layers as much as 10 cm thick.

Several beds of silicified bioclastic packstone, 5 to 8 cm thick, punctuate the section; these beds contain abundant disarticulated brachiopod valves and lesser crinoid ossicles, spicules, and phosphatic clasts. Some shells are rimmed with borings filled with brown or black mud (fig. 7D).

Tundra covers the highest beds of the Lisburne Group along Otuk Creek. The contact between the Lisburne and the overlying Siksikuk Formation is not exposed along the line of our measured section, but is preserved in an isolated outcrop 100 m to the southeast (fig. 1, sample locality 85ASi14-18; see also "Age and Biofacies" below). The stratigraphic relationship between this outcrop and our measured section is uncertain, but it most likely represents strata at least in part equivalent to the uppermost beds of the measured section. The total thickness of the Lisburne Group in the Ivotuk Hills is probably no more than 250 m.

## AGE AND BIOFACIES

### KAYAK SHALE

A sample from the 2-m-thick dolomitic packstone bed at the base of the section in the Kayak Shale yielded conodonts of late Early Mississippian (early Osagean) age (fig. 8D, P-T). The fauna represents a polygnathid-bispathodid biofacies, which generally indicates a relatively shallow-water, normal-marine platform or shelf depositional environment. The two predominant species, however, are *Polygnathus communis* and *Bispathodus* sp. indet. (a single-row morphotype that is either *B. stabilis* (Branson and Mehl) or *B. utahensis* Sandberg and Gutschick). These are pelagic forms (Sandberg and Gutschick, 1984) that are widespread in most normal-marine Early Mississippian environments, but are most abundant in the more basinal and (or) anoxic to dysaerobic environments (Sandberg and Gutschick, 1984; Dumoulin and others, this volume).

The collection from the Kayak Shale also contains a few representatives of species characteristic of shallow-water (but not the shallowest water) biofacies such as *Bispathodus aculeatus anteposicornis* (fig. 8T) and *Syncladognathus geminus* (Hinde) (fig. 8D), as well as representatives of shallow- to slightly deeper water platform or shelf biofacies such as *Hindeodus crassidentatus* (fig. 8S), *Pseudopolygnathus* sp. indet., and *Kladognathus* sp. indet. Of note is the absence of deeper water (outer shelf or slope) early Osagean genera such as gnathodids and scaliognathids. Taken together, the species association and preservation characteristics suggest postmortem transport within or from a moderate to shallow depth platform or shelf environment.

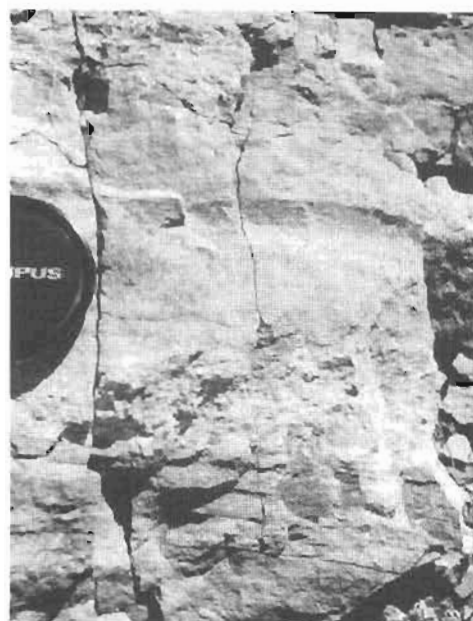
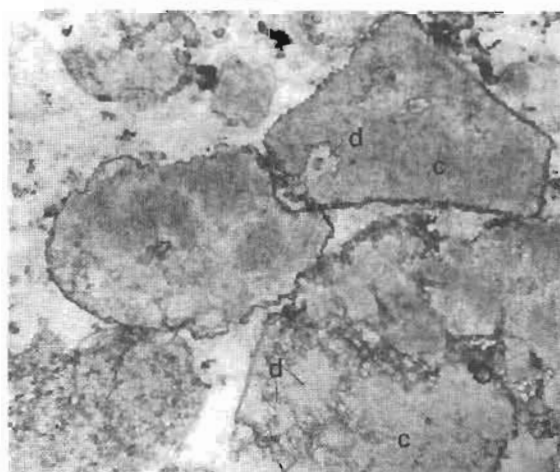
### LISBURNE GROUP

Two samples from the lower unit of the Lisburne Group in the Ivotuk Hills section produced conodonts of early Late Mississippian (late Meramecian) age, as did a sample from the massive middle unit. Samples taken 54 and 66 m above the base of the section are from dolostone with relict crinoidal pack/grainstone texture. Conodonts are relatively sparse, virtually all are incomplete (the ratio of generically determinate to indeterminate elements ranges from 1:3 to 1:2) and bispathodids (fig. 8I-K) and kladognathids (fig. 8M) predominate. The collections contain a few diagnostically shallow-water forms such as *Syncladognathus geminus* (fig. 8E, F) and cavusgnathids (fig. 8N, O). Overall species association and preservation characteristics suggest postmortem transport within or from a relatively shallow-water platform or shelf environment.

The sample taken from the middle massive unit at 115.4 m above the base of the section is from a dolomitic bryozoan-crinoidal wackestone. Conodonts are few, somewhat more complete than in samples from the lower unit, and consist chiefly of representatives of the pelagic species *Bispathodus utahensis*, with lesser numbers of *Kladognathus* sp. indet. and a few fragments of cavusgnathids (fig. 8G, H, and L). The species association and preservation characteristics suggest a normal-marine depositional environment with somewhat less postmortem transport than in the two samples from the lower unit.

Thin-bedded dolostone in the upper unit of the Lisburne Group, 190 m above the base of the section, was barren of conodonts. Another sample from the upper unit taken about 267 m above the base of the section produced only a few indeterminate conodont fragments. However, a sample collected by J.P. Siok (Terrasat, Anchorage, Alaska) from an isolated outcrop about 100 m southeast of our measured section provides a date for the uppermost part of the Lisburne Group in the Ivotuk Hills. This outcrop exposes a few tens of meters of the uppermost strata of the Lisburne Group, as well as strata of the overlying Siksikuk Formation. A sample of thin-bedded, fine-

Figure 4. Sedimentary features of Kayak Shale. A, Dolostone lens in black shale, 6.1 m above base of section. B, Photomicrograph of dolomitic mudstone lens, 8.4 m above base of section. C, Photomicrograph of layer rich in calcareous sponge spicules, 22 m above base of section. D, Dolomitic bioclastic packstone layer containing abundant crinoid columnals (c) and solitary corals (r), 21 m above base of section. E, Photomicrograph of bioclastic packstone lens shown in 4D; note clast of spiculitic mudstone (s), and crinoid ossicles (c) replaced by silica. F, Photomicrograph of bioclastic packstone lens 0.5 m above base of section; note phosphatic fish debris (p), and crinoid ossicles (c) replaced by dolomite.

*A**B**C**D**E**F*



grained carbonate rock taken 11 m below the stratigraphic top of the Lisburne Group at this outcrop yields representatives of *Gnathodus bilineatus* (Roundy), *G. defectus* Dunn, and *G. girtyi simplex* Dunn (fig. 8A–C). The collection restricts the age of the uppermost part of the Lisburne in this area to the latest Late Mississippian (latest Chesterian).

## DEPOSITIONAL ENVIRONMENT

### KAYAK SHALE

The Kayak Shale in the Ivotuk Hills accumulated in relatively quiet water, below fair-weather wave base. Preservation of laminae and rarity of bioturbation in these strata suggest that conditions inimical to bottom fauna, such as high turbidity and (or) low oxygen content, prevailed during deposition. Rocks rich in sponge spicules form both in shallow-water, restricted platform and deeper water, outer shelf or basin environments (Murchey and others, 1988; Dumoulin and Harris, 1992). Spiculites in the Kayak probably formed in deeper water, because they contain rare radiolarians and lack features characteristic of shallow-water, restricted settings (for example, peloids, algal stromatolites, and fenestral fabric).

Concretions and lenses of finely crystalline dolostone in the Kayak Shale resemble dolomitic lenses in the Kuna Formation, a deeper water facies of the Lisburne Group widely distributed in the western Kilik River and eastern Howard Pass quadrangles (Mull and others, 1982). Dolomite in the Kuna appears to have formed during early diagenesis as a result of marine microbial activity in relatively organic-rich sediments (Dumoulin and others, this volume); dolomite concretions in the Kayak were probably similarly produced.

Bioclastic packstone beds in the Kayak Shale were not generated in place, but were redeposited, probably by storm waves and (or) turbidity currents. Bouma sequences were not observed in these beds, but typical tempestite features (Flügel, 1982) such as graded bedding, shale rip-up

clasts, and a mix of fossils derived from various shallow-water biofacies characterize these strata. Conodont elements in these layers are mostly incomplete, indicating transport during high-energy conditions. Storm waves may have produced atypically well-oxygenated bottom conditions, because bioturbation in the Kayak appears confined to tempestite layers. Packstone beds may have been dolomitized by the same processes which produced the finely crystalline dolomite concretions, but could also have formed during later (reflux related?) dolomitization events.

Lithologic and faunal evidence thus suggest that the Kayak Shale in the Ivotuk Hills formed in moderately deep water on a middle to outer platform or shelf setting. The depositional environment was characterized by persistent influx of pelitic detritus and periodic accumulation of tempestites rich in calcareous bioclasts. These bioclasts were probably derived from the leading edge of a prograding carbonate platform.

### LISBURNE GROUP

The Lisburne Group in the Ivotuk Hills represents progradation of a carbonate bank across a shelf or platform setting. Fine-grained dolostone and spiculitic mudstone beds in the lower unit of the Lisburne are similar to those in the underlying Kayak Shale, but the lower unit contains less pelitic detritus and more bioclastic carbonate material than the Kayak. Both units were probably deposited in similar water depths, but the lower unit accumulated closer to the source of the carbonate debris. "Background" sediment in the lower unit consists of finely laminated noncarbonate mudstone, chert, and diagenetic dolomite; sponge spicules and rare radiolarians are the only bioclasts in these beds. Subordinate layers of skeletal packstone, like those in the underlying Kayak Shale, have features indicative of tempestite origin, such as graded bedding, shale rip-up clasts, and bioclasts derived from several biofacies. Some conodonts (cavusgnathids) and skeletal grains (foraminifers) indicate input from shallow- to very shallow-water depositional environments.

The massive middle unit appears to have formed in a shallower water setting and (or) during maximum progradation of the carbonate platform. Skeletal (chiefly crinoidal) packstone and lesser bryozoan wackestone dominate this unit and probably formed in sand shoals and crinoid-bryozoan gardens of the middle to inner shelf. Sedimentologic or paleontologic evidence of very shallow-water, restricted environments, such as mud cracks, peloids, fenestral fabric, stromatolites, calcispheres, or conodonts representative of the mestognathid biofacies, have not been found in this unit. If any part of the middle unit was deposited in shallow subtidal to supratidal environments, evidence of these settings has been obliterated by later dolomitization and (or) silicification.

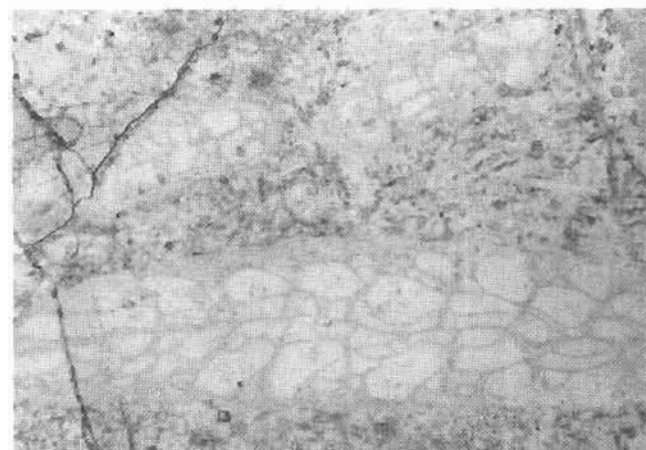
Figure 5. Sedimentary features, lower unit of Lisburne Group. A, Thinly interbedded light-weathering dolostone and dark-weathering spiculitic chert, 79 m above base of section. B, Photomicrograph of spiculitic mudstone, 45.7 m above base of section; light-colored layer is concentration of siliceous sponge spicules. C, Photomicrograph of spiculitic chert with minor rhombs of dolomite, 45.9 m above base of section. D, Graded bed of crinoidal packstone, 65 m above base of section. E, Photomicrograph of packstone shown in 5D; small dolomite crystals (d) grow inside calcite crinoid ossicles (c) in a matrix of spiculitic mudstone. F, Photomicrograph of bioclastic packstone, 54.5 m above base of section; crinoidal debris here has been partly pyritized and replaced by silica.



A

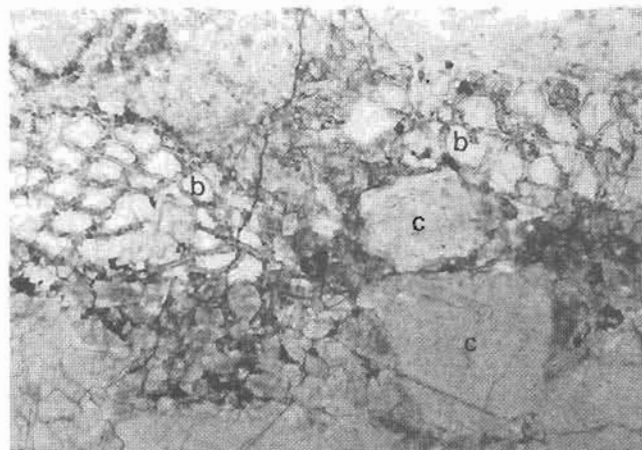


B



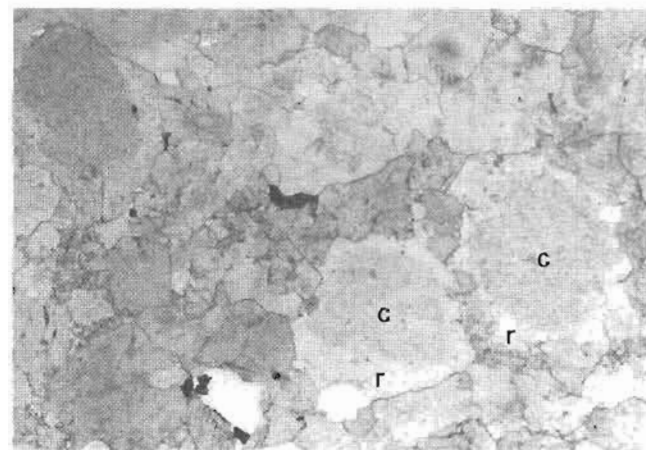
C

0 0.5 MILLIMETER



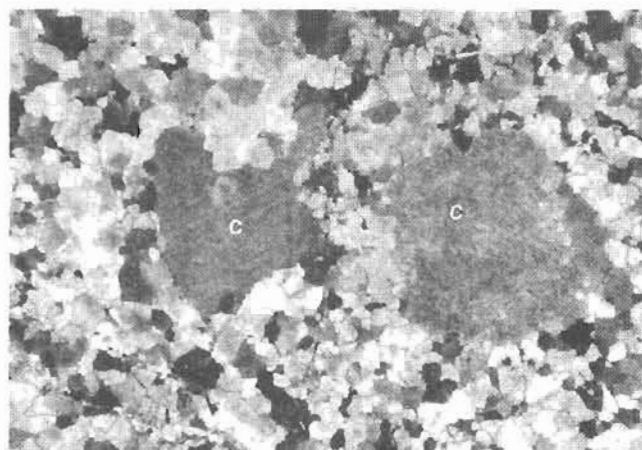
D

0 0.5 MILLIMETER



E

0 0.5 MILLIMETER



F

0 0.5 MILLIMETER

**Figure 6.** Sedimentary features, middle unit of Lisburne Group. *A*, Massive dolostone (bioclastic pack/grainstone) overlies dark-weathering bryozoan wackestone with irregular chert bands; contact between the two lithologies (marked by arrow) is 117 m above base of section. *B*, Silicified dolostone with irregular vugs (arrow) filled with hydrocarbons, 114 m above base of section. *C*, Photomicrograph of bryozoan wackestone with a matrix of spiculitic chert, 104 m above base of section. *D*, Photomicrograph of crinoids (c) and silicified bryozoans (b) in skeletal

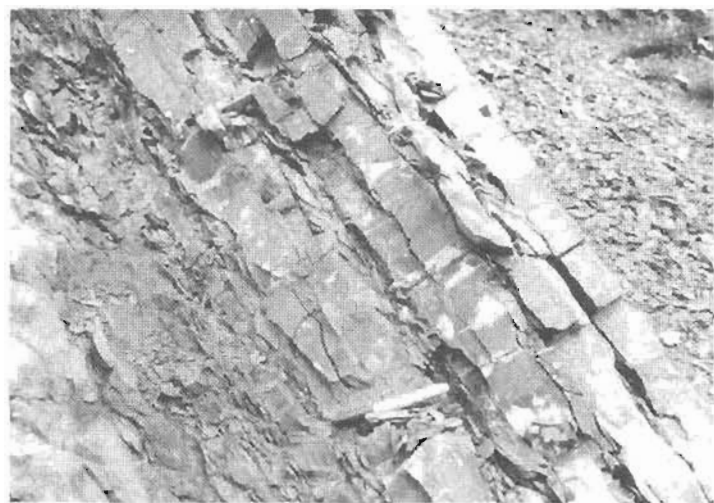
packstone, 102 m above base of section; pyrite outlines some bryozoan zoecia. *E*, Photomicrograph of dolomitized crinoidal grainstone 118 m above base of section; crinoid ossicles (c), associated rim cement overgrowths (r), and sparry matrix have all been replaced by dolomite. *F*, Photomicrograph of dolomitized crinoidal wackestone 135 m above base of section; crinoid ossicles (c) are still calcite but matrix and other skeletal grains have been replaced by dolomite.

The upper unit of the Lisburne Group was deposited chiefly below wave-base in deeper water, middle to outer shelf environments that received little input from carbonate banks. Well-laminated dolomitic mudstone, spiculite, and lesser shale characterize this unit. Rare packstone layers rich in brachiopods probably represent storm deposits; shells in these layers are locally bored, probably by algae prior to tempestite deposition. A conodont collection from the uppermost part of this unit produced exclusively gnathodids, forms typical of outer shelf and slope environments.

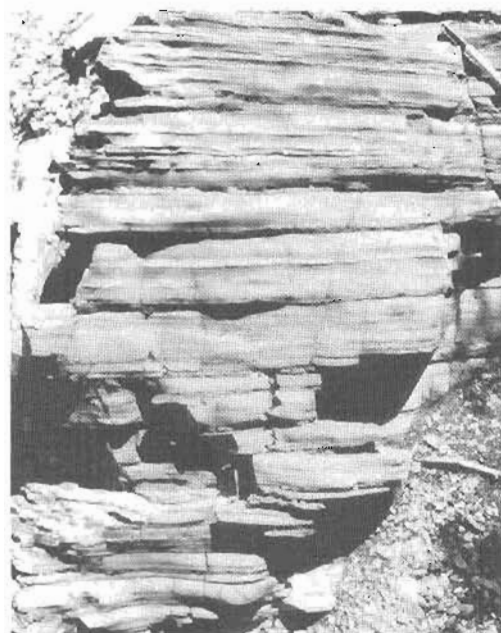
## CORRELATION

### KAYAK SHALE

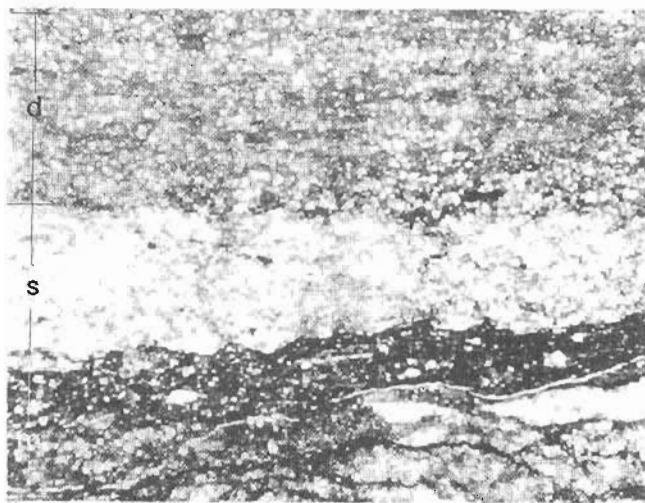
The Kayak Shale in the Ivotuk Hills resembles the Kayak Shale elsewhere in the Killik River-Howard Pass area, but also has some lithologic and faunal similarities to the Kuna Formation of the Lisburne Group. Both the Kayak Shale and the Kuna Formation consist chiefly of black to dark-gray shale, but shale in the Kuna Formation



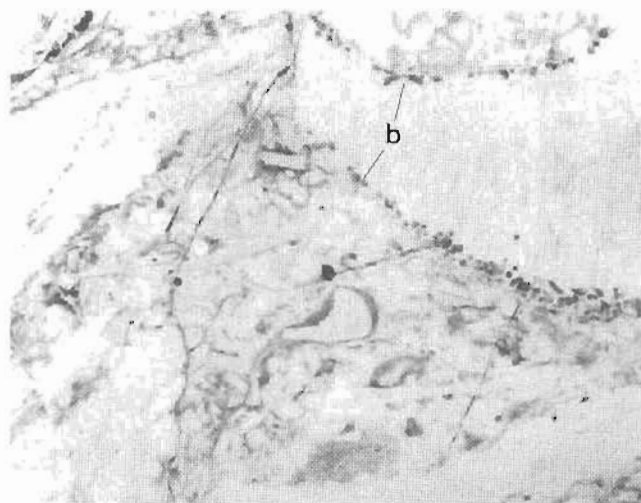
A



B



C



D

Figure 7. Sedimentary features, upper unit of Lisburne Group. A, Thin-bedded dolostone with shale partings, 262 m above base of section. B, Laminae rich in siliceous spicules weather out of dolomitic mudstone, 180 m above base of section. C, Photomicrograph of interval shown in 7B; dark mudstone layer with

scattered dolomite crystals (m) overlain by layers of spiculitic chert (s) and dolomite (d). D, Photomicrograph of silicified brachiopod packstone (probable tempestite), 199.2 m above base of section. Brown mud-filled borings (b) thru shell on right side of photograph.

**Figure 8.** Mississippian conodonts from measured section of uppermost part of the Kayak Shale and the Lisburne Group, Ivotuk Hills, Killik River B-5 quadrangle, western Brooks Range, Alaska (scanning electron micrographs). See figures 1 and 3 for location of samples and stratigraphic column and table 1 for conodont species distribution.

A-C, Latest Mississippian (latest Chesterian) conodonts from 11 m below top of the Lisburne Group (sample of grayish-black micrite to sparite collected by J.P. Siok, field no. 85ASI4-18), USGS colln. 29892-PC.

A, *Gnathodus bilineatus* (Roundy), incomplete Pa element, upper view,  $\times 60$ , USNM 473816. Specimens of *G. bilineatus* in this collection are juveniles or, like this specimen, lack diagnostic posterior part of platform and thus cannot be identified to subspecies. *G. bilineatus* subspp. range from the early Chesterian into the earliest Morrowan (into the *noduliferus-primus* Zone).

B, *Gnathodus defectus* Dunn, Pa element, upper view,  $\times 40$ , USNM 473817. This species ranges from within the Chesterian (probably latest Chesterian) into the earliest Morrowan (into the *noduliferus-primus* Zone).

C, *Gnathodus girryi simplex* Dunn, Pa element, upper view,  $\times 50$ , USNM 473818. This latest Chesterian species extends to the very top of the Chesterian, and probably not into the Morrowan. It restricts the highest sample of the Lisburne Group in the Ivotuk Hills to the Chesterian.

D, P-T, Early Osagean conodonts from crinoidal packstone bed in the Kayak Shale, 43 m below the base of the Lisburne Group, and 1.7 m above base of the measured section, USGS colln. 31734-PC,  $\times 40$ .

D, *Syncladognathus geminus* (Hinde), Pa element, outer lateral view, USNM 473819. The species ranges from the Osagean into the early Chesterian.

P, Q, *Polygnathus lacinatus circaperipherus* Rhodes, Austin, and Druce, Pa element, upper and lower views, USNM 473820. The species occurs in strata equivalent to the Osagean in the British Avonian (Rhodes and others, 1969).

R, *Polygnathus communis communis* Branson and Mehl, Pa element, oblique upper view, USNM 473821; a long-ranging Famennian through Osagean species.

S, *Hindeodus crassidentatus* (Branson and Mehl), Pa element, outer lateral view, USNM 473822. Late Kinderhookian through at least Osagean species.

T, *Bispathodus aculeatus anteposicornis* (Scott), Pa element, inner lateral view, USNM 473823. Latest Famennian to early Osagean species. The occurrence of this species with *Syncladognathus geminus* (fig. 8D) possibly restricts the age of the sample to the early Osagean.

E, F, N, O, Late Meramecian conodonts from crinoidal pack/grainstone, 9 m above the base of the lower unit of the Lisburne Group and 54 m above the base of the measured section, USGS colln. 31735-PC,  $\times 40$ .

E, F, *Syncladognathus geminus* (Hinde), Sa and Sb elements, posterior and inner lateral views, USNM 473958, 59.

N, O, *Cavusgnathus* sp. indet., Pa element fragments, lateral and upper views, USNM 473960, 61. This form combined with conodonts from underlying and overlying beds restricts the collection to the upper half of the Meramecian.

G, H, L, Late Meramecian conodonts from bryozoan-crinoidal wackestone, 20 m above the base of the middle massive unit of the Lisburne Group and 115.4 m above the base of the measured section, USGS colln. 31737-PC,  $\times 40$ .

G, H, *Bispathodus utahensis* Sandberg and Gutschick, Pa element, inner lateral and upper views, USNM 473962. Representatives of this species, mostly incomplete Pa elements, are the most abundant forms in this collection and in USGS colln. 317736-PC.

L, *Kladognathus* sp., Sc element, inner lateral view, USNM 473963.

I-K, M, Late Meramecian conodonts from dolomitized crinoidal pack/grainstone, 21 m above the base of the lower unit of the Lisburne Group and 66 m above the base of the measured section, USGS colln. 31736-PC,  $\times 40$ .

I-K, *Bispathodus utahensis* Sandberg and Gutschick, Pa and Sb elements, outer lateral, upper, and inner lateral views, USNM 473964, 65, respectively.

M, *Kladognathus* sp., P element, inner lateral view, USNM 473966.

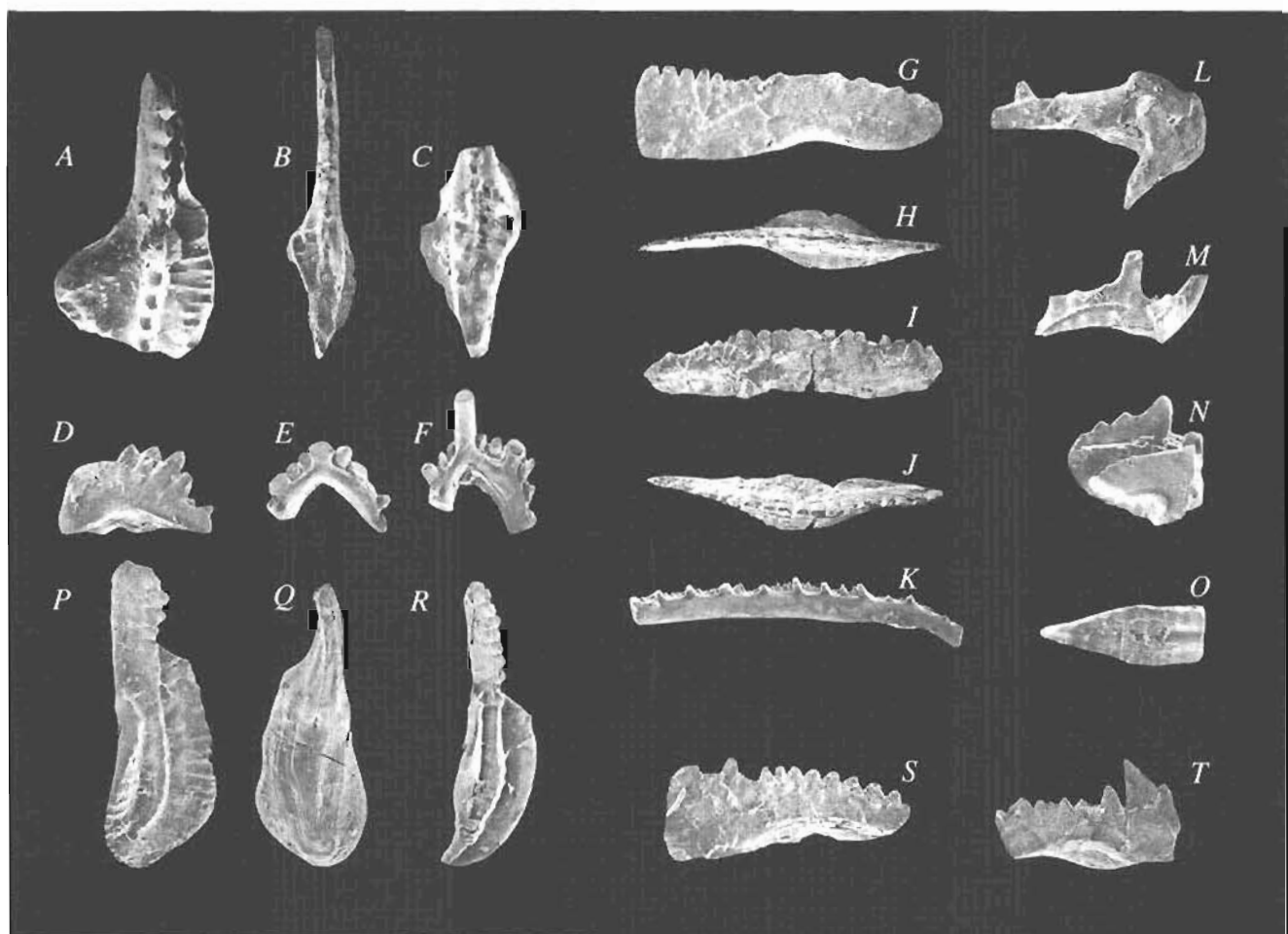


Table 1. Conodont faunules and lithologies, upper part of Kayak Shale and Lisburne Group, western Ivotuk Hills, Killik River B-5 quadrangle, Alaska

[See figures 1 and 3 for geographic and stratigraphic relationships. CAI, color alteration index]

UNIT	FIELD NO. (USGS COLLN.NO.) AND POSITION ABOVE BASE OF SECTION	LATITUDE N/ LONGITUDE W.	LITHOLOGY AND CONODONT FAUNULE	FOSSIL AGE, BIOFACIES, AND CAI	REMARKS
Kayak Shale	90AD59C (31734-PC); 1.7 m	68°28'50"/ 155°42'45" (base of section); 68°28'38"/ 155°42'45" (top of section)	Crinoidal packstone. 5 Pa elements <i>Bispathodus aculeatus anteposicornis</i> (Scott) (fig. 8T) 66 Pa element fragments <i>Bispathodus</i> sp. indet. <i>Hindeodus crassidentatus</i> (Branson and Mehl) (fig. 8S) 12 Pa and 1 Sc elements <i>Kladognathus</i> sp. 6 P, 14 M, 10 Sa and 17 Sc elements 73 Pa elements <i>Polygnathus communis</i> Branson and Mehl (fig. 8R) 2 Pa elements <i>Polygnathus lacinatus circaperipherus</i> Rhodes, Austin, and Drice (fig. 8P, Q) 8 Pa element fragments <i>Pseudopolygnathus</i> spp.? indet. <i>Syncladognathus geminus</i> (Hinde) 7 Pa, 1 Pb and 1 S elements (fig. 8D) <u>UNASSIGNED ELEMENTS:</u> 1 Pb, 58 M (3+ morphotypes), 6 Sa (2 morphotypes), 3 Sb, and 16 Sc (2+ morphotypes) 100+ indet. bar, blade, and platform fragments	late Early Mississippian (early Osagean). Postmortem transport from or within the polygnathid- hispathodid biofacies; faunule has some elements representing a variety of platform or shelf biofacies. CAI=1.5	All samples prefixed 90AD59 are from a measured section (see fig. 1). Virtually all conodonts are partly to completely coated by adventitious organic matter.
Lisburne Group (lower unit)	90AD59-S4 (31735-PC); 54 m		Crinoidal packstone/grainstone. 9 Pa element fragments <i>Bispathodus utahensis</i> Sandberg and Gutschick? 3 Pa element fragments <i>Cavusgnathus</i> sp. indet. (fig. 8N, O) <i>Kladognathus</i> sp. indet. 2 Sa and 7 Sc elements <i>Syncladognathus geminus</i> (Hinde) (fig. 8E, F) 1 M and 1 Sb elements <u>UNASSIGNED ELEMENTS:</u> 1 Pb and 3 M 74 indet. bar, blade, and platform fragments	early Late Mississippian (late Meramecian). Biofacies indeterminate: faunule represents postmortem mixing of shallow- to deeper water and (or) pelagic species. CAI=1-1.5	



Table 1. Conodont faunules and lithologies, upper part of Kayak Shale and Lisburne Group, western Ivotuk Hills, Killik River B-5 quadrangle, Alaska—Continued

UNIT	FIELD NO. (USGS COLLN. NO.) AND POSITION ABOVE BASE OF SECTION	LATITUDE N/ LONGITUDE W.	LITHOLOGY AND CONODONT FAUNULE	FOSSIL AGE, BIOFACIES, AND CAI	REMARKS
Lisburne Group (lower unit)	90AD59-66 (31736-PC); 66 m	68°28'50"/ 155°42'45" (base of section); 68°28'38"/ 155°42'45" (top of section)	Crinoidal packstone/grainstone. 47 Pa element fragments <i>Bisapthodus utahensis</i> Sandberg and Gutschick (fig. 8I-K) <i>Kladognathus</i> sp. indet. (fig. 8M) 7 unassigned M elements 94 indet. bar, blade, and platform fragments	early Late Mississippian (late Meramecian). Biofacies indeterminate: faunule represents postmortem mixing of shallow- to deeper water and (or) pelagic species. CAI=1-1.5	
Lisburne Group (middle unit)	90AD59-115.4 (31737-PC); 115.4 m		Bryozoan crinoidal wackestone. 19 Pa elements <i>Bisapthodus utahensis</i> Sandberg and Gutschick (fig. 8G, H) 2 Pa element fragments <i>Cavusgnathus</i> sp. <i>Kladognathus</i> sp. indet. (fig. 8L) 3 Sa and 5 Sc elements 1 unassigned Sc element 52 indet. bar, blade, and platform fragments	early Late Mississippian (late Meramecian). <i>Bisapthodid</i> (?) biofacies or mixing of pelagic and shallow- water elements. CAI=1-1.5	Representatives of <i>B.</i> <i>utahensis</i> are more complete than in the collections from the lower unit suggesting considerably less postmortem transport.
Lisburne Group (upper unit)	90AD59-190; 190 m		Thin-bedded dolostone. Barren.		
	92AD41A (31766-PC)	68°28'36"/ 155°42'30"	Dolostone containing sparse bioclasts and gray, noncalcareous to slightly calcareous shale partings. 3 indet. bar and blade fragments	Probably late Late Mississippian (Chesterian) on the basis of conodonts in USGS colln. 29982-PC (see below). Biofacies indeterminate. CAI=1-1.5	Sample is about 1 m below top of exposure and may be uppermost part of Lisburne; about 30 m of cover separates this sample from the top of the measured section.
Lisburne Group	85ASi14-18 (29892-PC)	68°28'33"/ 155°42'25"	Thin-bedded, fine-grained carbonate rocks. 5 incomplete and (or) juvenile Pa elements <i>Gnathodus</i> <i>bilineatus</i> (Roundy) (fig. 8A) 4 Pa elements <i>Gnathodus defectus</i> Dunn (fig. 8B) 1 Pa element <i>Gnathodus girtyi simplex</i> Dunn (fig. 8C) 15 indet. bar, blade, and platform fragments	Very latest Mississippian (latest Chesterian). Too few specimens for biofacies analysis, but faunule indicates normal-marine depositional environment. CAI=1.5	Sample from 11 m below top of Lisburne Group. Base of Siksikpuk Formation exposed at this locality. Sample may be equivalent to a level within the highest covered interval (see fig. 3) in measured section 90AD59. Samples with the prefix 85ASi were collected by J.P. Siok, Terrasat Corporation, Anchorage, AK, while he was a graduate student at the University of Alaska Fairbanks.
	85ASi14-14		Barren.		Sample from uppermost part of Lisburne Group, immediately beneath Siksikpuk Formation.



is richer in organic material; shale in the Ivotuk Hills is chiefly dark-gray and more like the Kayak Shale. Siliceous mudstone rich in sponge spicules, however, is characteristic of the Kuna (Dumoulin and others, this volume) and occurs in the Kayak in the Ivotuk Hills; this lithology has not been reported from other Kayak outcrops, although lime mudstone with minor sponge spicules occurs locally in the Kayak (Armstrong, 1974; Armstrong and Bird, 1976). Quartzose sandstone is typical of the Kayak, but is absent from the Ivotuk Hills section and the Kuna. This could be due to removal of the lower part of the Kayak in the Ivotuk Hills by thrusting; sandstone is generally most abundant in the basal beds of the Kayak (C.G. Mull, written commun., 1992).

Both the Kayak Shale and the Kuna Formation contain carbonate concretions. Concretions in the Ivotuk Hills section appear less iron-rich than typical Kayak concretions, but do not contain calcitized radiolarite as do many Kuna concretions (Dumoulin and others, this volume). Orange-weathering, bioclastic carbonate beds, locally rich in phosphatic grains and interpreted as tempestites, occur in the Kayak Shale in the Ivotuk Hills and elsewhere but are rare or absent in the Kuna (Bowsher and Dutro, 1957; Dumoulin, unpublished data).

Conodont faunas from the Kayak Shale in the Ivotuk Hills correspond both with faunas from other Kayak outcrops and from the Kuna Formation. In the central and western Brooks Range, carbonate beds in the Kayak are poorly to abundantly productive of conodonts. Regardless of yield, the predominant conodonts are double-rowed bispathodids such as *Bispathodus? plumulus nodosus* (Rhodes, Austin, and Druce) and lesser representatives of *B. stabilis*, polygnathids, hindeodids, and rare pseudopolygnathids (Dumoulin and others, this volume, and A.G. Harris, unpublished U.S. Geological Survey conodont collections). The Kuna Formation is generally poorly productive of conodonts, but rare abundant samples produce single-row bispathodids (*B. utahensis*) to the virtual exclusion of all other conodonts (Dumoulin and others, this volume). Like typical Kuna conodonts, conodonts from the Kayak Shale in the Ivotuk Hills are coated with organic matter and include abundant single-row bispathodids. The Ivotuk Hills conodont fauna is more diverse than that typically found in either the Kayak or the Kuna, however, and probably represents postmortem hydraulic mixing of elements from several biofacies.

Lithologic and faunal similarities of the Kayak Shale in the Ivotuk Hills to both the Kayak Shale and the Kuna Formation may be explained by deposition in an environment intermediate between that typical of the two formations. The shale section in the Ivotuk Hills probably formed in a platform or shelf setting in water somewhat deeper than that in which most of the Kayak Shale accumulated, but better oxygenated than that characteristic of the Kuna Formation.

## LISBURNE GROUP

The Lisburne Group in the Ivotuk Hills has been correlated (Martin, 1970; Armstrong, 1970; Mayfield and others, 1988) with Carboniferous sections several tens of kilometers to the west at Lisburne Ridge and Mount Bupto (fig. 1); these correlations are based on generalized lithologic columns and sparse megafossil collections. Detailed petrologic data and conodont faunas reported here allow more precise comparisons to be made.

Based on data presently available, the Lisburne Group in the Ivotuk Hills correlates better with the section at Lisburne Ridge than that at Mount Bupto. The general lithologic pattern at Lisburne Ridge is a threefold division like that in the Ivotuk Hills: thin-bedded chert and dolostone overlie and underlie an interval of more massive dolostone (Armstrong, 1970; Dumoulin, unpublished data). Conodonts from Lisburne Ridge indicate an age of early to middle Late Mississippian (late Meramecian to early Chesterian?) (Dumoulin and others, this volume, and unpublished data). The Lisburne Group at Mount Bupto contains megafossils interpreted by Armstrong (1970) as Osagean or Meramecian and probably Meramecian in age, but consists mostly of thin-bedded chert and lesser dolostone; a massive middle interval like that seen in the Ivotuk Hills has not been described.

The Lisburne Test Well No. 1 was drilled (to a total depth of 17,000 feet) about 1.5 km northeast of the Ivotuk Hills measured section; five thrust plates, each containing several hundred meters of Carboniferous strata, were encountered (Legg, 1983). Carboniferous rocks in these thrust plates consist of dolostone, limestone, subordinate chert, and lesser shale and glauconitic siltstone to sandstone. Carbonate lithologies are primarily bioclastic packstone and wackestone rich in crinoids and bryozoans. Foraminifers indicate an age of Late Mississippian for these strata (Mamet Zones 14 to 16 for the upper interval and 12 and 13 for the lower; equivalent to the late Meramecian to early Chesterian and the middle Meramecian, respectively). Foraminifers and lithofacies suggest that deposition took place primarily in open platform to bank environments, with some intervals of deposition under more restricted (lagoonal?) conditions.

Strata in these subsurface thrust plates thus appear roughly coeval with the Lisburne Group exposed in the Ivotuk Hills. However, at least parts of the subsurface sections may have formed in somewhat shallower water, more restricted depositional environments than those documented for the section along Otuk Creek.

## REFERENCES CITED

- Armstrong, A.K., 1970, Mississippian dolomites from Lisburne Group, Killik River, Mount Bupto Region, Alaska: Ameri-

- can Association of Petroleum Geologists Bulletin, v. 54, p. 251-264.
- 1974, Preliminary Carboniferous carbonate depositional models, lithofacies, and paleotectonic maps, Arctic Alaska: American Association of Petroleum Geologists Bulletin, v. 58, p. 621-645.
- Armstrong, A.K., and Bird, K.J., 1976, Carboniferous environments of deposition and facies, Arctic Alaska, in Miller, T.P., ed., Symposium on Recent and Ancient Sedimentary Environments in Alaska: Alaska Geological Society Symposium Proceedings, p. A1-A16.
- Armstrong, A.K., and Mamet, B.L., 1977, Carboniferous microfacies, microfossils, and corals, Lisburne Group, Arctic Alaska: U.S. Geological Survey Professional Paper 849, 129 p.
- Bowsher, A.L., and Dutro, J.T., Jr., 1957, The Paleozoic section in the Shainin Lake area, central Brooks Range, Alaska: U.S. Geological Survey Professional Paper 303-A, p. 1-39.
- Dickson, J.A.D., 1966, Carbonate identification and genesis as revealed by staining: *Journal of Sedimentary Petrology*, v. 36, p. 491-505.
- Dumoulin, J.A., and Harris, A.G., 1992, Devonian-Mississippian carbonate sequence in the Maiyumerak Mountains, western Brooks Range, Alaska: U.S. Geological Survey Open-File Report 92-3, 83 p.
- Epstein, A.G., Epstein, J.B., and Harris, L.D., 1977, Conodont color alteration—An index to organic metamorphism: U.S. Geological Survey Professional Paper 995, 27 p.
- Flügel, E., 1982, *Microfacies analysis of limestones*: New York, Springer-Verlag, 633 p.
- Legg, G.W., 1983, Geological report on the Lisburne Test Well No. 1, Husky Oil NPR Operations Inc., 17 p.
- Martin, A.J., 1970, Structure and tectonic history of the western Brooks Range, De Long Mountains and Lisburne Hills, Northern Alaska: *Geological Society of America Bulletin*, v. 81, p. 3605-3622.
- Mayfield, C.F., TAILLEUR, I.L., and ELLERSIECK, INYO, 1988, Stratigraphy, structure, and palinspastic synthesis of the western Brooks Range, northwestern Alaska, in Gryc, George, ed., *Geology and exploration of the National Petroleum Reserve in Alaska, 1974-1982*: U.S. Geological Survey Professional Paper 1399, p. 143-186.
- Mull, C.G., 1989, Generalized stratigraphy and structure of the Brooks Range and Arctic Slope, in Mull, C.G., and Adams, K.E., eds., *Dalton Highway, Yukon River to Prudhoe Bay, Alaska*: Alaska Division of Geological and Geophysical Surveys, Guidebook 7, v. 1, p. 31-46.
- Mull, C.G., Harris, E.E., and TAILLEUR, I.L., in press, Preliminary geologic map of the Killik River quadrangle: U.S. Geological Survey Open-File Report, scale 1:125,000.
- Mull, C.G., TAILLEUR, I.L., Mayfield, C.F., ELLERSIECK, INYO, and Curtis, S.M., 1982, New upper Paleozoic and lower Mesozoic stratigraphic units, central and western Brooks Range, Alaska: American Association of Petroleum Geologists Bulletin, v. 66, p. 348-362.
- Murchey, B.L., Jones, D.L., Holdsworth, B.K. and Wardlaw, B.R., 1988, Distribution patterns of facies, radiolarians, and conodonts in the Mississippian to Jurassic siliceous rocks of the northern Brooks Range, Alaska, in Gryc, George, ed., *Geology and exploration of the National Petroleum Reserve in Alaska, 1974 to 1982*: U.S. Geological Survey Professional Paper 1399, p. 697-724.
- Rhodes, F.H.T., Austin, R.L., and Druce, E.C., 1969, British Avonian (Carboniferous) conodont faunas and their value in local and intercontinental correlation: *Bulletin of the British Museum (Natural History) Geology Supplement* 5, 313 p.
- Sandberg, C.A., and Gutschick, R.C., 1984, Distribution, microfauna, and source-rock potential of Mississippian Delle Phosphatic Member of Woodman Formation and equivalents, Utah and adjacent states, in Woodward, Jane, and others, eds., *Hydrocarbon source rocks of the Greater Rocky Mountain region*: Denver, Colorado, Rocky Mountain Association of Geologists, p. 135-178.

Reviewers: A.K. Armstrong and C.G. Mull

# DEPOSITIONAL SEQUENCES IN LOWER CRETACEOUS ROCKS, ATIGUN SYNCLINE AND SLOPE MOUNTAIN AREAS, ALASKAN NORTH SLOPE

By Christopher J. Schenk and Kenneth J. Bird

## ABSTRACT

Sequence stratigraphy provides a framework in which conformable successions of strata deposited within one sea-level cycle can be used to predict the distribution of reservoir rocks, reservoir seals, and source rocks within a sequence. Five sequence boundaries that separate systems tracts are tentatively identified in Lower Cretaceous strata in the central part of the Alaskan North Slope, consisting of the Kemik Sandstone, Fortress Mountain Formation, Torok Formation, the Gilead Creek sandstone unit, and the Nanushuk Group (part). Many more sequence boundaries may be present within this part of the Cretaceous section, but their recognition awaits more detailed field observations. Structural complexity and the general lack of continuous outcrop combine to make regional tracing of possible sequence boundaries difficult to impossible.

## INTRODUCTION

This study represents a preliminary attempt at dividing the Lower Cretaceous stratigraphic section in the Atigun syncline-Slope Mountain area of the Alaskan North Slope into depositional sequences (fig. 1). A depositional sequence is defined as a genetically related succession of strata bounded by unconformities or their correlative conformities (Mitchum, 1977). Each depositional sequence can be further divided into systems tracts, which form in response to the general position of sea level during a depositional sequence. Each system tract is defined by its position within a sequence and the distribution and stacking patterns of parasequences and facies associations within it. Parasequences are the building blocks of systems tracts and sequences, and are defined as genetically related succession of beds or bedsets bounded by marine flooding surfaces or their correlative surfaces (Van Wagoner and others, 1990; Mitchum and Van Wagoner, 1991). Systems tracts provide a high degree of facies predictability within the framework of sequence boundaries, which is important for the analysis of reservoir rocks and seals within a basin or field (Van Wagoner and others, 1990).

Systems tracts include lowstand, transgressive, and highstand tracts (fig. 2). Lowstand tracts form on the unconformity developed during relative sea-level fall, and consist of basin floor and slope submarine fans and clastics of the lowstand wedge. The lowstand wedge includes progradational strata formed during falling sea level, incised valley fill deposits, and associated lowstand shoreline deposits. Valley fills commonly consist of fluvial and estuarine sandstone and mudstone, but can also include coal, shallow-marine sandstone and shelf mudstone. The boundaries of the lowstand tract are the lower sequence boundary at the base and the first major transgressive surface (ravinement or flooding surface) at the top. Thus, the lowstand wedge includes strata deposited during the lowstand but also strata deposited prior to the development of the transgressive surface. In more proximal parts of a sequence, the first deposits above a sequence boundary may be part of the transgressive systems tract (fig. 2).

Transgressive systems tracts are found between the first transgressive surface and the downlap surface of the highstand tract. Downlap surfaces, however, are difficult to recognize in shelf or ramp settings. The transgressive tract consists of a retrogradational parasequence set, and can include shelf mudstone, shallow-marine sandstone, and coastal plain mudstone, sandstone, and coal. However, in some documented sequences the transgressive tracts are thin or absent (Embry, 1989). Condensed sections occur in the transition from the upper transgressive tract to the lower highstand tract (Van Wagoner and others, 1990).

Highstand tracts are bounded below by the downlap surface and above by the sequence boundary, and consist of a progradational parasequence set. The parasequences can contain shelf mudstone, shallow-marine sandstone, and coastal plain mudstone and sandstone, including coal. Van Wagoner and others (1990) concluded that many clastic highstand tracts are significantly truncated by the next unconformity and that, if preserved, are thin and shaly. They also concluded that many hydrocarbon reservoirs are found in lowstand tracts.

Critical to the delineation of systems tracts and sequences is the recognition of parasequence stacking patterns and the regional recognition of sequence boundaries.

The recognition of sequence boundaries is nontrivial, and includes observing (1) subaerial erosion as incised valleys, subaerial exposure or laterally equivalent submarine erosion, (2) onlap of coastal strata onto sequence boundary,

(3) abrupt basinward shift of facies immediately above the sequence boundary, and (4) that one or more of the above occurs regionally. In the Alaskan North Slope, sequence boundaries are interpreted with difficulty because of the

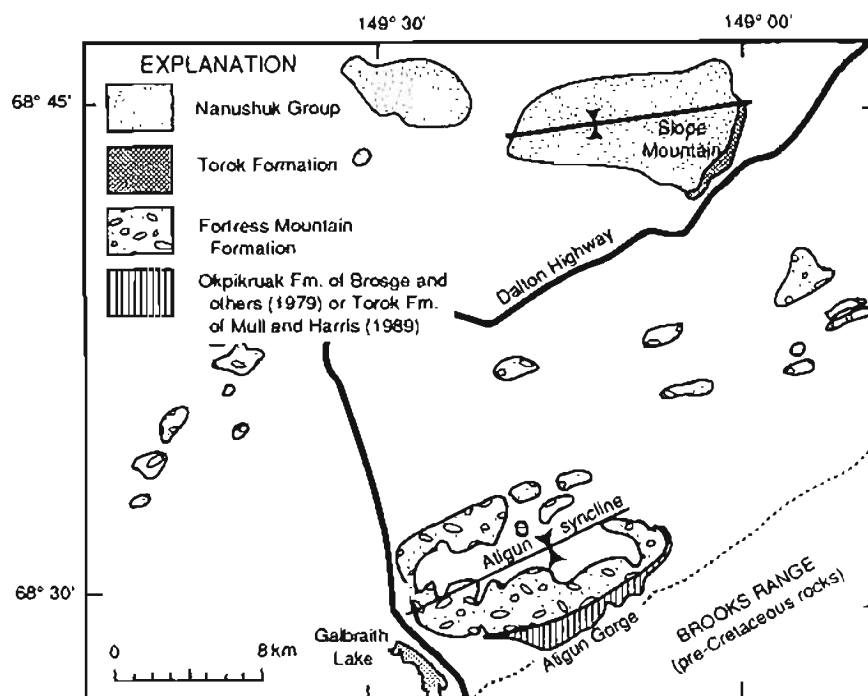
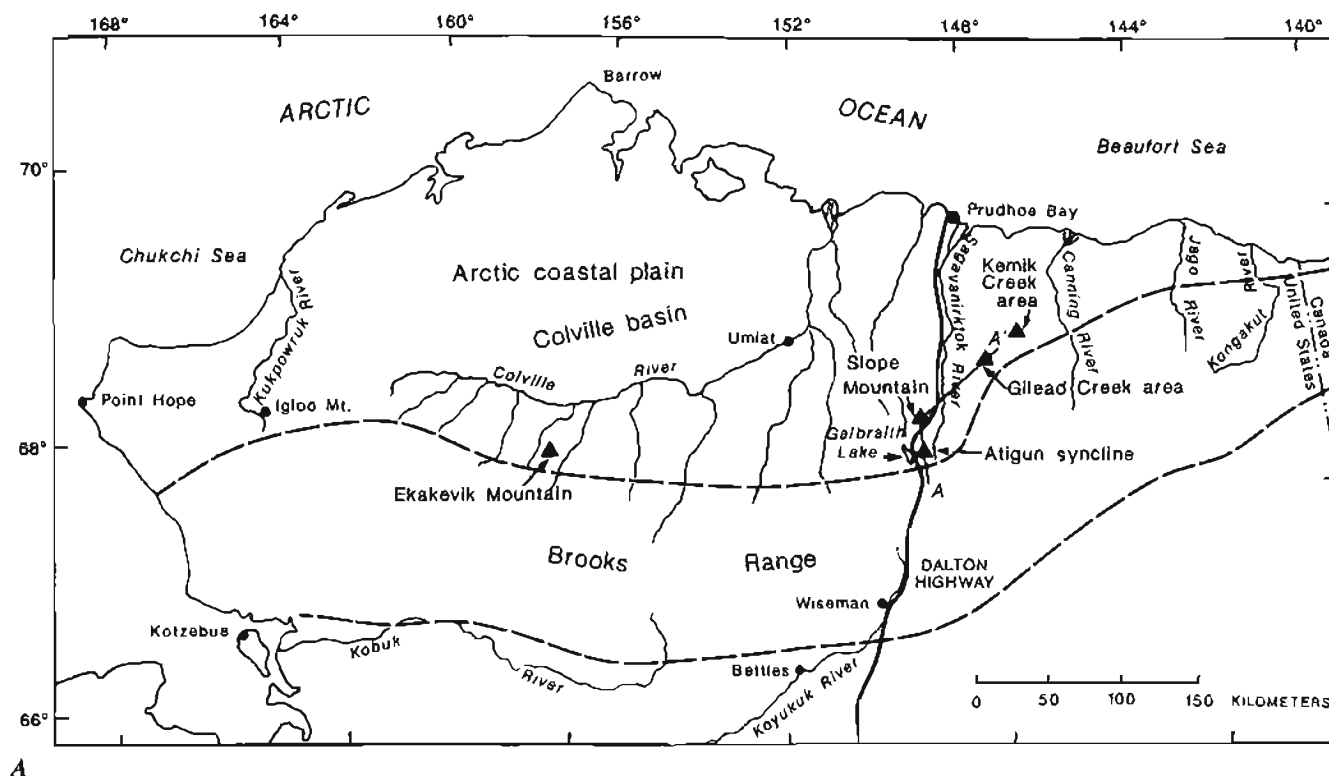


Figure 1. A, Location map of northern Alaska. Line of cross section A-A' is shown schematically in figure 3. B, Location map of study area around Slope Mountain, Atigun Gorge, and Atigun syncline. Dashed line approximates extent of Brooks Range.

general lack of continuous outcrop, paucity of close biostratigraphic control in many units, general lack of borehole control, and structural overprint of many units.

## INTERPRETATION OF SEQUENCE BOUNDARIES

Several stratigraphic units were examined during this study, including the Fortress Mountain Formation (Aptian? and Albian; Bird and Molenaar, 1992), Torok Formation (Aptian to Cenomanian; Weimer, 1987), the Nanushuk Group (Albian and Cenomanian; Mull, 1985), and the Gilead Creek sandstone unit (Albian? and Cenomanian?). This work, combined with a survey of available literature, forms the basis for the following discussion of sequences and the five sequence boundaries interpreted during this study (fig. 3).

### SEQUENCE BOUNDARY 1

The first sequence boundary considered for this study is the widely recognized Lower Cretaceous unconformity (LCU) and its equivalent down-dip conformable surface. In the foothills of the northeastern Brooks Range, the LCU cuts rocks as young as Valanginian and is overlain by rocks as old as probable Hauterivian (Molenaar, 1983).

The unconformity bevels the Jurassic and Cretaceous Kingak Shale and older rocks in a northerly direction (Molenaar, 1983; Bird and Molenaar, 1987). To the south, the unconformity dies out and is represented by a conformable surface extending southward into the axis of the basin (fig. 4). Several sandstone units were deposited on this surface. Because of their quartzose composition, indicating a northerly provenance, and their close association with hydrocarbon source rocks, these sandstones are attractive exploration targets.

The sequence model suggests the occurrence of lowstand shelf and deeper marine lowstand fan deposits south of the southern limit of the LCU. An apparent example of a shelf sandstone is the upward-coarsening sandstone beneath the pebble shale unit penetrated in the Tunalik well in the western part of the National Petroleum Reserve in Alaska (NPR) (Magoon and others, 1988, plate 19.2). Furthermore, we speculate that the quartzose sandstones of the Tingmerkpuk subunit of the Ipewik unit of Crane and Wiggins (1976), as mapped in the northern part of the DeLong Mountains (Curtis and others, 1990; Ellersieck and others, 1990), represent a lowstand fan deposit, perhaps derived from the Tunalik shelf region (fig. 4).

Subaerial erosion creating the LCU is likely to have produced incised valleys, controlled in part by structure (Noonan, 1987). As sea level rose, the valley system would have aggraded by fluvial and estuarine depositional processes, whereas shallow-marine processes would have

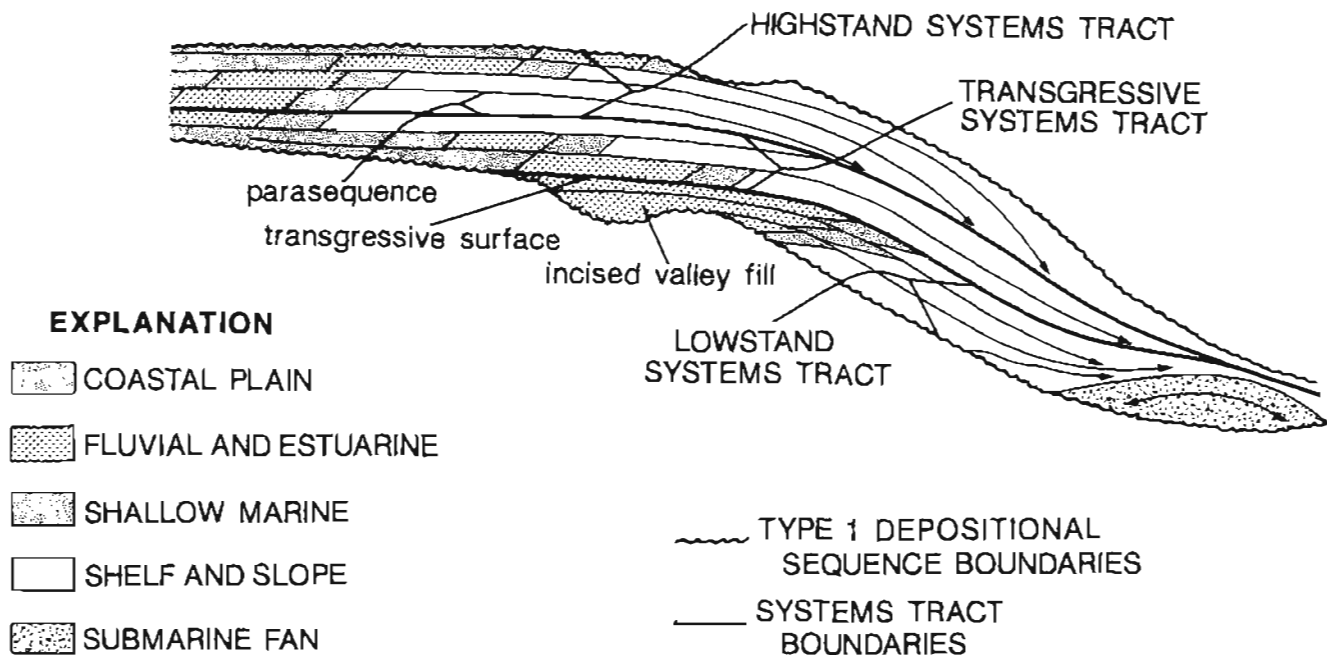


**Figure 2.** Diagram of systems tracts and parasequence stacking patterns in type 1 depositional sequence (after Mitchum and Van Wagoner, 1991). Lowstand tract contains submarine fan deposits and prograding deposits of lowstand wedge, consisting of incised valley fill of fluvial and estuarine sandstones. These deposits are overlain by transgressive surface and retrogradational

parasequence set of transgressive system tract. In marine sections, transition from upper part of transgressive systems tract to lower part of highstand tract commonly contains condensed section. Highstand tract contains progradational parasequence set (after Mitchum and Van Wagoner, 1991). Lower sequence boundary and transgressive surface can merge in updip direction.

predominated during the overall transgression. Several sandstone units were deposited on the LCU, including the Put River sand, the Thomson sand, and the Walakpa sandstone (all of local usage), as well as the Kemik Sandstone (Melvin, 1986; Mull, 1987) and the upper part of the Kuparuk Formation (fig. 4). Additional unnamed sandstones at this stratigraphic position are penetrated by numerous wells, but their areal extent is unknown (Bird, 1986, fig. 7).

The Put River sand (Jamison and others, 1980; Bird, 1988), located just west of Prudhoe Bay (fig. 4), has an areal extent of about 25 square kilometers, a maximum thickness of about 21 m, and an elongated north-south sinuous outline consistent with either a channel or bar deposit (see isopach map in McIntosh, 1977, or the outline map in Bird, 1986, fig. 8). The Thomson sand (Gautier, 1987; Bird and others, 1987; Bird, 1988) consists of as much as 90 m of sandstone composed of more than 50 percent detrital dolomite grains, and locally includes pebble, cobble, and boulder conglomerate with boulders as large as 1.4 m (Gautier, 1987). These deposits are certainly of local derivation and may represent a nonmarine channel sandstone deposited in an incised valley as part of

the lowstand wedge. Just south of Barrow (fig. 1), the Walakpa sandstone (Schindler, 1988) is poorly known, although recent drilling in the area suggests that the Walakpa sandstone is more sheetlike than the Put River sand (R. Glenn, personal communication, 1992). The Kemik Sandstone (Mull, 1987) is one of the thickest and most widespread of these sandstones (Bird and others, 1987, fig. 7.11). The upper member of the Kuparuk Formation (Carman and Hardwick, 1983) (equivalent to the Kuparuk River Formation of Masterson and Paris, 1987) overlies the LCU and was deposited in a marine shelf setting during a period of extensional faulting. This part of the Kuparuk displays considerable stratigraphic complexity including two transgressive episodes and two regressive episodes plus the cutting of an intra-unit unconformity. The interplay of eustatic sea-level change and tectonism has yet to be resolved for these rocks.

The lowstand systems tract depositional model predicts the occurrence of sets of sandstone-filled channels at the LCU. Their thickness and preservation depends on a number of factors, including competency of the fluvial system, a source of sediment, and preservation of the valley fill during transgression with limited reworking and

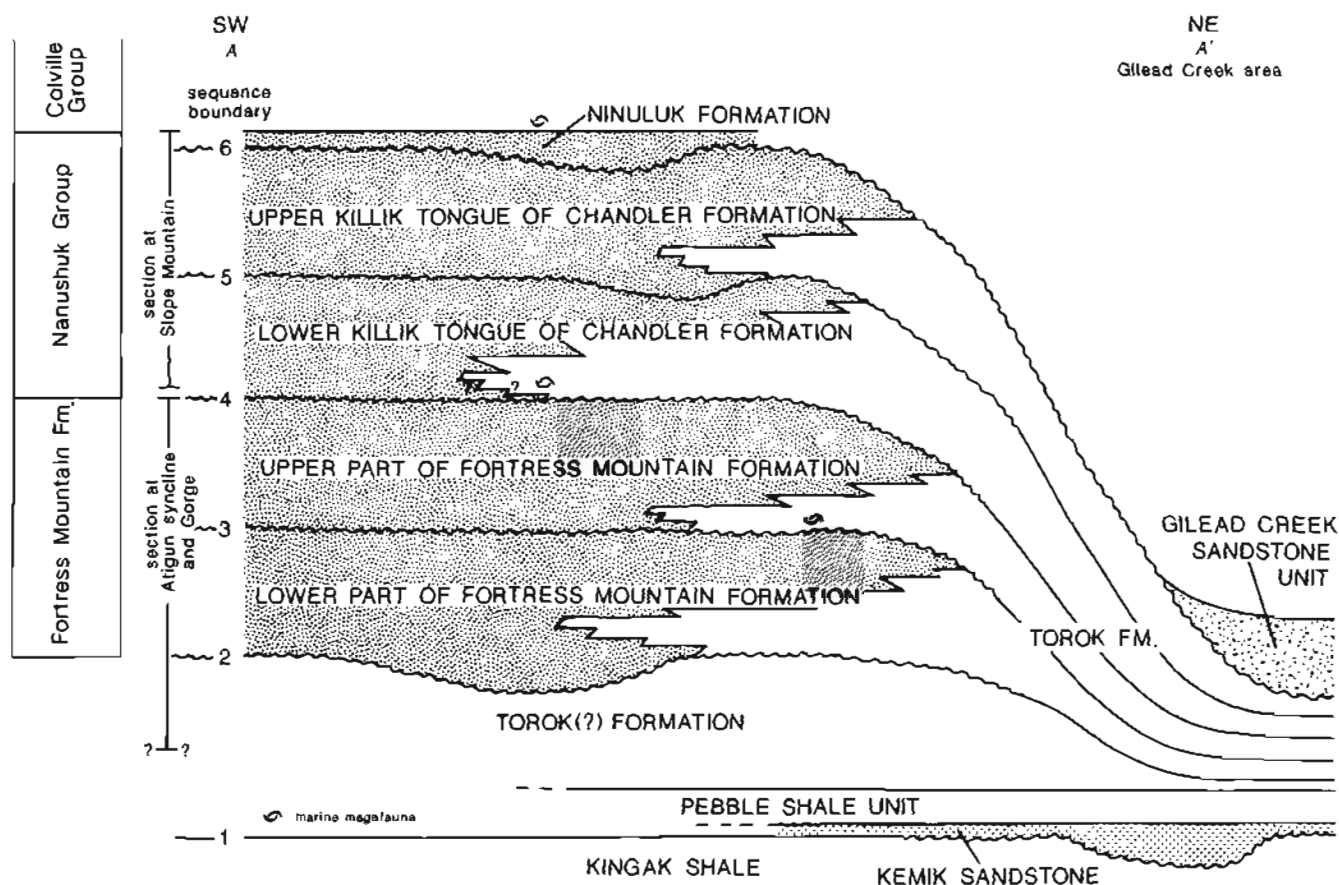
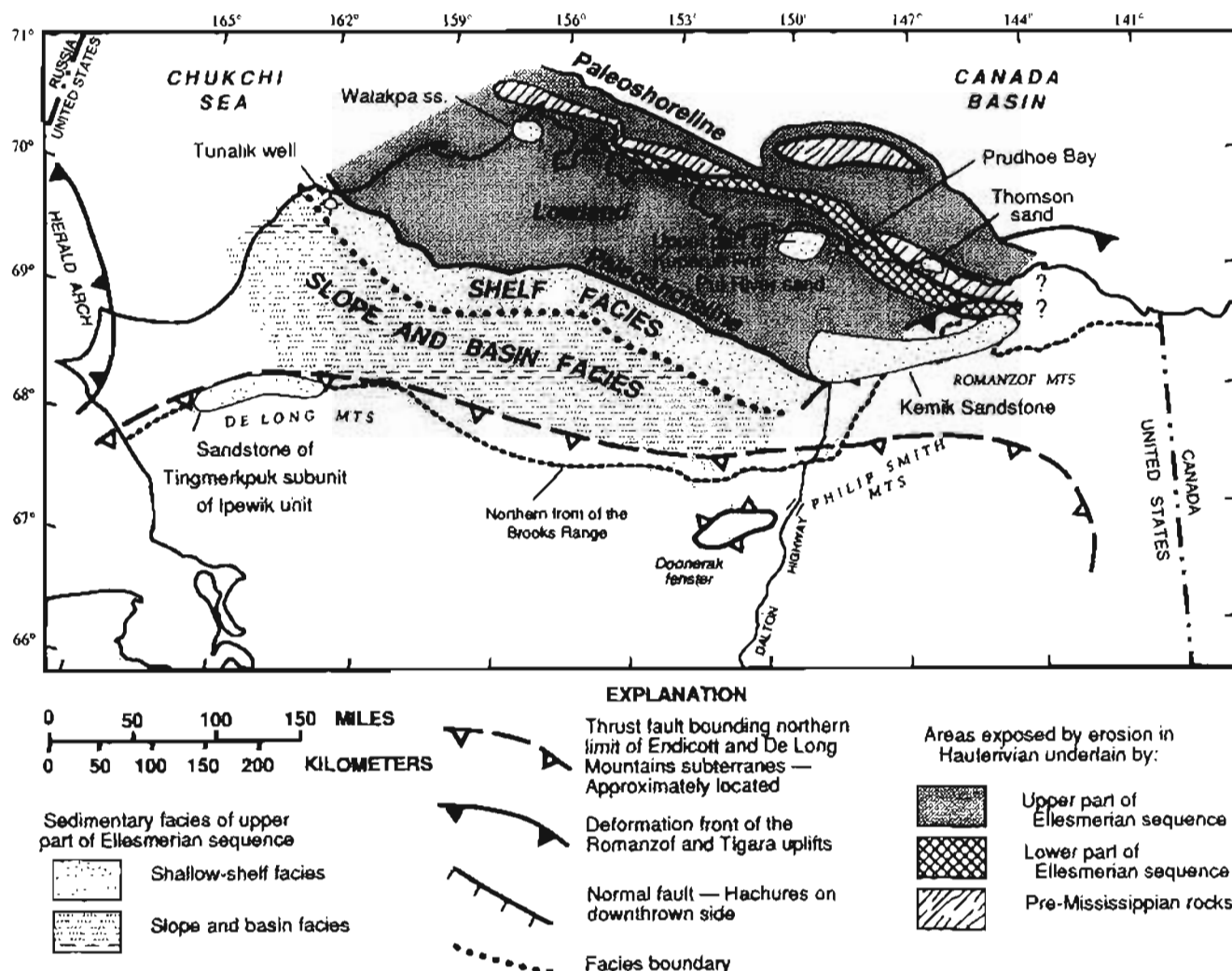


Figure 3. Summary schematic diagram of five depositional sequence boundaries tentatively identified in this study. Sequence boundary 6 is early(?) Cenomanian depositional sequence boundary described by Phillips and others (1990). Nomenclature for units in the Nanushuk Group slightly revised from Huffman (1989, fig. 227).

redistribution. The thickest of the known sandstones is about 90 m, which approaches the limit of seismic-reflection resolution. Mapping the channels may be possible only if additional borehole data become available. Certainly, the overall low density of exploratory drilling of the LCU interval allows for, or cannot preclude, such an occurrence.

The lowstand and transgressive sandstones of sequence 1 were covered by mudstones of the pebble shale unit (Bird and Molenaar, 1992), which is also part of the transgressive systems tract. The pebble shale unit, an important hydrocarbon source rock and seal along the North Slope (Bird, 1991), represents the youngest rock unit of northern derivation. The pebble shale unit was covered by distal mudstones of the southerly-derived Brookian (tectonostratigraphic) sequence of latest Jurassic(?) to

Holocene age. These distal mudstones are variously assigned to the gamma-ray zone, the uppermost part of the pebble shale unit in the western part of the North Slope, or to the Hue Shale in the eastern part of the North Slope (Molenaar and others, 1987). These mudstones, which represent increasing amounts of time in a northeasterly direction, include deposits assigned to the highstand systems tract, but they probably represent so much time that they must include all systems tracts developed from the Albian to the Campanian in the eastern area, near the Arctic National Wildlife Refuge. Thus, sequence 1, extending from the LCU to the gamma-ray zone, spans the transition from the Ellesmerian (equivalent to the Beaufortian sequence of some authors) sequence to the Brookian (tectonostratigraphic) sequence.



**Figure 4.** Paleogeography and paleogeology of North Slope at time of maximum regression in Early Cretaceous (Valanginian and Hauterivian) time. This figure, modified from Moore and others (1992), shows interpreted lowstand and transgressive systems tracts sandstones associated with sequence 1 of this report. Exposed area shows extent of Lower Cretaceous unconformity

and underlying rocks. Lowstand deposits may include shelf sandstone in Tunalik #1 well, and Tingmerkpuk subunit of Ipewik unit of Crane and Wiggins (1976). Transgressive and partly lowstand sandstones consist of Walakpa sandstone of local usage, upper part of Kuparuk Formation, Put River sand of local usage, Thomson sand of local usage, and Kemik Sandstone.



## SEQUENCE BOUNDARY 2

The exposure of the Fortress Mountain Formation along the north wall of Atigun Gorge is one of the few places where the lower contact of the Fortress Mountain may be examined. At this locality the Fortress Mountain Formation overlies at least 600 m of gray concretion-bearing mudstone and thin-bedded sandstone that has been mapped as the Neocomian Okpikruak Formation by Brosigé and others (1979) or the Albian Torok Formation by Mull and Harris (1989, fig. 99). No direct paleontologic determinations of the age of these strata at Atigun Gorge are known. Whereas the base of the Fortress Mountain Formation is clearly unconformable in areas to the west, such as at Ekakavik Mountain and Castle Mountain (Mull, 1985), the lower contact of the Fortress Mountain Formation was not mapped as unconformable in the Atigun Gorge area (Brosigé and others, 1979). The implication is that sedimentation may have been continuous throughout Early Cretaceous time in this area. However, the lower contact of the Fortress Mountain Formation in the Atigun area was reported to be unconformable by Crowder (1989, p. 296). Our preliminary work suggests that sandstone and mudstone of the basal part of the Fortress Mountain Formation appear to fill what may be a valley incised into the underlying mudstone of the Torok or Okpikruak Formations. Figure 5 is a panoramic view of part of the north wall of Atigun Gorge illustrating these relationships. The possible incisement of marine mudstone and later fill by fluvial and marine deposits led us to place a sequence boundary at this position in Atigun Gorge. The lower part of the Fortress Mountain Formation may be nonmarine to shallow marine in origin. These deposits were then

covered by marine mudstone and sandstone as transgression progressed. This possible sequence boundary and the associated sedimentary deposits as exposed along Atigun Gorge require more study in terms of parasequences and depositional environments. The lower part of this sequence in west-facing slopes at Atigun syncline was referred to as Unit A by Crowder (1989) and Lithosome 4 by Goff (1990), and was interpreted by them to be marine in origin. Sandstones of the Fortress Mountain Formation in a similar stratigraphic position in the west-central part of the North Slope were interpreted as deep marine in origin (Molenaar and others, 1988).

The marine sandstones grade up into channelized conglomerate and conglomeratic sandstone (unit B of Crowder, 1989; Lithosome 6 of Goff, 1990; Ryherd, 1990) at Atigun syncline east of Galbraith Lake (fig. 1B). Some of the sandstones we examined in the west-facing exposures displayed excellent examples of lateral-accretion bedding, formed as the result of the migration of sinuous channels. Some of the conglomerate and conglomeratic sandstones containing lateral-accretion bedding were stacked, forming composite conglomeratic sandstone bodies. The near-lack of mudstone and shale in this part of the section was noted by Ryherd (1990), who interpreted these conglomerates and conglomeratic sandstones as fan-deltaic deposits. The lack of turbidites and shales interbedded with the channel sandstones and the abundance of plant debris suggest that the majority of channel sandstones in this interval are nonmarine in origin. These same deposits have been interpreted as being of submarine fan origin, which is easy to understand given the poor exposure and lack of definitive sedimentologic criteria (Goff, 1990).

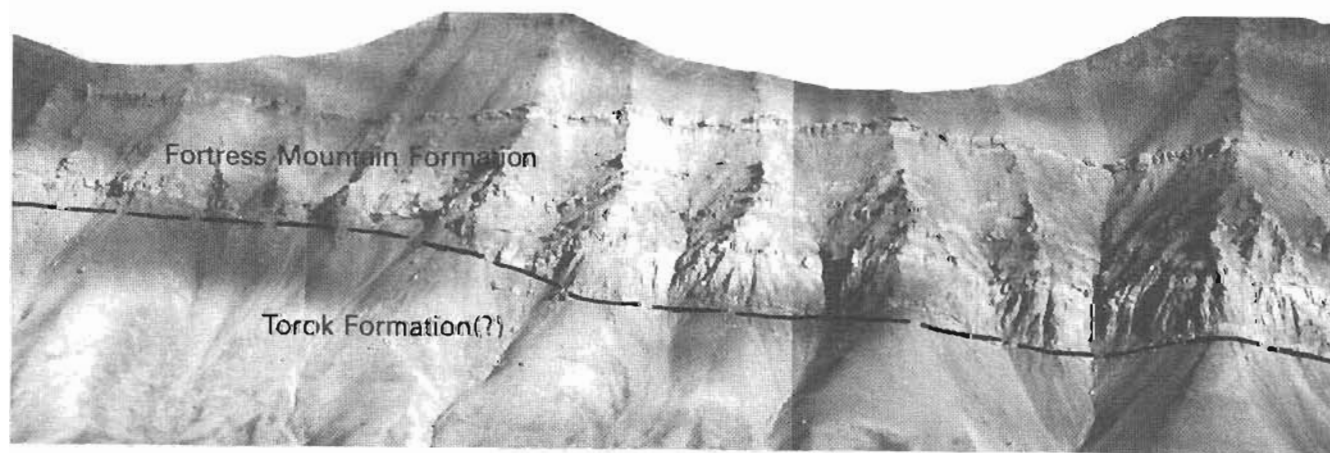


Figure 5. Photomosaic illustrating possible position of sequence boundary 2 along south-facing slope, north side of Atigun Gorge. Sandstones and mudstones of basal part of the Fortress Mountain Formation appear to onlap mudstones of the Torok(?) Formation. Although latter rocks were mapped as deformed strata of the Okpikruak Formation in this area by Brosigé and

others (1979), mudstones do not appear to be deformed for several hundred meters below contact, thus the Torok(?) Fm. designation for them in this figure. Photomosaic taken looking north from south side of Atigun Gorge, approximately 7.5 km east-northeast of Atigun River bridge. Bottom width of mosaic represents approximately 2.5 km.

## SEQUENCE BOUNDARY 3

Sequence boundary 3 was interpreted on the basis of sedimentologic discussions of Crowder (1987, 1989) and Goff (1990), who divided the Fortress Mountain Formation at Atigun syncline into various units based on gross sedimentology (fig. 6). Approximately at midpoint in the exposure of the Fortress Mountain Formation are thin coal beds overlain by sandstone and mudstone interpreted as marine in origin (Goff, 1990). The coals could belong to the highstand systems tract of sequence 2 (below sequence boundary 3), or they may belong to a valley fill in the lowstand tract of sequence 3 (above sequence boundary 3). We include the coals tentatively as part of the highstand tract of sequence 2, based on our preliminary observations,

although many coals in the Cretaceous of the Western Interior are part of lowstand systems tracts (Van Wagoner and others, 1990). We recognize that more work needs to be done to define the placement of a sequence boundary in this position. The mudstones containing the marine pelecypods that overlie the coals were placed in the transgressive systems tract of sequence 3. In sections that are proximal to the basin margin, as the Fortress Mountain Formation probably is, the first deposits above the sequence boundary are commonly part of the transgressive systems tract (fig. 2).

The marine sandstones and mudstones are overlain by a thick sequence of channelized conglomerates and conglomeratic sandstones interpreted generally as fan-deltaic or fluvial in origin. The sedimentologic characteristics of

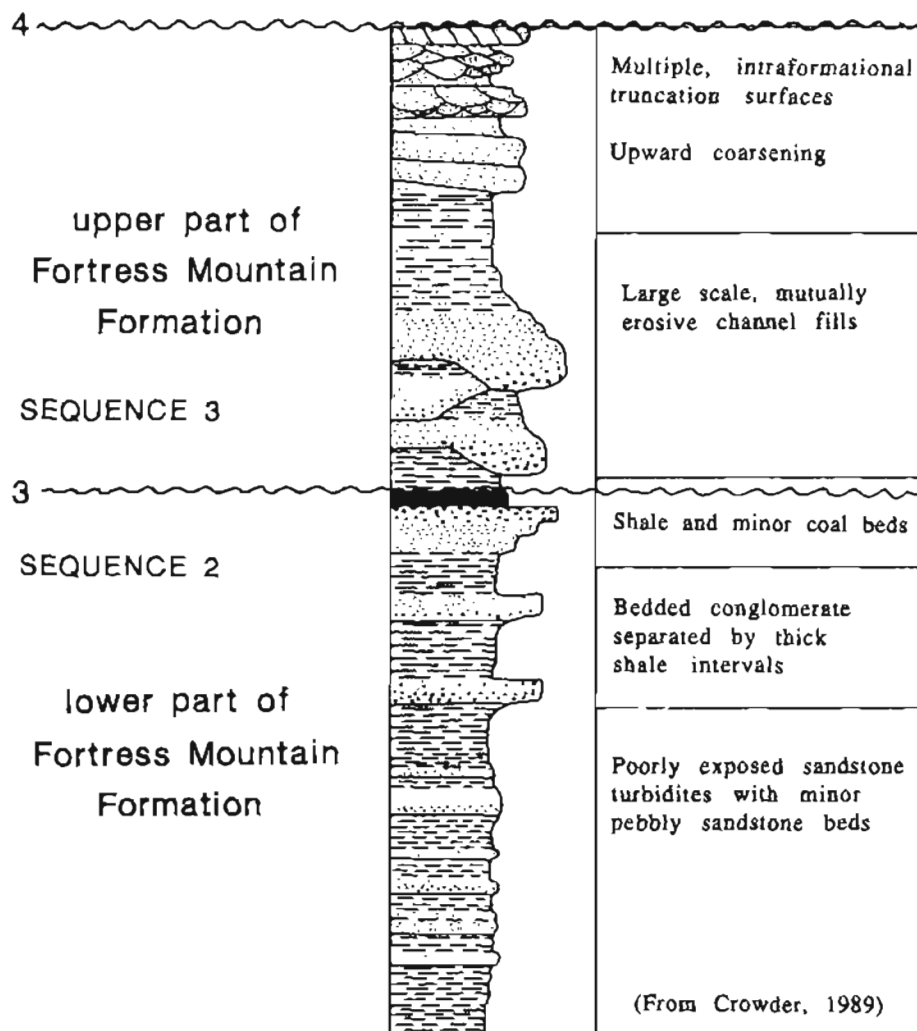


Figure 6. Schematic diagram showing general sedimentology of the Fortress Mountain Formation along west-facing slopes of Atigun syncline (from Crowder, 1989), to which sequence boundaries have been added. Sequence boundary 3 is tentatively placed where sandstone and coal are overlain by marine sandstone and mudstone, as reported by Crowder (1989) and Goff (1990). Sequence boundary 4 is tentatively placed at the top of Fortress Mountain Formation, but below Torok Formation.

the sandstones, as described by Crowder (1989) and Goff (1990), suggest that the sandstones formed in low-sinuosity channels on an extensive braidplain, possibly on a fan delta. This is Unit C of Crowder (1989) and the upper part of Lithosome 6 of Goff (1990). The sandstones are overlain by more sheetlike, finer grained channel sandstones that possibly represent deposits of sinuous fluvial channels.

#### SEQUENCE BOUNDARY 4

The fourth Early Cretaceous sequence boundary is postulated on the basis of regional considerations. This boundary in the Atigun syncline area is placed either within the uppermost part of the Fortress Mountain Formation, where depositional conditions change from fluvial below to marine above as observed at Ekakevik Mountain (Hunter and Fox, 1976; Molenaar and others, 1988), or higher in the section where the Fortress Mountain Formation is overlain by the Torok Formation, as is the case in the Igloo Mountain area (Chapman and Sable, 1960, fig. 8). The Atigun Gorge-Slope Mountain area is typical of much of the foothills of the Brooks Range in that the uppermost part of the Fortress Mountain Formation and the lowermost part of the Torok Formation are not preserved. At Atigun syncline, for example, the uppermost part of the Fortress Mountain Formation is composed of upward-

coarsening conglomerate, sandstone, and siltstone recording fluvial deposition (Crowder, 1989).

#### SEQUENCE BOUNDARY 5

Sequence boundary 5 at Slope Mountain is tentatively placed within the lower part of the Killik Tongue of the Chandler Formation of the Nanushuk Group (fig. 7), as defined in this area by Huffman and others (1985) and Huffman (1989). The placement of the sequence boundary in this position is tentative and requires more sedimentologic definition of the enclosing lithologies and extent of erosion on this possible sequence boundary, as is being done in the Upper Cretaceous Seabee Formation in this area (Phillips and others, 1990). Channels cutting into the lower part of the Killik Tongue were observed on south-facing exposures at Slope Mountain. These channels are either part of an incised valley fill or they simply represent distributary channels in a prograding deltaic shoreline. More work needs to be done on defining the magnitude and downcutting relationships of these channels to determine if they indeed are distributaries or the lower part of an incised valley fill. The upper part of the Torok Formation and the lower part of the Tuktu Formation at Slope Mountain contain several stacked progradational parasequences in shelf deposits, suggesting that they represent part of the highstand systems tract of the underlying sequence.

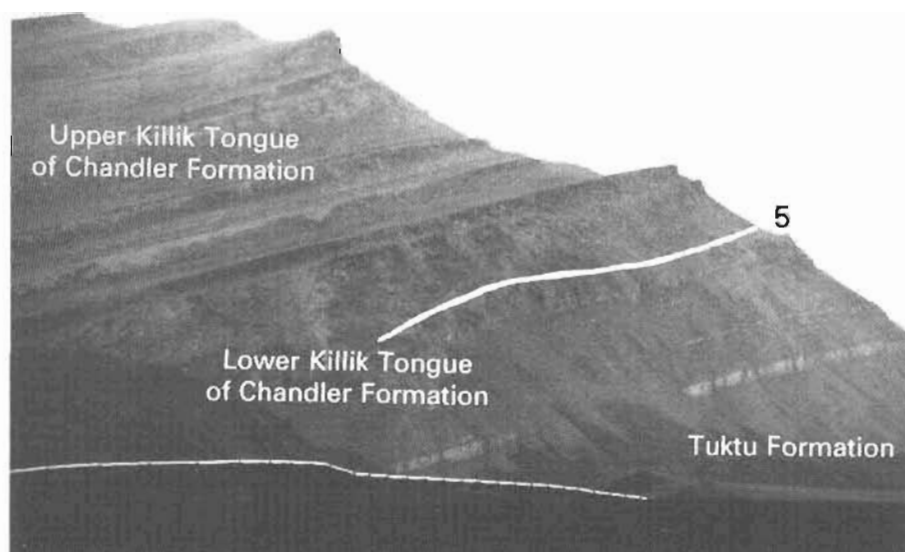


Figure 7. View northeastward of the Nanushuk Group at Slope Mountain (Dalton Highway Mile Marker 297) to which sequence boundary 5 has been added. Placement of sequence boundary 5 is speculative, and needs to be fully documented in the field to determine extent of channeling at this position. Sequence boundary is placed within lower Killik Tongue of Huffman (1989) of the Chandler Formation. Other sequence boundaries may be present in this section, but their interpretation awaits further field investigation. Structure at bottom is the Trans-Alaska pipeline.

Additional sequence boundaries may be present within the Chandler Formation at Slope Mountain, but given the relatively poor exposure of the lithologies between sandstones and the fair exposure of the sandstones, they are not outlined for this study. More definition of the environments represented by the Chandler Formation would help to define these sequence boundaries, if present.

#### GILEAD CREEK SANDSTONE UNIT

The informally named Gilead Creek sandstone unit (Reifenstuhel, 1989; Pessel and others, 1990) is exposed in the foothills about 60 km northeast of Slope Mountain (figs. 1, 3). This sandstone interval, 600–900 m thick, is anomalous in that it lies in close proximity to the Kingak Shale. Although exposures are poor, present mapping does not allow for hundreds to thousands of meters of mudstones of the Torok or Okpikruak Formations that typically occur in this position. Because this is a structurally complex area, it is possible that these mudstones, once present, are now faulted out. Such faulting, however, would require either a normal fault (in a dominantly compressional regime) or a thrust fault that places younger over older strata. We have no evidence to support either of these possibilities. We suggest that the Gilead Creek sandstone unit is the stratigraphic equivalent of part of the Torok Formation, or that it is somewhat younger and has scoured away an unknown amount of the Torok. Such relations could be explained by a lowstand fan deposit.

During relative sea-level low stands, the depositional sequence model predicts the development of lowstand fans in a downdip position at the same time that canyons and valleys are cut in an updip position. We concur with the interpretation of Molenaar and others (1984) of the Gilead Creek sandstone unit as composed mainly of turbidites. Such an interpretation is consistent with a lowstand fan deposit.

The age of the Gilead Creek sandstone unit is constrained by a marine pelecypod identified by W.P. Elder (personal communication, 1992) as *Inoceramus dunveganensis* of Cenomanian age from the upper part of the Gilead Creek sandstone unit (R. Reifenstuhel, personal communication, 1991) and marine pelecypods *Buchia* of Valanginian age from the underlying Kingak Shale (Pessel and others, 1990). With such age constraints, the Gilead Creek sandstone unit could represent a Cenomanian lowstand fan that scoured away Albian and Aptian mudstones, or it more likely represents an amalgamation of lowstand fan deposits spanning several depositional sequences.

#### DISCUSSION

Five depositional sequence boundaries have been outlined from exposures of the Fortress Mountain Formation,

Torok Formation, and the Chandler Formation of the Nanushuk Group in the area from Atigun syncline and Slope Mountain, and from examination of other sandstones including the Gilead Creek sandstone unit. These are not the only sequence boundaries possible in this stratigraphic interval; only these five are postulated from limited field observations. Other sequence boundaries may be present within the Fortress Mountain Formation and the Nanushuk Group, and their interpretation will have to be based on detailed field examination of these exposures.

One of the questions that arose during our field work was the stratigraphic relationship between the Fortress Mountain Formation and the Nanushuk Group in the Atigun syncline–Slope Mountain area. In this area there is a strong similarity of lithologic composition between these stratigraphic units, and one could argue that the Fortress Mountain at Atigun Gorge is simply the more proximal facies of the Nanushuk Group at Slope Mountain. Although the Fortress Mountain Formation–Torok Formation–Nanushuk Group transition is illustrated across the North Slope in cross sections (Molenaar, 1988), actual field evidence showing this succession is limited, as far as we could ascertain, to the area of Igloo Mountain near the Kokolik River, which was described by Chapman and Sable (1960). In the Igloo Mountain area (fig. 1A), the Fortress Mountain Formation appears to be in depositional contact with the Torok Formation, which is overlain by the Kukpowruk Formation (part of the Nanushuk Group). As the Kokolik River area is approximately 550 km west of the Atigun syncline area, the stratigraphic relationships between these three stratigraphic units are not clear. We speculate that the two sequences outlined in the Fortress Mountain Formation at Atigun syncline could be equivalent to two sequences of the Nanushuk Group at Slope Mountain, given the lack of good stratigraphic and biostratigraphic control. Although many seismic lines are available in the NPRA (Molenaar, 1985, 1988), none are properly positioned to resolve these stratigraphic relationships.

We attempted to point out the possible sequence boundaries that were present in this part of the stratigraphic section based on limited field work. We did not attempt to relate these boundaries to a causal mechanism, such as tectonics or eustasy. The Albian to Cenomanian section in the Western Interior Seaway of the United States contains many sequence boundaries ascribed by some to eustatic mechanisms (Haq and others, 1988), or to purely tectonic effects in the active Colville basin (Noonan, 1987) or in similar-aged rocks in Arctic Canada (Embry, 1989). Others have developed hybrid tectonic-eustatic models for the formation of depositional sequences in the Brookian sequence of Alaska (Rudolph and others, 1990). Whatever the cause, relative base-level changes had a significant effect on the depositional sequences as they developed in the Lower Cretaceous section of the Colville basin.

## CONCLUSIONS

Limited field work in the Atigun syncline-Slope Mountain area of the North Slope has led us to interpret five possible depositional sequence boundaries. Many more such boundaries may be present in the rocks examined, which were the Fortress Mountain Formation and Nanushuk Group, but require detailed sedimentologic examination of the entire section, and possible attempts to follow such boundaries regionally. The Gilead Creek sandstone unit was placed within a context of a lowstand submarine fan, based on its possible age, sedimentology, and geographic location relative to the Fortress Mountain and Nanushuk environments. Future work should focus on more closely defining the biostratigraphic and sedimentologic aspects of these units.

## REFERENCES CITED

- Bird, K.J., 1986, A comparison of the play analysis technique as applied in hydrocarbon resource assessments of the National Petroleum Reserve in Alaska and the Arctic National Wildlife Refuge, in Rice, D.D., ed., *Oil and gas assessment methods and applications*: American Association of Petroleum Geologists Studies in Geology 21, p. 133-142.
- , 1988, Alaskan North Slope stratigraphic nomenclature and data summary for government-drilled wells, in Gryc, George, ed., *Geology and exploration of the National Petroleum Reserve in Alaska*: U.S. Geological Survey Professional Paper 1399, p. 317-353.
- , 1991, North Slope of Alaska, in Gluskoter, H.J., Rice, D.D., and Taylor, R.B., eds., *Economic geology of the United States: Boulder*, Geological Society of America, *Geology of North America*, v. P-2, p. 447-462.
- Bird, K.J., and Molenaar, C.M., 1987, Stratigraphy, in Bird, K.J., and Magoon, L.B., eds., *Petroleum geology of the northern part of the Arctic National Wildlife Refuge, northeastern Alaska*: U.S. Geological Survey Bulletin 1778, p. 37-59.
- , 1992, The North Slope foreland basin, Alaska, in Macqueen, R.W., and Leckie, D.A., eds., *Foreland basin and foldbelts*: American Association of Petroleum Geologists Memoir 55, p. 363-393.
- Bird, K.J., Griscom, S.B., Bartsch-Winkler, S., and Giovannetti, D.M., 1987, Petroleum reservoir rocks, in Bird, K.J., and Magoon, L.B., eds., *Petroleum geology of the northern part of the Arctic National Wildlife Refuge, northeastern Alaska*: U.S. Geological Survey Bulletin 1778, p. 79-99.
- Brosigé, W.P., Reiser, H.N., Dutro, J.T., Jr., and Determan, R.L., 1979, Bedrock geologic map of the Phillip Smith Mountains quadrangle, Alaska: U.S. Geological Survey Miscellaneous Field Investigations Map MF 879-B, 2 sheets, scale 1:250,000.
- Carman, G.J., and Hardwick, P., 1983, Geology and regional setting of the Kuparuk oil field, Alaska: American Association of Petroleum Geologists Bulletin, v. 67, no. 6, p. 1014-1031.
- Chapman, R.M., and Sable, E.G., 1960, Geology of the Utukok-Corwin region, northwestern Alaska: U.S. Geological Survey Professional Paper 303-C, p. 47-167.
- Crane, R.C., and Wiggins, V.D., 1976, Ipewick Formation, significant Jurassic-Neocomian map unit in the northern Brooks Range foldbelt (abs.): American Association of Petroleum Geologists Bulletin, v. 60, no. 12, p. 2177.
- Crowder, R.K., 1987, Cretaceous basin to shelf transition in northern Alaska: deposition of the Fortress Mountain Formation, in Tailleir, I., and Weimer, P., eds., *Alaskan North Slope geology: Bakersfield*, Society of Economic Paleontologists and Mineralogists, Pacific Section, Book 50, v. 1, p. 449-458.
- , 1989, Deposition of the Fortress Mountain Formation, in Mull, C.G., and Adams, K.E., eds., *Dalton Highway, Yukon River to Prudhoe Bay, Alaska*: Alaska Division of Geological and Geophysical Surveys, Guidebook 7, Volume 2, p. 293-301.
- Curtis, S.M., Ellersieck, Inyo, Mayfield, C.F., and Tailleir, I.L., 1990, Reconnaissance geologic map of the De Long Mountains A-1 and B-1 quadrangles and part of the C-1 quadrangle, Alaska: U.S. Geological Survey Miscellaneous Investigations Series Map I-1930, 2 sheets, scale 1:63,360.
- Ellersieck, Inyo, Curtis, S.M., Mayfield, C.F., and Tailleir, I.L., 1990, Reconnaissance geologic map of the De Long Mountains A-2 and B-2 quadrangles and part of the C-2 quadrangle, Alaska: U.S. Geological Survey Miscellaneous Investigations Map I-1931, 2 sheets, scale 1:63,360.
- Embry, A.F., 1989, A tectonic origin for third-order depositional sequences in extensional basins—Implications for basin modeling, in Cross, T.A., ed., *Quantitative dynamic stratigraphy*: New York, Prentice-Hall, p. 491-501.
- Gautier, D.L., 1987, Petrology of Cretaceous and Tertiary reservoir sandstones in the Point Thomson area, in Bird, K.J., and Magoon, L.B., eds., *Petroleum geology of the northern part of the Arctic National Wildlife Refuge, northeastern Alaska*: U.S. Geological Survey Bulletin 1778, p. 117-122.
- Goff, R.A., 1990, Stratigraphy and sedimentology of the Fortress Mountain Formation at Atigun syncline, northern Alaska: Fairbanks, University of Alaska, M.S. thesis, 122 p.
- Haq, B.U., Hardenbol, J., and Vail, P.R., 1988, Mesozoic and Cenozoic chronostratigraphy and cycles of sea-level change, in *Sea level changes—An integrated approach*: Society of Economic Paleontologists and Mineralogists Special Publication 42, p. 71-108.
- Huffman, A.C., Jr., 1989, The Nanushuk Group, in Mull, C.G., and Adams, K.E., eds., *Dalton Highway, Yukon River to Prudhoe Bay, Alaska*: Alaska Division of Geological and Geophysical Surveys Guidebook 7, v. 2, p. 303-309.
- Huffman, A.C., Jr., Ahlbrandt, T.S., Pasternak, I., Stricker, G.D., and Fox, J.E., 1985, Depositional and sedimentologic factors affecting the reservoir potential of the Cretaceous Nanushuk Group, central North Slope, Alaska: U.S. Geological Survey Bulletin 1614, p. 61-74.
- Hunter, R.E., and Fox, J.E., 1976, Interpretation of depositional environments in the Fortress Mountain Formation, central Arctic Slope: U.S. Geological Survey Circular 733, p. 30-31.
- Jamison, H.C., Brockett, L.D., and McIntosh, R.A., 1980, Prudhoe Bay—A 10-year perspective, in Halbouty, M.T., ed., *Giant oil fields of the decade 1968-1978*: American Association of Petroleum Geologists Memoir 30, p. 289-314.

- Magoon, L.B., Bird, K.J., Claypool, G.E., Weitzmann, D.E., and Thompson, R.H., 1988, Organic geochemistry, hydrocarbon occurrence, and stratigraphy in government drilled wells, North Slope, Alaska, in Gryc, George, ed., *Geology and exploration of the National Petroleum Reserve in Alaska, 1974 to 1982: U.S. Geological Survey Professional Paper 1399*, p. 483-487.
- Masterson, W.D., and Paris, C.E., 1987, Depositional history and reservoir description of the Kuparuk River Formation, North Slope, Alaska, in Tailleir, L., and Weimer, P., eds., *Alaskan North Slope geology: Bakersfield, Society of Economic Paleontologists and Mineralogists, Pacific Section, Book 50, v. 1*, p. 95-107.
- McIntosh, R.A., 1977, Prudhoe Bay Unit operating plan, reservoir description: Alaska Oil and Gas Conservation Commission, May 5th Conservation Hearing No. 145, Exhibit No. 8, Anchorage.
- Melvin, J., 1986, Kemik Sandstone; inner shelf sand from northeast Alaska [abs.]: *American Association of Petroleum Geologists Bulletin*, v. 70, p. 620.
- Mitchum, R.M., 1977, Seismic stratigraphy and global changes of sea level, Part 1: glossary of terms used in sequence stratigraphy, in Payton, C.E., ed., *Seismic stratigraphy—Application to hydrocarbon exploration: American Association of Petroleum Geologists Memoir 26*, p. 205-212.
- Mitchum, R.M., and Van Wagoner, J.C., 1991, High-frequency sequences and their stacking patterns; sequence-stratigraphic evidence of high-frequency eustatic cycles: *Sedimentary Geology*, v. 70, p. 131-160.
- Molenaar, C.M., 1983, Depositional relations of Cretaceous and Lower Tertiary rocks, northeastern Alaska: *American Association of Petroleum Geologists Bulletin*, v. 67, p. 1066-1080.
- , 1985, Subsurface correlations and depositional history of the Nanushuk Group and related strata, North Slope, Alaska: *U.S. Geological Survey Bulletin 1614*, p. 37-59.
- , 1988, Depositional history and seismic stratigraphy of Lower Cretaceous Rocks in the National Petroleum Reserve in Alaska and adjacent areas, in Gryc, George, ed., *Geology and exploration of the National Petroleum Reserve in Alaska, 1974 to 1982: U.S. Geological Survey Professional Paper 1399*, p. 593-621.
- Molenaar, C.M., Bird, K.J., and Kirk, A.R., 1987, Cretaceous and Tertiary stratigraphy of northeastern Alaska, in Tailleir, L., and Weimer, P., eds., *Alaskan North Slope geology: Bakersfield, Society of Economic Paleontologists and Mineralogists, Pacific Section, Book 50, v. 1*, p. 513-528.
- Molenaar, C.M., Egbert, R.M., and Krystinik, L.F., 1988, Depositional facies, petrography, and reservoir potential of the Fortress Mountain Formation (Lower Cretaceous), central North Slope, Alaska, in Gryc, George, ed., *Geology and exploration of the National Petroleum Reserve in Alaska, 1974 to 1982: U.S. Geological Survey Professional Paper 1399*, p. 257-280.
- Molenaar, C.M., Kirk, A.R., Magoon, L.B., and Huffman, A.C., 1984, Twenty-two measured sections of Cretaceous-Lower Tertiary rocks, eastern North Slope, Alaska: *U.S. Geological Survey Open-File Report 84-695*, 19 p.
- Moore, T.E., Wallace, W.K., Bird, K.J., Karl, S.M., Mull, C.G., and Dillon, J.T., 1992, Stratigraphy, structure, and geologic synthesis of northern Alaska: *U.S. Geological Survey Open-File Report 92-330*, 183 p.
- Mull, C.G., 1985, Cretaceous tectonics, depositional cycles, and the Nanushuk Group, Brooks Range and Arctic Slope, Alaska, in Huffman, A.C. Jr., ed., *Geology of the Nanushuk Group and related rocks, North Slope, Alaska: U.S. Geological Survey Bulletin 1614*, p. 7-36.
- , 1987, Kemik Sandstone, Arctic National Wildlife Refuge, northeastern Alaska, in Tailleir, L., and Weimer, P., eds., *Alaskan North Slope geology: Bakersfield, Society of Economic Paleontologists and Mineralogists, Pacific Section, Book 50, v. 1*, p. 405-430.
- Mull, C.G., and Harris, E.E., 1989, Road log from Chandalar Shelf (Mile 237.1) to Prudhoe Bay (Mile 414), in Mull, C.G., and Adams, K.E., eds., *Dalton Highway, Yukon River to Prudhoe Bay: Alaska Division of Geological and Geophysical Surveys Guidebook 7, v. 1*, p. 101-131.
- Noonan, W.G., 1987, Post-Ellesmerian depositional sequences of the North Slope subsurface, in Tailleir, L., and Weimer, P., eds., *Alaskan North Slope geology: Bakersfield, Society of Economic Paleontologists and Mineralogists, Pacific Section, Book 50, v. 1*, p. 459-477.
- Pessel, G.H., Robinson, M.S., Clough, J.G., Imm, T.A., Reifensuhl, R.R., Ryherd, T.J., Myers, M.D., and Mull, C.G., 1990, Preliminary geologic map of the Gilead Creek area, Sagavanirktok A-2 quadrangle, Arctic Foothills, Alaska: Alaska Division of Geological and Geophysical Surveys Public-Data File 90-18, 6 p.
- Phillips, S., Decker, J., Shane, J.D., Hite, D.M., and Bergman, S.C., 1990, Recognition of depositional sequences in the Upper Cretaceous Seabee Formation, central North Slope, Alaska [abs.]: *American Association of Petroleum Geologists Bulletin*, v. 74, no. 5, p. 740.
- Reifensuhl, R.R., 1989, Measured stratigraphic section of the "Gilead Creek sandstone," northeastern Alaska: Alaska Division of Geological and Geophysical Surveys Public-Data File 89-26b, 16 p.
- Rudolph, K.W., Rassman, B.A., Abrams, M.A., Ando, C.M., Carter, J.B., Ferdinand, K.J., and Lorber, P.M., 1990, Relationship of sedimentary cycles to tectonic events and subsidence; an example from north Alaska [abs.]: *American Association of Petroleum Geologists Bulletin*, v. 74, p. 753.
- Ryherd, T.J., 1990, Fan-delta deposition in the Cretaceous (Albian) Fortress Mountain Formation, central North Slope, Alaska [abs.]: *American Association of Petroleum Geologists Bulletin*, v. 74, p. 753.
- Schindler, J.F., 1988, History of exploration in the National Petroleum Reserve in Alaska, with emphasis on the period from 1975 to 1982, in Gryc, George, ed., *Geology and exploration of the National Petroleum Reserve in Alaska, 1974 to 1982: U.S. Geological Survey Professional Paper 1399*, p. 13-76.
- Van Wagoner, J.C., Mitchum, R.M., Campion, K.M., and Rahmanian, V.D., 1990, Siliciclastic sequence stratigraphy in well logs, cores, and outcrops: *American Association of Petroleum Geologists Methods in Exploration Series 7*, 55 p.
- Weimer, P., 1987, Seismic stratigraphy of three areas of lower slope failure, Torok Formation, northern Alaska, in Tailleir, L., and Weimer, P., eds., *Alaskan North Slope geology: Bakersfield, Society of Economic Paleontologists and Mineralogists, Pacific Section, Book 50, v. 1*, p. 481-496.



# U-Pb AGES OF ZIRCON, MONAZITE, AND SPHENE FROM DEVONIAN METAGRANITES AND METAFELSITES, CENTRAL BROOKS RANGE, ALASKA

By John N. Aleinikoff, Thomas E. Moore, Marianne Walter, and Warren J. Nokleberg

## ABSTRACT

Six samples of metagneous rocks from the Coldfoot and Hammond terranes of the central Brooks Range have been individually dated by the U-Pb method. Zircons from two hornblende-biotite orthogneisses (Geroe Creek orthogneiss body and Horace Mountain plutons) yield simple isotopic systematics that indicate ages of  $391 \pm 1$  and  $393 \pm 5$  Ma, respectively. Zircons in two 2-mica orthogneisses (Baby Creek orthogneiss body and Middle Fork Koyukuk River orthogneiss body) have complex systematics, including significant inherited components and modern Pb loss; we infer poorly constrained ages of Early to Middle Devonian for these bodies. Zircons from two metafelsites from the Hammond terrane have tightly constrained ages of  $393 \pm 2$  and  $389 \pm 3$  Ma. The data confirm previous studies by J.T. Dillon who suggested, based on composite discordias composed of data from several samples, that the ages of most of the igneous rocks of the Brooks Range are about  $390 \pm 20$  Ma. These granitic rocks are part of a large, discontinuous belt of middle Paleozoic plutonic and volcanic rocks that occur throughout the North American Cordillera.

## INTRODUCTION

The central and eastern Brooks Range of northern Alaska has been divided into several lithotectonic zones, including, from south to north, the Angayucham terrane, Coldfoot terrane (also called the schist belt), the Hammond terrane (also called the central belt), the Endicott Mountains terrane, and the North Slope terrane. Excluding the Angayucham terrane (of oceanic origin), the other four terranes comprise the major part of the Arctic Alaska superterrane (Moore, 1992; fig. 1). The Coldfoot and Hammond terranes both are of Paleozoic age and of continental origin but have different protolith compositions and metamorphic and deformational histories, permitting their designation as separate lithotectonic blocks or units (Moore and others, 1992).

The most prominent belt of plutonic rocks in northern Alaska is located near the boundary between the Hammond and Coldfoot terranes in the southern Brooks Range (fig. 1). These rocks consist of deformed and metamorphosed, medium- to coarse-grained metaluminous to peraluminous granitic rocks. Metamorphosed hypabyssal to extrusive felsic igneous are also locally present in the southern Brooks Range, but because of poor age and structural control, the relation of the felsic rocks to the metagranites is uncertain.

The age of magmatic activity in the southern Brooks Range has been a matter of controversy for decades. Mertie (1923) was the first to conclude that some of the granites were emplaced in the Paleozoic. Biotite and hornblende from many plutons in the southern Brooks Range have yielded Cretaceous K-Ar ages (Turner and others, 1979). However, these minerals define metamorphic fabrics in strongly foliated rocks, leading to the interpretation that the rocks were deformed and metamorphosed in the mid-Cretaceous (Nelson and others, 1979). Dillon and others (1980), using the U-Pb zircon and Rb-Sr whole-rock methods, obtained Devonian ages from several plutons in the southern Brooks Range and concluded that the plutons were emplaced in the Devonian and metamorphosed in the mid-Cretaceous. Although Dillon and others (1980) found no evidence for Cretaceous magmatism, Tailleux (1984) concluded that field relations require Cretaceous emplacement ages for the plutons, and suggested that the granites contain Devonian xenocrystic zircons. Subsequent U-Pb zircon dating of plutons in the central and eastern Brooks Range by Dillon and others (1987) confirmed the earlier geochronology indicating Devonian ages for most of the plutons; they also found three bodies that were emplaced in the Late Proterozoic.

Although the U-Pb zircon data of Dillon and others (1980, 1987) strongly suggest ages of 370–390 Ma for the foliated plutonic rocks of the southern and central-eastern Brooks Range, a major weakness in both studies is that U-Pb isotopic data from zircon fractions of several different bodies (including both metaluminous and peraluminous plutons) were plotted together. Plutons in the eastern



Brooks Range yield a composite discordia with an upper intercept age of  $390 \pm 20$  Ma (Dillon and others, 1987). The degree of discordance of Pb/U ages ranges from about 5 to 60 percent, with most of the data plotting about one-third of the way down a discordia between 391 and 53 Ma. Similarly, Dillon and others (1987) regressed U-Pb isotopic data from five metavolcanic rock samples, obtaining an age of  $396 \pm 20$  Ma.

The purpose of our study is to individually date four metagranites from the Coldfoot terrane and two metafelsites from the Hammond terrane. New geologic mapping along the Trans Alaska Crustal Transect (TACT) route has distinguished several distinct granite bodies that Dillon and others (1980) grouped as Chandalar-area granite in the Chandalar quadrangle of the eastern Brooks Range. Three of these plutons, plus an isolated pluton in the southeastern Wiseman quadrangle, were sampled. Our geochronologic results are incorporated with existing and

new mapping to discuss tectonic models for the origin of the eastern Brooks Range.

## REGIONAL GEOLOGY

The Brooks Range is a north-directed fold and thrust belt formed by collision of an oceanic arc and subduction assemblage with a south-facing (present coordinates) passive continental margin in the Late Jurassic and Early Cretaceous (Roeder and Mull, 1978; Box, 1985; Moore and others, 1992). The collision resulted in obduction of oceanic rocks, including ophiolite of the Angayucham terrane, imbrication and folding of latest Devonian to Cretaceous passive-margin sedimentary rocks in the northern Brooks Range (North Slope and Endicott Mountains terranes), and ductile deformation and metamorphism of Devonian and older continental rocks in the metamorphic core of the

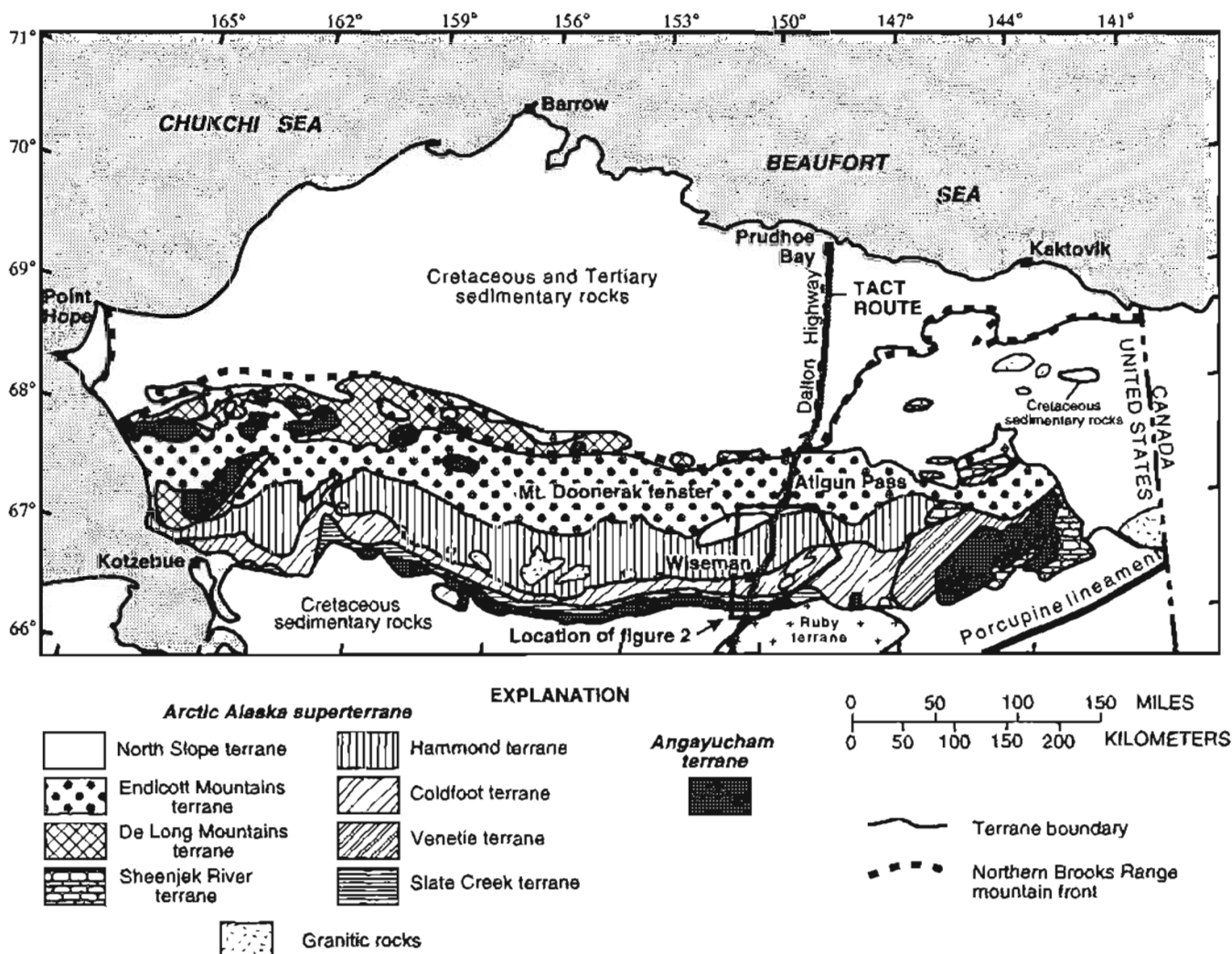


Figure 1. Tectonic map of northern Alaska.

orogen in the southern Brooks Range (Coldfoot and Hammond terranes). Subsequent uplift, closure of the K-Ar system, and erosion of the metamorphic core, all perhaps from extension as a consequence of the crustal thickening, occurred principally in mid-Cretaceous time.

The metamorphic core of the Brooks Range orogen consists of a southern belt of schist (schist belt) and a northern assemblage of schist and phyllite (central belt of Till and others, 1988; fig. 1). The stratigraphy of both of these units is largely obscured by extensive deformation and metamorphism. On the basis of contrasts in texture and lithology, the schist belt was assigned to the Coldfoot terrane and the schist and phyllite assemblage to the Hammond terrane (Jones and others, 1987; Moore and others, 1992; Moore, 1992). Nonetheless, the contact between the Coldfoot and Hammond terranes is ambiguous in many places (Till and others, 1988), although in the TACT corridor near Wiseman, the contact has been located at the south-dipping Wiseman or Minnie Creek thrust (Oldow and others, 1987; Grantz and others, 1991; Moore and others, 1992). On the basis of new mapping by the TACT project we now consider the contact to be located about 10 kilometers to the north of the Wiseman thrust on a north-dipping fault that extends east-west along the northern margin of the metagranitic rocks in the Chandalar quadrangle. The Coldfoot terrane was emplaced as a crustal wedge by thrusting either into, or beneath, the Hammond terrane (Oldow and others, 1987; Moore and others, 1992).

Stretching over 700 km westward from the Canadian border is a belt of nine groups of deformed and metamorphosed granitic bodies of Devonian age (Dillon and others, 1980, 1987). The metagranites occur along the contact between the Coldfoot and Hammond terranes and have been assigned to either or both of those units by various workers (for example, Moore and others, 1992). On the basis of the new mapping by the TACT project and high pressure-low temperature metamorphic assemblages in the plutons (B. Patrick, oral commun., 1990), all of the metagranitic bodies in the TACT study area (fig. 2) are here regarded as part of the Coldfoot terrane. Felsic and silicic metavolcanic rocks, inferred to be cogenetic with the metagranitic rocks (Dillon and others, 1980, 1987), are present in both terranes, but in neither terrane do they have a close spatial relationship. Compositionally, the metagranitic bodies consist of granite and granodiorite that is largely peraluminous, but locally metaluminous (Newberry and others, 1986). The felsic metavolcanic rocks of the study area typically are albite-quartz phyllite that is structurally interleaved with carbonate rocks and quartz-rich schist and phyllite. Samarium-neodymium (Nelson and others, in press) and lead data (Aleinikoff and others, 1991) from outside the study area indicate variable involvement of Precambrian crust in the genesis of the metagranitic rocks.

## COLDFOOT TERRANE

Along the TACT transect, the Coldfoot terrane consists chiefly of pelitic and semipelitic, quartz-mica schist that contains minor lenses of metabasite and albite schist (fig. 2). Locally map-scale units of calcareous schist and marble, quartz-poor greenschist, amphibole-rich schist, metabasite, quartzite, and metagranitic rocks also are present along the northern margin of the Coldfoot terrane. Low-angle discordances indicate that gently to moderate-dipping faults bound most of these units, including the metagranitic rocks, but in a few places intrusive contacts may be preserved. In most places, the Coldfoot terrane is characterized by a penetrative foliation and complete recrystallization. Metamorphic assemblages throughout the Coldfoot terrane are chiefly greenschist facies, but evidence of an earlier high pressure-low temperature metamorphism is widely preserved in some schists (Till and others, 1988; Gottschalk, 1990; Till and Moore, 1991) and in the metagranitic rocks (B. Patrick, oral commun., 1990). The protolith ages of the schists are largely unknown, although conodonts of Early Devonian age, and Silurian or Devonian age have been recovered from dolomitic calcschist at three localities southwest of Wiseman (A.G. Harris, written commun., 1990). Quartz-mica schist in the TACT corridor has yielded white mica with  $^{40}\text{Ar}/^{39}\text{Ar}$  ages as old as 120–130 Ma (Blythe and others, 1990), and metagranitic rocks in the Chandalar quadrangle have yielded K-Ar ages of 100–125 Ma (Brosge and Reiser, 1964).

Orthogneisses sampled for U-Pb dating include three large bodies in the Chandalar quadrangle about 20 to 40 km east of the Dalton highway and a small metagranitic body on the west side of the Middle Fork of the Koyukuk River, about 10 km south of Wiseman (Brosge and Reiser, 1964; Dillon and others, 1986; Dillon and Reifenhuth, 1990) (fig. 2; table 1). The Chandalar bodies were subdivided on the basis of composition into the Horace Mountain plutons and Baby Creek batholith by Newberry and others (1986). The Horace Mountain plutons are a string of small metagranitic bodies along the northern margin of the Coldfoot terrane that are largely metaluminous, porphyritic, biotite±hornblende granite and hornblende-biotite granodiorite (Newberry and others, 1986). These metagranitic rocks are bounded by faults that dip northward at moderate angles. The larger metagranitic bodies to the southwest were included in the Baby Creek batholith which consists dominantly of peraluminous, porphyritic, biotite±garnet±white mica granite (Newberry and others, 1986). The Baby Creek batholith of Newberry and others (1986) consists of at least two large metagranitic bodies that are separated by east-west-trending thrust faults. To the north is the Geroe Creek orthogneiss body, which consists of white mica ±biotite±hornblende granite and granodiorite. To the south are orthogneiss bodies at Baby Creek and Twin Lakes, which appear to be physically connected

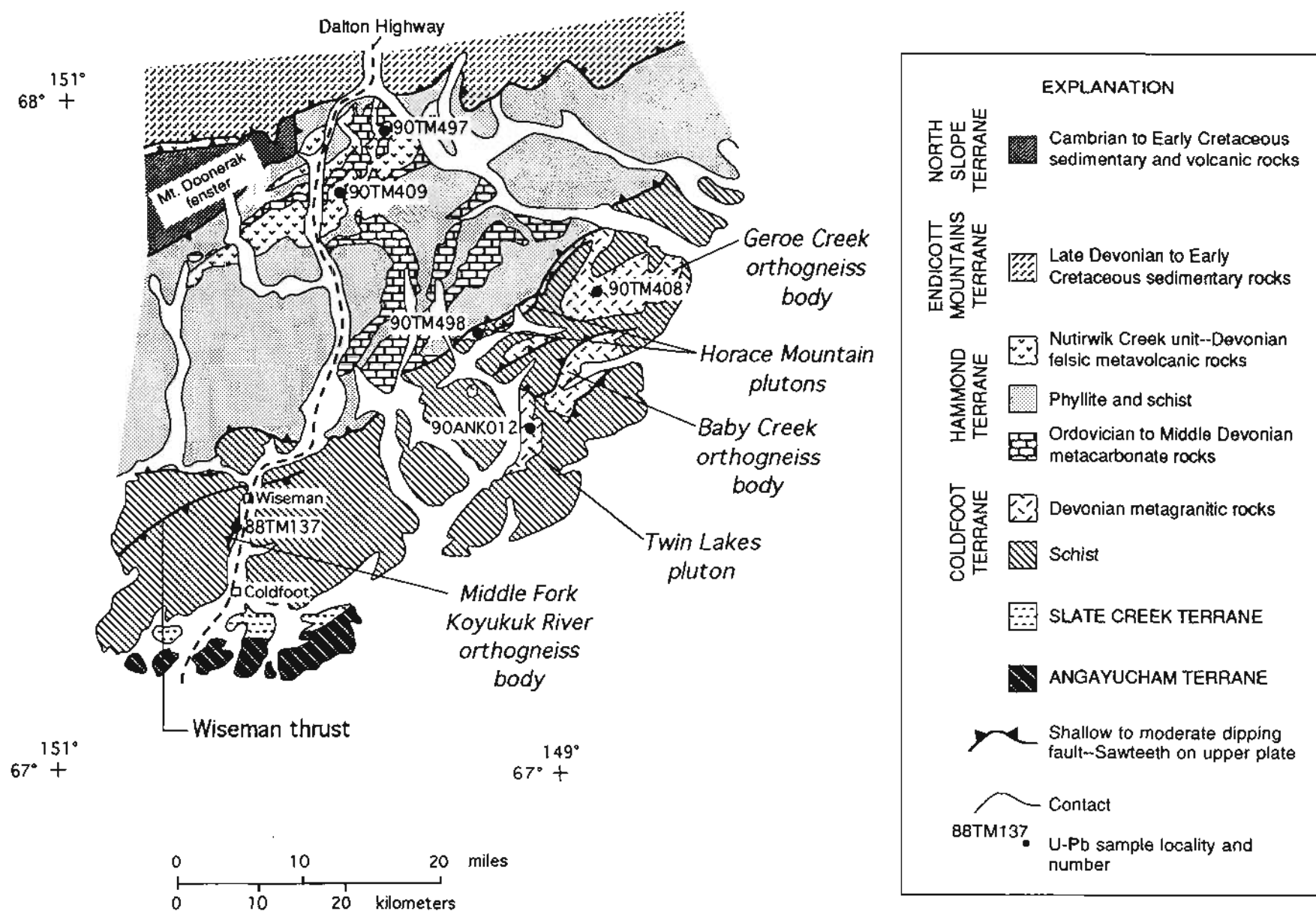


Figure 2. Simplified geologic map of part of eastern Brooks Range, Alaska (modified from Dillon and others, 1986; Brosgé and Reiser, 1964; and unpublished mapping of the TACT program). Many units have been combined within each terrane.

Table 1. Description of rocks and minerals from dated samples

Sample number	Name and minerals dated	Brief description
<b>COLDFOOT TERRANE</b>		
90TM408	Geroe Creek orthogneiss	Coarse-grained, quartz-K-feldspar-plagioclase-hornblende-biotite; strongly foliated, with quartz-sericite shear bands; fine-grained mosaic quartz; strained large quartz grains.
	zircon	Euhedral, medium-brown, length-to-width ratio (l/w) 3–5, mottled faces.
	spene	Pale yellow, adamantine, euhedral fragments.
90TM498	Horace Mountain plutons	Coarse-grained, quartz-K-feldspar-plagioclase-hornblende-biotite; some amphiboles contain relict cores of clinopyroxene; all feldspars are highly sericitized; strongly foliated, mortar structure, mosaic texture; strained quartz.
	zircon	Euhedral, light brown, l/w 2–4, adamantine.
	spene	Pale yellow, adamantine, euhedral fragments.
90ANK012	Baby Creek orthogneiss	Medium-grained, quartz-microcline-plagioclase-biotite-muscovite; phenocrysts of microcline; strongly foliated, with shear bands of quartz-sericite-biotite; fine-grained mosaic quartz.
	zircon	Medium-brown, l/w 2–6, mottled faces.
	monazite	Subhedral, pale yellow-orange, opaque.
88TM137	Middle Fork Koyukuk River orthogneiss body	Coarse-grained, quartz-muscovite-microcline-plagioclase-calcite-garnet; strongly foliated coarse-grained knots of clinozoisite-quartz-muscovite.
	zircon	Subhedral, dark brown, l/w 1–5, deformed.
<b>HAMMOND TERRANE</b>		
90TM409	dacite porphyry (Nutirwik Creek unit)	Fine-grained, buff, strongly foliated, phenocrysts of quartz and plagioclase, now rotated and polygonized; stretched fragments; altered to sericite and carbonate.
	zircon	Euhedral, light pink, l/w 2–4, adamantine.
90TM497	plagioclase porphyry (Nutirwik Creek unit)	Fine-grained, light green; phenocrysts of plagioclase and hornblende; slightly foliated to unfoliated; hornblende replaced by epidote and chlorite; groundmass is fine-grained mosaic of quartz and feldspar, with abundant needles of pale amphibole.
	zircon	Euhedral, light pink, l/w 4–8, adamantine.

and lithologically correlative. For the purpose of this paper, we geographically restrict the Baby Creek batholith (hereafter referred to as the Baby Creek orthogneiss body) to the two southern orthogneiss bodies at Baby Creek and to the nearby Twin Lakes body. The Baby Creek orthogneiss body appears to be a thick but tabular, fault-bounded body that is locally intrusive into adjacent metamorphosed mafic volcanic rocks. The Horace Mountain plutons, Geroe Creek orthogneiss body, and Baby Creek orthogneiss body display strong foliation, local mylonite zones, and gneissic textures along their outer contacts. Although foliated, relict igneous features such as xenoliths and megacrysts of potassium feldspar are locally retained in the cores of most of the bodies.

The small, poorly exposed orthogneiss body located on the Middle Fork of the Koyukuk River (hereafter referred to as the Middle Fork Koyukuk River orthogneiss body for convenience) south of Wiseman is medium- to coarse-grained, gneissic, muscovite-biotite quartz monzonite. This body locally contains garnet and megacrysts of microcline (Dillon and Reifenstahl, 1990). Its contact with overlying calcschist is unexposed, but the absence of dikes or stocks suggests that the contact is a low-angle fault.

Metagranitic rocks of the central Brooks Range are associated with porphyry, polymetallic vein, and skarn mineral deposits. Lode occurrences include polymetallic quartz veins with base-metal sulfides, tin skarns with disseminated cassiterite and base-metal sulfides, Cu-Pb-Zn skarns with disseminated iron and base-metal sulfides, and porphyry copper and molybdenum (Newberry and others, 1986; Nokleberg and others, 1988). These granitic magmatism-related deposits are part of a 900-km-long belt of mineral deposits in the Coldfoot, Hammond, and North Slope terranes.

## HAMMOND TERRANE

The Hammond terrane in the TACT corridor consists of a variety of lenticular, mostly fine-grained metaclastic, metavolcanic, and carbonate units that are completely to incompletely recrystallized to greenschist assemblages (fig. 2). In the southern part of the study area, rocks of the Hammond terrane display ductile folds, but to the north the rocks are deformed by imbricate thrusts. Primary textures are locally present and increase in abundance northward.

The Hammond terrane characteristically contains widespread bodies of thick, massive, Ordovician to Middle Devonian metacarbonate rocks. Other major fault-bounded lithologic packages in the southern part of the Hammond terrane in the TACT corridor include undated, fine-grained quartz schist, quartz-chlorite schist, and calcareous schist that contains minor layers and lenses of marble and metasandstone. To the north, thrust imbricates in the Hammond terrane consist of units of metamorphosed lithic conglomerate and sandstone, metamorphosed shale, siltstone, and lower Upper Devonian limestone that are intruded by diabase and gabbro, thin-bedded black Middle Ordovician phyllite and limestone, and a heterogeneous phyllitic volcanogenic assemblage, informally referred to here as the Nutirwik Creek unit.

The Nutirwik Creek unit is a thick, northeast-southwest-trending, disrupted and metamorphosed unit that is exposed chiefly south and east of the Mount Doonerak fenster. The principal lithology in this unit is soft, micaceous phyllite that is brightly colored purple and green. Enclosed within the purple and green phyllite are recrystallized, fine- to coarse-grained, lithic-quartz-feldspar sandstone, flattened argillite-pebble conglomerate, and lenses and blocks of feldspar porphyry. Euhedral crystals, clasts with relict volcanic textures, and feldspar-rich compositions are common in the metasandstones and indicate a volcanogenic protolith. Flattened white pebbles, locally abundant in some conglomerates, consist of mosaics of quartz and feldspar that may represent recrystallized pumice. Blocks of andesite and dacite porphyry commonly are present in groups in restricted areas in the phyllite, suggesting that they represent disrupted dikes, stocks, sills, or flows. The andesite and dacite blocks typically contain numerous phenocrysts of albitized feldspar and altered amphibole and locally contain quartz phenocrysts.

Although mostly recrystallized, moderately to strongly foliated, and structurally disrupted, the sparse relict volcanic textures indicate that the Nutirwik Creek unit is predominantly a volcanoclastic deposit shed from a volcanic source of intermediate composition whose location is unknown. The rocks composing the Nutirwik Creek unit were assigned to the Beaucoup Formation by Dutro and others (1979) and Brosge and others (1979) and to the informally named Whiteface Mountains volcanics by Dillon and others (1988). Two samples, 90TM497 and 90TM409, from widely separate localities of deformed porphyritic volcanic flows or hypabyssal rocks, were collected for U-Pb age dating (fig. 2; table 1).

## ANALYTICAL PROCEDURE AND RESULTS

Zircon, sphene, and monazite were extracted from about 25 kg of each sample by standard mineral separation

techniques, using a Wilfley table, magnetic separator, and methylene iodide. Fractions composed of the best-preserved zircons were prepared by hand-picking in alcohol, followed by abrasion (technique of Krogh, 1982, using an abrader described in Aleinikoff and others, 1990), and a final hand-picking. All analyzed fractions contain zircons that originally were greater than 200-mesh size (most grains were coarser than about 100  $\mu\text{m}$ ). Monazite and sphene grains were also hand-picked in alcohol and abraded.

Zircon fractions, weighing between 0.020 and 0.110 mg, were spiked with a mixed  $^{205}\text{Pb}$ - $^{233}\text{U}$ - $^{236}\text{U}$  tracer and were dissolved in microcapsules within standard Parr digestion bombs (method of Parrish, 1987) with concentrated HF and  $\text{HNO}_3$  in an oven at about 220°C for about 3 days. Sphene and monazite were dissolved in concentrated HF and  $\text{HNO}_3$  in screw-top containers on a hot-plate at about 175°C for several days. Pb and U were extracted using procedures modified from Krogh (1973). Total chemistry Pb blanks decreased during the course of the study from about 250 pg to about 20 pg. Pb and U isotopic ratios were measured, using single-filament silica gel- $\text{H}_3\text{PO}_4$  and triple filament assemblies, respectively, on a VG-Micro-Mass 54E single-collector mass spectrometer with a Daly collector. Isotopic data were reduced (table 2) and plotted (figs. 3 and 4) using the programs of Ludwig (1991a, 1991b).

## ORTHOGNEISSES OF THE COLDFOOT TERRANE

U-Pb isotopic data from zircons in the two hornblende-biotite granite gneiss samples of the Horace Mountain plutons and Geroe Creek orthogneiss body (90TM408 and 90TM498) are similar and fairly simple. In both rocks, most fractions contain about 220–260 ppm U. In sample 90TM408, zircons are euhedral, medium-brown, have mottled faces and length-to-width ratios (l/w) of 3–5 (table 1). Two fractions are concordant at about 390 Ma, and two fractions have slightly older  $^{207}\text{Pb}/^{206}\text{Pb}$  ages of 396 and 402 Ma (table 2, fig. 3A). The weighted average of the four  $^{206}\text{Pb}/^{238}\text{U}$  ages is  $391 \pm 1$  Ma. Coexisting sphene has Pb/U ages of 385 and 386 Ma and a  $^{207}\text{Pb}/^{206}\text{Pb}$  age of 393 Ma. Because the common Pb content is high (a typical characteristic of sphene), the  $^{207}\text{Pb}/^{235}\text{U}$  age has a higher uncertainty than data from the zircon fractions (see large error ellipse in figure 3A). Thus, we do not know if the Pb/U ages represent the time of cooling through the closure temperature for the U-Pb system in sphene (about 550°C; Hanson and others, 1971) or if the sphene is slightly discordant, implying a crystallization age of about 393 Ma.

Zircons in sample 90TM498 are euhedral, light brown, adamantine, and have l/w of 2–4 (table 1). One fraction is concordant at about 393 Ma; three other fractions have slightly older  $^{207}\text{Pb}/^{206}\text{Pb}$  ages between 396 and 412 Ma (table 2, fig. 3B). Sphene from this rock is nearly concor-

**Table 2.** U-Pb isotopic data from zircon, monazite, and sphene in igneous rocks of central Brooks Range, Alaska[Constants:  $^{235}\lambda = 9.8485 \cdot 10^{-10} \text{ yr}^{-1}$ ;  $^{238}\lambda = 1.55125 \cdot 10^{-10} \text{ yr}^{-1}$ ;  $^{238}\text{U}/^{235}\text{U} = 137.88$  (Steiger and Jäger, 1977)]

Fraction <sup>1</sup> (mesh size)	Weight (mg)	Concentrations (ppm)		Pb composition <sup>2</sup>			Ratios (percent error) <sup>3</sup>			Ages (Ma) <sup>4</sup>		
				<sup>206</sup> Pb	<sup>206</sup> Pb	<sup>206</sup> Pb	<sup>206</sup> Pb	<sup>207</sup> Pb	<sup>207</sup> Pb	<sup>206</sup> Pb	<sup>207</sup> Pb	<sup>207</sup> Pb
		U	Pb	<sup>204</sup> Pb	<sup>207</sup> Pb	<sup>208</sup> Pb	<sup>238</sup> U	<sup>235</sup> U	<sup>206</sup> Pb	<sup>238</sup> U	<sup>235</sup> U	<sup>206</sup> Pb
COLDFOOT TERRANE												
90TM408 (Geroe Creek orthogneiss body)												
(-100+150)NMECA	.062	417.8	27.73	13217	18.010	5.6295	.0625(.38)	.4687(.40)	.0544(.12)	391	390	388
(-100+150)NMECA	.078	514.4	34.22	6521.3	17.643	5.7400	.0626(.28)	.4701(.30)	.0544(.10)	392	391	389
(-100+150)NMECA	.080	250.8	16.74	8370.3	17.743	5.4629	.0624(.39)	.4702(.41)	.0546(.12)	390	391	396
(-100+150)NMECA	.110	259.6	17.40	7918.3	17.674	5.4644	.0627(.34)	.4731(.35)	.0547(.09)	392	393	402
sphene	.207	179.8	21.08	273.14	9.2426	1.0617	.0614(.28)	.4623(.62)	.0545(.53)	385	386	393
90TM498 (Horace Mountain plutons)												
(-100+150)NMECA	.063	239.8	18.31	569.57	12.472	3.4174	.0625(.32)	.4697(.40)	.0545(.23)	391	391	393
(-100+150)NMECA	.084	230.3	16.50	1760.1	15.838	4.1996	.0633(.29)	.4785(.32)	.0548(.15)	396	397	406
(-100+150)NMECA	.036	232.9	22.94	160.88	6.8615	2.2231	.0633(.55)	.4801(.65)	.0550(.32)	396	398	412
(-100+150)NMECA	.082	251.9	17.55	5502.9	17.466	4.1797	.0622(.32)	.4682(.34)	.0546(.12)	389	390	396
sphene	.137	222.4	18.29	510.10	12.016	2.5327	.0622(.46)	.4683(.54)	.0546(.28)	389	390	395
90ANK012 (Baby Creek orthogneiss body)												
(-100+200)NMECA	.034	1168	67.45	5765.6	17.452	14.080	.0593(.19)	.4481(.23)	.0548(.14)	372	376	403
(-100+200)NMECA	.037	644.2	39.69	60232	17.956	11.911	.0628(.34)	.4804(.35)	.0554(.11)	393	398	430
(-100+200)NMECA	.028	409.8	25.19	5119.9	17.393	9.3428	.0611(.35)	.4606(.37)	.0546(.12)	383	385	398
(-100+200)NMECA	.012	1056	63.55	2785.0	16.695	12.246	.0609(.53)	.4590(.56)	.0547(.18)	381	384	398
(-150+200)NMECA	.062	869.9	54.85	7145.5	17.210	12.305	.0642(.32)	.4962(.28)	.0561(.11)	401	409	455
monazite	.104	1503	1219	1093.2	14.766	.06846	.0587(.24)	.4396(.27)	.0544(.11)	367	370	386
monazite	.020	1614	1156	15844	18.156	.08006	.0610(.23)	.4552(.29)	.0542(.17)	381	381	378
88TM137 (Middle Fork Koyukuk River orthogneiss body)												
(-100+150)NMEA	.060	375.8	28.42	1683.1	15.752	3.0433	.0624(.47)	.4714(.50)	.0548(.19)	390	392	404
(-100+150)NMEA	.024	437.8	31.39	3255.8	16.949	3.4025	.06119(.47)	.4599(.51)	.0545(.19)	383	384	392
(-150+200)NMEA	.030	333.8	21.80	2922.3	16.443	3.962	.0574(.59)	.4418(.62)	.0558(.21)	360	372	445
(-150+200)NMEA	.051	351.6	27.85	1315	14.030	4.5234	.0702(.28)	.5830(.34)	.0602(.19)	437	466	612
HAMMOND TERRANE												
90TM409 (felsite)												
(-100)NMEA	.020	431.4	29.35	4382.8	17.297	5.0166	.0626(.41)	.4704(.44)	.0545(.15)	392	391	391
(-100)NMEA	.066	986.7	66.52	19567	18.081	5.2182	.0628(.24)	.04722(.28)	.0546(.13)	392	393	394
(-100+150)A	.066	570.0	38.65	2446.5	16.521	5.1262	.0623(.49)	.4684(.57)	.0546(.28)	389	390	394
90TM497 (plagioclase porphyry)												
(-150+200)ECA	.023	222.5	15.37	5512	17.436	4.6753	.0629(.51)	.4745(.57)	.0547(.24)	393	394	400
(-150+200)ECA	.025	279.4	25.24	244.21	8.6136	2.9628	.0666(.60)	.5182(.66)	.0564(.27)	416	424	469
(-150+200)ECA	.028	273.8	19.47	799.71	13.785	4.2084	.0616(.63)	.4606(.77)	.0543(.41)	385	385	382

<sup>1</sup>Abbreviations: NM, nonmagnetic; E, elongate; C, clear; A, abraded.<sup>2</sup>Blank and fractionation (0.11±.04%/a.m.u.) corrected. Pb blank decreased during study from about 0.250 to about 0.020 (±50%) ng. Blank lead composition used in calculations is 1:18.7:15.6:37.2.<sup>3</sup>2σ uncertainties.<sup>4</sup>Common lead corrections from the Stacey and Kramers (1975) model 390-Ma lead isotopic composition.

dant, with somewhat poorly constrained Pb/U ages of 389 and 390 Ma and a  $^{207}\text{Pb}/^{206}\text{Pb}$  age of 395 Ma. We conclude that the ages of the Geroe Creek orthogneiss body and Horace Mountain plutons are  $393 \pm 2$  Ma.

U-Pb data from zircons in two bodies of biotite-muscovite granite gneiss are more complicated than the results from the hornblende-biotite orthogneisses. Zircons in sample 90ANK012 (Baby Creek orthogneiss body) are euhedral, medium-brown, have mottled faces, and have  $l/w$  of 2–6 (table 1). Uranium concentrations are high (410

to 1,500 ppm) and the  $^{207}\text{Pb}/^{206}\text{Pb}$  and Pb/U ages are quite variable (ranging from 398 to 455 Ma and 381 to 409 Ma, respectively) (table 2, fig. 3C). The data do not form a linear array, and thus we cannot calculate an intercept age. The reference chord shown in figure 3C is constructed through the two fractions with the youngest  $^{207}\text{Pb}/^{206}\text{Pb}$  age, suggesting a maximum age of about 398 Ma for this rock. The scatter in the data is caused by a combination of inheritance of radiogenic Pb and Pb loss. One fraction of monazite is concordant at about 381 Ma; a second fraction

is discordant, having Pb/U ages of 367 and 370 Ma and a  $^{207}\text{Pb}/^{206}\text{Pb}$  age of 386 Ma. The concordant monazite date of about 381 Ma is regarded as a minimum age for emplacement of the pluton because this date may represent (1) the time of cooling through the closure temperature of the U-Pb system in monazite ( $\sim 720^\circ\text{C}$ ; Parrish, 1990) or (2) the time of growth of metamorphic monazite. In either case, the crystallization age of the pluton must be equal to or older than the monazite age. We thus constrain the time of emplacement of the Baby Creek orthogneiss body to be between 381 and 398 Ma.

In contrast to the euhedral, light- to medium-brown zircons in other orthogneisses, the zircons in sample 88TM137 (Middle Fork Koyukuk River orthogneiss body) are subhedral, dark brown, and deformed (table 1). Isoto-

pic data from four fractions are scattered, with  $^{207}\text{Pb}/^{206}\text{Pb}$  ages between 392 and 612 Ma and Pb/U ages ranging from 360 to 466 Ma (table 2, fig. 3D). They have uranium concentrations (333 to 438 ppm; table 2) intermediate between those of the hornblende-biotite orthogneisses and the Baby Creek (two-mica) orthogneiss body. No sphene or monazite was found in this sample. The poor preservation of the zircon and the scattered isotopic systematics preclude determining a precise date for this rock. However, the fraction with the youngest  $^{207}\text{Pb}/^{206}\text{Pb}$  age (about 392 Ma) is only about 2 percent discordant. Thus, we suggest a maximum age of emplacement for the Middle Fork Koyukuk River orthogneiss body of about 392 Ma. The absence of sphene or monazite prevents an independent verification of this assumed age.

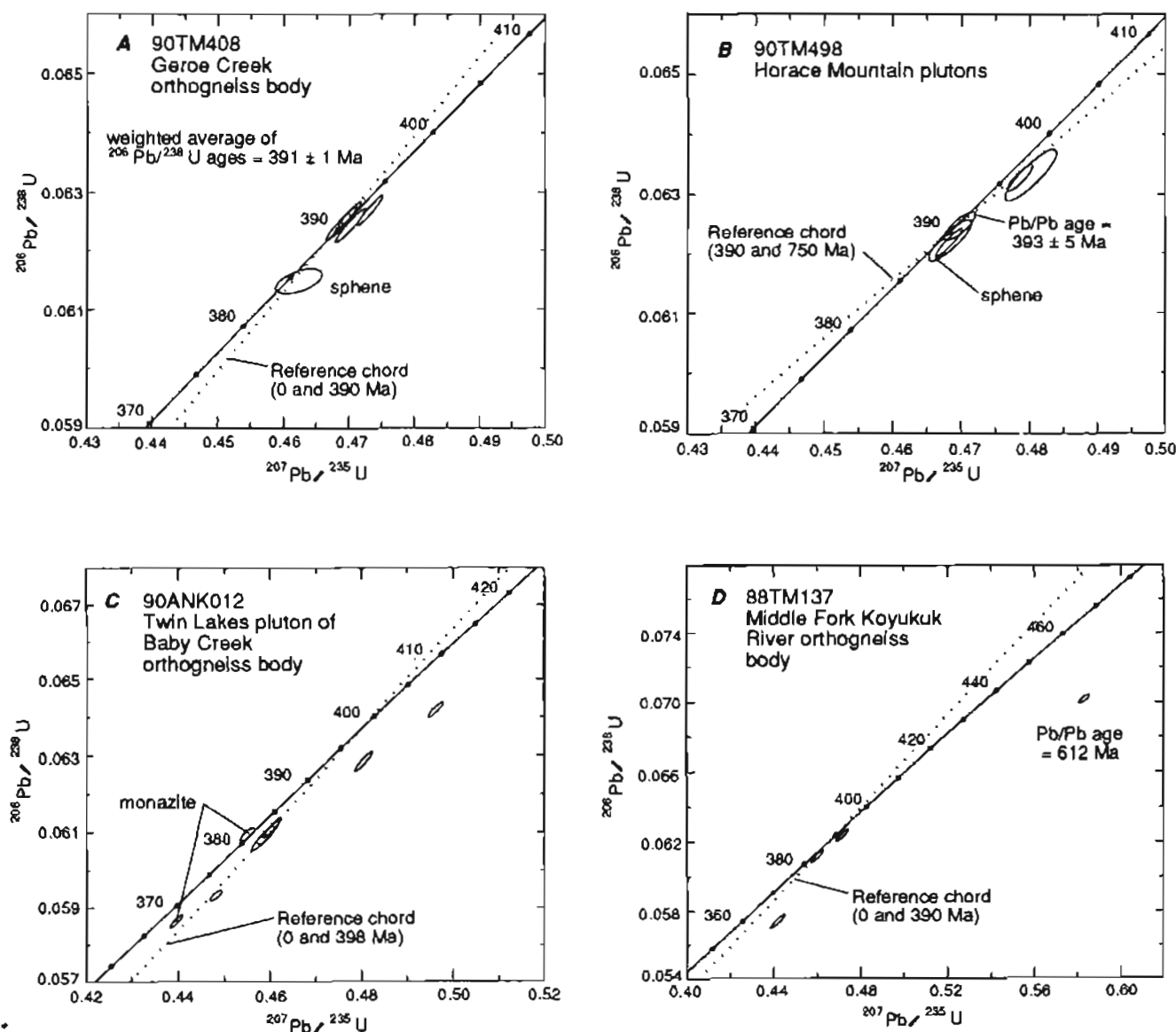


Figure 3. Concordia plots of U-Pb data from orthogneiss of the Coldfoot terrane, eastern Brooks Range. Sample localities shown on figure 2.



## METAFELSITES OF THE HAMMOND TERRANE

Two samples of fine-grained, foliated, porphyritic rocks (identified as felsites in the field) were collected from the Nutirwik Creek unit of the Hammond terrane to test their temporal correlations with granitic orthogneisses in the Coldfoot terrane. One or both of the samples may be metavolcanic in origin and thus may also provide constraints for the age of the stratigraphic section. Isotopic data from zircons from eight samples of fine-grained felsic rocks in the southern and eastern Brooks Range have yielded a composite discordia with an upper intercept age of  $396 \pm 20$  Ma (Dillon and others, 1987). Two of their

samples, from Whiteface Mountain and Wiehl Mountain, are about 25 km west and 30 km south, respectively, of our sample 90TM409.

Sample 90TM409 is a buff-colored, strongly foliated felsic rock. It is about 25–40 cm thick and is interlayered with gray, green, and purple shale, and interfolded (or faulted) with limestone and marble. It is compositionally homogeneous and contains augen of partly polygonized quartz phenocrysts, albitized feldspar phenocrysts, and volcanic rock fragments in a fine-grained, foliated matrix of metamorphic quartz, feldspar, calcite, and white mica. The lithologic characteristics and field occurrence have led to the interpretation that this rock is volcanic (extrusive) in origin, although it is possible, given the superimposed deformation and very limited outcrop, that it is a sill. Zircons from our sample are euhedral, light pink, adamantine, and have  $l/w$  of 2–4 (table 1). We analyzed three fractions, all of which are concordant (fig. 4A), despite having fairly high uranium concentrations of 431–987 ppm. The weighted average of the  $^{207}\text{Pb}/^{206}\text{Pb}$  ages is  $393 \pm 2$  Ma, interpreted as the time of crystallization of the rock.

Sample 90TM497 is a plagioclase porphyry (table 1) interpreted in the field as a hypabyssal felsite plug, flow, or sill. It contains feldspar and amphibole phenocrysts in a fine-grained groundmass and has been metamorphosed under apparent static conditions to albite, epidote, quartz, white mica, and pale amphibole. Zircons from this sample are similar in morphology to zircons in metafelsite sample 90TM409 (euhedral, light pink, adamantine) except that they are more prismatic with  $l/w$  of 4–8 (table 1). One fraction is concordant at about 385 Ma; two other fractions have  $^{207}\text{Pb}/^{206}\text{Pb}$  ages of 400 and 469 Ma (table 2). The isotopic data define a chord with a lower-intercept age of  $389 \pm 3$  Ma (fig. 4B); the upper-intercept age of  $1.015 \pm 103$  Ma may be geologically meaningless because the oldest known rocks in the central and eastern Brooks Range are Late Proterozoic (Dillon and others, 1987; Karl and others, 1989; Karl and Aleinikoff, 1990). Thus, the age of the sample may be best estimated by the  $^{206}\text{Pb}/^{238}\text{U}$  age ( $385 \pm 2$  Ma) of the concordant fraction.

In summary, all six samples dated in this study are Early to Middle Devonian in age. The ages of the hornblende-biotite orthogneisses are identical within uncertainty ( $391 \pm 1$  and  $393 \pm 5$  Ma) and the rocks may be related. The two-mica orthogneisses were more difficult to date, because of inheritance of radiogenic Pb, high uranium contents, and poorly preserved zircon grains. However, concordant monazite and two discordant zircon fractions in the Baby Creek orthogneiss body constrain the emplacement age to be between 381 and 398 Ma. A slightly discordant zircon fraction in the Middle Fork Koyukuk River orthogneiss body suggests a maximum crystallization age of about 390 Ma. The ages of the two metafelsites are  $393 \pm 2$  Ma and probably about 385–390 Ma, respectively.

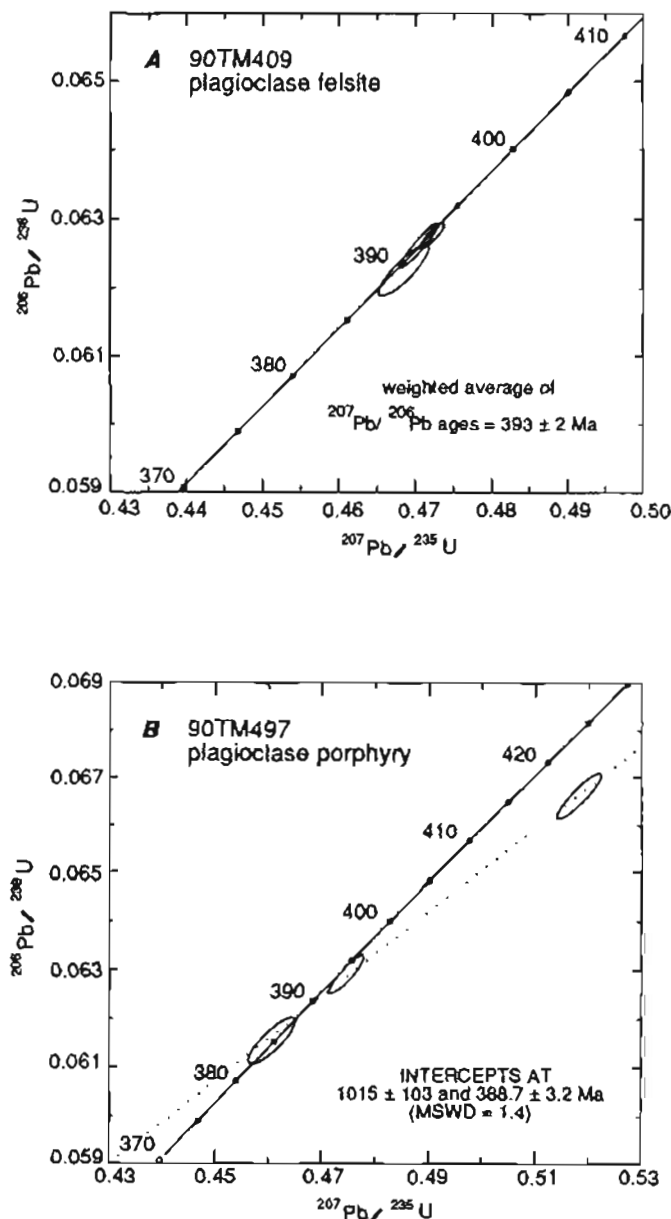


Figure 4. Concordia plots of U-Pb data from metafelsites of the Hammond terrane, eastern Brooks Range. Sample localities shown on figure 2. MSWD, mean square of weighted deviates.

## DISCUSSION AND TECTONIC IMPLICATIONS

Despite the unwise practice of using data from several plutons to calculate a composite regression and concordia intercept age, the Devonian age ( $391 \pm 20$  Ma) of Dillon and others (1987) for orthogneisses in the eastern Brooks Range is accurate. Our new data for each pluton are more precise; much of our data are concordant, and other fractions are mostly less than 10 percent discordant. However, despite very careful hand-picking of very small samples, we were unable to avoid some grains that contain inheritance of older radiogenic Pb, in even the most pristine zircon grains. The age of inheritance is unknown, although the only known older rocks are Late Proterozoic (about 700–750 Ma). Zircons in the hornblende-biotite orthogneisses (fig. 3A, B) contain only small amounts of inherited material, as evidenced by  $^{207}\text{Pb}/^{206}\text{Pb}$  ages 393 and 412 Ma. Zircon fractions in the two-mica orthogneisses (fig. 3C, D) have a much broader range of  $^{207}\text{Pb}/^{206}\text{Pb}$  ages (398 to 612 Ma), and we were unable to obtain concordant data from any fraction. Although these plutons are not S-type granites in the strict sense because their mineralogic and chemical characteristics were later found to be nondiagnostic (Dillon, 1989, p. 183), they are peraluminous and probably were derived from pelitic sediments. Detrital zircons in sedimentary rocks may be derived from many provenances (for example, quartzite in the Yukon-Tanana terrane contains zircons that range in age from 1.2 to 3.4 Ga; Mortensen, 1990), and thus, inherited material in the zircons may be a mixture of many ages.

The orthogneisses are strongly foliated, a deformation that apparently occurred in the middle Mesozoic on the basis of K-Ar ages (Armstrong and others, 1986). Our U-Pb data on sphene indicate that this metamorphism did not exceed about 550°C, because the sphenes have not been reset to a Mesozoic age. The sphene and monazite may be igneous minerals that cooled through their closure temperatures shortly after emplacement of the magmas, or they may have formed during a penetrative deformation in the Devonian. The coarse-grained, euhedral morphology of these minerals suggests that they are igneous in origin.

The ~390-Ma ages of the felsites may provide constraints for the age of the stratigraphic section. Sample 90TM409 (precisely dated at  $393 \pm 2$  Ma) particularly looks like an interbedded metavolcanic rock and thus would date the time of deposition of the purple and green phyllites of the Nutirwik Creek unit. However, geologic mapping shows that the purple and green phyllite is allochthonous relative to other rocks of the Hammond terrane and hence its stratigraphic significance is not understood. All contacts may be a complex interleaving of fault slivers.

On the basis of their contrasting composition and mineralogy, Newberry and others (1986) concluded that the metagranitic rocks of the Chandalar quadrangle comprise

peraluminous and metaluminous magmatic suites that are distinct and unrelated to each other. However, the similar U-Pb ages derived from samples from these suites, the present spatial proximity of the metagranitic bodies, and their similar porphyritic textures suggests to us that the Horace Mountain plutons, Geroe Creek orthogneiss body, and Baby Creek orthogneiss body once formed parts of a large Early Devonian batholith that was dismembered during the Brookian orogeny in the Jurassic or Early Cretaceous. This interpretation is supported by the tabular shapes of the metagranitic bodies and the presence of gently dipping faults both above and below several of the bodies. The compositional differences between the orthogneisses may be due to assimilation of different amounts of pelitic wall rocks. The assimilation of pelitic material is supported by the broad range of the  $^{207}\text{Pb}/^{206}\text{Pb}$  ages for the Baby Creek orthogneiss body discussed above. Thus, we suggest that the various orthogneisses represent different parts of a variably contaminated batholith.

Although the Coldfoot and Hammond terranes have different stratigraphies and different metamorphic and deformational histories, the almost exact agreement in ages of the orthogneisses and felsic metavolcanic rocks begs the question of the relationship between the two terranes. Dillon and others (1987) and Dillon (1989) suggested that the volcanogenic rocks that comprise the Nutirwik Creek unit represent the extrusive volcanic centers of the metagranitic rocks in the Coldfoot terrane to the south. Balanced cross sections through the Brooks Range, which regard the Coldfoot and Hammond terranes as basement for the imbricated passive continental deposits of the Endicott Mountains terrane to the north, support this view by placing the Coldfoot terrane beneath the Hammond terrane in their reconstruction (Oldow and others, 1987). The Early Devonian Nutirwik Creek unit, however, is intimately interleaved with, and possibly may have been deposited on, Ordovician to Devonian carbonate platform deposits. The Coldfoot terrane into which the metagranitic rocks were emplaced, in contrast, consists partly of calcareous quartz schist of Silurian (?) and Early Devonian age. Taken at face value, these relations suggest that the volcanic rocks were deposited in a different early to middle Paleozoic stratigraphic setting than the metagranitic rocks and thus may not be consanguineous. Alternatively, if they are assumed to be consanguineous, then large-displacement faults must divide the igneous rocks from the dated metasedimentary rocks in either or both terranes.

The Devonian metagranitic rocks of the central Brooks Range are part of an extensive, discontinuous, linear belt of middle Paleozoic plutonic and volcanic rocks that occur in various accreted terranes in the North American Cordillera (Rubin and others, 1990). In the Brooks Range, Devonian granitic rocks in the Coldfoot, Hammond, and North Slope terranes crop out in a belt of over 900 km. Elsewhere in Alaska and western Canada,

similar middle Paleozoic granitic rocks occur in the Cassiar, Kootenay, Seward, and Yukon-Tanana terranes. These terranes consist mainly of continental-margin, mostly miogeoclinal, sedimentary rocks of Late Proterozoic and Paleozoic age that are locally intruded by middle Paleozoic granitic rocks and that locally contain middle Paleozoic intermediate and felsic volcanic rocks. Various isotopic and geochemical data suggest that the middle Paleozoic igneous rocks formed above continentward-dipping subduction zone(s) (Rubin and others, 1990). It is unknown whether these terranes all formed in the same, extensive linear subduction zone along the former North American continental margin (Rubin and others, 1990) or if some of these terranes formed elsewhere and subsequently accreted to, and still later were dispersed by strike-slip faulting along, the North American continental margin.

The Devonian U-Pb ages of metagranitic rocks in the central Brooks Range provide important age constraints on the origin of a major metallogenic belt of associated granitic magmatism-related mineral deposits, mainly porphyry, polymetallic vein, and skarn deposits. Most of the Devonian orthogneisses that are associated with these lode deposits are highly evolved, peraluminous and meta-luminous biotite and two-mica granites. Most interpretations favor formation of the granitic rocks above a continental-margin subduction zone (Newberry and others, 1986). Possibly associated with the belt of granitic magmatism-related deposits are Devonian(?) Kuroko-type massive sulfide deposits that occur mainly in the Ambler sequence of interbedded Devonian(?) bimodal volcanic rocks and marine sedimentary rocks in the Coldfoot terrane in the western and central Brooks Range (Nokleberg and others, 1987, 1988).

**Acknowledgments.**—We thank Nina Bashir for petrographic analysis and Alison Till for help with sample collection.

## REFERENCES CITED

- Aleynikov, J.N., Moore, T.E., Karl, S.M., and Dillon, J.T., 1991, Pb isotopic ratios in Late Proterozoic and Devonian granitic rocks of the Brooks Range, Alaska: *Eos, Transactions American Geophysical Union*, 1991 Fall Meeting, Program and Abstracts, v. 72, no. 44, p. 299–300.
- Aleynikov, J.N., Winegarden, D.L., and Walter, M., 1990, U-Pb ages of zircon rims: A new analytical method using the air-abrasion technique: *Chemical Geology (Isotope Geoscience Section)*, v. 80, p. 351–363.
- Armstrong, R.L., Harakal, J.E., Forbes, R.B., Evans, B.W., and Thurston, S.P., 1986, Rb-Sr and K-Ar study of metamorphic rocks of the Seward Peninsula and Southern Brooks Range, Alaska: *Geological Society of America Memoir* 164, p. 185–203.
- Blythe, A.E., Wirth, K.R., and Bird, J.M., 1990, Fission track and  $^{40}\text{Ar}/^{39}\text{Ar}$  ages of metamorphism and uplift, Brooks Range, northern Alaska: *Geological Association of Canada, Program and Abstracts*, v. 15, p. A-12.
- Box, S.E., 1985, Early Cretaceous orogenic belt in northeastern Alaska: Internal organization, lateral extent, and tectonic interpretation, in Howell, D.G., ed., *Tectonostratigraphic terranes of the circum-Pacific region: Circum-Pacific Council for Energy and Mineral Resources (American Association of Petroleum Geologists), Earth Science series*, no. 1, p. 137–145.
- Brosigé, W.P., and Reiser, H.N., 1964, Geologic map and section of the Chandalar quadrangle, Alaska: *U.S. Geological Survey Miscellaneous Geologic Investigations Map* 1-375, scale 1:250,000.
- Brosigé, W.P., Reiser, H.N., Dutro, J.T., Jr., and Detterman, R.L., 1979, Bedrock geologic map of the Philip Smith Mountains quadrangle, Alaska: *U.S. Geological Survey Miscellaneous Field Studies Map* MF-897B, scale 1:250,000.
- Dillon, J.T., 1985, Structure and stratigraphy of the southern Brooks Range and northern Koyukuk basin near the Dalton Highway, in Mull, C.G., and Adams, K.E., eds., *Dalton Highway, Yukon River to Prudhoe Bay, Alaska: Alaska Division of Geological and Geophysical Surveys Guidebook* 7, v. 2, p. 157–187.
- Dillon, J.T., Brosigé, W.P., and Dutro, J.T., Jr., 1986, Generalized geologic map of the Wiseman quadrangle, Alaska: *U.S. Geological Survey Open-File Report* OF 86-219, scale 1:250,000.
- Dillon, J.T., Harris, A.G., and Dutro, J.T., Jr., Solie, D.N., Blum, J.D., Jones, D.L., and Howell, D.G., 1988, Preliminary geologic map and section of the Chandalar D-6 and parts of the Chandalar C-6 and Wiseman C-1 and D-1 quadrangles, Alaska: *Alaska Division of Geological and Geophysical Surveys Report of Investigations* 88-5, scale 1:63,360.
- Dillon, J.T., Pessel, G.H., Chen, J.H., and Veach, N.C., 1980, Middle Paleozoic magmatism and orogenesis in the Brooks Range, Alaska: *Geology*, v. 8, p. 338–343.
- Dillon, J.T., and Reifensstuhl, R.R., 1990, Geologic map of the Wiseman B-1 quadrangle, south central Brooks Range, Alaska: *Alaska Division of Geological and Geophysical Surveys Professional Report* 101, scale 1:63,360.
- Dillon, J.T., Tilton, G.R., Decker, J., and Kelly, M.J., 1987, Resource implications of magmatic and metamorphic ages for Devonian igneous rocks in the Brooks Range, in Taillefer, I.L., and Weimer, Paul, eds., *Alaskan North Slope geology: Bakersfield, California, Pacific Section Society of Economic Paleontologists and Mineralogists and Alaska Geological Society*, Book 50, p. 713–723.
- Dutro, J.T., Jr., Brosigé, W.P., Reiser, H.N., and Detterman, R.L., 1979, Beaucoup Formation, a new Upper Devonian stratigraphic unit in the central Brooks Range, northern Alaska, in Sohl, N.F., and Wright, W.B., eds., *Changes in stratigraphic nomenclature by the U.S. Geological Survey: U.S. Geological Survey Bulletin* 1482-A, p. A63–A69.
- Gottschalk, R.R., 1990, Structural evolution of the schist belt, south-central Brooks Range fold and thrust belt: *Journal of Structural Geology*, v. 12, p. 453–469.
- Grantz, Arthur, Moore, T.E., and Roeske, S.M., 1991, Continent-ocean transect A-3: Gulf of Alaska to Arctic Ocean: Boulder, Colorado, *Geological Society of America Centennial Continent-Ocean Transect* 15, 72 p., scale 1:500,000, 3 sheets.

- Hanson, G.N., Catanzaro, E.J., and Anderson, D.H., 1971, U-Pb ages for sphene in a contact metamorphic zone: *Earth and Planetary Science Letters*, v. 12, p. 231-237.
- Jones, D.L., Silberling, N.J., Coney, P.J., and Plafker, George, 1987, Lithotectonic terrane map of Alaska: U.S. Geological Survey Miscellaneous Field Studies Map MF-1874A, scale 1:2,500,000, 1 sheet.
- Karl, S.M., and Aleinikoff, J.N., 1990, Proterozoic U-Pb zircon age of granite in the Kallarichuk Hills, western Brooks Range Alaska: Evidence for Precambrian basement in the Schist Belt, in Dover, J.H., and Galloway, J.P., eds., *Geologic studies in Alaska by the U.S. Geological Survey*, 1989: U.S. Geological Survey Bulletin 1946, p. 95-100.
- Karl, S.M., Aleinikoff, J.N., Dickey, C.F., and Dillon, J.T., 1989, Age and chemical composition of the Proterozoic intrusive complex at Mount Angayukaqsaq, western Brooks Range, Alaska, in Dover, J.H., and Galloway, J.P., eds., *Geologic studies in Alaska by the U.S. Geological Survey*, 1988: U.S. Geological Survey Bulletin 1903, p. 10-19.
- Krogh, T.E., 1973, A low-contamination method for hydrothermal decomposition of zircon and extraction of U and Pb for isotopic age determination: *Geochimica et Cosmochimica Acta*, v. 37, p. 485-494.
- , 1982, Improved accuracy of U-Pb zircon ages by the creation of more concordant systems using an air abrasion technique: *Geochimica et Cosmochimica Acta*, v. 46, p. 637-649.
- Ludwig, K.R., 1991a, PBDAT—A computer program for processing Pb-U-Th isotope data, version 1.20: U.S. Geological Survey Open-File Report 88-542, Revision of March 19, 1991, 34 p.
- , 1991b, ISOPLOT—A plotting and regression program for radiogenic-isotope data: U.S. Geological Survey Open-File Report 91-445, 41 p.
- Mertie, J.B., Jr., 1923, Geology and gold placers of the Chandalar district, in Brooks, A.H., ed., *Mineral resources of Alaska*: U.S. Geological Survey Bulletin 773, p. 215-265.
- Moore, T.M., 1992, The Arctic Alaska superterrane, in Bradley, D.C., and Dusel-Bacon, Cynthia, *Geologic studies in Alaska by the U.S. Geological Survey*, 1991: U.S. Geological Survey Bulletin 2041, p. 238-244.
- Moore, T.E., Wallace, W.K., Bird, K.J., Karl, S.M., Mull, C.G., and Dillon, J.T., 1992, Stratigraphy, structure, and geologic synthesis of northern Alaska: U.S. Geological Survey Open-File Report OF 92-330, 183 p., 1 map sheet, scale 1:2,500,000.
- Mortensen, J.K., 1990, Significance of U-Pb ages for inherited and detrital zircons from Yukon-Tanana terrane, Yukon and Alaska: *Geological Association of Canada-Mineralogical Association of Canada Program with Abstracts*, v. 15, p. A91.
- Nelson, S.W., Grybeck, D., Silberman, M.L., and Brookins, D., 1979, Cataclastic granitic rocks in the central Brooks Range, Alaska: *Geological Society of America Abstracts with Programs*, v. 11, p. 119.
- Nelson, B.K., Nelson, S.W., and Till, A.B., in press, Nd- and Sr-isotope evidence for Proterozoic and Paleozoic crustal evolution of the Brooks Range, northern Alaska: *Journal of Geology*.
- Newberry, R.J., Dillon, J.T., and Adams, D.D., 1986, Regionally metamorphosed, calc-silicate-hosted deposits of the Brooks Range, northern Alaska: *Economic Geology*, v. 81, p. 1728-1752.
- Nokleberg, W.J., Bundtzen, T.K., Berg, H.C., Brew, D.A., Grybeck, Donald, Robinson, M.S., Smith, T.E., and Yeend, Warren, 1987, Significant metalliferous lode deposits and placer districts of Alaska: U.S. Geological Survey Bulletin 1786, 104 p.
- , 1988, Metallogeny and major mineral deposits of Alaska: U.S. Geological Survey Open-File Report 88-73, 97 p., 2 plates, scale 1:5,000,000.
- Oldow, J.S., Seidensticker, C.M., Phelps, J.C., Julian, F.E., Gottschalk, R.R., Boler, K.W., Handschy, J.W., and Ave Lallemand, H.G., 1987, Balanced cross sections through the central Brooks Range and North Slope, Arctic Alaska: *American Association of Petroleum Geologists publication*, 19 p., 8 plates, scale 1:200,000.
- Parrish, R.R., 1987, An improved micro-capsule for zircon dissolution in U-Pb geochronology: *Chemical Geology (Isotope Geoscience Section)*, v. 66, p. 99-102.
- , 1990, U-Pb dating of monazite and its implication to geological problems: *Canadian Journal of Earth Sciences*, v. 27, p. 1431-1450.
- Roeder, Dietrich, and Mull, C.G., 1978, Tectonics of Brooks Range ophiolites, Alaska: *American Association of Petroleum Geologists Bulletin*, v. 62, p. 1696-1702.
- Rubin, C.M., Miller, M.M., and Smith, G.M., 1990, Tectonic development of Cordilleran mid-Paleozoic volcano-plutonic complexes: Evidence for convergent margin tectonism, in Harwood, D.S., and Miller, M.M., eds., *Paleozoic and early Mesozoic paleogeographic relations: Sierra Nevada, Klamath Mountains, and related terranes*: Boulder, Colorado, Geological Society of America Special Paper 255, p. 1-16.
- Stacey, J.S., and Kramers, J.D., 1975, Approximation of terrestrial lead isotope evolution by a two-stage model: *Earth and Planetary Science Letters*, v. 26, p. 207-226.
- Steiger, R.H., and Jäger, E., 1977, Subcommittee on geochronology, convention on the use of decay constants in geo- and cosmochronology: *Earth and Planetary Science Letters*, v. 36, p. 359-362.
- Tailleux, I.L., 1984, Argument for Cretaceous instead of Devonian plutonism in the Brooks Range, northern Alaska: *Geological Society of America Abstracts with Programs*, v. 16, no. 5, p. 336.
- Till, A.B., and Moore, T.E., 1991, Tectonic relations of the schist belt, southern Brooks Range, Alaska [abs.]: *Eos, Transactions American Geophysical Union*, v. 72, no. 44, supplement, p. 295.
- Till, A.B., Schmidt, J.M., and Nelson, S.W., 1988, Thrust involvement of metamorphic rocks, southwestern Brooks Range, Alaska: *Geology*, v. 10, p. 930-933.
- Turner, D.L., Forbes, R.B., and Dillon, J.T., 1979, K-Ar geochronology of the south-western Brooks Range, Alaska: *Canadian Journal of Science*, v. 16, p. 1789-1804.

Reviewers: Steven W. Nelson and Wayne R. Premo

# APPEAL FOR NONPROLIFERATION OF ESCALATING TERRANE NOMENCLATURE

By Susan M. Karl and Charles G. Mull

## ABSTRACT

Terrane nomenclature in northern Alaska is expanding at a faster pace than geologic knowledge. The Arctic Alaska and Angayuchan terranes are appropriately defined terranes because it has been clearly demonstrated that they have different basements and different geologic histories. Subterrane nomenclature does not contribute to the geologic understanding of the Arctic Alaska terrane because subterrane boundaries cannot be clearly drawn for both sedimentary and structural reasons. The elevation of the Arctic Alaska terrane to superterrane status is inappropriate because the components of the Arctic Alaska "superterrane" share stratigraphic units and have similar geologic histories. Terranes are tectonostratigraphic units that are useful but unregulated, and as such cannot be used as stratigraphic tools.

## INTRODUCTION

The concept of terranes is a widely recognized and fundamentally useful tool in geologic interpretation and synthesis. The dangers of terrane implementation lie in the fact that terrane nomenclature is totally uncontrolled, not rigorously reviewed, and not bound by any formal code of usage. There are many assorted definitions of the term "terrane." The published definitions of the term have evolved almost annually (see, for example, Berg and others, 1978; Beck and others, 1980; Coney and others, 1980; Jones and others, 1981; Silberling and Jones, 1984; Howell and others, 1985; Jones and others, 1987; Monger and Berg, 1987; W. Nokleberg, written commun., 1992). The term has recently evolved from essentially a fault-bounded microplate extending to the Moho (Beck and others, 1980) to something that includes fault slivers less than a kilometer in map width and tens of meters in thickness (Nokleberg and others, 1985). Once it was important whether a terrane had continental or oceanic basement; now no basement is required. Originally, adjacent terranes were required to have a different geologic history (Coney and others, 1980); now some workers have expanded the definition such that some terranes may be faulted facies

equivalents of other terranes (W.J. Nokleberg, oral presentation, September 1992). This is permitted by the definition of Howell and others (1985), which "is preferred to the earlier one of Coney and others, 1980, which has been construed by some to mean that tectonostratigraphic units are not terranes if they may be explained or interpreted as facies equivalents of one another or cratonal North America" by Moore (1992, p. 238). The utility of the term is rapidly diminishing. In addition, as Sengör (1990) cautioned, geologists are distracted from geologic advances by the "pseudo-progress" of subdividing terranes. Moreover, inaccurate or inappropriate terrane delineation interferes with objective geologic analysis, and the validity of designated terranes cannot be tested (Sengör, 1990; Dover, 1990).

## DISCUSSION

In this short article, we make four points concerning the use of terrane terminology in northern Alaska: (1) The Arctic Alaska and Angayuchan terranes are appropriately defined terranes (Jones and others, 1987). (2) The term "subterrane" is inappropriately used within the Arctic Alaska terrane (Jones and others, 1987) because faulted sedimentary facies changes are the criteria by which the terrane boundaries were drawn, and in many places the subterrane boundaries are stacked thrust sheets and allochthons and their boundaries are not, and probably cannot be, clearly drawn due to the gradational nature of sedimentary facies changes. (3) The elevation of the Arctic Alaska terrane to superterrane status (Moore, 1992) is also inappropriate because the "terrane" within the "Arctic Alaska superterrane" share common stratigraphic and structural characteristics and have *similar* geologic histories. (4) Terranes are tectonostratigraphic units that are unregulated and should not be confused with stratigraphic units or used as stratigraphic tools. Terrane terminology should be employed to recognize different geologic histories between geologic entities.

1. *Retain appropriately defined terranes.*—We are two of the authors referred to by Moore (1992), who opposed the use of subterrane in a recent synthesis of the geology of northern Alaska (Moore and others, 1992). All

of the authors of that paper agreed that the Arctic Alaska terrane and the Angayucham terrane were well-defined, fault-bounded geologic entities with entirely different stratigraphies and geologic histories with respect to each other and to adjacent geologic entities. The Arctic Alaska terrane is interpreted to have stratigraphic affinities with North America, but is not located in its original orientation with respect to North America (Mayfield and others, 1988; Moore and others, 1992). The Arctic Alaska terrane is a continental margin lithologic succession with continental basement; the Angayucham terrane is oceanic. Each terrane has a long independent history prior to their juxtaposition in the Mesozoic.

2. *Subterrane* are inappropriate.—Application of the term "subterrane" (Silberling and Jones, 1984) added an unnecessary layer of complication to the discussion of the geology of Arctic Alaska. Some of the subterrane boundaries of Jones and others (1987) were drawn along the same (controversial) boundaries as the allochthons defined by Mayfield and others (1983), with major local inconsistencies that Moore and others (1992) tried to correct. Mayfield and others (1983) pointed out that these particular geologic entities have long been recognized as tectonostratigraphic units. They were first named "thrust tectonic units" (Snelson and TAILLEUR, 1968; TAILLEUR and Brosge, 1970), in which specific stratigraphic sequences were recognized (Martin, 1970). Consequently they were referred to as "thrust sequences" by Mayfield and others (1978), and repackaged as allochthons and parautochthons by Mayfield and others (1983, 1988), Mull and others (1987), and Mull (1989). "Modernization" of the terminology by again repackaging these thrust sheets, allochthons, and parautochthons as subterrane (Jones and others, 1987)(table 1) added no new information, insights, or understanding to the geology of the area. In fact, subterrane nomenclature obscures the fact that some of the subterrane are thrust sheets, some are single allochthons, some include several allochthons, some are metamorphic belts, some are structural belts, and some are belts of autochthonous or parautochthonous rocks. In other words, the single term (subterrane) represents apples, oranges, and watermelons. Moreover, (1) in many places in the Brooks Range, these "subterrane" are stacked; (2) in many places these "subterrane" are fault slivers only a few meters thick; and (3) in many places different "subterrane" are intimately imbricated, rendering their use locally impractical. To our way of thinking, thrust sequences, allochthons, and metamorphic belts convey a lot more useful (and still objective) information to other geologists than do "subterrane."

Figure 1 is a tectonic map of northern Alaska showing the various structural belts within the Arctic Alaska terrane. These structural belts are stratigraphically related, but have distinct structural character and styles of deformation. These belts are tectonic components of a larger

tectonostratigraphic entity. Allochthons and thrust sheets are tectonostratigraphic components of some of these belts, but are too small to be mapped at a regional scale. We emphasize that figure 1 is a tectonic map and *not* a substitute for a geologic map; it shows the application of the tectonostratigraphic terminology we propose.

3. *Superterrane* are inappropriate.—Recently Moore, (1992), recognizing "problems of the subterrane nomenclature as applied in northern Alaska," proposed that these thrust sheets and allochthons, or subterrane, be elevated to terrane status, which requires elevation of the Arctic Alaska terrane to superterrane status. This results, for example, in one terrane, the Endicott Mountains "terrane," which is a single imbricated rootless thrust sheet, or allochthon, and another terrane, the DeLong Mountains "terrane," which includes four previously identified allochthons. Such terrane designation gives faults with lesser amounts of displacement (such as the Endicott-Picnic Creek allochthon boundary) the same weight as major sutures (such as the boundary between the Arctic Alaska and Angayucham terranes). In addition, four, and possibly five of these new "terrane" in the Arctic Alaska "superterrane" (Moore, 1992) contain the same stratigraphic units. The same formations within the Endicott, Lisburne, and Etivluk Groups occur on several adjacent thrust sheets, or "terrane" of Moore (1992). For example, the Endicott Group is found in the "Endicott Mountains terrane" and the "DeLong Mountains terrane," and the Nakolik River unit has been identified as a depositional link between the Baird Group of the "Hammond terrane" and the Endicott Group of the "Endicott Mountains terrane" (Dumoulin and Harris, 1987).

If the Endicott, Lisburne, and Etivluk Groups have a different basement in each "terrane," then they are technically part of an "overlap assemblage." Since the pre-Devonian or pre-Mississippian basement of a large number of thrust sheets is missing due to faulting, it will be necessary to erect a large number of "suspect terrane," one for each of these thrust sheets, because the nature of their basement may never be known for certain. The implications of pursuing terrane to this level of detail are staggering because at present terrane boundaries are drawn along Mesozoic structures, and it would be necessary to identify all the pre-Mississippian structures instead.

If the Endicott, Lisburne, and Etivluk Groups do not have different basements in different terrane, terrane designation in this case subordinates the recognition of facies changes and a formal stratigraphic relationship between Endicott, Lisburne, and Etivluk rocks that link different thrust sheets or allochthons or "terrane." Does the Lisburne Group indeed have a different geologic history in one place from the Lisburne Group in another place? Admittedly this may be a semantic problem—every grain of sand on this earth probably has a unique history with respect to every other grain of sand—but where do we draw the line?



Moore's (1992) discussion of the Hammond "terrane" is another case in point. Moore (1992) maintained that terrane nomenclature simplifies and facilitates discussion of geologic entities, yet he stated that the Hammond "terrane" may in fact be two terranes, or it may actually be the North Slope "terrane." The Hammond "terrane" occupies the structural core of the Brooks Range and has been called a variety of names (table 1). This area is perhaps the least studied component of the Arctic Alaska terrane, and its boundaries remain controversial. It consists of rocks as old as Proterozoic, commonly referred to as the Franklinian sequence (Lerand, 1973). Franklinian rocks have been loosely correlated around the Arctic, and numerous workers have identified regional variation in these rocks. Lane (1992), Pelka and others (1992), and Cecile and Harrison (1992) have inferred that the Franklinian rocks in Arctic Canada, Alaska, and Chukchi province represent an unknown number of Precambrian terranes that were amalgamated by Devonian time and accreted to North America during the Ellesmerian orogeny (Lane, 1992). It is not known how many Precambrian terranes

are represented by Franklinian rocks in the Arctic Alaska terrane. The most detailed stratigraphic and paleontologic work in the Arctic Alaska terrane to date suggests that these rocks represent a single Precambrian to Paleozoic continental margin (Dumoulin and Harris, in press). There currently is no geologic evidence to define boundaries for subdividing these pre-Devonian rocks.

The Coldfoot "terrane" of Moore (1992), located on the southern flank of the Brooks Range, is composed in part of a 600-km-long belt of polydeformed metamorphic rocks well established in the literature as the "schist belt" (Gilbert and others, 1977; Grybeck and Nelson, 1981; Mull, 1982; Till and others, 1988). The boundary between the north margin of the schist belt, or Coldfoot "terrane," and the internal metamorphic belt, or Hammond "terrane," is obscure, controversial, and of uncertain structural significance. Dillon and others (1987), Dumoulin (1988), Karl and others (1989), and Moore and others (1992) noted that some of the carbonate rocks, bimodal volcanic rocks, and plutonic rocks in the schist belt (Coldfoot "terrane") are similar in composition, texture, and age to rocks

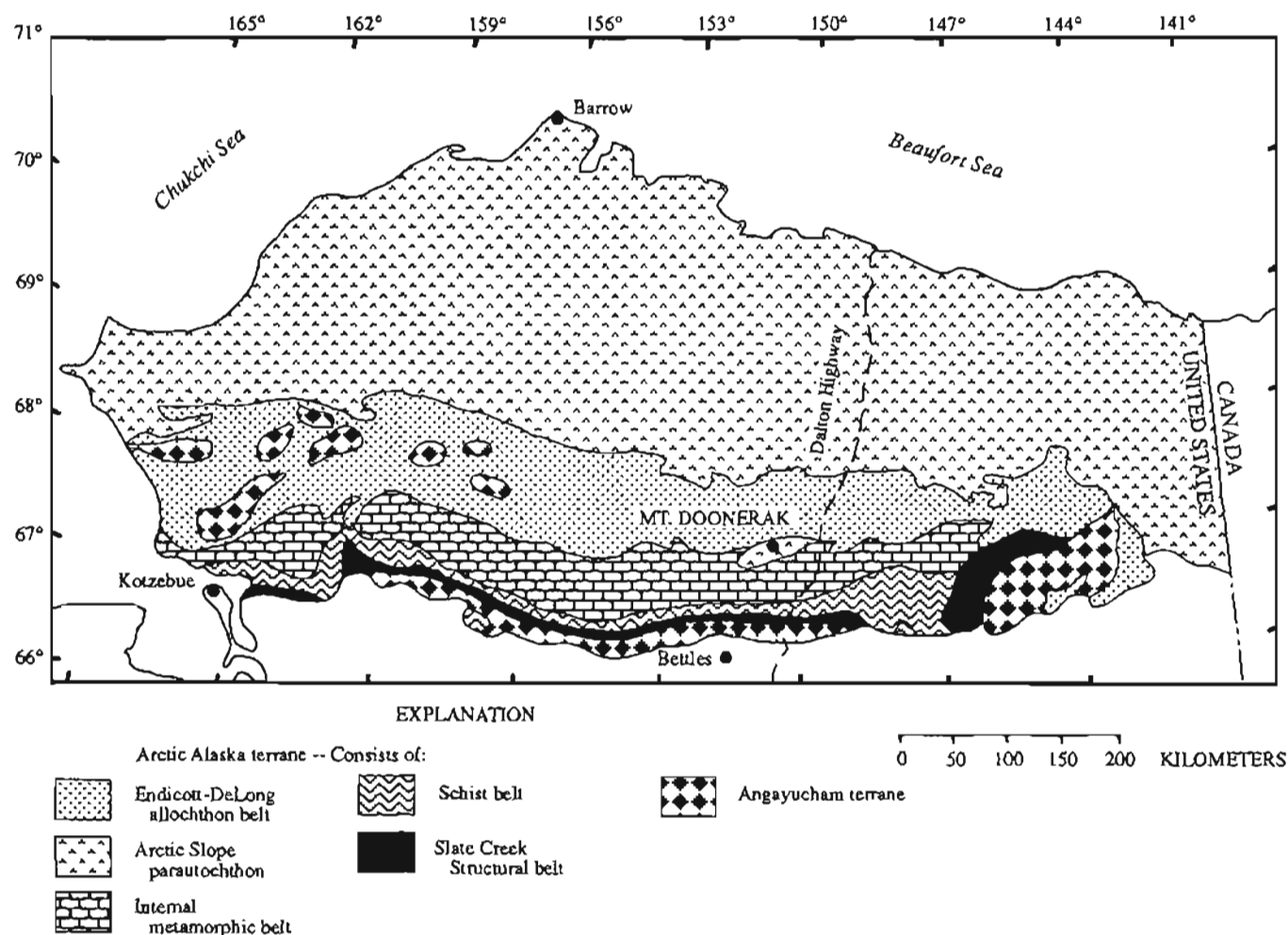


Figure 1. Tectonic components of Arctic Alaska and Angayucham tectonostratigraphic terranes in northern Alaska.



**Table 1.** Selected stages of evolution of nomenclature in northern Alaska and their sources

[Symbols: AT, Angayucham terrane; AAT, Arctic Alaska terrane; AAS, Arctic Alaska superterrane]

Snelson and Tailleux, 1968	Martin, 1970	Lerand, 1973	Pessel and others, 1973	Mayfield and others, 1978	Mull, 1982	Mayfield and others, 1983, 1988
Misheguk thrust tectonic unit	Ultrabasic pluton sequence			Misheguk Mountain thrust sequence	Misheguk Mountain allochthon	Misheguk Mountain allochthon
Misheguk thrust tectonic unit	Ultrabasic pluton sequence			Misheguk Mountain thrust sequence	Copter Peak allochthon	Copter Peak allochthon
Nuka Ridge thrust tectonic unit	Nuka Ridge sequence			Nuka Ridge thrust sequence	Nuka Ridge allochthon	Nuka Ridge allochthon
Ipsnavik River thrust tectonic unit	Ipsnavik River sequence			Ipsnavik River thrust sequence	Ipsnavik River allochthon	Ipsnavik River allochthon
Kelly thrust tectonic unit	DeLong sequence			Kelly River thrust sequence	Kelly River allochthon	Kelly River allochthon
Wulik thrust tectonic unit				Northwestern Brooks Range thrust sequence		Picnic Creek allochthon
Foothills thrust tectonic unit	Brooks Range sequence and Ivotuk Hills sequence			Northwestern and north-central Brooks Range thrust sequences	Endicott Mountains allochthon	Brooks Range allochthon
		Franklinian, Ellesmerian, and Brookian sequences			autochthon	autochthon
	Franklinian sequence					Schwatka sequence
			Schist belt			Schwatka sequence
						Schwatka sequence
						Copter Peak and Misheguk Mountain allochthons

Table 1. Selected stages of evolution of nomenclature in northern Alaska and their sources—Continued

[Symbols: AT, Angayucham terrane; AAT, Arctic Alaska terrane; AAS, Arctic Alaska superterrane]

Jones and others, 1987	Till and others, 1988	Patton and Box, 1989	Mull, 1989	Moore and others, 1992	Moore, 1992	This report
Angayucham terrane		Angayucham terrane	Misheguk Mountain allochthon (AT)	Angayucham terrane	Angayucham terrane	Brooks Range ophiolite allochthon (AT?)
Angayucham terrane		Angayucham terrane	Copter Peak allochthon (AT)	Angayucham terrane	Angayucham terrane	Brooks Range basalt allochthon (AT?)
DeLong Mountains subterrane (AAT)			Nuka Ridge allochthon (AAT)	DeLong Mountains subterrane (AAT)	DeLong Mountains terrane (AAS)	Endicott-DeLong allochthon belt* (AAT)
DeLong Mountains subterrane (AAT)			Ignavik River allochthon (AAT)	DeLong Mountains subterrane (AAT)	DeLong Mountains terrane (AAS)	Endicott-DeLong allochthon belt* (AAT)
DeLong Mountains subterrane (AAT)			Kelly River allochthon (AAT)	DeLong Mountains subterrane (AAT)	DeLong Mountains terrane (AAS)	Endicott-DeLong allochthon belt* (AAT)
DeLong Mountains subterrane (AAT)			Picnic Creek allochthon (AAT)	DeLong Mountains subterrane (AAT)	DeLong Mountains terrane (AAS)	Endicott-DeLong allochthon belt* (AAT)
Endicott Mountains subterrane (AAT)			Endicott Mountains allochthon (AAT)	Endicott Mountains subterrane (AAT)	Endicott Mountains terrane (AAS)	Endicott-DeLong allochthon belt* (AAT)
North Slope subterrane (AAT)			Autochthon and parautochthon (AAT)	North Slope subterrane (AAT)	North Slope terrane (AAS)	Arctic Slope parautochthon (AAT)
Hammond subterrane (AAT)	Central belt		Internal metamorphic and plutonic belt (AAT)	Hammond subterrane (AAT)	Hammond terrane (AAS)	Internal metamorphic belt (AAT)
Hammond and Coldfoot subterrane (AAT)	Schist belt		Schist belt (AAT)	Coldfoot subterrane (AAT)	Coldfoot terrane (AAS)	Schist belt (AAT)
Coldfoot subterrane (AAT)		Slate Creek thrust panel (AT)	Schist belt (AAT)	Slate Creek subterrane (AAT)	Slate Creek terrane (AAS)	Slate Creek structural belt (AAT)
Angayucham terrane		Narvak and Kanuti thrust panels (AT)	Narvak and Kanuti thrust panels (AT)	Angayucham terrane	Angayucham terrane	Narvak and Kanuti thrust panels (AT)

\*The Endicott-DeLong allochthon belt includes the Endicott, Picnic Creek, Kelly River, Ignavik River, and Nuka Ridge allochthons, but these individual tectonic units are too small to be mapped at small scales.

in the internal metamorphic belt (Hammond "terrane"). These lithologic relationships suggest that these two belts may have a fundamental stratigraphic and paleogeographic relationship to each other; terrane designation obscures recognition of their common characteristics. Most authors who have published work on the southern Brooks Range since Jones and others (1987) continue to refer to the "schist belt" (Dusel-Bacon and others, 1989; Karl and others, 1989; Gottschalk, 1990; Miller and Hudson, 1991; Blythe and others, in press; Little and others, in press; Law and others, in press), and we suggest that the term "schist belt" conveys information concerning the lithology and structural character of the belt without interpretations concerning genesis or regional structural relationships.

The Slate Creek "terrane" of Moore (1992) is a structural assemblage (Gottschalk, 1990; Murphy and Patton, 1988; Karl and others, 1989; Dillon, 1989) between the schist belt (Coldfoot "terrane") and the Angayucham terrane that extends for the full length of the schist belt along its southern boundary. This structural assemblage locally contains sandstone turbidites of probable Devonian age (Murphy and Patton, 1988), but has no internal stratigraphy. Patton and Box (1989) associated the Slate Creek "thrust panel" with the Angayucham terrane, but most other workers consider the Slate Creek structural assemblage to be part of the Arctic Alaska terrane (summarized in Moore and others, 1992). Moore (1992) suggested that the term "Slate Creek terrane" allows consideration of all models of origin, yet he includes it within the Arctic Alaska superterrane; we suggest that the term "Slate Creek structural belt" serves the purpose better because it is descriptive and is more informative with respect to its origin.

4. *Tectonostratigraphic terms are distinct from stratigraphic terms.*—Finally, the distinction between tectonostratigraphic units and stratigraphic units should be maintained and consciously honored. Stratigraphic units, such as formations and groups, have a stratigraphic basis of origin, consisting of a well-defined stratigraphic sequence, type or principal reference section, area, or locality, and age, as required by the Code of Stratigraphic Nomenclature. This basis provides their strength as stratigraphic tools for local and regional correlation. Tectonostratigraphic units are unregulated, informal terms that are not rigorously defined and that can be assigned and reassigned without any stratigraphic basis. Thus terranes should not be confused with formal stratigraphic units and have no validity as stratigraphic tools. Stratigraphic units can be correlated. Terranes contain sequences of stratigraphic units; correlation of terranes requires correlation of their entire stratigraphic sequences. Moore (1992, p. 241) suggested that "correlation of the Hammond terrane with the North Slope terrane is plausible because of the presence of Ellesmerian rocks in the Schwatka Mountains." Correlation requires a similar geologic history, and by definition, terranes have "a different

geologic history." Terranes are useful *precisely because* they indicate different geologic histories.

It is also critical to maintain the distinction between tectonostratigraphic maps with structural units and geologic maps with stratigraphic units. Both types of maps are important to regional syntheses, but they are not interchangeable.

## CONCLUSIONS

The geologic community as a whole needs to agree on a definition of the term "terrane" and stick to it. We think that the term will have the most utility if we go back to the standards set by Jones and others (1981):

A tectonostratigraphic terrane is defined as a fault-bounded geologic entity, usually of regional extent, that is characterized by a distinctive stratigraphic sequence or rock assemblage that differs markedly from those of nearby, partly or entirely coeval neighbors. In terrane definition and analysis, the entire preserved stratigraphic sequence or assemblage must be considered, and comparisons made on the basis of the total record of sedimentation and structural history up until the time of accretion. If two unlike sequences are linked by intermediate facies, then the entire assemblage is considered to form one terrane.

In summary, we agree with Moore (1992) that the subterrane nomenclature does not work as applied in northern Alaska, and we recognize the complexity within the Arctic Alaska terrane. However, we recommend against inflicting a new layer of nomenclature on northern Alaskan geology before the relationship between various thrust sequences is adequately understood. The regional terminology must remain simple, descriptive, nongenetic, and objective (Dover, 1990). New nomenclature in itself does not simplify, facilitate, clarify, or push back the frontiers of geology; without new information it only muddies the water.

## REFERENCES CITED

- Beck, Myrl, Cox, Allan, and Jones, D.L., 1980, Penrose Conference Report: Mesozoic and Cenozoic microplate tectonics of western North America: *Geology*, v. 8, p. 454-456.
- Berg, H.C., Jones, D.L., and Coney, P.J., 1978, Map showing tectonostratigraphic terranes of southeastern Alaska and adjacent areas: U.S. Geological Survey Open-File Report 78-1085, 2 sheets, scale 1:1,000,000.
- Blythe, Ann E., Bird, John M., and Onar, Gonea, I., in press, Constraints on the cooling history of the central Brooks Range, Alaska from fission-track and  $^{40}\text{Ar}/^{39}\text{Ar}$  analyses: paper submitted to GSA Memoir volume on the Central Brooks Range.

- Cecile, M.P., and Harrison, J.C., 1992, Wrangel Island, East Siberian and Chukchi Seas, N.E. R.S.F.S.R., in Tracy, K.V., Ankes, E.M., Ryan, C., and Hoffman, V., eds., International Conference on Arctic Margins [abs.]: Alaska Geological Society, p. 9.
- Coney, P.J., Jones, D.L., and Monger, J.W.H., 1980, Cordilleran suspect terranes: *Nature*, v. 288, p. 329-333.
- Dillon, J.T., 1989, Structure and stratigraphy of the southern Brooks Range and northern Koyukuk basin near the Dalton Highway, in Mull, C.G., and Adams, K.E., eds., Guidebook to bedrock geology along the Dalton Highway, Yukon River to Prudhoe Bay, Alaska: Alaska Division of Geological and Geophysical Surveys Guidebook 7, p. 157-190.
- Dillon, J.T., Tilton, G.R., Decker, John, and Kelley, M.J., 1987, Resource implications of magmatic and metamorphic ages for Devonian igneous rocks in the Brooks Range, in Tailleux, Irv., and Weimer, Paul, eds., Alaska North Slope Geology: Society of Economic Paleontologists and Mineralogists, Pacific Section, and Alaska Geological Society, v. 2, p. 713-723.
- Dover, J.H., 1990, Problems of terrane terminology — Causes and effects, *Geology*, v. 18, no. 6, p. 487-488.
- Dumoulin, J.A., 1988, Stromatolite- and coated-grain-bearing carbonate rocks of the western Brooks Range, in Galloway, J.P., and Hamilton, T.D., eds., Geologic studies in Alaska by the U.S. Geological Survey during 1987: U.S. Geological Survey Circular 1016, p. 31-34.
- Dumoulin, J.A., and Harris, A.G., in press, Depositional framework and regional correlation of pre-Carboniferous metacarbonate rocks of the Snowden Mountain area, central Brooks Range, northern Alaska: U.S. Geological Survey Professional Paper, 120 p.
- Dusel-Bacon, Cynthia, Brosge, W.P., Till, A.B., Doyle, E.O., Mayfield, C.F., Reiser, H.N., and Miller, T.P., 1989, Distribution, facies, ages, and proposed tectonic associations of regionally metamorphosed rocks in northern Alaska: U.S. Geological Survey Professional Paper 1497-A, 44 p., 2 plates.
- Gilbert, W.G., Wiltse, M.A., Carden, J.R., Forbes, R.B., and Hackett, S.W., 1977, Geology of Ruby Ridge, southwestern Brooks Range, Alaska: Alaska Division of Geological and Geophysical Surveys Geologic Report 58, 16 p.
- Gotschalck, R.R., Jr., 1990, Structural evolution of the schist belt, south-central Brooks Range fold and thrust belt, Alaska: *Journal of Structural Geology*, v. 12, p. 453-469.
- Grybeck, D., and Nelson, S.W., 1981, Structure of the Survey Pass quadrangle, Brooks Range, Alaska: U.S. Geological Survey Miscellaneous Field Studies Map MF-1176-B, 8 p., scale 1:250,000.
- Howell, D.G., Jones, D.L., and Scermer, E.R., 1985, Tectonostratigraphic terranes of the circum-Pacific region, in Howell, D.G., ed., Tectonostratigraphic terranes of the Pacific region: Houston, Circum-Pacific Council for Energy and Mineral Resources, Earth Science Series, v. 1, p. 3-30.
- Jones, D.L., Silberling, N.J., Berg, H.C., and Plafker, George, 1981, Tectonostratigraphic terrane map of Alaska, Part 3—summary description of terranes: U.S. Geological Survey Open-File Report 81-792, 2 sheets, scale 1:2,000,000, 20 p.
- Jones, D.L., Silberling, N.J., Coney, P.J., and Plafker, George, 1987, Lithotectonic terrane map of Alaska (west of the 141st meridian): U.S. Geological Survey Miscellaneous Field Studies Map MF 1874-A, 1 sheet, scale 1:2,500,000.
- Karl, S.M., Dumoulin, J.A., Ellersieck, Inyo, Harris, A.G., and Schmidt, J.M., 1989, Preliminary geologic map of the Baird Mountains quadrangle, Alaska: U.S. Geological Survey Open-File Report 89-551, 65 p., scale 1:250,000, 1 sheet.
- Lane, L.S., 1992, Kaltag fault, northern Yukon, Canada: Constraints on evolution of Arctic Alaska: *Geology*, v. 20, p. 653-656.
- Law, R.D., Miller, E.L., Little, T.A., and Lee, Jeffrey, in press, Extensional original ductile fabrics in the schist belt central Brooks Range, Alaska—II, Microstructural and petrofabric evidence: *Journal of Structural Geology*.
- Lerand, Monti, 1973, Beaufort Sea, in McCrossam, R.G., ed., The future petroleum provinces of Canada—their geology and potential: Canadian Society of Petroleum Geology Memoir 1, p. 315-386.
- Little, T.A., Miller, E.L., Lee, Jeffrey, and Law, R.D., in press, Extensional origin of ductile fabrics in the schist belt, central Brooks Range Alaska—I, Geologic and structural studies: *Journal of Structural Geology*.
- Martin, A.J., 1970, Structure and tectonic history of the western Brooks Range, DeLong Mountains and Lisburne Hills, northern Alaska: *Geological Society of America Bulletin*, v. 81, p. 3605-3622.
- Mayfield, C.F., Tailleux, I.L., Mull, C.G., and Sable, E.G., 1978, Bedrock geologic map of the south half of the National Petroleum Reserve in Alaska: U.S. Geological Survey Open-File Report 78-70B, scale 1:500,000, 2 sheets.
- Mayfield, C.F., Tailleux, I.L., and Ellersieck, Inyo, 1983, Stratigraphy, structure, and palinspastic synthesis of the western Brooks Range, northwestern Alaska: U.S. Geological Survey Open-File Report 83-779, 58 p., 5 plates, scale 1:1,000,000.
- 1988, Stratigraphy, structure, and palinspastic synthesis of the western Brooks Range, northwestern Alaska, Chapter 7, in Gryc, George, ed., Geology and exploration of the National Petroleum Reserve in Alaska, 1974-1982: U.S. Geological Survey Professional Paper 1399, p. 143-186.
- Miller, E.L., and Hudson, T.L., 1991, Mid-Cretaceous extensional fragmentation of a Jurassic-Early Cretaceous compressional orogen, Alaska: *Tectonics*, v. 10, p. 781-796.
- Monger, J.W.H., and Berg, H.C., 1987, Lithotectonic terrane map of western Canada and southeastern Alaska: U.S. Geological Survey Miscellaneous Field Studies Map MF-1874-B, 1 sheet, scale 1:2,500,000, 12 p.
- Moore, T.E., 1992, The Arctic Alaska super terrane, in Bradley, D.C., and Dusel-Bacon, C., eds., Geologic studies in Alaska by the U.S. Geological Survey, 1991: U.S. Geological Survey Bulletin 2041, p. 238-244.
- Moore, T.E., Wallace, W.K., Bird, K.J., Karl, S.M., Mull, C.G., and Dillon, J.T., 1992, Stratigraphy, structure, and geologic synthesis of northern Alaska: U.S. Geological Survey Open-File Report 92-330, 283 p., 1 pl.
- Mull, C.G., 1982, The tectonic evolution and structural style of the Brooks Range, Alaska: an illustrated summary, in Powers, R.B., ed., Geologic studies of the Cordilleran thrust belt: Denver, Rocky Mountain Association of Geologists, v. 1, p. 1-45.
- 1989, Generalized geologic map of the Brooks Range and Arctic Slope, Alaska, in Mull, C.G., and Adams, K.E.,

- eds., Guidebook to bedrock geology along the Dalton Highway, Yukon River to Prudhoe Bay, Alaska: Alaska Division of Geological and Geophysical Surveys Guidebook 7, sheet 1, scale 1:2,850,000.
- Mull, C.G., Roeder, D.H., Tailleur, I.L., Pessel, G.H., Grantz, Arthur, and May, S.D., 1987, Geologic sections and maps across the Brooks Range and Arctic Slope to Beaufort Sea, Alaska: Geological Society of America Maps and Charts Series MC 28-S, scale 1:500,000, 1 sheet.
- Murphy, J.M., and Patton, W.W., 1988, Geologic setting and petrography of the phyllite and metagraywacke thrust panel, north-central Alaska: Geologic studies by the U.S. Geological Survey in Alaska during 1987, U.S. Geological Survey Circular 1016, p.104-108.
- Nokleberg, W.J., Jones, D.L., and Silberling, N.J., 1985, Origin and tectonic evolution of the Maclaren and Wrangellia terranes, eastern Alaska Range, Alaska, Geological Society of America Bulletin, v. 96, p. 1251-1270.
- Patton, W.W., Jr., and Box, S.E., 1989, Tectonic setting of the Yukon-Koyukuk basin and its borderlands, western Alaska: Journal of Geophysical Research, v. 94, p. 15,807-15,820.
- Pelka, G.J., Sauve, J.A., and Walsh, T.P., 1992, Franklinian tectonic framework controls on post Devonian basin development, Chukchi Province, USA sector, in Tracy, K.V., Ankes, E.M., Ryan, C., and Hoffman, V., eds., International Conference on Arctic Margins [abs]: Abstracts, Alaska Geological Society, p. 49.
- Pessel, G.H., Eakins, G.R., and Garland, R.E., 1973, Geology and geochemistry of the southeastern Ambler River quadrangle, in Alaska Division of Geological and Geophysical Surveys 1972 Annual Report, p. 7-9.
- Sengör, A.M.C., 1990, Lithotectonic terranes and the plate tectonic theory of orogeny: a critique of the principles of terrane analysis, in Wiley, T.J., Howell, D.G., and Wong, F.L., eds., Terrane analysis of China and the Pacific rim: Houston, Circum-Pacific Council for Energy and Mineral Resources, Earth Sciences Series, v. 13, p. 9-44.
- Silberling, N.J., and Jones, D.L., eds., 1984, Lithotectonic terrane maps of the North American Cordillera: U.S. Geological Survey Open-File Report 84-523.
- Snelson, Sigmund, and Tailleur, I.L., 1968, Large-scale thrusting and migrating cretaceous foredeeps in western Brooks Range and adjacent regions of northwest Alaska [abs.]: American Association of Petroleum Geologists Bulletin, v. 52, p. 567.
- Tailleur, I.L., and Brosgé, W.P., 1970, Tectonic history of northern Alaska, in Adkison, W.L., and Brosgé, M.M., eds., Proceedings of the geological seminar on the North Slope of Alaska: American Association of Petroleum Geologists Pacific Section Meeting, Los Angeles, p. E1-E19.
- Till, A.B., Schmidt, J.M., and Nelson, S.W., 1988, Thrust involvement of metamorphic rocks, southwestern Brooks Range, Alaska: Geology, v. 10, p. 930-933.

Reviewers: Dwight C. Bradley and Steven W. Nelson

# FAVORABLE AREAS FOR METALLIC MINERAL RESOURCES IN AND NEAR THE HORN MOUNTAINS, SLEETMUTE QUADRANGLE, SOUTHWESTERN ALASKA

By John E. Gray, Peter M. Theodorakos, Leon A. Bradley, and John H. Bullock, Jr.

## ABSTRACT

In a reconnaissance geochemical survey of the Horn Mountains area in the western Sleetmute quadrangle, stream-sediment and heavy-mineral-concentrate samples were collected from 138 sites. Stream-sediment samples were analyzed by semiquantitative emission spectrography, atomic absorption spectrophotometry, and visual spectrophotometry; heavy-mineral-concentrate samples were analyzed by semiquantitative emission spectrography and microscopically examined for their mineralogical content. These resulting data were interpreted to identify favorable areas for metallic mineral resources in the Horn Mountains and surrounding areas.

Twelve areas were delineated as favorable for the presence of mineral deposits. In two areas within the volcanoplutonic complex of the Horn Mountains considered favorable for polymetallic vein deposits, Late Cretaceous and Tertiary intermediate to felsic intrusive rocks of the Horn Mountains stock cut coeval mafic to felsic volcanic rocks and Cretaceous sedimentary rocks of the Kuskokwim Group. Samples collected in these two areas are geochemically anomalous in Au, Ag, As, Sb, Hg, Pb, Cu, W, Bi, Cd, B, or Te reflecting the possibility of undiscovered polymetallic vein deposits. Deposits of this type containing base-metal sulfides, sulfosalts, or gold are observed in these two areas, as in other volcanoplutonic complexes in southwestern Alaska.

Eight areas delineated as favorable for the presence of epithermal mercury-rich vein deposits lie outside of the Horn Mountains, where Cretaceous sedimentary rocks of the Kuskokwim Group are most common, but where Late Cretaceous and Tertiary mafic to felsic volcanic rocks and intrusions are found locally. In these eight areas, the most consistent anomalies are Hg in stream-sediment samples and cinnabar in heavy-mineral-concentrate samples. These results suggest that the eight areas are favorable for undiscovered cinnabar-bearing vein deposits, a deposit type common throughout southwestern Alaska. A single site containing placer gold and an area with anomalous Au, Sn, Ba, W, and Pb were also delineated, but data are insufficient to evaluate the areas further.

## INTRODUCTION

The Horn Mountains are located about 50 km northeast of Aniak in the northwestern Sleetmute quadrangle. The Horn Mountains are considered favorable for metallic mineral resources (Miller and others, 1989), because they are similar in geology and geochemistry to the nearby Russian Mountains in the Russian Mission quadrangle, and the Beaver Mountains in the Iditarod quadrangle (fig. 1), where polymetallic vein deposits are known (Bundtzen and Gilbert, 1983; Bundtzen and Laird, 1991). In addition, the geology surrounding the Horn Mountains is similar to that where epithermal mercury-rich vein deposits are found such as the Red Devil deposit (MacKevett and Berg, 1963). However, few metallic mineral deposits have been discovered, probably because few geologic, geochemical, and geophysical studies have been conducted in the area. In the summer of 1992, a geochemical survey was conducted in the western part of the Sleetmute quadrangle as part of the Alaskan Mineral Resource Appraisal Program (AMRAP). The survey covered approximately 1,500 km<sup>2</sup> and included the Horn Mountains and surrounding areas.

Reconnaissance drainage basin geochemical surveys are a rapid and efficient means of locating upstream areas with possible mineral deposits. The objective of this study was to use geochemical data from stream-sediment samples, and geochemical and mineralogical data from heavy-mineral-concentrate samples, to identify areas favorable for the presence of mineral deposits. This report delineates drainage basins containing samples with anomalous concentrations of a suite of elements (Au, Ag, Hg, Sb, As, Cu, Pb, Zn, Sn, Bi, Cd, Ba, B, W, or Te) considered pathfinders for mineral deposit types commonly found in southwestern Alaska such as epithermal mercury-rich vein deposits and polymetallic vein deposits (Bundtzen and Gilbert, 1983). The data used in this report are listed in Theodorakos and others (1992).

## GEOLOGY

The Horn Mountains are underlain by one of several Late Cretaceous and Tertiary volcanoplutonic complexes

typical of those found in southwestern Alaska (fig. 1). Volcanic rocks of these complexes generally overlie or are in fault contact with coeval plutons that intrude and partially assimilate the volcanic rocks (Bundtzen and Gilbert, 1983). The plutonic rocks in the Horn Mountains (fig. 2) are part of a stock of mostly quartz monzonite that intrudes Late Cretaceous and Tertiary mafic to felsic tuff, lava, and breccia and sedimentary rocks of the Cretaceous Kuskokwim Group (Cady and others, 1955). In contact-

metamorphic aureoles adjacent to the plutons, sedimentary and volcanic rocks are converted to hornfels. The rocks of the Horn Mountains are proposed to be part of a caldera with a surrounding ring fracture zone and densely welded ash-flow tuffs (Doherty and Bergman, 1987). Igneous rocks in the Horn Mountains have not been dated, but K-Ar studies of similar volcanoplutonic complexes in southwestern Alaska yield ages of 73 to 59 Ma for the plutons and 77 to 58 Ma for the associated volcanic rocks (Decker

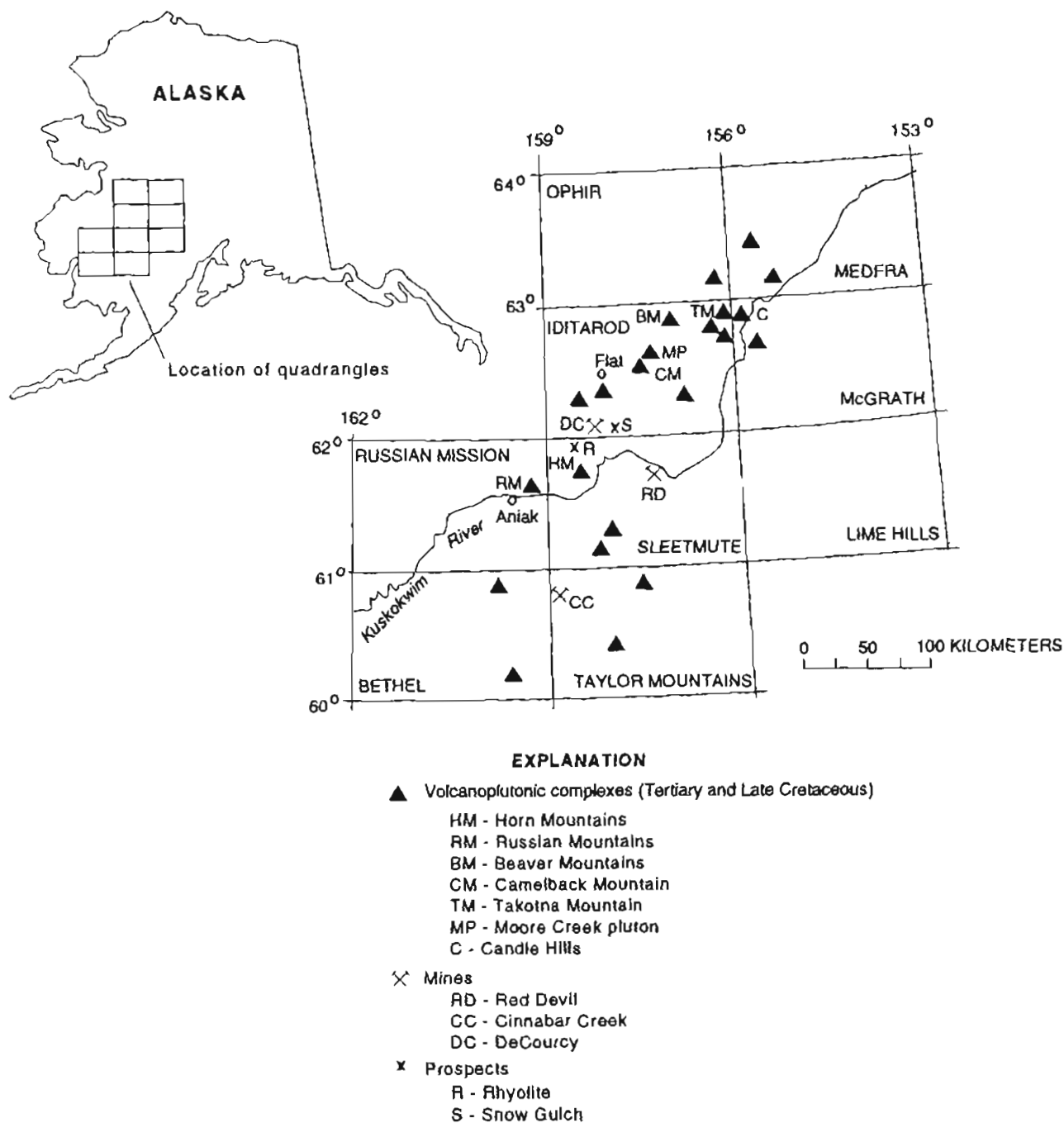


Figure 1. Volcanoplutonic complexes and selected mines and prospects in southwestern Alaska (compiled from Cady and others, 1955; Bundtzen and Gilbert, 1983; Miller and others, 1989; Miller and Bundtzen, 1992; Box and others, in press).



and others, 1984; Reifensuhl and others, 1984; Robinson and Decker, 1986; Miller and Bundtzen, 1993).

Intermediate to mafic dikes and granite porphyry intrusions cut all rock types in the study area, but most commonly intrude sedimentary rocks of the Kuskokwim Group (fig. 2). The intermediate to mafic dikes are generally small and local, typically less than 1 meter thick, discontinuous along strike, and difficult to trace for more than 10 meters (Cady and others, 1955; Miller and Bundtzen,

1993). The largest exposure of granite porphyry is at Juninggulra Mountain approximately 20 km north of the Horn Mountains. Intermediate to mafic dikes and granite porphyry intrusions are typically found near other volcanoplutonic complexes in southwestern Alaska (Cady and others, 1955; Bundtzen and Gilbert, 1983; Miller and others, 1989), suggesting that they are Late Cretaceous and Tertiary in age. Granite porphyries in southwest Alaska range in age from 72 to 62 Ma (Robinson and Decker,

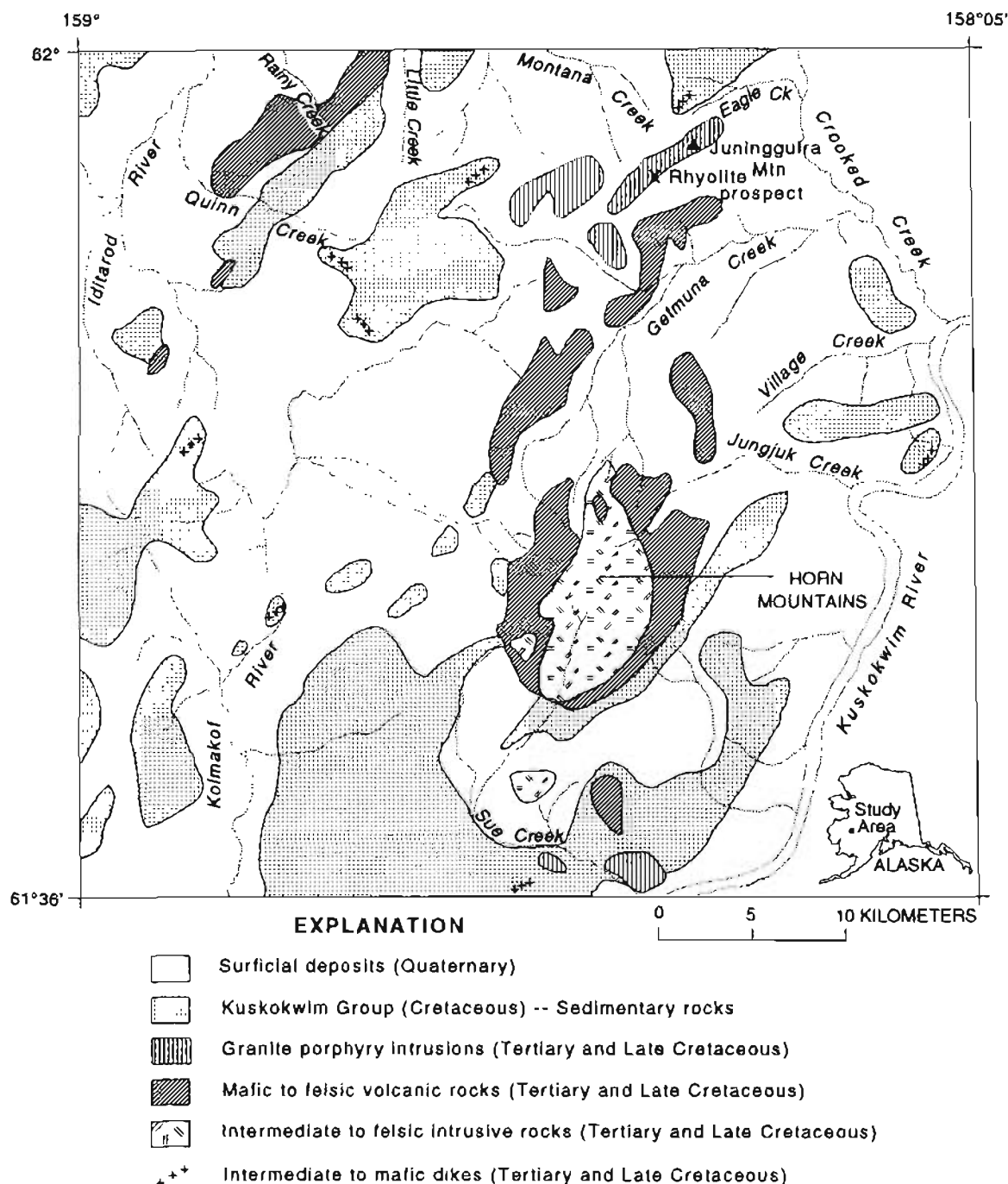


Figure 2. Geology of Horn Mountains area (simplified from Cady and others, 1955).

1986; Reifenhuth and others, 1984; Miller and Bundtzen, 1993); ages for intermediate to mafic dikes are poorly constrained because they are commonly altered, but one dike is 71 Ma (Miller and Bundtzen, 1993).

Rocks of the Cretaceous Kuskokwim Group surround the Horn Mountains. The Kuskokwim Group consists predominantly of sedimentary rocks, but also contains minor interbedded volcanic tuffs and flows in the Iditarod quadrangle (Miller and Bundtzen, 1993). The Kuskokwim Group is a unit of flysch representing turbidite fan, foreslope, shallow-marine, and shelf facies deposited in a Late Cretaceous basin (Bundtzen and Gilbert, 1983; Miller and Bundtzen, 1992). Cady and others (1955) first described and named rocks of the Kuskokwim Group, suggesting that graywacke and lesser siltstone compose almost all of the sequence; conglomerates are found locally. Rocks of the Kuskokwim Group are deformed into broad open folds, and locally into tight chevron folds, but they are not regionally metamorphosed (Miller and others, 1989).

## MINERAL OCCURRENCES

Few mineral occurrences have been recognized in the Horn Mountains study area. The Rhyolite prospect on Juninggulra Mountain is the only epithermal mercury-rich vein deposit known in the study area (fig. 2). Cinnabar-rich quartz-carbonate veins cut granite porphyry at this locality. The Rhyolite prospect was part of a larger study of epithermal cinnabar-stibnite-bearing deposits in the region (Gray and others, 1991). Other deposits of this type near the study area include the stibnite-rich Snow Gulch lode and the cinnabar-rich DeCourcy mercury mine, both about 7 km north of the Sleetmute quadrangle in the Iditarod quadrangle (fig. 1). Numerous epithermal mercury-rich vein lodes are scattered over several hundred thousand square kilometers in southwestern Alaska, in which cinnabar and stibnite are the dominant ore minerals, with lesser amounts of realgar, orpiment, native mercury, pyrite, gold, limonite, and hematite (Sainsbury and MacKevett, 1965; Gray and others, 1990). Scheelite, arsenopyrite, and base-metal-sulfide minerals are rare, but are found with cinnabar in some occurrences such as those near Flat (Bundtzen and others, 1992). Gangue is typically quartz, carbonate, and dickite. The deposits are found in all sedimentary and igneous rock types in the region, but typically show a close spatial association with Late Cretaceous and Tertiary igneous rocks. Many of these deposits are small, consisting of veins a few centimeters wide and extending for strike lengths of only a few meters, but in the Red Devil deposit veins exceeded a meter in width and 100 m in length (MacKevett and Berg, 1963). Red Devil produced approximately 35,000 flasks of mercury (1 flask = 76 lb or 34.5 kg) and total production from southwest Alaska is about 41,000 flasks of mercury (Miller and others, 1989).

Mercury, Sb, and As in minus-80-mesh stream-sediment samples, and cinnabar in nonmagnetic heavy-mineral-concentrate samples are the most consistently anomalous data in samples collected around epithermal cinnabar-stibnite-bearing deposits in southwestern Alaska (Gray and others, 1991).

Polymetallic veins were recently discovered in the Horn Mountains (Bundtzen and others, 1993) near the headwaters of Jungjuk Creek, Getmuna Creek, and Whitewing Valley (fig. 3), and are base-metal-sulfide-bearing with anomalous gold or silver. The Whitewing Valley occurrence cuts rocks of the Horn Mountain pluton, and the Jungjuk and Getmuna Creek occurrences are found in volcanic rock hornfels. Similar polymetallic vein lodes are found in other volcanoplutonic complexes in southwestern Alaska including the Russian Mountains (Bundtzen and Laird, 1991), Beaver Mountains (Bundtzen and Laird, 1982), the Flat area (Mertie, 1936; Bull and Bundtzen, 1987; Bundtzen and others, 1988c), Camelback Mountain (Bundtzen and others, 1988b), and the Moore Creek pluton (Bundtzen and others, 1988b). The mineralized veins are found in faults, shear zones, and breccias within cupolas of monzonite stocks or in surrounding sedimentary- and volcanic-rock hornfels aureoles (Bundtzen and Gilbert, 1983; Bundtzen and others, 1988a). The lodes contain arsenopyrite, pyrite, chalcopyrite, bornite, sphalerite, galena, marcasite, tetrahedrite, gold, bismuthanite, stephanite, cassiterite, scheelite, barite, or wolframite. Quartz, tourmaline, axinite, and fluorite comprise most of the gangue. Stream-sediment samples collected around volcanoplutonic complexes with known polymetallic vein deposits in the Iditarod quadrangle contain anomalous concentrations of Au, Ag, As, Cu, Pb, Zn, Mo, Sn, Hg, B, Bi, or Be; heavy-mineral-concentrate samples contain anomalous Au, Ag, Cu, Pb, Zn, Mo, Sn, Sb, As, W, Bi, Ba, B, or Nb, and may contain gold and scheelite, but rarely base-metal sulfides or cinnabar (Gray and others, 1988; Bennett and others, 1988). However, anomalous concentrations of base metals in drainage basin samples collected around some of the volcanoplutonic complexes are inconsistent with the mineralogy of polymetallic veins known in the areas. For example, in the Beaver Mountains, chalcopyrite- and galena-bearing veins are known (Bundtzen and Laird, 1982), but heavy-mineral concentrates collected from the area show no anomalous Cu and Zn (Gray and others, 1988). This probably reflects the small-scale nature of the polymetallic veins, sampling distance from the vein deposits, and mechanical breakdown of the sulfides in the weathering environment.

Placer gold mines are not known in the study area, but approximately 1,500 oz of gold was recovered from a placer mine on New York Creek, about 5 km south of the study area (Madden, 1915; Cady and others, 1955; Miller and others, 1989). In addition, approximately 25,000 oz of gold has been produced from placer mines in the Donlin-

Crooked Creek area about 7 km north of the study area (Bundtzen and others, 1988a). Placer gold and cinnabar have also been reported on Little Creek near the northern Sleetmute quadrangle boundary (fig. 3) (Cady and others, 1955), but no production is known from this locality, and its location is not known with certainty (the locality may be in the Iditarod or Sleetmute quadrangle, or possibly in both quadrangles). Minor placer gold also has been reported on American Creek in the Iditarod quadrangle,

approximately 4 km north of the study area (Bennett and others, 1988). In these areas, Cretaceous sedimentary rocks of the Kuskokwim Group are cut by small Late Cretaceous and Tertiary intermediate to mafic dikes and granite porphyry intrusions. The spatial association of placer gold occurrences with igneous rocks suggests that the Horn Mountains area is favorable for placer gold.

The only other mineral occurrence in the Horn Mountains is a placer scheelite occurrence reported at the western foot of

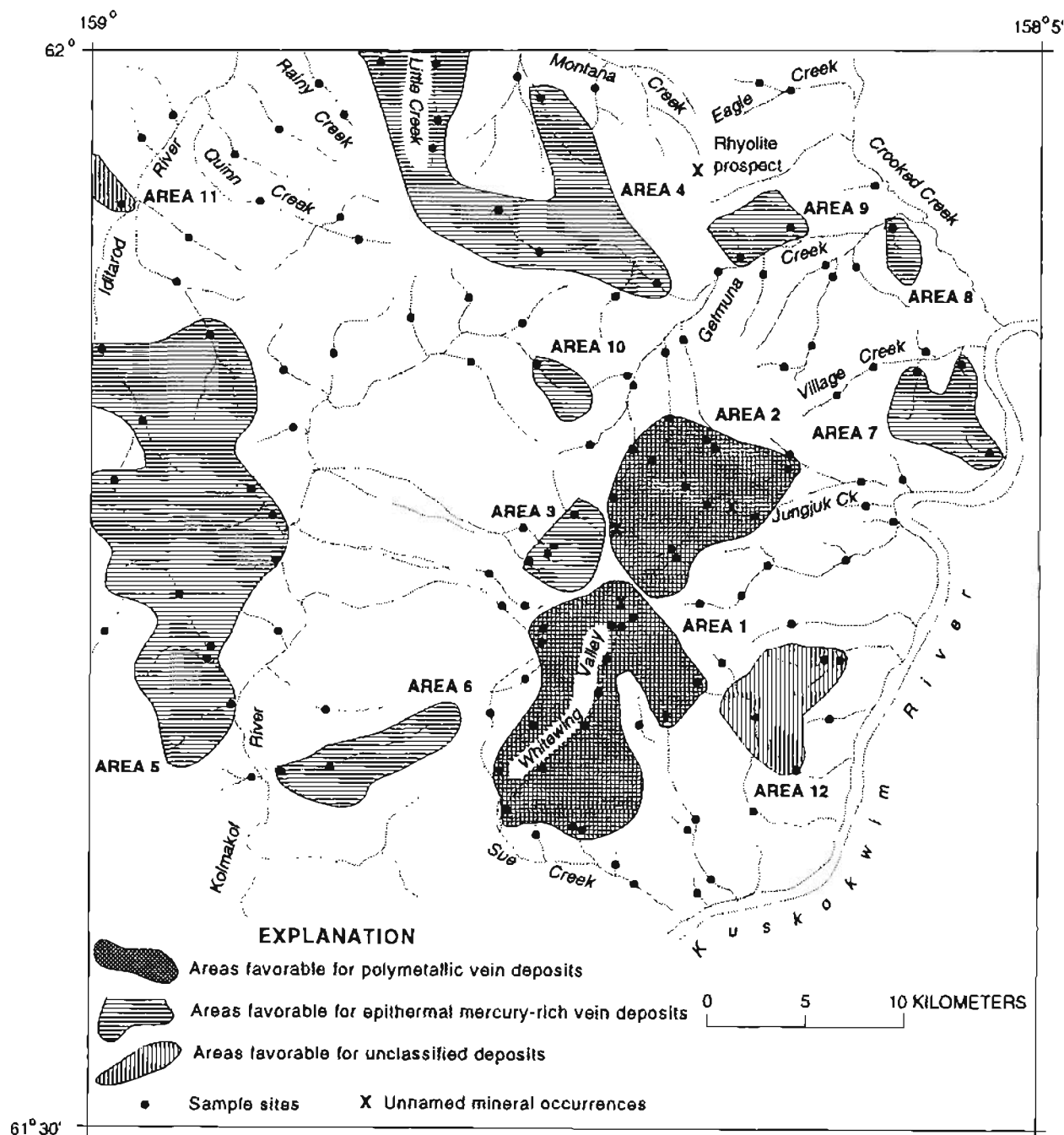


Figure 3. Areas favorable for metallic mineral resources in the Horn Mountains and surrounding areas.

the mountains (Cady and others, 1955). However, its location is poorly defined, and no further data are known for this mineral occurrence.

## GEOCHEMICAL SAMPLING TECHNIQUES AND SAMPLE PREPARATION

Stream-sediment and heavy-mineral-concentrate samples were collected from the active stream channel at 138 sites (fig. 3). Stream sediment was screened to minus-10 mesh and collected in a stainless steel gold pan. Approximately 2 kg of sediment was taken from the pan and saved as the stream-sediment sample. The pan was refilled with stream sediment and panned until most of the less dense minerals, organic materials, and clay were removed. This panned sample was saved as the heavy-mineral-concentrate sample.

In the laboratory, each stream-sediment sample was dried below 50°C, sieved to minus-80 mesh, pulverized, and chemically analyzed. The heavy-mineral-concentrate samples were further separated using bromoform to remove any remaining lighter minerals, primarily quartz and feldspar, and then separated magnetically into magnetic, paramagnetic, and nonmagnetic fractions. The nonmagnetic fractions were ground and chemically analyzed, and splits were evaluated microscopically for their mineralogical content. Only one heavy-mineral-concentrate sample had insufficient material for geochemical analysis. All of the 138 heavy-mineral-concentrate samples collected were examined microscopically for their mineralogical content.

## ANALYTICAL TECHNIQUES

### SEMIQUANTITATIVE EMISSION SPECTROSCOPY

The stream-sediment and nonmagnetic-heavy-mineral-concentrate samples were analyzed by a semiquantitative, direct-current arc emission spectrographic (SQS) technique adapted from Grimes and Marranzino (1968). The 35 elements Ag, As, Au, B, Ba, Be, Bi, Ca, Cd, Co, Cr, Cu, Fe, Ga, Ge, La, Mg, Mn, Mo, Na, Nb, Ni, P, Pb, Sb, Sc, Sn, Sr, Ti, Th, V, W, Y, Zn, and Zr were determined in samples analyzed by SQS. In addition, Pd and Pt were determined in the heavy-mineral-concentrate samples by SQS.

### ATOMIC ABSORPTION SPECTROPHOTOMETRY

Concentrations of Au, Te, and Tl in the stream-sediment samples were determined by an atomic absorption spectrophotometry (AAS) technique adapted from Hubert

and Chao (1985). The samples were digested using a series of hydrogen peroxide, hydrofluoric acid, aqua regia, and hydrobromic acid-bromine solutions. Gold, Te, and Tl were separated and concentrated by extraction into methyl isobutyl ketone and determined by flame AAS. Concentrations for Au in the range of 0.002 to 0.050 ppm were determined by graphite furnace atomic absorption spectrophotometry (GFAAS) on samples that were shown to be less than 0.050 ppm by the flame AAS technique. The GFAAS technique for Au was adapted from Meier (1980).

Mercury was measured in the stream-sediment samples using a modified version of the cold vapor AAS technique (Kennedy and Crock, 1987). The samples were decomposed with nitric acid and sodium dichromate. Mercury was then reduced to elemental Hg with hydroxylamine hydrochloride/sodium chloride and stannous chloride in a continuous flow system that releases the Hg vapor directly into an atomic absorption spectrophotometer. Tungsten was determined by a visible spectrophotometric (VS) method by decomposing the sample with nitric, hydrofluoric, and hydrochloric acids (Welsch, 1983).

### INDUCTIVELY COUPLED PLASMA-ATOMIC EMISSION SPECTROSCOPY

Concentrations of Ag, As, Sb, Bi, Cd, Cu, Mo, Pb, and Zn were determined in the stream-sediment samples by inductively coupled plasma-atomic emission spectroscopy (ICP) using the procedure developed by Motooka (1988). The sediments were decomposed with concentrated hydrochloric acid and hydrogen peroxide in a hot-water bath. The metals were extracted in diisobutyl ketone (DIBK) in the presence of ascorbic acid and potassium iodide. The DIBK phase was then aspirated directly into the plasma and element concentrations were determined simultaneously with a multichannel ICP instrument.

### MINERALOGICAL ANALYSIS

The nonmagnetic fraction of the heavy-mineral-concentrate samples contains sulfide minerals, gold, and some nonmagnetic oxides and silicates. Mineral identifications were made with a binocular microscope, recording the amounts of particular minerals in the following way: class 1, less than 1 percent; class 2, 1–5 percent; class 3, 5–20 percent; class 4, 20–50 percent; and class 5, greater than 50 percent. If a particular mineral was not observed, an "N" was recorded. This approach was used to identify the general abundance of minerals in the concentrates that were diagnostic of possible upstream mineral deposits. Cinnabar, gold, scheelite, and barite were the most useful for this study.

## RESULTS

Anomalous concentrations of elements and minerals used in this study were determined by identifying breaks in the frequency distribution of each data set, usually between the 90th and 98th percentiles. Anomalous concentrations were also based on background concentrations of various lithologies in the Iditarod quadrangle (McGimsey and others, 1988), where rock types are similar to those exposed in the Horn Mountains area. Table 1 summarizes data used in this report and selected anomalous concentrations. Some elements and minerals were not included in table 1 because they were not considered pathfinders for metallic mineral resources in this study area, or because no samples contained anomalous values for that element or mineral.

Cinnabar is common in the heavy-mineral-concentrate samples; 56 percent of the concentrates contain microscopically visible cinnabar. Heavy-mineral-concentrate samples containing greater than 1 percent cinnabar are considered diagnostic of possible upstream mineralized areas, and all of these samples cluster in specific areas considered favorable for epithermal Hg-rich deposits. Most samples with less than 1 percent cinnabar are found as single-site anomalies that are difficult to evaluate; however, a few of these samples help delineate areas favorable for Hg-rich deposits when samples from these areas also contain element anomalies typical of this deposit type.

## INTERPRETATION

### AREAS FAVORABLE FOR POLYMETALLIC VEIN DEPOSITS

Two areas surrounding the Horn Mountains are favorable for polymetallic vein deposits (fig. 3). Delineation of these areas is based on bedrock geology and geochemically or mineralogically anomalous stream-sediment or heavy-mineral-concentrate samples.

#### AREA 1

Area 1 is located in the southern Horn Mountains (fig. 3), where mafic to felsic volcanic rocks and sedimentary rocks of the Kuskokwim Group are cut by intermediate to felsic intrusions of the Horn Mountains stock (fig. 2). Stream-sediment samples collected in this area contain as much as 0.70 ppm Au, 0.68 ppm Ag, 120 ppm Cu, 54 ppm Pb, 370 ppm As, 35 ppm Sb, 0.81 ppm Hg, 16 ppm W, 1.9 ppm Cd, 150 ppm B, and 0.2 ppm Te. Heavy-mineral concentrates collected in area 1 contain as much as 30 ppm Au, 15 ppm Ag, 2,000 ppm Pb, 300 ppm Sb, 1,000 ppm Bi, 7,000 ppm Ba, and 700 ppm W, and several contain microscopically visible gold, scheelite, and barite.

This area is consistent with an upstream polymetallic vein occurrence found near the headwaters of Whitewing Valley (Bundtzen and others, 1993); additional similar undiscovered veins are possible in this area.

#### AREA 2

A geochemical anomaly on the northern side of the Horn Mountains includes several samples collected from tributaries of Getmuna and Jungjuk Creeks (fig. 3). In area 2, intermediate to felsic intrusions of the Horn Mountains stock cut mafic to felsic volcanic rocks (fig. 2). Stream-sediment samples collected in the area contain as much as 0.026 ppm Au, 0.95 ppm Ag, 290 ppm As, 57 ppm Sb, 4.0 ppm Hg, 5 ppm W, 57 ppm Pb, 6.4 ppm Bi, 1.5 ppm Cd, 200 ppm B, and 0.6 ppm Te; heavy-mineral-concentrate samples contain as much as 30 ppm Au, 5 ppm Ag, 1,500 ppm Bi, 500 ppm Pb, 200 ppm Sb, 1,000 ppm W, 1,000 ppm B, and 1 percent scheelite.

Two polymetallic vein occurrences are known in area 2 (Bundtzen and others, 1993) along Getmuna and Jungjuk Creeks (fig. 3). With the exception of Pb, base-metal anomalies are lacking in samples collected from area 2. However, as previously mentioned, base-metal anomalies in samples collected around volcanoplutonic complexes are sometimes inconsistent with the base-metal-sulfide-bearing nature of known polymetallic vein deposits. Although base-metal anomalies are not predominant, area 2 is considered favorable for polymetallic vein deposits on the basis of other geochemical anomalies and bedrock geology consistent with areas where polymetallic veins have been recognized.

### AREAS FAVORABLE FOR EPITHERMAL MERCURY-RICH VEIN DEPOSITS

Data from the Horn Mountains area suggest that eight areas are favorable for epithermal mercury-rich vein deposits. Lode deposits of this type are not known in these areas, but geochemical anomalies in samples from these areas and rocks that host known epithermal Hg-rich vein deposits in southwest Alaska are similar to that in these eight areas.

#### AREA 3

Four sample sites delineate area 3 on the western side of the Horn Mountains (fig. 3). Bedrock geology in this area consists of mafic to felsic volcanic rocks and minor sedimentary rocks of the Kuskokwim Group that are adjacent to the Horn Mountains pluton (fig. 2). Anomalous stream-sediment samples contain as much as 1.7 ppm Hg, 120 ppm As, and 7 ppm W; a heavy-mineral-concentrate sample contains 500 ppm Au, 20 ppm Ag, microscopically

Table 1. Summary of selected stream-sediment and heavy-mineral-concentrate geochemical data

[AAS, atomic absorption spectrophotometry; ICP, inductively coupled plasma-atomic emission spectroscopy; VS, visible spectrophotometry; SQS, semiquantitative emission spectrography; MIN, mineralogical analysis; N, not detected at concentration shown; L, detected but less than concentration shown; G, greater than concentration shown; —, not applicable; <, less than. All concentrations shown in parts per million (ppm)]

	Detection ratio <sup>1</sup>	N <sup>2</sup>	L <sup>3</sup>	G <sup>4</sup>	Minimum concentration	Percentile concentrations				Maximum concentration	Selected anomalies <sup>5</sup>
						50th	90th	95th	98th		
Stream sediments											
Au-AAS .....	0.22	96	11	0	0.002N	0.002N	0.010	0.027	0.13	0.70	0.010
Hg-AAS .....	1.00	0	0	0	.02	.12	1.1	2.3	4.8	8.0	.75
Ag-ICP .....	.30	96	0	0	.067N	.067N	.15	.25	.56	.95	.5
As-ICP .....	.96	6	0	0	.67N	8.3	135	215	315	370	50
Cu-ICP .....	1.00	0	0	0	5.8	14	25	34	62	120	100
Pb-ICP .....	1.00	0	0	0	3.6	8.0	15	23	44	57	50
Sb-ICP .....	.54	64	0	0	.67N	.74	12	26	35	57	10
Bi-ICP .....	.11	123	0	0	.67N	.67N	.71	1.7	3.1	6.4	2.0
Cd-ICP .....	1.00	0	0	0	.075	.15	.42	.65	.81	1.9	1.0
Ba-SQS .....	1.00	0	0	0	200	500	700	700	1,000	2,000	3,000
B-SQS .....	.62	15	38	0	10N	10	70	100	150	200	150
W-VS .....	.96	5	0	0	1.0N	2.0	4.0	5.0	7.0	16	5.0
Te-AAS .....	.23	106	0	0	.05N	.05N	.10	.20	.25	.60	.20
Concentrates											
Au-SQS .....	.04	130	2	0	20N	20N	20N	20N	20	500	20
Ag-SQS .....	.04	131	1	0	1N	1N	1N	1N	3	20	3
Sb-SQS .....	.03	130	3	0	200N	200N	200N	200N	200	300	200
Pb-SQS .....	.15	85	31	0	20N	20N	20	50	300	2,000	200
Zn-SQS .....	.02	135	0	0	500N	500N	500N	500N	500N	700	700
Bi-SQS .....	.10	123	0	0	20N	20N	200N	200	700	1,500	200
Sn-SQS .....	.34	80	11	0	20N	20N	300	500	1,000	1,500	500
W-SQS .....	.10	115	8	0	50N	50N	50L	100	500	1,000	50
Ba-SQS .....	.99	0	0	2	50	300	2,000	3,000	10,000	10,000G	5,000
B-SQS .....	.45	48	27	0	20N	20L	50	70	150	1,000	1,000
Gold-MIN .....	.04	132	—	—	N	N	N	N	N	1%	Gold <sup>6</sup>
Cinnabar-MIN ...	.55	61	—	—	N	< 1%	< 1%	1–5%	5–20%	20–50%	1–5%
Scheelite-MIN ...	.18	113	—	—	N	N	< 1%	< 1%	< 1%	1–5%	Scheelite <sup>6</sup>
Barite-MIN .....	.31	95	—	—	N	N	< 1%	< 1%	1–5%	1–5%	Barite <sup>6</sup>

<sup>1</sup>Number of uncensored values (those not qualified with N, L, or G) divided by total number of samples analyzed.

<sup>2</sup>Number of samples in which concentrations could not be detected at lower limit of determination.

<sup>3</sup>Number of samples in which concentrations were reported as observable but less than lower limit of determination.

<sup>4</sup>Number of samples in which concentrations were reported as observable but greater than upper limit of determination.

<sup>5</sup>Anomalous concentrations were selected by identifying breaks in frequency distribution of each data set.

<sup>6</sup>Any amount of visible gold, scheelite, or barite in heavy-mineral-concentrate samples is considered anomalous.

visible gold, and two concentrates contain less than 1 percent cinnabar. The designation of area 3 as favorable for epithermal Hg-rich vein deposits is somewhat uncertain. Although the geochemical association of Hg, As, Au, and Ag is similar to many epithermal Hg-rich vein deposits in the region, anomalous W in stream-sediment samples and microscopically visible gold in heavy-mineral concentrates are less commonly associated with this deposit type. However, anomalous W has been noted in cinnabar-rich vein samples from the Iditarod quadrangle (McGimsey and others, 1988) and geochemically anomalous gold or native gold has also been noted in cinnabar-rich vein samples from southwestern Alaska (Hawley and others, 1969; Clark and Sorg, 1971; Gray and others, 1990; Frost and

others, 1992). It is unlikely that area 3 is the same locality as the placer scheelite occurrence from the western side of the Horn Mountains (Cady and others, 1955) because heavy-mineral-concentrate samples collected in area 3 did not contain scheelite.

#### AREA 4

Area 4 is defined primarily by anomalous cinnabar in heavy-mineral-concentrate samples collected from Little, Getmuna, and Montana Creeks (fig. 3). Sedimentary rocks of the Kuskokwim Group predominate in the area, but mafic to felsic volcanic rocks, and granite porphyry intrusions also crop out (fig. 2). Mafic to felsic dikes cut

sedimentary rocks of the Kuskokwim Group near the headwaters of Getmuna Creek. Heavy-mineral-concentrate samples collected in area 4 contain as much as 20 percent cinnabar and 1 percent scheelite. In addition, one stream-sediment sample contains 0.100 ppm Au and 79 ppm As. As discussed above, minor placer gold and cinnabar has been reported on Little Creek (Cady and others, 1955), but no lode deposits are known in area 4. Scheelite is not typically associated with epithermal mercury-rich deposits, but is found with cinnabar in veins in the Flat area (Bundtzen and others, 1992); placer cinnabar and scheelite are found together in concentrates collected from streams in the Flat, Moore Creek, Takotna Mountain, and Candle areas (Bundtzen and others, 1988a). Data presented here suggest that the area is favorable for mercury-rich mineral deposits and includes portions of Montana and Getmuna Creeks, as well as Little Creek, as delineated on figure 3.

#### AREA 5

Samples with anomalous cinnabar and Hg collected from tributaries of the Iditarod and Kolmakof Rivers define area 5. Rocks in the area consist predominantly of sedimentary rocks of the Kuskokwim Group, with minor exposures of mafic to felsic volcanic rocks and intermediate to mafic dikes. Stream-sediment samples contain as much as 3.4 ppm Hg, 22 ppm Sb, 72 ppm As, 0.028 ppm Au, and 0.3 ppm Te; heavy-mineral-concentrate samples contain as much as 20 percent cinnabar, 5 percent barite, 1 percent scheelite, 10,000 ppm Ba, and 700 ppm Zn. Anomalous Ba, barite, Zn, and Te in samples collected from area 5 are unusual associations for Hg-rich vein deposits, although sphalerite and anomalous Ba were reported from the Cinnabar Creek mine (Clark and Sorg, 1971). However, highly anomalous Hg, Sb, and As in stream-sediment samples and cinnabar in heavy-mineral-concentrate samples strongly suggest that the area is favorable for epithermal Hg-rich vein deposits.

#### AREA 6

Area 6 is a mercury anomaly defined by two sample sites on a small tributary on the eastern side of the Kolmakof River. Area 6 is underlain by sedimentary rocks of the Kuskokwim Group. Stream-sediment samples collected from these sites contain 5.6 and 0.75 ppm Hg, and the concentrates contain as much as 50 percent cinnabar.

#### AREA 7

Two sample sites on tributaries of Village Creek and another on a nearby tributary of the Kuskokwim River delineate area 7. Sedimentary rocks of the Kuskokwim Group predominate in the area, but mafic to intermediate

dikes cut the sedimentary rocks at one locality. Two stream-sediment samples collected from this area contain 3.4 and 1.2 ppm Hg, and one stream-sediment sample contains 0.012 ppm Au; one heavy-mineral-concentrate sample contains 1,500 ppm Sn, and two concentrates contain less than 1 percent microscopically visible scheelite. The stream-sediment samples are highly anomalous in Hg and suggest the area is favorable for epithermal Hg-rich vein deposits, although Sn and scheelite are not commonly associated with this deposit type.

#### AREA 8

A stream-sediment sample collected from a tributary of Getmuna Creek delineates area 8. Only sedimentary rocks of the Kuskokwim Group are found in this area. The stream-sediment sample collected from this site contains 6.7 ppm Hg, and the heavy-mineral-concentrate sample contains less than 1 percent cinnabar. Although this is a single-site anomaly, the stream-sediment sample is highly anomalous in Hg, suggesting that this drainage basin is favorable for epithermal Hg-rich vein deposits.

#### AREA 9

Area 9 is defined by a Hg-W anomaly. Mafic to felsic volcanic rocks underlie area 9. In this area, one stream-sediment sample contains 2.4 ppm Hg, a second contains 5 ppm W, and up to 1 percent cinnabar was found in the concentrate sample corresponding to the Hg stream-sediment anomaly. As discussed for area 3, W is only rarely associated with cinnabar in epithermal vein deposits, but is found in some cinnabar-rich vein deposits (McGimsey and others, 1988). The stream-sediment Hg anomaly indicates that the area is favorable for epithermal Hg-rich deposits.

#### AREA 10

A single stream-sediment sample containing anomalous Hg delineates area 10. Rocks in the area consist exclusively of mafic to felsic volcanic rocks. The stream-sediment sample contains 1.5 ppm Hg, and the heavy-mineral-concentrate sample collected from this site contains less than 1 percent cinnabar.

### UNCLASSIFIED ANOMALIES

#### AREA 11

A single-site gold anomaly is found on a small tributary of the Iditarod River. Lithologies in this area are poorly known because the terrain is primarily low and swampy; however, small highly weathered pebbles of sedimentary rock were found at this site, suggesting that the



area is underlain by sedimentary rocks of the Kuskokwim Group. The heavy-mineral-concentrate sample collected from this site contains several grains of microscopically visible gold, but gold was not detected analytically in either the stream-sediment or concentrate sample. The significance of this single-site placer gold anomaly is poorly defined.

#### AREA 12

Samples collected from unnamed tributaries of the Kuskokwim River delineate area 12. Sedimentary rocks of the Kuskokwim Group are the only bedrock in the area. In this area, two stream-sediment samples contain 0.018 and 0.012 ppm Au; heavy-mineral concentrates contain up to 1,000 ppm Sn, 10,000 ppm Ba, 200 ppm Pb, and microscopically visible gold, scheelite, and barite. The geochemical anomalies of Au, Sn, Ba, and Pb, as well as the presence of gold, scheelite, and barite in heavy-mineral-concentrates, are perhaps most similar to those in the Horn Mountains (areas 1 and 2). This anomaly is enigmatic because the geology is inconsistent with the anomaly. The data suggest that poorly exposed or concealed intrusive rocks may be present in area 12, some of which may be mineralized. Another possibility is that the anomaly is of glacial derivation from the nearby Horn Mountains.

#### CONCLUSIONS

The reconnaissance geochemical study of the Horn Mountains area identified 12 geochemically anomalous areas. Two of these areas are considered favorable for polymetallic vein deposits, eight areas are interpreted as being favorable for epithermal mercury-rich vein deposits, and two areas are unclassified. The two areas favorable for polymetallic vein deposits are found within or around the Horn Mountains where intermediate to felsic intrusions cut mafic to felsic volcanic rocks and sedimentary rocks of the Kuskokwim Group. Stream-sediment samples collected in these areas are anomalous in Au, Ag, As, Cu, Pb, Hg, Sb, W, Cd, Bi, B, or Te; heavy-mineral concentrates are anomalous in Au, Ag, Pb, Sb, W, Bi, Ba, or B, and contain microscopically visible gold, scheelite, or barite. The Horn Mountains are similar geologically and geochemically to other areas in southwestern Alaska such as the Russian and Beaver Mountains, where base-metal-sulfide-, sulfosalt-, and gold-bearing polymetallic vein deposits are known. Polymetallic vein lodes are known in the Horn Mountains, and the geochemical anomalies surround these occurrences.

Eight areas are designated as favorable for epithermal mercury-rich vein deposits. Cretaceous sedimentary rocks of the Kuskokwim Group are most common in these areas,

but Late Cretaceous and Tertiary mafic to felsic volcanic rocks and intrusions are found locally. Anomalous concentrations of Hg in stream-sediment samples and cinnabar in heavy-mineral-concentrate samples are most consistent in these areas. Stream-sediment samples containing anomalous Sb, As, Au, W, or Te, and heavy-mineral-concentrate samples containing anomalous Au, Ag, Ba, Zn, or Sn, and microscopically visible gold, scheelite, or barite are less consistently found in these areas. Numerous epithermal mercury-rich vein deposits are found throughout southwestern Alaska in areas with similar geology and geochemistry, suggesting that undiscovered deposits of this type are possible in the areas delineated.

Two additional areas are delineated in the study. One area is a single-site placer gold occurrence on a tributary of the Iditarod River. In the final area, stream-sediment samples are anomalous in Au, whereas heavy-mineral-concentrate samples contain anomalous Pb, Sn, Ba, and microscopically visible gold, scheelite, and barite. Data are presently insufficient to classify these two deposits.

*Acknowledgments.*—The authors would like to thank Phil Hageman, Bruce Roushey, Craig Motooka, and Jerry Motooka for chemical analyses; Danny Abrams for sample preparation; and Jimmy Carter Borden for assistance with sample collection.

#### REFERENCES CITED

- Bennett, G.J., Gray, J.E., and Taylor, C.D., 1988, Mineralogy and sample locality map of the nonmagnetic, heavy-mineral-concentrate samples, Iditarod quadrangle, Alaska: U.S. Geological Survey Open-File Report 88-32, 37 p., 1 plate, scale 1:250,000.
- Box, S.E., Moll-Stalcup, E.J., Frost, T.P., and Murphy, J.R., in press, Preliminary geologic map of the Bethel and southern part of the Russian Mission 1:250,000 quadrangles, Alaska: U.S. Geological Survey Miscellaneous Field Studies Map 2226-A, scale 1:250,000.
- Bull, K.F., and Bundtzen, T.K., 1987, Greisen and vein Au-W mineralization of the Black Creek stock, the Flat area, west-central Alaska: Geological Society of America Abstracts with Programs, v. 19, p. 362.
- Bundtzen, T.K., Cox, B.C., and Veach, N.C., 1988a, Heavy mineral provenance studies in the Iditarod and Innoko districts, western Alaska, in Process Mineralogy VII: Metallurgical Society, SME/AIME joint meeting, Denver, Colorado, proceedings, p. 221-245.
- Bundtzen, T.K., and Gilbert, W.G., 1983, Outline of geology and mineral resources of upper Kuskokwim region, Alaska: Journal of the Alaska Geological Society, v. 3, p. 101-119.
- Bundtzen, T.K., Laird, G.M., Harris, B.E., Kline, J.T., and Miller, M.L., 1993, Geologic map of Sleetmute C-7, D-7, C-8, and D-8 quadrangles, Horn Mountains area, southwestern Alaska: Alaska Division of Geological and Geophysical Surveys Public-Data File 93-47, 1 plate, scale 1:63,360.
- Bundtzen, T.K., and Laird, G.M., 1982, Geological map of the

- Iditarod D-2 and eastern D-3 quadrangles, Alaska: Alaska Division of Geological and Geophysical Surveys Geologic Report 72, 1 plate, scale 1:63,360.
- 1991, Geology and mineral resources of the Russian Mission C-1 quadrangle, southwest Alaska: Division of Geological and Geophysical Surveys Professional Report 109, 24 p.
- Bundtzen, T.K., Laird, G.M., and Lockwood, M.S., 1988b, Geologic map of the Iditarod C-3 quadrangle, Alaska: Alaska Division of Geological and Geophysical Surveys Professional Report 96, 13 p., 1 plate, scale 1:63,360.
- Bundtzen, T.K., Miller, M.L., Bull, K.F., and Laird, G.M., 1988c, Geology and mineral resources of the Iditarod mining district, Iditarod B-4 and B-5 quadrangles, westcentral Alaska: Alaska Division of Geological and Geophysical Surveys Public-data File 88-19, 44 p., 1 plate, scale 1:63,360.
- Bundtzen, T.K., Miller, M.L., Laird, G.M., and Bull, K.F., 1992, Geology and mineral resources of the Iditarod mining district, Iditarod B-4 and B-5 quadrangles, westcentral Alaska: Alaska Division of Geological and Geophysical Surveys Professional Report 97, 46 p.
- Cady, W.M., Wallace, R.E., Hoare, J.M., and Webber, E.J., 1955, The central Kuskokwim region, Alaska: U.S. Geological Survey Professional Paper 268, 132 p.
- Clark, A.L., and Sorg, D.H., 1971, Mineralogy and geochemistry of the Cinnabar Creek quicksilver mine, central Kuskokwim region, Alaska [abs.]: Geological Society of America Abstracts with Programs, v. 3, no. 2, p. 96-97.
- Decker, John, Robinson, M.S., Murphy, J.M., Reifensuhl, R.R., and Albanese, M.D., 1984, Geologic map of the Steetmute A-6 quadrangle: Alaska Division of Geological and Geophysical Surveys Report of Investigations 84-8, scale 1:40,000.
- Doherty, D.J., and Bergman, S.C., 1987, Late Cretaceous-early Tertiary calderas in western Alaska [abs.]: Geological Society of America Abstracts with Programs, v. 19, no. 7, p. 645.
- Frost, T.P., Bradley, L.A., O'Leary, R.M., and Motooka, J.M., 1992, Geochemical results and sample locality map for rock samples from the Bethel and southern part of the Russian Mission 1:250,000 quadrangles, Alaska: U.S. Geological Survey Open-File Report 92-316, 229 p.
- Gray, J.E., Arbogast, B.F., and Hudson, A.E., 1988, Geochemical results and sample locality map of the stream-sediment and nonmagnetic, heavy-mineral-concentrate samples for the Iditarod quadrangle, Alaska: U.S. Geological Survey Open-File Report 88-221, 69 p., 1 plate, scale 1:250,000.
- Gray, J.E., Frost, T.P., Goldfarb, R.J., and Detra, D.E., 1990, Gold associated with cinnabar- and stibnite-bearing deposits and mineral occurrences in the Kuskokwim River region, southwestern Alaska, in Goldfarb, R.J., Nash, T.J., and Stoeser, J.W., eds., *Geochemical studies in Alaska* by the U.S. Geological Survey, 1989: U.S. Geological Survey Bulletin 1950, p. D1-D6.
- Gray, J.E., Goldfarb, R.J., Detra, D.E., and Slaughter, K.E., 1991, Geochemistry and exploration criteria for epithermal cinnabar and stibnite vein deposits in the Kuskokwim River region, southwestern Alaska: *Journal of Geochemical Exploration*, v. 41, p. 1-24.
- Grimes, D.J., and Marranzino, A.P., 1968, Direct-current arc and alternating-current spark emission spectrographic field methods for the semiquantitative analysis of geological materials: U.S. Geological Survey Circular 591, 6 p.
- Hawley, C.C., Martinez, E.E., and Marinenko, J., 1969, Geochemical data on the south ore zone, White Mountain mine and on the gold content of other mercury ores, southwestern Alaska: U.S. Geological Survey Circular 615, p. 16-20.
- Hubert, A.E., and Chao, T.T., 1985, Determination of gold, indium, tellurium and thallium in the same sample digestion of geological materials by atomic-absorption spectroscopy and two-step solvent extraction: *Talanta*, v. 32, p. 383-387.
- Kennedy, K.R., and Crock, J.G., 1987, Determination of mercury in geological materials by continuous flow, cold-vapor, atomic-absorption spectrophotometry: *Analytical Letters*, v. 20, p. 899-908.
- MacKevett, E.M., Jr., and Berg, H.C., 1963, Geology of the Red Devil quicksilver mine, Alaska: U.S. Geological Survey Bulletin 1142-G, p. G1-G16.
- Maddren, A.G., 1915, Gold placers of the lower Kuskokwim, with a note on copper in the Russian Mountains, in Brooks, A.H., and others, *Mineral resources of Alaska—report on progress of investigations in 1914*: U.S. Geological Survey Bulletin 622, p. 292-360.
- McGimsey, R.G., Miller, M.L., and Arbogast, B.F., 1988, Paper version of analytical results, and sample locality map for rock samples from the Iditarod quadrangle, Alaska: U.S. Geological Survey Open-File Report 88-421-A, 110 p., 1 plate, scale 1:250,000.
- Meier, A.L., 1980, Flameless atomic-absorption determination of gold in geological materials: *Journal of Geochemical Exploration*, v. 13, p. 77-85.
- Mertie, J.B., Jr., 1936, Mineral deposits of the Ruby-Kuskokwim region, Alaska: U.S. Geological Survey Bulletin 864-C, p. 115-247.
- Miller, M.L., Belkin, H.E., Blodgett, R.B., Bundtzen, T.K., Cady, J.W., Goldfarb, R.J., Gray, J.E., McGimsey, R.G., and Simpson, S.L., 1989, Pre-field study and mineral resource assessment of the Steetmute quadrangle, southwestern Alaska: U.S. Geological Survey Open-File Report 89-363, 115 p., 3 plates, scale 1:250,000.
- Miller, M.L., and Bundtzen, T.K., 1992, Geologic history of the post-accretionary rocks, Iditarod quadrangle, west-central Alaska [abs.]: Geological Society of America Abstracts with Programs, v. 24, no. 5, p. 71.
- 1993, Geologic map of the Iditarod quadrangle, Alaska: U.S. Geological Survey Miscellaneous Field Studies Map MF-2219-A, 1 plate, scale 1:250,000.
- Motooka, J.M., 1988, An exploration geochemical technique for the determination of preconcentrated organometallic halides by ICP-AES: *Applied Spectroscopy*, v. 42, no. 7, p. 1293-1296.
- Reifensuhl, R.R., Robinson, M.S., Smith, T.E., Albanese, M.D., and Allegro, G.A., 1984, Geologic map of the Steetmute B-6 quadrangle, Alaska: Alaska Division of Geological and Geophysical Surveys Report of Investigations 84-12, scale 1:40,000.
- Robinson, M.S., and Decker, John, 1986, Preliminary age dates and analytical data for selected igneous rocks from the

- Sleetmute, Russian Mission, Taylor Mountains, and Bethel quadrangles, southwestern Alaska: Alaska Division of Geological and Geophysical Surveys Public-Data File 86-99, 9 p.
- Sainsbury, C.L., and MacKevett, E.M., Jr., 1965, Quicksilver deposits of southwestern Alaska: U.S. Geological Survey Bulletin 1187, 89 p.
- Theodorakos, P.M., Borden, J.C., Bullock, J.H., Jr., Gray, J.E., and Hageman, P.L., 1992, Analytical data and sample locality map of stream-sediment and heavy-mineral-concentrate samples collected from the Horn Mountains area, Sleetmute quadrangle, southwest Alaska: U.S. Geological Survey Open-File Report 92-708-A, 36 p.
- Welsch, E.P., 1983, A rapid geochemical spectrophotometric determination of tungsten with dithiol: *Talanta*, v. 30, p. 876-878.
- Reviewers: Karen D. Kelley and Richard J. Goldfarb

# GOLD AND CINNABAR IN HEAVY-MINERAL CONCENTRATES FROM STREAM-SEDIMENT SAMPLES COLLECTED FROM THE WESTERN HALF OF THE LIME HILLS 1° × 3° QUADRANGLE, ALASKA

By Robert G. Eppinger

## ABSTRACT

Geochemical sampling in the western half of the Lime Hills 1° × 3° quadrangle has revealed the presence of visible gold and cinnabar in numerous heavy-mineral-concentrate samples. This widespread fine-grained gold has not been reported previously. Further, there are no mines or prospects in the area. The area is underlain predominantly by clastic rocks of the post-accretionary Cretaceous Kuskokwim Group and by Paleozoic clastic and carbonate rocks of the Dillinger, Mystic, and Nixon Fork terranes.

Gold was identified in 100 of the 396 heavy-mineral concentrate samples collected. Megascopic gold was observed in 30 samples, the largest grain being about 1 mm in diameter. Gold grains usually are less than 0.3 mm in the longest dimension. The grains are commonly flat and rounded to subrounded, and less frequently are elongate. Less commonly, gold grains have delicate shapes with angular or jagged edges, embayments, and protrusions. Euhedral gold grains were not observed. The variations in gold grain morphology may indicate distal and local sources for the gold.

Anhydrous cinnabar was identified in 45 of the concentrate samples. Megascopic grains of cinnabar rarely were observed. Cinnabar grain size typically is in the range of a few tenths of a millimeter.

Two distinct sample populations are evident. Samples in the northern half of the study area contain cinnabar ± gold. This area is underlain almost entirely by carbonate and clastic rocks of the Dillinger terrane. Diorite, granite, granite porphyry, and quartz porphyry are common in alluvium, but rare in outcrop in the area. The cinnabar ± gold in concentrates may reflect small epithermal cinnabar- and stibnite-bearing vein deposits such as those found elsewhere throughout southwestern Alaska.

Samples in the southern half of the study area contain gold, but generally lack cinnabar. The southern area is underlain by platform carbonate rocks of the Nixon Fork terrane and marine clastic rocks of the Kuskokwim Group. As in the northern part of the study area, igneous rocks are

common in alluvium, but rare in outcrop. The presence of gold and paucity of cinnabar in concentrates in the southern area suggest an origin different from that of the cinnabar ± gold in concentrates to the north.

## INTRODUCTION

A geochemical survey of the Lime Hills 1° × 3° quadrangle is in progress by the U.S. Geological Survey, as part of the Alaska Mineral Resource Assessment Program (AMRAP). Reconnaissance sampling in the western half of the quadrangle was undertaken during the summers of 1991 and 1992 (fig. 1). This sampling has revealed visible gold and cinnabar in numerous heavy-mineral-concentrate samples collected from stream sediment. There are no published reports of widespread gold occurring in this area. Geochemical studies of the samples collected in the study area are in progress.

Previous work in the quadrangle includes geologic mapping, stream-sediment geochemical surveys, and geochronologic studies in the Alaska Range (Reed and Elliot, 1970; Reed and Lanphere, 1969, 1972, 1973; and Lanphere and Reed, 1985) and mapping and geochemical studies in the northwestern part of the quadrangle (Gilbert, 1981). Geochemical studies of the quadrangle were undertaken during the National Uranium Resource Evaluation (NURE) program (Jacobson and others, 1979; Hinderman, 1982). Geochemical data for samples collected in the eastern half of the Lime Hills quadrangle as part of the AMRAP program are reported in Allen and others (1990), Allen and Slaughter (1990), Malcolm and others (1990), and Motooka and others (1990). These geochemical data were used in an interpretive report on gold anomalies and occurrences in the eastern half of the Lime Hills quadrangle (Allen, 1990).

Terrain in the western half of the Lime Hills quadrangle consists dominantly of heavily vegetated, swampy lowlands with elevations of 300 m or less. Interspersed among these areas are small, rolling, mountainous areas,

the largest found to the south around Cairn Mountain (1,158 m) and to the north in the Lyman Hills, with elevations above 1,200 m.

## GEOLOGY

The geology of the western half of the Lime Hills quadrangle has not been studied in detail. Descriptions and lithotectonic terrane designations used here are taken largely from Wallace and others (1989) and from Jones

and others (1987). The western half of the Lime Hills quadrangle is underlain by three lithotectonic terranes and by the Kuskokwim Group of sedimentary rocks (fig. 2). These three terranes, the Nixon Fork, Mystic, and Dillinger, have recently been combined as separate parts of the Farewell terrane (Decker and others, in press).

The Nixon Fork terrane is found as a thin northeast-trending belt of isolated outcrops in the southwestern quadrant of the Lime Hills quadrangle. The Nixon Fork terrane in the quadrangle is fault-bounded and composed of thick Cambrian to Middle Devonian calcareous

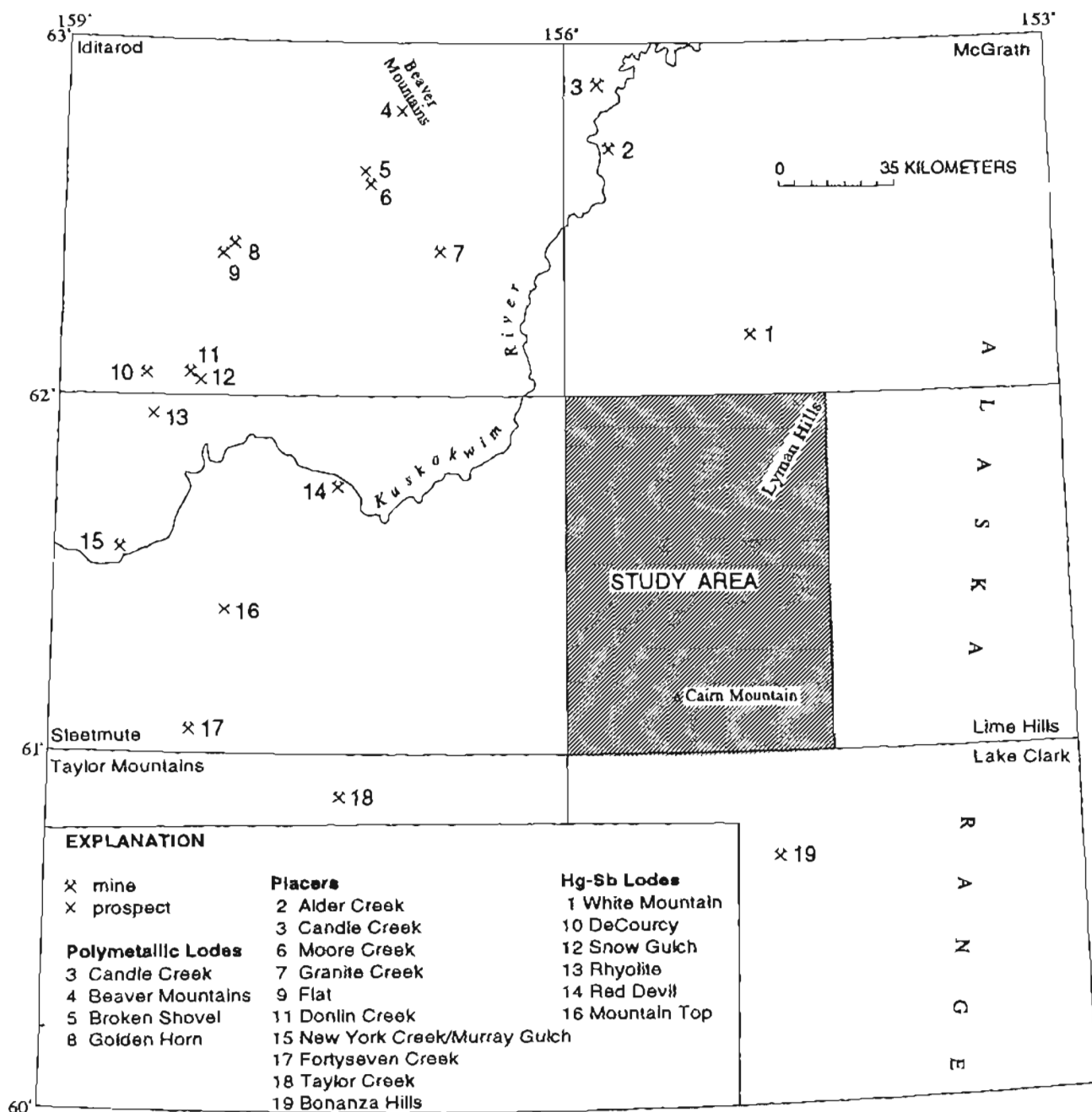


Figure 1. Location of study area and selected mines and prospects in adjacent quadrangles.

mudstone and limestone, representing carbonate platform deposits (Churkin and others, 1984; Wallace and others, 1989).

Rocks of the Mystic terrane are found in the west-central and north-central parts of the Lime Hills quadrangle as isolated outcrops of Upper Devonian to Permian clastic rocks, carbonate rocks, and chert (Wallace and others, 1989; Gilbert and others, 1990). These rocks represent shallow-water marine to nonmarine depositional environments (Gilbert and Bundtzen, 1984).

The Dillinger terrane covers an extensive area of the northern and northwestern parts of the Lime Hills quadrangle and includes graptolitic shale, basinal carbonate rocks, calcareous sandstone, and minor chert and conglomerate. Rocks of the Dillinger terrane are Cambrian to Middle Devonian in age (Wallace and others, 1989). Rocks of the Dillinger terrane represent a shallowing-upward regime that includes basinal, fan turbidite, and foreslope depositional environments (Gilbert and Bundtzen, 1984).

Sandstone, shale, and conglomerate of the Cretaceous Kuskokwim Group (Cady and others, 1955) are found throughout much of the southwestern part of the Lime Hills quadrangle, and in small outcrops in the northwestern corner of the quadrangle. This post-accretionary sequence, more than 10 km thick, is composed primarily of deep-marine turbidites, with subordinate shallow-marine and fluvial rocks, and has been deformed generally into broad open folds (Cady and others, 1955; Decker and others, in press; Moore and Wallace, 1985).

Igneous rocks in the western half of the Lime Hills quadrangle consist of Tertiary dikes of andesitic to basaltic composition and porphyritic to equigranular texture, found in the northern part of the study area (Gamble and others, 1988); small bodies of Tertiary(?) sericitically altered quartz porphyry (B.L. Reed, written commun., 1990), found in the central part of the study area; and Triassic to Jurassic pillow basalts capping rocks of the Mystic terrane (Wallace and others, 1989), found in the north-central part of the study area (Gamble and others, 1988). A small body of Tertiary(?) intrusive rhyolite to fine-grained granite was mapped south of Cairn Mountain near the southern edge of the quadrangle (John Decker, 1984, unpub. mapping). Extensive bodies of syn- to post-accretionary, Cretaceous to Tertiary, mafic to felsic, plutonic and volcanic rocks of the Alaska Range batholith crop out immediately east of the study area in the eastern half of the Lime Hills quadrangle and throughout the Alaska Range (Gamble and others, 1988).

Unconsolidated Quaternary deposits are extensive in the western half of the Lime Hills quadrangle and severely limit bedrock exposure in many areas. Glacial features are common in some areas. Glacial deposits in the area have not been mapped, but are evident on aerial photographs (B.M. Gamble, oral commun., 1992).

## MINERAL DEPOSITS AND OCCURRENCES

There are no mines or identified mineral resources in the Lime Hills quadrangle. Gamble and others (1988) listed 67 mineral occurrences in the quadrangle. Four of these are within the study area, and are based on isolated rock samples collected in the northern Lyman Hills (fig. 2). Occurrence 1 is a NURE rock sample containing anomalous As, Mo, Fe, Ni, Sn, and U (Hinderman, 1982). Occurrence 2 is vaguely described as a "deposit around spring," where two rock samples contain anomalous Ag, Zn, and Mo (Gilbert, 1981). During the present study, the area around these two occurrences was explored. Near occurrence 1 were thin quartz-pyrite veinlets up to 0.6 cm thick along a shear zone cutting cleaved, iron-oxide-stained, black, shaly, well-indurated argillite. Occurrence 3 is a gossan sample with anomalous Ag, Cu, and Zn, and occurrence 4 is a malachite-stained diorite dike with anomalous Au, Cu, and Ni (Gilbert, 1981). An additional occurrence is found on a hill called Center, in the southeast quadrant of the study area, where quartz veins cut sericitically altered quartz porphyry. Quartz float and vein quartz from outcrop contain anomalous Ag, As, and Sb (B.L. Reed, written commun., 1991).

Additional occurrences listed by Gamble and others (1988) are east of the study area, scattered throughout the Alaska Range in the eastern half of the Lime Hills quadrangle. These occurrences typically are rock samples containing pyrite, base-metal sulfides, or molybdenite, or having geochemical anomalies for Cu, Pb, Zn, Mo, Au, and Ag. Many of the occurrences are in quartz veins, and most are associated spatially with plutonic rocks of intermediate to felsic composition (Gamble and others, 1988). Additional gold anomalies and gold-bearing vein occurrences, generally in the northeastern part of the quadrangle, were described by Allen (1990).

While no mineral deposits are found in the Lime Hills quadrangle, many are found in adjacent quadrangles, in rocks correlative with those exposed in the study area (fig. 1). Numerous placer gold deposits and occurrences are found in contiguous quadrangles, and these contain varied amounts of cinnabar, scheelite, and locally cassiterite (Eberlein and others, 1977; Bundtzen and others, 1988). Productive gold placers include Flat, Ganes Creek, Moore Creek, Granite Creek, and Donlin Creek in the Iditarod quadrangle (Mertie, 1936; Cady and others, 1955; Bundtzen and others, 1986); New York Creek/Murray Gulch and Fortyseven Creek in the Sleetmute quadrangle (Cady and others, 1955); Alder Creek and Candle Creek in the McGrath quadrangle (Mertie, 1936; Eberlein and others, 1977); Taylor Creek in the Taylor Mountains quadrangle (Cady and others, 1955); and Bonanza Hills in the Lake Clark quadrangle (Nelson and others, 1985).










Epithermal cinnabar- and stibnite-bearing vein deposits and occurrences are found scattered over much of southwestern Alaska (Sainsbury and MacKevett, 1965). Selected deposits near the study area include those at the Red Devil mine (Hg, Sb), Mountain Top (Hg, Sb), and Rhyolite (Hg) in the Sleetmute quadrangle; the White Mountain mine (Hg) in the McGrath quadrangle; and the DeCourcy mine (Hg, Sb) and Snow Gulch (Sb) areas in the Iditarod quadrangle (Cady and others, 1955; Sainsbury and MacKevett, 1965; Sorg and Estlund, 1972). These deposits are hosted primarily in sedimentary rocks of the Kuskokwim Group or in igneous rocks intruding rocks of the Kuskokwim Group, except for the White Mountain mine, which is in shale and limestone of the Holitna Group, in the Dillinger terrane. A common spatial association is found between cinnabar-stibnite deposits and Late Cretaceous to Tertiary dikes, sills, and small stocks of mafic to felsic composition. Cinnabar and stibnite are the dominant ore minerals, with lesser amounts of realgar, orpiment, native mercury, pyrite, and gold (Sainsbury and

MacKevett, 1965; Gray and others, 1990). Gangue minerals include quartz, carbonate, dickite, limonite, and hematite.






A variety of polymetallic vein deposits are found in southwestern Alaska. While many of the deposits have their own unique characteristics, several features are common to all. These features include (1) a spatial association with volcanoplutonic complexes, (2) intrusions of monzonitic composition, (3) veins, breccias, and stockworks that occupy joints, faults, or shear zones, (4) mineralized veins in intermediate to felsic stocks and in the surrounding sedimentary and volcanic rocks, and (5) hornfels aureoles surrounding the stocks. Mineralogy of these deposits is varied and includes arsenopyrite, bismuthinite, bornite, cassiterite, chalcopyrite, galena, gold, marcasite, pyrite, scheelite, sphalerite, stephanite, tetrahedrite, and wolframite, in a gangue of quartz, tourmaline, axinite, and fluorite (Bundtzen and Gilbert, 1983; Bundtzen and Laird, 1982; Bundtzen and others, 1988; Miller and others, 1989). Polymetallic vein deposits include those in the Beaver Mountains, at the Golden Horn mine, and Broken

## EXPLANATION

## POST-ACCRETIONARY ROCKS

-  Alluvial, colluvial, and glacial deposits, undivided (Quaternary)
-  Quartz porphyry (Tertiary?)--Commonly sericitically altered quartz porphyry. Bodies crop out in central part of map area
-  Dikes (Tertiary?)--Porphyritic to equigranular, mafic to intermediate dikes. Dikes present in northern part of map area
-  Fine-grained granite (Tertiary?)--Granite body present in southern part of map area
-  Kuskokwim Group (Cretaceous)--Sandstone, shale, graywacke, and conglomerate. Conglomerate is most abundant in the Cairn Mountain and Sparrevohn areas. Chiefly marine basin and fan deposits

## ACCRETIONARY ROCKS

-  Pillow basalt, argillite, and chert (Jurassic to Triassic)--Pillow basalt interbedded with minor argillite and chert. Present in north-central part of map area  
Dillinger terrane
-  Limestone, sandstone, and shale (Devonian and Silurian)--Argillaceous limestone, calc-sandstone, and graptolitic shale. Slope to basinal deposits
-  Shale, siltstone, argillite, and limestone (Devonian to Cambrian)  
Nixon Fork terrane
-  Mudstone and carbonate rocks (Devonian and Silurian)--Calcareous mudstone and limestone algal reef complex. Carbonate platform deposits  
Mystic terrane
-  Limestone (Permian to Devonian)--Thick-bedded limestone. Open-marine shelf deposits

## Symbols

- Concentrate sample site
- ⊙ Sample containing rounded to subrounded gold
- ⊠ Sample containing angular, subangular, and delicate gold
- ✕ Sample containing cinnabar

For the above symbols, adjacent number is the number of grains observed. No number is shown for samples containing one grain. Numbers in italics are for cinnabar. M indicates at least one megascopic grain; no M indicates all grains are microscopic.

- Area discussed in text
- ◇<sub>2</sub> Mineral occurrence described in text
- △ Cultural feature as shown on USGS 1:250,000-scale topographic map of Lime Hills quadrangle
- ~ Contact, approximately located
- - - Fault, approximately located
- ~ River

Figure 2. Continued.

Shovel lode in the Iditarod quadrangle (Bundtzen and Gilbert, 1983; Bundtzen and others, 1988) and at Candle Creek in the McGrath area (Bundtzen and Gilbert, 1983).

## METHODS

Reconnaissance geochemical samples of the western half of the Lime Hills quadrangle include minus-80-mesh stream sediments collected from 427 sites, heavy-mineral concentrates from stream sediment (hereafter called concentrates) collected from 396 of these same sites, and 186 rock samples collected from alluvium, float, and outcrops throughout the area. Chemical analyses of these samples are not completed at the time of writing. Data used here are from hand-lens inspection of concentrates in the field and microscopic examination of selected samples. Gold data collected in the NURE program are also used.

Concentrates were collected whenever possible at stream-sediment sample sites. Sampling was confined generally to first- and second-order drainages in areas of adequate relief. Broad, swampy lowland areas were avoided. Thus, sampling density varies throughout the study area. When possible, samples were collected in areas likely to collect heavy minerals, such as behind boulders, on point bars, and along the inside of curves in the stream. Moderately coarse gravel was the preferred sample medium at these sites.

Concentrates were collected by filling a 36 cm (14 inch) gold pan with minus-10-mesh, active stream sediment. The approximate 7.25 kg sample was panned at the site until about 100 g of sample remained. The concentrate was swirled in the pan until a heavy mineral trail developed. This trail was examined with a 10 $\times$  hand lens for gross mineral content and specifically for gold and cinnabar. Numbers of grains of these minerals were recorded in the field notes. In the laboratory, selected samples were examined for their mineral content using a petrographic microscope under plain white and ultraviolet light. For selected samples, field and laboratory identifications of gold and cinnabar were verified by X-ray diffraction.

## DATA

The number of gold and cinnabar grains identified in concentrates and their locations are shown in figure 2. Only samples for which these minerals were identified with certainty are plotted. Uncertainties in identification of cinnabar and, to a lesser extent, gold occurred in a few instances when the grain size approached the limits of resolution with the hand lens.

Gold was identified in 100 of the 396 concentrate samples collected. Grain size for gold most commonly is microscopic. Megascopic gold, defined here as gold

visible with the unaided eye, was observed in 30 samples, and the largest grain was estimated in the field to be about 1 mm in diameter. Gold grains usually are less than 0.3 mm in the longest dimension.

Gold grain morphology varies, but grains most commonly are flat and rounded to subrounded. Spherical or equant grains are rare. Flat elongate gold grains commonly were observed under microscope, all less than 0.35 mm in the longest dimension. Measurements of elongate grains reveal that the length approximately is double the width. Less commonly, gold grains were seen with angular or jagged edges. Some gold grains have complex morphologies, such as thin protrusions and embayments, sometimes with sharp edges. These grains are termed delicate in this study. A small number of gold grains have embayments with angular cavities resembling molds, interpreted to be the result of interstitial gold precipitation around crystals that had been removed. Euhedral gold grains were not observed.

Cinnabar was identified in 45 of the concentrate samples. Megascopic grains of cinnabar rarely were seen. Cinnabar grain size typically is in the range of a few tenths of a millimeter, although quantitative measurements were not made. All of the cinnabar is anhedral, due no doubt to the relative softness and friable nature of the mineral. Further, the frequently observed dull luster of the cinnabar suggests a friable variety (Palache and others, 1946).

Gold geochemical data from 382 stream and pond sediments collected in the study area during the NURE program were evaluated and compared to the visual gold found in this study. NURE samples from the area were not analyzed for mercury. Gold, determined by neutron activation, was found at six widely scattered NURE sites, ranging from 0.06 to 0.12 parts per million. Three of the gold-bearing samples were collected far from outcrop, in flat, alluvium-covered areas not sampled during this study. However, the other three gold-bearing samples are from areas containing visible gold and cinnabar, as described below.

## DISCUSSION

Two distinct sample populations are evident in figure 2, roughly separated by the Swift River. To the north are samples in the Lyman Hills containing cinnabar  $\pm$  gold and to the south are samples typically containing gold without cinnabar. Within these two large areas are five smaller areas, shown in figure 2, which contain clusters of samples with multiple grains of gold or cinnabar. One of the areas contains abundant cinnabar plus gold, while the other four areas contain gold alone.

Cinnabar in the study area is most common in concentrates from the Lyman Hills. Cinnabar also was found in concentrates from the eastern part of the Lyman Hills by

Allen and Slaughter (1990). The Lyman Hills are underlain almost entirely by limestone, sandstone, and shale of the Dillinger terrane. Rocks observed in drainages and outcrops include locally calcareous siltstone and shale, limestone, and graywacke. Quartz and quartz-carbonate fragments are common in alluvium, but typically constitute less than 1 percent of the alluvium. These fragments commonly are vuggy, druse-lined, and banded, and are interpreted to be derived from quartz veins. Scant to abundant igneous rocks are common in alluvium and include diorite, granite, granite porphyry, and quartz porphyry. However, only one igneous rock outcrop, diorite, was seen in the area.

Area 1, along the Gagaryah River in the Lyman Hills (fig. 2), contains a cluster of five samples with the largest number of cinnabar grains in the study area. This area differs from most cinnabar-bearing drainages in the Lyman Hills, in that it also contains a large number of gold grains. Many of the gold grains are megascopic. Abundant cobbles of quartz porphyry were identified at four of the sites. However, bedrock was not found upstream of the sample sites. Nearby bedrock along the Gagaryah River, less than 1 km to the east, is a red- and orange-colored cliff of limestone with abundant iron-oxide-coated joints and shears.

Approximately 17 km north-northeast of area 1, a concentrate containing megascopic gold was collected. The flat, rounded gold grain, about 1 mm in diameter, was one of the largest found in the study. A nearby NURE sediment sample collected downstream and west of this site contained 0.12 ppm gold, the highest gold concentration in NURE samples from the western half of the quadrangle. Downstream and northwest of these sites are numerous cinnabar-bearing concentrate sample sites.

South of the Swift River is a large area containing gold-bearing concentrates (fig. 2). This area is underlain by limestone and calcareous mudstone of the Nixon Fork terrane along its western edge, and shale, sandstone, graywacke, and conglomerate of the Kuskokwim Group elsewhere. In most concentrates from the area, only a single grain of flat, rounded gold was observed. However, four clusters of samples contain multiple grains of megascopic gold. Two of these clusters contain gold grains exhibiting delicate morphologies, suggesting a relatively local source.

Area 2 is centered about a hill called Anchor, in the east-central part of the study area, and contains seven samples with gold. In five of these the gold is megascopic. Multiple grains of gold are found in four samples from the northern part of area 2. Further, gold in the northern part varies from subangular to angular. In the sample from which four gold grains were found, one of the grains is about 1 mm long and very delicate, having a sharp serrated texture along one edge. These features suggest that the gold from drainages in this area did not travel far. Alluvium from the northern part of area 2 consists of

well-indurated shale, green siltstone, minor granite boulders, and about 1 percent vuggy, drusy, banded vein quartz pebbles. The granite likely has been glacially transported from the Alaska Range to the east. Gray and white quartz stockwork with veins up to about 1 cm thick was observed cutting siltstone in cobbles. The veins locally are vuggy and brecciated, containing small gray vein quartz fragments and siltstone clasts floating in a quartz matrix. The fragments and clasts are rimmed by white quartz. Thus, repeated movement and quartz precipitation are implied. Ridges in the northern part of area 2 were traversed and rock samples were collected. Abundant quartz veins up to 5 cm thick cutting shale, sandstone, green hard siltstone, lesser conglomerate, and diorite were observed locally in float along the traverse. Fresh pyrite and rare red tourmaline were seen in one of the veins, although clots of iron-oxide (after pyrite?) were more common. A NURE sediment sample, collected southeast and downstream of drainages in area 2, contained 0.08 ppm gold.

Area 3 is located adjacent to the Stony River, centered about a hill called Only in the southeastern corner of the study area. Six of the seven concentrates from the area contain multiple grains of gold and three concentrates contain megascopic gold. Gold grains from one of the sites has sharp edges, from a second site has embayments and delicate features, and from a third site has an overall texture that suggests a mold. Alluvium in area 3 is dominantly dark gray to green shale, siltstone, and graywacke of the Kuskokwim Group. Traces to small amounts of quartz porphyry and fragments of vein quartz cutting siltstone were seen in alluvium at the three sites containing from three to five grains of gold. One site with two gold grains contains a small amount of aplitic granite cobbles. Volcanic rocks of intermediate composition and diorite were seen in minor amounts in alluvium at several sites. All the drainages contain from 5 to 30 percent leucocratic granite in alluvium. Glacial drift-mantled slopes paralleling the Stony River along the northwest side of area 3 suggest that most, possibly all, of the granite is derived from the Alaska Range to the east. Further mapping is necessary to determine whether other igneous rocks observed have a local source. Allen and Slaughter (1990) showed isolated gold anomalies in stream-sediment and concentrate samples several kilometers upstream of area 3 along the Stony River. However, it is unlikely that the gold seen here was transported along the Stony River, as the delicate features described above imply a short distance of transport.

Areas 4 and 5 are located north of Cairn Mountain and northwest of Sparrevohn Air Force Station, respectively. Each of these areas contains several concentrates with multiple grains of gold. Megascopic gold is found in three concentrates from each area. Unlike at areas 2 and 3, gold grains from these sites are well-rounded and flat, except for subrounded grains in area 5 at the site containing cinnabar. A NURE sediment sample collected from

the southwest edge of area 4 contained 0.07 ppm gold. Shale, siltstone, graywacke, and lesser conglomerate of the Kuskokwim Group are the predominant alluvium in the two areas. Minor quartz pebbles are common in alluvium. The quartz locally is vuggy and cuts siltstone in some of the larger pebbles. Granite and volcanic rocks of intermediate composition are present in varying amounts in alluvium from all of the drainages. Granite glacial erratics are present and till-mantled slopes are likely in both areas.

Conglomerate of the Kuskokwim Group is abundant in outcrop in areas 4 and 5, in the upper reaches of drainages. The conglomerates typically have round to locally angular clasts from 1 to 10 cm in diameter. Clast compositions include siltstone, sandstone, shale, graywacke, and clear to white, locally drusy, quartz pebbles. Vein quartz cutting the conglomerate was observed at one site. Two 9-kg bulk conglomerate samples were collected from each area. These samples were ground coarsely and panned in the laboratory. No gold was found during visual examination of the panned samples.

## CONCLUSIONS

Concentrate samples from the large area in the Lyman Hills containing cinnabar  $\pm$  gold in concentrates may reflect small epithermal cinnabar- and stibnite-bearing vein deposits such as those found elsewhere throughout the Kuskokwim basin of southwestern Alaska. The White Mountain mine, in the Lyman Hills about 30 km to the north of the study area, is hosted in similar shale and limestone of the Dillingter terrane and may provide the closest analog.

The general abundance of gold and paucity of cinnabar in concentrates south of the Swift River suggest a source different from that of the cinnabar  $\pm$  gold in concentrates to the north. Variations in the quantity, size, and morphology of the gold grains may reflect multiple sources.

The presence of such widespread generally fine-grained gold is paradoxical. The present data preclude the determination of sources and origins of the gold. It is unlikely that such widespread fine gold could be the result solely of glacial or fluvial transport from the Alaska Range to the east. If this were the case, one would expect many more gold occurrences and anomalies in the southeastern part of the Lime Hills quadrangle than those identified by Allen and Slaughter (1990). Further, the delicate morphologies found in areas 2 and 3 suggest local sources for the gold in these areas.

While visible gold was not found in the two bulk samples of conglomerate from the Kuskokwim Group collected in areas 4 and 5, this potential source of gold cannot be conclusively ruled out. However, paleoplacer gold derived from rocks of the Kuskokwim Group has not been

reported elsewhere. Yet, 76 of the 85 gold-bearing concentrates collected south of the Swift River are from drainages containing outcrops where only sedimentary rocks of the Kuskokwim Group are known. Three of the remaining nine concentrates were collected in drainages underlain by limestone of the Nixon Fork terrane, but are downslope and within 3 km of isolated outcrops of rocks of the Kuskokwim Group. A strong spatial association is evident between gold in concentrates and sedimentary rocks of the Kuskokwim Group in the area. Whether the gold is derived from rocks of the Kuskokwim Group or has been introduced by subsequent mineralization is not clear.

The western half of the Lime Hills quadrangle has not been mapped in detail. In contrast, detailed geologic mapping exists for the adjacent Iditarod quadrangle (Miller and Bundtzen, 1993). The Iditarod quadrangle is underlain principally by rocks of the Kuskokwim Group, but detailed ground traverses have revealed the presence of numerous mafic to felsic dikes. Further, Late Cretaceous to early Tertiary volcanoplutonic complexes and related igneous bodies are the major sources of lode and placer deposits in the Iditarod quadrangle (Bundtzen and others, 1985; Miller and Bundtzen, 1987). Similar unrecognized intrusive bodies may exist in the western Lime Hills quadrangle.

This study suggests favorability for epithermal cinnabar  $\pm$  stibnite deposits in the Lyman Hills and for gold-bearing vein or placer deposits in rocks of the Kuskokwim Group south of the Swift River. Precious metal and pathfinder geochemical analyses of samples collected in the western half of the Lime Hills quadrangle will help to clarify relations and may further delineate targets.

*Acknowledgments.*—I thank Elizabeth Bailey, Carter Borden, Barrett Cieutat, and Greg Lee for their help in sample collection and field identification. Steve Sutley performed X-ray diffraction analyses.

## REFERENCES CITED

- Allen, M.S., 1990, Gold anomalies and newly identified gold occurrences in the Lime Hills quadrangle, Alaska, and their association with the Hartman sequence plutons, in Goldfarb, R.J., Nash, J.T., and Stoeser, J.W., eds., *Geochemical studies in Alaska by the U.S. Geological Survey, 1989*; U.S. Geological Survey Bulletin 1950-F, p. F1-F16.
- Allen, M.S., Malcolm, M.J., Motooka, J.M., and Slaughter, K.M., 1990, Geologic description, chemical analyses and sample locality map for rock samples collected from the eastern part of the Lime Hills quadrangle, Alaska: U.S. Geological Survey Open-File Report 90-69, 49 p.
- Allen, M.S., and Slaughter, K.M., 1990, Mineralogical data and sample locality map of nonmagnetic, heavy-mineral-concentrate samples collected from the eastern part of the Lime Hills quadrangle, Alaska: U.S. Geological Survey Open-File Report 90-67, 64 p.

- Bundtzen, T.K., and Gilbert, W.G., 1983. Outline of geology and mineral resources of upper Kuskokwim region, Alaska: *Journal of the Alaska Geological Society*, v. 3, p. 101-119.
- Bundtzen, T.K., and Laird, G.M., 1982. Geological map of the Iditarod D-2 and eastern D-3 quadrangles, Alaska: Alaska Division of Geological and Geophysical Surveys Geologic Report 72, 1 pl., scale 1:63,360.
- Bundtzen, T.K., Miller, M.L., Bull, K.F., and Laird, G.M., 1988. Geology and mineral resources of the Iditarod mining district, Iditarod B-4 and B-5 quadrangles, westcentral Alaska: Alaska Division of Geological and Geophysical Surveys Public-Data File 88-19, 44 p., 1 pl., scale 1:63,360.
- Bundtzen, T.K., Miller, M.L., and Kline, J.T., 1985. Geology of heavy mineral placer deposits of the Iditarod and Innoko precincts, western Alaska, in Madonna, J.A., ed., *Conference on Alaskan Placer Mining*, 7th. Proceedings: Fairbanks, Alaska Prospectors Publishing Company, p. 35-41.
- Bundtzen, T.K., Miller, M.L., and Laird, G.M., 1986. Prospect examination of the Wyrick placer/lode system, Granite Creek, Iditarod-George mining district, Iditarod B-2 quadrangle, Alaska: Alaska Division of Geological and Geophysical Surveys Public-Data File 86-29, 10 p., 1 pl., scale 1:63,360.
- Cady, W.M., Wallace, R.E., Hoare, J.M., and Webber, E.J., 1955. The central Kuskokwim region, Alaska: U.S. Geological Survey Professional Paper 268, 132 p.
- Churkin, Michael, Jr., Wallace, W.K., Bundtzen, T.K., and Gilbert, W.G., 1984. Nixon Fork-Dillinger terranes: A dismembered Paleozoic craton margin in Alaska displaced from Yukon Territory: *Geological Society of America Abstracts with Programs*, v. 16, no. 5, p. 275.
- Decker, John, Bergman, S.C., Blodgett, R.B., Box, S.E., Bundtzen, T.K., Clough, J.G., Coonrad, W.L., Gilbert, W.G., Miller, M.L., Murphy, J.M., Robinson, M.S., and Wallace, W.K., in press. Geology of southwestern Alaska: Boulder, Geological Society of America, *Geology of North America series*, v. F1, chapter II-F.
- Eberlein, G.D., Chapman, R.M., Foster, H.L., and Gassaway, J.S., 1977. Table describing known metalliferous and selected nonmetalliferous mineral deposits in central Alaska: U.S. Geological Survey Open-File Report 77-168D, 132 p.
- Gamble, B.M., Allen, M.S., McCammon, R.B., Root, D.H., Scott, W.A., Griscom, A., Krohn, M.D., Ehmann, W.J., and Southworth, S.C., 1988. Lime Hills quadrangle, Alaska—An AMRAP planning document: U.S. Geological Survey Administrative Report, 167 p.
- Gilbert, W.G., 1981. Preliminary geologic map and geochemical data, Cheeneetuk River area, Alaska: Alaska Division of Geological and Geophysical Surveys Open-File Report 153, 10 p., 2 pl., scale 1:63,360.
- Gilbert, W.G., and Bundtzen, T.K., 1984. Stratigraphic relationship between Dillinger and Mystic terranes, western Alaska Range, Alaska: *Geological Society of America Abstracts with Programs*, v. 16, no. 5, p. 286.
- Gilbert, W.G., Bundtzen, T.K., Kline, J.T., and Laird, G.M., 1990. Preliminary geology and geochemistry of the southwest part of the Lime Hills D-4 quadrangle, Alaska: Alaska Division of Geological and Geophysical Surveys Report of Investigations 90-6, scale 1:63,360.
- Gray, J.E., Frost, T.P., Goldfarb, R.J., and Detra, D.E., 1990. Gold associated with cinnabar- and stibnite-bearing deposits and mineral occurrences in the Kuskokwim River region, southwestern Alaska, in Goldfarb, R.J., Nash, J.T., and Stoesser, J.W., eds., *Geochemical studies in Alaska by the U.S. Geological Survey*, 1989: U.S. Geological Survey Bulletin 1950-D, p. D1-D6.
- Hinderman, T.K., 1982. National Uranium Resource Evaluation, Lime Hills quadrangle, Alaska [National Uranium Resource Evaluation program, PGJ/F-057(82)]: Grand Junction, Colo., U.S. Department of Energy, 18 p., 14 plates, scale 1:500,000.
- Jacobson, S.I., Aamodt, P.L., and Sharp, R.R., 1979. Uranium hydrogeochemical and stream sediment reconnaissance of the Lime Hills and Tyonek NTMS quadrangles, Alaska, including concentrations of forty-three additional elements: Los Alamos Scientific Laboratory Informal Report LA-7348-MS, 224 p.
- Jones, D.L., Silberling, N.J., Coney, P.J., and Plafker, George, 1987. Lithotectonic terrane map of Alaska (west of the 141st meridian): U.S. Geological Survey Miscellaneous Field Studies Map MF-1874-A, scale 1:2,500,000.
- Lanphere, M.A., and Reed, B.L., 1985. The McKinley sequence of granitic rocks—A key element in the accretionary history of southern Alaska: *Journal of Geophysical Research*, v. 90, no. B13, p. 11413-11430.
- Malcolm, M.J., Allen, M.S., and Slaughter, K.E., 1990. Analytical results and sample locality map of the nonmagnetic, heavy-mineral-concentrate samples collected from the eastern part of the Lime Hills quadrangle, Alaska: U.S. Geological Survey Open-File Report 90-68, 83 p.
- Mertie, J.B., 1936. Mineral deposits of the Ruby-Kuskokwim region, Alaska: U.S. Geological Survey Bulletin 864-C, p. 115-255.
- Miller, M.L., Belkin, H.E., Blodgett, R.B., Bundtzen, T.K., Cady, J.W., Goldfarb, R.J., Gray, J.E., McGimsey, R.G., and Simpson, S.L., 1989. Pre-field study and mineral resource assessment of the Sleetmute quadrangle, southwestern Alaska: U.S. Geological Survey Open-File Report 89-363, 115 p.
- Miller, M.L., and Bundtzen, T.K., 1993. Geologic map of the Iditarod quadrangle, Alaska: U.S. Geological Survey Miscellaneous Field Studies Map MF-2219-A, scale 1:250,000.
- 1987. Geology and mineral resources of the Iditarod quadrangle, west-central Alaska, in Sachs, J.S., ed., *USGS research on mineral resources—1987 program and abstracts*, Third Annual V.E. McKelvey Forum on Mineral and Energy Resources: U.S. Geological Survey Circular 995, p. 46-47.
- Moore, T.E., and Wallace, W.K., 1985. Submarine-fan facies of the Kuskokwim Group, Cairn Mountain area, southwestern Alaska: *Geological Society of America Abstracts with Programs*, v. 17, p. 371.
- Motooka, J.M., Allen, M.S., Malcolm, M.J., and Slaughter, K.E., 1990. Analytical results and sample locality map for stream-sediment samples collected from the eastern part of the Lime Hills quadrangle, Alaska: U.S. Geological Survey Open-File Report 90-70, 103 p.
- Nelson, W.H., King, H.D., Case, J.E., Tripp, R.B., Crim, W.D., and Cooley, E.F., 1985. Mineral resource map of the Lake Clark quadrangle, Alaska: U.S. Geological Survey Miscella-

- neous Field Studies Map MF-1114-B, scale 1:250,000.
- Palache, C., Berman, H., and Frondel, C., 1946, *The system of mineralogy of James Dwight Dana and Edward Salisbury Dana*, Yale University, 1837-1892, seventh edition, v. 1: New York, John Wiley & Sons, 834 p.
- Reed, B.L., and Elliot, R.L., 1970, Reconnaissance geologic map, analyses of bedrock and stream sediment samples, and an aeromagnetic map of parts of the southern Alaska Range: U.S. Geological Survey Open-File Report 70-271, 24 p., 3 sheets, scale 1:250,000.
- Reed, B.L., and Lanphere, M.A., 1969, Age and chemistry of Mesozoic and Tertiary plutonic rocks in south-central Alaska: *Geological Society of America Bulletin*, v. 80, p. 23-44.
- , 1972, Generalized geologic map of the Alaska-Aleutian Range batholith showing potassium-argon ages of plutonic rocks: U.S. Geological Survey Miscellaneous Field Studies Map MF-372, 2 sheets, scale 1:100,000.
- , 1973, Alaska-Aleutian Range batholith—Geochronology, chemistry, and relation to circum-Pacific plutonism: *Geological Society of America Bulletin*, v. 84, p. 2583-2610.
- Sainsbury, C.L., and MacKevett, E.M., Jr., 1965, Quicksilver deposits of southwestern Alaska: U.S. Geological Survey Bulletin 1187, 89 p.
- Sorg, D.H., and Estlund, M.B., 1972, Geologic map of the Mountain Top mercury deposit, southwestern Alaska: U.S. Geological Survey Miscellaneous Field Studies Map MF-449, scale 1:600.
- Wallace, W.K., Hanks, C.L., and Rogers, J.F., 1989, The southern Kahlitna terrane: Implications for the tectonic evolution of southwestern Alaska: *Geological Society of America Bulletin*, v. 101, p. 1389-1407.

Reviewers: John E. Gray and Richard J. Goldfarb

# EARLY CENOZOIC DEPOSITIONAL SYSTEMS, WISHBONE HILL DISTRICT, MATANUSKA COAL FIELD, ALASKA

By Romeo M. Flores and Gary D. Stricker

## ABSTRACT

Vertical and lateral facies architecture of the coal-bearing Chickaloon and conglomeratic Wishbone Formations in the Wishbone Hill district of the Matanuska coal field reflect evolution of depositional systems from low- to high-gradient streams during Paleocene and Eocene time. Low-gradient, bedload meandering and mixed-load anastomosed streams principally drained the Matanuska area during the Paleocene. Low-lying mires formed on abandoned belts of meandering streams during lateral aggradation, a process influenced by tectonic stability and autocyclic processes. In contrast, low-lying mires in anastomosed streams developed during vertical aggradation, which was controlled by regional basin subsidence. Growth faulting promoted prolonged paludification of mires on the upthrown area and fluvial-channel capture on the downthrown area. Overthickened fluvial deposits and intervening coal zones, and coal-zone splitting reflect episodic interaction of intrabasin allocyclic processes (basin relative stability and subsidence), autocyclic processes (avulsion and abandonment of stream courses), and effects of growth faulting, all of which controlled basin dynamics. As extrabasinal uplift of the provenance area influenced the basin dynamics, steepening of gradients produced braided streams and mountain-front alluvial fans during the early Tertiary. Climate probably slightly controlled basin dynamics because megaflores of these fluvial deposits represent subtropical and warm-temperate conditions.

## INTRODUCTION

Historically, the Paleocene and Eocene Chickaloon Formation is one of the major coal-producing rock units in Alaska. The Chickaloon Formation is exposed in the Matanuska coal field (fig. 1). Here the Wishbone, Chickaloon, and Anthracite Ridge coal districts combined produced as much as 6,130,000 metric tons from 1915 to 1967 (Merritt and Belowich, 1984). Surface and underground coal mines were concentrated in the Wishbone Hill district (Barnes, 1951; Barnes and Payne, 1956). Surface mining in the Evan Jones Coal Mine between the Moose

and Eska Creeks near Jonesville (fig. 2) and north of the Wishbone Hill syncline created strip-mine highwalls that are continuous for over 3 km. We carried out facies investigations along these highwalls. Although drill-hole data near the strip mine was collected by Barnes and Payne (1956), no description of the highwall geology was ever recorded. Recent reclamation proposals led to an urgent need to collect stratigraphic and facies data in the strip mine, and plans to open an underground mine near the Evan Jones strip mine (Bohn and Schneider, 1992, p. 32) necessitated a better understanding of the coal-bearing facies. During the summer of 1992 we described 46 stratigraphic sections and assembled photomosaics with complementary sketches of seven highwalls at the Evan Jones strip mine.

## REGIONAL GEOLOGY

The Matanuska coal field is located in the Matanuska River valley at the northeast head of Cook Inlet. The valley is bounded to the north by the high-angle Castle Mountain fault (Martin and Katz, 1912) and Talkeetna Mountains, which contain granitic and gneissic rocks. To the south, the valley is bounded by the Chugach Mountains, which consist of greenstone, diorite, and interbedded slate and graywacke (Barnes and Payne, 1956; Winkler, 1992). The Castle Mountain fault (fig. 2) was interpreted by Grantz (1966) as a right-lateral fault during Mesozoic through early Tertiary time and a reverse vertical fault from Oligocene time to the present. Dettmerman and others (1976) suggested that the Castle Mountain fault was active for millions of years and recorded at least several kilometers net displacement. Payne (1955) characterized the Matanuska River valley as part of a geosynclinal trough 50 km wide, which extends beyond the Copper River to the east and into Cook Inlet to the southwest.

Mapping of the Matanuska River valley by Capps (1927), Barnes and Payne (1956), Grantz and Jones (1960), and Barnes (1962) shows that Tertiary nonmarine clastic sedimentary rocks are generally concentrated along the central part of the geosynclinal trough. Subordinate amounts of the Tertiary rocks are of hypabyssal intrusive and



volcanic (basaltic flow) origin. These rocks are flanked to the north, south, and east by Jurassic and Cretaceous rocks, which are mainly marine to nonmarine clastic sedimentary rocks and subordinate volcanic and plutonic rocks.

The canoe-shaped Wishbone Hill syncline, with an axis striking S. 55°–80° W. and plunging to the southwest, is the most prominent structural element in the Wishbone Hill coal district (Patsch, 1981). Rocks exposed along its flanks include mainly the Tertiary Chickaloon and Wishbone Formations. In the Evan Jones coal mine, highwall exposures of these formations along the northern limb of the Wishbone syncline were the focus of this study. Northeast-oriented left-lateral oblique-slip faults have dissected this syncline. At least six of these faults, commonly with an up-to-the-west displacement component, occur in the study area (fig. 2). Here, horizontal displacements range from a few centimeters to 120 m and vertical displacement is as much as 15 m. The orientation of these oblique-slip faults with respect to the Castle Mountain fault suggests that they probably represent oblique-slip faults rotated as much as 30° clockwise from the ideal R' Riedel shear orientation (Tchalenko, 1970) (fig. 3). The observed arrangement of the structures does not necessarily conform to those predicted by the Riedel model because rocks are heterogeneous, structures are developed sequentially rather than instantaneously, and early formed structures tend to be rotated during protracted deformation (Christie-Blick and Biddle, 1989). We suggest that these faults must have been active from the early stages of deformation of the Castle Mountain fault during Mesozoic through early Tertiary time when the Chickaloon Formation was deposited. These faults do not represent pure strike-slip as most have a dip-slip component as well. Mi-

nor faults, which probably splay from these faults, are also present in the study area and a few may have been avenues for gabbroic dikes (as thick as 7.6 m) that intruded the interval.

## STRATIGRAPHY AND COAL GEOLOGY

The Chickaloon Formation, which is as much as 1,500 m thick, consists mainly of interbedded sandstone, conglomeratic sandstone, siltstone, mudstone, carbonaceous shale, and coal (Martin and Katz, 1912). This formation rests unconformably on the Cretaceous Matanuska Formation and, in general, is conformably overlain by the Wishbone Formation. The Wishbone Formation is as much as 900 m thick and consists mainly of conglomerate and sandstone, and minor amounts of siltstone and mudstone (Barnes and Payne, 1956). However, this formation exhibits locally unconformable basal contacts where the conglomerate and sandstone are incised into the underlying Chickaloon Formation. The conglomerate comprises pebble to boulder sizes of igneous and metamorphic rocks as well as chert, vein quartz, and jasper fragments. Studies of the palynology and megafossils by Ames and Riegel (1962) and by Wolfe and others (1966) noted the Chickaloon Formation to be entirely Paleocene in age. However, the overlying Wishbone Formation, which has not yielded identifiable plant fossils, was interpreted as consisting partly of Paleocene rocks, due to its regional conformable relationship with the Paleocene Chickaloon Formation by Wolfe and others (1966). These later workers also reported the Wishbone Formation to be, in part, Eocene(?) in age. A more precise position of the Paleocene–Eocene contact

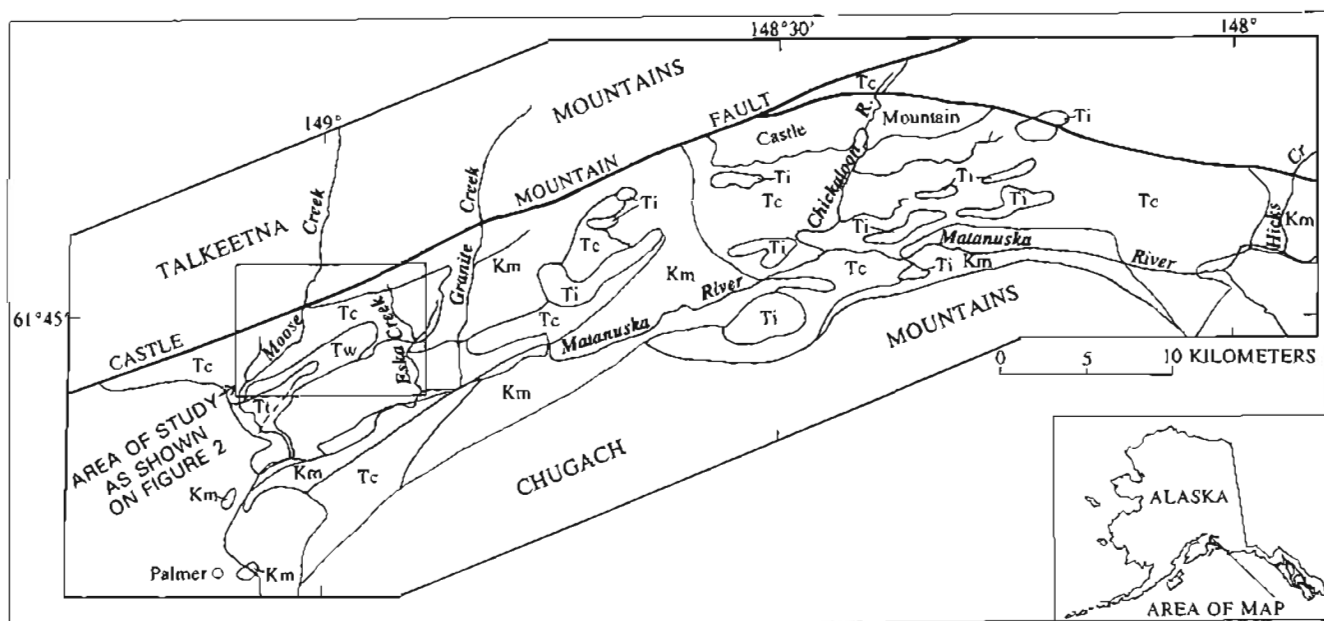


**Figure 1.** Location and generalized geology of Matanuska coal field, Alaska. Modified from Grantz (1966). Ti, intrusive rocks (Tertiary); Tw, Wishbone Formation (Eocene); Tc, Chickaloon Formation; Km, Matanuska Formation (Cretaceous).

within the Chickaloon Formation, based on radiometric age dating, was identified by Triplehorn and others (1984). The investigation of megaflores by Wolfe and others (1966) indicates that these Paleocene and Eocene deposits accumulated in a subtropical, warm-temperate climate.

Economic coalbeds are concentrated in the upper 425 m of the Chickaloon Formation. A few thin, scattered coalbeds occur in the lower part. The upper part of the Chickaloon Formation was subdivided by Barnes and Payne (1956) into four major coal-bearing groups generally separated by noncoaly intervals. The upper three of these coal groups, identified in this study as coal zones, from bottom to top include the Eska, Premier, and Jonesville coal zones (fig. 4). The Midway coalbed, between the Eska and Premier coal zones, occurs 25 to 23 m below the base of the Premier zone. The study interval includes these four coal zones of the uppermost part of the Chickaloon Formation (about 160 m) and the overlying lowermost part of the Wishbone Formation (15–23 m).

The coal zones, which range from 18 to 80 m in thickness, are separated by coal-free sequences that are as thick as 84 m in the Wishbone Hill district.

Although the Premier and Jonesville coal zones were strip mined in the study area, reserves of about 102 million metric tons are estimated to remain in the Wishbone Hill syncline (Barnes, 1967, p. 11). These coal zones consist of single and dull- to bright-banded coalbeds interbedded with carbonaceous shale, bony coal, mudstone, tonstein beds, and ironstone concretions. In the Evan Jones coal mine, the coal quality on an as-received basis varies between the Premier and Jonesville coal zones (Barnes and Payne, 1956). The as-received heat-of-combustion of the coals range from 10,290 to 11,650 Btu/lb for the Jonesville coal zone and from 10,450 to 11,890 Btu/lb for the Premier coal zone. Apparent rank of coals is high-volatile B bituminous. Ash contents range from 14 to 20 percent for the Jonesville coal zone and from 12 to 22 percent for the Premier coal zone. Sulfur contents range from 0.3 to

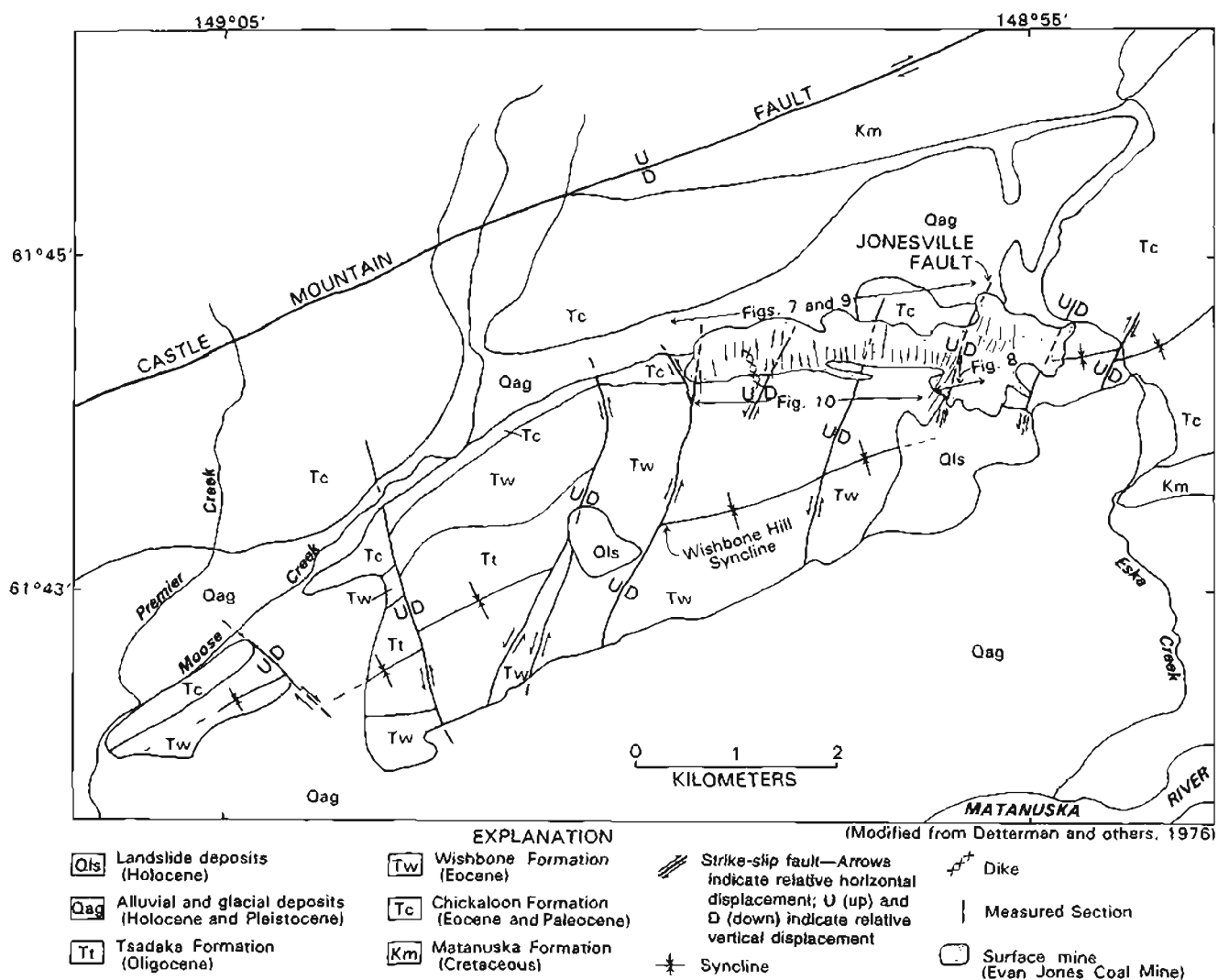


**Figure 2.** Detailed geologic and structural maps of study area in Wishbone Hill district of Matanuska coal field. Locations of measured sections and cross sections (figs. 7–10) shown in strip mine.

0.5 percent for the Jonesville coal zone and from 0.2 to 0.5 percent for the Premier coal zone. For comparison, analyses of coals in the Wishbone Hill district show heats-of-combustion from 10,400 to 13,200 Btu/lb, ash contents from 4 to 22 percent, and sulfur contents from 0.2 to 1.0 percent. Coals in the Wishbone Hill district also have apparent rank of high-volatile B bituminous.

## LITHOTYPES

Lithotypes from below the Eska to above the Jonesville coal zones of the Chickaloon Formation are fine-grained dominated compared to those of the Wishbone Formation, which is coarse-grained dominated (fig. 4). Mudstone and siltstone are dominant over sandstone, coal, and carbonaceous shale in the Chickaloon Formation. In contrast, conglomerate is dominant over sandstone, siltstone, and mudstone in the Wishbone Formation.

## MUDSTONE AND SILTSTONE

The mudstone lithotype is light gray to dark gray; the latter color reflects higher organic content. This lithotype

displays "popcorn" texture in weathered surface, indicating smectitic clay content; however, fresh surfaces show nonbedded, blocky, and mottled appearance. Root marks, whole to partial fragments of plant stems, trunks, and leaves, and vertical to horizontal animal burrows are abundant. Crude laminations marked by macerated plant fragments and silty grains are common. Diagenetic mineralization in the form of carbonate and siderite concretions and spherules are common and range in diameter from a few centimeters to greater than 1.5 m. Siderite spherules often contain plant remains and weather dark brown to reddish. Vitrain lenses often mark coalified roots, stems, and trunks; "coffee grounds" composed of finely macerated plant fragments form wispy lenses in the mudstone.

The siltstone lithotype is light gray to dark gray with the latter color enhanced by dispersed fine organic material in the silty matrix. This lithotype is commonly parallel to subparallel laminated and ripple laminated (climbing and current microlaminations). These sedimentary structures are commonly intercalated with mud drapes. Vertical and horizontal animal burrows and root marks commonly destroy the original sedimentary structures. Carbonized woody fragments, leaves and stems, and coal spars are scattered in the siltstone. Diagenetic carbonate concretions, from a few to 30 cm in diameter, are scattered throughout the siltstone.

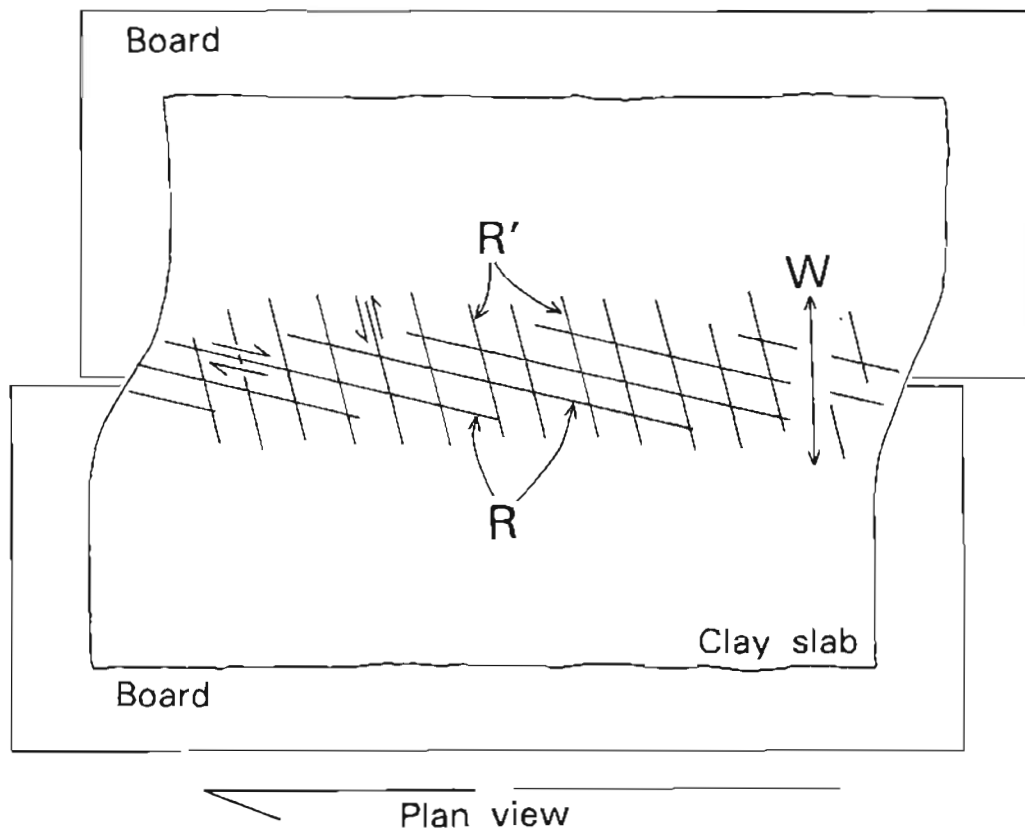


Figure 3. Structural model of deformation of Riedel experiment showing Riedel shear (R) and conjugate Riedel shear (R'). W, width of shear zone. Modified from Tchalenko (1970).

## SANDSTONE AND CONGLOMERATE

The sandstone lithotype is light gray to buff colored, ranges from very fine to coarse grained, and may contain thin, basal lag grits or conglomerates. The sandstone is feldspathic and the accompanying basal lag conglomerates include pebble-dominated fragments of volcanic, metamorphic, and sedimentary rocks (for example, coal, chert, mudstone, ironstone, and siltstone fragments); the latter rock types were probably recycled from Jurassic, Cretaceous, and older Tertiary sedimentary rocks. The basal lag grits consist of granules to fine pebbles of vein quartz, feldspar, chert, mudstone, and coal. Sedimentary structures in the sandstone include trough crossbeds (as much as 1 m in height), tabular crossbeds (as much as 0.5 m in height and 15 m long), convolute laminations, and current ripple laminations. Sigmoidal macroforms are common and separated by mud drapes. Laminiae of cross stratifications are defined by carbonaceous matter. The lithotype contains abundant plant fragments, and stems and trunk impressions along bedding planes. Trough-crossbed foreset measurements ( $n=24$ ) show west-southwest dip orientation.

The conglomerate lithotype occurs either as thin basal lag deposits (mainly in the Chickaloon Formation) or as thick bodies (as much as 15 m) that contain a few thin (up to several centimeters thick) sandstone beds. Thick conglomerate beds are common in the Wishbone Formation in

the Wishbone Hill coal district. The conglomerate interval contains from 25 to 75 percent conglomerate beds (Clardy, 1974). This conglomerate consists predominantly of pebbles and cobbles, with some boulders. The phenoclasts include abundant volcanic rocks (60 percent), common sedimentary rocks (chert and jasper), and rare plutonic fragments (Clardy, 1974). The conglomerates are framework-clast supported and loosely to tightly packed. Sand fills pore spaces between clasts. Texturally, the clasts are poorly to well sorted and of unimodal pebble size. Clasts are rounded to subrounded and range from spherical to rodlike in shape. The conglomerates are crudely to well imbricated, exhibiting east-northeast dip orientation (A axis). Trough-crossbed foresets in the sandstone interbeds show west-southwest orientation (Clardy, 1974).

## COAL AND CARBONACEOUS SHALE

The coal and carbonaceous shale lithotypes are the least common units within the total rock volume of the Chickaloon Formation. The apparent ranks of coalbeds in this formation range from subbituminous to anthracite, but are mainly bituminous in the study area (Barnes and Payne, 1956). As many as 30 single and dull- to bright-banded coalbeds, as much as 3.5 m thick, were recognized in the upper 450 m of the Chickaloon Formation by Barnes and Payne (1956) and Merritt (1986). These coalbeds are interbedded with bony coal, bone, carbonaceous shale, coaly mudstone-ironstone, and tonstein partings and thus are grouped as coal zones. Petrographic analyses by Rao and Wolff (1980) and Merritt (1985) in the Premier mine about 8 km southwest of the study area indicate that the coals are dominantly woody (92.7 percent vitrinite, 3 percent liptinite, and 4.3 percent inertinite).

Carbonaceous shale, consisting of fissile, black mudstone laminated by abundant macerated plant fragments and as thick as 1.8 m, is the most common coalbed parting. Proportions of carbonaceous-shale impurities in the coalbeds yield various gradations from bony coal to bone. The bony coal contains evenly disseminated impurities yielding dull luster and dark-gray to black color as well as some carbonaceous-shale laminae, which yield dull bands of impure coaly material. Bone is dark gray to black and commonly contains alternating carbonaceous-shale laminae or coaly mudstone lenses in coal, yielding a heavier and tougher coaly material than the pure coal. Tonstein beds, which are white to light green and bentonitic in composition, are as thick as 1.8 m and the least common type of parting. Ironstone or siderite (carbonate) partings occur as reddish-brown nodules, concretions, and irregular knobby lenses containing abundant plant fragments and tree trunks. The Premier coal zone, in particular, contains abundant carbonaceous shale and tonstein and ironstone partings.

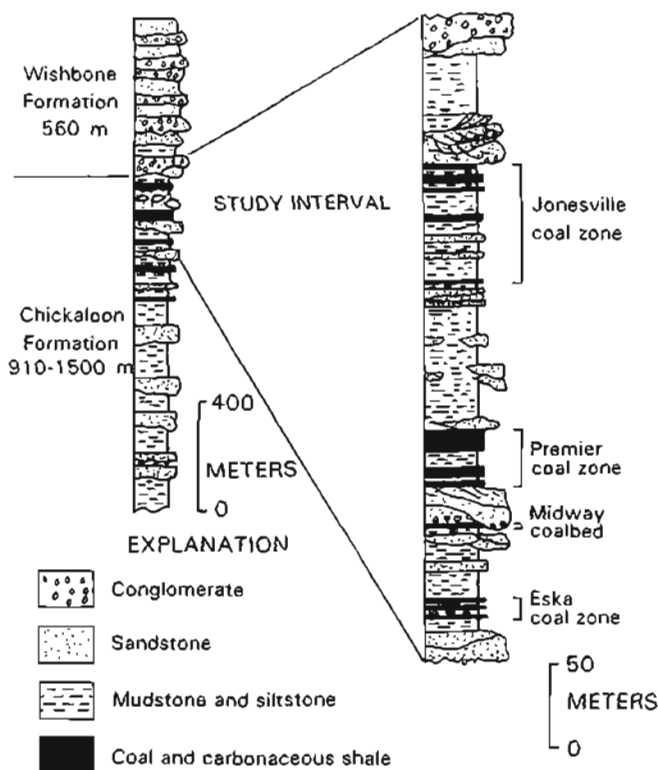


Figure 4. Composite Tertiary stratigraphic section showing study interval in Chickaloon and Wishbone Formations.

## SEDIMENTARY FACIES

Sedimentary facies of the Chickaloon and Wishbone Formations may be described by their vertical- and lateral-facies architecture. Vertical-facies architecture is represented by sequence profiles, and lateral-facies architecture includes facies associations and relationships.

## VERTICAL-FACIES ARCHITECTURE

Composite vertical variations of the study interval in the Chickaloon Formation divide into three major facies-sequence profiles: (1) the Eska-Midway-Premier coal interval, (2) the Premier-Jonesville coal zone interval, and (3) the interval above the Jonesville coal zone (fig. 5).

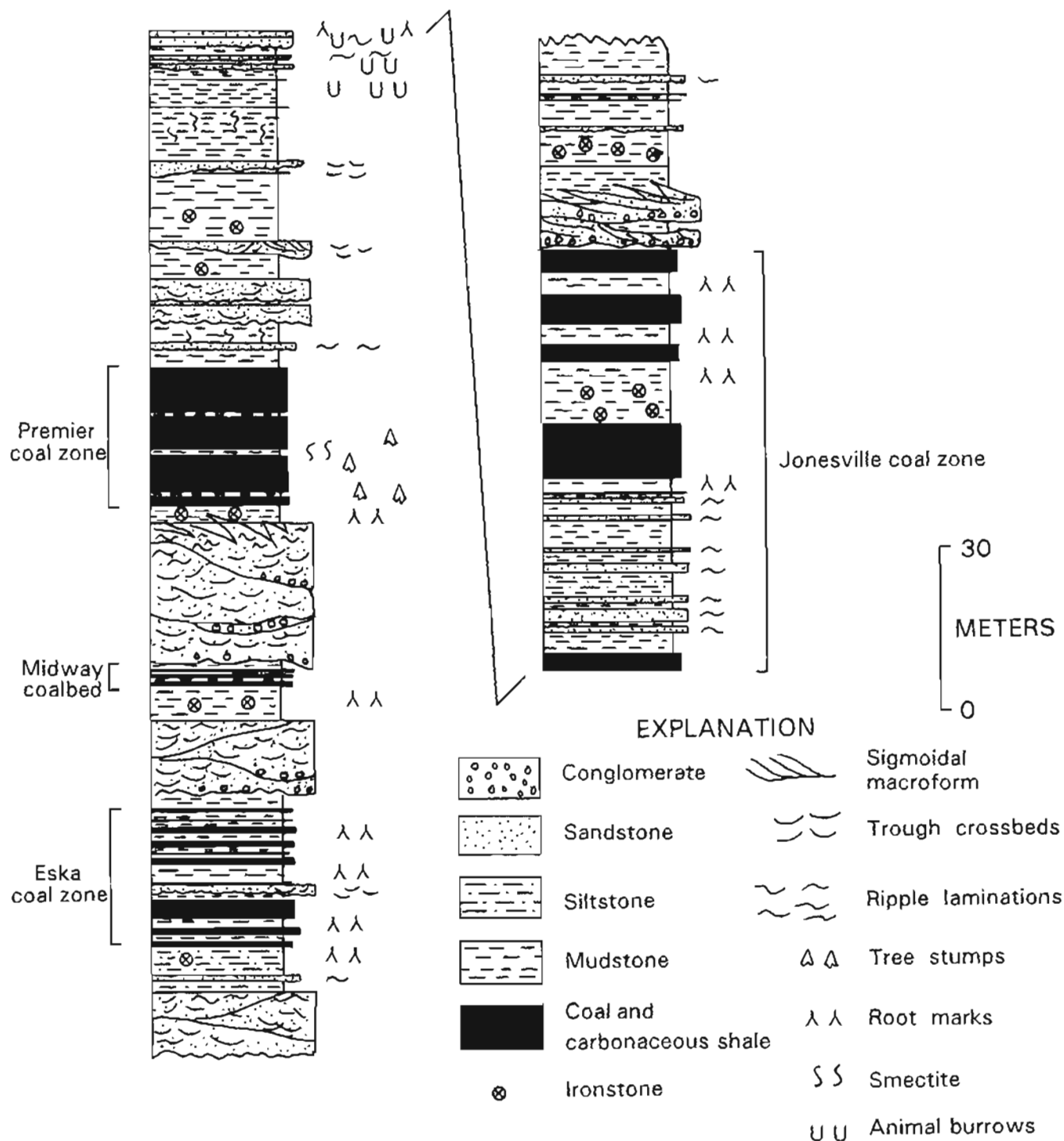


Figure 5. Composite vertical-facies profile of Chickaloon Formation from below Eska coal zone to above Jonesville coal zone.

The first and third of these profiles are dominated by erosional-based, fining-upward sandstones. These sandstones are vertically stacked bodies (as much as 30 m thick) bounded by multiple-scoured surfaces, each overlain by basal lag conglomerates. Each scour-based sandstone body contains crude (in the Eska-Midway-Premier facies profile) to well-developed (in the facies profile above the Jonesville coal zone) sigmoidal macroforms separated by mudstone drapes, which extend along part or the entire length of the macroforms. The sigmoidal macroforms are laterally offset, alternating with wedge-shaped mudstone drapes, which thicken toward the upper ends of the macroforms. These mudstone drapes, in turn, are interbedded with and grade upward into rippled, root-marked sandstones and siltstones. Each sigmoidal macroform contains trough and tabular crossbeds, with convolute laminations in the lower end, and asymmetrical ripple laminations in the upper end.

The facies-sequence profile between the Premier and Jonesville coal zones is dominated by mudstone and siltstone, which is distributed either as thin randomly interbedded units or as alternating thick couplets. These fine-grained sedimentary deposits encase coarsening-upward and fining-upward sandstones. Coarsening-upward sandstones, as much as 6 m thick, conformably underlie and overlie the siltstone and mudstone. The sandstones are ripple laminated (climbing ripple laminations) in the lower parts and small-scale (7 centimeters in height) trough crossbedded in the upper parts. Fining-upward sandstones are small, lenticular bodies (4 to 10 m thick and 7 to 55 m wide) and are scoured into underlying mudstone and siltstone or coarsening-upward sandstone. These lenticular sandstone bodies, in turn, are composed of smaller, compound bodies marked by scoured surfaces. Each small sandstone body comprises steeply dipping, ripple-laminated, trough-crossbed foresets that are interbedded with siltstone and mudstone. A large fining-upward sandstone, as much as 15 m thick and greater than 150 m wide, also occurs in the facies-sequence profile.

The facies-sequence profile in the lowermost part of the Wishbone Formation (fig. 6) consists of interbedded thin to thick (15 cm to 30 m) conglomerates and thin to thick (30 cm to 2.4 m) sandstones in the lower part and a very thick (greater than 7.5 m) conglomerate in the upper part. Both conglomerates and sandstones in the lower part of the facies are mainly basally scoured. However, a few sandstone bodies exhibit sharp to gradational basal contacts. The thin sandstones are ripple laminated and the thick sandstones are trough (30 cm in height) and planar (30 to 60 cm in height) crossbedded. The conglomerates in the upper part of the facies-sequence profile are partitioned by internal scour surfaces. These scour surfaces are overlain by fining-upward conglomerates with poorly to well-developed imbrication. These conglomerates show various states of framework-grain to matrix support.

## LATERAL-FACIES ARCHITECTURE

In the Eska-Midway-Premier sandstone-dominated facies-sequence profile, the multiscoured, fining-upward conglomeratic sandstones display amalgamated, multilateral, and multistory architecture over a lateral distance of 2 km (fig. 7). Poorly developed sigmoidal macroforms are mainly present in the uppermost fining-upward sandstones. The conglomeratic sandstones grade laterally into interbedded rippled sandstones, rooted mudstones and siltstones, and carbonaceous shales. Conglomeratic sandstones separate the Eska, Midway, and Premier coal zones. The upper part of the Eska coal zone grades upward into an

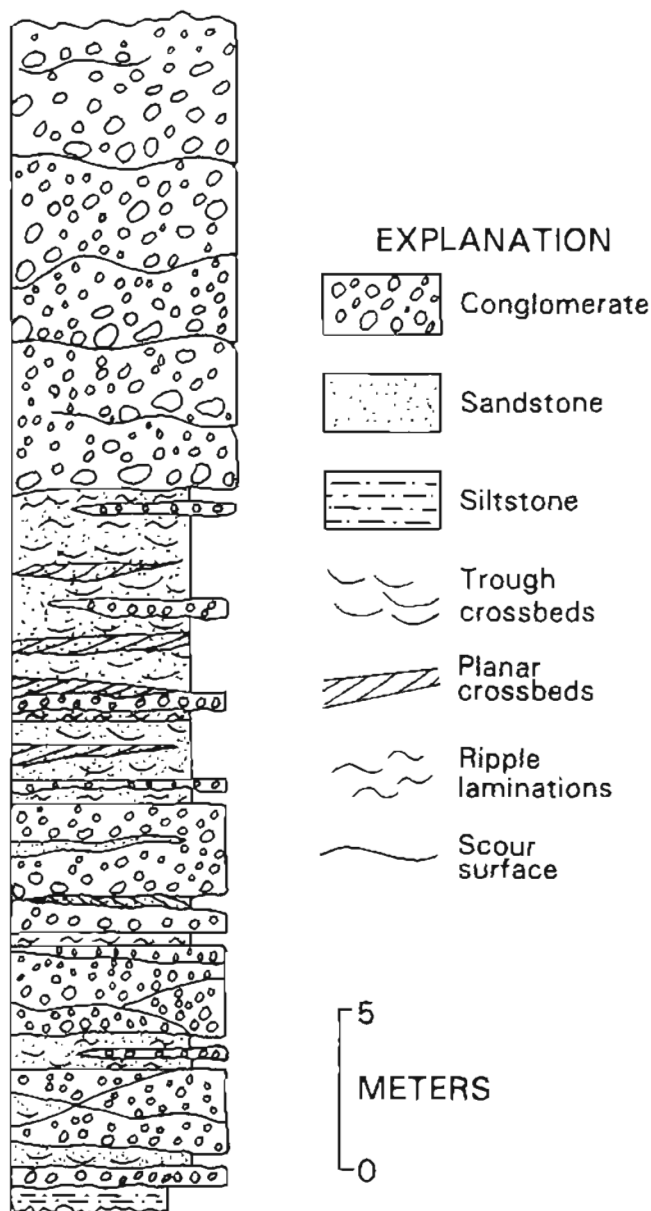
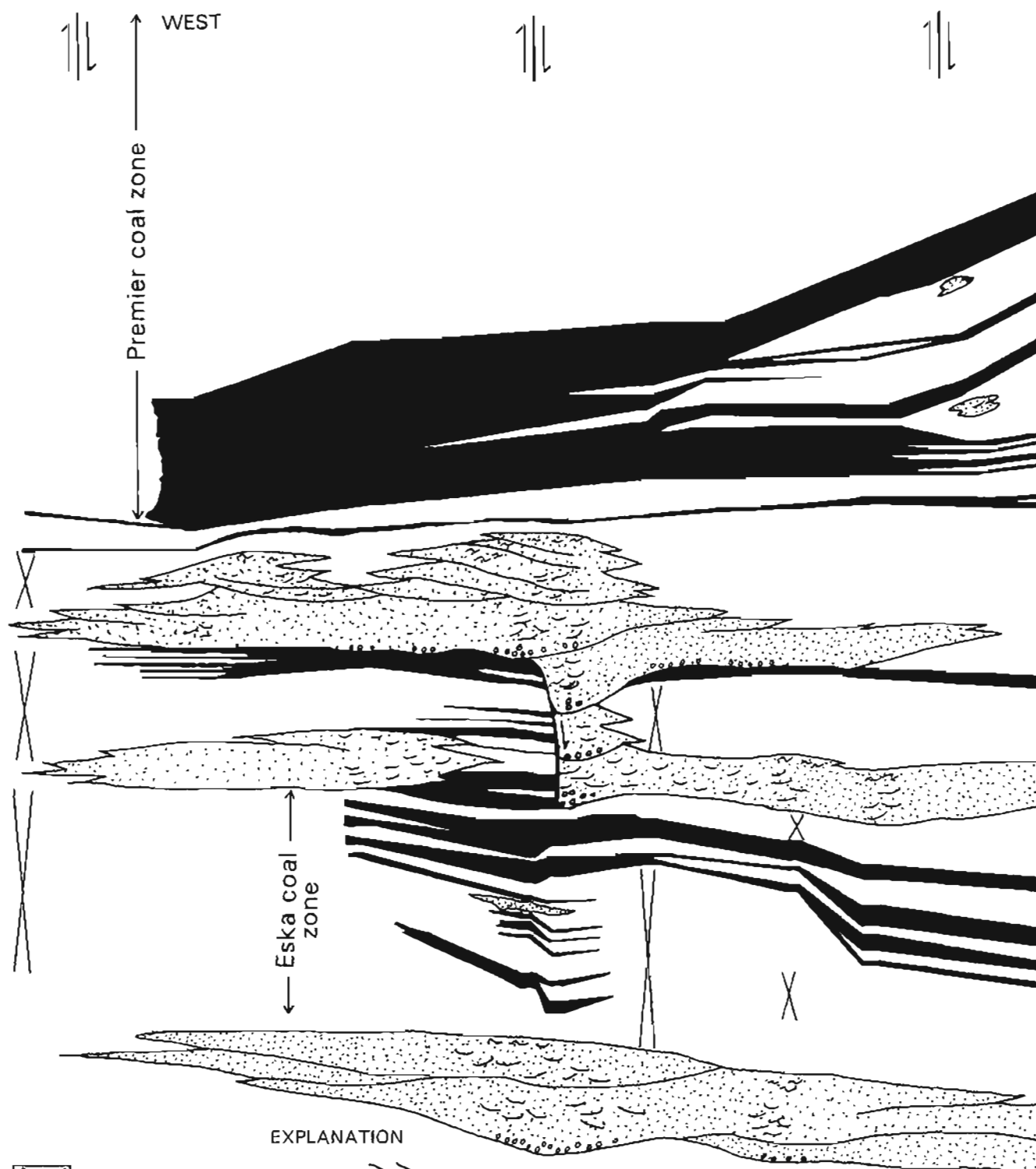
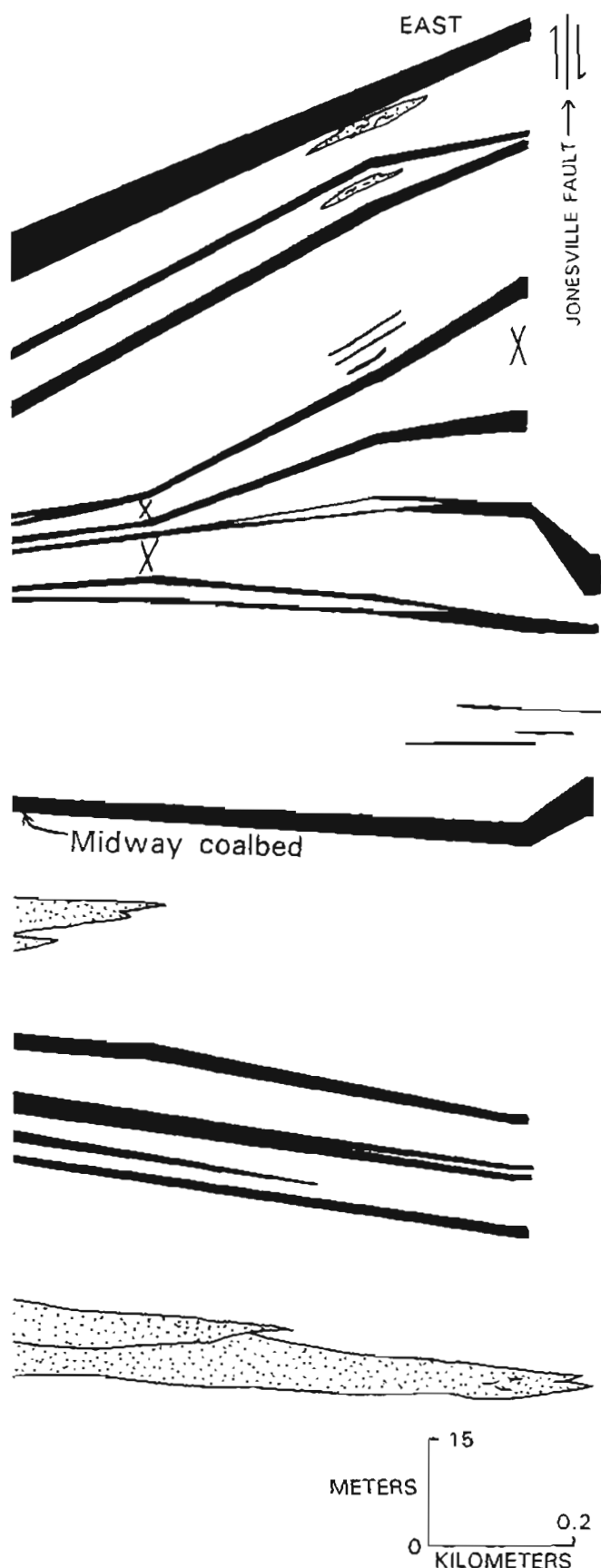


Figure 6. Composite vertical-facies profile of lowermost part of Wishbone Formation.







overthickened Midway coalbed, which abuts against a conglomeratic sandstone immediately to the east. This conglomeratic sandstone, in turn, merges upward with a conglomeratic sandstone that elsewhere overlies the Midway coalbed (fig. 7). This lateral-facies variation is recorded where a left-lateral, oblique-slip fault is developed.

The Premier coal zone contains six coalbeds interbedded with thin carbonaceous shale, mudstone, ironstone, and tonsteins. These coalbeds and coal-free interbeds are, in turn, separated by similar but thicker noncoaly intervals. In general, the lower four coalbeds contain more thick coal-free interbeds than the upper two coalbeds, which comprise more bone and bony coal interbeds (Barnes and Payne, 1956). Laterally, the six coalbeds of the Premier coal zone merge to the west. The thickness of intervening noncoaly interbeds is expanded by erosional-based, fining-upward sandstones and coarsening-upward sandstones (fig. 7). The eastward overthickening of the Premier coal zone and splitting of the coalbeds coincides with the occurrence of left-lateral, oblique-slip faults.

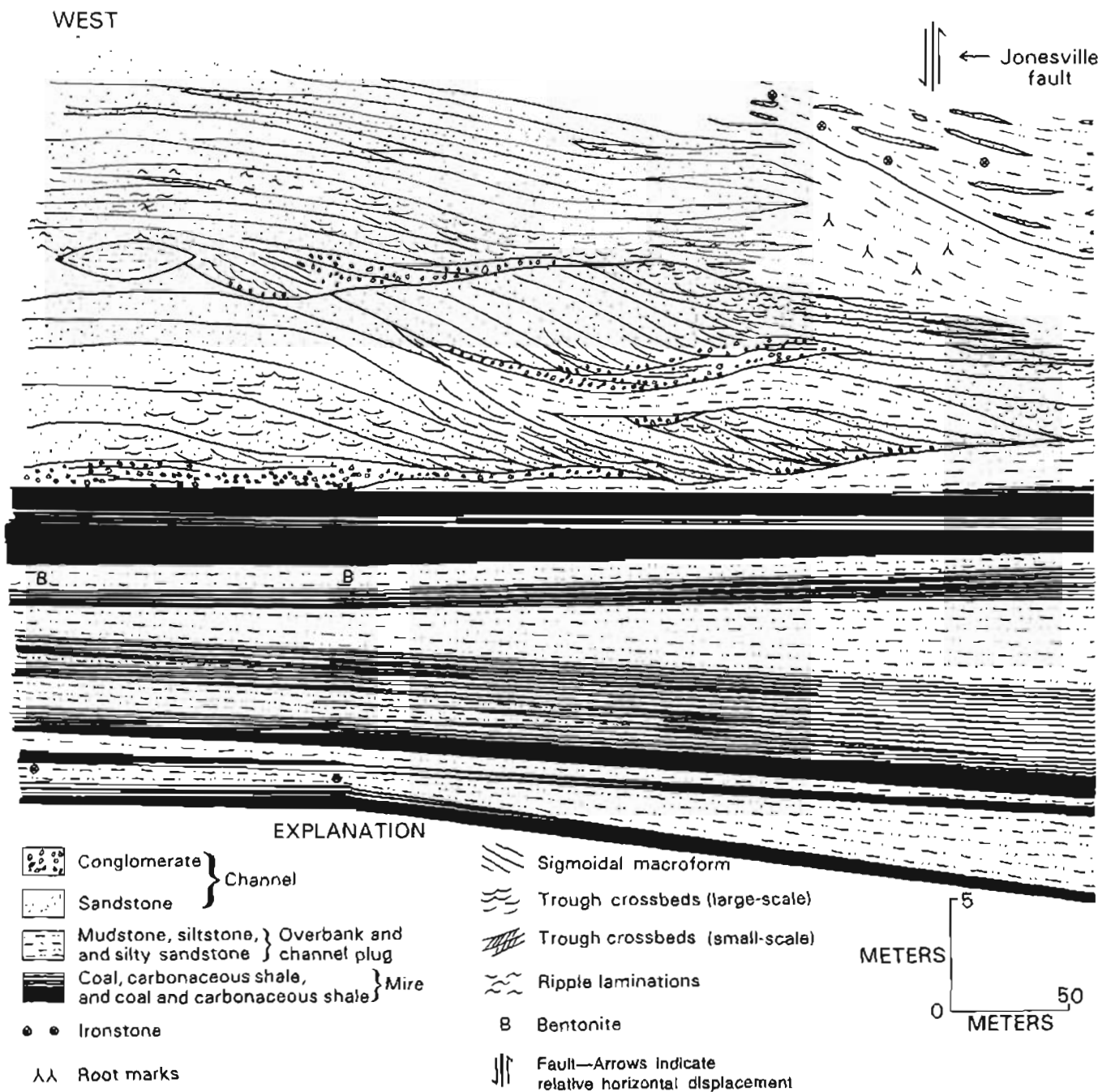
In the erosional-based, fining-upward, conglomeratic sandstone above the Jonesville coal zone, the conglomeratic sandstone consists of an amalgamated, multistory, and multilateral architecture over the 800-m lateral extent shown in figure 8. However, the complex is interrupted by erosional-based bodies of interbedded mudstone, siltstone, and sandstone. The internal organization of the sigmoidal macroforms within this conglomeratic-sandstone also varies laterally. Sigmoidal macroforms, which are well developed in all the conglomeratic-sandstone bodies, generally show west-northwest dip orientation at the west end of the cross section and east-southeast dip orientation at the east end. Laterally to the west, the conglomeratic-sandstone complex grades into interbedded rooted mudstone and rippled siltstone and sandstone. The conglomeratic sandstones unconformably overlie the Jonesville coal zone, which consists of four coalbeds interbedded with carbonaceous shale, mudstone, ironstone, and tonstein units (fig. 8). The lowermost coalbed and interbedded noncoaly units are separated from the upper three coalbeds by very thick (1.5 to 4.5 m) interbedded mudstones, siltstones, and sandstones that locally thicken from east to west. However, in the section shown in figure 9 these clastic interbeds regionally thicken eastward in the direction of occurrence of the left-lateral, oblique-slip faults. The uppermost coalbed and thin noncoaly units (fig. 8) are separated from the middle coalbeds by thin to thick (15 cm to 1.5 m) mudstones and

Figure 7. Lateral-facies architecture of interval from below Eska coal zone to Premier coal zone in the Chickaloon Formation. Architecture is restored from vertical component of movement of left-lateral, oblique-slip faults whose locations are shown in upper part of diagram.

siltstones. The middle coalbeds commonly contain bone in contrast to the uppermost coalbed, which commonly contains bony coal. The conglomeratic sandstones (see fig. 8) grade upward into a thick (as much as 10 m) mudstone with some siltstone interbeds, which in turn, is unconformably overlain by conglomerates of the Wishbone Formation.

In the mudstone-siltstone dominated facies sequence between the Premier and Jonesville coal zones, the facies sequence consists of a wide, erosional-based, fining-upward sandstone complex at the west highwall and grades eastward to coeval narrow, thin, multierosional, fining-

upward sandstones associated with coarsening-upward mudstones, siltstones, and sandstones as well as thin to thick, discontinuous coal and carbonaceous shale beds (fig. 9). Abundant vertical petrified tree trunks, as much as 6 m in height, occur along the extent of this facies sequence. The tree trunks are primarily associated with fining-upward sandstones and a coarsening-upward mudstone, siltstone, and sandstone complex. The uppermost part of the facies sequence lying immediately below the Jonesville coal zone consists of an interbedded mudstone, siltstone, and silty sandstone complex that thickens eastward. This complex is parallel to ripple laminated where not



destroyed by nondescript poor to intense vertical and horizontal burrows.

In the lowermost part of the conglomeratic Wishbone Formation over a distance of 1.4 km, a continuous erosional contact is recognized between mudstone of the Chickaloon Formation and the erosional-based conglomerate and sandstone of the Wishbone Formation (fig. 10). Conglomerates lie directly on top of the Chickaloon mudstones, however, interbedded gritty sandstones and conglomerates occur at the eastern part of the cross section. This conglomerate-gritty sandstone complex is overlain across the extent of the cross section by a thick, internally

scoured conglomerate complex. Thus, the lowermost part of the Wishbone Formation may be divided into two major subfacies: (1) a lower conglomerate-sandstone-dominated subfacies merging with a conglomerate-dominated facies, both of which are locally distributed, and (2) an upper conglomerate-dominated subfacies that is regionally distributed.

## FACIES INTERPRETATIONS

Facies characteristics of (1) the Eska-Midway-Premier coal zone interval, (2) Premier-Jonesville coal zone interval, (3) the interval above the Jonesville coal zone of the Chickaloon Formation, and (4) the lowermost part of the Wishbone Formation indicate deposits of (1) low-gradient high sinuosity (meandering) bedload, (2) low-sinuosity anastomosed streams, (3) high-gradient braided streams, and (4) alluvial fans, respectively. The coal zones occur alternately above fining-upward- and coarsening-upward-dominated fluvial sequences suggesting development of topogenous mires in vertically and laterally aggrading fluvial systems.

## CHICKALOON FORMATION

The Eska-Midway-Premier facies sequence, which consists of multiscoured, multistory, multilateral, fining-upward, conglomeratic sandstones with crude sigmoidal macroforms, reflects fluvial deposits of high-sinuosity (meandering) streams. Dominance of sand bedload (less than 5 percent silt and clay channel-fill sediment), traction currents (trough crossbeds), and lack of channel bars suggest deposition in bedload streams affected by seasonal discharge that favored preservation of sinuous-crested dune bedforms (Schumm, 1972, 1977; Ethridge and Schumm, 1978). Amalgamation of these channel sandstones suggests a long-term development of a relatively stable meander belt in which lateral aggradation by downstream meander migration was dominant over channel cut-offs and shifting (avulsion) of channels. Subsidence and slow rates of vertical aggradation in the surrounding flood plain prevented preservation of point bars (sigmoidal macroforms), which were successively eroded from older channels by younger migrating channels. Trough crossbeds in the channel sandstones indicate a west-southwest flow direction for these meandering streams. Overthickening of the Eska and Midway coal zones against laterally coeval,

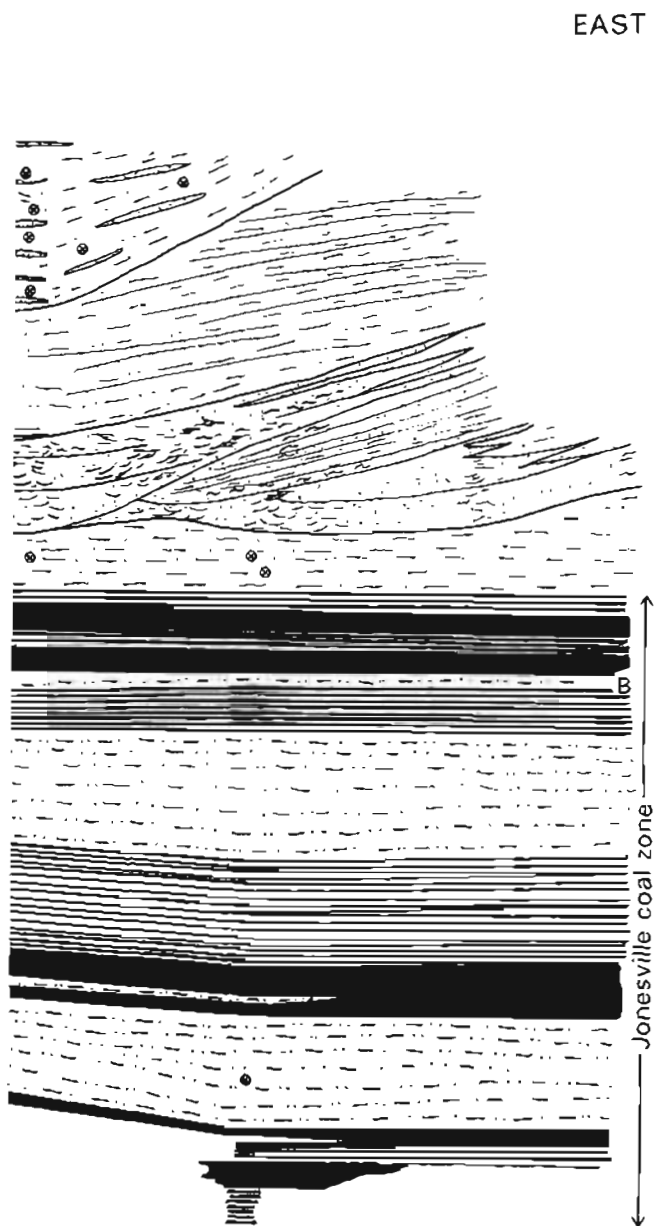
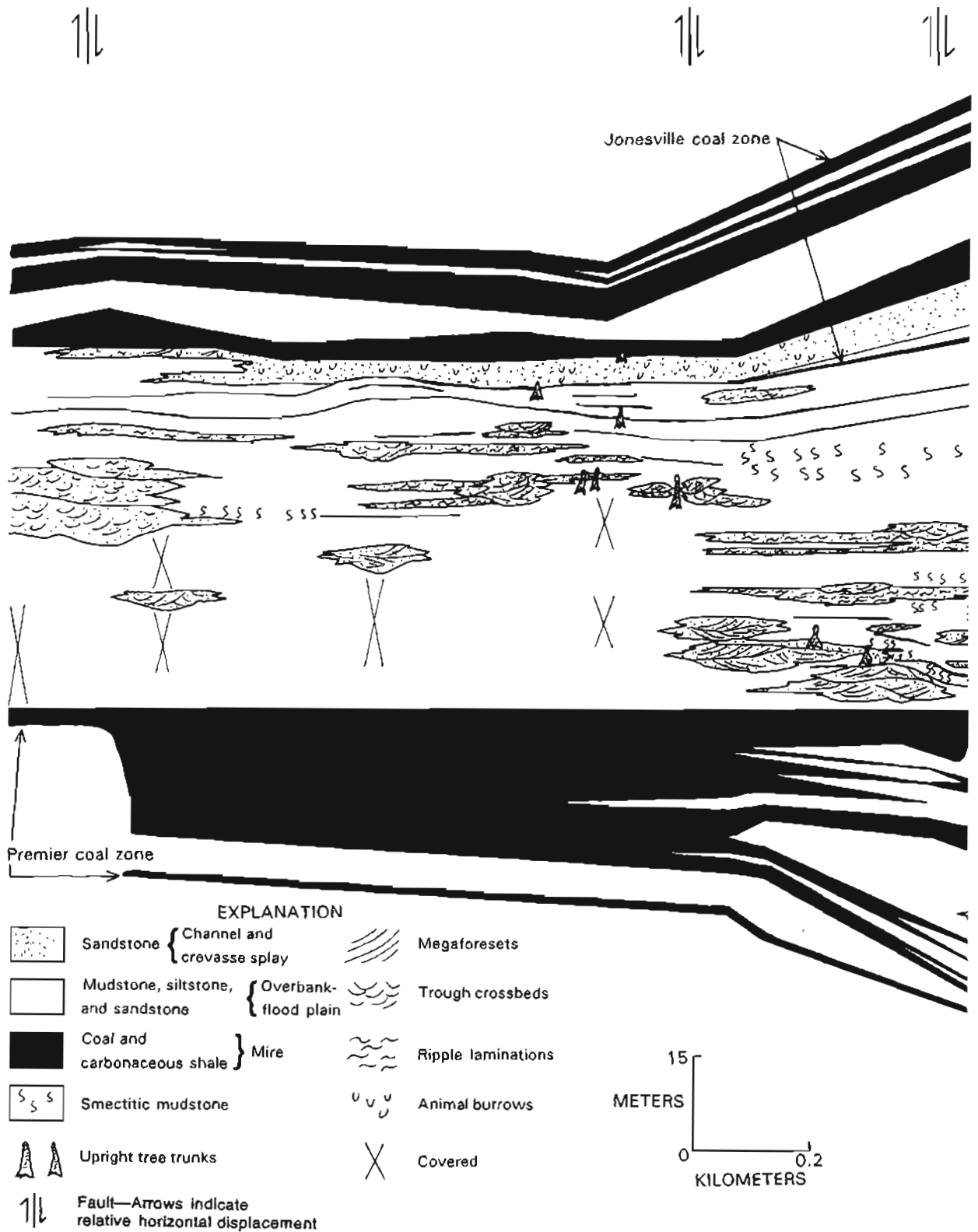
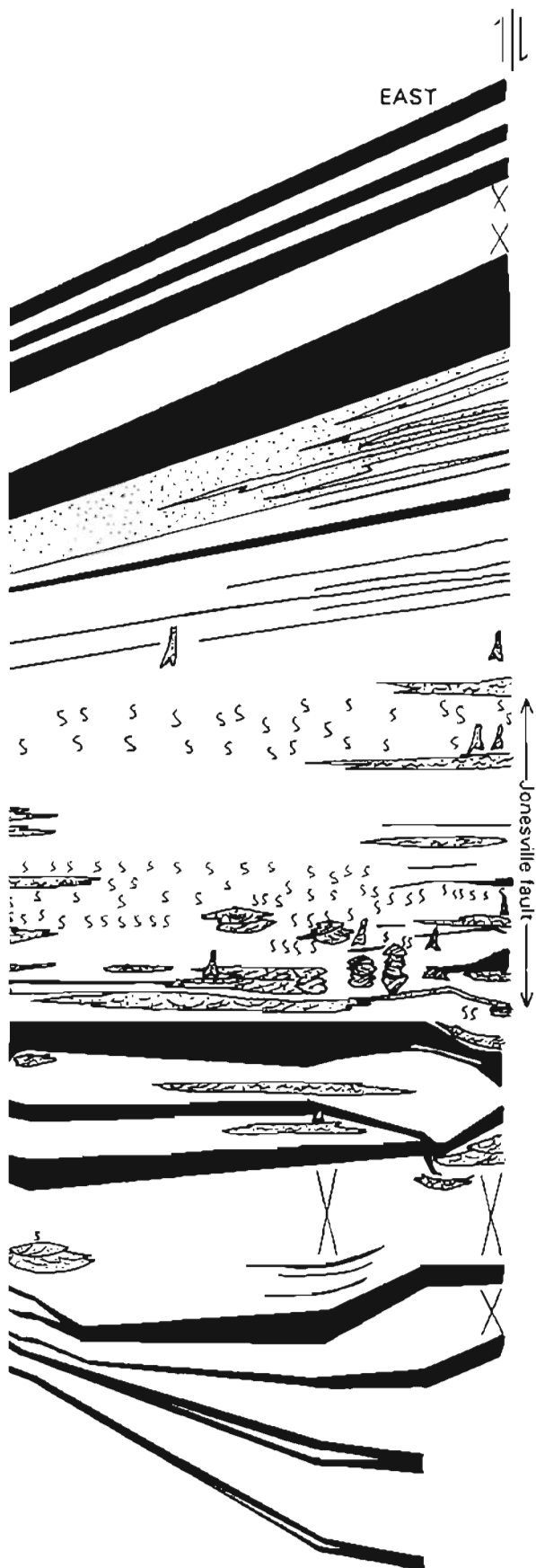


Figure 8. Lateral-facies architecture of Jonesville coal zone of the Chickaloon Formation and overlying sedimentary interval. Architecture is restored from vertical component of movement of Jonesville left-lateral, oblique-slip fault whose location is shown in upper part of diagram.

WEST





multiscoured, conglomeratic sandstones, deposited where left-lateral, oblique-slip faults were developed, suggests that the vertical component of movement during deposition (growth faulting) controlled the position of fluvial channels and equivalent mires. That is, fluvial channels were captured and incised within downthrown areas, while mire development was prolonged on upthrown areas. A series of growth faults may also account for the overthickening and splitting of the Premier coal zone by diversion of fluvial drainages into the downthrown areas. Here, the greater proportion of clastic sequences and coal splits suggests a dominance of crevasse-splay deposition that was localized by the fault structures. Similar fault-controlled fluvial and mire development was described by Flores (1984) and Weisenfluh and Ferm (1984).

In contrast to the facies of the interval above the Jonesville coal zone, the multiscoured, multistory, multilateral, fining-upward, conglomeratic sandstones with well-developed sigmoidal macroforms represents fluvial deposits of high-sinuosity (meandering) streams. Channel width-to-depth ratios of greater than 40 (60 to 90 for the well-developed sigmoidal macroforms or point bars) indicate deposition in stable bedload channels (Ethridge and Schumm, 1978). However, the occurrence of less than 5 percent silt and clay channel-fill sediments associated with the point-bar sandstones suggests a mixed sediment load. Amalgamation of channel deposits suggests that cut-offs (reflected by mixed-load or channel-plug deposits) and shifts (represented by the bedload or point-bar sandstones) of channels were the dominant process of lateral aggradation within the confines of the meander belt. Vertical aggradation in the surrounding flood plain due to sediment compaction influenced preservation of well-developed point-bar sandstones. Stream flow, based on trough crossbeds, was towards the west-southwest.

Facies between the Premier and Jonesville coal zones, characterized by coarsening-upward sequences associated with coeval, thin, narrow, fining-upward sandstones and enclosed by thick muddy and silty sediments, indicate fluvial deposits of anastomosed streams and related flood basins. Coarsening-upward sequences were formed by crevasse splays that spilled into low-lying flood basins during high discharges of a low-sinuosity stream. Crevasse channels drained the splays, and continued progradation of splay lobes permitted bifurcation and merging of the channels. Subsidence and confinement of these crevasse channels produced vertically aggrading, low-gradient channels and wooded levees. Low thickness-to-width ratios of the fining-upward channel sandstones, which

**Figure 9.** Lateral-facies architecture of interval from Premier to Jonesville coal zones of the Chickaloon Formation. Architecture is restored from vertical component of movement of left-lateral, oblique-slip faults whose positions are shown in upper part of diagram.

range from 1:4 to 1:30, are within the range for anastomosed streams suggested by Smith (1983). The common occurrence of mud drapes between steeply dipping silty sandstone foresets and the vertical stacking of these channel-fill units with low thickness-to-width ratios (1:4 to 1:6) are also characteristic of anastomosed streams (Galloway and Hobday, 1983). Widespread bioturbated mudstone, siltstone, and silty sandstone deposited in lacustrine settings suggest a close association of the anastomosed channels with flood-basin lakes.

Coal zones immediately below and above deposits of these fluvial systems represent organic accumulation in mires which developed on abandoned meander (Premier coal zone) and anastomosed (Jonesville coal zone) belts. The high ash content (as much as 25 percent) and abundant carbonaceous shale and mudstone interbeds associated with the coalbeds indicate that these mires were low lying or topogenous. Although mires formed on topographically high meander belts such as that below the Premier coal zone, base level must have been lowered periodically to permit drowning by detrital influxes. However, detrital in-

fluxes were probably short lived, allowing for the reestablishment of the mires, until a final sustained influx terminated peat accumulation. Since the meander-belt deposits represent deposition in relatively stable, laterally aggrading channels probably controlled by stable tectonic condition, we suggest that the lowering of base level was caused by local subsidence due to sediment compaction. Furthermore, splitting of the Premier coal zone by meander-belt-overbank deposits and the corresponding thinning of the underlying meander-belt deposits indicates that shifts or avulsion of stream courses promoted differential compaction of laterally offset channel sandstones and fine-grained flood-plain sediments. In addition, channel avulsion and diversion of crevasse splays may have been enhanced by vertical components of movement along contemporaneous left-lateral, oblique-slip faults. In contrast, the lowering of base level in association with the mires in which the Jonesville coal zone accumulated may have been controlled by regional tectonic subsidence. Regional lowering of base level probably started during sedimentation of the anastomosed streams, whose vertical aggradation is related

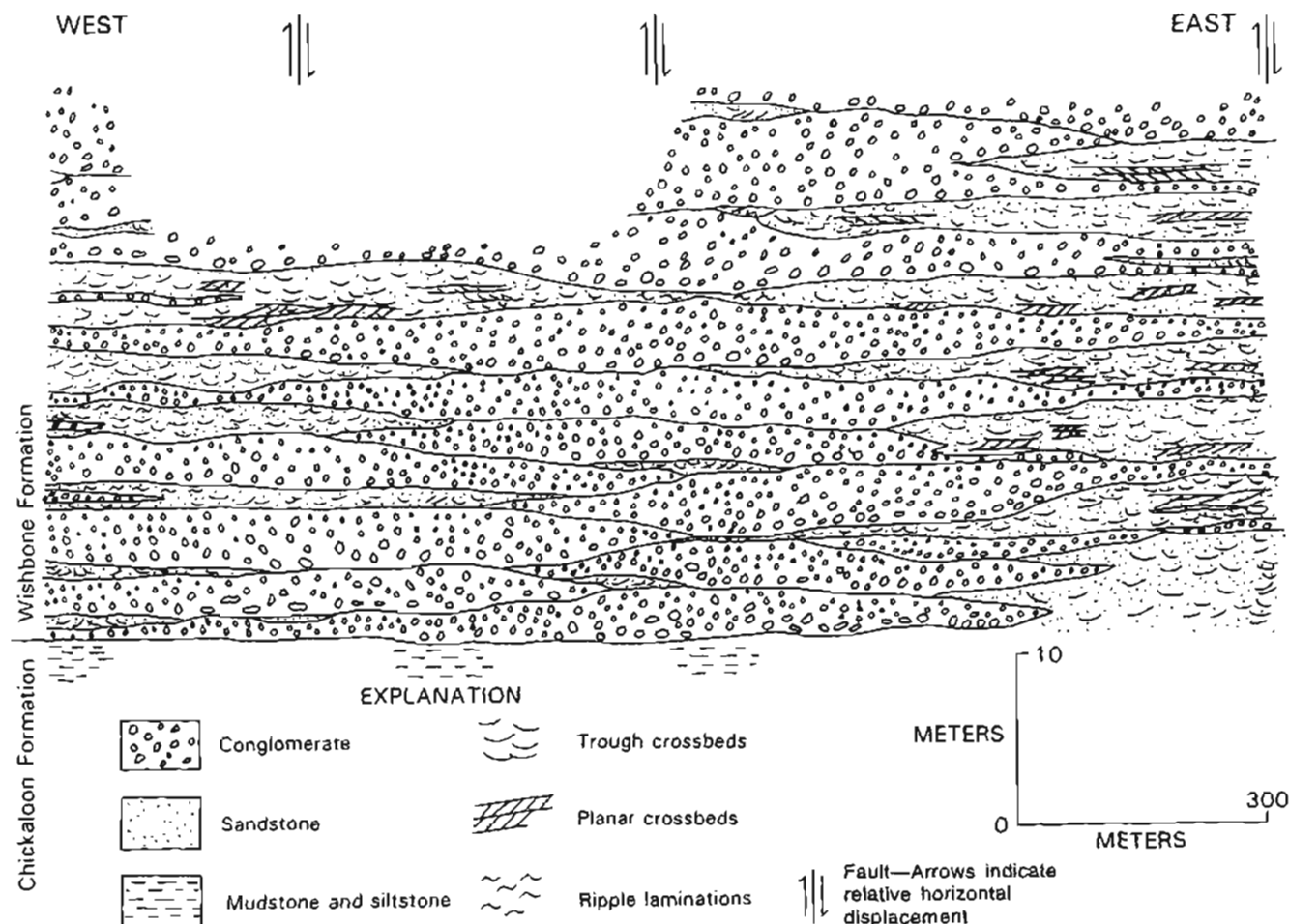


Figure 10. Lateral-facies architecture of lowermost part of Wishbone Formation. Architecture is restored from vertical component of movement of left-lateral, oblique-slip faults whose positions are shown in upper part of diagram. Reconstruction based in part on stratigraphic data of Clardy (1974).

to rapid basin subsidence (Smith, 1983). Thus, the vertical repetition of coal zones in the Chickaloon Formation reflects an intrabasin interaction of autocyclic (avulsion and abandonment of stream courses influenced by local sediment compaction) and allocyclic (regional basin subsidence) processes.

### WISHBONE FORMATION

Facies characteristics of the lowermost part of the Wishbone Formation, which consists mainly of framework-supported conglomerates and subordinate gritty sandstones, indicate deposition in high-gradient braided streams and alluvial fans. Steepening of stream courses at this time reflects extrabasinal or provenance uplift (Clardy, 1974). The multiscoured, imbricated, pebbly conglomerates were deposited as gravel bars by traction currents in channelized flows. Fining-upward conglomerate suggests gradual infilling of active channels by migrating gravel during floods. Waning stages of floods are reflected by ripple-laminated gritty sandstone caps on these gravel bars. Interbedded conglomerates and sandstones reflect the flashy discharge of the braided streams. Erosional-based sandstones interbedded with the conglomerates, which are trough and planar crossbedded, are attributed to sand-bar accretions marginal to or on top of gravel-bars during waning flows. Vertical stacking of the conglomerates suggests their deposition in laterally shifting, diverging, and converging channels such as in a broad-belt braided stream.

The lower part of the study interval in the Wishbone Formation probably reflects a dichotomy of braiding by sand and gravel bars. The sandy braid bars suggest development of a passive belt of braided streams contemporaneous to gravelly braid bars, which represent active belts of braided streams. This dichotomous relationship of bedload sediments in a depositional continuum reflects gravel-bar sedimentation during flood periods succeeded by prolonged gradual waning periods, which resulted in infilling of gravel belt margins of braided streams by sand bars. Waxing and waning depositional events in the braided streams are in contrast to the upper part of the study interval, which was deposited during perennial flood periods. This facies sequence indicates sedimentation at distal and proximal areas of humid alluvial fans (Clardy, 1974). Pebble imbrication and crossbed directions (Clardy, 1974) suggest westerly flow of the braided streams and south-westerly flow of streams within the alluvial fans.

### SUMMARY

Facies architecture indicates that the fluvial deposition of west-southwest-flowing meandering to anastomosed streams in the Chickaloon Formation was

succeeded by westerly flowing braided streams and south-westerly prograding alluvial fans in the Wishbone Formation. The meandering and anastomosed streams probably were a part of a flow-through, trunk-tributary, fluvial system that drained the "Matanuska geosyncline" (fig. 11). These streams may have been propagated under varying base-level conditions influenced by basin subsidence (allocyclic), avulsion due to sediment compaction (autocyclic), and growth faulting. When subsidence rates were low, lateral aggradation by meandering streams occurred in stable, confined meander belts. This was accompanied by flood-plain clastic accretion and organic accumulation in topogenous mires, which developed on abandoned meander belts removed from detrital influx. In areas dissected by left-lateral, oblique-slip faults, vertical movements localized aggradation by streams captured on downthrown areas. In addition, probable diversion of crevasse splays on downthrown areas caused splitting of the coalbeds accompanied by overthickened interburden intervals. In contrast, mires on upthrown areas, where thick coalbeds accumulated, were undisturbed by detrital influx.

Flood-plain sedimentation by crevasse splays during flood discharges from meandering streams initiated the process of anastomosis. Progradation of crevasse splays into the flood plain permitted bifurcation and merging of crevasse channels. This process, influenced by a high rate of basin subsidence, expanded areas of anastomosis and flood-basin lake development, and enhanced vertical aggradation of crevasse channel-overbank sediments. Topogenous mires formed in flood basins enlarged onto abandoned sites of anastomosis. As anastomosis matured, a crevasse channel was transformed into a major conduit and through time, developed from a low- to a high-sinuosity stream, leading to the onset of a meandering stream and repetition of the fluvial cycle. However, we propose that these streams occurred alternately through time and geographically coexisted in the drainage basin. Vertical and lateral aggradation of these streams were affected by local subsidence due to sediment compaction (autocyclic) and regional basin subsidence (allocyclic).

During raising and steepening of the regional base level (due to extrabasinal factors), the mire-prone, meandering and anastomosed fluvial systems were replaced by high-gradient, braided streams and transverse alluvial fans. Uplift of the Talkeetna Mountains along the Castle Mountain fault north of the Matanuska Valley controlled the gradient of the streams and their sediment supply (Grantz, 1966; Clardy, 1974). Mountain-front, alluvial-fan conglomerates represent localized deposits from intermittent movements along the fault. These alluvial fans supplied sediments to the lower-gradient, non-mire-forming, braided streams. Bimodal sediment loads in the braided streams reflect either episodic flash floods due to seasonal climatic changes or periodicity of provenance uplift.



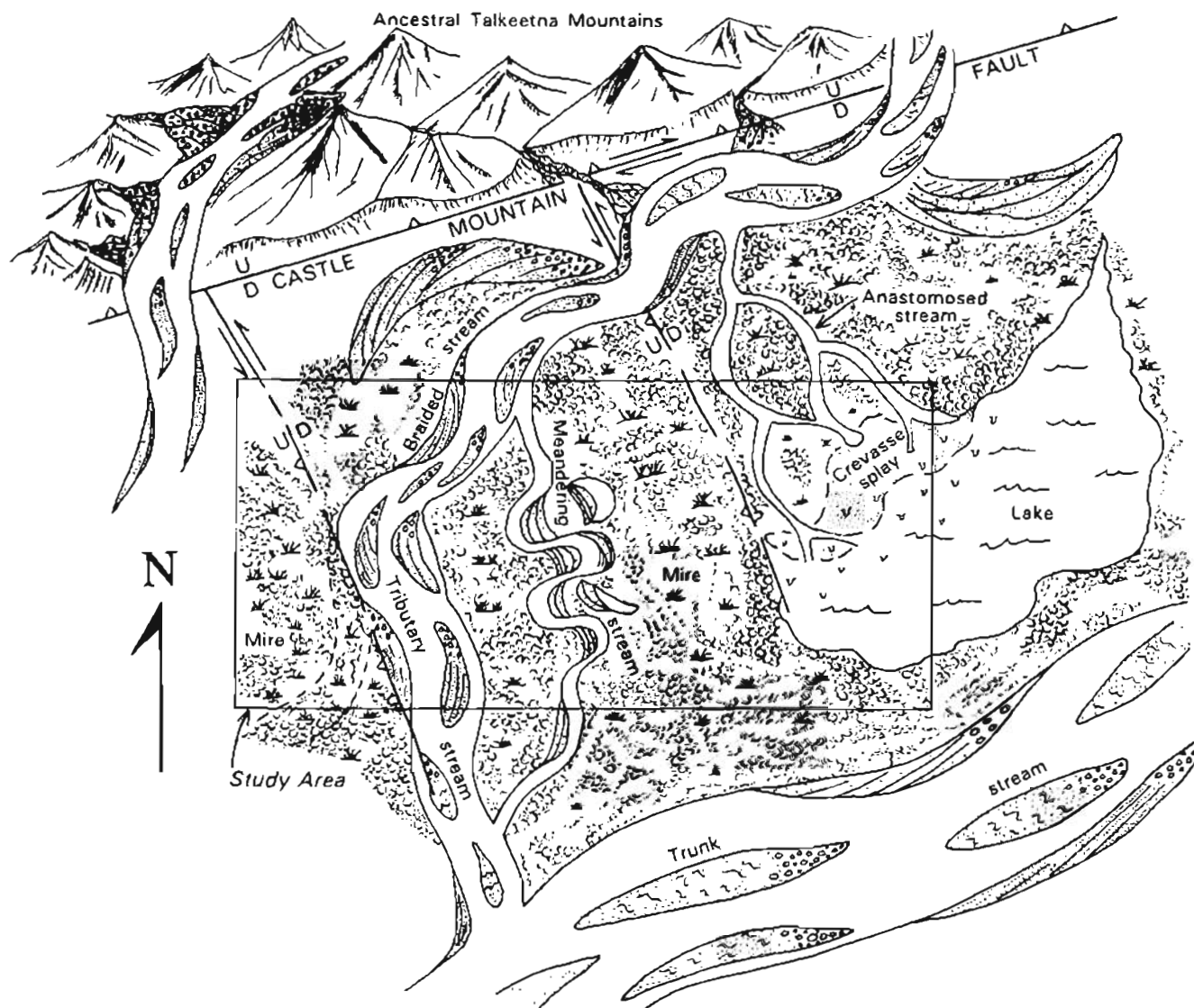


Figure 11. Idealized reconstruction of fluvial environments during deposition of Chickaloon Formation in study and outlying areas.

## REFERENCES CITED

- Ames, H., and Riegel, W., 1962, Palynological investigation of coals from the Chickaloon Formation [abs.]: *Pollen et Spores*, v. 4, p. 328.
- Barnes, F.F., 1951, Mining and exploration in 1945 in the Wishbone Hill coal district, Matanuska Valley, Alaska, in Barnes, F.F., and others, eds., *Coal investigations in south-central Alaska*: U.S. Geological Survey Bulletin 962-E, p. 193-201.
- , 1962, *Geologic map of lower Matanuska Valley, Alaska*: U.S. Geological Survey Miscellaneous Geologic Investigations Map I-359, scale 1:63,360.
- , 1967, *Coal resources of Alaska*: U.S. Geological Survey Bulletin 1242-B, 36 p.
- Barnes, F.F., and Payne, T.G., 1956, *The Wishbone Hill district, Matanuska coal field, Alaska*: U.S. Geological Survey Bulletin 1016, 88 p.
- Bohn, Diedra, and Schneider, J.L., eds., 1992, 1992 annual report on Alaska's mineral resources: U.S. Geological Survey Circular 1091, 65 p.
- Capps, S.R., 1927, *Geology of the upper Matanuska Valley, Alaska*: U.S. Geological Survey Bulletin 791, 92 p.
- Christie-Blick, Nicholas, and Biddle, K.T., 1989, Deformation and basin formation along strike-slip faults, in Foster, N.H., and Beaumont, E.A., *Structural concepts and techniques II (basement-involved deformation)*: American Association of Petroleum Geologists Treatise of Petroleum Geology reprint series 10, p. 239-272.
- Clardy, B.I., 1974, *Origin of the lower and middle Tertiary Wishbone and Tsadaka Formations, Matanuska Valley*: Fairbanks, University of Alaska, M.S. thesis, 74 p.
- Dettmerman, R.L., Plafker, George, Tysdal, R.G., and Hudson, Travis, 1976, *Geology and surface features along part of the Talkeetna segment of the Castle Mountain-Caribou fault system*: U.S. Geological Survey Miscellaneous Field

- Studies Map MF-738, scale 1:63,360.
- Ethridge, F.G., and Schumm, S.A., 1978, Reconstructing paleochannel morphologic and flow characteristics: methodology, limitations, and assessments, in Miall, A.D., ed., *Fluvial sedimentology*: Canadian Society of Petroleum Geologists, p. 703-721.
- Flores, R.M., 1984, Comparative analysis of coal accumulation in Cretaceous alluvial deposits, southern United States Rocky Mountain basins, in Stott, D.F. and Glass, D.J., eds., *The Mesozoic of middle North America*: Canadian Society of Petroleum Geologists Memoir 9, p. 373-385.
- Galloway, W.E., and Hobday, D.K., 1983, Terrigenous clastic depositional systems, applications to petroleum, coal, and uranium exploration: New York, Springer-Verlag, 423 p.
- Grantz, Arthur, 1966, Strike-slip faults in Alaska: U.S. Geological Survey Open-File Report 267, 82 p.
- Grantz, Arthur and Jones, D.L., 1960, Stratigraphy and age of the Matanuska Formation, south central Alaska: *American Association of Petroleum Geologists Bulletin*, v. 45, p. 1762-1765.
- Martin, G.C., and Katz, F.J., 1912, Geology and coal fields of the lower Matanuska Valley, Alaska: U.S. Geological Survey Bulletin 500, 98 p.
- Merritt, R.D., 1985, Coal atlas of the Matanuska Valley, Alaska: Alaska Division of Geological and Geophysical Surveys Public Data File 85-45, 270 p.
- , 1986, Paleoenvironmental and tectonic controls in major coal basins of Alaska, in Lyons, P.C., and Rice, C.L., eds., *Paleoenvironmental and tectonic controls in coal-forming basins of the United States*: Geological Society of America Special Paper 210, p. 173-200.
- Merritt, R.D., and Belowich, M.A., 1984, Coal geology and resources of the Matanuska Valley, Alaska: Alaska Division of Geological and Geophysical Surveys Report of Investigations 82-24, 64 p.
- Patsch, B.J.G., 1981, Remaining coal resources of the Matanuska field, in Rao, P.D., and Wolff, E.N., eds., *Focus on Alaska's coal '80*: Mineral Industry Research Laboratory Report 63, p. 1-60.
- Payne, T.G., 1955, Mesozoic and Cenozoic tectonic elements of Alaska: U.S. Geological Survey Miscellaneous Geological Investigations Map I-84, scale 1:250,000.
- Rao, P.D., and Wolff, E.N., 1980, Petrographic, mineralogical and chemical characterization of certain Alaskan coals and washability products, in Rao, P.D., and Wolff, E.N., eds., *Focus on Alaska's coal '80*: Mineral Industry Research Laboratory Report 63, p. 194-235.
- Schumm, S.A., 1972, Fluvial paleochannels, in Rigby, J.K., and Hamblin, W.K., eds., *Recognition of ancient sedimentary environments*: Society of Economic Paleontologists and Mineralogists Special Publication 16, p. 98-107.
- , 1977, *The fluvial system*: New York, John Wiley and Sons, 338 p.
- Smith, D.G., 1983, Anastomosed fluvial deposits: modern examples from western Canada, in Collinson, J.D., and Lewin, J., eds., *Modern and ancient fluvial systems*: International Association of Sedimentologists Special Publication 6, Blackwell Scientific Publications, p. 155-168.
- Tchalenko, J.S., 1970, Similarities between shear zones of different magnitudes: *Geological Society of America Bulletin*, v. 81, p. 1625-1640.
- Triplehorn, D.M., Turner, D.L., and Naeser, C.W., 1984, Radiometric age of the Chickaloon Formation of south-central Alaska—Location of the Paleocene-Eocene boundary: *Geological Society of America Bulletin*, v. 95, p. 740-742.
- Weisenfluh, G.A., and Ferm, J.C., 1984, Geologic controls on deposition of the Pratt seam, Black Warrior Basin, Alabama, U.S.A., in Rahmani, R.A., and Flores, R.M., eds., *Sedimentology of coal and coal-bearing sequences*: International Association of Sedimentologists Special Publication 7, p. 317-330.
- Winkler, G.R., 1992, Geologic map and summary geochronology of the Anchorage 1°x3° quadrangle, southern Alaska: U.S. Geological Survey Miscellaneous Investigations Map I-2283, 1 sheet, scale 1:250,000.
- Wolfe, J.A., Hopkins, D.M., and Leopold, E.B., 1966, Tertiary stratigraphy and paleobotany of the Cook Inlet region, Alaska: U.S. Geological Survey Professional Paper 398-A, p. A1-A29.
- Reviewers: William J. Perry, Jr. and Stephen B. Roberts

# RESERVOIR FRAMEWORK ARCHITECTURE IN THE CLAMGULCHIAN TYPE SECTION (PLIOCENE) OF THE STERLING FORMATION, KENAI PENINSULA, ALASKA

By Romeo M. Flores and Gary D. Stricker

## ABSTRACT

The coal-bearing Kenai Group in the Cook Inlet and Kenai Peninsula is a significant gas-producing unit. A large percentage of the nonassociated gas, particularly in the upper part of the Kenai Group, is generated from mudstones and coalbeds. Study of sandstones and associated coaly sequences of the Sterling Formation in the upper part of the Kenai Group has revealed reservoir and source rock characteristics.

Lithostratigraphic sequences and facies associations of the Clamgulchian Sterling Formation were formed in fluvial systems consisting of framework braided channels and overbank-flood-plain matrix overlapped by mires. Braided channel sandstones exhibit different levels of reservoir heterogeneity based on the hierarchy, nature, continuity, and arrangement of bounding surfaces. Fining-upward sandstones formed in bedload, low-sinuosity braided channels provide homogeneous and less compartmentalized reservoir systems. Fining-upward sandstones formed in mixed bedload and suspended load, moderately high-sinuosity braided channels yield heterogeneous and highly compartmentalized reservoir systems. Coaly sequences related to the low-sinuosity braided channel sandstones are thicker than those related to the mixed bedload and suspended load channel sandstones. Mixed load fluvial systems readily supplied suspended sediments that suffocated organic accumulation in low-lying mires.

## INTRODUCTION

The upper Miocene and Pliocene Sterling Formation is a coal-bearing unit within the Kenai Group in the Cook Inlet area, Alaska (fig. 1). Thin to thick coalbeds are common in the lower and middle parts, and thin and sparse in the upper part of the Sterling Formation on the Kenai Peninsula (Barnes and Cobb, 1959; Calderwood and Fackler, 1972; Merritt and others, 1987). This formation is best exposed along the northern coast of Kachemak Bay and eastern coast of Cook Inlet (figs. 1 and 2). The Sterling Formation is as thick as 2,100 m and consists of inter-

bedded sandstone, siltstone, mudstone, carbonaceous shale, and coal (fig. 3). Although Sterling coalbeds have not been mined for commercial use, methane gas associated with these coals is produced commercially (Kelly, 1963, 1968). Most nonassociated gas in the late Tertiary sandstone reservoirs is produced from methane gas generated from the coalbeds (Kelly, 1968). Multiple sandstone beds in the upper part of the Kenai Group at the Kenai and Swanson River fields, 25 and 65 km north of the study area, respectively (fig. 4), are the most consistent reservoir of methane gas (Kelly, 1968). These sandstone reservoirs, which are found at depths of 1,060–1,520 m, are clean, fine to medium grained, locally conglomeratic, poorly consolidated units and are separated commonly by gray shale and rarely by lignite. A stratigraphic correlation by Church and others (1969) through the Kenai and Swanson River fields and nearby fields along the western part of Kenai Peninsula indicates that these sandstone reservoirs are within the Sterling Formation. The Kenai and Swanson River fields combined produced a total of 78,559,687 million cubic feet of gas from 1963 to 1967 in the upper part of the Kenai Group (Kelly, 1968).

We made assessments of Tertiary coal and associated unconventional gas resources in Alaska in general, and of the coal-bearing Kenai Group in particular, during the summers of 1991 and 1992. We targeted the Kenai Group because of its abundant subbituminous coalbeds in the Tyonek and Beluga Formations, where these beds are as thick as 15 m. In addition, these coalbeds and associated shales and mudstones were the source rocks for condensate and microbial (biogenic) gas for late Tertiary sandstone reservoirs in the Cook Inlet basin (Kelly, 1968; Magoon and Anders, 1990). Thus, knowledge of the paleoenvironments of these coalbeds and associated sandstones, particularly in the upper part of the Tertiary Kenai Group, is necessary to understand the accumulation and distribution of these organic deposits and related biogenic gas as well as the character of reservoir systems. The study focuses on the stratigraphic interval in the upper part of the Sterling Formation from 3.1 km south to 2.2 km north of Clam Gulch (fig. 2), where potential sandstone reservoirs are well developed and exposed in two

dimensions. In addition, occurrences of these sandstone reservoirs are directly related to the presence of thin coalbeds in the Clamgulchian type section. This relationship is best demonstrated by a genetic stratigraphic framework based on 30 measured sections described during the summer of 1992.

### STRATIGRAPHIC AND SEDIMENTOLOGIC SETTING

Merritt (1986) indicated that coal accumulation in the Kenai Group was related to a low-energy sedimentation during a Miocene sea-level stillstand, which was succeeded

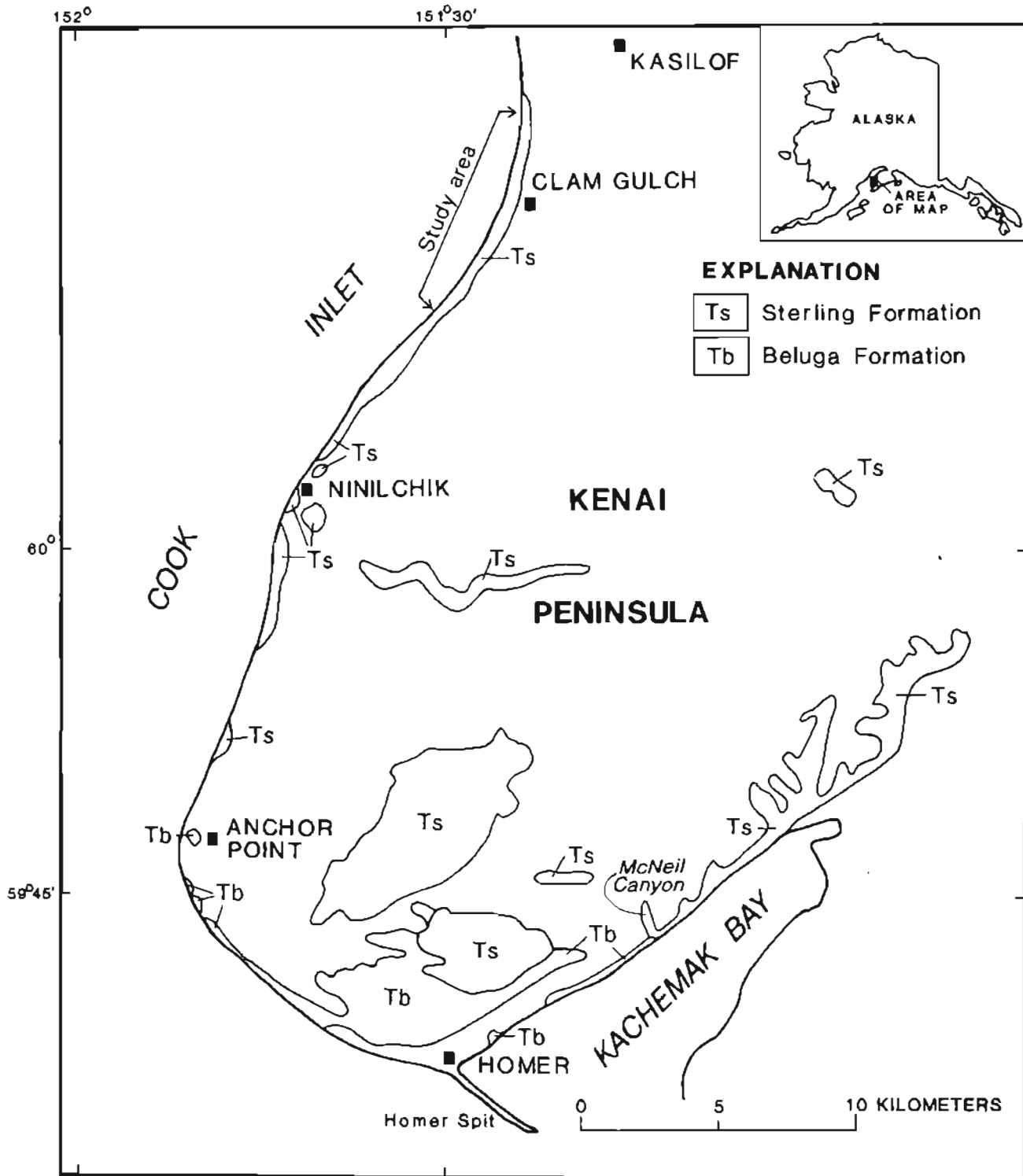


Figure 1. Location map showing study area in eastern part of Cook Inlet basin, Alaska.

during the Pliocene by a regressive phase. The stillstand period resulted in deposition of the upper part of the Tyonek Formation and lower part of the Beluga Formation. Cyclical sequences of fining-upward sandstone, underclay, and coal in these formations were interpreted by Merritt (1986) as deposits formed during periods of source-rock uplifts and rapid basin subsidence. Consequent to sea-level fall or uplift, regression followed with deposition of the upper part of the Beluga Formation and Sterling Formation. Uplift occurred in the Kenai-Chugach Mountains east of the Cook Inlet basin during deposition of the Beluga Formation (Hartman and others, 1972; Hayes and others, 1976). However, uplift along the Aleutian-Alaska Range provided detritus during deposition of the Sterling Formation (Hartman and others, 1972; Hayes and others, 1976).

The Beluga and Sterling Formations were interpreted by Hite (1975, 1976) and by Hayes and others (1976) as deposits of small, high-gradient braided streams flowing on alluvial fans and broad alluvial plains during Miocene and Pliocene time; subsequently these were replaced by large, meandering streams on broad alluvial plains during Pliocene time. Flores and Stricker (1992) modified these interpretations to include anastomosed streams in the upper part of the Beluga Formation and small meandering streams in the upper and middle parts of the Sterling For-

mation. Flores and Stricker (1992) suggested that coal accumulation was better developed in mires associated with anastomosed streams as compared to those mires related to the small meandering streams. These meandering and anastomosed streams probably were an integral part of fluvial networks of the river drainage basins, which were temporally related to the braided and large, meandering streams.

Parts of the Beluga and Sterling Formations exposed along the east shore of the Cook Inlet and along the north shore of Kachemak Bay are, based on megafossil content, Homerian Stage or late Miocene in age (Wolfe and others, 1966). Type Homerian flora reflect a cool, temperate climate. The upper part of the Sterling Formation in the Clam Gulch area, from Happy Creek (13 km south of Ninilchik) northward to a point 6.4 km north of Clam Gulch on the east shore of Cook Inlet, is Clamgulchian Stage or Pliocene in age (Wolfe and others, 1966). In this study this area is informally called the Clamgulchian type section. The Clamgulchian megafossils reflect a cool, temperate climate but one cooler than the Homerian climate and considerably warmer than that of Cook Inlet today. The Clamgulchian cool climate was not a significant factor in organic-matter preservation or coal accumulation, because peat is preserved and accumulated in modern cool-climate mires (Martini and Glooschenko, 1985). Thus, the sparse coalbeds in the Clamgulchian type section of the Sterling Formation may be explained by depositional rather than climatic factors.

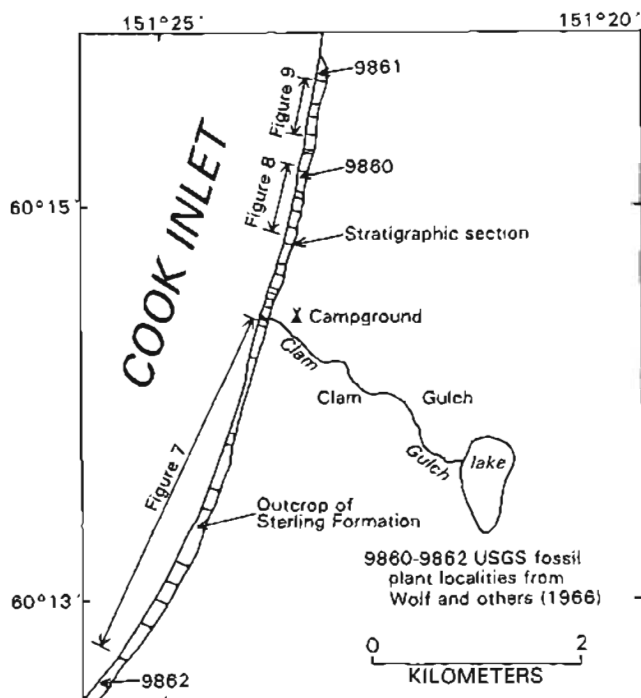


**Figure 2.** Map of study area in vicinity of Clam Gulch showing outcrops of the Sterling Formation along beach coast, locations of measured sections, and paleobotanical sampling localities of Wolfe and others (1966).

## GENETIC STRATIGRAPHIC ANALYSIS

Genetic stratigraphic analysis of the Clamgulchian type section of the Sterling Formation may be described in a hierarchical approach that consists of the following, from the smallest to largest rock properties: (1) internal sedimentary structures, grain size, and color, (2) nature of contacts, (3) lateral and vertical facies organizations or architecture, and (4) cross-sectional geometry. This analytical approach permits interpretation, at different scales, of the depositional systems of lithostratigraphic sequences and facies associations. A lithostratigraphic sequence is a rock type or a grouping of rock types that have similar grain size (or grain size variation) and lithic composition. Facies association is the vertical and lateral variations between lithostratigraphic sequences.

## LITHOSTRATIGRAPHIC SEQUENCES

Lithostratigraphy of the Clamgulchian type section of the Sterling Formation may be grouped into (1) a lower coaly and sandy sequence and (2) an upper coal-poor and sandstone-and-mudstone-dominated sequence. Volumetric

cally these sequences comprise as much as 75 percent sandstone, about 24 percent siltstone and mudstone, and 1 percent coal, carbonaceous shale, and tonsteins.

#### SANDSTONE SEQUENCES

Sandstone occurs in fining-upward sequences ranging from coarse to fine grained, light gray to buff, and locally include lag conglomerates of coal spars and pebble- to boulder-size mudstones. These sandstones are, in turn, amalgamated into multiscoured bodies with the internal scour bases locally marked by lag conglomerates. These multiscoured sandstones are up to 65 m in thickness and more than 3 km long. The sandstone bodies display

megaforesets as high as 3.5 m and common trough crossbeds as high as 1.2 m and 23 m long. A few planar crossbeds as high as 1.5 m occur in cross sets up to 3 m high. Convolute laminations as high as 3 m occur in zones as much as 6.7 m in height. Ripple laminations (climbing and current ripples) either locally cap sandstone complexes or occur within scoured sandstone bodies.

Very fine grained sandstone occurs as tabular bodies with sharp to gradational bases and gradational tops. They commonly exhibit climbing and current ripple laminations. In places, a few narrow (a few millimeters across) and short (a few centimeters long) vertical and horizontal burrows have destroyed some or all of the ripple laminations. These sandstones, which are as thick as 2.5 m, are either

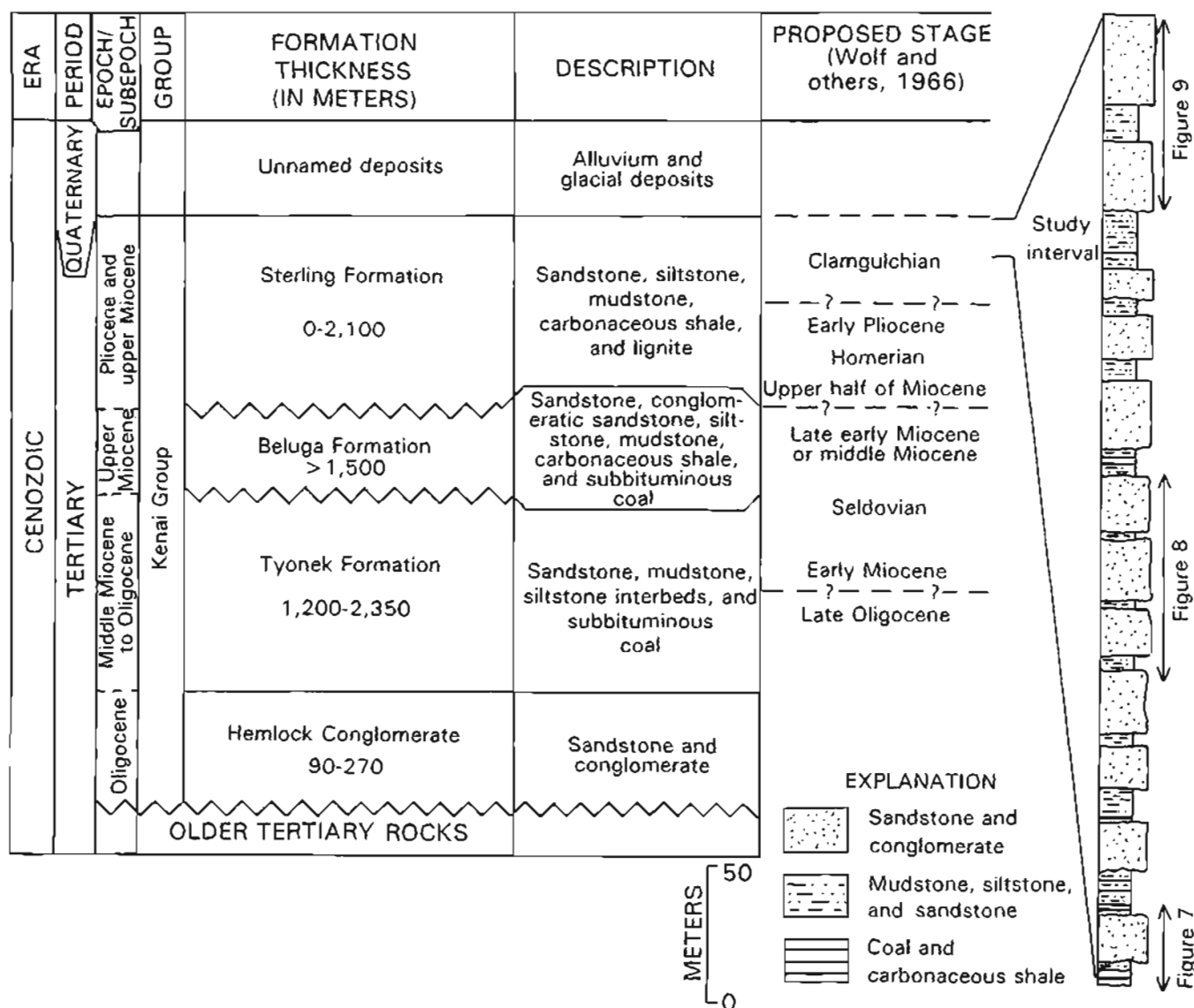


Figure 3. Generalized stratigraphic column of Kenai Group in the Kenai Peninsula showing stage subdivisions of Wolfe and others (1966) and position of study interval in upper part of Clamgulchian type section of the Sterling Formation. Study interval is shown in composite stratigraphic section to left. Detailed facies associations of lower, middle, and upper parts of study interval are shown in figures 5-7.

randomly interbedded with mudstone and siltstone, or coarsening-upward sequences of mudstone and siltstone.

#### MUDSTONE AND SILTSTONE SEQUENCES

Mudstone is dark to light gray and commonly displays popcorn-weathered texture indicating that it is composed of smectitic clay (Moore, 1976; Reinink-Smith, 1990). It contains abundant macerated plant fragments that are frequently concentrated as discontinuous laminae. The mudstones are mainly massive but locally contain plant root marks and some nondescript vertical and horizontal burrows. This lithologic unit is as much as 7 m thick and is volumetrically more common than siltstone.

Siltstone is dark to light gray, sandy, and contains current and climbing ripple laminations. These ripple laminations are frequently crosscut by root marks of coalified plants and tubelike vertical burrows. It contains abundant plant fragments and "coffee ground" (finely macerated organic matter) laminations. This lithologic unit is as much as 3 m thick.

The mudstone and siltstone occur either as (1) randomly interbedded sequences with silty to very fine-grained sandstone or (2) coarsening-upward sequences of mudstone, grading upward into siltstone and tabular, very fine grained sandstone. These two types of sequences are, in turn, commonly interbedded with each other.

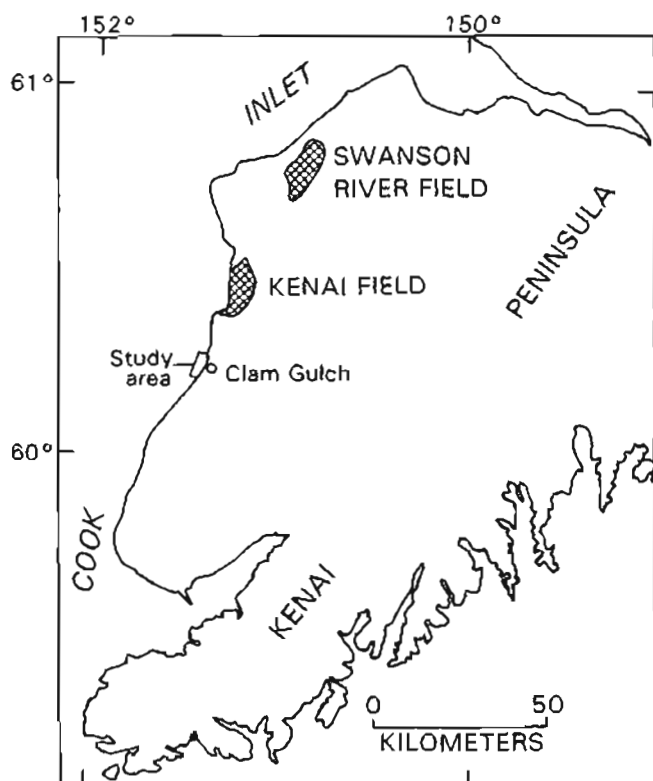


Figure 4. Map showing locations of the Kenai and Swanson River gas fields.

#### COAL, CARBONACEOUS SHALE, AND TONSTEIN SEQUENCES

Coal in the Clamgulchian type section of the Sterling Formation consists entirely of lignite (average vitrinite reflectance is 0.32 percent; Merritt and others, 1987) with abundant carbonaceous shale partings and a few tonstein partings. Woody fragments with well-preserved internal structures and tree stumps are the common composition of the coal. Merritt and others (1987) described the maceral composition of Sterling coal on the eastern side of Cook Inlet as comprising mainly 85.3 percent huminite, 9.6 percent liptinite, and 5.1 percent inertinite. These workers indicated that Sterling coalbeds have increased levels of inertinites compared to coalbeds of the Beluga Formation. The coalbeds in the Clamgulchian type section range from a few centimeters to 1.4 m in thickness and thin upward with increased carbonaceous shale interbeds. The thickest coalbed in the lowermost part of the Clamgulchian type section is exposed for more than 3.1 km.

Carbonaceous shale is dark-gray to black, fissile mudstone mixed with abundant macerated plant-fragment laminae and occurs as single beds or as partings in the coalbeds. It commonly contains coalified plant root marks, woody fragments, and tree stumps. The carbonaceous shale laterally grades into coalbeds and commonly replaces coalbeds in the uppermost part of the Clamgulchian type section of the Sterling Formation. A few, nonbedded, white to yellowish tonstein beds up to a few centimeters thick occur as partings in the coalbeds. A rippled tonstein bed, which is bentonitic in composition and mixed with mudstone, and as thick as 1.5 m, is interbedded with the coalbed in the lowermost part of the Clamgulchian type section. This tonstein bed is similar to the tonstein partings described by Reinink-Smith (1990) that are interbedded with Sterling coalbeds, which she interpreted to be volcanic ash. Sequences of coal, carbonaceous shale, and tonstein occur as interbeds in mudstone and siltstone sequences.

#### FACIES ASSOCIATIONS

Lithostratigraphic sequences may be organized vertically into facies associations, as displayed in figures 5–7. These facies associations pass from one to the other either in a preferred or random order. A facies association may grade into another or be bounded by an erosional surface. The facies associations are grouped in order to interpret them as genetically related neighbors. Thus, the Clamgulchian type section of the Sterling Formation was grouped into three facies associations according to their similarities and differences.

The lower part of the composite Clamgulchian type section of the Sterling Formation consists of (1) interbedded fining-upward sandstone, (2) mudstone and



siltstone, and (3) coal, carbonaceous shale, and tonstein-facies associations (fig. 5). The fining-upward sandstones, which average 20 m in thickness, are interbedded with mudstone and siltstone sequences that average 9.5 m in thickness, and with coal, carbonaceous shale, and tonstein sequences that average 2.8 m in thickness. The lowermost coal, carbonaceous shale, and tonstein sequences are as thick as 5.2 m and contain as many as four coalbeds; however, they are interbedded with the mudstone and siltstone sequences. The fining-upward sandstones are composed of as many as three tiers (multistory) of amalgamated multiscoured (as many as four internal scour bases) bodies. These sandstone bodies are separated by thick mudstone and siltstone sequences that occasionally contain coarsening-upward sandstone. The multiscoured sandstones, in turn, exhibit a series of stacked bodies separated by a few thin, scour-based mudstone-siltstone lenses (see lowermost

sandstone complex in fig. 5). In addition, these multiscoured sandstone bodies are laterally offset, displaying a multilateral architecture.

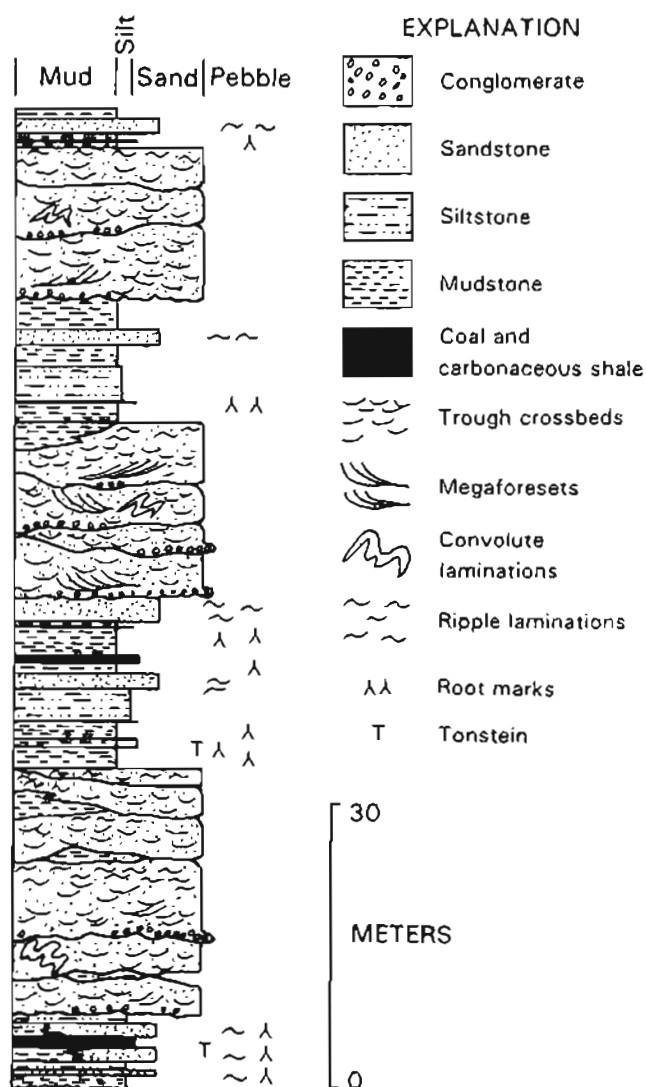


Figure 5. Composite vertical facies association in lower part of Clamgulchian type section of the Sterling Formation.

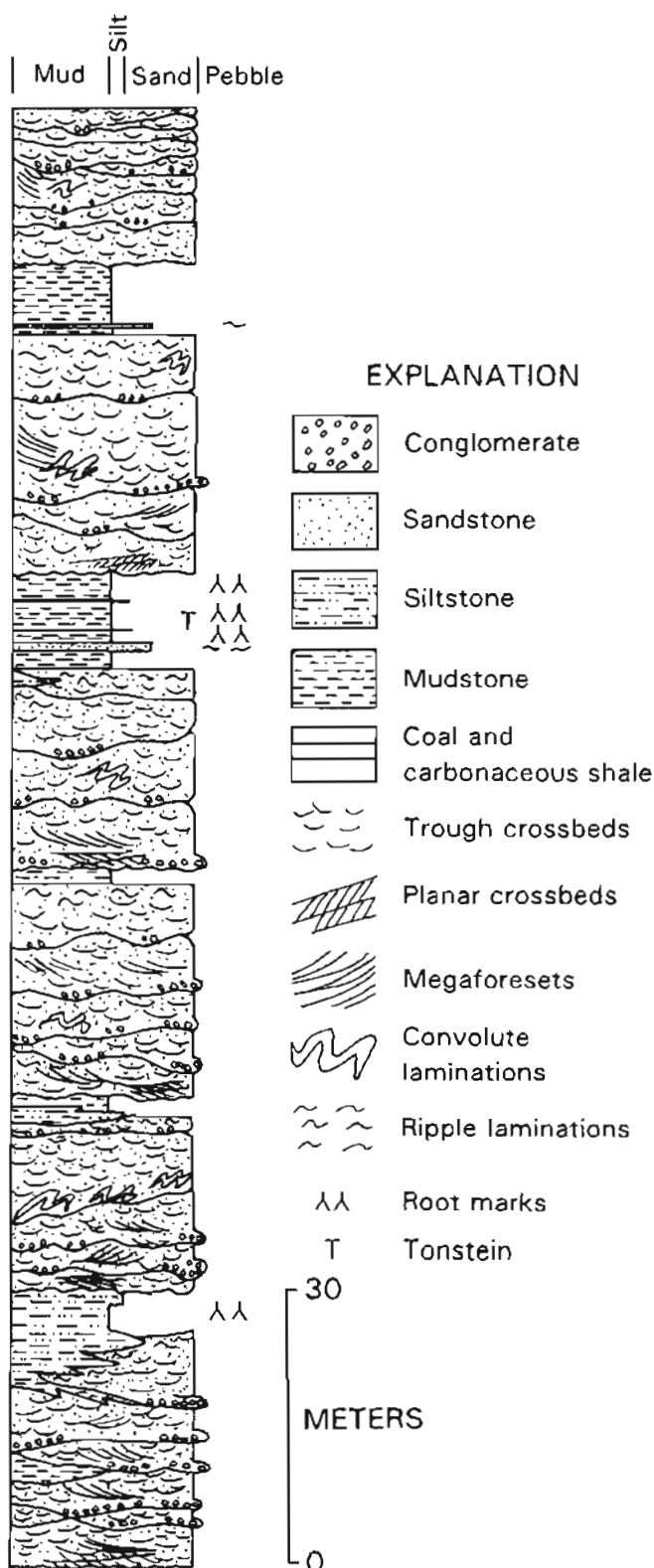


Figure 6. Composite vertical facies association in middle part of Clamgulchian type section of the Sterling Formation.

The middle part of the Clamgulchian type section of the Sterling Formation is composed of alternating fining-upward sandstone, and mudstone and siltstone facies associations (fig. 6). Fining-upward sandstones average 27 m in thickness and the mudstone and siltstone sequences average 3 m in thickness. The fining-upward sandstones are amalgamated into multiscoured (as many as five internal scour bases) bodies and are interbedded with thin to thick interbedded mudstone and siltstone sequences. Although the multiscoured sandstone bodies display multistory (six tiers) and multilateral architecture as in the lower interval, here the multistacked sandstone bodies are commonly separated by thin mudstone-siltstone lenses with basal scours. The mudstone and siltstone sequences, which

contain coarsening-upward sandstone, are also laterally gradational into the fining-upward sandstones particularly in the upper parts of the multistacked sandstone complexes.

The upper part of the Clamgulchian type section of the Sterling Formation consists of interbedded fining-upward sandstone, mudstone and siltstone, and coal, carbonaceous shale, and tonstein facies associations (fig. 7). The fining-upward sandstones range from 18 to 38 m in thickness and like those in the lower and middle intervals also occur as amalgamated multiscoured bodies. The multiscoured sandstones are also multistory (three tiers) and interbedded with thin to thick (1.5 to 31 m) mudstone and siltstone sequences and thin (0.4 m) coal, carbonaceous shale, and tonstein sequences. The multiscoured sandstone bodies in the upper part of the interval consist of as many six internal scour bases and are locally interrupted by numerous scour-based mudstone and siltstone lenses. The amalgamated multiscoured sandstones also exhibit multilateral architecture, but have more pronounced offset or en echelon lateral arrangements than those in the middle interval. However, as in the middle interval, the fining-upward sandstones also locally grade laterally into mudstone and siltstone and coarsening-upward sandstone sequences.

The three groups of facies associations include both the fining-upward sandstone and mudstone and siltstone sequences throughout the stratigraphic interval. The coal, carbonaceous shale, and tonstein sequence is not present throughout and generally thins upward in the stratigraphic interval. Although the coal, carbonaceous shale, and tonstein sequences occur in thick mudstone and siltstone sequences, thin and less coaly sequences are associated with the thinner mudstone and siltstone sequences. In addition, the thick coal, carbonaceous shale, and tonstein sequences are interbedded with thin fining-upward sandstones.

## RESERVOIR ARCHITECTURE

Successions of the fining-upward sandstones throughout the stratigraphic interval show both upward thickening and changes in reservoir architecture. The fining-upward sandstones increase twofold in thickness upward from the lower to the upper part of the study interval. This is accompanied by increased multistory and internal heterogeneity of the sandstone complexes. The number of multistacked, fining-upward sandstones increases threefold upward and is accompanied by an upward increase in the frequency of internal bounding surfaces (compare for example the multistory and internal basal scours in figs. 5–7). Sedimentary structures within sandstone bodies bounded by scour surfaces range from homogeneous trough crossbeds in the lower part and ripple laminations in the upper part to heterogeneous, haphazardly arranged convolute laminations, megafosets, trough and planar crossbeds in the lower part and ripple laminations in the

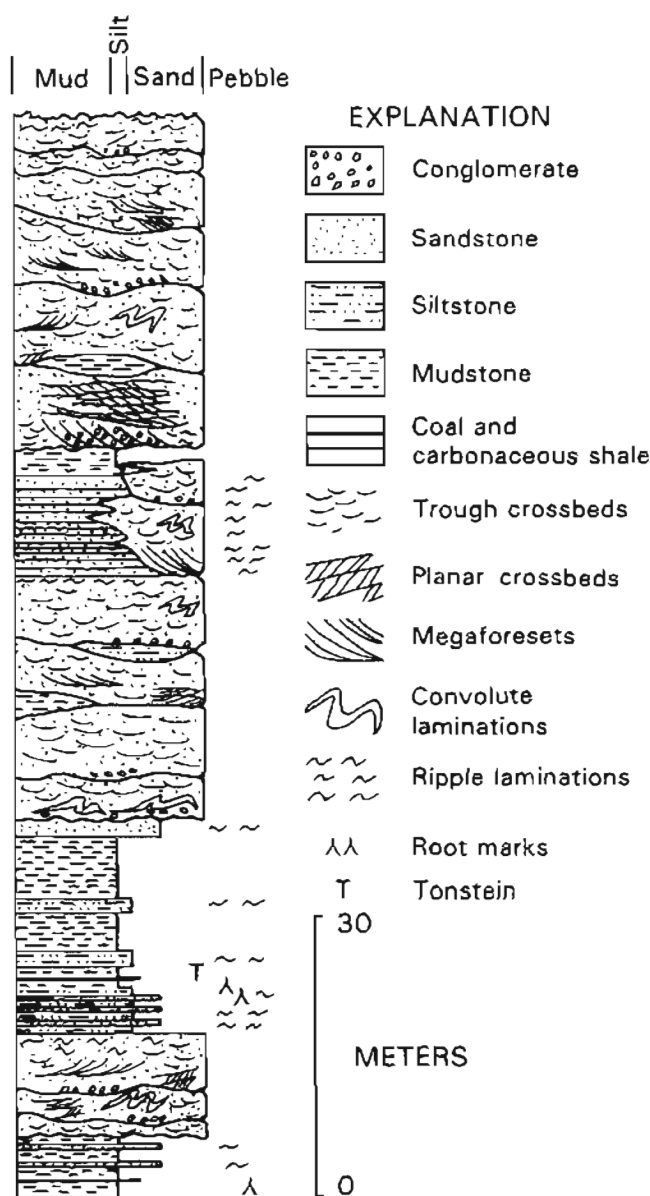


Figure 7. Composite vertical facies association in upper part of Clamgulchian type section of the Sterling Formation.

upper part (see figs. 8–10). Framework architecture of the thick complexes of sandstones in the upper part of the stratigraphic interval also records inclusion of more basally scoured mudstone and siltstone lenses (see figs. 5–7).

Thus, framework architecture of the fining-upward sandstone reservoir system indicates different levels of heterogeneity, based on the hierarchy, nature, continuity, and arrangement of bounding surfaces. The thin fining-upward sandstone reservoir system with fewer multistacked sandstone bodies and accompanying bounding scour surfaces in the lower part of the Clamgulchian type section of the Sterling Formation is a more homogeneous and less compartmentalized reservoir system (fig. 8). That is, compartmentalization by permeability barriers (such as bounding surfaces) subdivides a potential reservoir system into many smaller individual reservoirs of more homogeneous properties. First-order bounding surfaces that compartmentalized the fining-upward sandstone reservoir system include a continuous sharp basal scour surface, and gradational marginal and upper contact with surrounding fine-grained sediments. Second-order bounding surfaces are the internal, discontinuous sharp basal scour surfaces of the multistacked sandstone bodies. Third-order bounding surfaces

within the multistacked sandstone bodies are short, discontinuous bounding surfaces of single bedforms such as trough crossbeds, megaforesets, convolute laminations, and ripple laminations. Fourth-order bounding surfaces within these bedforms include very short, asynchronous laminae surfaces. The transition from the trough-crossbedded lower part to the ripple-laminated uppermost part of the sandstone bodies is locally disrupted by some megaforeset and large-scale convolute bedforms. In addition, the upper part of the sandstone reservoir system is locally interrupted by subordinate basally erosional lenses of mudstone and siltstone. Juxtaposition of the reservoir sandstone system with thick, potential source rocks for gas consisting of the coal, carbonaceous shale, and mudstone sequences and thick impermeable rocks consisting of mudstone and siltstone sequences make them ideal targets for exploration.

In contrast, the thick fining-upward sandstones in the middle and upper parts of the Clamgulchian type section of the Sterling Formation, which consist of a larger number of stacked, single sandstone bodies with accompanying bounding scour surfaces and multiple, unorganized bedforms, represent very heterogeneous and highly compartmentalized reservoir systems (figs. 9, 10). Although

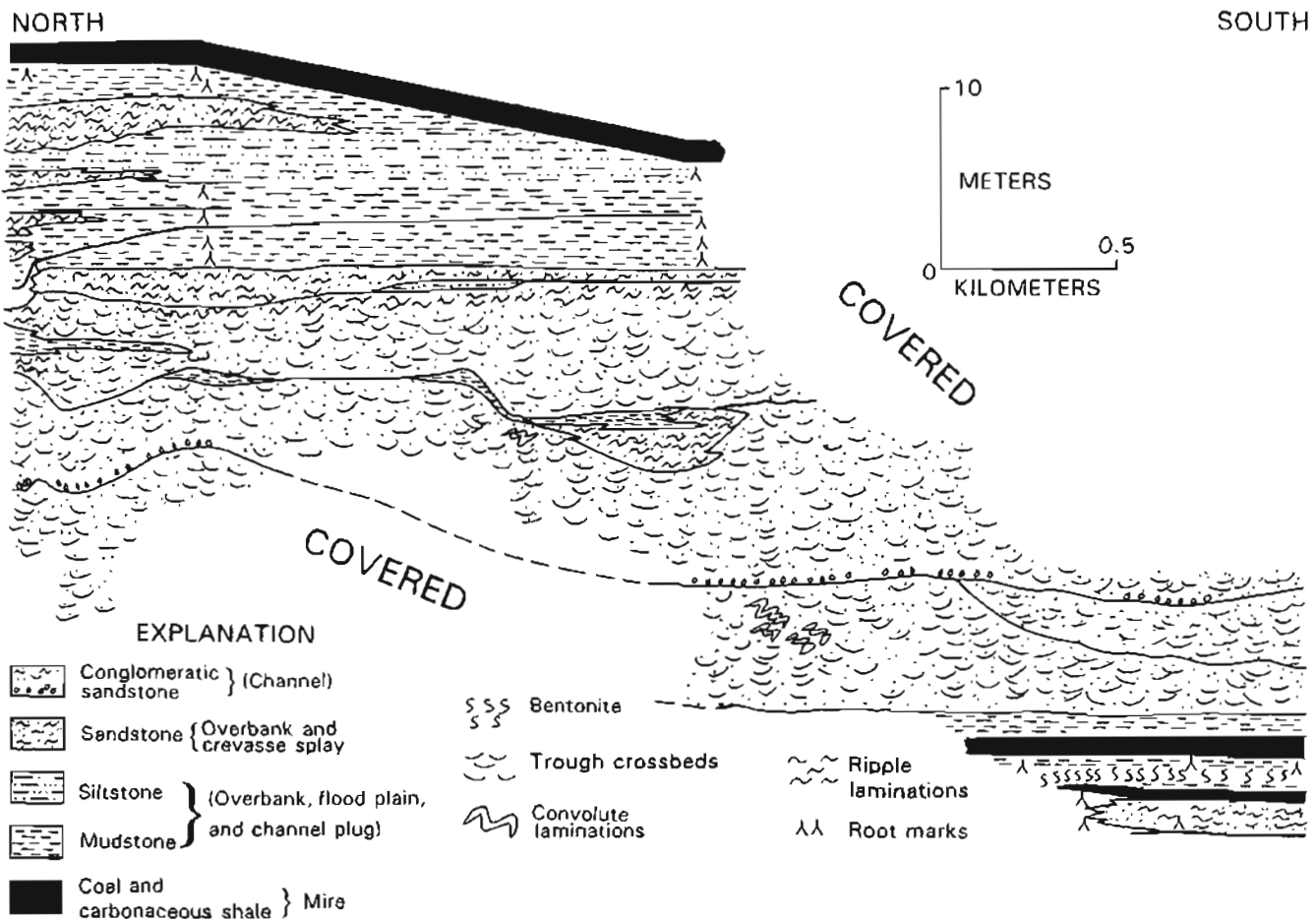


Figure 8. Sandstone reservoir framework architecture in lower part of Clamgulchian type section of the Sterling Formation.

these sandstone reservoir systems contain all four orders of bounding surfaces, their extent and continuity are less predictable than those of the reservoir system in the lower part of the study interval. For example, numerous second-order internal scour surfaces bounding the stacked sandstone bodies truncate each other more commonly and are shorter than those in the reservoir system of the lower part of the Clamgulchian type section. Also, haphazard arrangement of the megaforesets, trough and planar crossbeds, convolute laminations, and ripple laminations produces random patterns of the third- and fourth-order bounding surfaces, resulting in poor interconnectedness and chaotic internal plumbing within the multistacked sandstone bodies. Heterogeneity of the reservoir systems is enhanced by random inclusion of numerous lenses of scour-based mudstone and siltstone. These fine-grained lenses disrupt communication between multistacked sandstone bodies as well as acting as a local impermeable layer. Paucity of potential source rocks (coal, carbonaceous shale, and mudstone sequences) juxtaposed with these sandstone reservoir systems make them less significant as targets for exploitation.

## DISCUSSIONS OF FACIES AND ENVIRONMENTS

The lithostratigraphic sequences and facies associations of the Clamgulchian type section of the Sterling Formation provide a knowledge of their depositional facies, environments, and systems. Depositional facies are interpreted from the facies associations, relying to a great extent on sedimentary models (Schumm, 1977; Galloway

and Hobday, 1983; Reading, 1986). Comparison of physical attributes of the depositional facies to those formed by modern processes defines environments of related depositional systems. Thus, environmental interpretations result from a range of process-response models in the context of the genetic stratigraphy and facies.

In general, the lithostratigraphic sequences and facies associations in the study interval reflect various fluvial environments. The fluvial environments are represented by (1) the fining-upward sandstone sequence deposited in a fluvial channel, (2) the mudstone and siltstone sequence deposited in an overbank-flood-plain environment, and (3) the coal, carbonaceous shale, and tonstein deposited in a mire environment. These sequences, grouped as facies associations, suggest that the fluvial environments were overlapped through time and space. That is, a fluvial system composed of these discrete environments changed in character through time during deposition of the Clamgulchian type section of the Sterling Formation. More specifically, the fluvial-channel morphology changed temporally (fig. 11) from low-sinuosity, bedload stream resulting in deposition of homogeneous sandstone reservoirs to high-sinuosity mixed bedload and suspended-load streams resulting in deposition of heterogeneous sandstone reservoirs.

The lithostratigraphic sequences and facies associations in the lower part of the type section suggest that the fluvial system comprised well-developed mires that were associated with the flood plain. However, interbedding of coal, carbonaceous shale, and tonstein sequences with mudstone and siltstone sequences indicates that the mires were low lying or topogenous to permit detrital influx during floods. Relatively thin mudstone and siltstone sequences indicate diminished suspended load of the fluvial

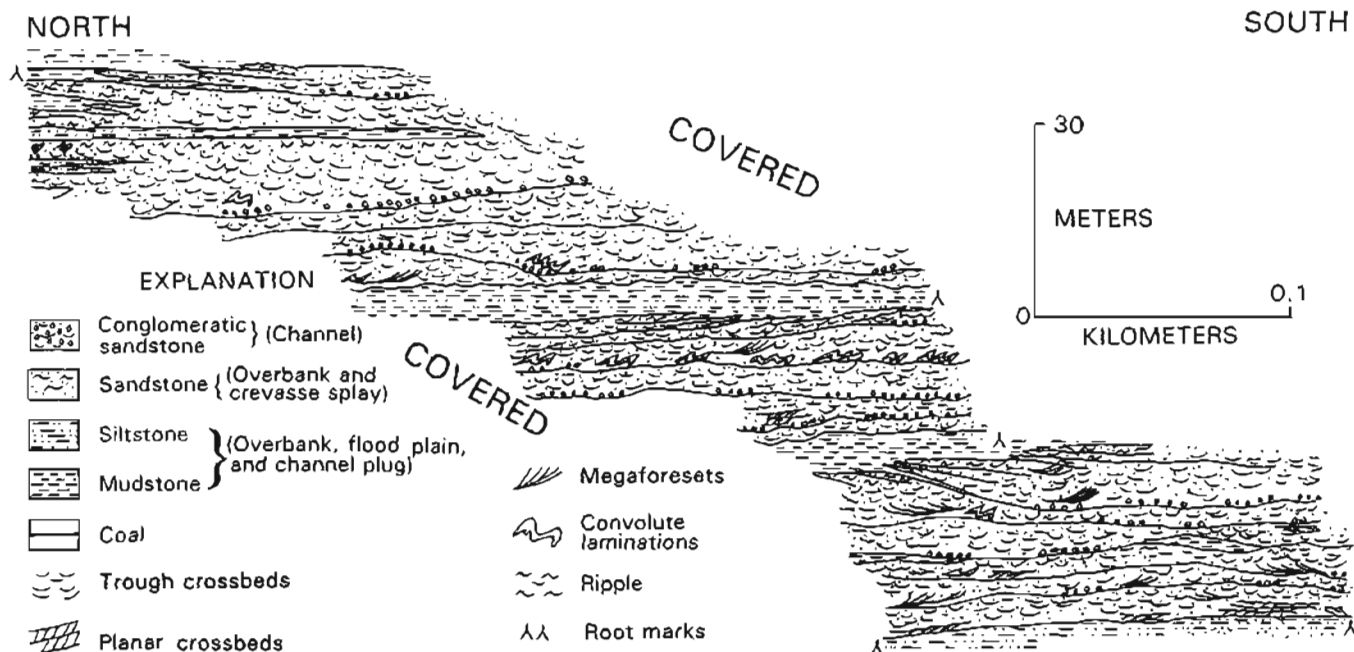


Figure 9. Sandstone reservoir framework architecture in middle part of Clamgulchian type section of the Sterling Formation.

channels; thus, fewer fine-grained sediments were available to choke organic accumulation in the low-lying mires. The presence of a few coarsening-upward sandstones (for example, the units below coalbeds in fig. 5) in mudstone and siltstone sequences represents crevasse splays during floods, which are possible avenues for the limited detrital influxes to the mires in distal areas of the flood plains. Point sources of crevasse splays were moderately low-sinuosity bedload streams in which downstream migration by lateral and mid-channel bars was the dominant process of channel infilling as indicated by the multistory, multilateral, fining-upward sandstones.

In the middle part of the study interval the fluvial system was dominated by fluvial channel and overbank-flood-plain environments. The absence of coal, carbonaceous shale, and tonstein sequences in this facies association suggests that mires were not developed or were outside these fluvial channel, overbank, and flood-plain belts. The multistory, multilateral fining-upward sandstones with a few scour-based mudstone and siltstone sequences represent active bedload and passive suspended load fluvial channel fills. In the active-bedload fluvial-channel fill, alternating lateral and mid-channel sand bars form downstream-migrating bars. This is indicated by scour-based sandstone bodies with megafosets and trough crossbeds. In the passive suspended-load fluvial-channel fill, channel diversion or avulsion is punctuated by deposition of volumetrically minor channel plugs consisting of thin, discontinuous, scour-based mudstone and siltstone sequences. This fining-upward sandstone complex, which was formed in relatively low-sinuosity

braided channels, grades laterally and vertically into mudstone and siltstone sequences formed in channel margins and interchannel flood plains by bank overflow or bank breaches. Thin mudstone and siltstone sequences suggest redistribution of fine-grained suspended load farther into the outlying flood plains, which may have contributed to choking organic accumulation in topogenous mires. Alternating braidbelt, channel margin, and interchannel flood-plain deposits in the middle part of the Clamgulchian type section of the Sterling Formation reflect reoccupation and consequent stacking of channel-overbank-flood-plain sediments. This may be due to influence by either local subsidence resulting from tectonism, sediment auto-compaction, or confinement by relatively resistant fine-grained flood-plain sediments.

In the upper part of the Clamgulchian type section of the Sterling Formation, the lithostratigraphic sequences and facies associations represent fluvial braidbelt-overbank-flood-plain deposits similar to those of the middle part of the interval. However, a difference lies in the occurrence of minor coal, carbonaceous shale, and tonstein sequences in the lower part of the interval and in the framework architecture of the fining-upward sandstone complex in the upper part of the interval. The coal, carbonaceous shale, and tonstein sequences probably represent accumulations in topogenous mires that formed in distal parts of the interchannel flood plains, which consequently encroached on abandoned braidbelt-overbank-flood-plain deposits. However, thick mudstone and siltstone sequences with accompanying coarsening-upward sandstone suggest abundant suspended-load

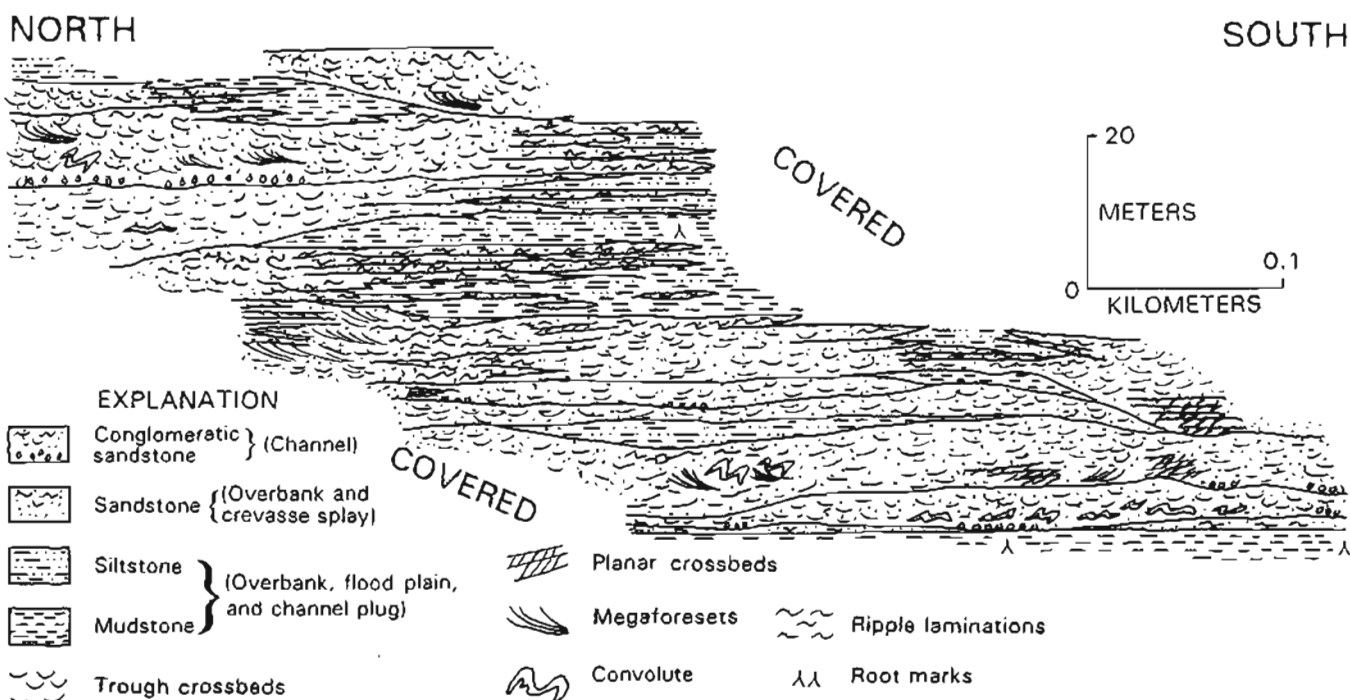


Figure 10. Sandstone reservoir framework architecture in upper part of Clamgulchian type section of the Sterling Formation.

sediments transmitted through crevasse splays, which choked organic accumulation in the topogenous mires. The fining-upward sandstone complex, which consists of numerous scour-based mudstone and siltstone sequences and sandstone bodies with highly variable sedimentary structures, reflects deposition in moderately high-sinuosity braided channels. The numerous stacked, scour-based fining-upward sandstone bodies indicate that these channels were infilled by multiple braid bars of bedload sediments. Associated abandoned braid channels were infilled by suspended-load sediments represented by the discontinuous, scour-based mudstone and siltstone sequences. Offset arrangement of fining-upward sandstone complexes suggest repeated shifts of the braided stream by avulsion via channel-bank breaches and subsequent abandonment of stream courses on which overbank-flood-plain and mire relocate.

### SUMMARY

The Clamgulchian type section of the Sterling Formation represents deposits of a fluvial system that consisted

of integrated drainage networks. These networks consist mainly of bedload and subordinate suspended-load channels bounded by overbank and interchannel flood-plain-crevasse splay and mire environments. This fluvial system displays a systematic evolution in response to changes in sediment supply, flow discharges, gradient, avulsion, and basin or local subsidence. Through time, the Clamgulchian fluvial system evolved from bedload to mixed bedload and suspended-load channels. Bedload fluvial channels exhibit low sinuosity characterized by lateral- and mid-channel bars. Mixed bedload and suspended-load fluvial channels display moderately high sinuosity with multiple braid bars and abandoned channel plugs. Facies association shows that the interchannel flood plain, which is related to the bedload fluvial system, favored development of topogenous mires where organic accumulation is directly due to sparse influx of suspended-load sediments. In the mixed bedload and suspended-load system, redistribution during floods of suspended-load sediments into low-lying mires choked organic accumulation. Presence of tonsteins in the coal and carbonaceous shale sequences indicates that ash from

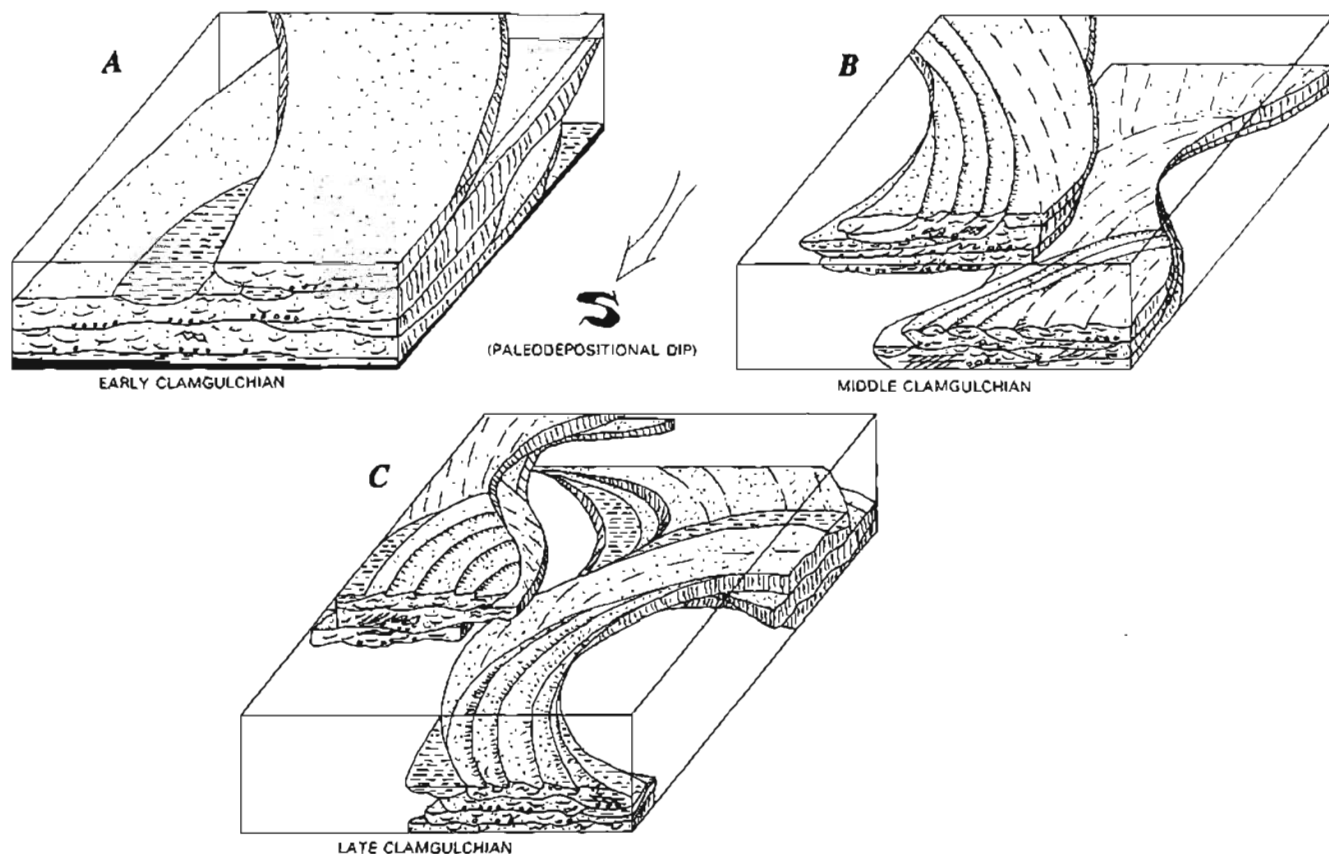


**Figure 11.** Idealized three-dimensional framework architecture, geometry, vertical and lateral distributions, and internal structures of sandstone reservoir systems in Clamgulchian type section of the Sterling Formation. Sandstone reservoirs were deposited within: A, bedload; B, mixed bedload; and C, suspended-load fluvial systems. Sinuosity of fluvial systems increased from bedload to mixed fluvial systems. See figures 7–10 for explanation of symbols.



volcanism along the Aleutian-Alaskan Ranges frequently interrupted organic accumulation in the mires (Reinink-Smith, 1990).

Depositional system analysis of the Clamgulchian sandstones provides insights into the framework architecture of reservoir systems that control accumulation and production of hydrocarbons. Fining-upward sandstone complexes formed by the bedload fluvial system are the most homogeneous and least compartmentalized reservoir systems. Fining-upward sandstone complexes containing abandoned channel plugs and highly variable sedimentary structures formed by the mixed bedload and suspended-load fluvial system are heterogeneous and highly compartmentalized reservoir systems. Finally, close facies association of the bedload fluvial-system sandstones with coal and carbonaceous shale sequences, which serve as source rocks for biogenic gas, provide the best potential targets for hydrocarbon exploitation.

## REFERENCES CITED

- Barnes, F.F., and Cobb, E.H., 1959, Geology and coal resources of the Homer district, Kenai coal field, Alaska: U.S. Geological Survey Bulletin 1058-F, p. 217-260.
- Calderwood, K.W., and Fackler, W.C., 1972, Proposed stratigraphic nomenclature for the Kenai Group, Cook Inlet basin, Alaska: American Association of Petroleum Geologists Bulletin, v. 56, p. 739-754.
- Church, R.E., Crick, R.W., Kirschner, C.E., Lian, E.B., Fackler, W.C., and Vigoren, L.L., 1969, South to north stratigraphic correlation section, Anchor Point to Campbell Point, Cook Inlet basin, Alaska: Anchorage, Alaska Geological Society, 1 pl.
- Flores, R.M., and Stricker, G.D., 1992, Some facies aspects of the upper part of the Kenai Group, southern Kenai Peninsula, Alaska, in Bradley, D.C., and Dusel-Bacon, Cynthia, eds., Geologic studies in Alaska by the U. S. Geological Survey, 1991: U.S. Geological Survey Bulletin 2041, p. 160-170.
- Galloway, W.E., and Hobday, D.K., 1983, Terrigenous clastic depositional systems, application to petroleum, coal, and uranium exploration: New York, Springer-Verlag, 423 p.
- Hartman, D.C., Pessel, G.H., and McGee, D.L., 1972, Preliminary report on stratigraphy of Kenai Group of upper Cook Inlet, Alaska: Alaska Division of Geological and Geophysical Surveys Special Report 5, 4 p.
- Hayes, J.B., Harms, J.C., and Wilson, T.W., 1976, Contrasts between braided and meandering stream deposits, Beluga and Sterling Formations (Tertiary), Cook Inlet, Alaska, in Miller, T.P., ed., Recent and ancient sedimentary environments in Alaska: Alaska Geological Society Proceedings, p. J1-J27.
- Hite, D.M., 1975, Some sedimentary aspects of the Kenai Group, Cook Inlet, Alaska, in Sisson, A., ed., Guide to the geology of the Kenai Peninsula, Alaska: Anchorage, Alaska Geological Society, p. 3-19.
- , 1976, Some sedimentary aspects of the Kenai Group, Cook Inlet, Alaska, in Miller, T.P., ed., Recent and ancient sedimentary environments in Alaska: Alaska Geological Society Proceedings, p. 11-123.
- Kelly, T.E., 1963, Geology and hydrocarbons in Cook Inlet basin, Alaska, in Childs, O.E., and Beebe, B.W., eds., Backbone of the Americas: American Association of Petroleum Geologists Memoir, v. 2, p. 278-296.
- , 1968, Gas accumulations in nonmarine strata, Cook Inlet basin, Alaska, in Beebe, B.W., and Curtis, B.F., eds., Natural gases of North America: American Association of Petroleum Geologists Memoir, v. 9, p. 49-64.
- Magoon, L.B., and Anders, D.E., 1990, Oil-source rock correlation using carbon isotope data and biological marker compounds, Cook Inlet-Alaska Peninsula, Alaska: American Association of Petroleum Geologists Bulletin, v. 74, p. 711.
- Martini, I.P., and Glooschenko, W.A., 1985, Cold climate peat formation in Canada, and its relevance to lower Permian coal measures of Australia: Earth-Science Reviews, v. 32, p. 141-172.
- Merritt, R.D., 1986, Paleoenvironmental and tectonic controls in major coal basins of Alaska, in Lyons, P.C. and Rice, C.L., eds., Paleoenvironmental and tectonic controls in coal-forming basins in the United States: Geological Society of America Special Paper 210, p. 173-200.
- Merritt, R.D., Lueck, L.L., Rawlinson, S.E., Belowich, M.A., Goff, K.M., Clough, J.C., and Reinink-Smith, L.M., 1987, Southern Kenai Peninsula (Homer district) coal-resource assessment and mapping project: Alaska Division of Geological and Geophysical Surveys Public-Data File 87-15, 125 p.
- Moore, W.L., 1976, The stratigraphy and environments of deposition of the Cretaceous Hell Creek Formation (reconnaissance) and the Paleocene Ludlow Formation (detailed), southwestern North Dakota: North Dakota Geological Survey Report of Investigations No. 56, 40 p.
- Reading, H.G., ed., 1986, Sedimentary environments and facies: Oxford, Blackwell Scientific Publications, 615 p.
- Reinink-Smith, L.M., 1990, Relative frequency of Neogene volcanic events as recorded in coal partings from the Kenai lowland, Alaska: A comparison with deep-sea core data: Geological Society of America Bulletin, v. 102, p. 830-840.
- Schumm, S.A., 1977, The fluvial system: New York, John Wiley & Sons, 338 p.
- Wolfe, J.A., Hopkins, D.M., and Leopold, E.B., 1966, Tertiary stratigraphy and paleobotany of the Cook Inlet region, Alaska: U.S. Geological Survey Professional Paper 398-A, p. A1-A29.

Reviewers: C. William Keighin and Richard G. Stanley



# GEOCHEMISTRY OF OPHIOLITIC ROCKS FROM KNIGHT ISLAND, PRINCE WILLIAM SOUND, ALASKA

By Steven W. Nelson and Matthew S. Nelson

## ABSTRACT

The geology of Knight Island consists of the oceanic crustal component of an ophiolite suite of rocks assigned to the early Tertiary Orca Group, a thick deep-sea-fan flysch complex. The upper part of the ophiolite is a 5,000-m-thick section of westward-dipping pillow and massive basalt. The central part of the island is made up of a thick sheeted dike unit with massive gabbro plugs, plagiogranite, and rare blocks of ultramafic rock. All the analyzed rocks retain their primary igneous textures despite low-grade metamorphism characterized by chlorite, prehnite, pumpellyite, and actinolite. Geochemical and discrimination diagrams suggest several tectonic environments for the formation of the ophiolite: a dominant MORB-type setting (based on  $La/Ta = 14-30$ ,  $FeO^*/MgO$  vs  $TiO_2 = 1$ , high Ti classification, and flat REE abundances between 10 and 20 times chondrite), ocean-island tholeiite, and various arc settings. Our favored interpretation to account for the range of settings and the known geology is that the ophiolite formed in a ridge/trench region similar to the present-day Juan de Fuca Ridge and involved migration and injection of sediment-contaminated basaltic magmas upward along a partially subducted ridge and eruption of pillow lavas along the unsubducted ridge segment. Geochemical analyses of eight basalt samples from Drier Bay show no significant stratigraphic variation within the pillow basalt section sampled.

## INTRODUCTION

Ophiolitic rocks of the Prince William Sound area (fig. 1) include various oceanic crustal components in the Chugach and Prince William lithotectonic terranes of Jones and others (1987). The Chugach terrane is made up of two fault-bounded Mesozoic belts (Jones and others, 1981). The northern belt consists of a discontinuous melange named the McHugh Complex (Clark, 1973). The southern belt consists of Late Cretaceous deep-sea fan turbidites and oceanic crust of the Valdez Group (Plafker and others, 1977).

Summaries of the geologic and geochemical interpretations of the ophiolitic rocks in the Chugach terrane indicate several tectonic settings. Volcanic blocks from the melange of the McHugh Complex suggest both normal and enriched MORB as well as within-plate tectonic settings (Nelson and Blome, 1991; Plafker and others, 1989). Basaltic rocks from the Valdez Group are interpreted to have formed in a mid-ocean ridge basalt (MORB) setting (Crowe and others, 1992) or primitive island-arc setting (Lull and Plafker, 1990).

The Prince William terrane lies adjacent to and south of the Chugach terrane, and it is separated from it by the Contact fault system (Plafker and others, 1986). The terrane is composed of the Orca Group, an accreted late Paleocene through early middle Eocene deep-sea-fan complex, and ophiolitic and volcanic units of similar age (Winkler, 1976; Nelson and others, 1985; Plafker and others, 1985).

Paleomagnetic and fossil data from the two terranes indicate that they originated south of their present position. There are no paleomagnetic data from the McHugh Complex, but paleogeographic data based on radiolarian fauna from the melange, although not precise, suggest large northward displacements for Triassic cherts and suggest that Jurassic and Early Cretaceous cherts were displaced to near their present position by the Late Cretaceous (Blome and others, 1990). There is no paleomagnetic or paleogeographic data from the Valdez Group, and early data from the Orca Group are contradictory (Hillhouse and others, 1985; Plumley and Plafker, 1985). Careful analyses by Bol and others (1992) on rocks of the Orca Group from the Resurrection Peninsula ophiolite (fig. 1) indicate 13 degrees of northward displacement. Most workers agree that the Chugach and Prince William terranes are allocthonous and that they were nearly in place (with respect to the rest of North America) by early Tertiary time (Plafker and others, in press).

In the Prince William terrane, the igneous rocks of the Orca Group include three ophiolites (fig. 1) referred to as the Resurrection Peninsula, Knight Island, and Glacier Island ophiolites (Crowe and others, 1992; Nelson and others, 1985). These are the youngest and most complete ophiolites in Alaska. In a composite section (Nelson, 1992) from top to bottom are a pillow basalt unit, locally

interbedded with turbidites, volcanic breccia, and tuff, a sheeted dike unit, and a layered gabbro unit. Minor amounts of ultramafic rocks and plagiogranite are also present.

## KNIGHT ISLAND OPHIOLITE

Knight Island, located in western Prince William Sound (fig. 2), is composed of oceanic crustal rocks typical of the upper part of an ophiolite sequence (Coleman, 1977; Nelson and others, 1987). These rocks include a sequence of pillow and massive basalt (5,000 m thick) (fig. 3) and sheeted dikes with minor related rocks including plagiogranite (figs. 4, 5), peridotite, massive gabbro, and diorite stocks. Gravity data suggest that the ophiolite may extend as much as 10 km below sea level (Case and others, 1966).

In a previous study, Tysdal and others (1977) recognized that the Knight Island ophiolite complex has geologic characteristics of oceanic spreading ridges and of ophiolites, yet occurs within flysch deposits along the present continental margin. They raised several questions: (1) do these rocks represent remnants of a major oceanic spreading center such as the Kula ridge, (2) are they products of incipient island-arc volcanism, or (3) are they products of tholeiitic magmatic activity in a fore-arc subduction setting?

In a regional study of major- and minor-element geochemistry of the volcanic rocks of the Orca Group in Prince William Sound, Crowe and others (1992) recognized two groupings: (1) an ophiolite sequence consisting of several complexes (including Knight Island) with pillow basalt, sheeted dikes, layered and massive gabbro, and ultramafic bodies, and (2) a nonophiolitic sequence containing mixed mafic volcanic rocks and various sedimentary rocks.

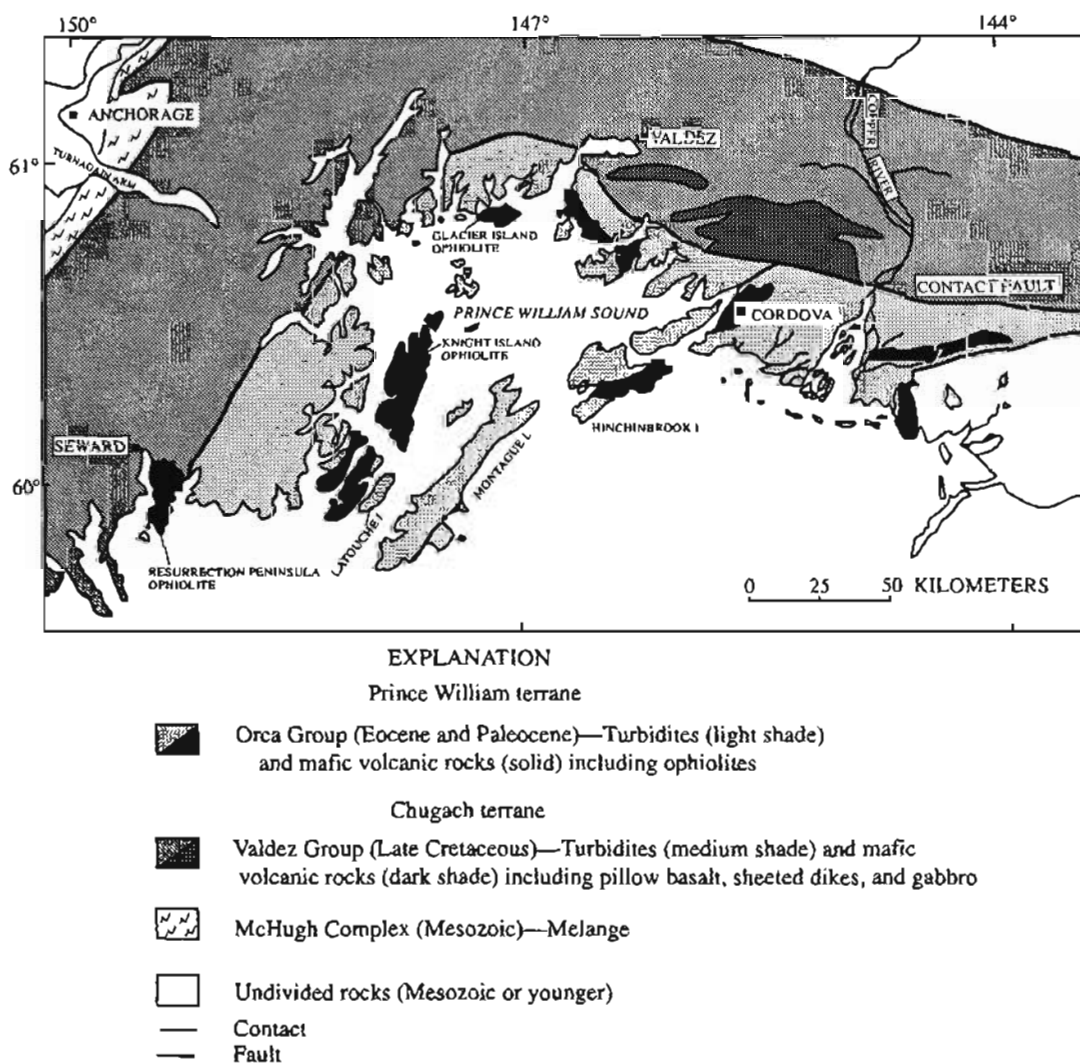


Figure 1. Location map of Prince William Sound region, southcentral Alaska, showing major lithologic units and ophiolite localities mentioned in text (modified from Crowe and others, 1992).

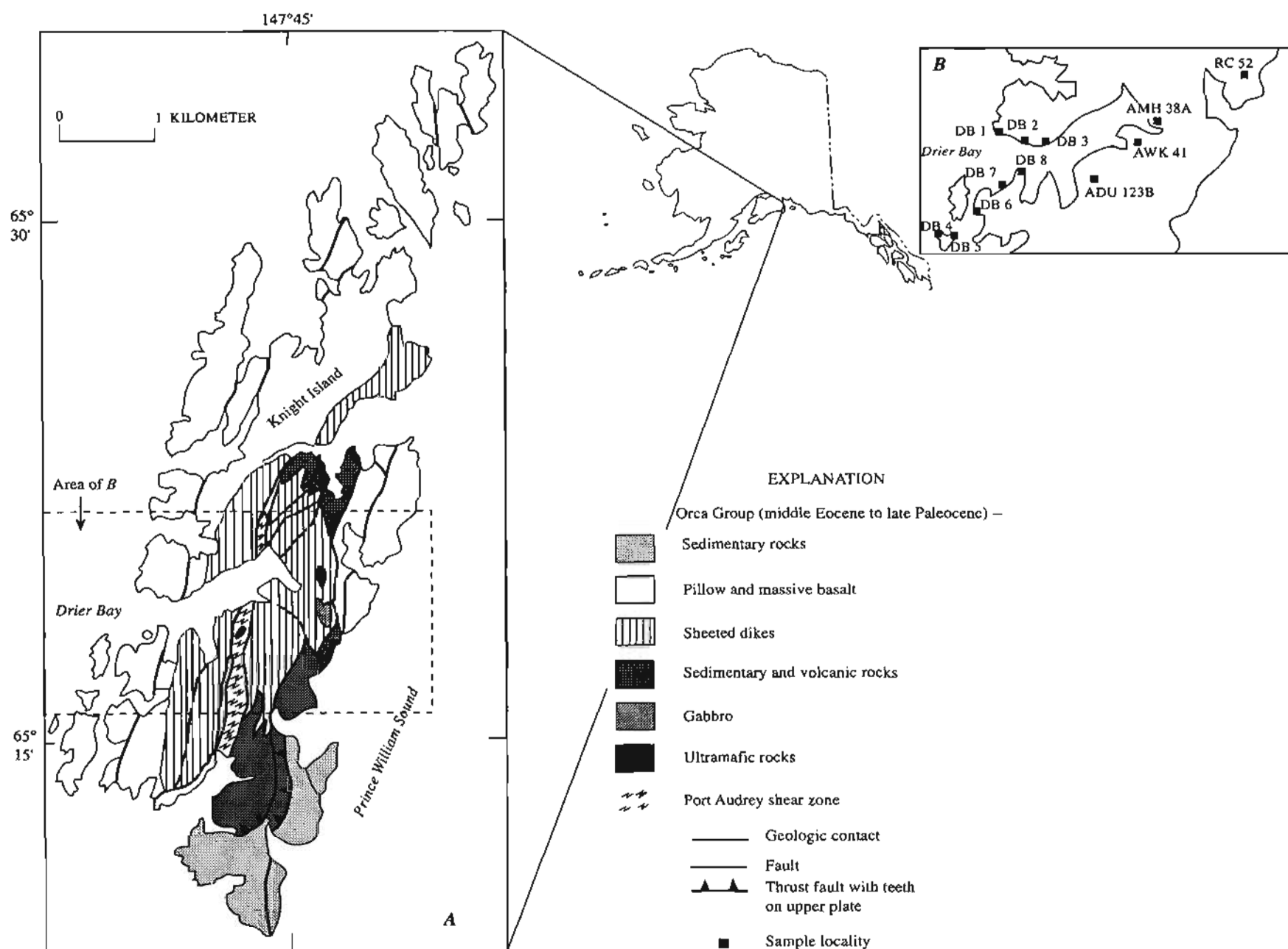


Figure 2. Geologic Map (A) and sample locality map (B) of Knight Island. Geology from Nelson and others (1985).

Crowe and others' (1992) study of the geochemistry suggested several possible tectonic environments of formation for the ophiolites, including MORB and island-arc settings. They suggested generation in a spreading ridge/subduction zone area and possible contamination of the mafic magmas by sediments to account for the geochemical variation.

In this study, we focus on the geochemistry of samples from the different units of the Knight Island ophiolite. The purpose is to better understand the

geochemical signature of the ophiolite and how its geochemistry relates to the regional geochemical interpretations of the earlier studies. Eight samples of basalt were collected in Drier Bay (fig. 2) from different intervals within a 5,000-m-thick, west-dipping stratigraphic section (Richter, 1965; Tysdal and others, 1977). These samples, within the basalt section, were used to test for geochemical changes stratigraphically. Additionally, analyses of four samples from Crowe and others (1992, table 1) on Knight Island are included in the geochemical diagrams of this report.

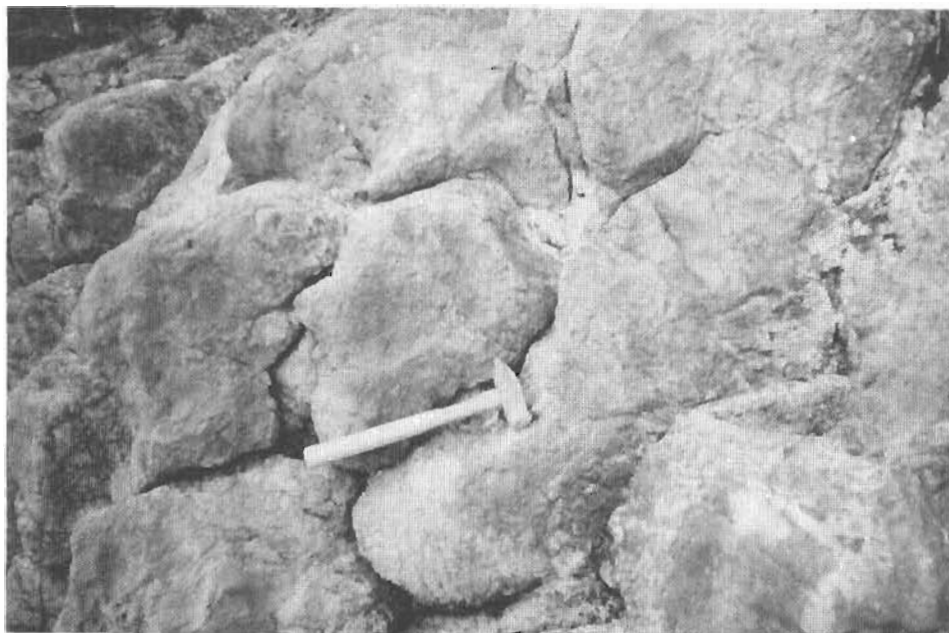


Figure 3. Pillow basalt at locality DB 2, Drier Bay, Knight Island.



Figure 4. Glaciated outcrop of sheeted dikes from central Knight Island.

The additional samples are from a gabbro body (ADU123B) and two sheeted dikes (AMH 38A, AWK 41) from the Drier Bay area, and a diorite plug (RC 52) intruding pillow basalt in the Rua Cove mine (fig. 2B). Analyses of ultramafic rocks from Knight Island are listed in Crowe and others (1992) and are not considered in this paper. Plagiogranite samples from Knight Island are presently being analyzed.

## PETROGRAPHY

Five samples of the pillow basalt are fine to medium grained and porphyritic. They contain rare phenocrysts of plagioclase and clinopyroxene in a hyalopilitic or pilotaxitic groundmass containing laths of plagioclase, commonly with swallow-tail or belt-buckle morphologies. These plagioclase laths float in a brown cloudy matrix with interstitial clinopyroxene, chlorite, and opaque minerals. The samples contain rare amygdules of chlorite, and some have minor calcite. All samples contain one or more

of the low-grade metamorphic minerals chlorite, prehnite, or pumpellyite. The only secondary fabric is rare veins of calcite and quartz or prehnite. Pillows range in size from 0.5 m to 1 m in diameter.

Three of the basalt samples are from massive flows, 3-4 m thick interlayered with pillow basalt. All three exhibit fine-grained intergranular texture with plagioclase laths and interstitial subhedral clinopyroxene and chlorite patches. All contain the low-grade metamorphic minerals chlorite+pumpellyite or chlorite+epidote.

The two diabase samples from sheeted dikes are fine grained with ophitic or diabasic texture. The diabase contains rare phenocrysts of well-zoned plagioclase. Altered clinopyroxene occurs in the groundmass. No secondary fabric was observed, and both samples contain chlorite and actinolite.

The gabbro sample is a medium-grained rock with relatively fresh plagioclase and actinolite pseudomorphs after pyroxene. This sample is from the Port Audrey shear zone (Richter, 1965; Nelson and others, 1985) and is strongly fractured. Plagioclase shows strong undulatory extinction.

No thin section was available for the diorite sample from the Rua Cove mine.

## GEOCHEMICAL SAMPLING AND RESULTS

The chemical analyses for the eight samples of basaltic rock collected from shoreline outcrops in Drier Bay are presented in table 1. As mentioned above, analyses for the other samples used in this report are from Crowe and others (1992, table 1). To minimize any secondary influences only fresh-appearing samples were collected. The cores of pillows were analyzed to minimize the effect of contact with seawater, and weathering and obvious veins were cut from the sample. The petrographic observations above indicate that these rocks have undergone low-grade regional metamorphism, but retain primary igneous textures.

The degree of alteration was evaluated using the alteration test of Miyashiro (1975). Three of the basalt samples (5A, 6A, and 8A) and the two sheeted dike samples are unaltered (fig. 6). Basalt samples 2A, 4A, and 7A plot in the altered field, indicating a loss of  $K_2O$ . Basalt sample 1A and the diorite sample plot just inside the altered field, indicating possible minor loss of  $K_2O$ . The rare-earth element (REE) diagram (fig. 7) shows the abundances of these relatively immobile trace elements. The flat or light REE depleted patterns indicates that there has been no LREE-enrichment due to weathering (Ludden and Thompson, 1978). In the following diagrams, the "unaltered" sample plots usually overlap the values for all samples, and so we conclude that the net effect of any element mobility on the overall geochemical interpretation is minor.



Figure 5. Plagiogranite (light color) occurrences in sheeted dike unit from central Knight Island.

Table 1. Major-oxide and minor-element compositions of basaltic rocks from Drier Bay, Knight Island

[Major oxides analyzed by Z.A. Brown and E.A. Bailey by rapid rock method; minor elements except Zr, Y, and Nb by G.A. Wandless using INAA; Zr, Y, and Nb by J. Kent using EDXRF]

Sample	90DBN01A	90DBN02A	90DBN03A	90DBN04A	90DBN05A	90DBN06A	90DBN07A	90DBN08A
Major oxides (in weight percent)								
SiO <sub>2</sub>	52.0	50.0	47.5	53.9	48.9	51.5	53.5	51.2
Al <sub>2</sub> O <sub>3</sub>	16.0	16.1	16.3	15.6	16.8	15.6	16.4	18.0
Fe <sub>2</sub> O <sub>3</sub>	1.7	2.2	1.7	2.1	2.0	2.3	1.9	1.4
FeO	5.4	7.0	8.0	5.1	6.6	7.4	6.2	6.0
MgO	6.7	8.1	7.9	6.3	8.8	7.6	7.7	8.1
CaO	8.4	8.1	9.3	8.4	9.3	8.9	5.5	6.8
Na <sub>2</sub> O	5.0	4.4	3.4	5.6	2.1	3.2	5.5	3.8
K <sub>2</sub> O	.46	.12	<.05	<.05	.2	.34	.15	1.4
TiO <sub>2</sub>	.95	1.2	1.4	.99	1.2	1.4	.91	.88
P <sub>2</sub> O <sub>5</sub>	.14	.14	.15	.13	.13	.15	.08	.11
MnO	.11	.11	.10	.12	.12	.16	.11	.14
Total	96.86	97.47	95.75	98.24	96.15	98.55	97.95	97.83
Minor elements (in parts per million)								
La	5.3	4.8	4.5	4.0	3.9	5.3	3.9	4.8
Ce	13	12	12	10	10	13	9.2	12
Nd	8.6	8.6	8.9	6.3	8.8	8.4	7.4	8.4
Sm	2.7	3.1	3.4	2.5	3.2	3.6	2.3	2.5
Eu	.89	.97	1.19	.74	1.05	1.15	.72	.76
Tb	.63	.74	.8	.64	.74	.89	.56	.56
Yb	2.5	2.8	3	2.4	2.9	3.2	2.3	2.3
Lu	.34	.41	.42	.37	.4	.46	.34	.32
Ba	66	41	78	<31	84	110	60	1100
Sr	100	150	250	<60	140	170	120	180
Co	32.3	36.7	43.5	32.1	39.5	36.4	33.3	33.9
Ni	110	80	110	77	110	94	99	100
Cr	241	278	255	220	272	227	273	297
Cs	<.14	<.16	<.5	<.15	.29	<.16	<.15	.31
Hf	2.17	2.28	2.57	1.97	2.3	2.67	1.71	2
Rb	9.5	<4	<4	<5	<4	9.5	11	25
Sb	.17	<.10	.14	.14	<.18	.21	.21	.13
Ta	.22	.25	.24	.22	.19	.22	.17	.24
Th	1.1	.87	.71	1.1	.63	.91	1.1	1.5
U	.51	.29	.31	.45	.38	.36	.43	.64
Zr	96	100	112	94	90	112	74	84
Sc	27.7	36.9	34.6	31.4	35.5	32.5	30.4	29.6
Zn	61	90	97	72	74	84	75	69
Cu	56	64	126	78	66	46	48	66
Y	24	32	32	30	26	34	22	24
Nb	<10	<10	<10	<10	<10	<10	<10	<10

### MAJOR OXIDES

The eight basalt samples from Drier Bay have a range of SiO<sub>2</sub> of 49 to 54 percent (major-oxide values in text recalculated to 100 percent) and using the classification of Cox and others (1979), three are subalkalic basalt, four are alkalic basalt, and one is basaltic andesite. The sheeted dike and gabbro samples have SiO<sub>2</sub> values of 49 and 50 percent and are classified as subalkalic basalt. The average SiO<sub>2</sub> content for these samples is greater than that typical of oceanic tholeiite and is in the range

of values from Knight Island reported by Tysdal and Case (1977). The diorite sample plots as basaltic andesite and has the highest SiO<sub>2</sub> (55 percent) of the entire sample set.

On the AMF plot (fig. 8) all samples except the sheeted dike samples and one basalt sample plot in the calc-alkaline field. The general distribution of values appears to show a calc-alkaline trend. This trend contrasts with the more typical tholeiitic iron-enrichment trend shown regionally in samples from several other ophiolite complexes of the Orca Group (Nelson, 1992).

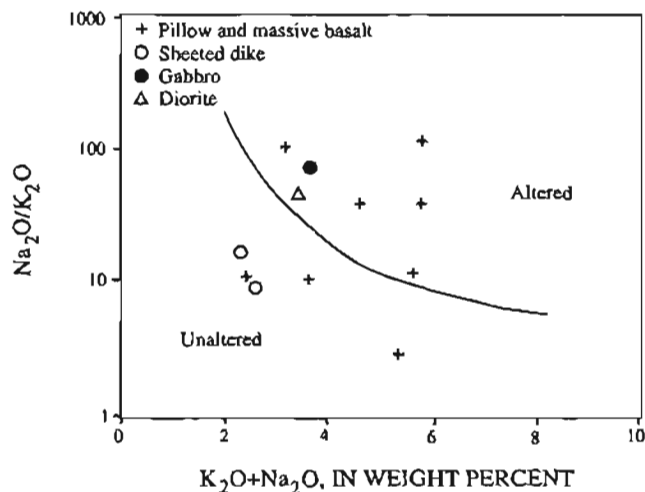


Figure 6. Alteration test based on  $\text{Na}_2\text{O}$  and  $\text{K}_2\text{O}$  variation (after Miyashiro, 1975).

On several major-oxide variation diagrams, the samples generally plot in a tight cluster sometimes overlapping different tectonic settings. Figure 9 ( $\text{CaO}$  and  $\text{Al}_2\text{O}_3$  vs  $\text{TiO}_2$ ) shows a MORB-like pattern that contrasts with arc rocks and several classic ophiolites, such as those at Betts Cove and Troodos (Sun and Nesbitt, 1978), that are now thought to have formed in a suprasubduction zone setting.  $\text{FeO}^*$  (total iron as  $\text{FeO}$ )/ $\text{MgO}$  vs  $\text{TiO}_2$  (fig. 10) also shows a strong cluster of the samples in the MORB field. In a plot of  $\text{TiO}_2$  vs  $\text{FeO}^*/\text{FeO}^* + \text{MgO}$  (fig. 11), the samples plot in the field of high-Ti ophiolites, which Serri (1981) considered typical of several tectonic settings including back-arc basins, ensialic back-arc basins, or major ocean basins, as well as spreading centers along transcurrent plate boundaries. Other alternatives are suggested by the  $\text{TiO}_2$ - $\text{MnO}$ - $\text{P}_2\text{O}_5$  discrimination diagram (fig. 12) of Mullen (1983), which shows that these samples plot in three fields: mid-ocean ridge basalt (MORB), ocean-island tholeiite (OIT), and island-arc tholeiite (IAT).

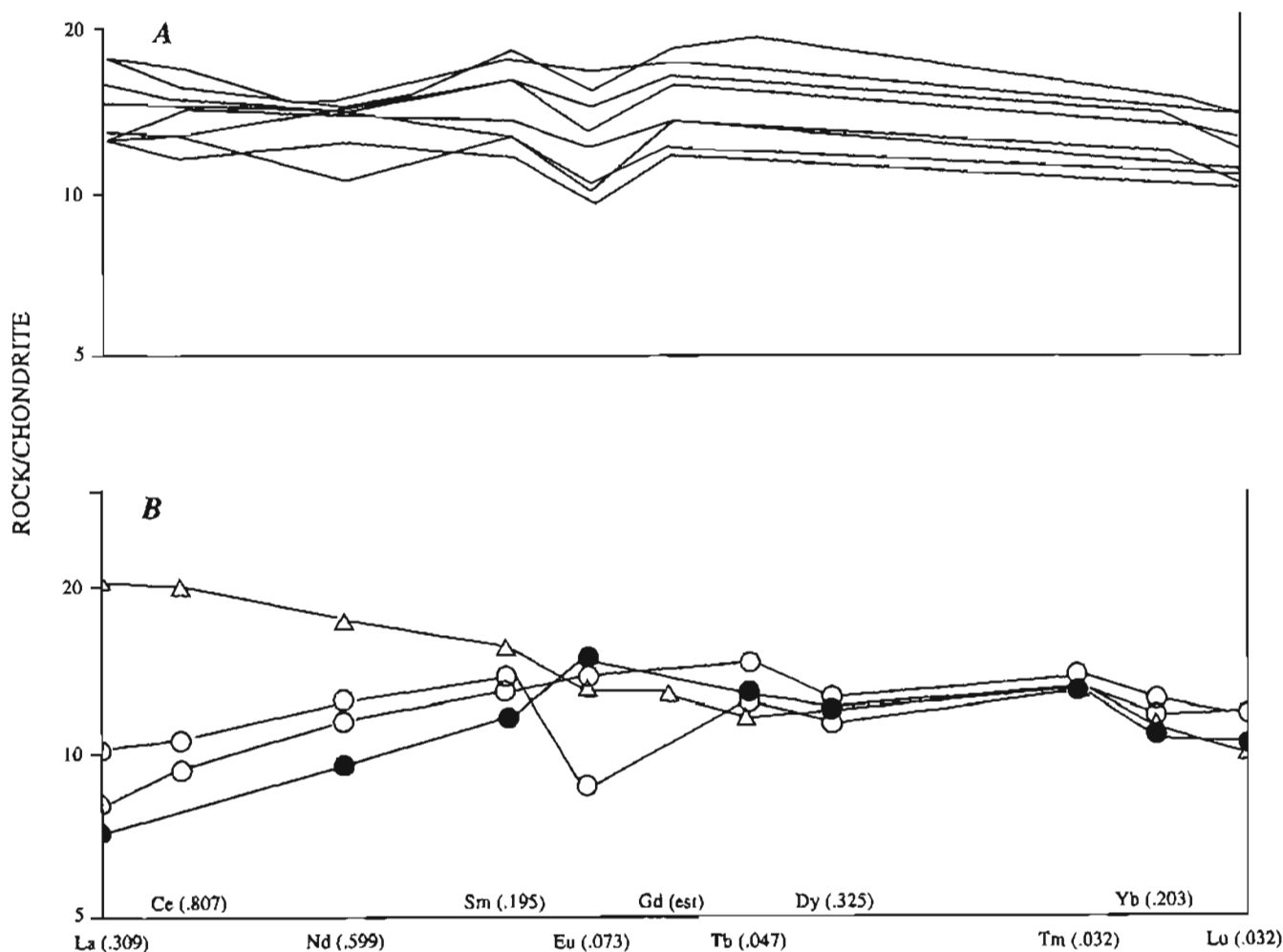
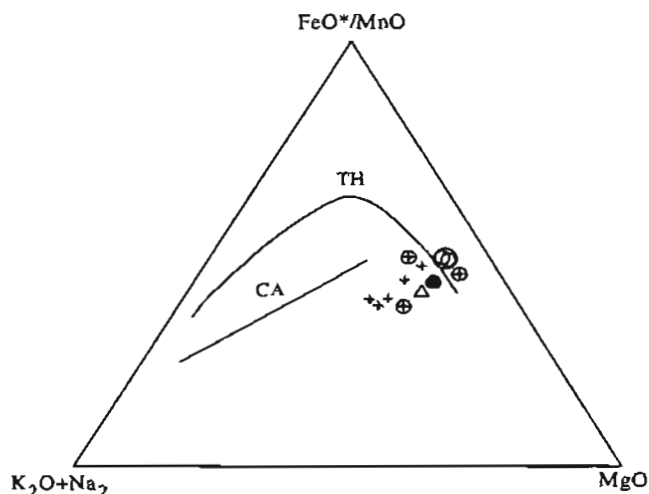
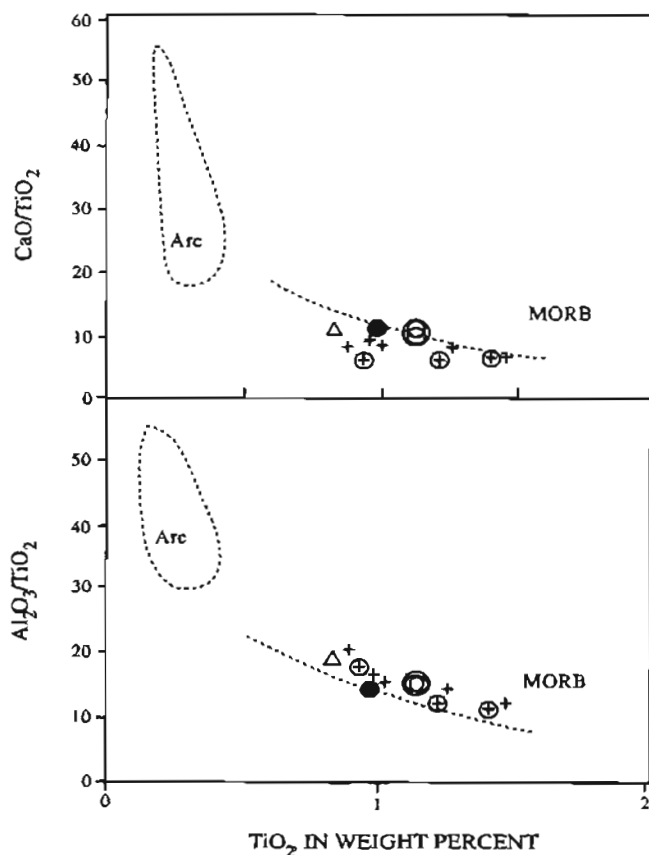


Figure 7. Chondrite-normalized rare-earth element abundances of samples from Knight Island. Normalization constants shown for each element; Gd values are estimates (G.A. Wandless, 1991, written commun.). A, Pillow and massive basalts. B, Symbols same as on figure 6.





**Figure 8.** AMF diagram for samples from Knight Island. Tholeiitic (TH) and calc-alkaline (CA) trends after Wilson (1989). Same symbols as on figure 6. Circled values are "unaltered" samples from figure 6.



**Figure 9.**  $\text{CaO}/\text{TiO}_2$  and  $\text{Al}_2\text{O}_3/\text{TiO}_2$  vs  $\text{TiO}_2$  for samples from Knight Island. Based on Sun and Nesbitt (1978). Same symbols as on figure 6. Circled values are "unaltered" samples from figure 6. MORB, mid-ocean ridge basalt; arc, arc rocks.

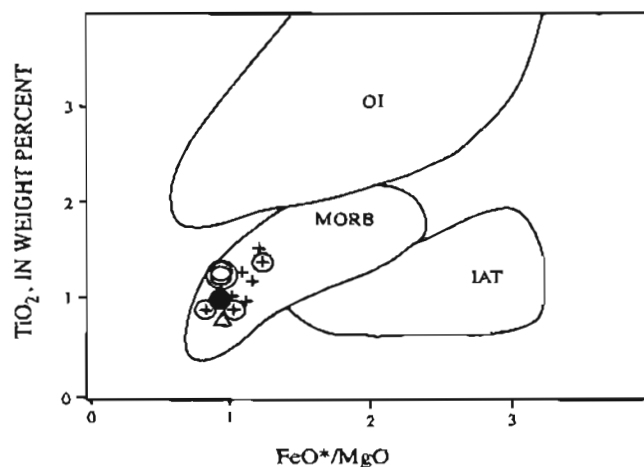


**Figure 10.**  $\text{FeO}^*/\text{MgO}$  vs  $\text{TiO}_2$  for samples from Knight Island (after Glassley, 1974). Symbols same as on figure 6. Circled values are "unaltered" samples from figure 6. MORB, mid-ocean ridge basalt; OI, ocean island rocks; IAT, island-arc tholeiite.

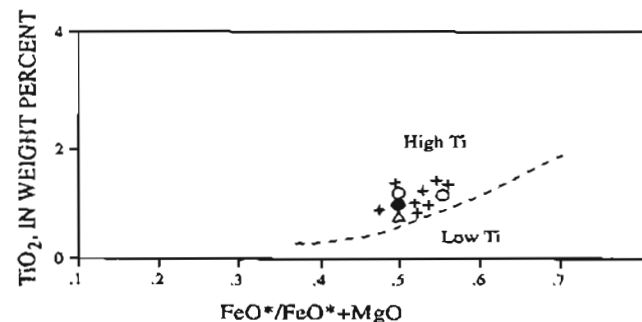


**Figure 11.** High-titanium vs low-titanium classification of samples from Knight Island (after Serri, 1981). Symbols same as on figure 6.

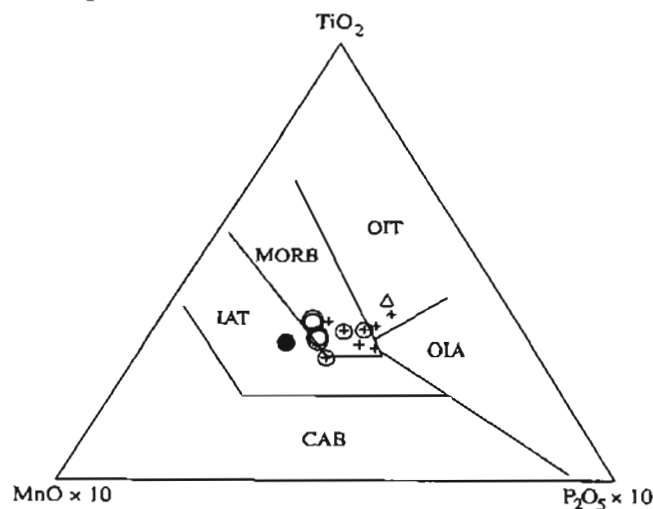


**Figure 12.**  $\text{TiO}_2$ - $\text{MnO}$ - $\text{P}_2\text{O}_5$  (weight percent) ternary diagram for samples from Knight Island. Fields based on Mullen (1983). OIT, ocean-island tholeiite; MORB, mid-ocean ridge basalt; LAT, island-arc tholeiite; OIA, ocean-island alkaline basalt; CAB, calc-alkaline basalt. Same symbols as on figure 6. Circled values are "unaltered" samples from figure 6.

## MINOR ELEMENTS

Chondrite-normalized rare-earth element (REE) abundances for the Drier Bay basaltic rocks show relatively flat patterns between 10 and 20 times chondrite (fig. 7). The basalt samples and one sheeted dike sample have a weak negative europium anomaly suggesting plagioclase fractionation. The sheeted dike and gabbro samples have a light-REE depleted pattern, and their overall abundances are slightly lower than the basaltic rocks. The diorite sample shows minor light REE enrichment, otherwise the values for the other REE are similar to the Drier Bay basalts. The flat REE pattern is similar to REE abundances of ophiolitic rocks from the Orca Group in other localities (Crowe and others, 1992) and is typical of ophiolite rocks in general (Coleman, 1977).

MORB-normalized incompatible trace-element abundances for all samples (fig. 13) have MORB values (near 1) for the nonmobile elements Ta to Yb and variably enriched or depleted values for the more mobile elements Sr, K, Rb, and Th. Abundances of these elements from flysch of the Orca Group (Barker and others, 1992) show an enrichment of Sr, K, Rb, Ba, and Th similar to the basalt samples (fig. 13). This suggests to us an addition of mobile elements to a magma of MORB composition perhaps related to fluids generated in a subduction zone. The high values of Ba and Th, similar to Orca flysch, strongly suggest contamination in a convergent margin setting (Pearce, 1983).

Variation diagrams based on trace-element ratios have been found useful in separating subduction-related components from mantle components in the petrogenesis of magmas (Pearce, 1982). In one (fig. 14), midocean ridge basalts (MORB) and uncontaminated intraplate basalts plot within a narrow zone because mantle-enrichment processes concentrate Ta and Th equally. The use of Yb as the denominator tends to reduce the effect of variations due to partial melting and fractional crystallization. In this diagram, the samples plot in the area typical of oceanic island arc rocks. This suggests that the samples were derived from a depleted mantle source, similar to the source for MORB, but either subduction-zone fluids or contamination from eroded arc material resulted in Th enrichment (Pearce, 1982) and a chemical signature more similar to island-arc rocks.

The provenance of sedimentary rocks involved in magmas can result in misleading tectonic interpretation. This was recognized by Barker and others (1992) in their study of the Eocene plutons intruding the flysch of the Orca Group. They showed conclusively that the granodiorite plutons were derived from large melt components of Orca flysch. With this source in mind, the plutonic rocks should have an S-type classification (Chappell and White, 1974) indicating that the magmas were derived from melted sedimentary rocks. Instead, Barker and others

(1992) found that the plutonic rocks are I-type and chemically similar to volcanic-arc granite. They concluded that the magmas took on the chemical characteristics of the igneous parentage of the Orca sedimentary rocks which, in this case, is considered the Coast Plutonic Complex of Richards and McTaggart (1976) of southeastern Alaska and British Columbia (Farmer and others, 1989).

With this idea in mind we compared the Th/Ta data to similar data from the more regional study of ophiolitic rocks of the Orca Group from Crowe and others (1992). Ratios of Th/Yb and Ta/Yb in the data of Crowe and others (1992) suggest three groups (not shown but refer to fig. 14). The first group is represented by gabbroic rocks which have the lowest ratios (nearly equal to N-MORB values but less than the gabbro sample from Knight Island shown in figure 14). The second group has ratios similar

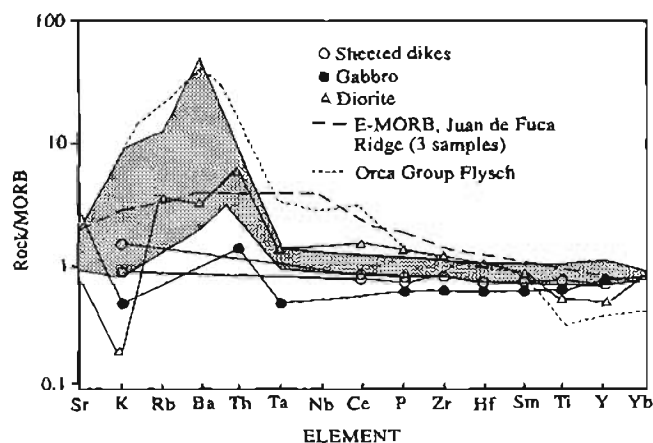


Figure 13. MORB-normalized incompatible trace-element patterns for Knight Island rocks and flysch of the Orca Group. Shaded area is eight pillow and massive basalts. E-MORB values from Karsten and others (1990); Orca flysch average from Barker and others (1992). E-MORB, enriched mid-ocean ridge basalt.

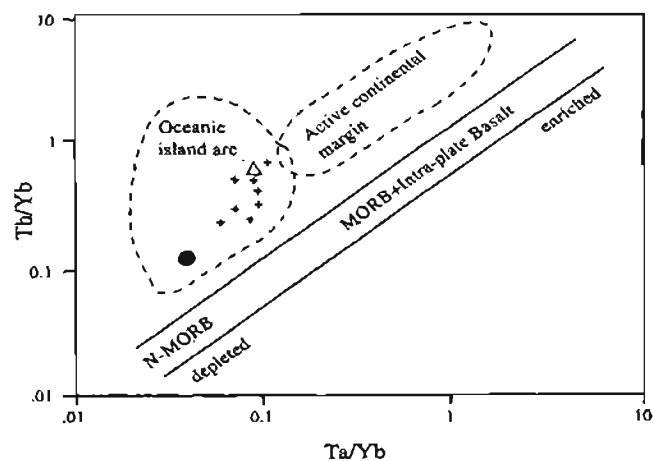


Figure 14. Th/Yb vs Ta/Yb variation diagram for samples from Knight Island. Based on Pearce (1983). Ta not detected in sheeted dikes. Symbols same as on figure 6. N-MORB, normal mid-ocean ridge basalt.

to the basalts from Drier Bay and includes both basalt and sheeted dike samples. The third group has the highest ratios and equals the value for the diorite sample from Knight Island and plagiogranite from the Resurrection Peninsula ophiolite. This vertical distribution of Th/Yb values is compatible with contamination processes (Pearce, 1983). If crustal contamination is the dominant factor accounting for the increase of the ratios from gabbro to dikes and basalt—and finally to diorite and plagiogranite—then this contamination probably took place in the gabbroic magmas that formed the sheeted dikes, basalts, diorite, and possibly the plagiogranite.

Several minor-element discrimination diagrams have been proposed to aid in the determination of the tectonic environment for the generation of various igneous rocks (Pearce and Cann, 1973; Wood, 1980; Wood and others,

1979). These diagrams are useful when combined with geologic knowledge of the area. Using La/Ta variation for all but the sheeted dike samples (fig. 15), all plot in the zone  $\text{La}/\text{Ta} = 14\text{--}30$  that is typical for MORB (Wood and others, 1979). On discrimination diagrams using Ti-Zr-Y (fig. 16) and Ti vs Zr (fig. 17) the samples plot in several fields. On figure 16 the Drier Bay basaltic rocks, gabbro, and sheeted dikes plot in the MORB/island-arc tholeiite overlap field. On figure 17, however, the basalts and sheeted dikes plot either in the ocean-floor basalt (MORB) or calc-alkaline field and the gabbro plots in the MORB/island-arc overlap region. Diorite plots in the calc-alkaline field on both diagrams. In the Hf-Th-Ta diagram (fig. 18), the samples plot in the island-arc tholeiite and calc-alkaline fields. Crowe and others (1992) reported a similar

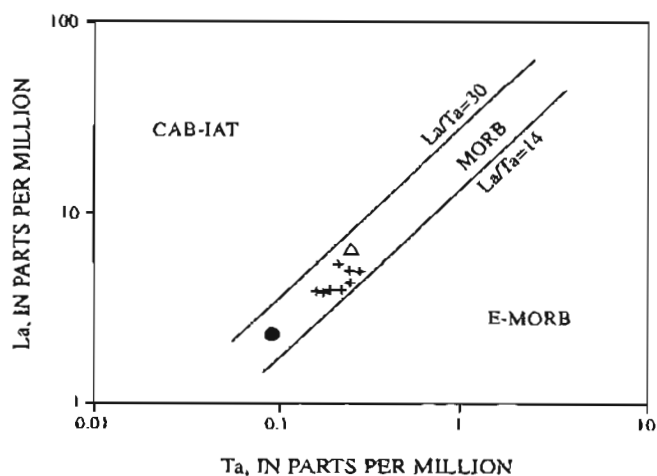


Figure 15. La/Ta variation for samples from Knight Island. Based on Wood and others (1979). Ta not detected in sheeted dikes. Symbols and abbreviations same as on figures 6, 12, and 13.

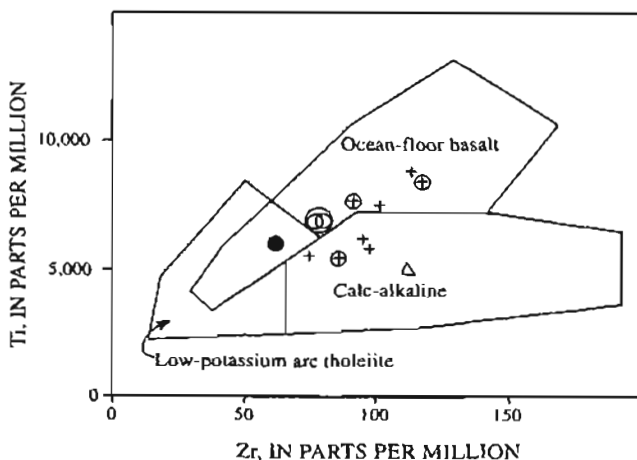


Figure 17. Ti vs Zr variation diagram for samples from Knight Island. Based on Pearce and Cann (1973). Symbols same as on figure 6. Circled values are "unaltered" samples from figure 6.

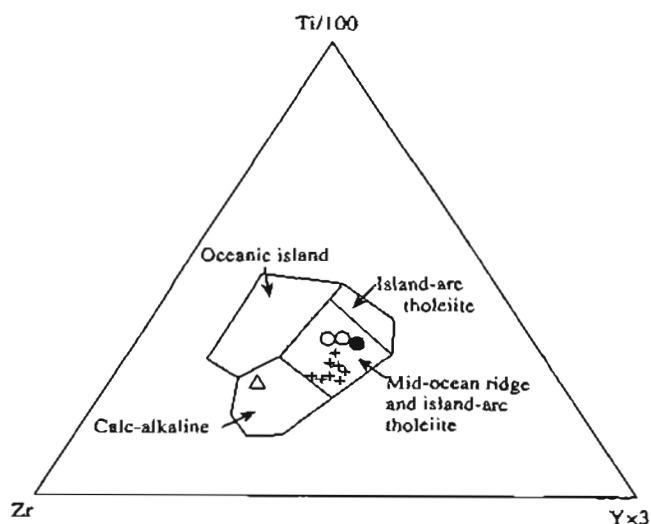


Figure 16. Ti-Zr-Y ternary diagram for sample from Knight Island. Based on Pearce and Cann (1973). Symbols same as on figure 6.

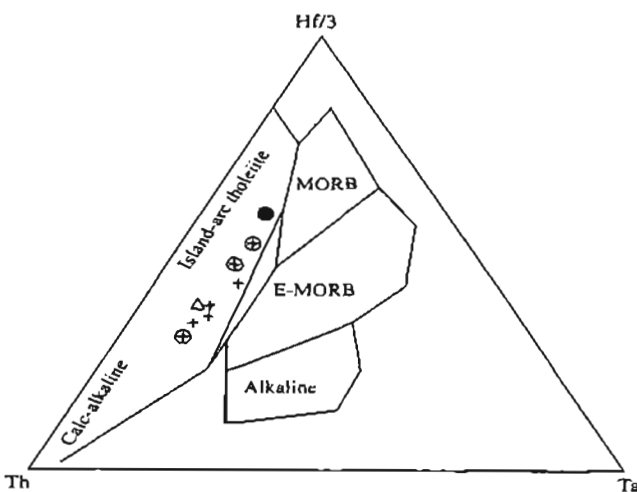


Figure 18. Hf-Th-Ta ternary plot for samples from Knight Island. Based on Wood (1980). Ta not detected in sheeted dikes. Symbols and abbreviations same as on figures 6, 12, and 13. Circled values are "unaltered" samples from figure 6.

overlap for ophiolitic rocks of the Orca Group with additional samples plotting in the MORB region. Clearly there is a significant range of values for the Orca rocks both locally and regionally.

### STRATIGRAPHIC GEOCHEMICAL VARIATION

Several of the geochemical values from this study were evaluated to see if there were any significant changes in values from samples stratigraphically low to high in the Drier Bay basalt section. At all sites, the stratigraphic up direction is to the west. The data were divided into three geographic groupings (fig. 2): group 1 consists of samples 1, 2, 3 from the north side of Drier Bay, group 2 consists of samples 7 and 8 from the south side of Drier Bay, and group 3 consists of samples 4, 5, 6 from near the mouth of Drier Bay. Within each group the low-numbered sample is the stratigraphically higher one, and group 3 samples are the stratigraphically highest group from this study (fig. 2A). Geochemical values examined consist of both major oxides ( $\text{SiO}_2$ ,  $\text{Na}_2\text{O}$ ,  $\text{K}_2\text{O}$ ,  $\text{FeO}^*$ ,  $\text{TiO}_2$ ) and trace elements (Ba and Zr). Groups 1 and 2 show either increases or decreases of the elements stratigraphically, although the same element may not change the same way stratigraphically ( $\text{FeO}^*$  decreases up section in group 1, but increases in group 2). In group 3, three of the elements ( $\text{K}_2\text{O}$ ,  $\text{FeO}$ , and  $\text{TiO}_2$ ) decrease up section and the other three elements show no trend. None of the elements shows the same trend in each of the groups. Therefore, we find no systematic geochemical changes within the stratigraphic section sampled.

### TECTONIC INTERPRETATION

Table 2 summarizes the tectonic classification from the discrimination and selected variation diagrams presented above. Five of the figures show plots suggesting that the rocks formed in a midocean-ridge setting. The rest of the figures suggest some overlap between arc, MORB, or primitive arc tectonic settings. The data from Knight Island show similar geochemical variations as observed in other ophiolites in Prince William Sound (Crowe and others, 1992). This overlap of MORB and arc-like chemistry is permissive of a back-arc basin basalt (BABB) (Hawkesworth and others, 1977; Dick, 1982; and Donato, 1991). Crowe and others (1992) suggested, however, that the variation of basalt chemistry in the ophiolites of Prince William Sound was due to the contamination of their magmas by sediments in a ridge/trench setting.

How then do we resolve the arc, back-arc, and ridge settings? Petrographic (Dumoulin, 1987) and isotopic evidence (Farmer and others, 1989) from the sedimentary rocks of the Orca Group suggests that they were derived

from an eroding arc inboard of their present position, possibly the Coast Plutonic Complex of southeastern Alaska and British Columbia. Seismic studies of deep crustal structure beneath the Chugach terrane shows evidence for underplated oceanic crust and upper mantle(?), but no clear evidence for a subducted island arc (Plafker and others, 1989). In other words, geologic evidence suggests an inboard arc but no former existence of an island arc outboard of Prince William Sound.

The ophiolites of the Orca Group show a great compositional diversity. Basalt, basaltic andesite, diorite, and plagiogranite compositions are reported (this report and Crowe and others, 1992). These variations are consistent with sediment contamination of a MORB magma such as in a ridge/trench setting (Lull and Plafker, 1990).

As mentioned above, the present-day setting of the ophiolitic rocks in Prince William Sound is in an accretionary prism or fore-arc setting. It seems incompatible with the strong MORB-like geochemical signature and the presence of sheeted dikes that these rocks could have formed in a contractional fore-arc region. It appears more likely that the ophiolites were derived from a subducting oceanic ridge in a setting similar to the present-day Juan de Fuca ridge.

Several workers have called upon sediment contamination to account for variable volcanic rock compositions in an accretionary setting (Moore and others, 1983; Cole and Basu, 1992; Crowe and others, 1992). What is not always addressed is where or how the contamination took place. For Knight Island the possibilities are: (1) contamination of ridge magmas before subduction, (2) contamination of ridge magmas after subduction, or (3) contamination in a partially subducted ridge segment. Possibility 1 seems unlikely because of the difficulty of getting the sedimentary deposits from the surface down into a magma zone. Possibility 2 seems unlikely because it would require that the ophiolite form in a subduction zone below the accretionary prism and therefore it would be impossible for 5,000 m of pillow lavas to form. Possibility 3 seems reasonable, as discussed next.

The composition of rocks along the Endeavor Segment of the Juan de Fuca Ridge are of two types (Karsten and others, 1990). These types are geochemically classified as E-MORB (enriched-MORB) or transitional MORB. The enriched rocks were collected north of the Cobb Offset. The enriched composition described by Karsten and others (1990) differ from the Knight Island rocks in that they contain greater than MORB values for more elements (fig. 13) and are chemically similar to the compositions of rocks forming in a within-plate setting (Pearce, 1983).

Although the compositions of the enriched rocks found along the Endeavor Segment of the Juan de Fuca Ridge do not match those from Knight Island, the mechanism suggested by Karsten and others (1990) for their emplacement could explain the Knight Island compositions.

**Table 2.** Summary of discriminant diagrams for rocks from the Knight Island ophiolite

[Classification abbreviations: OIT, ocean-island tholeiite; MORB/OFB, mid-ocean ridge basalt or ocean floor basalt; CA, calc-alkaline; LKAT/OFB, low potassium arc tholeiite/ocean floor basalt overlap; IAT, island arc tholeiite. Numbers are number of samples from this report in indicated classification]

Method	Classification					
	OIT	MORB/OFB	MORB/IAT	CA	LKAT/OFB	IAT
TiO <sub>2</sub> -MnO-P <sub>2</sub> O <sub>5</sub> .....	3	7	—	—	—	2
CaO/TiO <sub>2</sub> vs TiO <sub>2</sub> .....	—	12	—	—	—	—
Al <sub>2</sub> O <sub>3</sub> /TiO <sub>2</sub> vs TiO <sub>2</sub> .....	—	12	—	—	—	—
TiO <sub>2</sub> vs FeO*/MgO .....	—	12	—	—	—	—
La vs Ta .....	—	10	—	—	—	—
Ti vs Zr .....	—	6	—	5	1	—
Hf-Th-Ta .....	—	—	—	6	—	4
Ti-Zr-Y .....	—	—	11	1	—	—

Karsten and others (1990) suggested that magmas from a centralized region below the ridge are laterally injected along the ridge segment. In this process, we propose that magmas could be contaminated by sediments in a partially subducted ridge and laterally migrate to the unsubducted part of the ridge. This is the scenario, as in possibility 3 above, that best accounts for both the geologic and chemical features of the rocks from Knight Island.

## REFERENCES CITED

- Barker, Fred, Farmer, G.L., Ayuso, R.A., Plafker, George, and Lull, J.S. 1992, The 50 Ma granodiorite of the eastern Gulf of Alaska: Melting in an accretionary prism in the forarc: *Journal of Geophysical Research*, v. 97, no. 85, p. 6757-6778.
- Blome, C.D., Nelson, S.W., and Karl, S.M., 1990, Accretionary history of chert-rich McHugh Complex, southern Alaska: Geological Society of America, Program with Abstracts, v. 22, p. A321.
- Bol, A.J., Coe, R.S., Gromme, C.S., and Hillhouse, J.W., 1992, Paleomagnetism of the Resurrection Peninsula, Alaska: Implications for the tectonics of southern Alaska and the Kula-Parallon ridge: *Journal of Geophysical Research*, v. 97, no. B12, p. 17,213-17,232.
- Case, J.E., Barnes, D.F., Plafker, George, and Robbins, S.L., 1966, Gravity survey and regional geology of the Prince William Sound epicenter region, Alaska: U.S. Geological Survey Professional Paper 543-C, 12 p.
- Chappell, B.W., and White, A.J.R., 1974, Two contrasting granite types: *Pacific Sciences*, v. 8, p. 173-174.
- Clark, S.H.B., 1973, The McHugh Complex of south-central Alaska: U.S. Geological Survey Bulletin 1372-D, p. D1-D11.
- Cole, R.B., and Basu, A.R., 1992, Middle Tertiary near-trench volcanism from ridge-trench collisions along west-central California: Geological Society of America, Abstracts with Programs, v. 24, no. 7, p. A42.
- Coleman, R.G., 1977, *Ophiolites*: New York, Springer-Verlag, 229 p.
- Cox, K.G., Bell, J.D., Pankhurst, R.J., 1979, *The interpretation of igneous rocks*: London, Allen and Unwin, 450 p.
- Crowe, D.E., Nelson, S.W., Brown, P.E., Shanks, W.C., III, and Valley, J.W., 1992, *Geology and geochemistry of volcanogenic massive sulfide deposits and related igneous rocks, Prince William Sound, southcentral, Alaska*: *Economic Geology*, v. 7, no. 7, p. 1722-1746.
- Dick, H.J.B., 1982, The petrology of two back-arc basins of the northern Philippine Sea: *American Journal of Sciences*, v. 282, p. 644-700.
- Donato, M.M., 1991, Geochemical recognition of a captured back-arc basin metabasaltic complex, southwestern Oregon: *Journal of Geology*, v. 99, p. 711-728.
- Dumoulin, J.A., 1987, Sandstone composition of the Valdez and Orca Groups, Prince William Sound, Alaska: U.S. Geological Survey Bulletin 1774, 37 p.
- Farmer, G.L., Barker, Fred, Plafker, George, and Nokleberg, W.J., 1989, Isotopic evidence on the provenance of Tertiary metasedimentary rocks and on the origin of Eocene granites in the Prince William terrane, southcentral, Alaska [abs.]: *Eos, Transactions American Geophysical Union*, v. 70, no. 43, p. 1336.
- Glassley, William, 1974, *Geochemistry and tectonics of Crescent volcanic rocks, Olympic Peninsula, Washington*: Geological Society of America Bulletin, v. 85, p. 785-794.
- Hawkesworth, C.J., O'Nions, R.K., Pankhurst, R.J., Hamelton, P.J., and Evensen, N.M., 1977, A geochemical study of island-arc and back-arc tholeiites from the Scotia Sea: *Earth and Planetary Science Letters*, v. 36, p. 253-262.
- Hillhouse, J.W., Grommé, C.S., and Csejtey, Béla, 1985, Tectonic implications of paleomagnetic poles from lower Tertiary volcanic rocks, south central Alaska: *Journal of Geophysical Research*, v. 90, p. 12,523-12,535.
- Jones, D.L., Howell, D.G., Coney, P.J., and Monger, J.W.H., 1981, Recognition, character, and analyses of tectonostratigraphic terranes in western North America: U.S. Geological Survey Open-File Report 81-792, 18 p., with map.
- Jones, D.L., Silberling, N.J., Coney, P.J., and Plafker, George, 1987, Lithotectonic terrane maps of Alaska (west of the 141st meridian): U.S. Geological Survey Miscellaneous Field Studies Map 1874-A.

- Karsten, J.L., Delaney, J.R., Rhodes, J.M., and Liios, R.A., 1990, Spatial and temporal evolution of magmatic systems beneath the Endeavor Segment, Juan de Fuca Ridge: Tectonic and petrologic constraints: *Journal of Geophysical Research*, v. 95, no. B12, p. 19,235-19,256.
- Ludden, J.N., and Thompson, Geoffrey, 1978, Behavior of rare earth elements during submarine weathering of tholeiitic basalt: *Nature*, v. 274, p. 147-149.
- Lull, J.S., and Plafker, George, 1990, Geochemistry and paleotectonic implications of metabasaltic rocks in the Valdez Group, southern Alaska, in Dover, J.H., and Galloway, J.P., eds., *Geologic studies in Alaska by the U.S. Geological Survey, 1989: U.S. Geological Survey Bulletin 1946*, p. 29-38.
- Miyashiro, Akiho, 1975, Classification, characteristics, and origin of ophiolites: *Journal of Geology*, v. 83, p. 249-281.
- Moore, J.C., Byrne, T., Plumley, P.W., Reid, M., Gibbons, H., and Coe, R.S., 1983, Paleogene evolution of the Kodiak Islands, Alaska—consequences of ridge-trench interaction in a more southerly latitude: *Tectonics*, v. 2, p. 265-293.
- Mullen, E.D., 1983,  $\text{MnO}/\text{TiO}_2/\text{P}_2\text{O}_5$ : A minor element discriminant for basaltic rocks of oceanic environments and its implications for petrogenesis: *Earth and Planetary Science Letters*, v. 62, p. 53-62.
- Nelson, S.W., 1992, Ophiolitic complexes of the Gulf of Alaska: U.S. Geological Survey Open-File Report 92-20C, 9 p.
- Nelson, S.W., and Blome, C.D., 1991, Preliminary geochemistry of volcanic rocks from the McHugh Complex and Kachemak terrane, southern Alaska: U.S. Geological Survey Open-File Report 91-134, 14 p.
- Nelson, S.W., Dumoulin, J.A., and Miller, M.L., 1985, Geologic map of the Chugach National Forest, Alaska: U.S. Geological Survey Miscellaneous Field Studies Map MF-1645-B, scale 1:250,000, 15 p.
- Nelson, S.W., Miller, M.L., and Dumoulin, J.A., 1987, Resurrection Peninsula and Knight Island ophiolites and recent faulting on Montague Island, southern Alaska: *Geological Society of America Centennial Field Guide-Cordilleran Section*, p. 433-438.
- Pearce, J.A., 1982, Trace element characteristics of lavas from destructive plate boundaries, in Thorpe, R.S., ed., *Andesites: orogenic andesites and related rocks*: Chichester, Wiley, p. 525-548.
- , 1983, The role of sub-continental lithosphere in magma genesis at destructive plate margins, in Hawkesworth, C.J., and Norry, M.J., eds., *Continental basalts and mantle xenoliths*: Nantwich, Shiva, p. 230-249.
- Pearce, J.A., and Cann, J.R., 1973, Tectonic setting of basic volcanic rocks determined using trace element analyses: *Earth and Planetary Science Letters*, v. 19, p. 220-300.
- Plafker, George, Jones, D.L., and Pessagno, E.A., 1977, A Cretaceous accretionary flysch and melange terrane along the Gulf of Alaska margin, in Blean, K.M., ed., *United States Geological Survey in Alaska: Accomplishments during 1976: U.S. Geological Survey Circular 751-B*, p. B41-B43.
- Plafker, George, Keller, Gerta, Nelson, S.W., Dumoulin, J.A., and Miller, M.L., 1985, Summary of data on the age of the Orca Group, Alaska, in Bartsch-Winkler, Susan, ed., *The United States Geological Survey in Alaska: Accomplishments during 1984: U.S. Geological Survey Circular 967*, p. 74-76.
- Plafker, George, Moore, J.C., and Winkler, G.R., [in press], *Geology of the southern Alaska margin*: Boulder, Geological Society of America, *Decade of North American Geology (DNAG) Series*.
- Plafker, George, Nokleberg, W.J., and Lull, J.S., 1989, Bedrock geology and tectonic evolution of the Wrangellia, Peninsular, and Chugach terranes along the Trans-Alaska Crustal Transect in the Chugach Mountains and southern Copper River Basin, Alaska: *Journal of Geophysical Research*, v. 94, p. 4255-4295.
- Plafker, George, Nokleberg, W.J., Lull, J.S., Roeske, S.M., and Winkler, G.W., 1986, Nature and timing of deformation along the Contact fault system in the Cordova, Bering Glacier, and Valdez quadrangles, Alaska: *U.S. Geological Survey Circular 978*, p. 74-77.
- Plumley, P.W., and Plafker, George, 1985, Additional estimate of paleo-latitude for the Paleocene/Eocene Prince William terrane Orca volcanics: *Geological Society of America Abstracts with Programs*, v. 17, p. 401.
- Richards, T.A. and McTaggart, K.C., 1976, Granitic rocks of the southern Coast Plutonic Complex and northern Cascades of British Columbia: *Geological Society of America Bulletin*, v. 87, no. 6, p. 935-953.
- Richter, D.H., 1965, *Geology and mineral deposits of central Knight Island, Prince William Sound, Alaska*: Alaska Division of Mines and Minerals *Geologic Report 16*, 37 p.
- Serri, Giancarlo, 1981, The petrochemistry of ophiolite gabbroic complexes: A key for the classification of ophiolites into low-Ti and high-Ti types: *Earth and Planetary Science Letters*, v. 52, p. 203-212.
- Sun, Shen-Su, and Nesbitt, R.W., 1978, Geochemical regularities and genetic significance of ophiolitic basalts: *Geology*, v. 6, p. 689-693.
- Tysdal, R.G., Case, J.E., Winkler, G.R., and Clark, S.H.B., 1977, Sheeted dikes, gabbro, and pillow basalt in flysch of coastal southern Alaska: *Geology*, v. 5, p. 377-383.
- Wilson, Marjorie, 1989, *Igneous petrogenesis*: London, Unwin Hyman, 466 p.
- Winkler, G.W., 1976, Deep-sea fan deposition of the lower Tertiary Orca Group, eastern Prince William Sound, Alaska, in Miller, T.P., ed., *Recent and ancient sedimentary environments in Alaska*: Anchorage, Alaska Geological Society Symposium Proceedings, p. R1-R20.
- Wood, D.A., 1980, The application of a Th-Hf-Ta diagram to problems of tectonomagmatic classification and to establishing the nature of crustal contamination of basaltic lavas of the British Tertiary Volcanic Province: *Earth and Planetary Science Letters*, v. 50, p. 11-30.
- Wood, D.A., Joron, Jean-Louis, and Treuil, Michel, 1979, A reappraisal of the use of trace elements to classify and discriminate between magma series erupted in different tectonic settings: *Earth and Planetary Science Letters*, v. 45, p. 326-336.

Reviewers: Peter Haeussler and William W. Patton, Jr.

# STRUCTURAL EVOLUTION OF THE CHUGACH-PRINCE WILLIAM TERRANE AT THE HINGE OF THE OROCLINE IN PRINCE WILLIAM SOUND, AND IMPLICATIONS FOR ORE DEPOSITS

By Peter J. Haeussler and Steven W. Nelson

## ABSTRACT

The Chugach-Prince William terrane is a Mesozoic through Tertiary accretionary complex that lies along coastal southern and southeastern Alaska. In Prince William Sound, the regional structural fabric bends about 90°, forming an orocline. Rocks at the hinge of the orocline consist of turbidites, conglomerate, and minor volcanic rocks and limestone. The structural geology in the hinge region defines a number of domains (each >15 km<sup>2</sup>) consisting of kilometer-scale tight folds. Adjacent domains may have up to a 90° difference in the strike of bedding and trend of fold axes. Four granite to tonalitic or gabbro plutons are dated or inferred to be about 35 Ma in age, and all were emplaced after regional folding. Base-metal sulfide mineral occurrences, barren quartz veins, and strike-slip late faults locally cut the plutons and generally strike north-south. The mineral occurrences often have a dendritic network of quartz veinlets adjacent to the mineralized zone and brecciated wall rock within the zone. Oroclinal bending, in the style of bending a bar, is consistent with the origin of the complicated domainal geometry of the structures. The Contact fault, thought by some workers to juxtapose two parts of the accretionary prism, truncates one of these 35-Ma plutons with strike-slip offset, but previous reverse motion cannot be ruled out. A magmatic source for the ore-forming fluids is consistent with the structural and mineralogical data. The north-south orientation of mineralized zones suggests that east-west extension occurred possibly during release of fluids from the plutons, which locally hydrofractured the wall rocks and allowed migration of ore-forming fluids along pre-existing fractures.

## INTRODUCTION

The geology of coastal south-central Alaska is dominated by rocks of a vast accretionary prism of Late

Cretaceous to Eocene(?) age (Plafker and others, 1989). In Prince William Sound, the regional strike of bedding and cleavage changes by about 90° from the east side to the west side (Nelson and others, 1985). This change in orientation of the structural grain defines the orocline of southern Alaska (Carey, 1955) (fig. 1). At the hinge of the orocline, previous studies recognized (1) regions where the strike of bedding was discordant from the regional strike, and (2) Zn-, Cu-, Pb-rich mineral occurrences that are not found elsewhere in the accretionary prism (Nelson and others, 1984, 1985; MacKevett and Halloway, 1977a, 1977b). Most mineral occurrences in the prism consist of syngenetic volcanogenic massive sulfide deposits associated with ophiolites (Crowe and others, 1992), or, turbidite-hosted epigenetic lode-gold deposits in structurally simple regions of harmonic folds with subhorizontal fold axes (for example, see Mitchell, 1979). Because of the presence of the unique Zn-, Cu-, Pb-rich veins described above and to support the Chugach National Forest management plan, the U.S. Geological Survey and the U.S. Bureau of Mines recommended additional study in this area. Funds for this work were provided by the U.S. Forest Service. This paper presents the structural geology of the Chugach National Forest Special Study Area based upon 1:63,360-scale (1 inch = 1 mile) mapping in the area between Columbia Glacier and Unakwik Inlet (fig. 2) and discusses the structural and tectonic development at the hinge area of the orocline in addition to the relationship between structure, magmatism, and mineral occurrences.

## REGIONAL GEOLOGY

Rocks in the vicinity of Prince William Sound largely consist of siliciclastic turbidites (Dumoulin, 1987) of the Orca and Valdez Groups (figs. 1 and 2). The rocks of the Valdez Group are thought to have originated as trench-fill deposits at the margin of an Andean-type arc (Nilsen and Zuffa, 1982; Plafker and others, 1989), and the rocks of



the Orca Group have been interpreted as a deep-sea fan by Winkler (1976). Bedding and cleavage generally dip northward in both the Valdez and Orca Groups, with dips to the northeast or northwest on the east and west sides, respectively, of the hinge of the orocline. The study area includes a segment of the Contact fault, which according to Plafker and others (1977) separates higher grade Late Cretaceous rocks of the Valdez Group to the north, from lower grade Paleocene and Eocene rocks of the Orca Group to the south (Plafker and others, 1985). However, several workers have noted that the change from inboard, more deformed and metamorphosed rocks, to outboard, less deformed and less metamorphosed rocks, in northern and western Prince William Sound is locally complex with no clear lithologic break, which indicates that the Orca and Valdez Groups represent parts of a continuously evolving accretionary prism (Dumoulin, 1987; Gibbons, 1988; Bol and Gibbons, 1992). Therefore, following the suggestion of Bol and Gibbons (1992) and the terminology of Bol and others (1992), we use the term "Chugach-

Prince William terrane" for the terrane designation of these rocks.

In addition to the turbidites, a belt of ophiolites that stretches from Elrington Island northeast to the Copper Mountain-Ellamar area is found in Prince William Sound (Crowe and others, 1992) (fig. 1). One of these ophiolites is located on Glacier Island in the southern part of the study area (fig. 2); we will not consider these ophiolites further.

Plutons of two ages intrude the accretionary prism in the Prince William Sound region. Granite to granodiorite plutons of the Sanak-Baranof belt (Hudson and others, 1979) that are dated by K-Ar as approximately 50–55 Ma in age (Nelson and others, 1985; Tysdal and Case, 1979) are located in eastern Prince William Sound, also near Girdwood, as well as further to the southwest on the Kenai Peninsula (fig. 1). Granite to diorite and gabbro plutons dated by K-Ar at ~35 Ma (Nelson and others, 1985; Tysdal and Case, 1979) are located only in the western part of Prince William Sound.

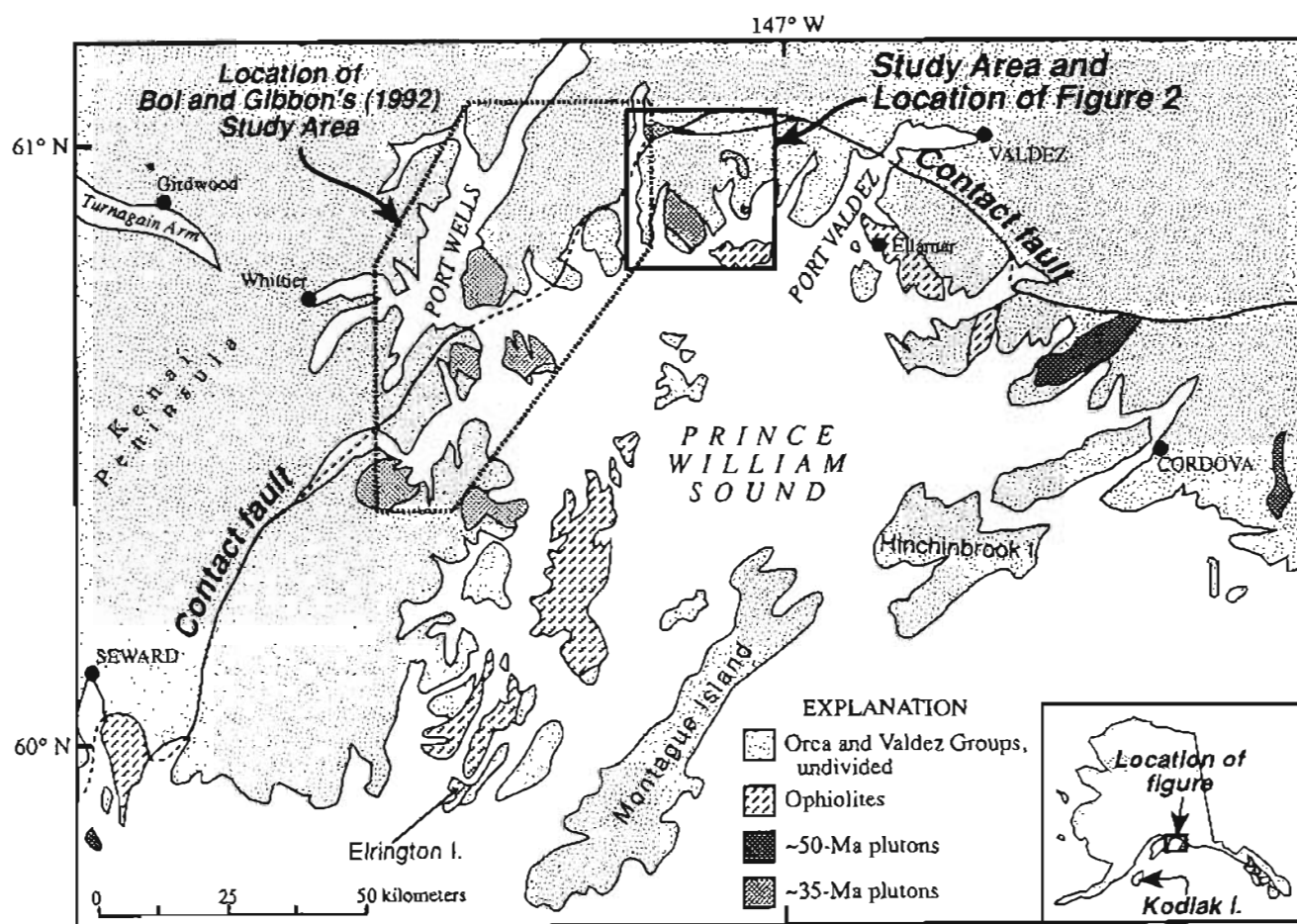
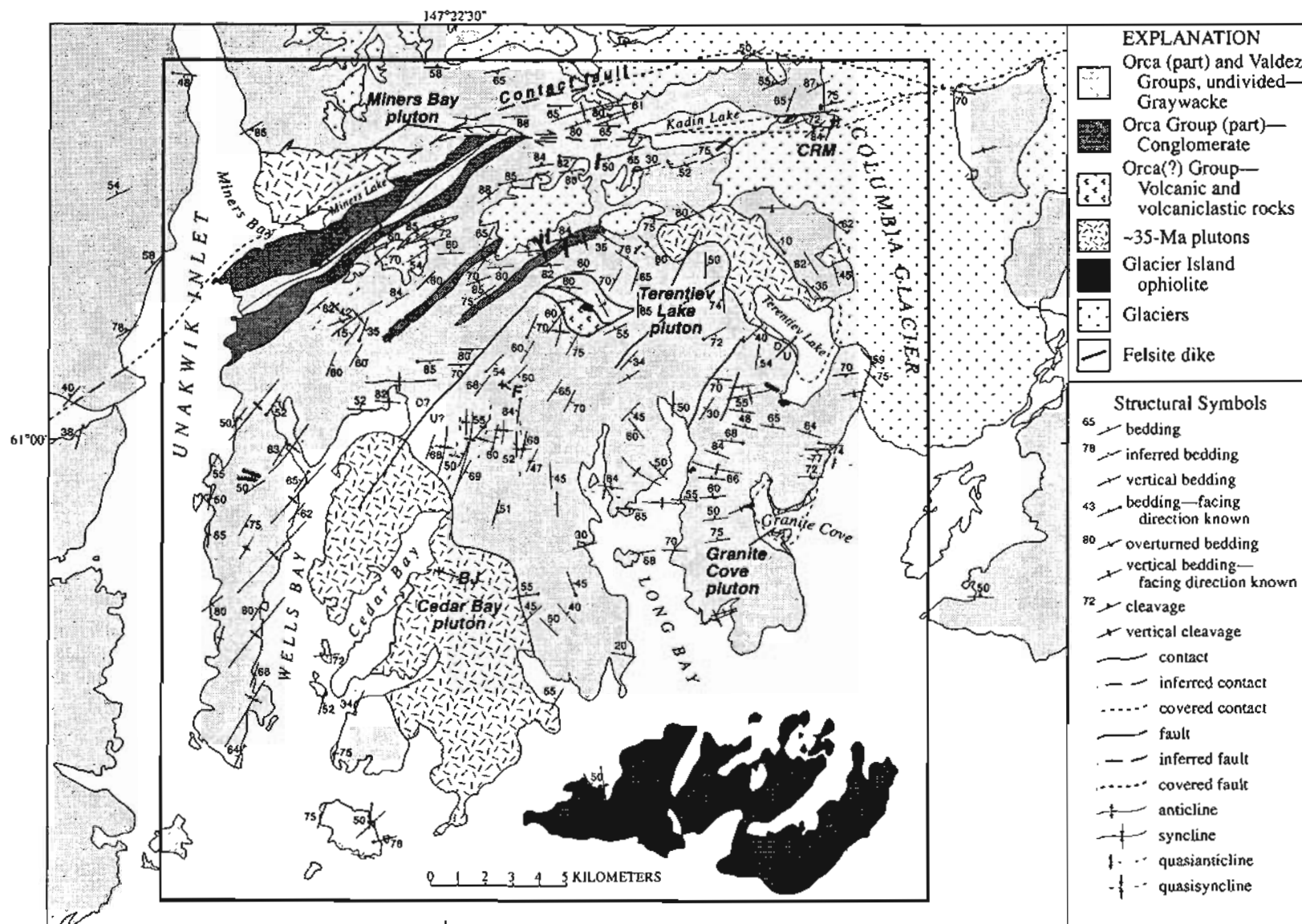


**Figure 1.** Regional geologic map of south-central Alaska showing present study area and study area of Bol and Gibbons (1992). Rocks north of Contact fault belong to Valdez Group and those to the south belong to Orca Group. In general, strike of bedding and cleavage is subparallel to Contact fault.



## GEOLOGY IN THE STUDY AREA

The sedimentary rocks within the study area are dominantly turbidites of Mutti and Ricci-Lucci (1978) facies B and C, with less common facies A and D. The map pattern of lithofacies is roughly symmetric about a northeast-southwest-trending axis that extends from the south end of Wells Bay to the east end of Kadin Lake (S. Nelson, unpublished mapping, 1992). Bedding thicknesses range from about 3 cm to about 3 m. Conglomerates (facies A) up to about 300 m thick are present in the northwest (fig. 2). There are also conglomerates adjacent to the Columbia Red Metals massive sulfide occurrence (CRM, fig. 2), but are too small to be shown on our map. Volcaniclastic sedimentary rocks, broken pillow breccia, rare pillow lava, and limestone was found at two small localities (fig. 2), one about 3 km southeast of Miners Lake and the other west of Terentiev Lake and north of Long Bay.

There are four felsic to intermediate plutons within the study area, informally named: the Cedar Bay, Granite Cove, Terentiev Lake (which has an apophysis along the Columbia Glacier), and Miners Bay plutons (fig. 2). The first three of these are texturally homogenous, fine-grained, equigranular granite. The Cedar Bay pluton has some tonalite. The other pluton, the Miners Bay, has two compositional phases, with the main (western) part that consists chiefly of gabbro and diorite, and the eastern "tail" is granite. This pluton is the only one in the study area that has been radiometrically dated, with K-Ar ages on biotite and hornblende of 32 and 38 Ma, respectively (Nelson and others, 1985).

Nelson and others (1985) correlated the Cedar Bay, Terentiev Lake, and Granite Cove plutons with the other Paleocene to Eocene plutons in Prince William Sound based upon petrography. However, recent major-, minor-, and trace-element geochemical analyses (S. Nelson, unpublished data) indicate that these plutons are distinct from the Paleocene to Eocene plutons and are most similar to the ~35-Ma plutons in the western part of Prince William Sound. We thus consider all the plutons in the study area to be in that group.

Dikes of several compositions are present in the study area. There are pegmatite and autobrecciated granitic dikes (discussed below) associated with the Granite Cove pluton. Felsite dikes with a fine-grained sugary texture are present throughout the study area south of the Contact fault (fig. 2). Two dikes on the peninsula between Unakwik Inlet and Wells Bay contain phenocrysts of centimeter-size K-feldspar and quartz in a fine-grained matrix. Dikes with this distinct texture and composition are only found in the vicinity of Unakwik Inlet (Nelson and others, 1985). Because of the spatial association of all the dikes with the plutons, they are probably related and the same age.

Metamorphism in the study area is generally to the laumontite to mid-greenschist facies (white mica  $\pm$  chlorite

$\pm$  epidote  $\pm$  incipient biotite) in lithic graywackes (Goldfarb and others, 1986). Macroscopic metamorphic minerals were not observed outside of contact aureoles, and slaty cleavage was not commonly observed in the field or in thin section. When present, it was a weak pressure-solution cleavage, like that documented in correlative rocks to the southwest (Gibbons, 1988) (fig. 1). Mapping by Nelson and others (1985) indicates that a slaty cleavage was observed to the north of the study area. The contact aureoles of the plutons are upper greenschist to amphibolite facies in pelitic rocks (biotite + muscovite + quartz  $\pm$  staurolite  $\pm$  andalusite  $\pm$  cordierite  $\pm$  garnet), and are generally no more than 0.5 km wide. The aureoles are up to 2 km wide on the north side of the Terentiev Lake pluton and 2.5 km wide along the southwest side of the Cedar Bay pluton, which suggests that the plutons may extend beneath these outcrops. Mapping around Terentiev Lake demonstrates that the erosion level coincides with the top of the Terentiev Lake pluton. The contact between the igneous rocks and the overlying sedimentary rocks is subhorizontal, and is spectacularly exposed in outcrops recently revealed by a 100-m drop of lake level within the last 10 years due to retreat of the Columbia Glacier.

## STRUCTURAL GEOLOGY

The early structural history of the rocks in the study area involved minor soft-sediment deformation and the development of web structure. Fine-grained clastic dikes up to 2 cm wide and 5–6 cm long intrude mudstone and fine-grained siltstone at one locality, and similar soft-sediment features were observed outside of the study area. Web structure (Cowan, 1982; Byrne, 1984) was not observed in the field but was seen in thin sections, and has also been reported in correlative rocks to the southwest by Bol and Gibbons (1992; Gibbons, 1988; see fig. 1).

We have divided the study area into 11 structural domains for analysis (fig. 3). We define each domain by roughly consistent strike of bedding, and domain boundaries are defined by discordances in bedding (figs. 3, 4). Therefore, each domain should be characterized by cylindrical folds with the trend of fold axes in each domain discordant to those in adjacent domains. In one case, fold axes be traced between domains (B and C) because these domains were divided on the basis of the overall change in the strike of bedding between the west end of domain B and the east end of domain C, despite no drastic change in strike at the B-C boundary (fig. 3). We also separated domain A from those to the south by the Miners Bay-Kadin Lake splay of the Contact fault, in order to examine the differences between the domains on either side of the fault. Several other domain boundaries can be demonstrated to be faults. Domain F is bounded by a high-angle fault on its

southwestern margin and inferred faults on its other margins. A northeast-southwest-striking fault corresponds with the boundary between domain D and domains F and H. A fault with a similar orientation roughly corresponds with the domain I-J boundary.

## FOLDS

Folding in the study area is indicated by rocks dipping in opposite directions, but having the same strike and facing direction. The wavelength of these folds based upon our mapping (fig. 2) is commonly 1.5 to 2.5 km, but may range from 1 to 4.5 km. The amplitude of the folds is not known, although it is almost certainly greater than their wavelength. Because the wavelength is so large, fold hinges were not generally observed. However, between Miners Lake and Wells Bay in domain C there are gentle undulations of bedding with a wavelength of about 100 m

that are probably at the crest of an anticline (M-folds). We generally do not have enough data to trace fold axes laterally more than 2 to 3 km. In domain C, however, conglomerate marker beds allow a fold to be traced for 12 km.

Stereograms of poles to bedding in each domain help to define the geometry of the folds, and we determined a best-fit fold axis for each domain, if enough data had been collected to define a girdle. Four of the eleven domains did not have sufficient data ( $N \geq 20$ ) to clearly discriminate fold axes. Although the trends of the best-fit fold axes are variable between domains, these fold axes are sub-horizontal, except in domain F, which has a different structural style and is discussed separately below. Outside of domain F, 12 mesoscale fold axes were measured, and in most cases these fold axes do not coincide with the best-fit fold axes determined from the girdle of poles to bedding. In correlative rocks to the southwest Bol and Gibbons (1992) (fig. 1) found that mesoscale fold hinges were oriented similarly to the best-fit fold axis determined from the

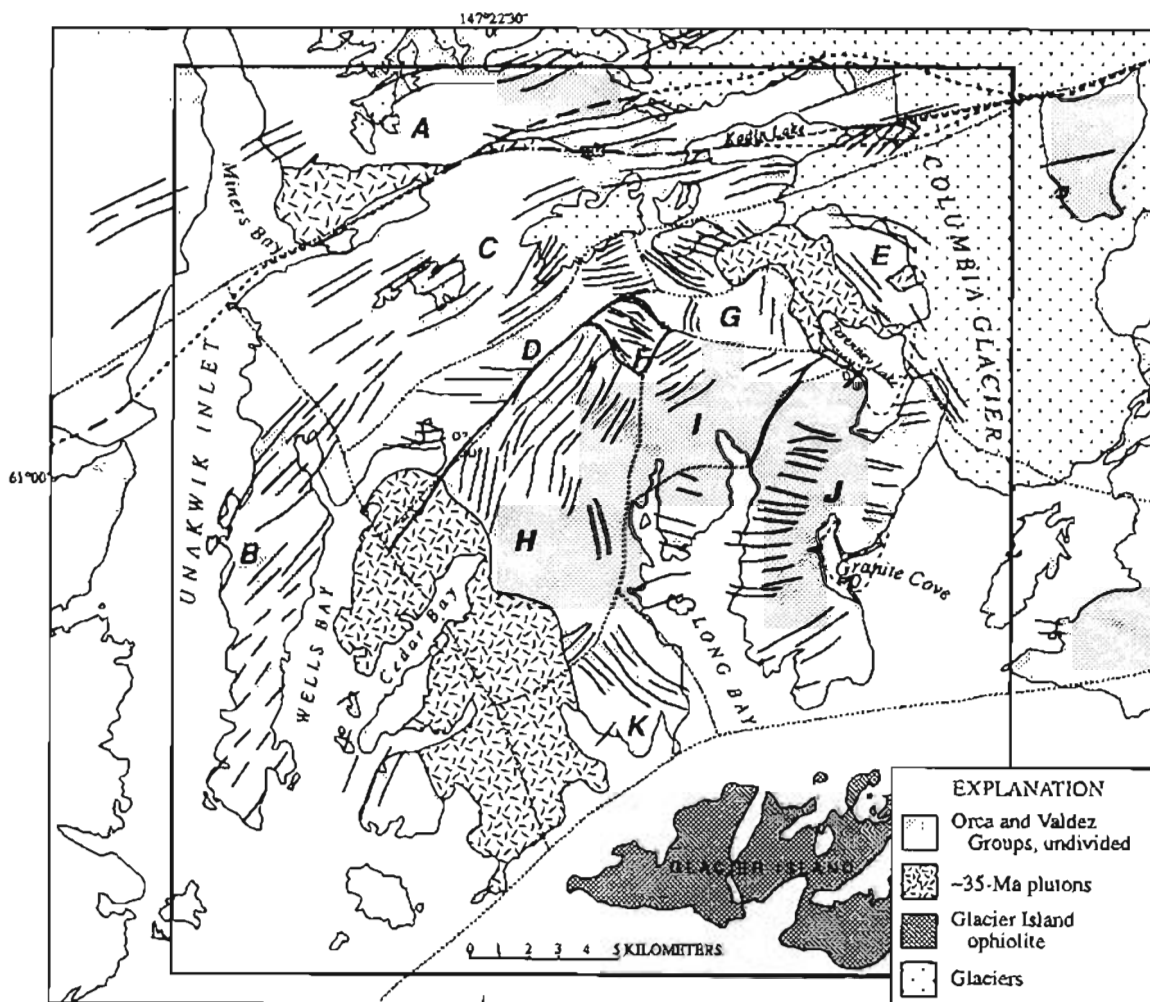
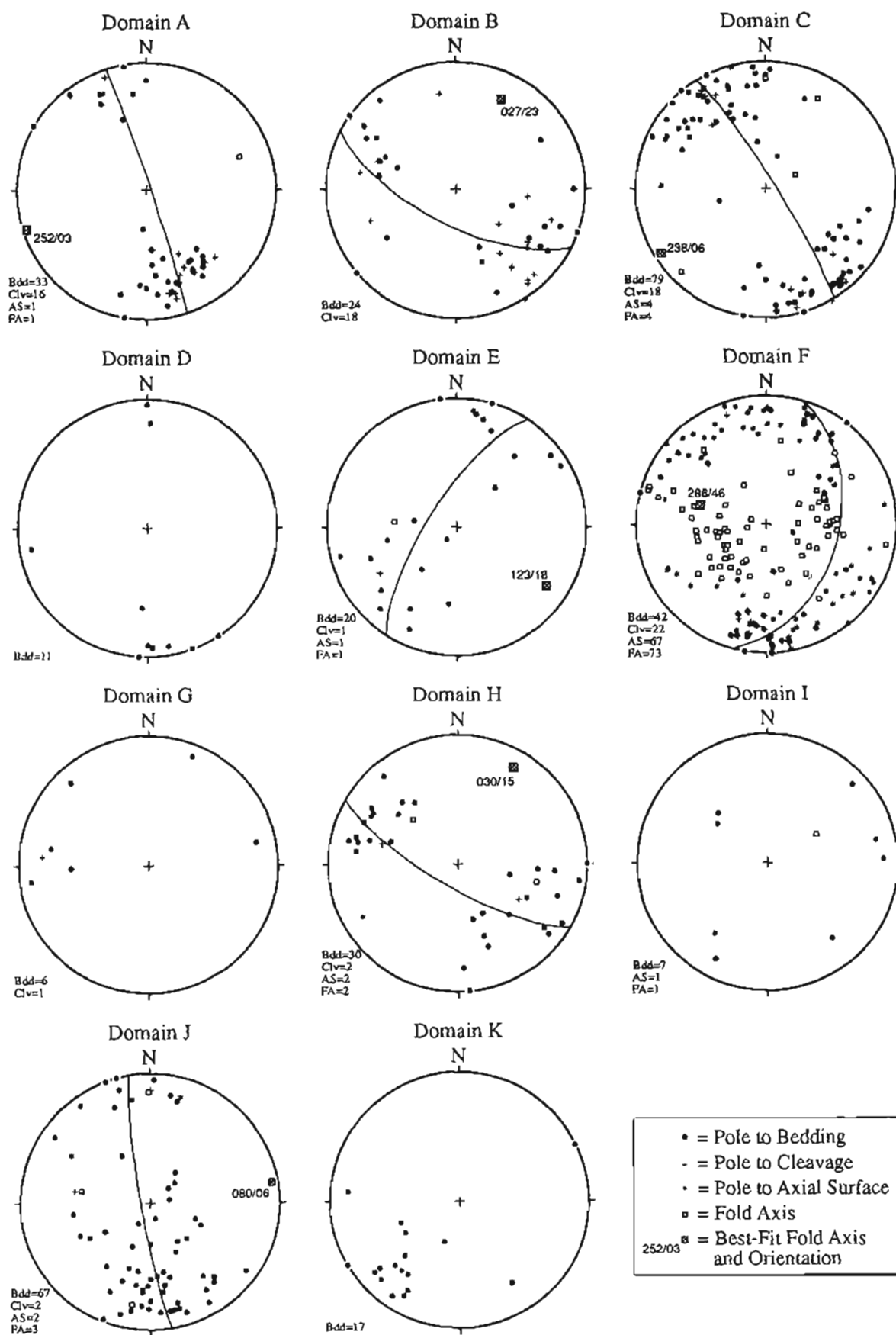


**Figure 3.** Form-line map of interpretive strike of bedding (solid lines) and structural domains, A to K (dotted lines). Data for domains A and B also taken from unpublished mapping in Anchorage A-2 and Seward D-2 quadrangles north and west of study area by S.W. Nelson, M. Miller, J. Dumoulin, G. Winkler, S. Karl, and J. Case.



girdle of poles to bedding. Therefore, the discordance that we find between the observed and best-fit fold axes is unusual and might be explained several ways. (1) The outcrop-scale fold axes might be slump folds, not tectonic folds. Because the folded rocks at several localities were Mutti and Ricci-Lucci (1978) D facies turbidites, which are often found in slump folds, this possibility appears likely. (2) The outcrop-scale folds may not reflect the strain regime of the macroscale structures, and thus there was heterogeneous strain. Because cleavage is uncommon, significant lateral strain variations probably are not present, and thus there most likely was not heterogeneous strain. (3) There may have been more than one period of folding, but there is no other evidence for polyphase ductile deformation with a similar structural style.

The stereograms also indicate that the folds are open to isoclinal, but tight folds are the most common, with interlimb angles from 20° to 70°. The mean interlimb angle determined from stereograms is approximately 40°. For reference, we will refer to the main period of folding that generated the kilometer-scale folds with subhorizontal fold axes as  $F_m$ .

In domain F, which contains the volcanic and volcanoclastic rocks and limestone, and in an interval about 300 m wide between domains I and J, the rocks have a distinctive structural style with outcrop-scale chevron folds and (or) stratally disrupted bedding (fig. 5). Where the rocks are stratally disrupted, centimeter-size phacoid-shaped pieces of silicified sandstone and basaltic tuff define a melange-like planar fabric and are surrounded by fine-grained siltstone and mudstone (fig. 5A). The volcanoclastic section in domain F had the highest degree of stratal disruption, and in the turbidites to the northeast, stratal disruption was not as extreme as bedding could be traced for several meters. A felsic dike intruded the stratally disrupted rocks in domain F parallel to the vertical fabric and was locally boudinaged; boudin axes are subvertical. Where there are folds, either the melange-like fabric or 2- to 4-m-long lozenges of bedding define folds with a wavelength of 0.5 m to several meters and an amplitude of about 3 cm to several meters (fig. 5B). The interlimb angles observed in outcrop were commonly 90°. The folds defined by fragment foliation are asymmetric and disharmonic, but no dominant sense of asymmetry was noted. Stereograms of structural data from domain F (fig.

6) show that the pole to the best-fit plane of the poles to bedding gives a steeply plunging fold axis (46°), in contrast to the other domains (fig. 4). The axial planes to the folds are subvertical and strike ENE-WSW. Stereograms of the fold axes show two maxima plunging 60° (fig. 6).

We digress briefly to discuss eight localities within the study area that have what we refer to as "quasi-fold" geometry (see figs. 7 and 2). On the map scale, there is apparent fanning of bedding planes, without a change of facing direction. Heterogeneous strain is one way to explain this geometry, but because no cleavage was generally observed, large differences in strain intensity are unlikely. A more favorable explanation is possible tilting to near vertical of hanging-wall or footwall thrust-fault cutoffs (fig. 8). As shown in figure 8, quasi-fold geometry can be generated by tilting of fault-bend folds to near vertical. This interpretation requires a thrust fault at a low angle to bedding between the upright and overturned rocks and later tilting. Although we favor this interpretation, no field evidence for these particular thrust faults was observed. Two possible reasons for this are that (1) abundant vegetation and snow cover critical locations and (2) bedding-parallel thrust faults are difficult to recognize, because elsewhere in the Chugach-Prince William terrane they may form narrow shear zones less than 1 m wide (Sample and Moore, 1987; Bol and Gibbons, 1992).

## INTRUSIVE BODIES

All of the plutons in the study area were intruded after folding, but before faulting ceased. This timing relationship is indicated by bedding and rare solution cleavage that does not become parallel to the pluton margins, porphyroblasts in the contact aureoles that appear postdeformational (fig. 9A), a weak to nonexistent magmatic foliation, and little evidence for low-temperature solid-state deformation of the plutons (fig. 9B). Therefore, there is no outcrop or microstructural evidence for significant ductile deformation of either the wall rocks or the plutons during or after emplacement of the intrusions. We discuss the timing of pluton emplacement relative to particular faults in the following section.

The Granite Cove pluton has associated dikes and an apophysis of an unusual granitic autobreccia (fig. 10). In the apophysis of the pluton on the west side of Granite Cove, we observed a gradational contact between unbrecciated granite and intensely brecciated rock over a lateral interval of about 50 m. Two dikes of the breccia were also found at the north end of Granite Cove within graywacke. The breccia clasts, which apparently have no minimum size, consist of micrographic intergrowths of potassium feldspar and quartz, with only minor alteration of the feldspars to clay. There are no reaction rims or embayment of the clasts to suggest alteration by hydrothermal

⇐

Figure 4. Equal-area stereographic plot of fold axes and poles to bedding, cleavage, and axial surfaces for each domain. Domain F attitudes are more clearly shown in figure 6. Bdd, bedding; Clv, cleavage; AS, axial surface; FA, fold axis. Where the plot of poles to bedding displayed a girdle, a best-fit plane through the poles and the pole to that plane, the inferred fold axis, and its orientation are shown.



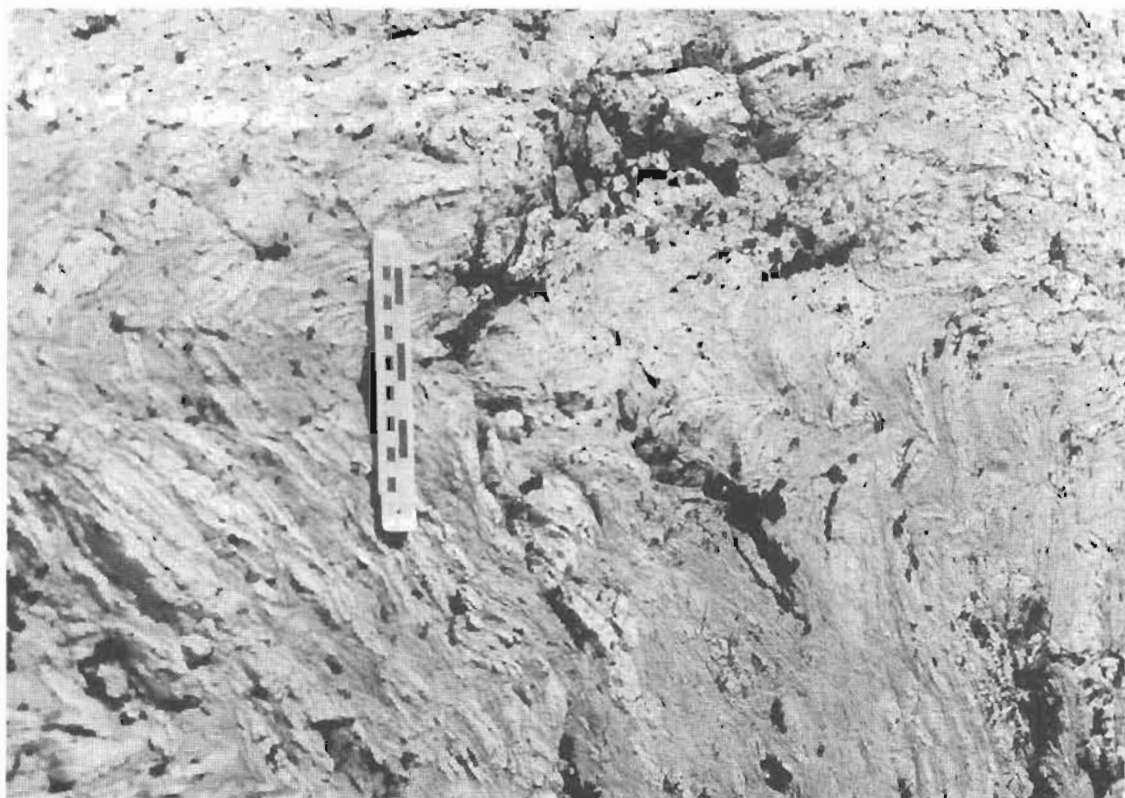
*A**B*

Figure 5. Structural style in domain F. *A*, Stratal disruption. *B*, Disharmonic chevron folds.



fluids. There is a minor amount of chlorite between clasts, and even less white mica(?); these minerals constitute less than 2 percent of the rock. The clasts are randomly oriented, and there is no indication that the breccia is fault related as there are no throughgoing slip surfaces. Some clasts can be seen to be at the initial stage of breaking up, with some clasts slightly rotated relative to the others.

Because the mineralogy of the breccia is unaltered and because clasts are rotated with respect to each other, brecciation is probably not related to hydrothermal processes. We suggest that the breccia was formed by a magmatic

autobrecciation process, in which a magmatic fluid brecciated previously crystallized fine-grained granite at the margin of the pluton. The Granite Cove pluton has the highest potassium and silica content of any intrusion in Prince William Sound in either the ~35-Ma or ~50- to 55-Ma age groups (S. Nelson, unpublished data). Finally, the Granite Cove pluton has a narrow contact aureole, but thin sections show that chlorite and epidote are found in fractures up to 2 km from the pluton. This evidence suggests that the present exposures of the pluton are near its top, one phase of the pluton was fluid-rich, and after emplacement and

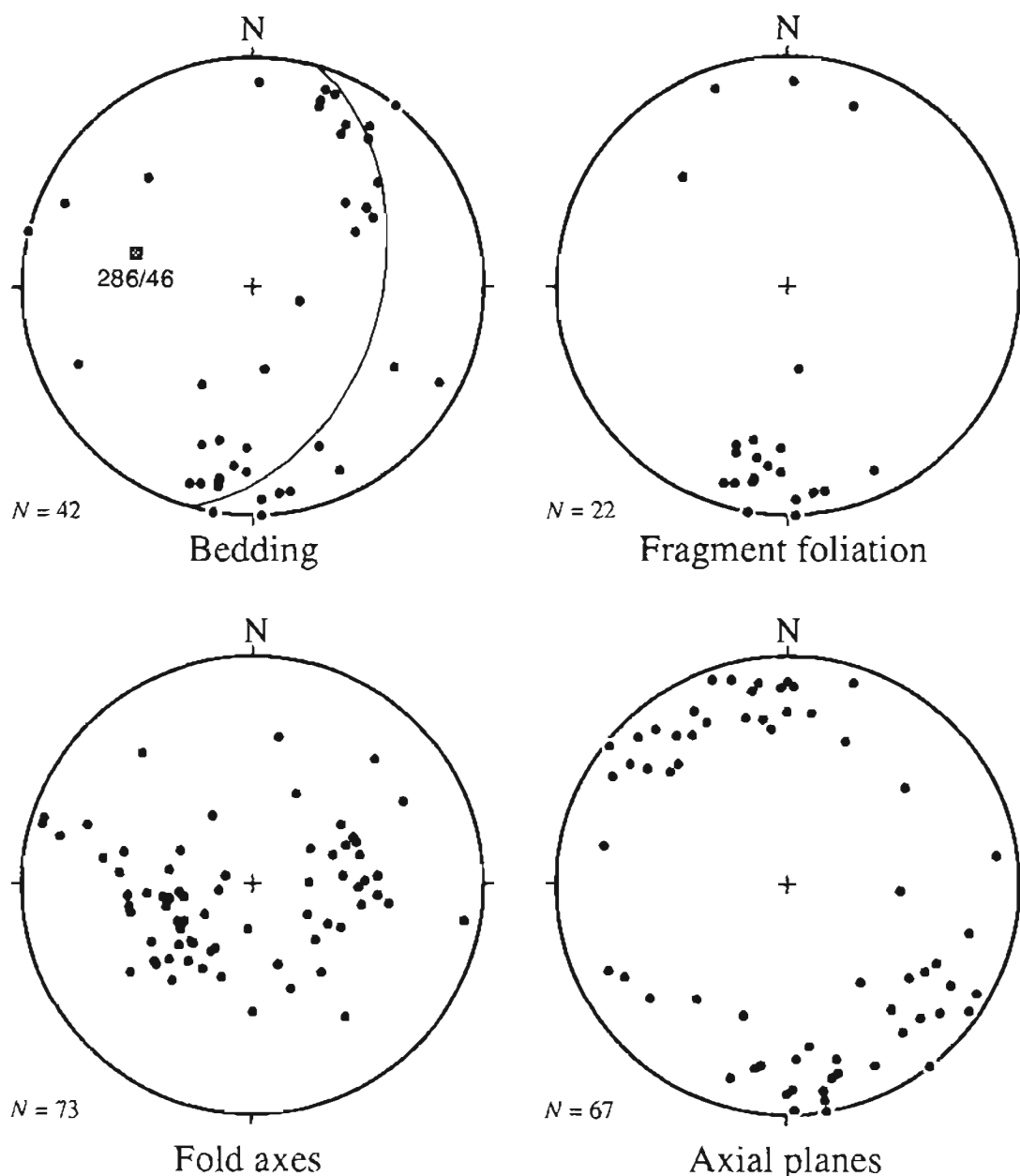


**Figure 6.** Equal-area stereograms of poles to bedding, cleavage, fold axes, and axial planes from domain F. Also shown is the best-fit plane through the poles to bedding and the pole to that plane, the inferred fold axis, and its orientation. *N*, number of samples; +, pole to bedding; ◻, best-fit fold axis and orientation.

crystallization, the release of magmatic fluids affected the wall rocks around the pluton.

The felsite dikes in the study area are subvertical and generally strike northwest-southeast, but the strikes range from east-west to north-south (fig. 11). The dikes near Unakwik Inlet with K-feldspar and quartz phenocrysts strike east-west (fig. 11). Pegmatite and autobrecciated granitic dikes associated with the Granite Cove pluton strike northwest-southeast (fig. 11). As mentioned earlier, a dike in domain F is slightly boudinaged with subvertical boudin axes. This is the only indication of ductile deformation of any of the dikes.

### FAULTS

Steeply dipping brittle faults with quartz veins, brecciated wall rock, and clayey gouge less than several centimeters thick are found throughout the study area. The orientation of these faults is roughly the same in all domains, and thus we consider them together. A plot of all known fault orientations and their sense of offset (fig. 12), where it was determined, demonstrates that (1) the most common fault orientation is north-south- or NNW-SSE-striking and subvertically dipping, and (2) most of these faults (18 of 24 with known offset) are strike-slip faults. North-south-striking sinistral-slip faults cut the Cedar Bay pluton, and north-south-striking dextral- and sinistral-slip faults cut the Granite Cove pluton. It is puzzling that both dextral and sinistral faults have approximately the same orientation but the opposite sense of slip.

Abundant geomorphic lineaments cross the study area, and many of these have a north-south or NNW-SSE trend. Lineaments with the same orientation cut the Miners Bay, Cedar Bay, and Terentiev Lake plutons. The Cedar Bay pluton, in particular, has a strong NNW-SSE-striking set. The fractures are subvertical, as indicated by their linear trace across topography. The strikes of fractures in the southern half of the study area were measured from Condon and Cass's (1958) compilation of linear geologic features in western Prince William Sound (fig. 13). The lineaments strike north-south to NNW-SSE, similar to the

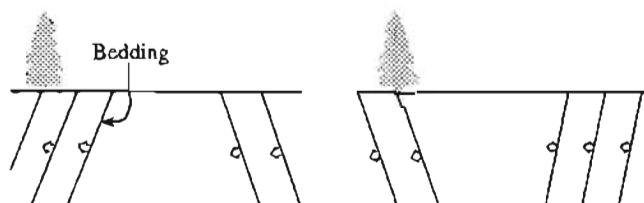


**Figure 7.** Eight localities within study area show quasi-fold geometry, which at 1:63,360-map scale show apparent fanning of bedding planes, although facing direction remains the same. This figure shows in cross-sectional view our use of the term "quasi-fold" and the two types of geometry observed in the field. Arrows show upward-facing direction of rocks.

most common orientation of faults, and thus we interpret the lineaments as fractures that are probably strike-slip faults with minor offset.

The amount of offset on these north-south to NNW-SSE-striking brittle faults probably is not significant because no pluton contact or stratigraphic horizon is offset along them. However, there may be approximately 11 km of dextral map separation along a (ENE-WSW-striking) splay of the Contact fault (Winkler, 1992) that runs between Miners Bay and Kadin Lake (fig. 2). Conglomerate south of Miners Lake (fig. 2) strikes into the Miners Bay-Kadin Lake splay, and the closest conglomerate on the north side of the splay is located near the Columbia Red Metals prospect (CRM, fig. 2) between Kadin Lake and the Columbia Glacier. This fault also truncates the ~35-Ma Miners Bay pluton. Traverses across the Miners Bay-Kadin Lake splay of the Contact fault did not reveal areas of high ductile strain. In conglomerate adjacent to the fault, clasts were not noticeably flattened. No brittle faults were observed in the vicinity of the fault at either the east or west end of Kadin Lake, but numerous subvertical lineaments along the splay indicate that there has been some

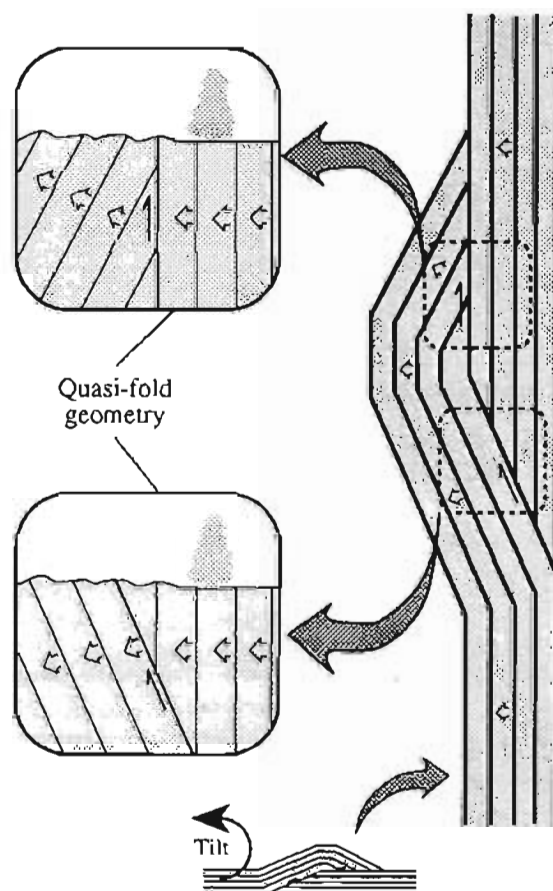


**Figure 8.** Quasi-folds may be explained by tilting of hanging-wall and footwall cutoffs of fault-bend folds. Arrows show upward-facing direction of sedimentary section.

motion along steeply dipping faults. At the east end of Kadin Lake, a silicic dike with disseminated sulfides may have been dextrally offset about 1 km along one of these

faults. Along the trace of the "true" Contact fault in the northwestern part of the study area (Winkler, 1992), the Miners Bay pluton has apparent *sinistral* offset of about

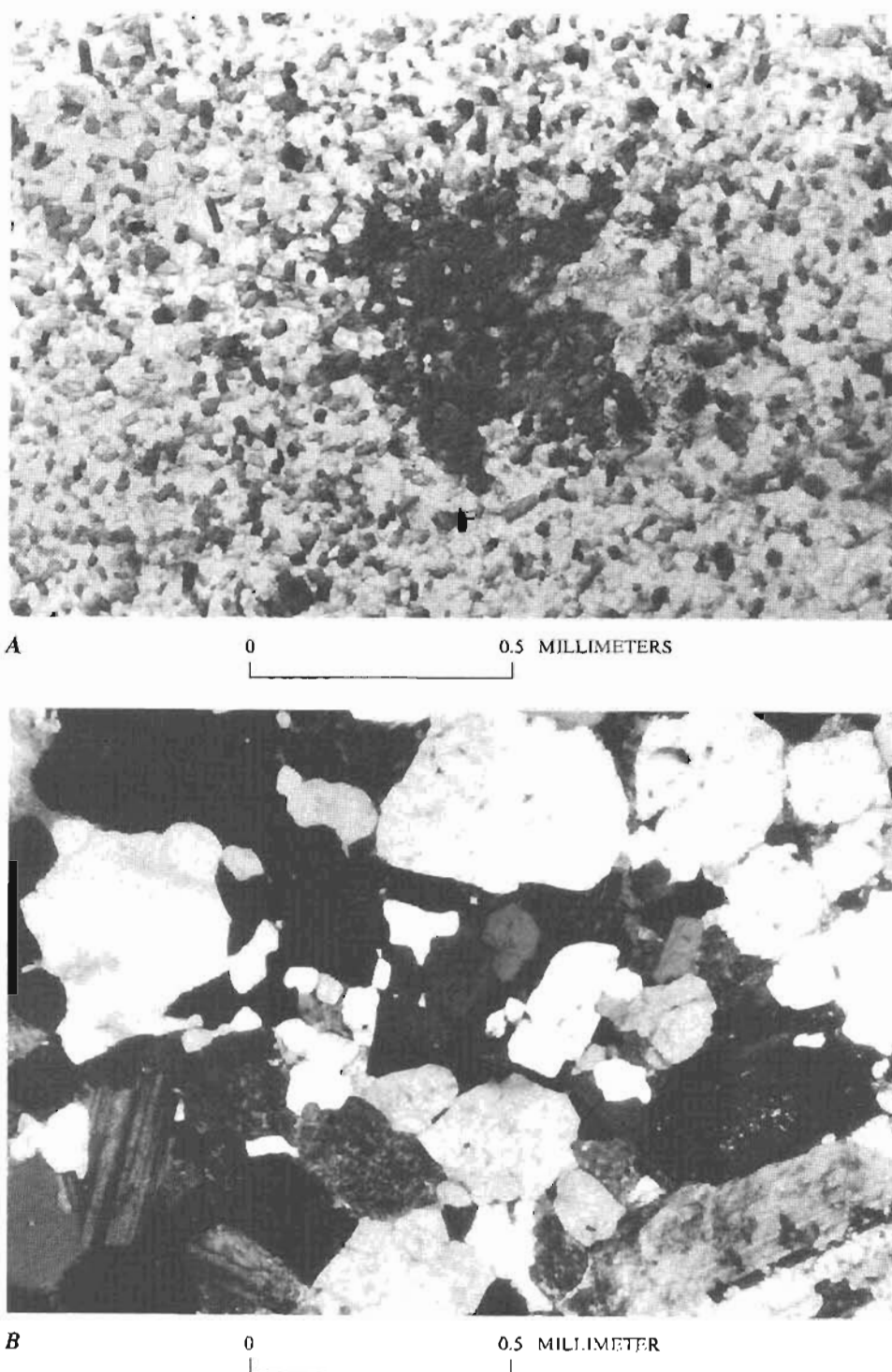


Figure 9. A, Staurolite porphyroblast in matrix of biotite and quartz in metasedimentary rocks near margin of Terentiev Lake pluton. There is no indication that there was ductile deformation during or after emplacement of plutons. Plane-polarized light. B, Typical primary igneous hypidiomorphic-granular texture of granite of Terentiev Lake pluton. There is only minor evidence of later deformation. All plutons are similarly undeformed in thin section.

2.5 km along the Contact fault. However, the part of the pluton south of the fault is granite, but the part to the north is gabbro. We are uncertain how these two compositionally different parts of the pluton are structurally related.

Northeast-southwest-striking faults cut and displace the Terentiev Lake and Cedar Bay plutons (fig. 2). A fault that cuts the Terentiev Lake pluton is nearly vertical and has about 30 m of apparent southeast-side-up motion. The fault that cuts the Cedar Bay pluton is not exposed, but the topography on the northwest side of the fault is about 100 m lower than that on the southeast side, which suggests that its motion is also southeast-side-up. This fault is at least 12 km long and is the structural boundary between domain D on the northwest and domains F and H on the southeast.

### QUARTZ VEINS

Quartz veins are found throughout the study area and typically dip steeply and strike north-south or NNW-SSE (fig. 14). We noted no veins parallel to bedding or cleavage as reported by Goldfarb and others (1986) in rocks of the Valdez Group. The quartz veins are generally less than 2 cm wide, but some are up to 2 m. Some veins are planar and contain coarsely crystalline quartz, in contrast to

others that are planar and have dendritic offshoots or are a series of en echelon tension fractures. There was no discernible shearing across most veins.

## STRUCTURAL GEOLOGY OF MINERAL OCCURRENCES

### BLACKJACK PROSPECT

The two prospects in the study area from which we have the most structural information are the Blackjack and the Columbia Red Metals (fig. 2) (Jansons and others, 1984). The Blackjack is the largest epigenetic zinc prospect in Prince William Sound and is hosted by the Cedar Bay pluton. It consists of an east-west trending adit about 90 m long with a small ( $\leq 3$  m to the east and to the west) drift along a 1.5-m-wide silicified zone striking north-south, located a few meters from the end of the main drift. Within the silicified zone, the tonalitic host rock has been recrystallized into fine-grained medium-gray material that is iron stained on most surfaces. There has been no exploration along similar, but narrower ( $< 1$  m), silicified zones within the adit. Sulfide minerals in the silicified zones are dominantly sphalerite and pyrite; minor pyrrhotite, chalcopyrite, and covellite have also been reported (Moffit and Fellows, 1950; Jansons and others, 1984). The only evidence for shear along the main mineralized zone is a fault (strike  $180^\circ$ , dip  $75^\circ$  W.) parallel to the zone with less than

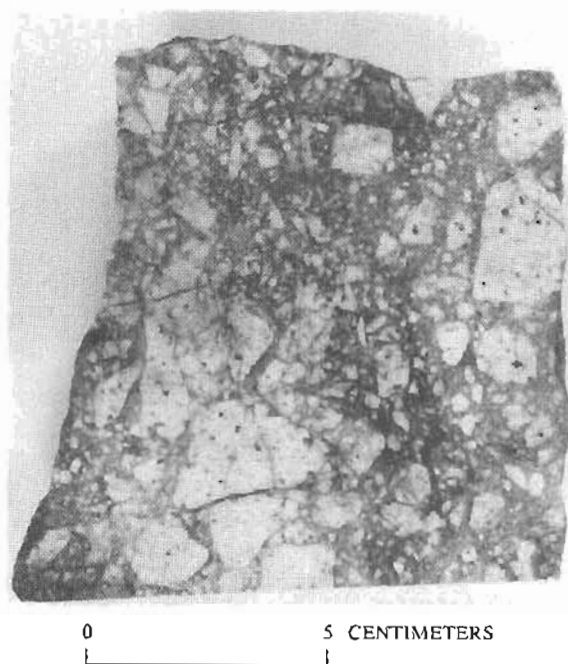


Figure 10. Polished slab of granitic autobreccia from apophysis on west side of Granite Cove pluton. Clasts consist of micrographic intergrowths of potassium feldspar and quartz. Finer grained groundmass consists of the same minerals, as well as minor chlorite and rare white mica.

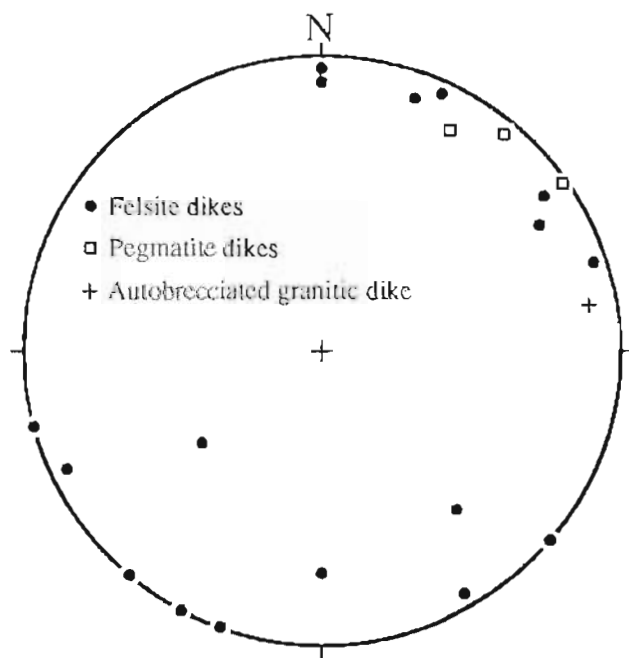


Figure 11. Equal-area stereogram of poles to felsite dikes, pegmatite dikes, and a granitic autobreccia dike from the Granite Cove pluton (fig. 2).

3 cm of gouge and with subhorizontal mullions, indicating strike-slip motion. We were unable to determine the sense of slip on this surface. In a 15-m-long upper adit, there has been probable left-lateral offset on structures with the same orientation. There was no other evidence for high strain within the mineralized zone, as there was no planar or linear fabric. The mineralizing fluids apparently followed pre-existing joints or faults. Jansons and others (1984) reported that the mineralized zone is traceable for 1.5 km.

### COLUMBIA RED METALS PROSPECT

The Columbia Red Metals prospect is a rust-weathering polymetallic vein occurrence located along the Miners Bay-Kadin Lake splay of the Contact fault (fig. 2); it lies within graywacke of the Orca Group, and conglomerate is present within and adjacent to the prospect. A small disseminated sulfide-bearing felsic stock and a dike are lo-

cated less than 0.5 km to the east. The mineralized zone is about 1 m thick and strikes  $015^\circ$  and dips  $52^\circ$  E. (fig. 15). It contains brecciated wall rock inclusions and planar zones of chalcopyrite with lesser pyrite, limonite, iron oxides and (or) Fe-S oxyhydroxides. Jansons and others (1984) also reported disseminated galena and sphalerite. They were able to trace the sulfide-bearing part of the occurrence 65 m along strike. The chalcopyrite is ribboned in places. Also within and adjacent to the mineralized zone are drusy quartz crystals up to a centimeter across and 2 cm long. Jansons and others (1984) described this occurrence as a shear zone. However, we found no evidence for differential slip within or along the walls of the mineralized zone. Adjacent to the mineralized zone there is a dendritic network of barren quartz veinlets (figs. 15 and 16); veinlets are less than a centimeter thick and locally surround blocks of wall rock less than 15 cm across. These veins are most abundant within several meters of the mineralized zone.

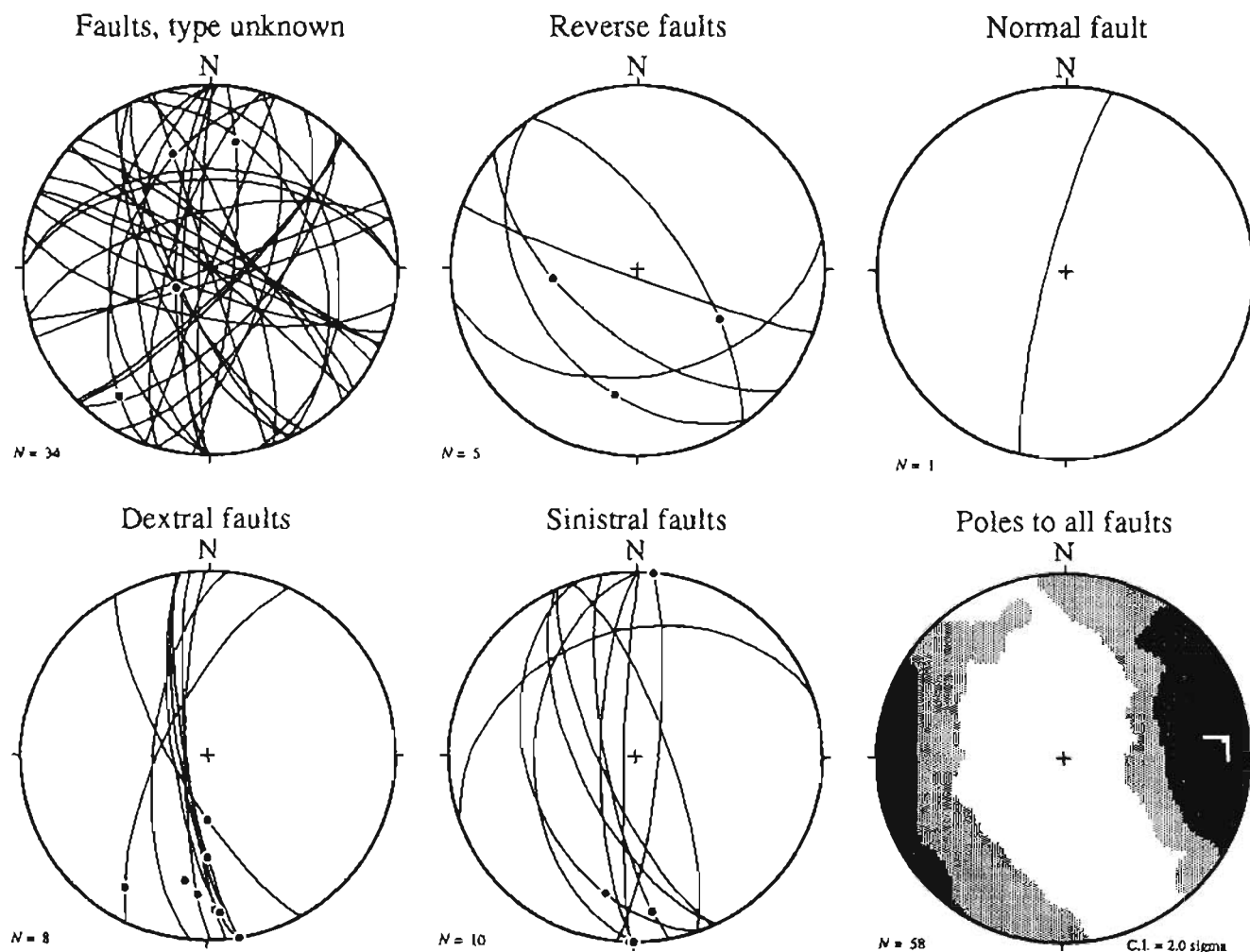


Figure 12. Equal-area stereograms of faults in study area. Dots show slip direction on faults in which it could be determined. Contoured plot is a Kamb contoured plot of poles to all faults. C.I., contour interval;  $N$ , number of samples.

### OTHER OCCURRENCES

Disseminated pyrrhotite, pentlandite, and chalcopyrite occur within quartz diorite of the Miners Bay pluton (Jansons and others, 1984). This syngenetic occurrence is distinct from the epigenetic Blackjack and Columbia Red Metals prospects, which are in mineralized zones that strike approximately north-south, have little or no shearing along the mineralized zone, and have dendritic quartz veinlets that locally brecciate the wall rock. The epigenetic occurrences are either within ~2 km of, or within, an intrusion.

There is one quartz-fluorite occurrence in the study area (fig. 2)—the only known occurrence of this type within the Chugach-Prince William terrane. The main vein consists of a 1- to 2-m-wide yellow-weathering zone that contains ~70 percent quartz and ~30 percent fluorite. Within the vein there is abundant vuggy quartz and crescent and phacoid-shaped blobs of fluorite up to 8 cm by 3–4 cm. The fluorite blobs are oriented parallel to the margins of the vein. The vein strikes NNW–SSE (fig. 14), is steeply dipping, and its exposed length is 300 m. There is a network of dendritic quartz veinlets adjacent to the main vein, and the margins of all veins are sharp with no

evidence of faulting or shearing. These veinlets are reminiscent of those at the Columbia Red Metals prospect, but they are more planar and continuous and generally subparallel the main quartz-fluorite vein.

### DISCUSSION OF STRUCTURAL AND TECTONIC HISTORY

Ductile deformation in the study area is characterized by kilometer-scale tight folds with steep bedding dips and an absence of cleavage. Bol and Gibbons (1992) studied the structural geology of a correlative belt of rocks southwest of our study area (fig. 1) (Bol and Gibbons' eastern belt) and found that bedding generally has moderate dips, in contrast to the steep dips in our study area, and a similar absence of cleavage. They favored the interpretation that these rocks are an incorporated slope basin, in order to explain its slightly deformed character. However, they stated that vitrinite reflectance and mineral assemblage data (Gibbons, 1988) indicate burial depths of 10 to 15 km, which might argue that the rocks were underplated, but escaped intense deformation. The steeper dips of bedding in our study area suggest that there are along-strike variations in the intensity of deformation and possibly that this belt of rocks is more deformed than Bol and Gibbons (1992) appreciated. Perhaps this greater degree of deformation indicates that these rocks were underplated. However, the roughly symmetric distribution of lithofacies in our study



Figure 13. Rose diagram of lineament trends in study area south of lat 61° N., and north of Glacier Island, from Condon and Cass (1958). *N*, number of samples.

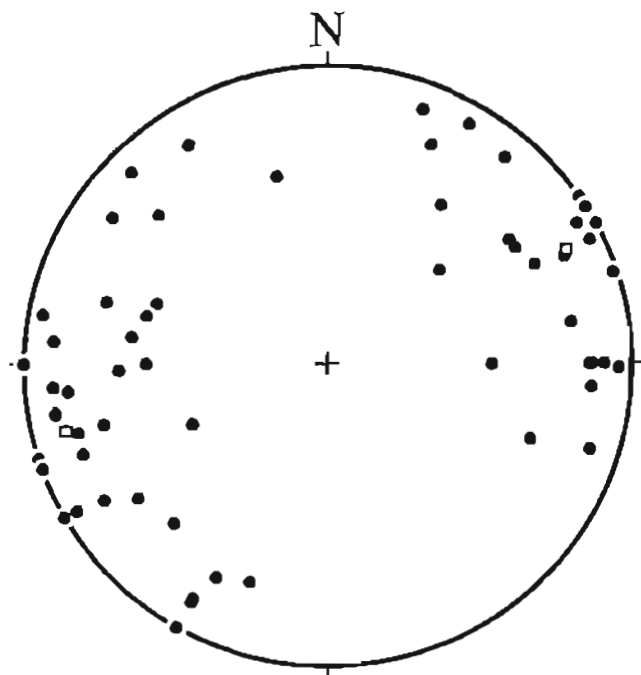


Figure 14. Equal-area stereogram of poles to quartz vein orientations (dots) and quartz-fluorite vein orientations (boxes).

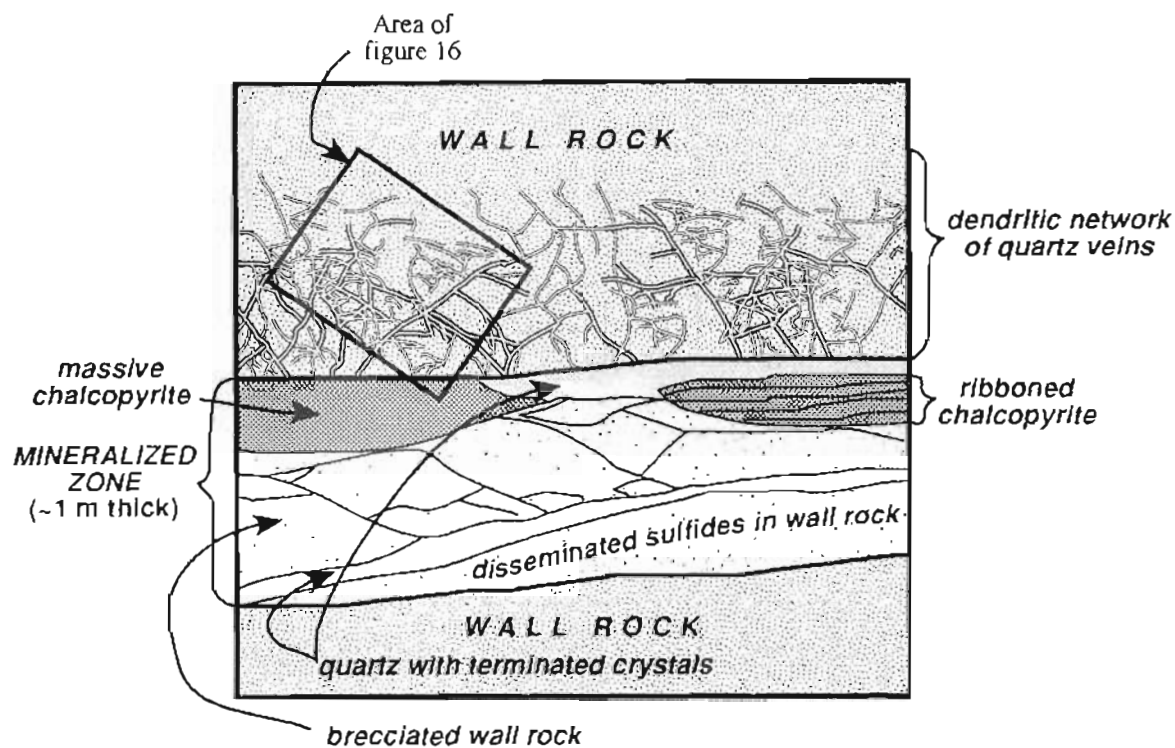


Figure 15. Simplified cross-sectional sketch of Columbia Red Metals prospect.



Figure 16. Dendritic quartz veins at upper margin of Columbia Red Metals prospect.



area is reminiscent of the pattern that might be expected in a slope basin. Therefore, the general intensity of deformation, the lack of cleavage, and the distribution of lithofacies is consistent with an incorporated slope basin, but the mineral assemblage and vitrinite reflectance data are enigmatic in such an interpretation.

Deformation in the study area began with soft-sediment disruption and the development of web structure, followed by folding and the formation of cleavage, intrusion of plutons, and finally high-angle brittle faulting, quartz veining, and sulfide mineralization. Because the plutons postdate ductile deformation, folding must have occurred before emplacement of these plutons. There is no evidence that precludes brittle faulting, quartz veining, and sulfide mineralization (at localities away from plutons) before intrusion of the plutons. However, in all cases where there are cross-cutting relationships, these events occurred afterward.

Perhaps one of the most significant questions one can ask about the structural geology of the area is, why is the strike of bedding so variable between domains? Answers can be categorized as either single-stage or multistage processes. A possible single-stage process is if the structures developed by underplating or deformation of a slope basin at a bend in the continental margin. In this scenario, we would expect fold axes and the strike of bedding and cleavage to simply wrap around the bend, such as in the Kashmir syntaxis (Bossart and others, 1988), but this is not what we observe.

Another possibility is that the domains with strikes discordant to regional trends represent lateral ramps on thrust faults. Although thrust faults have not been recognized in the study area, the structural style is characterized by folding not faulting. Also, the structural thickness of thrust packets in modern accretionary prisms is typically less than 2 km (for example, Karig, 1986; Moore and others, 1991; Westbrook and others, 1984), much less than the structural thickness of the domains in the study area. We cannot rule out that some domain boundaries are lateral ramps, but the geometry and scale of the structures do not compel us to argue for their existence. Therefore, we are led to examine multistage hypotheses, in which the  $F_m$  folds were generated in one event and reoriented in another.

We consider three other possible mechanisms to explain the various orientations of the domains within the hinge of the orocline of southern Alaska: vertical-axis block rotation caused by dextral slip on strands of the Contact fault, indentation, and oroclinal bending. Vertical-axis block rotation has been documented by Bol and Roeske (1993) between strands of the Contact fault in eastern Prince William Sound. They report that the strike of bedding in that area is oriented clockwise from regional trends and that there has been vertical-axis block rotations caused by a broad system of right-lateral strike-slip faults. We do not find that domains in the study area are consistently

rotated clockwise from regional trends and do not consider dextral strike-slip faulting as a likely cause for the geometry of the structures.

Indentation of a tectonic block into the southern Alaska margin (for example, Tapponnier and others, 1982) could conceivably cause the domainal reorientation of structures. However, there is no manifestation of the orocline due south of the study area (Nelson and others, 1985), nor is there a large rock unit that may have acted as rigid indenter penetrating into the accretionary prism. The lack of an indenter leads us to conclude that this mechanism is unlikely.

Oroclinal bending of southern Alaska has been proposed on the basis of structural and paleomagnetic evidence (Grantz, 1966; Coe and others, 1985, 1989), and involves a roughly 45° counterclockwise bend of southwestern Alaska about a vertical axis. Bol and Gibbons (1992) proposed that the approximately 90° bend of the structural grain in Prince William Sound was caused by a roughly 45° oroclinal bend of southern and southwestern Alaska in conjunction with dextral strike-slip faulting along the Contact fault system in eastern Prince William Sound and thrust-faulting in western Prince William Sound, which resulted in an additional 45° of counterclockwise rotation. Paleomagnetic constraints upon the timing of oroclinal bending in Alaska indicate that it occurred between about 65 and about 35 Ma (Coe and others, 1989).

Oroclinal bending of a once-straighter continental margin with reorientation of domains in the study area along faults (some recognized, some unrecognized) at the domain boundaries can explain the observed geometry. If we imagine straightening out the structural grain in domains A, B, C, H, I, and J, then domains D, E, G, and K (F will be discussed later) need to have undergone rotations in order to accommodate strain between domains with a structural grain subparallel to the regional trends. The motion along specific domain-bounding faults is uncertain because we do not know the location of relative poles of rotation of adjacent domains. However, we can suggest the motion on faults between some domains. For example, the east-west strike of bedding in domain D may have been caused by dextral shear between domains C and H. The elongate shape of domain D may be due to several east-west-striking intradomainal antithetic sinistral strike-slip faults. The western part of domain E is rotated clockwise from the strike of bedding in the domains to the north. Dextral or dextral-thrust motion may have occurred along the domain E and C boundary.

We infer that most reorientation of domains occurred before intrusion of the plutons, because the Cedar Bay and Terentiev Lake plutons do not lie within a domain, but intrude several domains, and they are not highly deformed. The boudinaged dike in domain F and the joint set in the Cedar Bay pluton indicate that some deformation occurred

after emplacement of the intrusions. Therefore, if the intrusions are about 35 Ma in age, then the timing of reorientation of domains is consistent with the paleomagnetic constraints for oroclinal bending.

There is some evidence for reactivation of the domain bounding faults after emplacement of the plutons. For example, the fault along the domain D and H boundary also cuts the Cedar Bay pluton, but the pluton margin is not offset. Therefore, if the structures in domains D and H were initially parallel and later reoriented, then the reorientation process occurred before intrusion of the Cedar Bay pluton, and the fault was reactivated later.

The smooth curvature of the strike of bedding around the orocline in domains A, B, and C suggests that contractional deformation related to oroclinal bending was focused south of these domains. Therefore, the oroclinal bend in Prince William Sound may be modeled by the bending of a beam, with contractional deformation found on the inside of the beam (more precisely, inside the neutral surface—the surface along which there is no strain) and extensional deformation on the outside. However, mapping at 1:250,000 scale north of the study area has shown no such extensional deformation (Nelson and others, 1985; Winkler, 1992).

The development of the structures in domain F and how they relate to the other brittle and ductile structures is not obvious in any interpretation. Because volcanic rocks and limestones are not typically encountered within turbidite fans, we consider this fault-bounded block as exotic. It may have been part of a ridge, a seamount, or oceanic crust subducted beneath the accretionary prism. Because the melange-like foliation in domain F is folded, the fabric could be interpreted as the product of more than one phase of deformation. Polyphase deformation is also consistent with the fold axes clustering around two loci (fig. 6). Alternatively, the structures may have developed in one period of progressive deformation in which the fabric elements were refolded, but not sheath folded. Fold axes do not lie on a plane on a stereogram (fig. 6), but are more dispersed than would be expected in sheath folds (Cobbold and Quinquis, 1980). The fault between domains F and H juxtaposed the two, because a syncline in domain H is truncated by the fault (fig. 2). The steep plunge of fold axes in domain F suggests that the structures may have formed during strike-slip or oblique-slip motion. Also, the slightly sigmoidal shape of the domain (fig. 2) suggests a component of sinistral motion on faults along the northwest and southeast sides of the domain. Nonetheless, we are uncertain if the structures in domain F formed in one period of progressive deformation or two separate phases of deformation, and how the timing of deformation relates to the juxtaposition of domains F and H, and the development of  $F_m$  folds.

In eastern Prince William Sound, the dextral motion along the Contact fault system juxtaposes higher grade

polydeformed rocks against lower grade rocks that have undergone only one period of deformation (Bol and Roeske, 1993; Plafker and others, 1977). In western Prince William Sound to the southwest of the study area (fig. 1), Bol and Gibbons (1992) found that the previously mapped trace of the Contact fault shows thrust motion. As our study area lies between the areas examined by Bol and Gibbons (1992) and Bol and Roeske (1993), we might expect to find either thrust or dextral strike-slip motion, or both.

The Miners Bay–Kadin Lake splay of the Contact fault in the study area does not have the characteristics of the Contact fault in eastern Prince William Sound. Rocks on either side of the fault are low angle and are not polydeformed. There is probably about 11 km of dextral offset on the splay, based upon correlating the conglomerate outcrop at the Columbia Red Metals mineral occurrence with the conglomerate near Miners Lake. This motion was along steeply dipping brittle faults. No ductile deformation was found in the vicinity of the splay, and thus the Contact fault is probably a high-angle strike-slip fault. Alternatively, the Contact fault (proper) may have slightly different characteristics than the Miners Bay–Kadin Lake splay of the Contact fault. Bol and Gibbons (1992) found that the Contact fault (their Eaglek fault) southwest of the study area (fig. 1) consists of a 10- to 100-m-wide zone of highly sheared rocks with numerous minor faults, downdip lineations, shear veins, and an extensional crenulation. We found none of these features.

The main trace of the Contact fault has about 2.5 km of sinistral map separation of the different compositional phases of the Miners Bay pluton. It is perplexing how the main fault could have sinistral offset of a couple kilometers, and a splay of the fault has probable dextral offset of about 11 km. It is possible that earlier motion on the fault was reverse—as described by Bol and Gibbons (1992)—and offset the different compositional phases of the Miners Bay pluton, and later dextral strike-slip motion along the Kadin Lake–Miners Bay splay offset the conglomerate. Nonetheless, because the Contact fault truncates the southern margin of the Miners Bay pluton, the age of some movement on the fault must be younger than 35 Ma. Deformation of the rocks of the Orca and Valdez Groups occurred prior to emplacement of the plutons, and thus these two rock units were juxtaposed sometime earlier. Therefore, recent motion on the Contact fault in the study area records strike-slip offset, rather than reverse motion that separates two pulses of accretion in the prism (Plafker and others, 1977).

There are probably multiple causes of brittle faulting in the study area. Some faulting, as just discussed, is related to strike-slip movement along the Contact fault and the Kadin Lake–Miners Bay fault, some faulting is probably related to the reorientation of domains possibly by oroclinal bending, and some faults may be like the late faults in the Turnagain Arm area (fig. 1) reported by

Bradley and Kusky (1990). They found four late-fault sets—a conjugate set of strike-slip faults at a large angle to the regional structural fabric, reverse faults parallel to the regional structural grain, and normal faults perpendicular to it. We do not find any conjugate sets of faults. However, the mean strike of the strike-slip faults that we observed is perpendicular to the regional (east-west-striking) structural grain as is the mean strike of the strike-slip faults described by Bradley and Kusky (1990). The reverse faults that we measured are parallel to the regional structural fabric, and are antithetic to the synthetic reverse faults along Turnagain Arm. Byrne (1984) recorded both synthetic and antithetic late faults parallel to the structural grain on Kodiak Island (fig. 1). The one normal fault that we measured is perpendicular to regional strike as are the normal faults along Turnagain Arm. Bradley and Kusky (1990) attributed the origin of these late-fault sets to subhorizontal shortening within the accretionary prism and to minor extension along its strike.

The north-south-striking strike-slip faults with both dextral and sinistral motion that cut the plutons in the study area are not easily interpreted. Because quartz veins, mineralized zones, and late faults have a similar orientation (compare figs. 12 and 14), veining, mineralization, and faulting are probably related. The north-south strike of quartz veins indicates there was north-south contraction or east-west extension in the study area. The orientations of the late faults are broadly consistent with this interpretation. Felsic dikes within the study area generally have northwest-southeast strikes, but orientations range from north-south, the same as the quartz veins, to east-west. Perhaps the orientation of most of the dikes also indicates east-west or northeast-southwest extension. Alternatively, our data may be biased toward the two or three domains in which the most faults with a known sense of offset were measured, or perhaps there is more than one generation of faulting.

## IMPLICATIONS FOR ORE DEPOSITS

Turbidite-hosted lode-gold deposits are the most common type of epigenetic mineral occurrence in the Chugach-Prince William terrane. The source of the ore-forming fluids has been argued to be from metamorphic dehydration reactions (Goldfarb and others, 1986) or the circulation of meteoric water (Silberman and others, 1981). Regardless of the origin of the fluids, most of these deposits are along late faults, do not show much evidence for hydrofracturing unrelated to faulting, and have common arsenic-bearing sulfides (for example, Mitchell, 1979; Richter, 1970; Pickthorn, 1982; Stuewe, 1986). In contrast, the prospects and occurrences in the study area have base-metal sulfides, no precious metals, little, if any, faulting or shearing across them, and abundant evidence of hydro-

fracturing. Most of the mineralized zones have a north-south strike, which is similar to the orientation of barren quartz veins and late strike-slip faults. Gold-bearing quartz veins to the east and west of the study area, in the Port Wells and Port Valdez mining districts (fig. 1), have somewhat different orientations, most commonly striking north-west-southeast. Both types of deposits postdate the plutons in the areas where they are found, and both are found along steeply dipping surfaces. However, the differences in vein mineralogy and structural setting indicate that the polymetallic vein systems have little in common with the gold vein systems.

The proximity of mineralized zones to intrusive bodies and the presence of the quartz-fluorite vein suggest a genetic link between magmatism and hydrothermal activity. The abundance of base-metal sulfides and lack of gold- and arsenic-bearing sulfides suggests that chloride complexes were dominant in the ore-forming fluids and that these may have had a magmatic origin. The autobrecciated granite associated with the Granite Cove pluton indicates that at least one of the plutons in the study area had a fluid phase that escaped the magma chamber after crystallization. The escape of fluids from the plutons, which may have also carried base-metal bearing complexes, locally and perhaps regionally hydrofractured the wall rocks to the plutons along a pre-existing joint set. This joint set may have developed if the rocks were within a regional stress field favoring orogen-parallel extension after oroclinal bending. Orogen-parallel extension during late faulting has been proposed by Bradley and Kusky (1990), and is broadly supported by the orientation of the late faults, quartz veins, and dikes in the study area. This scenario, in which fluids escaped from the plutons and hydrofractured the wall rocks along pre-existing fractures, possibly related to orogen-parallel extension, explains the origin of the ore-forming fluids, the lack of offset along most mineralized zones, brecciation of the wall rocks in mineralized zones, void-filling quartz in mineralized zones, and the roughly consistent orientation of most quartz veins. However, it does not explain why such mineralization does not occur elsewhere within the Chugach-Prince William terrane, even though the same rock types and same age and composition plutons are found outside the study area.

## REFERENCES CITED

- Bol, A.J., Coe, R.S., Grommé, C.S., and Hillhouse, J.W., 1992, Paleomagnetism of the Resurrection Peninsula, Alaska: Implications for the tectonics of southern Alaska and the Kula-Parallon ridge: *Journal of Geophysical Research* v. 97, p. 17,213-17,232.
- Bol, A.J., and Gibbons, H., 1992, Tectonic implications of out-of-sequence faults in an accretionary prism, Prince William Sound, Alaska: *Tectonics*, v. 11, p. 1288-1300.
- Bol, A.J., and Roeske, S.M., 1993, Strike-slip faulting and block

- rotation along the Contact fault system, eastern Prince William Sound, Alaska: *Tectonics*, v. 12, p. 49-62.
- Bossart, P., Dietrich, D., Greco, A., Ottiger, R., and Ramsay, J.G., 1988, The tectonic structure of the Hazara-Kashmir syntaxis, southern Himalayas, Pakistan: *Tectonics*, v. 7, p. 273-297.
- Bradley, D.C., and Kusky, T.M., 1990, Kinematics of late faults along Turnagain Arm, Mesozoic accretionary complex, south-central Alaska, in Dover, J.H., and Galloway, J.P., editors, *Geologic studies in Alaska by the U.S. Geological Survey*, 1989: U.S. Geological Survey Bulletin 1946, p. 3-10.
- Byrne, T., 1984, Structural geology of melange terranes in the Ghost Rocks Formation, in Raymond, L., ed., *Melanges: Their origin and significance*: Geological Society of America Special Paper 198, p. 21-51.
- Carey, S.W., 1955, The orocline hypothesis in geotectonics: *Proceedings of the Royal Society of Tasmania*, v. 89, p. 255-288.
- Cobbold, P., and Quinquis, H., 1980, Development of sheath folds in shear regimes, *Journal of Structural Geology*, v. 2, p. 119-126.
- Coe, R.S., Globerman, B.R., Plumley, P.W., and Thrupp, G., 1985, Paleomagnetic results from Alaska and their tectonic implications, in Howell, D.G., ed., *Tectonostratigraphic terranes of the Circum-Pacific region*: Houston, Circum-Pacific Council for Energy and Mineral Resources, *Earth Sci. Ser.*, vol. 1, p. 85-108.
- , 1989, Rotation of central and southern Alaska in the Early Tertiary: oroclinal bending by megakinking? in Kissel, C., and Laj, C., eds., *Paleomagnetic rotations and continental deformation*: Boston, Kluwer, NATO-ASI series, p. 327-339.
- Condon, W.H., and Cass, J.T., 1958, Map of a part of the Prince William Sound area, Alaska showing linear geologic features as shown on aerial photographs: U.S. Geological Survey Miscellaneous Investigations Map I-273.
- Cowan, D.S., 1982, Deformation of partly dewatered and consolidated Franciscan sediments near Piedras Blancas Point, California, in Leggett, J.K., ed., *Trench forearc geology*: Geological Society of London Special Publication 10, p. 439-458.
- Crowe, D.E., Nelson, S.W., Brown, P.E., Shanks, W.C., III, and Valley, J.W., 1992, Geology and geochemistry of volcanogenic massive sulfide deposits and related igneous rocks, Prince William Sound, south-central Alaska: *Economic Geology*, v. 87, p. 1722-1746.
- Dumoulin, J.A., 1987, Sandstone composition of the Valdez and Orca Groups, Prince William Sound, Alaska: U.S. Geological Survey Bulletin 1774, 37 p.
- Gibbons, H., 1988, Microstructures and metamorphism in an accretionary prism in Prince William Sound, Alaska: Santa Cruz, University of California Santa Cruz, M.S. thesis, 191 p.
- Goldfarb, R.J., Leach, D.L., Miller, M.L., and Pickthorn, W.J., 1986, Geology, metamorphic setting, and genetic constraints of epigenetic lode-gold mineralization within the Cretaceous Valdez Group, south-central Alaska, in Keppie, J.D., Boyle, R.W., and Haynes, S.J., eds., *Turbidite-hosted gold deposits*: Geological Association of Canada Special Paper 32, p. 87-105.
- Grantz, Arthur, 1966, Strike-slip faults in Alaska: U.S. Geological Survey Open-File Report 267, 82 p.
- Hudson, Travis, Plafker, George, and Peterman, Z.E., 1979, Paleogene anatexis along the Gulf of Alaska margin: *Geology*, v. 7, p. 573-577.
- Jansons, U., Hoekzema, R.B., Kurtak, J.M., and Fechner, S.A., 1984, Mineral occurrences in the Chugach National Forest, southcentral Alaska: U.S. Bureau of Mines Open File Report MLA 5-84.
- Karig, D.E., 1986, The framework of deformation in the Nankai Trough, in Karig, D.E., Kagami, H., and others, *Initial Reports of the Deep Sea Drilling Project*, volume 87: Washington, U.S. Government Printing Office, p. 927-940.
- MacKevett, E.M., Jr., and Holloway, C.D., 1977a, Metalliferous and selected non-metalliferous mineral deposits in the eastern part of southern Alaska: U.S. Geological Survey Open-File Report 77-169A, 99 p., 1 sheet, scale 1:1,000,000.
- , 1977b, Metalliferous mineral deposits in the western part of southern Alaska: U.S. Geological Survey Open-File Report 77-169-F, 38 p., 1 sheet, scale 1:1,000,000.
- Mitchell, P.A., 1979, *Geology of the Hope-Sunrise (gold) mining district, north-central Kenai Peninsula, Alaska*: Stanford, California, Stanford University, M.S. thesis, 243 p.
- Moffit, P.H., and Fellows, R.E., 1950, Copper deposits of the Prince William Sound district, Alaska: U.S. Geological Survey Bulletin 963-B, 80 p.
- Moore, J.C., Diebold, J., Fisher, M.A., Sample, J., Brocher, J., Taiwan, M., Ewing, J., von Huene, R., Rowe, C., Stone, D., Stevens, C., and Sawyer, D., 1991, EDGE deep seismic reflection transect of the eastern Aleutian arc-trench layered lower crust reveals underplating and continental growth: *Geology*, v. 19, p. 420-424.
- Mutti, E., and Ricci-Lucchi, F., 1978, Turbidites of the northern Apennines—introduction to facies analysis: *International Geology Review*, v. 20, p. 125-166.
- Nelson, S.W., Miller, M.L., Barnes, D.F., Dumoulin, J.A., Goldfarb, R.J., Koski, R.A., Mull, C.G., Pickthorn, W.J., Jansons, U., Hoekzema, R.B., Kurtak, J.M., and Fechner, S.A., 1984, Mineral resource potential of the Chugach National Forest, Alaska: U.S. Geological Survey Miscellaneous Field Studies Map MF-1645-A.
- Nelson, S.W., Dumoulin, J.A., and Miller, M.L., 1985, Geologic map of the Chugach National Forest, Alaska: U.S. Geological Survey Map MF-1645-B.
- Nilson, T.H., and Zuffa, G.G., 1982, The Chugach terrane, a Cretaceous trench-fill deposit southern Alaska, in *Trench-forearc geology—Sedimentation and tectonics on modern and ancient active plate margins*: Geological Society of London Special Publication 10, p. 213-227.
- Pickthorn, W.J., 1982, Stable isotope and fluid inclusion study of the Port Valdez district, southern Alaska: Los Angeles, University of California, M.S. thesis, 66 p.
- Plafker, George, Jones, D.L., and Pessagno, E.A., Jr., 1977, A Cretaceous accretionary flysch and melange terrane along the Gulf of Alaska margin, in Blean, K.M., ed., *The United States Geological Survey in Alaska—Accomplishments during 1976*: U.S. Geological Survey Circular 751-B, p. B41-B43.
- Plafker, George, Keller, Gerta, Nelson, S.W., Dumoulin, J.A., and Miller, M.L., 1985, Summary of data on the age of the Orca Group, Alaska, in Bartsch-Winkler, S. ed., *The United States Geological Survey in Alaska: Accomplish-*

- ments during 1984: U.S. Geological Survey Circular 967, p. 74-76.
- Plafker, George, Nokleberg, W.J., and Lull, J.S., 1989, Bedrock geology and tectonic evolution of the Wrangellia, Peninsular, and Chugach terranes along the Trans-Alaska Crustal Transect in the Chugach Mountains and southern Copper River basin, Alaska: *Journal of Geophysical Research*, v. 94, p. 4255-4295.
- Richter, D.H., 1970, Geology and lode-gold deposits of the Nuka Bay area, Kenai Peninsula, Alaska: U.S. Geological Survey Professional Paper 625G, 16 p.
- Sample, J., and Fisher, D., 1986, Duplex accretion and underplating in an ancient accretionary complex, Kodiak Islands, Alaska: *Geology*, v. 14, p. 160-163.
- Sample, J.C., and Moore, J.C., 1987, Structural style and kinematics of an underplated slate belt, Kodiak and adjacent islands, Alaska: *Geological Society of America Bulletin*, v. 19, p. 7-20.
- Silberman, M.L., Mitchell, P.A., and O'Neil, J.R., 1981, Isotopic data bearing on the origin and age of the epithermal lode gold deposits in the Hope-Sunrise mining district, northern Kenai Peninsula, Alaska: in Albert, N.R.D., and Hudson, T., eds., *the U.S. Geological Survey in Alaska—Accomplishments during 1979*: U.S. Geological Survey Circular 823B, p. B81-B84.
- Stuwe, K., 1986, Structural evolution of the Port Wells gold mining district, Prince William Sound, south central Alaska: *Implications for the origin of the gold lodes: Mineralium Deposita*, v. 21, p. 288-295.
- Tapponnier, P., Peltzer, G., Le Dain, A.Y., Armijo, R., and Cobbold, P., 1982, Propagating extrusion tectonics in Asia: New insights from simple experiments with plasticine: *Geology*, v. 10, p. 611-616.
- Tysdal, R.G., and Case, J.E., 1979, *Geologic map of the Seward and Blying Sound quadrangles, Alaska*: U.S. Geological Survey Miscellaneous Investigations Series I-1150, 12 p., 1 sheet, scale 1:250,000.
- Westbrook, G.K., Mascle, A., and Biju-Duval, B., 1984, Geophysics and the structure of the Lesser Antilles forearc, in Biju-Duval, B., Moore, J.C., and others, *Initial Reports of the Deep Sea Drilling Project*, v. 78A: Washington, U. S. Government Printing Office, p. 23-38.
- Winkler, G.R., 1976, Deep sea fan deposition of the lower Tertiary Orca Group, eastern Prince William Sound, Alaska, in Miller, T.P., ed., *Recent and ancient sedimentary environments in Alaska*: Anchorage, Alaska Geological Society Symposium Proceedings, p. R1-R20.
- , 1992, *Geologic map and summary geochronology of the Anchorage 1° × 3° quadrangle, southern Alaska*: U.S. Geological Survey Miscellaneous Investigations Map I-2283.

Reviewers: Dwight C. Bradley and Richard J. Goldfarb

# TIMING OF EARLY TERTIARY RIDGE SUBDUCTION IN SOUTHERN ALASKA

By Dwight C. Bradley, Peter J. Haeussler, and Timothy M. Kusky

## ABSTRACT

We present a new compilation of 158 isotopic ages from Tertiary plutons that intrude the accretionary prism (Chugach-Prince William composite terrane) of southern Alaska. Two broad plutonic age groups are present: Paleocene to Eocene (the Sanak-Baranof plutonic belt), and Oligocene to Miocene. Plutons of the Sanak-Baranof belt are broadly coeval with magmatism along the axis of an Andean-type arc that lay farther inboard. A plot of age versus position along strike shows that near-trench magmatism progressed from about 66–63 Ma in the west to about 50 Ma in the east. We interpret the near-trench magmatism as the product of subduction of the Kula-Farallon ridge (or another unidentified spreading center) and suggest that the age progression tracks a migrating trench-ridge-trench triple junction along the continental margin.

## INTRODUCTION

Subduction of the Kula-Farallon ridge beneath the North American continent is a fundamental feature of all marine-based global plate reconstructions for early Tertiary time (Byrne, 1979; Engebretson and others, 1985; Stock and Molnar, 1988; Lonsdale, 1988; Atwater, 1989). In all reconstructions, however, the position through time of the trench-ridge-trench triple junction between the Kula, Farallon, and North American plates, where ridge subduction occurred, has been hypothetical. Although none of the published reconstructions have placed the triple junction farther north than Vancouver Island, evidence does exist in southern Alaska that a spreading ridge—perhaps the Kula-Farallon, or perhaps another ridge—was subducted in early Tertiary time.

The near-trench position and geochemistry of plutons of the Sanak-Baranof belt of Hudson and others (1979) (fig. 1) have led several previous workers to link this magmatic event to subduction of the Kula-Farallon ridge (Hill and others, 1981; Helwig and Emmet, 1981; Moore and others, 1983). In this paper, we discuss another aspect of Sanak-Baranof magmatism that supports the ridge-subduc-

tion hypothesis: the age pattern of magmatism along the belt. Several previous workers have commented, without thorough documentation, on the spatial distribution of ages along the belt. Hudson and others (1979), Hudson (1983), and Barker and others (1992) have contended that there were two pulses: at about 60 Ma in the west (Sanak Island to Kodiak Island) and at about 50 Ma in the east (Prince William Sound to Baranof Island). Others have argued, also without much documentation, that these same ages show a progression from 65–60 Ma in the west to 50–45 Ma in the east (Hill and others, 1981; Helwig and Emmet, 1981; Moore and others, 1983). An age progression of near-trench magmatism would be most readily interpreted in terms of ridge subduction, whereas a bimodal age pattern might have a number of possible causes.

Accordingly, in this paper we present a compilation of isotopic ages from the Sanak-Baranof belt (table 1) and discuss some tectonic implications of these ages. The available data now span the entire Sanak-Baranof belt without major gaps; new  $^{40}\text{Ar}/^{39}\text{Ar}$  and U/Pb determinations fill what had been a crucial gap between Kodiak Island and Prince William Sound, where an age jump would occur if the age distribution were bimodal. The available data show that Sanak-Baranof magmatism progressed generally from west to east, in support of the ridge subduction model. This conclusion has implications for plate reconstructions, terrane displacement, orocline formation, gold mineralization, and deformation of the accretionary wedge.

## REGIONAL GEOLOGY

Plutons of the Sanak-Baranof belt intrude a complexly deformed Mesozoic and Cenozoic accretionary prism—the Chugach-Prince William composite terrane (the term “composite” is omitted below for brevity) (fig. 1)—along the seaward margin of the Peninsular-Wrangellia-Alexander composite terrane. Plafker and others (in press) provide a thorough review of the regional geology. The inboard part of the prism is a melange of relatively competent blocks and fault slices of basalt, chert, and graywacke, in an argillite matrix (Early Cretaceous Uyak Complex, Triassic to mid-Cretaceous McHugh Complex, and Late



Jurassic to mid-Cretaceous Kelp Bay Group; Connelly, 1978; Bradley and Kusky, 1992; Decker, 1980). Farther outboard is a belt of Upper Cretaceous flysch, assigned to the Shumagin Formation, Kodiak Formation, Valdez Group, and Sitka Graywacke (part) (Moore, 1973; Nilsen and Moore, 1979; Nilsen and Zuffa, 1982; Decker, 1980). Still farther outboard lie belts of flysch assigned to the Ghost Rocks Formation and Orca Group (Moore and others, 1983; Moore and Allwardt, 1980; Helwig and Emmet, 1981). The Ghost Rocks Formation and Orca Group contain mafic and, in the latter case, ultramafic rocks that will be mentioned below as one line of evidence for ridge subduction. Penetrative deformation in the accretionary prism (thrust imbrication, folding, melange formation) and regional metamorphism (typically prehnite-pumpellyite to greenschist facies) occurred during and shortly after subduction-accretion during the Cretaceous and early Tertiary. Near-trench plutons of the Sanak-Baranof belt were emplaced into the accretionary prism after this deformation. Another tract of accreted deep-sea turbidites (Eocene Sitkalidak Formation and the outboard part of the Orca Group; Moore and Allwardt, 1980; Helwig and Emmet, 1981) lies outboard of the Sanak-Baranof belt; these younger turbidites are not cut by the plutons, and hence are probably younger.

Paleocene to Eocene plutons of the Sanak-Baranof belt crop out discontinuously along the entire 2,200 km length of the Chugach-Prince William terrane. The plutons are mainly granodiorite, granite, and tonalite (Hudson, 1983). Some of the plutons are elongate parallel to structural grain of the accretionary prism; others are transverse. Some are enormous—the Kodiak batholith, for example, is

more than 100 km long and up to 10 km wide. In the eastern Chugach Mountains, magmatism was accompanied by high-grade regional metamorphism and anatectic melting of flysch (Hudson and Plafker, 1982; Sisson and others, 1989). Paleocene to Eocene intermediate to silicic dikes are plentiful in some regions, such as the Kenai Peninsula (Winkler, 1992; Bradley and Kusky, 1992). Oligocene to early Miocene plutons intruded the Chugach-Prince William terrane in southeastern Alaska and Prince William Sound; post-Eocene plutons have not been recognized from the Kenai Peninsula to Sanak Island.

### ISOTOPIC AGES FROM THE SANAK-BARANOF BELT

Isotopic ages from intrusive rocks in the Chugach-Prince William terrane are compiled in table 1. Most of these data are contained in recent compilations of much broader scope by Wilson and others (1991) for Alaska and by Dodds and Campbell (1988) for the Yukon and British Columbia. Alaskan ages from pre-1977 sources were recalculated by Wilson and others (1991) using decay constants recommended by Steiger and Jäger (1977). A few intrusions from the Peninsular-Wrangellia-Alexander composite terrane (Winkler, 1992; Loney and others, 1975) probably could be included in the Sanak-Baranof belt, but because a near-trench position during magmatism cannot be as readily demonstrated as for the Chugach-Prince William terrane, we have not tabulated these ages; in any case, their inclusion would not change our conclu-

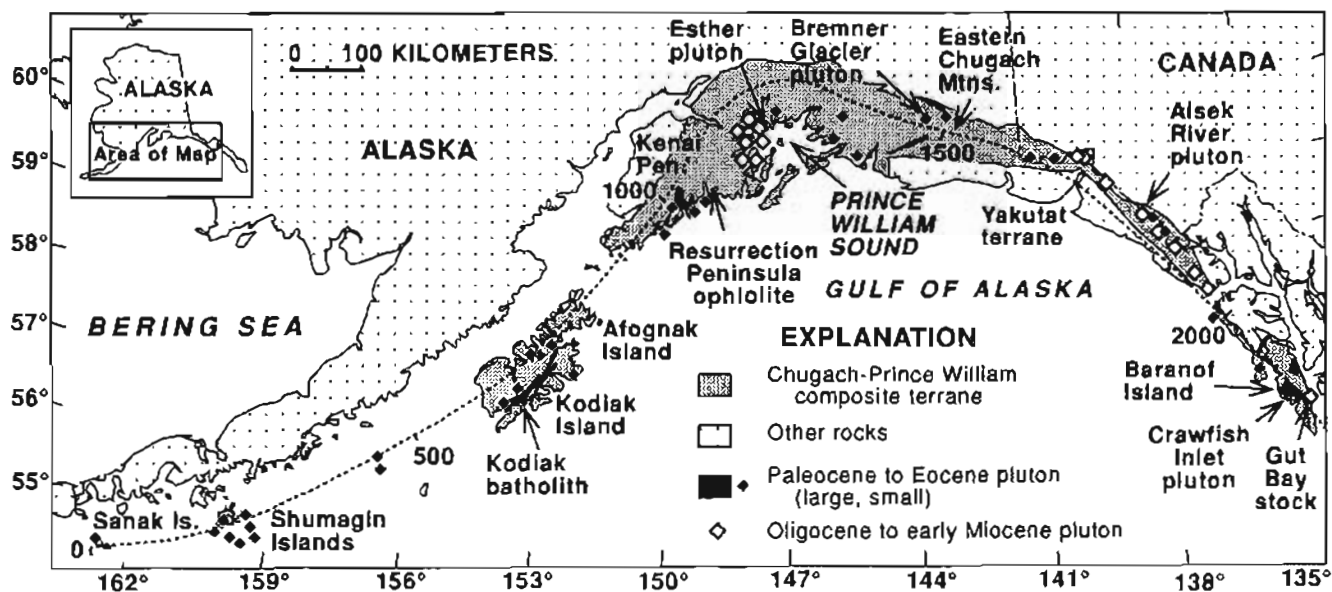


Figure 1. Generalized geologic map of southern Alaska showing plutons of Sanak-Baranof plutonic belt, Chugach-Prince William composite terrane, and localities mentioned in text. Numbers along dashed reference line show distance in kilometers from southern tip of Sanak Island to Baranof Island.

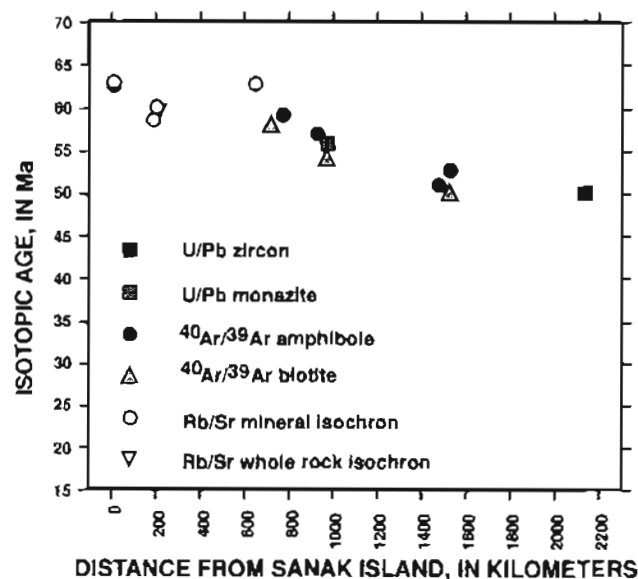


sions. We also have excluded data from the Yakutat terrane in southeastern Alaska (fig. 1), which is interpreted as a former southerly continuation of the Chugach-Prince William terrane that was translated about 600 km north with respect to the rest of the terrane during the Cenozoic (Plafker, 1987). Although the Sanak-Baranof belt as defined by Hudson and others (1979) is Paleocene to Eocene in age, table 1 includes ages ranging from Late Cretaceous to Miocene, as discussed below.

Of the 158 ages listed in table 1, 30 were rejected for inclusion in figure 2 for failure to meet the lenient selection criteria identified in the "Notes" column of table 1. Ages with errors greater than 10 percent were judged to be unacceptable. Ages from plutons with multiple determinations were either rejected if judged to be discordant, or accepted for inclusion in figure 2 if judged to be concordant or problematic. A pair of ages was considered to be discordant if the difference in ages was greater than 6 million years (m.y.), or greater than the sum of errors, using the more lenient standard in each case. The younger of a discordant pair was rejected. For three or more ages from the same pluton, discordance was determined starting from the oldest, by comparing one age with the next younger age only. For example, for a pluton with ages of 50, 46, and 43 Ma ( $\pm 2$  in all cases), all three ages would be accepted as concordant for present purposes. If, however, the only available ages were 50 and 43 Ma, the 43-Ma age would

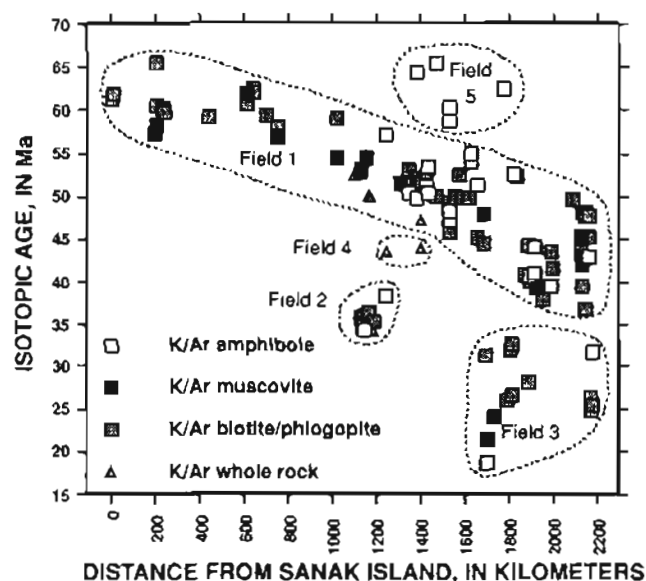
be rejected as discordant. There are a few problematic plutons in the eastern Chugach and St. Elias Mountains from which the oldest age, determined by conventional K/Ar on amphibole, is the questionable one. Problems with these amphibole ages, which define field 5 in figure 2B, are discussed below. For these plutons, all the ages—even those that we suspect are spurious—were accepted.

Two plots of isotopic age versus position along strike (excluding rejected data) are shown in figure 2. U/Pb,  $^{40}\text{Ar}/^{39}\text{Ar}$ , and Rb/Sr data (fig. 2A) show a general west-to-east age progression from 66–63 Ma in the west to 50 Ma in the east. Despite greater scatter, the same trend is also evident from conventional K/Ar data (field 1 in fig. 2B), especially west of Prince William Sound. From Prince William Sound eastward, K/Ar ages cluster in five fields (fields 1–5). Field 1 corresponds to the Sanak-Baranof belt as defined by Hudson and others (1979); fields 2–5 are discussed at greater length below. The timing of magmatism at the eastern end of the Sanak-Baranof belt is well constrained by a U/Pb zircon age of  $50.1 \pm 0.1$  Ma from the Crawfish Inlet pluton (Brew and others, 1991). The onset of magmatism at the opposite end of the belt is less tightly dated, because only conventional K/Ar and Rb/Sr isochron ages are available. The oldest age from the Sanak pluton at the extreme end of the belt is an Rb/Sr mineral isochron of  $63.1 \pm 1.2$  Ma (Hill and others, 1981); the oldest age from the Shumagin pluton, about 200



A

Figure 2. Plots of isotopic age versus distance along strike around Sanak-Baranof plutonic belt. Data are listed in table 1 and selection criteria for including in these plots are discussed in text. A, U/Pb,  $^{40}\text{Ar}/^{39}\text{Ar}$ , and Rb/Sr data. West-to-east age progression is consistent with triple junction migration. B, Conventional K/Ar data, showing same age progression (field 1) amidst scatter from a number of sources. Field 2, Oligocene



B

plutonic suite in Prince William Sound. Field 3, Oligocene to early Miocene plutonic suite in southeastern Alaska. Field 4, K/Ar whole-rock ages of dubious quality, probably subject to partial argon loss rather than a separate intrusive event. Field 5, Anomalously old hornblende ages from eastern Chugach and St. Elias Mountains, at least partly resulting from inherited argon.

km from the end of the belt, is a K/Ar muscovite age of  $65.6 \pm 3.3$  Ma (Burk, 1965). Lacking better data, we have picked an age in the range 66–63 Ma for the onset of magmatism at the western end of the belt.

We attribute two of the other fields in figure 2B to younger magmatic events. Field 2 corresponds to a suite of Oligocene plutons in Prince William Sound. In contrast to the Paleocene to Eocene tonalite to granite plutons of the Sanak–Baranof belt, the Oligocene plutons of Prince William Sound typically are composite bodies of gabbro and granite (Nelson and others, 1985; Tysdal and Case, 1979). A new, unpublished  $^{40}\text{Ar}/^{39}\text{Ar}$  biotite age of  $36.1 \pm 0.1$  Ma from the Esther pluton (L. Snee, written commun., 1993) suggests that the Oligocene conventional K/Ar ages from Prince William Sound are probably only a few million years younger than the age of intrusion. Field 3 includes K/Ar ages from seven plutons in southeastern Alaska. These plutons (for example, the Gut Bay stock and Alsek River pluton) have yielded Oligocene to early Miocene ages only; they record a magmatic event that is significantly younger than the Sanak–Baranof belt. Some other plutons in southeastern Alaska (for example, the Baranof Lake pluton) have yielded ages ranging from Eocene to Oligocene and even Miocene; we attribute these younger ages to cooling and (or) resetting rather than intrusion.

We attribute the remaining two fields in figure 2B to partial argon loss in one case and to inherited argon in the other. Field 4 in figure 2B includes two conventional K/Ar whole-rock ages of dubious quality. The ages are from dikes for which mineral ages were not obtained. Because none of the more reliable methods have yielded comparable ages in this region, the whole-rock ages probably record partial argon loss rather than a separate intrusive event. Field 5 is a group of amphibole ages from plutons in the eastern Chugach Mountains that fall above field 1. In a detailed case study, Onstott and others (1989) showed that amphiboles from two of these plutons had been contaminated by inherited argon. Actinolite/cummingtonite from the Bremner Glacier pluton yielded a conventional K/Ar age of  $64.1 \pm 7.0$  Ma (George Plafker, cited in Onstott and others, 1989), in close agreement with a  $^{40}\text{Ar}/^{39}\text{Ar}$  integrated (total gas) age of  $66.4 \pm 4.3$  Ma, but far older than a corresponding  $^{40}\text{Ar}/^{39}\text{Ar}$  plateau age of  $54.0 \pm 1.1$  Ma. A slightly more reliable age of  $51.2 \pm 4.3$  Ma (table 1) was determined from the intercept on a plot of  $^{36}\text{Ar}/^{40}\text{Ar}$  versus  $^{39}\text{Ar}/^{40}\text{Ar}$ ; this correction uses the calculated initial argon isotopic composition rather than an assumed atmospheric composition (Onstott and others, 1989). In general, the K/Ar data show a great deal of scatter. In more than a third of the samples in table 1 from which two or more minerals have been dated by the conventional K/Ar method, the expected age progression hornblende > muscovite > biotite (a function of progressively lower blocking temperatures; McDougall and Harrison, 1988) does not apply.

## DISCUSSION

### GEOLOGIC EFFECTS OF RIDGE SUBDUCTION

The term “ridge subduction” describes the subduction of a divergent plate boundary beneath a convergent plate boundary at a trench-ridge-trench or trench-ridge-transform triple junction. The term is restricted to subduction of an oceanic spreading center, regardless of the presence or absence of a morphologic ridge, and is not to be confused with “aseismic ridge subduction,” which applies to the subduction of seamounts. As discussed by Dickinson and Snyder (1979) and Thorkelson and Taylor (1989), a spreading center ceases to exist upon subduction. In its place, an ever-widening “slab window” opens down-dip of the triple junction. This window is an anomalously hot interface between the base of the overriding plate and asthenosphere that upwells from beneath the two subducted, but still diverging plates. Present understanding of the geologic effects of ridge subduction is derived from theoretical studies (Delong and Fox, 1977) as well as modern and ancient examples. There are two modern examples of “pure” ridge subduction (where the triple junction is of the trench-ridge-trench type): in the Chile trench (Forsythe and Nelson, 1985; Forsythe and others, 1986; Cande and Leslie, 1986; Scientific Party, 1992) and in the Solomon trench (Taylor and Exon, 1987; Perfit and others, 1987; Johnson and others, 1987). In addition, there are three examples of active “partial” ridge subduction along the west coast of North America, where the triple junctions are of the trench-ridge-transform type. Other Neogene ridge-subduction events have been identified in the Antarctic Peninsula (Barker, 1982) and in the Philippine Sea (Hibbard and Karig, 1990). The most striking geologic effect of ridge subduction is near-trench magmatism in a setting where low heat flow is the rule (Marshak and Karig, 1977).

### INTERPRETATION OF SANAK–BARANOF MAGMATISM AS THE PRODUCT OF RIDGE SUBDUCTION

Although a number of possible explanations have been advanced, most present workers believe that Sanak–Baranof magmatism was the product of ridge subduction (Marshak and Karig, 1977; Hill and others, 1981; Helwig and Emmet, 1981; Moore and others, 1983; Plafker and others, 1989; Sisson and others, 1989; Bradley and Kusky, 1992; Barker and others, 1992; Bol and others, 1992; Winkler, 1992). Five independent lines of evidence that support this interpretation are summarized below.

(1) *Near-trench position of plutons.*—Plutons of the Sanak–Baranof belt intruded recently deformed deep-sea turbidites (Shumagin, Kodiak, and Ghost Rocks Formations, Valdez Group, inboard part of the Orca Group, and

Sitka Graywacke) in an accretionary prism (Marshak and Karig, 1977). During the same time interval, a more landward belt of plutons was also emplaced along what has been interpreted as an Andean-type magmatic arc (Armstrong, 1988; Plafker and others, in press). Sanak-Baranof plutonism in southeastern Alaska was coeval with a major magmatic pulse in the Coast Plutonic Complex (of Douglas and others, 1970), a huge coast-parallel batholith 100–150 km to the east (Brew and Morrell, 1983; Armstrong, 1988). Similarly, from Prince William Sound to Kodiak Island, Sanak-Baranof magmatism was at least partly coeval with magmatism along the 74- to 55-Ma Alaska-Aleutian Range batholith (Reed and Lanphere, 1973; Wallace and Engebretson, 1984), which parallels the Sanak-Baranof belt but lies 200–300 km inboard of it.

(2) *Geochemistry of near-trench plutonic rocks.*—Petrogenetic modeling of Paleocene granitoids on Kodiak Island suggests interaction between a parent magma similar to mid-ocean ridge basalt (MORB-like) and anatectically melted flysch at the base of the accretionary prism (Hill and others, 1981). Barker and others (1992) invoked heat from a subducted spreading center to melt the base of accretionary prism as an explanation for the geochemistry and isotopic composition of Eocene granitoids in eastern Prince William Sound.

(3) *Obducted ophiolites in the accretionary prism.*—In the Resurrection Peninsula ophiolite (57 Ma) (Nelson and others, 1989), pillow lavas at the top of an ophiolite sequence are interbedded with flysch, suggesting proximity of a spreading center to a sediment source along the continental margin (Bol and others, 1992). The agreement between the ages of ophiolite genesis and near-trench magmatism in nearby, previously accreted rocks of the Valdez Group suggests that while the ophiolite was being generated, a slab window (the subducted part of the spreading center) heated the base of the adjacent accretionary prism. Interbedded mafic volcanic rocks and turbidites in the Ghost Rocks Formation have also been interpreted as having formed at a ridge-trench-trench triple junction (Moore and others, 1983). These volcanic rocks have geochemical signatures that suggest mixing between a MORB-like magma and melted flysch (Moore and others, 1983).

(4) *High-grade metamorphism in parts of the accretionary prism.*—Although accretionary prisms are typically subject to relatively low temperature-high pressure metamorphism, parts of the Chugach-Prince William terrane experienced the opposite—high temperature-low pressure metamorphism (Hudson and Plafker, 1982). In the eastern Chugach Mountains, peak metamorphism, at about 675°C and about 3 kilobars, occurred at 58–56 Ma and was followed by rapid cooling to about 350°C by 50 Ma (Sisson and others, 1989). On Baranof Island, conditions of 790°C at 4.4 kilobars (garnet-cordierite zone) were reached during the Eocene in a broad tract of regional contact metamorphism (Loney and Brew, 1987).

(5) *Age progression of near-trench magmatism.*—Ridge subduction is the one mechanism for near-trench magmatism that is compatible with the age progression documented in figure 2B. Any effects of ridge subduction should generally be diachronous along the strike of a subduction zone, except in the two special cases where the subducted ridge is either exactly parallel or exactly perpendicular to the subduction zone (McKenzie and Morgan, 1969). Conversely, the age progression is inconsistent with other models for Sanak-Baranof belt magmatism. Hudson and others (1979) invoked spontaneous anatectic melting of recently accreted sediments; this, however, would require the diachronous accretion of a thick wedge of flysch along the whole 2,200-km-long belt shortly before magmatism commenced, for which there is no evidence. Even ignoring geochemical evidence against an arc environment (for example, Barker and others, 1992), the suggestion by Kienle and Turner (1976) that the western segment of the belt is a magmatic arc fails to account for the migration of a short-lived magmatic pulse 2,200 km along the continental margin. Another possible cause of near-trench magmatism is overriding a seafloor hot spot. In general, however, this would cause magmatism in only one place in the accretionary prism, not along its entire length. Only in the unlikely case where the trend of the subduction zone was parallel to the relative motion of the overriding plate in a hot-spot reference frame would near-trench magmatism be diachronous along strike. Finally, localized transtension along a transform margin might also explain a magmatic pulse close to a former trench, but this model cannot account for the observed age progression.

## IMPLICATIONS FOR PLATE RECONSTRUCTIONS

The west-to-east age progression of near-trench magmatism suggests the migration of a triple junction (Helwig and Emmet, 1981; Moore and others, 1983) about 2,200 km along strike in about 13–16 m.y., at an average rate of about 140–170 km/m.y. It seems more likely that the triple junction was of the trench-ridge-trench type than a trench-ridge-transform type (McKenzie and Morgan, 1969), because accretion of the Valdez Group, Kodiak Formation, and Shumagin Formation immediately preceded near-trench magmatism, and accretion of the Sitkalidak Formation and outer part of the Orca Group immediately followed near-trench magmatism. Both accretionary episodes have been attributed to subduction, rather than to transform tectonics (Plafker and others, 1989; Moore and Allwardt, 1980).

Although most of the proponents of ridge subduction cited above have linked Sanak-Baranof magmatism to the Kula-Farallon ridge, the identity of the subducted ridge is debatable. As the triple junction migrated past a given point on the overriding accretionary prism, subduction of a

more easterly oceanic plate must have been succeeded by subduction of a more westerly oceanic plate (fig. 3). This statement is deliberately vague because it is unclear whether the Kula–Farallon ridge or a “West Kula–East Kula” ridge was subducted. The one ridge that *can* be eliminated is the Kula–Pacific (compare DeLong and others, 1978), because recently discovered magnetic anomalies indicate that it ceased to spread at about 40–41 Ma, when it was thousands of kilometers offshore in the Pacific, far from the North American or Alaskan margin where it could have been subducted (Lonsdale, 1988; Lonsdale’s age picks have been modified according to the new magnetic time scale of Cande and Kent, 1992). Simple plate circuitry among the North American, Pacific, Kula, and Farallon plates cannot further resolve the identity of the subducted ridge that we believe caused Sanak–Baranof magmatism, because so much ocean floor has been subducted since the early Tertiary (Atwater, 1989). Various reconstructions do agree, however, on the approxi-

mate offshore position of the Kula–Farallon–Pacific ridge–ridge triple junction at about 56 Ma (Engebretson and others, 1985; Stock and Molnar, 1988; Lonsdale, 1988; Atwater, 1989; Bol and others, 1992). These workers have inferred that the Kula–Farallon ridge trended from this triple junction toward the present coastal position of Vancouver Island. However, it might have been offset to the north or south by transforms (Bol and others, 1992)(fig. 3). Another possibility is that the Kula–Farallon ridge split into another ridge separating what could be called the “West Kula” and “East Kula” plates. Unfortunately, two postulated but poorly resolved onshore events complicate interpretations even further: (1) northward displacement of the Chugach–Prince William terrane by  $13 \pm 9^\circ$ , during the interval from about 57 to about 45 Ma (Coe and others, 1985; Bol and others, 1992) and (2) formation of the southern Alaska orocline by  $44 \pm 11^\circ$  counterclockwise rotation of southwestern Alaska some time between about 65 and about 35 Ma (Coe and others, 1989). If both events have been correctly interpreted from the paleomagnetic record, all of the Sanak–Baranof belt was displaced northward relative to stable North America, and the part west of Prince William Sound was oroclinally rotated, possibly during emplacement of the Sanak–Baranof plutons.

Although a general west-to-east age progression is evident from figure 2, the available data do not allow resolution of a number of tectonically important details. The data do not even allow identification of the major plate

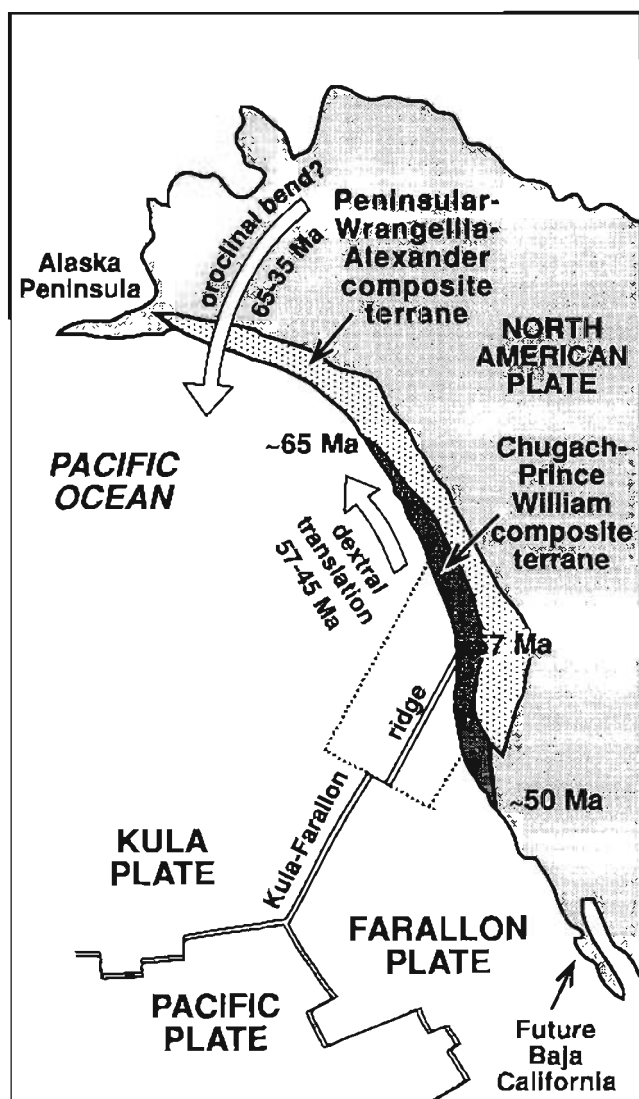


**Figure 3.** Early Tertiary plate reconstruction of northern Pacific, adapted from Bol and others (1992) and Engebretson and others (1985). Oroclinal bend has been straightened and Chugach–Prince William terrane has been restored to a more southerly position, following Bol and others (1992). Solid ridge–transform system shows inferred Kula–Farallon ridge configuration and position of triple junction at 57 Ma based on paleomagnetism (Bol and others, 1992). Relative positions of Kula–Farallon–North American triple junction at about 65 and about 50 Ma, based on the present study, are shown by numbers at either end of the Chugach–Prince William composite terrane in its restored position. Dashed ridge–transform systems are only two of an infinite number of possible alternative left-stepping and right-stepping ridge geometries. Two alternatives shown would suggest more northerly or more southerly positions of Kula–Farallon–North American triple junction, respectively. Small transform offset could have caused major shift in position of triple junction. Formation of orocline may not have spanned entire 65- to 35-Ma age range permitted by paleomagnetic data. Complete lack of data on seafloor-spreading history of northern part of area shown as Kula plate allows for possibility that Kula plate was, in fact, two plates—“East Kula” and “West Kula”—separated by yet another spreading ridge that has been entirely subducted.

reorganizations at about 54–52 Ma or 41–40 Ma seen in magnetic anomalies from the Pacific plate (these are the 56- and 42-Ma events of Engebretson and others, 1985, recalibrated to the new magnetic anomaly time scale of Cande and Kent, 1992). If Sanak–Baranof magmatism occurred at a migrating trench-ridge-trench triple junction, the presence of left-stepping or right-stepping transforms along the subducting ridge would be expected to affect the position of the triple junction through time, in a manner not unlike that described by Atwater (1989) for the Pacific–Farallon–North American triple junction in California. Depending on the relative ages and (or) magnitudes of oroclinal bending, northward strike-slip of the Chugach terrane, and ridge subduction, interaction between these events could yield a multitude of possible age patterns on a plot like figure 2. Indeed, with 10–20 new, high-precision U/Pb and  $^{40}\text{Ar}/^{39}\text{Ar}$  determinations from the Sanak–Baranof belt, such a plot might place some new, quantitative constraints on the early Tertiary tectonic evolution. The available data, however, only support qualitative conclusions. The claim by Hudson and others (1979) and some later workers that the Sanak–Baranof belt is divided by age into a westerly ~60-Ma half and an easterly ~50-Ma half definitely is not substantiated by figure 2. At most, figure 2 could be interpreted to show that magmatism was virtually coeval from Sanak to Kodiak Island, and progressively younger from there eastward (F. Wilson, written commun., 1993).

At least in southeastern Alaska, marine-based plate reconstructions imply that a transform margin existed after about 41–40 Ma (revised from 42 Ma using the new time scale of Cande and Kent, 1992) (Hyndman and Hamilton, 1990). Oligocene to Miocene plutonism in southeastern Alaska (field 3 in fig. 2B) is presumably somehow related to transform-margin tectonics along a Pacific–North American plate boundary. The cause of Oligocene plutonism in Prince William Sound (field 2 in fig. 2B) has not been investigated.

### SHALLOW-LEVEL EFFECTS OF RIDGE SUBDUCTION IN THE ACCRETIONARY PRISM

Several recent models have treated accretionary prisms as wedges of material with an equilibrium “critical taper,” much like a wedge of snow built up in front of a snowplow (for example, Davis and others, 1983; Platt, 1986). Subduction of a ridge at a migrating triple junction might be expected to have several disruptive effects on a critically tapered wedge. First, migration of a trench-ridge-trench triple junction past a given point would be accompanied by subduction of progressively more bouyant, topographically higher lithosphere, then less bouyant, topographically lower lithosphere. In addition, intrusion of large magma bodies into the prism would severely perturb

the stress field, because fluids cannot transmit shear stress. Finally, a change in rate and convergence direction would have to occur as the triple junction moved past a given place. Thus, passage of a triple junction would change the sense of obliquity of subduction, which in turn would change the sense and (or) rate of displacement of motion along trench-parallel faults in the forearc (Dewey, 1980).

Recent findings suggest that near-trench magmatism was coeval with regional-scale brittle deformation of the accretionary prism in the western part of the Sanak–Baranof belt (fig. 4), much as it was coeval with ductile deformation and metamorphism at deeper levels in the eastern Chugach Mountains (Sisson and others, 1989). In the southern Kenai Peninsula, dike trends indicate north-south extension, at about 45° to regional strike; one such dike yielded a  $^{40}\text{Ar}/^{39}\text{Ar}$  hornblende age of 57 Ma (Bradley and Kusky, 1992). Mutual cross-cutting relations reveal that these dikes are coeval with a set of conjugate strike-slip cross-faults that caused orogen-parallel extension (Bradley and Kusky, 1992). Kinematic analysis of correlative faults from the northern Kenai Peninsula also indicates orogen-parallel extension (Bradley and Kusky, 1990); curved slickenlines on these faults indicate that stress orientations changed markedly during faulting, probably as a consequence of uplift. The occurrence of similar fault sets on Afognak and Kodiak Islands (Sample and Moore, 1987; Byrne, 1984) suggests that at least the western limb of the orocline underwent extension subparallel to structural grain. Hibbard and Karig (1990) described remarkably similar late faults and dikes in Japan where a spreading center was subducted during the Miocene.

Epigenetic gold-bearing quartz veins are widespread throughout the Chugach terrane, from Kodiak to Baranof Island. Isotopic ages from three sites in the Kenai Peninsula indicate that gold mineralization was coeval with magmatism in this part of the Sanak–Baranof belt. Like the magmatism, the gold mineralization must have occurred in a near-trench setting (fig. 4). Sericite from a gold-quartz vein from the Beauty Bay Mine yielded a  $^{40}\text{Ar}/^{39}\text{Ar}$  age of  $55.6 \pm 0.17$  Ma (Borden and others, 1992). Two conventional K/Ar ages from hydrothermally altered, mineralized dikes farther north on the Kenai Peninsula have yielded similar results ( $53.2 \pm 1.6$  Ma and  $52.7 \pm 1.6$  Ma; Silberman and others, 1981). Accordingly, we suggest that the ore-forming fluids were generated and mobilized during subduction of a spreading center.

Shallow structures formed during subduction of a spreading ridge beneath the Chugach–Prince William accretionary prism are shown schematically in figure 4. At depth, partial melting of accreted sediments above a slab window led to intrusion of granitoids and high-grade metamorphism (as exposed in the eastern Chugach Mountains). At shallower levels, dike injection and movement on conjugate strike-slip faults together resulted in orogen-parallel

extension; some of these structures host lode gold. Owing to migration of the triple junction, the accretionary prism experienced a rapid succession of three very different tectonic regimes—before, during, and after ridge subduction.

**Acknowledgments.**—We thank the following people for providing unpublished ages: Dave Brew, Bill Clendenin, Randy Parrish, Sarah Roeske, Larry Snee, and Ric Wilson. Nora Shew provided a digital data base of Alaskan geochronology.

## REFERENCES

- Armstrong, R.L., 1988, Mesozoic and early Cenozoic magmatic evolution of the Canadian Cordillera: Geological Society of America Special Paper 218, p. 91.
- Atwater, Tanya, 1989, Plate tectonic history of the northeast Pacific and western North America, in Winterer, E.L., Hussong, D.M., and Decker, R.W., editors, *The geology of North America: The Eastern Pacific Ocean and Hawaii*:

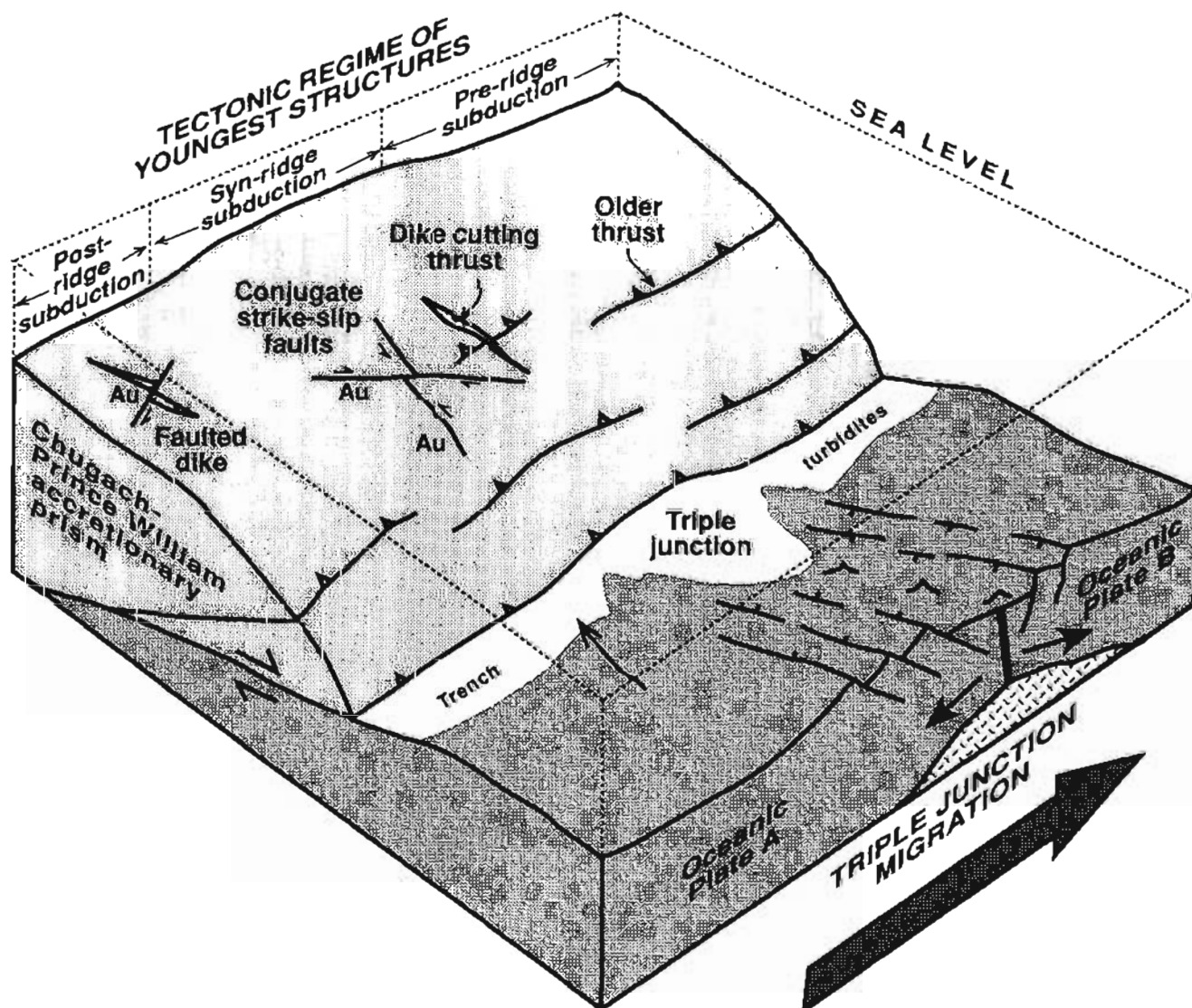


**Figure 4.** Schematic depiction of conditions during subduction of spreading ridge beneath Chugach-Prince William composite terrane. Oceanic plates A and B correspond, respectively, to Kula and Farallon plates, or to "West Kula" and "East Kula" plates. At depth within accretionary prism, partial melting of accreted rocks above a "slab window" leads to intrusion of granitoids. At shallower levels shown here, dike injection and movement on conjugate strike-slip faults together result in

orogen-parallel extension. Left-to-right migration of triple junction (inferred from age progression in fig. 2) subjects accretionary prism to succession of three very different tectonic regimes—before, during, and after ridge subduction. Structures that host lode gold (Au symbol) formed, at least in part, in ridge subduction environment. Adapted, in part, from unpublished figure by Steve Nelson.



- Geological Society of America DNAG Series, v. N, p. 21-72.
- Barker, F., Farmer, G.L., Ayuso, R.A., Plafker, George, and Lull, J.S., 1992, The 50 Ma granodiorite of the eastern Gulf of Alaska: Melting of the accretionary prism in the forearc: *Journal of Geophysical Research*, v. 97, p. 6757-6778.
- Barker, P., 1982, The Cenozoic subduction history of the Pacific margin of the Antarctic peninsula: ridge crest-trench interactions: *Journal of the Geological Society of London*, v. 139, p. 787-801.
- Beikman, H., 1980, Geologic map of Alaska: U.S. Geological Survey, scale 1:2,500,000.
- Bol, A.J., Coe, R.S., Grommé, C.S., and Hillhouse, J.W., 1992, Paleomagnetism of the Resurrection Peninsula, Alaska: Implications for the tectonics of southern Alaska and the Kula-Farallon Ridge: *Journal of Geophysical Research*, v. 97, p. 17,213-17,232.
- Borden, J.C., Goldfarb, R.J., Gent, C.A., Burruss, R.C., and Roushey, B.H., 1992, Geochemistry of lode-gold deposits, Nuka Bay district, southern Kenai Peninsula, in Bradley, D.C., and Dusel-Bacon, Cynthia, editors, *Geologic studies in Alaska by the U.S. Geological Survey, 1991: U.S. Geological Survey Bulletin 2041*, p. 13-22.
- Bradley, D.C., and Kusky, T.M., 1990, Kinematics of late faults along Turnagain Arm, Mesozoic accretionary complex, south-central Alaska, in Dover, J.H., and Galloway, J.P., editors, *Geologic studies in Alaska by the U.S. Geological Survey, 1989: U.S. Geological Survey Bulletin 1946*, p. 3-10.
- 1992, Deformation history of the McHugh Complex, Seldovia quadrangle, south-central Alaska, in Bradley, D.C., and Ford, A., editors, *Geologic studies in Alaska by the U.S. Geological Survey, 1990: U.S. Geological Survey Bulletin 1999*, p. 17-32.
- Brew, D.A., Hammarstrom, J.M., Himmelberg, G.R., Wooden, J.L., Loney, R.A., and Karl, S.M., 1991, Crawfish Inlet pluton, Baranof Island, southeastern Alaska—A north-tilted Eocene body or an untilted enigma?: *Geological Society of America Abstracts with Programs*, v. 23, no. 2, p. 8.
- Brew, D.A., and Morrell, R.P., 1983, Intrusive rocks and plutonic belts of southeastern Alaska, U.S.A.: *Geological Society of America Memoir 159*, p. 171-193.
- Burk, C.A., 1965, *Geology of the Alaska Peninsula—Island arc and continental margin*: Geological Society of America Memoir 99, parts 1-3, 250 p.
- Byrne, T., 1979, Late Paleocene demise of the Kula-Pacific ridge: *Geology*, v. 7, p. 341-344.
- 1984, Early deformation in mélange terranes of the Ghost Rocks Formation, Kodiak Islands, Alaska, in Raymond, L.A., ed., *Mélanges: Their nature, origin, and significance*: Geological Society of America Special Paper 198, p. 21-51.
- Cande, S.C., and Kent, D.V., 1992, A new geomagnetic polarity time scale for the Late Cretaceous and Cenozoic: *Journal of Geophysical Research*, v. 97, p. 13,917-13,951.
- Cande, S.C., and Leslie, R., 1986, Late Cenozoic tectonics of the southern Chile trench: *Journal of Geophysical Research*, v. 91, p. 471-496.
- Clark, S.H.B., Yount, M.E., and Bartsch, S.R., 1976, Reconnaissance geologic map and geochemical analyses of the Anchorage A-7 and A-8 quadrangles, Alaska: U.S. Geological Survey Miscellaneous Field Studies Map MF-765, 3 sheets, scale 1:63,360.
- Clendenin, W.S., 1991, Thermal history and vertical tectonics of the southern Alaska convergent margin: Ph.D. dissertation, Brown University, Providence, Rhode Island, 177 p.
- Coe, R.S., Globberman, B.R., Plumley, P.R., and Thrupp, G.A., 1985, Paleomagnetic results from Alaska and their tectonic implications, in Howell, D.G., editor, *Tectonostratigraphic terranes of the Circum-Pacific region*: Houston, Circum-Pacific Council for Energy and Mineral Resources, p. 85-108.
- 1989, Rotation of central and southern Alaska in the Early Tertiary: Oroclinal bending by megakinking?, in Kissel, C., and Laj, C., editors, *Paleomagnetic rotations and continental deformation*: Boston, Kluwer Academic Publishers, NATO-ASI series, p. 327-339.
- Connelly, W., 1978, Uyak Complex, Kodiak Islands, Alaska: A Cretaceous subduction complex: *Geological Society of America Bulletin*, v. 89, p. 755-769.
- Davis, D., Suppe, J., and Dahlen, F.A., 1983, Mechanics of fold-and-thrust belts and accretionary wedges: *Journal of Geophysical Research*, v. 88, p. 1153-1172.
- Decker, J.E., Jr., 1980, *Geology of a Cretaceous subduction complex, western Chichagof Island, southeastern Alaska*: Ph.D. dissertation, Stanford University, Stanford, California, 135 p.
- De Long, S., and Fox, P.J., 1977, Geological consequences of ridge subduction, in Talwani, M., and Pitman, W.C., editors, *Island arcs, deep sea trenches, and back-arc basins*: American Geophysical Union, Maurice Ewing Series 1, p. 221-228.
- De Long, S., Fox, P.J., and McDowell, F., 1978, Subduction of the Kula Ridge at the Aleutian trench: *Geological Society of America Bulletin*, v. 89, p. 83-95.
- Dewey, J.F., 1980, Episodicity, sequence, and style in convergent plate boundaries: *Geological Association of Canada Special Publication*, v. 20, p. 553-576.
- Dickinson, W.R., and Snyder, W.S., 1979, Geometry of triple junctions related to San Andreas transform: *Journal of Geophysical Research*, v. 84, 561-572.
- Dodds, C.J., and Campbell, R.B., 1988, Potassium-argon ages of mainly intrusive rocks in the Saint Elias Mountains, Yukon and British Columbia: *Geological Survey of Canada Paper 87-16*, 43 p.
- Douglas, R.J.W., Gabrielse, H., Wheeler, J.O., Stott, D.F., and Belyea, H.R., 1970, *Geology of western Canada*, in Douglas, R.J.W., editor, *Geology and economic minerals of Canada*: Geological Survey of Canada Economic Geology Report 1, p. 365-488.
- Engebretson, D.C., Cox, Allan, and Gordon, R.G., 1985, Relative motions between oceanic and continental plates in the Pacific Basin: *Geological Society of America Special Paper 206*, 59 p.
- Forsythe, R.D., and Nelson, E.P., 1985, Geological manifestations of ridge collision: evidence from the Golfo de Penas-Taitao basin, southern Chile: *Tectonics*, v. 4, p. 477-495.
- Forsythe, R.D., Nelson, E.P., Carr, M.J., Kaeding, M.E., Herve, M., Mpodozis, C., Soffia, J.M., and Harambour, S., 1986, Pliocene near-trench magnetism in southern Chile: A possible manifesta-



- tation of ridge collision: *Geology*, v. 14, 23–27.
- Helwig, J., and Emmet, P., 1981, Structure of the Early Tertiary Orca Group in Prince William Sound and some implications for the plate tectonic history of southern Alaska: *Journal of the Alaska Geological Society*, v. 1, p. 12–35.
- Hibbard, J.P., and Karig, D.E., 1990, Structural and magmatic responses to spreading ridge subduction: an example from southwest Japan: *Tectonics*, v. 9, p. 207–230.
- Hill, M., Morris, J., and Whelan, J., 1981, Hybrid granodiorites intruding the accretionary prism, Kodiak, Shumagin, and Sanak Islands, southwest Alaska: *Journal of Geophysical Research*, v. 86, p. 10569–10590.
- Himmelberg, G.R., Loney, R.A., and Nabelek, P.I., 1987, Petrogenesis of gabbro-norite at Yakobi and northwest Chichagof Islands, Alaska: *Geological Society of America Bulletin*, v. 98, p. 265–279.
- Hudson, Travis, 1983, Calc-alkaline plutonism along the Pacific rim of southern Alaska: *Geological Society of America, Memoir* 159, p. 159–169.
- Hudson, Travis, and Plafker, George, 1981, Emplacement age of the Crillon-LaPerouse pluton, Fairweather Range: U.S. Geological Survey Circular 823-B, p. B90–B94.
- , 1982, Paleogene metamorphism in an accretionary flysch terrane, eastern Gulf of Alaska: *Geological Society of America Bulletin*, v. 93, p. 1280–1290.
- Hudson, Travis, and Plafker, George, and Lanphere, M.A., 1977, Intrusive rocks of the Yakutat–St. Elias area, south-central Alaska: *Journal of Research of the U.S. Geological Survey*, v. 5, p. 155–172.
- Hudson, Travis, and Plafker, George, and Peterman, Z.E., 1979, Paleogene anatexis along the Gulf of Alaska margin: *Geology*, v. 7, p. 573–577.
- Hyndman, R.D., and Hamilton, T.S., 1990, Cenozoic relative plate motions along the northeastern Pacific margin and their association with Queen Charlotte area tectonics and volcanism: *Geological Survey of Canada Paper* 90–10, p. 107–126.
- Johnson, R.A., Jacques, A., Langmuir, C., Perfit, M., Staudigel, H., Dunkley, B., Chappell, B., Taylor, S., and Baekisapa, M., 1987, Ridge subduction and forearc volcanism: Petrology and geochemistry of rocks dredged from the western Solomon arc and Woodlark Basin, in Taylor, B., and Exon, N., editors, *Marine geology, geophysics, and geochemistry of the Woodlark Basin–Solomon Islands*: Houston, Circum-Pacific Council for Energy and Mineral Resources, Earth Science Series, v. 7, p. 155–226.
- Karl, S.M., Johnson, B.R., and Lanphere, M.A., 1988, New K–Ar ages for plutons on western Chichagof Island and on Yakobi Island: U.S. Geological Survey Circular 1016, p. 164–168.
- Kienle, Jürgen, and Turner, D.L., 1976, The Shumagin–Kodiak batholith — a Paleocene magmatic arc?, in *Short notes on Alaskan geology — 1976*: Alaska Division of Geological and Geophysical Surveys *Geologic Report* 51, p. 9–11.
- Lanphere, M.A., 1966, Potassium-argon ages of Tertiary plutons in the Prince William Sound region, Alaska, in *Geological Survey research 1966*: U.S. Geological Survey Professional Paper 550–D, p. D195–D198.
- Little, T.A., and Naeser, C.W., 1989, Tertiary tectonics of the border Ranges fault system, Chugach Mountains, Alaska: deformation and uplift in a forearc setting: *Journal of Geophysical Research*, v. 94, p. 4333–4359.
- Loney, R.A., and Brew, D.A., 1987, Regional thermal metamorphism and deformation of the Sitka Graywacke, southern Baranof island, southeastern Alaska: U.S. Geological Survey Bulletin 1779, 17 p.
- Loney, R.A., Brew, D.A., and Lanphere, M.A., 1967, Post-Paleozoic radiometric ages and their relevance to fault movements, northern southeastern Alaska: *Geological Society of America Bulletin*, v. 78, p. 511–526.
- Loney, R.A., Brew, D.A., Muffler, L.J.P., and Pomeroy, J.S., 1975, Reconnaissance geology of Chichagof, Baranof, and Kruzof Islands, southeastern Alaska: U.S. Geological Survey Professional Paper 792, 105 p.
- Loney, R.A., and Himmelberg, G.R., 1983, Structure and petrology of the La Perouse gabbro intrusion, Fairweather Range, southeastern Alaska: *Journal of Petrology*, v. 24, p. 377–423.
- Lonsdale, Peter, 1988, Paleogene history of the Kula plate: Off-shore evidence and onshore implications: *Geological Society of America Bulletin*, v. 99, p. 733–754.
- Marshak, R.S., and Karig, D.E., 1977, Triple junctions as a cause for anomalously near-trench igneous activity between the trench and volcanic arc: *Geology*, v. 5, p. 233–236.
- Marvin, R.F., and Dobson, S.W., 1979, Radiometric ages: Compilation B, U.S. Geological Survey: *Isochron/West*, no. 26.
- McDougall, Ian, and Harrison, T.M., 1988, *Geochronology and thermochronology by the  $^{40}\text{Ar}/^{39}\text{Ar}$  method*: Oxford Monographs on Geology and Geophysics no. 9, New York, Oxford University Press, 212 p.
- McKenzie, D.P., and Morgan, W.J., 1969, Evolution of triple junctions: *Nature*, v. 224, p. 125–133.
- Moore, J.C., 1973, Cretaceous continental margin sedimentation, southwestern Alaska: *Geological Society of America Bulletin*, v. 84, p. 595–614.
- , 1974a, Geologic and structural map of the Sanak Islands, southwestern Alaska: U.S. Geological Survey Miscellaneous Investigations Map I–817, scale 1:63,360.
- , 1974b, Geologic and structural map of part of the Outer Shumagin Islands, southwestern Alaska: U.S. Geological Survey Miscellaneous Investigations Series Map I–815, scale 1:63,360.
- Moore, J.C., and Allwardt, A., 1980, Progressive deformation of a Tertiary trench slope, Kodiak islands, Alaska: *Journal of Geophysical Research*, v. 85, p. 4741–4756.
- Moore, J.C., Byrne, T., Plumley, P.W., Reid, M., Gibbons, H., and Coe, R.S., 1983, Paleogene evolution of the Kodiak Islands, Alaska: consequences of ridge-trench interaction in a more southerly latitude: *Tectonics*, v. 2, p. 265–293.
- Nelson, S.W., Dumoulin, J.A., and Miller, M.L., 1985, Geologic map of the Chugach National Forest, Alaska: U.S. Geological Survey Miscellaneous Field Studies Map MF–1645–B, 14 p., 1 sheet, scale 1:250,000.
- Nelson, S.W., Miller, M.L., and Dumoulin, J.A., 1989, Resurrection Peninsula ophiolite, in Nelson, S.W., and Hamilton, T.W., editors, *Guide to the geology of Resurrection Bay, eastern Kenai Fiords area, Alaska*: Anchorage, Geological Society of Alaska, p. 10–20.
- Nilsen, T.H., and Moore, G.W., 1979, Reconnaissance study of Upper Cretaceous to Miocene stratigraphic units and sedimentary facies, Kodiak and adjacent islands, Alaska: U.S.

- Geological Survey Professional Paper 1093, 34 p.
- Nilsen, T.H., and Zuffa, G.G., 1982, The Chugach terrane, a Cretaceous trench-fill deposit, southern Alaska: *Special Publications of the Geological Society of London*, v. 10, p. 213-227.
- Onstott, T.C., Sisson, V.B., and Turner, D.L., 1989, Initial argon in amphiboles from the Chugach Mountains, southern Alaska: *Journal of Geophysical Research*, v. 94, p. 4361-4372.
- Perfit, M., Langmuir, C., Baekisapa, M., Chappell, B., Johnson, R., Staudigel, H., and Taylor, S., 1987, Geochemistry and petrology of volcanic rocks from the Woodlark basin: Addressing questions of ridge subduction, in Taylor, B., and Exon, N., editors, *Marine geology, geophysics, and geochemistry of the Woodlark Basin-Solomon Islands*: Houston, Circum-Pacific Council for Energy and Mineral Resources, *Earth Science Series*, v. 7, p. 113-154.
- Plafker, George, 1987, Regional geology and petroleum potential of the northern Gulf of Alaska continental margin, in Scholl, D.W., Grantz, Arthur, and Vedder, J.G., editors, *Geology and resource potential of the continental margin of western North America and adjacent ocean basins*: Houston, Circum-Pacific Council for Energy and Mineral Resources, *Earth Science Series* v. 6, p. 229-268.
- Plafker, George, Moore, J.C., Winkler, G.R., and Decker, J.E., in press, Geology of the southern Alaska margin, in *The geology of North America*: Geological Society of America DNAG Series, v. G-1.
- Plafker, George, Nokleberg, W.J., and Lull, J.S., 1989, Bedrock geology and tectonic evolution of the Wrangellia, Peninsular, and Chugach terranes along the Trans-Alaska Crustal Transect in the Chugach Mountains and southern Copper River basin: *Journal of Geophysical Research*, v. 94, p. 4255-4295.
- Platt, J.P., 1986, Dynamics of orogenic wedges and the uplift of high-pressure metamorphic rocks: *Geological Society of America Bulletin*, v. 97, p. 1037-1053.
- Reed, B.L., and Lanphere, M.A., 1973, Alaska-Aleutian Range batholith: geochronology, chemistry, and relation to circum-Pacific plutonism: *Geological Society of America Bulletin*, v. 84, p. 2583-2610.
- Reifenstahl, R.R., 1983, A geological and geophysical study of the Goddard hot springs area, Baranof Island, southeast Alaska: Fairbanks, University of Alaska, M.S. thesis, 113 p., 1 sheet, scale 1:250,000.
- Sample, J.C., and Moore, J.C., 1987, Structural style and kinematics of an underplated slate belt, Kodiak and adjacent islands, Alaska: *Geological Society of America Bulletin*, v. 99, p. 7-20.
- Scientific Party (ODP Leg 141), 1992, Geology and tectonics of the Chile triple junction: *Eos*, v. 73, no. 38, p. 404-405 and 410.
- Silberman, M.L., Mitchell, P.A., and O'Neil, J.R., 1981, Isotopic data bearing on the origin and age of the epithermal lode gold deposits in the Hope-Sunrise mining district, northern Kenai Peninsula, Alaska: U.S. Geological Survey Circular 823-B, p. B81-B84.
- Sisson, V.B., Hollister, L.S., and Onstott, T.C., 1989, Petrologic and age constraints on the origin of a low-pressure/high-temperature metamorphic complex, southern Alaska: *Journal of Geophysical Research*, v. 94, p. 4392-4410.
- Steiger, R.H., and Jäger, E., 1977, Subcommittee on geochronology: convention on the use of decay constants in geo- and cosmochronology: *Earth and Planetary Science Letters*, v. 36, p. 359-362.
- Stock, J., and Molnar, P., 1988, Uncertainties and implications of Late Cretaceous and Tertiary position of North America relative to the Farallon, Pacific, and Kula plates: *Tectonics*, v. 7, p. 1339-1384.
- Taylor, B., and Exon, N.F., 1987, An investigation of ridge subduction in the Woodlark-Solomons region: introduction and overview, in Taylor, B., and Exon, N., editors, *Marine geology, geophysics, and geochemistry of the Woodlark Basin-Solomon Islands*: Houston, Circum-Pacific Council for Energy and Mineral Resources, *Earth Science Series*, v. 7, p. 1-24.
- Thorkelson, D.J., and Taylor, R.P., 1989, Cordilleran slab windows: *Geology*, v. 17, p. 833-836.
- Tysdal, R.G., and Case, J.E., 1979, Geologic map of the Seward and Blyling Sound quadrangles, Alaska: U.S. Geological Survey Miscellaneous Investigations Series I-1150, 12 p., 1 sheet, scale 1:250,000.
- Udike, R.G., and Utery, C.A., 1988, Bedrock geology of the Anchorage (B7SE) quadrangle, Alaska: U.S. Geological Survey Open-File Report 88-418, 1 sheet, scale 1:25,000.
- Wallace, W.K., and Engebretson, D.C., 1984, Relationships between plate motions and Late Cretaceous to Paleogene magmatism in southwestern Alaska: *Tectonics*, v. 3, p. 295-315.
- Wilson, F.H., Shew, N., and DuBois, G.D., 1991, Map and tables showing isotopic age data, in *The geology of North America*: Geological Society of America DNAG Series, v. G-1, scale 1:2,500,000.
- Winkler, G.R., 1992, Geologic map and summary geochronology of the Anchorage 1° x 3° quadrangle, southern Alaska: U.S. Geological Survey Miscellaneous Investigations Series Map I-2283, 1 sheet, scale 1:250,000.
- Winkler, G.R., and Plafker, George, 1981, Geologic map and cross-sections of the Cordova and Middleton Island quadrangles, southern Alaska: U.S. Geological Survey Open-File Report 81-1164, 25 p., 1 sheet, scale 1:250,000.
- Winkler, G.R., Silberman, M.L., Grantz, A., Miller, R.L., and MacKevett, E.M., Jr., 1981, Geologic map and summary geochronology of the Valdez quadrangle, southern Alaska: U.S. Geological Survey Open-File Report 80-892-A, 2 sheets, scale 1:250,000.

Reviewers: Donald H. Richter and Alison B. Till

**Table 1.** Isotopic ages of intrusive rocks from the Sanak-Baranof belt, southern Alaska

[Abbreviations for 1:250,000-scale quadrangles: Afog, Afognak; Anc, Anchorage; BG, Bering Glacier; Bly, Blying Sound; Cor, Cordova; FP, False Pass; Kag, Kaguyak; Kod, Kodiak; MF, Mt. Fairweather; MSE, Mt. St. Elias; PA, Port Alexander; PM, Port Moller; Sel, Seldovia; Sew, Seward; Sim, Simeonof Island; Sit, Sitka; Skag, Skagway; Step, Stepovak Bay; Sut, Sutwik Island; Trin, Trinity Islands; Val, Valdez; Yak, Yakutat. Distance along strike was measured from the southern tip of Sanak Island on Beikman's (1980) geologic map of Alaska. Notes: 1, Not plotted in figure 2B, because error >10%; 2, Not plotted in figure 2B, because strongly discordant with older determination(s) from same pluton; 3, Problematic age from a pluton with multiple determinations; 4, Suspect, but plotted in figure 2B; 5, Recalculated using new decay constant (most recalculated values are from Wilson and others, 1991); 6, Glacial erratic assumed to have been derived from the Kodiak batholith]

Igneous body	Quad	Field number or location	Latitude	Longitude	Age (Ma)	Error (m.y.)	Notes	Method	Distance from Sanak Island (km)	Reference
Sanak pluton	FP	S-70	54°29.2'	162°45.8'	61.4	1.8	5	K/Ar biotite	5	Moore, 1974a
Sanak pluton	FP	S70	54°29.2'	162°45.8'	62.7	1.2		Rb/Sr min. isochron	5	Hill and others, 1981
Sanak pluton	FP	75089	~54°29'	~162°45'	62	1.9	5	K/Ar biotite	7	Kienle & Turner, 1976
Sanak pluton	FP	S9A	54°29.8'	162°45.1'	63.1	1.2		Rb/Sr min. isochron	7	Hill and others, 1981
Sanak pluton	FP	many	54°28.5'	162°45.0'	49.5	5.6	1,2	Rb/Sr w.r. isochron	7	Hill and others, 1981
Shumagin pluton	Sim	N131	54°52.8'	160°11.7'	58.7	1.2		Rb/Sr min. isochron	180	Hill and others, 1981
Shumagin pluton	PM	N20	55°02.7'	160°05.3'	60.4	2.6		Rb/Sr min. isochron	195	Hill and others, 1981
Shumagin pluton	PM	405M	55°03.2'	160°02.5'	57.4	2.9	5	K/Ar muscovite	195	Burk, 1965
Shumagin pluton	PM	406M	55°06.8'	160°01.7'	65.6	3.3	5	K/Ar muscovite	200	Burk, 1965
Shumagin pluton	PM	406B	55°06.8'	160°01.7'	58.4	2.9	5	K/Ar biotite	200	Burk, 1965
Shumagin pluton	PM	75092	55°05'	160°00'	60.7	1.8	5	K/Ar biotite	200	Kienle & Turner, 1976
Shumagin pluton	Step	many	~55°8'	~159°45'	59.8	3		Rb/Sr w.r. isochron	215	Hill and others, 1981
Shumagin pluton	Step	75088	55°08.9'	159°32.0'	60.2	1.8	5	K/Ar biotite	230	Kienle & Turner, 1976
Shumagin pluton	Sim	62AGz7	54°55.0'	159°14.4'	59.9	3.0	5	K/Ar biotite	235	Moore, 1974b
Chowiet pluton	Sut	75086	56°02.7'	156°41.3'	59.3	1.8	5	K/Ar biotite	435	Kienle & Turner, 1976
Kempf Bay pluton	Trin	62AMe120	56°55'	154°13'	61.9	2.9		K/Ar muscovite	610	Marvin & Dobson, 1979
Kempf Bay pluton	Trin	62AMe120	56°55'	154°13'	60.8	3		K/Ar biotite	610	Marvin & Dobson, 1979
Aliulik pluton	Kag	A2	56°59'	153°44'	63	3		Rb/Sr min. isochron	640	Moore and others 1983
Aliulik pluton	Kag	A2	56°59'	153°44'	62.6	0.6		K/Ar biotite	640	Moore and others 1983
Aliulik pluton	Kag	A2	56°59'	153°44'	62.1	0.6		K/Ar biotite	640	Moore and others 1983
Kodiak batholith	Kod	62AKa10	57°26'	152°58'	59.5		6	K/Ar biotite	700	Moore and others 1983
Kodiak batholith	Kod	Terror Lake	~57°40'	~153°00'	58.3	0.3		40/39(?) biotite	715	W. Clendenin, written comm., 1992
Stock, Anton Larsen Bay	Kod	78AWs1	57°52'	152°40'	58.1	1		K/Ar biotite	750	Wilson and others, 1991
Stock, Anton Larsen Bay	Kod	78AWs1	57°52'	152°40'	57.1	1		K/Ar muscovite	750	Wilson and others, 1991
Dike, Malina Bay	Afog	M-19-88	58°12.6'	153°00.1'	59.3	2.2		40/39 hornblende	765	Clendenin, 1991
Dike, Seldovia Bay	Sel	88ADw230	59°23.6'	150°39.9'	57	0.22		40/39 hornblende	920	Clendenin, in Bradley & Kusky, 1992
Nuka pluton	Sel	88ACy9	59°28.4'	150°20.2'	54.2	0.08		40/39 biotite	970	Clendenin, in Bradley & Kusky, 1992
Nuka pluton	Sel	88ACy9	59°28.4'	150°20.2'	56	0.5		U/Pb monazite	970	Parrish, in Bradley & Kusky, 1992
Aialik pluton	Bly	loc. 5	59°42.4'	149°31.4'	59.2	1.8		K/Ar biotite	1015	Tysdal and Case, 1979
Aialik pluton	Bly	loc. 5	59°42.4'	149°31.4'	54.6	1.6		K/Ar muscovite	1015	Tysdal and Case, 1979
Dike, Oracle Mine	Sew	81BS116C	60°37'	149°34.5'	52.5	1.6		K/Ar whole rock	1100	Nelson and others, 1985
Dike, Kenai Star Mine	Sew	2203N	60°50.7'	149°30.6'	52.7	1.6		K/Ar whole rock	1125	Silberman and others, 1981
Nellie Juan pluton	Sew	PW-9	60°29.5'	148°23.0'	36.1	0.9	5	K/Ar biotite	1125	Lanphere, 1966
Dike, Bear Creek	Sew	2237B	~60°52.7'	~149°31.6'	53.2	1.6		K/Ar muscovite	1130	Silberman and others, 1981
Dike, Potter Marsh	Anc	70ACs423	61°04.0'	149°47.5'	34.8	2.0		K/Ar hornblende	1135	Clark and others, 1976
Eshamy pluton	Sew	PW-8	60°27.0'	148°06.5'	36.2	1.0	5	K/Ar biotite	1140	Lanphere, 1966
Eshamy pluton	Sew	PW-8	60°27.0'	148°06.5'	34.4	1.2	5	K/Ar hornblende	1140	Lanphere, 1966
Crow Pass pluton	Anc	80AMS34	61°3.2'	149°6.1'	54.5	1.6		K/Ar muscovite	1150	Nelson and others, 1985
Crow Pass pluton	Anc	80KMS321	61°3.2'	149°6.1'	54.8	2.7		K/Ar whole rock	1150	Nelson and others, 1985
Sill, Eagle River	Anc	CKA-1	61°16.2'	149°17.1'	50.2	2.5		K/Ar whole rock	1165	Updike and Ulery, 1988
Passage Canal pluton	Sew	PW-1	60°50.0'	148°29.0'	36.6	1.0	5	K/Ar biotite	1165	Lanphere, 1966
Dike, Peters Creek	Anc	CKA-2	61°19.1'	149°18.7'	50	2.6		K/Ar whole rock	1170	Updike and Ulery, 1988

Igneous body	Quad	Field number or location	Latitude	Longitude	Age (Ma)	Error (m.y.)	Notes	Method	Distance from Sanak Island (km)	Reference
Esther pluton	Sew	PW-2	60°50.0'	148°03.0'	35.5	0.9	5	K/Ar biotite	1185	Lanphere, 1966
Perry Island pluton	Sew	80ANs60A	60°44.3'	147°57.5'	34.2	1.7		K/Ar whole rock	1185	Nelson and others, 1985
Sill, Gravel Creek area	Anc	none given	~61°40'	~147°55'	57.2	3.2		K/Ar hornblende	1240	Little and Nueser, 1989
Miners Bay pluton	Anc	81AMH69A	61°05.7'	147°30.2'	32.2	1.6	2	K/Ar biotite	1240	Nelson and others, 1985
Miners Bay pluton	Anc	81ANs82	61°05.7'	147°30.2'	38.4	1.9		K/Ar hornblende	1240	Nelson and others, 1985
Dike, Harvard Glacier	Anc	81AMH65A	61°23.2'	147°32.3'	43.6	1.6		K/Ar whole rock	1245	Nelson and others, 1985
Stock near Mt. Cameron	Val	79PW8	61°12.4'	144°46.5'	51.6	1.5		K/Ar muscovite	1305	Winkler and others, 1981
Sheep Bay pluton	Cor	71APr22	60°42'	146°08'	50.5	1.5		K/Ar hornblende	1345	Winkler and Plafker, 1981
Sheep Bay pluton	Cor	71APr22C	60°42'	146°08'	53.2	1.6		K/Ar biotite	1345	Winkler and Plafker, 1981
Rude River pluton (gabbro)	Cor	85ANk96B	60°41.8'	145°31.1'	64.5	2.1	3	K/Ar hornblende	1380	Plafker, in Wilson and others, 1991
Rude River pluton (granodiorite)	Cor	84APr8	60°42.1'	145°29.2'	49.9	1.5		K/Ar hornblende	1380	Plafker, in Wilson and others, 1991
Rude River pluton (granodiorite)	Cor	84APr8	60°42.1'	145°29.2'	52.3	1.6		K/Ar biotite	1380	Plafker, in Wilson and others, 1991
Dike, Cirque Creek	Val	84APe97	61°19.1'	144°53.2'	52.2	1.6		K/Ar biotite	1390	Plafker and others, 1989
Dike, Cirque Creek	Val	84APe97	61°19.1'	144°53.2'	43.6	3.1	2	K/Ar hornblende	1390	Plafker and others, 1989
McKinley Peak pluton	Cor	84APr9	60°34.4'	145°15.1'	51.4	1.5		K/Ar biotite	1400	Plafker, in Wilson and others, 1991
McKinley Peak pluton	Cor	67APr1	60°28'	145°20'	51.6	2		K/Ar phlogopite	1405	Winkler and Plafker, 1981
Dike, Cordova area	Cor	none given	60°28'	145°20'	44	—		K/Ar whole rock	1405	Barker and others, 1992
Dike, Cordova area	Cor	none given	60°28'	145°20'	47.2	—		K/Ar whole rock	1405	Barker and others, 1992
Dike, Cordova area	Cor	none given	60°28'	145°20'	52	—		K/Ar whole rock	1405	Barker and others, 1992
McKinley Pk pluton	Cor	85APr140	60°32.3'	145°11.2'	47.2	1.4	2	K/Ar whole rock	1405	Plafker, in Wilson and others, 1991
Pluton south of Miles Glacier	Cor	80ANs148A	60°29'	144°23'	52.7	1.6		K/Ar biotite	1425	Winkler and Plafker, 1981
Pluton south of Miles Glacier	Cor	80ANs148A	60°29'	144°23'	51.3	2.9		K/Ar hornblende	1425	Winkler and Plafker, 1981
Pluton, upper Miles Glacier	Cor	71APr20C	60°39'	144°10'	50.9	1.5		K/Ar biotite	1425	Winkler and Plafker, 1981
Pluton, upper Miles Glacier	Cor	71APr25C	60°29'	144°23'	53.5	1.6		K/Ar hornblende	1430	Winkler and Plafker, 1981
Pluton, upper Miles Glacier	Cor	71APr20B	60°36'	144°11'	50.6	1.5		K/Ar hornblende	1430	Winkler and Plafker, 1981
Bremner Glacier pluton	BG	74APr151-H	60°53.5'	143°27'	51.2	2.6		40/39 actinolite	1470	Sisson and others, 1989
Bremner Glacier pluton	BG	74APr151	60°53.5'	143°27'	65.7	7.2	3	K/Ar hornblende	1470	Plafker in Onstott and others (1989)
Bremner Glacier pluton	BG	74APr151	60°53.5'	143°27'	50.1	2.0		K/Ar biotite	1470	Plafker, in Wilson and others, 1991
Tana Glacier sill	BG	84ASn103-H1	60°44.5'	142°43'	52.8	0.8		40/39 hornblende	1520	Sisson and others, 1989
Tana Glacier sill	BG	84ASn103-B2	60°44.5'	142°43'	50.1	0.5		40/39 biotite	1520	Sisson and others, 1989
Tana Glacier sill	BG	84ASn103-P2	60°44.5'	142°43'	35.3	2.2	2	40/39 plagioclase	1520	Sisson and others, 1989
Bremner Glacier pluton	BG	73APr300	60°58.7'	143°21.6'	60.5	3.6	3	K/Ar hornblende	1525	Plafker, in Wilson and others, 1991
Bremner Glacier pluton	BG	73APr300	60°58.7'	143°21.6'	47.2	1.8		K/Ar biotite	1525	Plafker, in Wilson and others, 1991
Bremner Glacier pluton	BG	84APr198	60°56.4'	143°18.7'	49.4	1.5		K/Ar biotite	1530	Plafker, in Wilson and others, 1991
Bremner Glacier pluton	BG	84APr198	60°56.4'	143°18.7'	48.4	1.5		K/Ar hornblende	1530	Plafker, in Wilson and others, 1991
Pluton, upper Miles Glacier	BG	none given	60°43.7'	143°22'	59	—	3	K/Ar hornblende	1530	Onstott and others, 1989 (fig. 1 only)
Pluton, upper Miles Glacier	BG	none given	60°43.7'	143°22'	46	—		K/Ar biotite	1530	Onstott and others, 1989 (fig. 1 only)
Pluton north of Granite Ck.	BG	73AH275B	60°46.3'	142°04.0'	50.2	2.0		K/Ar biotite	1550	Plafker, in Wilson and others, 1991
Pluton south of Granite Ck.	BG	73AH274B	60°42.9'	141°54.5'	49.9	2.0		K/Ar biotite	1560	Plafker, in Wilson and others, 1991
Pluton south of Granite Ck.	BG	84APr197B	60°42.8'	141°54.3'	27.4	0.8	2	K/Ar biotite	1560	Plafker, in Wilson and others, 1991
Jeffries pluton	BG	73AH273A	60°41.5'	141°43.6'	52.6	2.0		K/Ar biotite	1570	Plafker, in Wilson and others, 1991
King Peak pluton	MSE	106Cac771	60°36.25'	140°51.9'	50	2.4		K/Ar biotite	1615	Dodds and Campbell, 1988
Mt. Newton pluton	MSE	69APr48A	60°19'	140°50'	27.4	22.9	1	K/Ar hornblende	1625	Dodds and Campbell, 1988
Mt. Saint Elias pluton	MSE	69APr54A	60°17'	140°53'	89.3	3.1	5,3	K/Ar biotite	1625	Hudson and others, 1977
Mt. Saint Elias pluton	MSE	69APr54A	60°17'	140°53'	54.2	1.7	5	K/Ar hornblende	1625	Hudson and others, 1977
Mt. Saint Elias pluton	MSE	69APr54A	60°17'	140°53'	56.1	9.5	1	K/Ar hornblende	1625	Dodds and Campbell, 1988
Mt. Saint Elias pluton	MSE	138Cac771	60°12.9'	140°56.1'	35.8	2.1	2	K/Ar biotite	1625	Dodds and Campbell, 1988
Mt. Saint Elias pluton	MSE	138Cac771	60°12.9'	140°56.1'	60.5	8.2	1	K/Ar hornblende	1625	Dodds and Campbell, 1988

Table 1. Isotopic ages of intrusive rocks from the Sanak-Baranof belt, southern Alaska—Continued

[Abbreviations for 1:250,000-scale quadrangles: Afog, Afognak; Anc, Anchorage; BG, Bering Glacier; Bly, Blying Sound; Cor, Cordova; FP, False Pass; Kag, Kaguyak; Kod, Kodiak; MF, Mt. Fairweather; MSE, Mt. St. Elias; PA, Port Alexander; PM, Port Moller; Sel, Seldovia; Sew, Seward; Sim, Simeonof Island; Sit, Sitka; Skag, Skagway; Step, Stepovak Bay; Sut, Sutwik Island; Trin, Trinity Islands; Val, Valdez; Yak, Yakutat. Distance along strike was measured from the southern tip of Sanak Island on Beikman's (1980) geologic map of Alaska. Notes: 1, Not plotted in figure 2B, because error >10%; 2, Not plotted in figure 2B, because strongly discordant with older determination(s) from same pluton; 3, Problematic age from a pluton with multiple determinations; 4, Suspect, but plotted in figure 2B; 5, Recalculated using new decay constant (most recalculated values are from Wilson and others, 1991); 6, Glacial erratic assumed to have been derived from the Kodiak batholith]

Igneous body	Quad	Field number or location	Latitude	Longitude	Age (Ma)	Error (m.y.)	Notes	Method	Distance from Sanak Island (km)	Reference
Mt. Saint Elias pluton	MSE	138CAc771	60°12.9'	140°56.1'	63.6	8.7	1	K/Ar hornblende	1625	Dodds and Campbell, 1988
Mt. Saint Elias pluton	MSE	138CAc771	60°12.9'	140°56.1'	34.7	1.1	2	K/Ar biotite	1625	Dodds and Campbell, 1988
Mt. Saint Elias pluton	MSE	138CAc771	60°12.9'	140°56.1'	55.1	1.8		K/Ar hornblende	1625	Dodds and Campbell, 1988
Mt. Saint Elias pluton	MSE	31CAc781	60°12.9'	140°56.1'	38.4	2.2	2	K/Ar biotite	1625	Dodds and Campbell, 1988
Mt. Saint Elias pluton	MSE	31CAc781	60°12.9'	140°56.1'	67.2	10.7	1	K/Ar hornblende	1625	Dodds and Campbell, 1988
Pluton, upper Seward Glacier	MSE	72CAc741	60°25.1'	140°15.8'	45.4	2.4		K/Ar biotite	1655	Dodds and Campbell, 1988
Pluton, upper Seward Glacier	MSE	72CAc741	60°25.1'	140°15.8'	51.5	3.0		K/Ar hornblende	1655	Dodds and Campbell, 1988
Mt. Vancouver pluton	MSE	69APr32A	60°18.1'	139°36.1'	48.0	1.0	5	K/Ar muscovite	1680	Hudson and others, 1977
Mt. Vancouver pluton	MSE	69APr32A	60°18.1'	139°36.1'	44.6	1.0	5	K/Ar biotite	1680	Hudson and others, 1977
Mt. Foresta pluton	MSE	69APr40A	60°13.3'	139°31'	31.4	1.0	5	K/Ar biotite	1690	Hudson and others, 1977
Valerie Glacier pluton	MSE	67APr78A	60°07.6'	139°28.5'	21.4	3.1	5	K/Ar muscovite	1700	Hudson and others, 1977
Valerie Glacier pluton	MSE	67APr78A	60°07.6'	139°28.5'	18.9	1.0	5	K/Ar hornblende	1700	Hudson and others, 1977
Pluton north of Nunatak Fiord	Yak	67APr57B1	59°52.1'	138°58.8'	24.1	0.7	5	K/Ar muscovite	1730	Hudson and others, 1977
Novatak Glacier pluton	Yak	68APr103B	59°37'	138°31'	62.5	2.0	5,3	K/Ar hornblende	1775	Hudson and others, 1977
Novatak Glacier pluton	Yak	68AMk108	59°31.8'	138°23.5'	26	1.0	5,3	K/Ar biotite	1785	Hudson and others, 1977
Alsek River pluton	Yak	67APr94C	59°25.5'	138°00'	23.1	2.0	5,2	K/Ar biotite	1810	Hudson and others, 1977
Alsek River pluton	Yak	67APr94C	59°25.5'	138°00'	21.2	2.8	2	K/Ar biotite	1810	Dodds and Campbell, 1988
Alsek River pluton	Yak	49CAc781	59°24.8'	138°01.5'	32.8	1.9		K/Ar biotite	1810	Dodds and Campbell, 1988
Pluton south of Alsek River	Skag	78AH70	59°21.3'	137°56.8'	26.6	1.1		K/Ar biotite	1810	Plafker, in Wilson and others, 1991
Konamoxi Glacier pluton	Skag	78AH69A	59°21.5'	137°49.7'	52.7	4.0		K/Ar hornblende	1815	Plafker, in Wilson and others, 1991
Konamoxi Glacier pluton	Skag	78AH69A	59°21.5'	137°49.7'	42.4	1.6	2	K/Ar biotite	1815	Plafker, in Wilson and others, 1991
Konamoxi Glacier pluton	Skag	78AH69B	59°21.5'	137°49.7'	42.3	1.6	2	K/Ar biotite	1815	Plafker, in Wilson and others, 1991
Konamoxi Glacier pluton	Skag	78AH69C	59°21.5'	137°49.7'	42.2	1.6	2	K/Ar biotite	1815	Plafker, in Wilson and others, 1991
Konamoxi Glacier pluton	Skag	114CAc781	59°21.6'	137°38.2'	52.4	1.8		K/Ar biotite	1830	Dodds and Campbell, 1988
Jarl Glacier pluton	Skag	113CAc781	59°09.8'	137°17.8'	41	2.2		K/Ar biotite	1865	Dodds and Campbell, 1988
Pluton near Mt. Quincy Adams	MF	77BJ029A	58°53.5'	137°22.0'	28.1	0.8		K/Ar biotite	1880	D. Brew, written commun., 1993
Pluton near Mt. Forde	Skag	77BJ038A	59°02.4'	137°07.4'	44.4	1.3		K/Ar biotite	1880	D. Brew, written commun., 1993
Pluton near Mt. Forde	Skag	77BJ038A	59°02.4'	137°07.4'	37.5	1.1	2	K/Ar hornblende	1880	D. Brew, written commun., 1993
Pluton, S. side J. Hopkins Inlet	MF	66AFD404	58°52.4'	137°02.9'	40.2	1.2		K/Ar biotite	1890	D. Brew, written commun., 1993
Pluton, head J. Hopkins Inlet	MF	66ABd699	58°50.2'	137°08.0'	30.7	0.9	2	K/Ar biotite	1890	D. Brew, written commun., 1993
Pluton, head J. Hopkins Inlet	MF	66ABd699	58°50.2'	137°08.0'	40.8	1.2		K/Ar hornblende	1890	D. Brew, written commun., 1993
La Perouse intrusion	MF	67A	58°35'	137°15'	41.1	2.2		K/Ar hornblende	1910	Hudson and Plafker, 1981
La Perouse intrusion	MF	67B	58°35'	137°15'	32.5	2.5	2	K/Ar hornblende	1910	Hudson and Plafker, 1981
La Perouse intrusion	MF	67C	58°35'	137°15'	22.8	0.9	2	K/Ar biotite	1910	Hudson and Plafker, 1981
La Perouse intrusion	MF	67D	58°35'	137°15'	19.3	0.7	2	K/Ar biotite	1910	Hudson and Plafker, 1981
La Perouse intrusion	MF	67F	58°35'	137°15'	44.2	3.3		K/Ar hornblende	1910	Hudson and Plafker, 1981
La Perouse intrusion	MF	none given	58°35'	137°10'	28.0	8.0	2,1	40/39 plagioclase	1915	Loney and Himmelberg, 1983
Pluton, west side Brady Glacier	MF	66AFD468	58°37.6'	136°53.5'	32.3	1.0	2	K/Ar biotite	1920	D. Brew, written commun., 1993
Pluton, west side Brady Glacier	MF	66AFD468	58°37.6'	136°53.5'	39.4	1.2		K/Ar muscovite	1920	D. Brew, written commun., 1993
Pluton, west side Taylor Bay	MF	76DB123A	58°20.3'	136°40.3'	38.2	1.1		K/Ar biotite	1950	D. Brew, written commun., 1993
Pluton, west side Taylor Bay	MF	76CN034A	58°17.9'	136°39.8'	30.5	0.9	2	K/Ar biotite	1955	D. Brew, written commun., 1993

Igneous body	Quad	Field number or location	Latitude	Longitude	Age (Ma)	Error (m.y.)	Notes	Method	Distance from Sanak Island (km)	Reference
Pluton on Yakobi Island	Sit	none given	57°59'	136°27'	34.0	1.0	2	K/Ar biotite	1990	Himmelberg and others, 1987
Pluton on Yakobi Island	Sit	none given	57°59'	136°27'	43.6	0.6		K/Ar biotite	1990	Himmelberg and others, 1987
Pluton on Yakobi Island	Sit	79BJ119A	57°59'	136°27'	34.0	1.0	2	K/Ar biotite	1990	Karl and others, 1988
Pluton on Yakobi Island	Sit	79BJ119A	57°59'	136°27'	39.6	1.2		K/Ar hornblende	1990	Karl and others, 1988
Pluton on Yakobi Island	Sit	79BJ108A	57°55'	136°33'	41.7	1.3		K/Ar biotite	1995	Karl and others, 1988
Kruzof Island pluton	Sit	61ABd713a	57°11.5'	135°49.5'	49.8	1.3	5	K/Ar biotite	2080	Loney and others, 1967
Baranof Lake pluton	Sit	62ABd332	57°11'	134°52.5'	43.6	1.1	5	K/Ar biotite	2120	Loney and others, 1967
Baranof Lake pluton	Sit	62ABd332	57°11'	134°52.5'	45.3	1.2	5	K/Ar muscovite	2120	Loney and others, 1967
Baranof Lake pluton	Sit	LK8203	57°06'	134°54.5'	42.1	0.8	5	K/Ar muscovite	2125	Loney and others, 1967
Baranof Lake pluton	Sit	LK8203	57°06'	134°54.5'	43.1	0.8	5	K/Ar muscovite	2125	Loney and others, 1967
Baranof Lake pluton	Sit	62ALy201	57°01'	135°02.5'	48.3	1.3	5	K/Ar biotite	2125	Loney and others, 1967
Baranof Lake pluton	Sit	LK82110	57°04'	134°47.5'	28.7	1.3	5,2	K/Ar biotite	2130	Loney and others, 1967
Baranof Lake pluton	Sit	62APy252	57°03'	134°51'	39.6	0.9	5	K/Ar biotite	2130	Loney and others, 1967
Crawfish Inlet pluton	PA	none given	~56°50'	~135°15'	50.1	0.1		U/Pb zircon	2130	Brew and others, 1991
Crawfish Inlet pluton	PA	81RR170	56°49.6'	135°11.2'	48.3	—		K/Ar biotite	2140	Reifensuhl, 1983
Crawfish Inlet pluton	PA	81RR170	56°49.6'	135°11.2'	48.0	—		K/Ar biotite	2140	Reifensuhl, 1983
Dike, Baranof Island	PA	LK8217	56°55'	134°43.5'	37.0	0.4	5	K/Ar biotite	2145	Loney and others, 1967
Crawfish Inlet pluton	PA	LK8211	56°44'	134°43'	47.9	0.5	5	K/Ar biotite	2145	Loney and others, 1967
Crawfish Inlet pluton	PA	63ABd41	56°46.5'	134°56.5'	45.3	1.1	5	K/Ar biotite	2150	Loney and others, 1967
Crawfish Inlet pluton	PA	LK8214	56°43'	134°57'	45.4	0.4	5	K/Ar biotite	2155	Loney and others, 1967
Crawfish Inlet pluton	PA	LK8215A	56°42'	134°53'	47.8	3.1	5	K/Ar biotite	2160	Loney and others, 1967
Crawfish Inlet pluton	PA	LK8215C	56°42'	134°53'	43.0	0.6	5	K/Ar hornblende	2160	Loney and others, 1967
Gut Bay stock	PA	62APy157	56°44'	134°43'	24.9	1.6	5	K/Ar biotite	2165	Loney and others, 1967
Gut Bay stock	PA	LK8202	56°42.5'	134°44.5'	26.4	0.6	5	K/Ar biotite	2165	Loney and others, 1967
Gut Bay stock	PA	LK8201	56°44'	134°38'	25.5	0.5	5	K/Ar biotite	2170	Loney and others, 1967
Gut Bay stock	PA	LK8201	56°44'	134°38'	31.9	0.5	5	K/Ar hornblende	2170	Loney and others, 1967

# GEOCHEMICAL EVALUATION OF STREAM-SEDIMENT DATA FROM THE BERING GLACIER AND ICY BAY QUADRANGLES, SOUTH-CENTRAL ALASKA

By Richard J. Goldfarb and J. Carter Borden

## ABSTRACT

Samples of stream sediment collected from the Bering Glacier and Icy Bay 1° × 3° quadrangles during the NURE survey were statistically evaluated. Factor analysis of the 436 samples was used to identify five significant geochemical associations accounting for 80 percent of the variance in the data. Samples with high concentrations of Hf, Lu, Cr, Mn, U, Th, La, Ti, and Dy are found across the Gulf of Alaska coastal plain, reflecting heavy-mineral concentrations within the Yakataga placer mining district. Relative enrichments of Co, Mg, Cu, Fe, Ni, and Sc characterize stream-sediment samples from the Wrangellia terrane. These enrichments reflect (1) the relatively high geochemical background levels for these elements in mafic volcanic rocks and (2) sulfide-bearing veins where samples are derived from the Jurassic Chitina Valley batholith. Highest concentrations of K, Ba, and Al in samples from the survey locally characterize some facies of the marine sedimentary rocks of the Valdez Group. Tertiary intrusive bodies in the Chugach terrane yield stream sediments with high concentrations of Sm, Ce, La, Dy, Pb, Eu, and Th. Samples that are relatively enriched in As and Ca, as well as depleted in Al and Na, delineate watersheds underlain by carbonate rocks within the Wrangellia and Alexander terranes.

The distribution of collected samples is erratic, limiting the usefulness of the NURE survey for assessing mineral resource potential. Most of the anomalous values in the data set reflect the relatively high geochemical background values of the less abundant rock units that crop out in the study area. However, two broad areas, not previously recognized as containing metallic mineral occurrences, are delineated as favorable for the presence of mineral resources. Anomalous amounts of Ag, As, Au, Co, Cu, Ni, and Fe in stream-sediment samples suggest that copper-porphyry- and molybdenum-porphyry-related vein systems are located throughout the Chitina Valley batholith. Highly anomalous arsenic values in samples collected between the Tana River and Twelvemile Creek likely reflect contributions from mesothermal gold-bearing quartz veins in metasedimentary rocks of the Valdez Group.

## INTRODUCTION

The Bering Glacier 1° × 3° quadrangle, and the limited land mass on the Icy Bay 1° × 3° quadrangle immediately to the south, are centered around the eastern part of the rugged Chugach-Kenai Mountains of south-central Alaska. Lode and related placer gold deposits, and volcanogenic massive sulfide deposits, are widespread farther to the west within Late Cretaceous and younger rocks of the mountain range (Moffit, 1954; Jansons and others, 1984; Nelson and others, 1984). Similar metallic mineral occurrences are, however, generally not known within the same rock units in the easternmost part of the Chugach Range. This might reflect a lack of hydrothermal ore-forming processes affecting the rocks that make up this part of the range. Alternatively, the relative remoteness of this highly glaciated area has historically hampered prospecting efforts and geologic data gathering landward of the Gulf of Alaska coastal plain. Except for a part of the Kenai quadrangle, the Bering Glacier and Icy Bay quadrangles are the only part of south-central Alaska between the St. Elias-Wrangell Mountain Ranges and Cook Inlet lacking 1:250,000-scale geochemical and geological studies typical of the Alaska Mineral Resources Assessment Program (AMRAP).

Stream-sediment samples were, however, collected over a large part of the Bering Glacier and Icy Bay quadrangles during the U.S. Department of Energy's National Uranium Resource Evaluation (NURE) program (Los Alamos National Laboratory, 1983). It was hoped that interpretation of the existing geochemical data from the NURE study might be useful in identifying some areas on the quadrangles favorable for the presence of metallic mineral occurrences. This report presents a statistical summary and factor analysis of the geochemical data, defines the distribution of geochemically anomalous samples, and identifies a few new areas favorable for the presence of metallic mineral occurrences in the eastern Chugach Mountains.



## GEOLOGY AND KNOWN MINERAL OCCURRENCES

The study area (fig. 1) is underlain by rocks of the Alexander, Wrangellia, Chugach, Prince William, and Yakutat terranes (Jones and others, 1987). Reconnaissance geologic mapping of the easternmost Chugach Mountains was conducted by Hudson and Plafker (1982), Gardner and others (1988), and Plafker and others (1989). Detailed geologic mapping of the entire Bering Glacier and Icy Bay quadrangles (at a scale of 1:250,000 or greater) has not yet been carried out.

The northeastern corner of the Bering Glacier quadrangle is underlain by a thick sequence of early Paleozoic through Early Jurassic rocks informally named the "Kaskawulsh Group" by Gardner and others (1988). This complex sequence of rocks, comprising the basement rocks of Alexander terrane, includes marble, limestone, schist, phyllite, siltstone, argillite, basic volcanic rocks, and felsic to intermediate intrusive bodies. Late Paleozoic basaltic to andesitic flow rocks, flow breccia, volcanic graywacke, tuff, and limestone of the Wrangellia terrane crop out south and west of the Alexander terrane. Prior to the Early to mid-Cretaceous docking of the amalgamated Alexander and Wrangellia terranes onto North America (Saleeby, 1983), Late Jurassic quartz monzodiorite, with lesser quartz diorite, granodiorite, and tonalite of the Chitina Valley batholith, intruded Triassic and older rocks of the Wrangellia terrane.

The Border Ranges fault system separates the Wrangellia terrane and the Chugach terrane to the south. The Chugach terrane underlies most of the northern half of the Bering Glacier quadrangle and was underthrust beneath the Wrangellia terrane in Late Cretaceous or early Tertiary time (Plafker and others, 1977). Within the study area, the Chugach terrane consists of highly deformed marine clastic rocks and subordinate interbedded basaltic units of the Cretaceous Valdez Group. The northern third of the Valdez Group is metamorphosed to greenschist facies, whereas the remainder consists of higher grade schist and gneiss of the informally named, high-temperature, low-pressure "Chugach Metamorphic Complex" of Hudson and Plafker (1982) (see also, Sisson and others, 1989). The Contact fault system separates the Chugach terrane from the early Eocene Prince William terrane, a similar turbidite-rich sequence of rocks (the Orca Group) that was tectonically underthrust by about 51 Ma (Plafker, 1987). Small, Eocene stocks and dikes of felsic to intermediate composition intrude rocks of both the Chugach and Prince William terranes.

The southern third of the Bering Glacier quadrangle and land areas on the Icy Bay quadrangle are underlain by bedded sedimentary rocks of the Yakutat terrane described by Winkler and Plafker (1981) and Plafker (1987). The Chugach-St. Elias fault system separates the Yakutat

terrane from the Prince William terrane. Units in the Yakutat terrane consist of the Eocene sandstone, siltstone, and shale of the alluvial-plain Kulthieth Formation, the deltaic Tokun Formation, and the pro-delta Stillwater Formation. A late Eocene to early Miocene marine transgression is recorded by the organic-shale-dominated Poul Creek Formation. This unit contains basaltic flows and related mafic intrusive rocks. Oligocene(?) and younger clastic strata of the Redwood and Yakataga Formations, reflecting glacially derived material from uplift of the Chugach and St. Elias Mountains, were deposited on top of the Poul Creek Formation in a continental-shelf environment.

The only known mineral deposits within the Bering Glacier and Icy Bay quadrangles are the river, beach, and marine terrace placer gold deposits of the Yakataga mining district. These placers stretch for approximately 50 km, from Cape Yakataga to eastward of longitude 141° (fig. 1). Fine-grained gold has been mined by small-scale placer operations from 1897 until the present, with an estimated 15,709 oz of gold recovered through 1959 (Koschmann and Bergendahl, 1968). Wave action has concentrated much of the gold within heavy-mineral layers in the beach sand and in raised terraces. Reimnitz and Plafker (1976) noted beach sand about 8 km east of the mouth of the White River that contained 1.87 ppm Au; a sample of sand just west of the mouth of the White River analyzed by Eyles (1990) contained 37 ppm Au. Gold in the placers has been speculated to have been reworked most recently from rocks of the Yakataga Formation, but ultimately the gold is interpreted to have been derived from bedrock sources in the Chugach and St. Elias Mountains (Maddren, 1914; Reimnitz and Plafker, 1976; Eyles, 1990). The gold-bearing heavy mineral layers are largely composed of garnet, with some chromite, native copper, magnetite, ilmenite, xenotime, rutile, sphene, ilmenite, zircon, platinum, and U- and Th-bearing minerals (Moxham and Nelson, 1952; Thomas and Berryhill, 1962).

A few isolated metallic lode occurrences are scattered throughout the Bering Glacier quadrangle. None of these are described in great detail, and it is impossible to relate these occurrences to specific mineral deposit models. Hydrothermal quartz-feldspar veins containing up to 20 percent graphite and pyrite cut bleached metamorphic rocks of the Wrangellia terrane about 1.5 km north of Slender Lake along the northern edge of the Bering Glacier quadrangle (Brabb and Miller, 1962). Along the southern shore of the lake, Brabb and Miller (1962) reported argillite containing hematite both disseminated and in fracture zones. In rocks of the Valdez Group within the Granite Range, minor gold was reported in what is probably a silicified felsic dike (60° 51' N., 142° 26' W.; Brabb and Miller, 1962). A few kilometers to the northeast of this occurrence, gold-bearing placers are recognized along the Kiagna River. Moffit (1918) described numerous quartz veins cutting metasedimentary and granitic rocks of the

Wrangellia terrane, as well as a large pyrite-rich vein or lens, in the area of the placer workings. South of the Granite Range, near Natural Arch in the center of the Bering Glacier quadrangle, native copper is found in volcanic rocks of the Orca Group and malachite and azurite occur in associated quartz veins (Brabb and Miller, 1962).

Whereas no placer gold occurrences are known in the northwest corner of the Bering Glacier quadrangle, small placer operations existed near the turn of the century on Golconda Creek a few kilometers north of the quadrangle and on the Bremner River a few kilometers west of the quadrangle (Moffit, 1914). MacKevett (1976) noted a few copper sulfide- and oxide-bearing vein occurrences cutting quartz diorite of the batholith 2–3 km north of the Bering Glacier quadrangle, between the Kiagna River and Goat Creek. The Cu-Mo-Ag-Au signature of these veins and the surrounding hydrothermal alteration in the McCarthy quadrangle led Singer and MacKevett (1977) to delineate this area as favorable for porphyry copper and molybdenum occurrences.

## GEOCHEMICAL METHODS

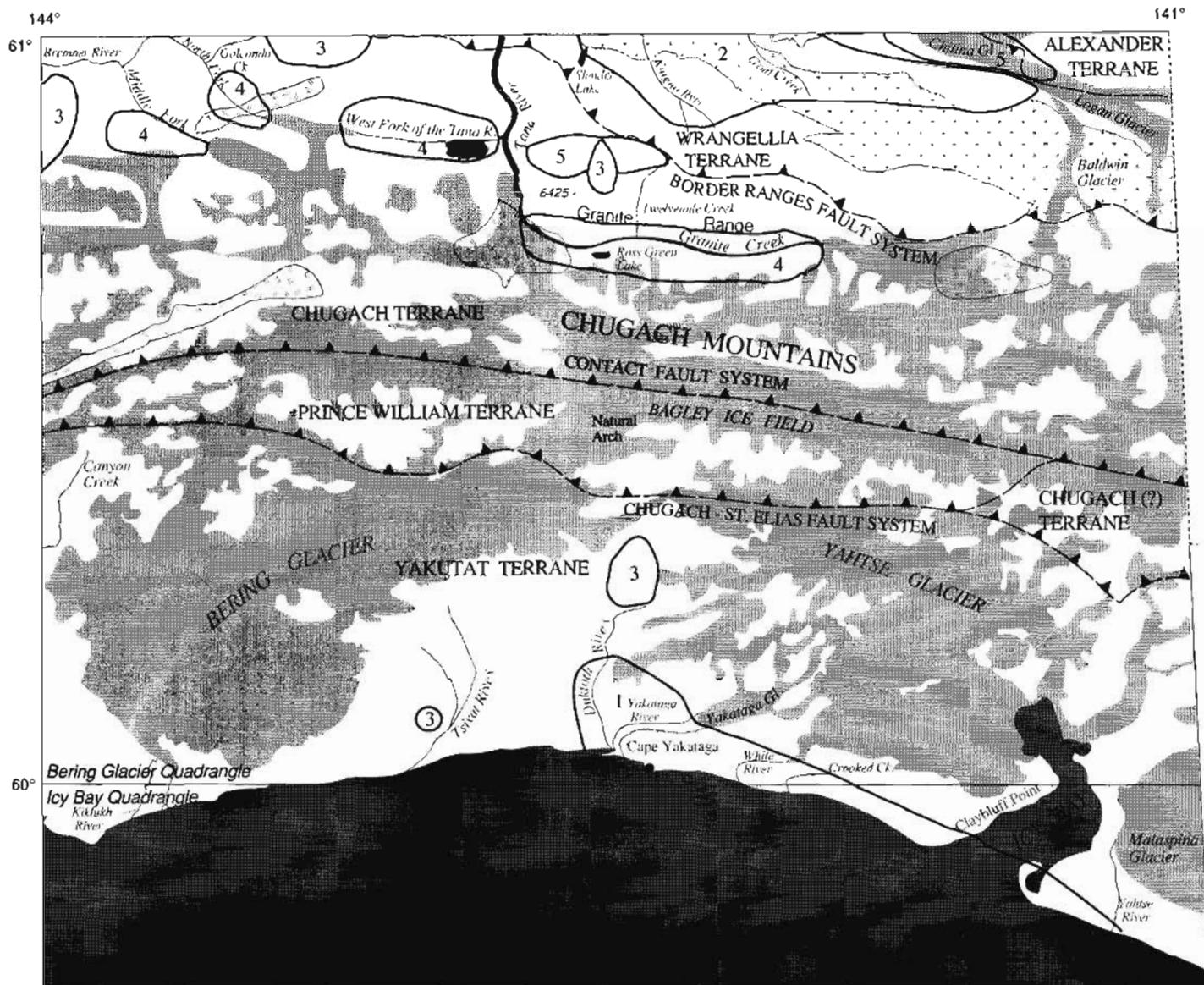
Analytical results evaluated in this study are contained in the U.S. Department of Energy's Hydrogeochemical and Stream Sediment Reconnaissance (HSSR) portion of the NURE program (Youngquist and others, 1981; Zinkl and others, 1981). A total of 406 minus-100-mesh stream-sediment samples were collected from the Bering Glacier quadrangle, and 30 samples were taken from the Icy Bay quadrangle. Latitudes and longitudes for the sample sites are included with the analytical results; however, the lack of a published sample site map often makes it difficult to determine whether samples were collected in major streams or at the mouth of tributaries to such streams. Approximately 1 kg of sediment was composited from three adjacent locations at each sample site. The collected sample size assured at least 25 g of material for chemical analysis subsequent to drying and sieving at the laboratory (Los Alamos National Laboratory, 1983). Samples were analyzed by the Department of Energy at Los Alamos National Laboratory for 41 elements by the methods included in table 1.

Data in table 1 summarize most of the results from the NURE survey. Lower determination limits are included for most elements in table 1. For elements determined by neutron activation analysis, the lower determination limit is a complex function of the total composition and mass of each individual sample. Presented lower limits (determined by Los Alamos National Laboratory, 1983) are average values for Alaska calculated on the basis of typical 4-g samples. Therefore, in many cases in table 1, the average estimate for an element's lower determination limit exceeds minimum values. No data are listed for niobium or selenium because all 436 analyses for these elements were below the lower determination limits of 20 ppm and 5 ppm, respectively.

## STATISTICAL EVALUATION OF NURE GEOCHEMICAL DATA

Minimum, median, 90th percentile, 95th percentile, 97.5th percentile, and maximum values are included in table 1 to present the range in the geochemical data. An anomalous element value is one that exceeds the normal or expected abundance of a given element, generally referred to as the geochemical background value. The 95th percentile included in table 1 has been chosen to approximate a threshold value for the stream-sediment population, with all values greater than the threshold being considered anomalous. For the elements Ag, Bi, Cd, Sn, Au, Sb, and Ta, more than 95 percent of the stream-sediment sample values were below lower determination limits. Therefore, all detected concentrations for these elements were determined to be anomalous. Anomalies in the data set may be interpreted to reflect rock types with relatively high geochemical background levels or concentrations of elements in mineral resources. Because much of the study area is underlain by marine clastic units, most stream-sediment concentrations reflect that lithology. Samples derived from less commonly exposed mafic volcanic, felsic to intermediate intrusive, or carbonate rocks, tend to be locally enriched in specific element suites relative to samples collected in watersheds underlain by clastic rocks. Local geology must be considered to distinguish enrichments reflecting variable rock types and anomalies representative of metallic mineral resources.

R-mode factor analysis with Varimax rotation was used to identify the dominant geochemical associations in the data set. The more highly censored elements (>67 percent of the values below the lower determination limit for the element in question) were removed from each data set. All values of an element qualified with an "L", signifying a level below determination limits, were changed to 0.5 of the lower limit of detection for that element. Factor analysis places similarly behaving experimental variables (elements) into groups termed "factors." Specific rock types or ore deposit types are commonly represented by distinct suites of trace elements. Therefore, certain factors composed of distinctive element suites can be used to identify stream-sediment samples derived from such rock types or mineral deposit systems in the study area. A five-factor model that explains 80 percent of the total variance (table 2) was selected to summarize broad geochemical trends in the NURE stream-sediment data. Factor loadings for the sediment data are listed in table 2. The factor loadings, which depict the influence of each variable on a factor, may be interpreted similarly to correlation coefficients. The optimal number of factors that were chosen was based on the breaks in slope on plots of factor number versus total variance. Factor scores, discussed below, measure the effect a particular factor has on each sample site. A high score for a given sample signifies that the element association represented by that factor is strong.



## EXPLANATION

—— Boundary of areas with high factor analysis scores:

Factor 1. Hf-Lu-Cr-Mn-U-Th-La-Ti-Dy

Factor 2. Co-Mg-Cu-Fe-Ni-Sc

Factor 3. K-Ba-Al-(Ca)

Factor 4. Sm-Ce-La-Dy-Pb-Eu-Th

Factor 5. As-(Al-Na)



▲▲▲ Thrust fault, approximate location; sawteeth on upper plate



Granitic rocks (Tertiary)



Chitina Valley batholith (Jurassic)—Granitic rocks



Glacier

**Figure 1.** Study area showing location of clusters of stream-sediment samples with anomalous factor scores. Geology generalized from Hudson and Plafker (1982) and Plafker (written commun., 1993).

**Table 1.** Statistical summary for 436 stream-sediment samples from the Bering Glacier and Icy Bay quadrangles, Alaska

[All values in are parts per million (ppm), except for Al, Ca, Fe, Mg, and Na which are in percent. Uranium was determined by delayed neutron counting; Ag, As, Bi, Cd, Cu, Ni, Pb, Sn, W, and Zr by X-ray fluorescence; and all other elements by neutron activation analysis. B, number of samples with no data reported. L, number of samples qualified with a "less than." LDL, lower determination limit (LDL) as listed in Los Alamos National Laboratory (1983, table 1). Limits were not given for Rb and Sm]

Element	B	L	LDL	Minimum	Median	Percentile			Maximum
						90	95	97.5	
U .....	0	0	0.01	0.8	2.3	3.9	6.1	8.4	55.2
Ag .....	10	419	5	5L	5L	5L	5L	5L	9
AS .....	10	80	5	5L	8	21	32	37	186
Bi .....	10	424	5	5L	5L	5L	5L	5L	8
Cd .....	10	425	5	5L	5L	5L	5L	5L	8
Cu .....	10	1	10	10L	34	64	73	88	178
Ni .....	10	94	15	15L	23	51	60	68	137
Pb .....	10	282	5	5L	5L	9	10	12	39
Sn .....	10	423	10	10L	10L	10L	10L	10L	16
W .....	10	420	15	15L	15L	15L	15L	15L	23
Zr .....	10	0	5	49	190	478	672	992	25,242
Al .....	0	0	.3	3.8	6.5	7.5	7.7	8.0	9.4
Au .....	0	418	.05	.04L	.07L	.10L	.14L	.20	69
Ba .....	0	66	150	145L	462	733	825	935	5,821
Ca .....	0	0	.1	.4	2.6	5.5	7.0	8.5	12.5
Ce .....	0	1	10	12L	53	86	106	147	299
Co .....	0	0	1.7	3.2	14	26	30	34	79
Cr .....	0	0	10	24	87	156	199	321	3,234
Cs .....	0	375	2	1.0L	1.9L	2.2	3.0	3.5	9.6
Dy .....	0	0	.7	2	4	6	7	9	21
Eu .....	0	0	.4	.6	1.3	1.8	2.1	2.3	4.3
Fe .....	0	0	.11	1.2	3.9	6.7	8.1	9.4	22.6
Hf .....	0	1	1.3	2.3L	7.1	20	29	45	662
K .....	0	107	.34	.3L	.9	1.4	1.5	1.7	5.0
La .....	0	2	7	5L	24	39	48	64	197
Lu .....	0	1	.1	.1L	.3	.5	.7	.9	8.2
Mg .....	0	5	.27	.2L	1.0	1.9	2.2	2.5	3.6
Mn .....	0	0	55	300	775	1,392	1,645	2,367	15,260
Na .....	0	0	.1	.2	2.2	2.5	2.5	2.6	3.0
Rb .....	0	400	—	22L	37L	60L	50	62	197
Sb .....	0	435	1	1L	2L	3L	3L	3L	2
Sc .....	0	0	.9	4.9	17	28	33	37	89
Sm .....	0	2	—	1.7L	4.5	6.8	8.4	10	18
Sr .....	6	381	400	213L	312L	314	418	483	836
Ta .....	0	428	1	1L	1L	2L	2L	2.5L	3
Tb .....	0	355	1	1L	1L	1	1	1	4
Th .....	0	0	1	1.4	5.7	11	15	20	90
Ti .....	0	3	750	605L	4,269	7,554	9,402	12,025	37,900
V .....	0	0	6	22	122	222	264	315	639
Yb .....	0	29	1	1.0L	3.2	4.8	5.9	8.7	64
Zn .....	13	290	100	16L	49L	117	142	160	498

## DISCUSSION OF GEOCHEMICALLY ANOMALOUS AREAS

Factor score values and plots of individual element concentrations were used to delineate the geochemically anomalous areas, which are discussed below, in the Bering Glacier and Icy Bay quadrangles (fig. 1). Samples with high scores for factor 1 are characterized by a Hf-Lu-Cr-Mn-U-Th-La-Ti-Dy signature. Twenty samples with high scores are located along the coastline between Cape

Yakataga and the Yahtse River and reflect the garnet-, chromite-, rutile-, and rare-earth-element-bearing beach placers of the Yakataga district. One sample at Cape Yakataga contained 22.6 percent Fe, 3.5 percent K, 3.7 percent Ti, 2.5 percent Zr, 15,260 ppm Mn (probably in spessartine), 3,234 ppm Cr, 662 ppm Hf, 639 ppm V, 299 ppm Ce, 197 ppm La, 90 ppm Th, 89 ppm Sc, 69 ppm Au, 64 ppm Yb, 55 ppm U, 21 ppm Dy, 14.9 ppm Sm, 8.2 ppm Lu, 4 ppm Tb, and 3 ppm Ta. These are the highest concentrations for most of these elements in NURE

**Table 2.** Factor loadings for first five factors after R-mode analysis with Varimax rotation of stream-sediment data

[Variance explained by five factors equals 80 percent. —, loadings less than 0.50 that have been omitted]

Element	1	2	3	4	5
Al .....	—	—	0.56	—	~0.64
As .....	—	—	—	—	.62
Ba .....	—	—	.77	—	—
Ca .....	—	—	~.50	—	—
Ce .....	0.61	—	—	0.74	—
Co .....	—	0.95	—	—	—
Cr .....	.96	—	—	—	—
Cu .....	—	.81	—	—	—
Dy .....	.70	—	—	.55	—
Eu .....	—	.52	—	.53	—
Fe .....	.52	.75	—	—	—
Hf .....	.97	—	—	—	—
K .....	—	—	.80	—	—
La .....	.75	—	—	.59	—
Lu .....	.96	—	—	—	—
Mg .....	—	.91	—	—	—
Mn .....	.90	—	—	—	—
Na .....	—	—	—	—	~.60
Ni .....	—	.74	—	—	—
Pb .....	—	—	—	.54	—
Sc .....	.56	.73	—	—	—
Sm .....	—	—	—	.84	—
Th .....	.79	—	—	.52	—
Ti .....	.73	.53	—	—	—
U .....	.85	—	—	—	—
Percent total variance....	40	21	8	7	4

stream-sediment samples from the two quadrangles. Samples with high scores for factor 1, collected from the toe of Yakataga Glacier and 12 km inland from the mouth of the Duktoth River, indicate that localized heavy-mineral concentrations continue inland from the coast. Eight of the 18 samples from the study area with anomalous gold were collected between Crooked Creek and the mouth of the Duktoth River.

Samples with high scores for factor 2 are enriched in Co-Mg-Cu-Fe-Ni-Sc and show a strong spatial correlation with both Late Jurassic intrusive bodies and outcrops of basaltic to andesitic volcanic rocks of the Wrangellia terrane. Stream-sediment samples containing as much as 12.8 percent Fe, 3.2 percent Mg, 50 ppm Co, 123 ppm Cu, 70 ppm Ni, and 45 ppm Sc cluster along the East and North Forks of the Kiagna River and throughout the Goat Creek watershed. Samples with high factor 2 scores scattered along the west side of Logan Glacier suggest that the source for the element enrichments extends perhaps 25 km east of Goat Creek. Many of the 30 sediment samples in this belt also contain anomalous amounts of Ag, As, Au, Cr, Mn, Ti, and V. A sediment sample, likely collected from medial moraine material, where Baldwin Glacier

joins Logan Glacier contained 149 ppm Cu and 186 ppm As, the latter being the highest arsenic concentration from the NURE survey.

Some of these high element concentrations in the north-central part of the Bering Glacier quadrangle reflect high geochemical background values for many elements in mafic country rocks. But many of the anomalous samples are from drainages within the Chitina Valley batholith. They hint at upstream mineral occurrences similar to the porphyry-related vein systems described by MacKevett (1976) a few kilometers to the north. A number of the stream-sediment samples with high scores for factor 2 are notably enriched in pathfinder elements for the Cu-rich veins and are the most suggestive samples of upstream metallic mineral occurrences in the Bering Glacier quadrangle. One sample on Goat Creek, 8 km below the toe of the unnamed glacier at its source, contained 50 ppm Co, 123 ppm Cu, and 10.5 percent Fe; another from 12 km below the glacier contained 49 ppm Co, 107 ppm Cu, 12.8 percent Fe, and 58 ppm As; a third from 4 km below the glacier contained 82 ppm As. It is uncertain whether these samples collected during the NURE survey were taken from Goat Creek or from tributary streams, but they most likely represent pyrite, chalcopyrite, or arsenopyrite within the area. The stream-sediment sample from the head of the North Fork of the Kiagna River contained 0.12 ppm Au. Very few samples were collected in the Chitina Valley batholith east of Goat Creek. However, the sample described above collected from near the toe of Baldwin Glacier indicates that Cu-dominant mineral occurrences likely continue far to the east. Four of the seven samples with detected silver are in the group of anomalous samples derived from the batholith, further suggesting the presence of hydrothermal mineral occurrences.

The East Fork of the Kiagna River defines the western boundary of this belt of samples with high scores for factor 2. A sample collected 2 km below the toe of the unnamed glacier at the head of the East Fork of the Kiagna River contained 108 ppm Cu, 8.8 percent Fe, 2,505 ppm Mn, 5 ppm Ag, 70 ppm As, and 0.19 ppm Au. Two other samples collected along the river were also anomalous in gold, as well as many of the siderophile and chalcophile elements. It is uncertain whether the source area for the gold-bearing sediment is also rocks of the Chitina Valley batholith, or instead may be the mafic volcanic rocks of the Wrangellia terrane and (or) rocks of the Chugach terrane near the crest of the Granite Range.

A single site with a high score for factor 2, either draining Ross Green Lake or a small, unnamed glacier immediately to the southwest, is defined by concentrations of 79 ppm Co, 178 ppm Cu, 11.7 percent Fe, 3.6 percent Mg, 137 ppm Ni, 37 ppm Sc, 2253 ppm Ba, 194 ppm Cr, 9.6 ppm Cs, 5.0 percent K, 197 ppm Rb, and 0.96 percent Ti. These are the highest concentrations of Co, Cu, Mg, Ni, Cs, K, and Rb determined for any of the 436 sediment

samples. The sample is derived from high-grade metamorphic rocks of the Valdez Group, and the reason for the multi-element anomaly is unknown.

In the Icy Bay quadrangle, two samples collected near Claybluff Point and a series of samples to the east of Icy Bay and south of Malaspina Glacier have high scores for factor 2. Additionally, 17 of the 30 samples collected in the quadrangle contained greater than 50 ppm Ni, and three of these contained 91–135 ppm Ni. Most of these samples with Ni concentrations above the 90th percentile also had Cu and Cr values above the 90th percentile. These high values for the mafic elements could be due to accumulations of mafic volcanic rocks transported down from the higher elevations of Malaspina Glacier to the east of the study area.

Samples with high scores for factor 3 contain relatively high concentrations of K, Ba, and Al and generally low amounts of Ca. This same geochemical association was described by Goldfarb (1984) for NURE stream-sediment samples collected in the Cordova quadrangle, adjacent and west of the Bering Glacier quadrangle. The association was suggested to indicate samples derived from clay-rich zones within marine metasedimentary rocks of the Orca Group. Within the Bering Glacier quadrangle, the Prince William terrane, which is composed of rocks of the Orca Group, lies in a belt across the high elevations of the Bagley Ice Field. No stream- or moraine-sediment samples were collected from this part of the quadrangle during the NURE survey. Samples with the highest scores for factor 3 are generally scattered through the medium- and high-grade metamorphic rocks of the Valdez Group in the northwestern part of the Bering Glacier quadrangle. These samples are probably derived from sedimentary facies within the turbidite sequence that have fewer mafic volcanic lithic fragments and plagioclase grains, and (or) greater amounts of potassium feldspar, muscovite, and detrital barite. A cluster of samples with high factor 3 scores from the headwaters of the Duktoth River may also be suggestive of similar facies variations within the Yakutat terrane.

An isolated stream-sediment sample with a high score for factor 3, collected from a marshy tributary to the Tsivat River, contained 5,821 ppm Ba. Pickthorn and others (1985) described barium soil anomalies and abundant barite in heavy-mineral concentrate samples from Kayak Island, a few kilometers west of the Icy Bay quadrangle. The source for the barite was shown to be glauconitic horizons in the upper part of the Poul Creek Formation of the Yakutat terrane. A similar source is feasible for the single-site anomaly 75 km northeast in the southern Bering Glacier quadrangle.

Factor 4 is dominated by a Sm-Ce-La-Dy-Pb-Eu-Th signature that reflects the distribution of some of the Tertiary felsic igneous rocks that intrude sedimentary units of the Valdez Group. Samples with high scores for factor 4 stretch along the Middle Fork of the Bremner River, the

West Fork of the Tana River, and Granite Creek. Those collected from the Middle Fork of the Bremner River are notably enriched in U and Th. Five stream-sediment samples from the watershed contained 23–31 ppm Th and 10–12 ppm U. Goldfarb and others (1989) identified similar thorium and uranium values along the South Fork of the Bremner River within the adjacent Cordova quadrangle to the west. These relative enrichments were attributed to the presence of monazite, apatite, allanite, and other accessory minerals that have likely been weathered from felsic igneous rocks.

Samples with high scores for factor 5 are enriched in As and depleted in Al and Na. They cluster in the northeast corner of the study area and in the region between the Tana River and Twelvemile Creek. In the former area, samples with highest scores have been derived from rocks of the Alexander and Wrangellia terranes along tributary valleys of the Chitina and Logan Glaciers. Samples that are most depleted in Al and Na commonly are some of the most Ca-enriched stream-sediment samples from the study area, suggesting detrital contributions from Paleozoic limestone and marble. Excluding the earlier described sample from Baldwin Glacier with 186 ppm As, most sediments collected in the northeast corner of the study area with high scores for factor 5 contain 15–33 ppm As. They show background amounts of all base and precious metals. Although the origin of the elevated arsenic values is unclear, they are not believed to reflect upstream metallic mineral occurrences. A single stream-sediment sample collected below the ridge on the north side of Logan Glacier contained high concentrations of Ba, Ce, Cs, K, La, Pb, Rb, Sb, Sm, Th, and U. The lead concentration of 39 ppm is the highest value detected from the study area. These data suggest the upstream presence of igneous rocks enriched in lithophile elements.

Anomalous samples between the Tana River and Twelvemile Creek target an area likely to contain gold-bearing quartz veins. Such veins are known to be scattered throughout medium-grade metamorphic rocks of the Valdez Group to the west of the Bering Glacier quadrangle (Goldfarb and others, 1986). V.B. Sisson (written commun., 1991) identified a closely spaced pattern of inverted isograds in rocks of the Valdez Group along the Tana River, changing from migmatite to biotite zone of the greenschist facies over only 5 km. Such a metamorphic setting is spatially associated with major gold deposits along the Juneau gold belt in southeast Alaska and at Valdez Creek to the south of the Alaska Range, and in general may be an important feature aiding in the development of mesothermal gold lodes (Goldfarb and others, 1993). Many of the stream-sediment samples collected immediately east of the Tana River contain 34–39 ppm As, likely reflecting arsenopyrite commonly found in the auriferous veins. A stream-sediment sample collected to the northeast of peak 6425 contained 62 ppm As. One stream-



sediment sample collected along the east side of the Tana River contained 0.24 ppm Au. An adjacent sample contained 201 ppm Zn, a highly anomalous value for the NURE survey and likely indicative of sphalerite associated with the precious metals.

A few additional isolated anomalies were identified through examination of single-element distribution maps. A stream-sediment sample containing 259 ppm Zn and 36 ppm As may be associated with the earlier described hydrothermal mineralization near Slender Lake. Four samples with anomalous zinc values extend along the southwestern edge of the Bering Glacier quadrangle in the Yakutat terrane. One sample collected from Canyon Creek contained 498 ppm Zn, the highest concentration from the NURE survey. These data suggest an eastward extension of sphalerite-bearing strata of the Poul Creek and Yakataga Formations delineated by Goldfarb and others (1985). Two samples with 42 ppm As were collected along the Kiktukh River in the southwestern corner of the Bering Glacier quadrangle. Five kilometers to the east a single stream-sediment sample from the Tashalich River contained 1.99 ppm Au. Since these three samples reflect glaciofluvial outwash from Bering Glacier, the anomalies could be derived from locations throughout half the study area, and these data are thus difficult to relate back to their source. One sample from the Bremner River on the western edge of the study area contained 0.28 ppm Au, indicative of the placer gold accumulations that are recognized within rocks of the Valdez Group a few kilometers downriver.

## CONCLUSIONS

Factor analysis of stream-sediment data from the NURE survey was used to aid in the delineation of geochemically anomalous samples within the Bering Glacier and Icy Bay quadrangles. Much of the variation in the geochemical data reflects differences in lithology. Samples enriched in the lithophile elements are largely derived from upstream outcrops of Tertiary granitic rocks within the Valdez Group, whereas many of the samples with high concentrations of chalcophile elements are derived from volcanic rocks of the Wrangellia terrane. Differences in content of K, Ba, and Al apparently reflect facies variations in marine sedimentary rocks. Samples derived from Paleozoic carbonate rocks in the Wrangellia and Alexander terranes are relatively enriched in As and Ca and depleted in Al and Na.

Elements enriched in refractory minerals, such as many of the rare earths, chromium, and titanium, occur in anomalous amounts in samples collected along the coastal plain. These samples delineate the area of well-studied gold and heavy-mineral beach placers of the Yakataga mining district. Two new areas, geochemically favorable for the presence of metallic mineral resources, have also

been identified through interpretation of the NURE data. Samples with anomalous values for Fe, Cu, Co, and Ni (likely indicating the presence of pyrite and chalcopyrite), as well as for gold, silver, and arsenic, are common throughout the Chitina Valley batholith. These anomalies suggest the presence of metal-bearing quartz veins associated with copper porphyry and molybdenum porphyry systems. To the east of this area, a cluster of samples with anomalous arsenic between the Tana River and Twelvemile Creek are suggested to reflect the upstream presence of mesothermal gold-bearing quartz veins within metasedimentary rocks of the Valdez Group.

Despite the fact that two new areas with favorability for the presence of metallic mineral resources have been delineated, the NURE stream-sediment data are generally inadequate for a comprehensive mineral resource assessment of the Bering Glacier and Icy Bay quadrangles. Stream-sediment samples were collected over less than half of the land area on the Bering Glacier quadrangle. Although much of the higher elevations of the quadrangle is glaciated and was ignored during the NURE survey, stream- or moraine-sediment sampling is still possible in these areas. In fact, not a single sediment sample was collected from within the Prince William terrane. Many of the collected stream-sediment samples were recovered on the more accessible large outwash plains and along major rivers, and thus their usefulness for identifying upstream sources is limited. Also, the lack of collection of heavy-mineral-concentrate samples during the NURE drainage survey further hinders its usefulness. Collection of such a sample medium, concentrating a relatively large stream volume, is critical when trying to detect a few metallic grains along a stretch of stream channel.

## REFERENCES CITED

- Brabb, E.E., and Miller, D.J., 1962, Reconnaissance traverse across the eastern Chugach Mountains, Alaska: U.S. Geological Survey Miscellaneous Geologic Investigations Map I-341, 1 sheet, scale 1:96,000.
- Eyles, N., 1990, Glacially derived, shallow-marine gold placers of the Cape Yakataga district, Gulf of Alaska: *Sedimentary Geology*, v. 68, p. 171-185.
- Gardner, M.C., Bergman, S.C., Cushing, G.W., MacKevett, E.M., Plafker, G., Campbell, R.B., Dodds, C.J., McClelland, W.C., and Mueller, P.A., 1988, Pennsylvanian pluton stitching of Wrangellia and the Alexander terrane, Wrangell Mountains, Alaska: *Geology*, v. 16, p. 967-971.
- Goldfarb, R.J., 1984, A preliminary geochemical interpretation of the Chugach Wilderness, southern Alaska, in Coonrad, W.L., and Elliott, R.L., eds., *The United States Geological Survey in Alaska—Accomplishments during 1981*: U.S. Geological Survey Circular 868, p. 89-92.
- Goldfarb, R.J., Leach, D.L., Miller, M.L., and Pickthorn, W.J., 1986, *Geology, metamorphic setting and genetic constraints*



- of epigenetic lode-gold mineralization within the Cretaceous Valdez Group, south-central Alaska, in Keppie, J.D., Boyle, R.W., and Haynes, S.J., eds., *Turbidite-hosted gold deposits: Geological Association of Canada Special Paper 32*, p. 87-105.
- Goldfarb, R.J., O'Leary, R.M., Sutley, S.J., and Tripp, R.B., 1989, Geochemical survey of the Cordova and Middleton Island 1° × 3° quadrangles, south-central Alaska: U.S. Geological Survey Bulletin 1865, 32 pages, 3 plates.
- Goldfarb, R.J., Snee, L.W., and Pickthorn, W.J., 1993, Orogenesis, high-T thermal events, and gold vein formation within metamorphic rocks of the Alaskan Cordillera: *Mineralogical Magazine*, in press.
- Goldfarb, R.J., Tripp, R.B., and Smaglik, S.M., 1985, Geochemical map showing distribution of barite, galena, and sphalerite within the Chugach National Forest, Alaska: U.S. Geological Survey Miscellaneous Field Studies Map 1645-C, scale 1:250,000.
- Hudson, Travis, and Plafker, George, 1982, Paleogene metamorphism of an accretionary flysch terrane, eastern Gulf of Alaska: *Geological Society of America Bulletin*, v. 93, p. 1280-1290.
- Jansons, Uldis, Hoekzema, R.B., Kurtak, J.M., and Fechner, S.A., 1984, Mineral occurrences in the Chugach National Forest, southcentral Alaska: U.S. Bureau of Mines Mineral Land Assessment Report 5-84, 43 p., 2 map sheets.
- Jones, D.L., Silberling, N.J., Coney, P.J., and Plafker, George, 1987, Lithotectonic terrane map of Alaska (west of the 141st meridian): U.S. Geological Survey Miscellaneous Field Studies Map, MF-1874-A, scale 1:2,500,000.
- Koschmann, A.H., and Bergendahl, M.H., 1968, Principal gold-producing districts of the United States: U.S. Geological Survey Professional Paper 610, 283 p.
- Los Alamos National Laboratory, 1983, The geochemical atlas of Alaska: Grand Junction, CO, Bendix Field Engineering Corp. Report GJBX-32(83), 57 p.
- MacKevett, E.M., Jr., 1976, Mineral deposits and occurrences in the McCarthy quadrangle, Alaska: U.S. Geological Survey Miscellaneous Field Studies Map MF 773-B, scale 1:250,000.
- Maddren, A.G., 1914, Mineral deposits of the Yakutat district: U.S. Geological Survey Bulletin 592, p. 119-153.
- Moffit, F.H., 1914, Geology of the Hanagita-Bremner region, Alaska: U.S. Geological Survey Bulletin 576, 56 p.
- , 1918, The upper Chiutna Valley, Alaska, with a description of igneous rocks: U.S. Geological Survey Bulletin 675, 82 p.
- , 1954, Geology of the Prince William Sound region, Alaska: U.S. Geological Survey Bulletin 989-E, p. 225-310.
- Moxham, R.M., and Nelson, A.E., 1952, Reconnaissance for radioactive deposits in south-central Alaska: U.S. Geological Survey Circular 184, 14 p.
- Nelson, S.W., Miller, M.L., Barnes, D.F., Dumoulin, J.A., Goldfarb, R.J., Koski, R.A., Mull, C.G., Pickthorn, W.J., Jansons, Uldis, Hoekzema, R.B., Kurtak, J.M., and Fechner, S.A., 1984, Mineral resource potential map of the Chugach National Forest, Alaska: U.S. Geological Survey Miscellaneous Field Studies Map MF-1645-A, scale 1:250,000.
- Pickthorn, W.J., Goldfarb, R.J., O'Leary, R.M., Butley, S.J., and Weaver, S., 1985, Kayak Island—Analysis of a geochemical anomaly, in Bartsch-Winkler, S., and Reed, K.M., eds., *The United States Geological Survey in Alaska—Accomplishments during 1983: U.S. Geological Survey Circular 945*, p. 82-83.
- Plafker, George, 1987, Regional geology and petroleum potential of the northern Gulf of Alaska continental margin, in Scholl, D.W., Grantz, A., and Vedder, J.G., eds., *Geology, and resource potential of the continental margin of western North America and adjacent ocean basins: Houston, Circum-Pacific Council for Energy and Mineral Resources Earth Sciences Series 6*, p. 229-268.
- Plafker, George, Jones, D.L., and Pessagno, E.A., Jr., 1977, A Cretaceous accretionary flysch along the Gulf of Alaska margin, in Blean, K.M., ed., *U.S. Geological Survey in Alaska—Accomplishments during 1976: U.S. Geological Survey Circular 751B*, p. B41-B43.
- Plafker, George, Nokleberg, W.J., and Lull, J.S., 1989, Bedrock geology and tectonic evolution of the Wrangellia, Peninsular, and Chugach terranes along the Trans-Alaska Crustal Transect in the Chugach Mountains and southern Copper River Basin, Alaska: *Journal of Geophysical Research*, v. 94, no. B4, p. 4255-4295.
- Reimnitz, Erik, and Plafker, George, 1976, Marine gold placers along the Gulf of Alaska margin: U.S. Geological Survey Bulletin 1415, 16 p.
- Saleeby, J.B., 1983, Accretionary terranes of the North American Cordillera: *Annual Review of Earth and Planetary Sciences*, v. 15, p. 45-73.
- Singer, D.A., and MacKevett, E.M., Jr., 1977, Mineral resources of the McCarthy quadrangle, Alaska: U.S. Geological Survey Miscellaneous Field Studies Map 773-C, scale 1:250,000.
- Sisson, V.B., Hollister, L.S., and Onstout, T.C., 1989, Petrologic and age constraints on the origin of a low-pressure/high-temperature metamorphic complex, southern Alaska: *Journal of Geophysical Research*, v. 94, no. B4, p. 4392-4410.
- Thomas, B.I., and Berryhill, R.V., 1962, Reconnaissance studies of Alaskan beach sands, eastern Gulf of Alaska: U.S. Bureau of Mines Report of Investigations 5986, 40 p.
- Winkler, G.R., and Plafker, George, 1981, Geologic map and cross sections of the Cordova and Middleton Island quadrangles, southern Alaska: U.S. Geological Survey Open-file Report 81-1164, 26 p.
- Youngquist, C.A., D'Andrea, R.F., Jr., Zinkl, R.J., Shettel, D.L., Jr., and Langfeldt, S.L., 1981, Uranium hydrogeochemical and stream sediment reconnaissance of the Bering Glacier NTMS quadrangle, Alaska: Grand Junction, Colorado, Bendix Field Engineering Corp. Report GJBX-189(81).
- Zinkl, R.J., Shettel, D.L., Langfeldt, S.L., Youngquist, C.A., and D'Andrea, R.F., Jr., 1981, Uranium hydrogeochemical and stream sediment reconnaissance of the Icy Bay NTMS quadrangle, Alaska: Grand Junction, Colorado, Bendix Field Engineering Corp. Report GJBX-186(81).

Reviewers: John E. Gray and Cliff D. Taylor

# NEWLY DISCOVERED MOLYBDENITE OCCURRENCES AT DORA BAY, PRINCE OF WALES ISLAND, SOUTHEAST ALASKA, AND PRELIMINARY SCANNING ELECTRON MICROSCOPE STUDIES

By John Philpotts, Cliff Taylor, John Evans, and Poul Emsbo

## ABSTRACT

Molybdenite was discovered at two sites that are located 3 km apart in the border facies of a syenite pluton at Dora Bay, Prince of Wales Island, southeast Alaska. At one of the localities, molybdenite is visible in a 5-m-wide zone; analyses of two molybdenite-rich bulk samples from this zone yielded 0.5 and 1.2 percent molybdenum, respectively. Rock samples were further studied using a scanning electron microscope with X-ray analysis capability. Chlorine-rich minerals occur at both localities. Sodic metasomatism and veining by iron-bearing minerals appear to have preceded potassic metasomatism and molybdenite crystallization. A mineral that contains potassium, iron, and molybdenum may offer insights on the transport of molybdenum and the characteristic association of potassic metasomatism with molybdenite.

## INTRODUCTION

In support of the U.S. Geological Survey's mineral resource assessment of Alaska, enrichments of rare earths and other lithophile trace elements associated with alkalic igneous activity in the vicinity of Dora Bay, Prince of Wales Island, southeast Alaska, were examined for several days in the summers of 1991 and 1992. In 1992 we noted molybdenite in a fragment of the gravel used to surface the logging road on the mountain on the west side of Dora Bay. The road gravel at this locality was further distinguished by a reddish coloration and by an increase in count rate on the scintillometer indicative of an increase in radioactivity. An employee at the local logging camp showed us the putative source of the road gravel, a small pit having both reddish rocks and increased scintillometer counts. Examination of the face of the pit revealed molybdenite in situ. As far as we are aware, this is the first report of a molybdenite occurrence in the immediate vicinity of Dora Bay. We refer to this occurrence as "Holly Moly" (hereafter HM). Following the HM discovery, examination of other rock samples

from the area resulted in the identification of molybdenite from a site 3 km to the south-southeast in a cliff face rising above the western shore of Dora Lake; we refer to this occurrence as "Cliff Moly" (CM).

The HM occurrence is located on the west side of Dora Bay at about lat  $55^{\circ}11'54''$  N. and long  $132^{\circ}15'45''$  W. at an elevation of about 265 feet; the CM site is at a known occurrence of eudialyte and is located at about  $55^{\circ}10'23''$  N.,  $132^{\circ}14'53''$  W. at an elevation of about 875 feet (figs. 1, 2). Both HM and CM lie within the Tongass

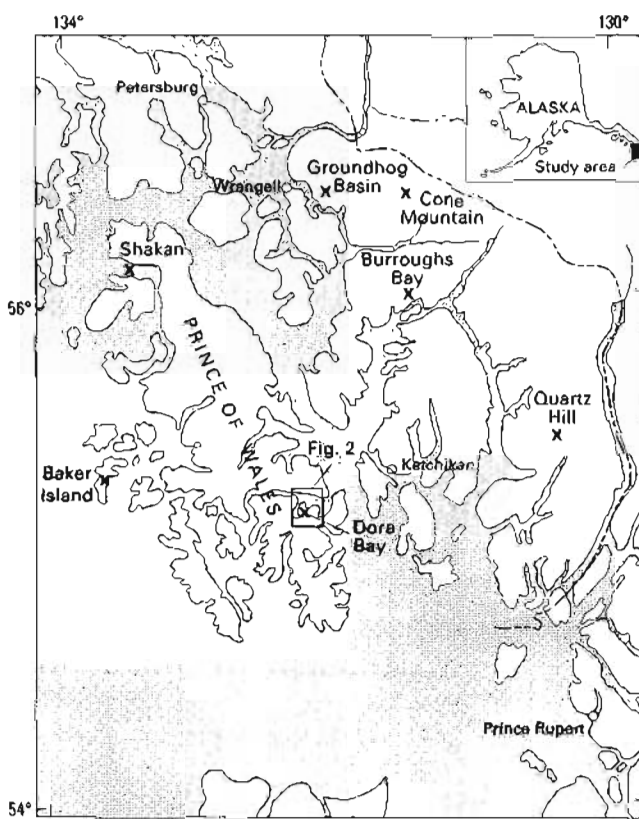


Figure 1. Dora Bay molybdenite localities on Prince of Wales Island in relation to known molybdenite localities ("X") in southeast Alaska. Area covered by figure 2 is outlined at center.

National Forest in an area designated as Land Use Designation III ("management for a variety of uses") in the U.S. Department of Agriculture Forest Service land management plan (1991). Apparently surface rights in the vicinity of HM were conveyed to the Kootznoowoo Native Corporation and Sealaska Native Corporation owns the subsurface rights in the area (written communication, Rick Harris, Vice President, Mineral Resources, Sealaska Corporation, Juneau, June 28, 1991).

This paper reports the molybdenite occurrences and the results of subsequent preliminary laboratory studies made on rock samples collected there. The report, based on only a few hours of field study at the two sites and on limited laboratory investigations, is necessarily of a rudimentary, preliminary, and speculative nature; nevertheless, a number of features of potential interest have come to light.

## GEOLOGIC FRAMEWORK

Prince of Wales Island lies within the Alexander tectonostratigraphic terrane (Brew and others, 1991). In the vicinity of Dora Bay, the Wales Group, composed of metamorphosed pre-Middle Ordovician sedimentary and volcanic rocks (Eberlein and others, 1983), is intruded by an igneous pluton (fig. 2). The highest resolution regional mapping in the area is that of Herreid and others (1978); however, their coverage extends eastward only to the westernmost margin of the intrusion, which they mapped as a part of their "granodiorite and related rocks (potassium-argon age  $102 \pm 3.0$  m.y.)." The map of Eberlein and others (1983) displays the complete intrusive body, which

is classified as Paleozoic and (or) Mesozoic nepheline-eudialyte-bearing syenite. Gehrels and Berg (1984) tentatively classified the body as Late Pennsylvanian and (or) Early Permian syenite. The HM occurrence is located in the northeast border zone of the intrusive body, which extends for about 4 km in its longest exposed dimension from northwest to southeast; the CM occurrence is located near the southeast extremity of the body (fig. 2).

The outline of the intrusion as shown in figure 2 is based on the map of Eberlein and others (1983). We have confirmed the location of the contact in the field in only a few places. The representation of the easternmost contact has been modified in light of the sketch-map presented by Barker and Mardock (1990). It is not clear whether the interfingering at the eastern margin is due to dike- or sill-like extensions, to faulting, or to topographic intersections. Outcrop exposure tends to be good only along the shoreline, at higher elevations, and on cliff faces.

## THE HOLLY MOLY AND CLIFF MOLY OCCURRENCES

The HM molybdenite-bearing samples were collected on the 5-m-high southern face of a roughly circular pit, that is about 30 m in diameter. The rocks in the pit are cut by a large number of joints and shears including a strong near-vertical set and several subhorizontal sets. The molybdenite appears to be concentrated on shears having intermediate dip. Because of the complexity of the fracture set and the limited field examination, we do not as yet have a good understanding of fracture history and its relation to the mineralization. A siliceous, eastward-dipping pegmatite, about 8 cm wide with a selvage of fluorite and biotite, appears to cut, and hence postdate, the molybdenite mineralization. Abundant visible molybdenite was noted in outcrop in a zone extending for about 5 m in an easterly direction from the vicinity of the pegmatite vein. Much of the pit face is discolored by tan- and rusty-weathering products that obscure the nature of the rocks present and their relationships. The molybdenite occurs in a gray rock that lacked features whereby it could be easily classified in the field. The western margin of the pit is defined by a well-jointed rock that readily breaks down into cubes 2 to 3 cm across with fully weathered dark surfaces. This rock is a breccia with a continuum of clast sizes ranging up to several centimeters across and little, if any, apparent porosity. The most visible of the clasts are of a distinctive fine-grained red lithology. Clasts of melanocratic syenite and other gray clasts are less well defined against a fine-grained gray matrix. The lack of sharp contacts on some of these clasts suggests that the breccia may have been heated. The eastern margin of the pit is composed of a dark porphyritic latite(?) with mafic phenocrysts and a bleached white albitized rock, both of which have weathered surfaces stained by iron oxide.

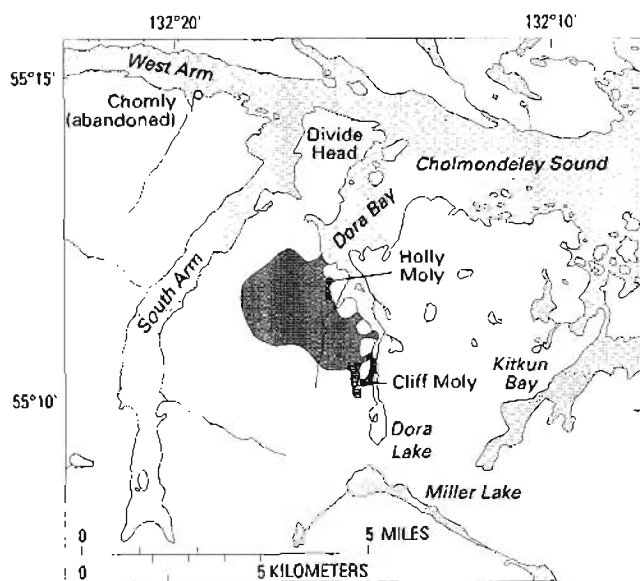


Figure 2. Locations of Holly Moly and Cliff Moly molybdenite occurrences at margin of Dora Bay syenite pluton (shaded area), Prince of Wales Island.

The CM site is located in a setting similar to that of HM at the boundary of the intrusive body. At the CM site, abundant syenite and pegmatitic syenite, some bearing eudialyte [ $\text{Na}_4(\text{Ca,Fe})_2\text{ZrSi}_6\text{O}_{17}(\text{OH,Cl})_2$ ], have thermally metamorphosed rocks of the Wales Group. Some of the igneous rock now occurs as a thick layer of gneiss. Breccia and porphyritic rocks lithologically similar to those at HM also occur at CM. The molybdenite was found in a rust-stained white rock that bears a striking resemblance to the white albite-rich rock at HM; they might well be the same border unit. The rock contains nebulous gray patches and may represent a more basic igneous rock that has been largely metasomatized to albite. Although not very abundant in the CM rock, the molybdenite is quite visible inasmuch as it occurs as reflective plates on natural fractures. The molybdenite was tentatively identified in this rock sample in the field, and its occurrence was subsequently corroborated by scanning electron microscopy.

Molybdenite is more abundant at HM. It occurs in three textural forms: disseminated, in clots, and in veins. Because these forms occur within the same rock, they may have originated at roughly the same time. Molybdenite is most easily seen in association with calcite in the clots and veins. Figure 3 shows a fragment of HM rock sample CDP-92-29 that illustrates the clot form of texture, in which molybdenite occurs on planes in calcite. Although not shown in figure 3, biotite is frequently present in this association in books up to a centimeter or more across; the molybdenite plates typically have somewhat smaller dimensions. More typically in rock sample CDP-92-29, molybdenite occurs disseminated within silicate minerals. Molybdenite is not the only sulfide that is disseminated in this rock. Figure 4 shows a fairly typical fragment of CDP-92-29 that is composed largely of a gangue mineral of greasy greenish-gray color. Reflections from cleavage surfaces of this gangue mineral reveal a surprisingly large grain size, up to 5 cm across. The large grain size is accentuated in places by the occurrence, apparently within individual grains, of roughly aligned

grains and veins of iron sulfide (fig. 4). Much of the iron sulfide appears to be pyrrhotite but X-ray diffraction on a whole-rock powder of another fragment of CDP-92-29 showed no pyrrhotite, only pyrite. Molybdenite also occurs disseminated in the gray mineral. Typically, the gangue mineral appears to include either molybdenite or iron sulfide, but not both phases; only rarely does molybdenite occur immediately adjacent to iron sulfide in CDP-92-29.

## WHOLE-ROCK MOLYBDENUM ABUNDANCES

Our Dora Bay rock samples have been analyzed for molybdenum by inductively coupled plasma optical-emission spectroscopy (ICP). A bulk sample (HM 92DB-17), containing the highest observed grade of vein molybdenite, yielded 1.2 percent molybdenum. Another bulk sample was prepared so as to be representative of HM rock CDP-92-29, which contains abundant disseminated molybdenite; separate portions of the same powdered sample of CDP-92-29 were analyzed by independent ICP techniques and yielded 0.38 and 0.54 percent molybdenum, respectively. Both of these rock samples were selected on the basis of their abundant molybdenite content, which is well within ore grade. No channel sample was collected through the mineralized zone owing to time constraints.

Analyses we have obtained on more than 50 other rock samples from the Dora Bay area yielded molybdenum abundances that are two orders of magnitude less than those of the two high-grade samples. Indeed, half of our rock samples were below the ICP detection limit of 1 part per million (ppm) by weight of molybdenum. It might be noted that the high-grade samples were prepared for



Figure 3. Fragment of HM rock sample CDP-92-29. Molybdenite occurs throughout the fragment. At bottom center, molybdenite occurs on planes in calcite. Sample is approximately 3 cm across. Photograph by Lewis V. Thompson

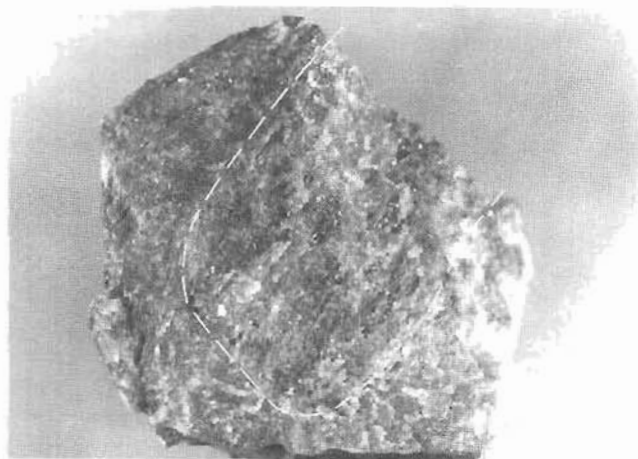


Figure 4. Fragment of HM rock sample CDP-92-29. Iron-sulfide grains in the center of the fragment, showing parallel orientation to the upper right, are included within a large grain of scapolite (dashed area) that has the same orientation of its long dimension. Sample is 5 cm across. Photograph by Lewis V. Thompson.

analysis after the other samples in order to minimize contamination. Of the other rock samples from the HM pit itself, bulk analyses of all but the albitized sample show measurable molybdenum, although all have less than 10 ppm; no molybdenite was noted in preliminary study of any of these samples. Only two of our rock samples from the Dora Bay area, other than the high-grade samples, had molybdenum contents exceeding 10 ppm, and then only barely (11 ppm). One of these was a sample of country rock with reddish coloration. The other was the albitized rock sample from CM in which molybdenite had been tentatively identified by visual examination. Interestingly, Barker and Mardock (1990), in a study of rare-earth enrichments in the Dora Bay area, reported their highest molybdenum value of 51 ppm from a sample collected at a site located at the narrows of Dora Lake close to the CM locality.

## SCANNING ELECTRON MICROSCOPY

Many of the features noted in hand specimen receive corroboration and amplification when viewed under a scanning electron microscope (SEM). Samples were hand polished on fresh abrasive paper and then carbon coated. The SEM used is an Etec Autoscan with a Kevex Delta Microanalysis Energy-Dispersive System (EDS) and Quantex software. Operating conditions of the SEM were accelerating voltage of 30 kV, filament current of about 125  $\mu$ A, and working distance of 14–18 mm. Output was in the form of backscattered-electron images, in which grains of higher average atomic number appear brighter, and X-ray spectra plots of relative intensity versus energy. Spectral assignments were made using the system's integral software. Because thick slabs were used in this SEM study in the interest of rapid and inexpensive sample preparation, there is very little a priori control or knowledge of what is being analyzed at depth below the surface of the slab. Some of the EDS spectra are no doubt reflecting compositional data from more than one mineral; however, consistency in ratios of peak intensities for analyses at neighboring spots can often be used as a criterion for evaluating whether a spectrum represents a single phase or a mixture of phases. Because of the lack of sampling control, we have not attempted to make the corrections to raw peak intensities necessary to convert these into quantitative element abundances. Because of the geometric constraint, the lack of corrections to the intensity data, and other problems inherent to SEM-EDS analysis (especially for elements of lower atomic number), any intimations of exact compositions must be considered tentative. It follows from this, and from the general lack of crystallographic information, that our SEM mineral "identifications" are reasonable but not definitive.

An abundant mineral in the HM molybdenite-bearing rock sample CDP-92-29 is a sodium-calcium-aluminum-

silicate containing some potassium and major amounts of chlorine. An EDS spectrum for this mineral is shown in figure 5. The mineral was tentatively identified as scapolite [ $3\text{NaAlSi}_3\text{O}_8 \cdot \text{NaCl} \cdot 3\text{CaAl}_2\text{Si}_2\text{O}_8 \cdot \text{CaCO}_3$ ]. Subsequent X-ray diffraction on a powdered whole-rock sample produced a complex spectrum, which indicated that scapolite was a likely major component. The scapolite appears to be partially altered and replaced by other phases. Under the SEM, the scapolite has a birds-eye appearance and is cut by numerous intersecting veins of both calcite and potassium feldspar. Figure 6 is a backscattered-electron image of altered and veined scapolite (dark gray). The area above and to the left of the scapolite consists largely of patches of potassium feldspar, biotite, and residual areas of scapolite. A number of accessory minerals can be seen in the figure, including sphene, apatite, and zircon; sphalerite and iron sulfide occur elsewhere in the sample. In the upper left corner of the scapolite grain in figure 6 is a small group of molybdenite grains (white) set within a calcite vein (gray). This indicates that some, at least, of the molybdenite is later in the paragenetic sequence than the scapolite.

Molybdenite also occurs as lenses and sheets, tens of micrometers thick and millimeters in length, composed of polycrystalline molybdenite in a matrix of potassium feldspar (fig. 7); the molybdenite is presumed to be filling small fractures. The molybdenite appears to be quite pure. The EDS spectrum reveals only molybdenum and sulfur peaks and trace peaks for silicon and aluminum. Although the latter are very small, they do appear consistently, and it may be that a fine-grained aluminum silicate (feldspar?) was crystallizing intermixed with the molybdenite. Potassium feldspar, in sizable grains, is a common associate of the molybdenite. It is usually quite pure, without any detectable sodium or calcium. Small amounts of pure albite also occur, but this mineral is at least an order of magnitude less abundant. The apparent lack of measurable solid solution in these feldspars suggests low-temperature crystallization. The accessory phases sphene, pyrrhotite, and sphalerite appear to be more abundant in potassium feldspar-rich regions. Pyrrhotite was not found immediately adjacent to molybdenite. Biotite is common, but irregularly distributed; EDS spectra show that the biotite contains minor titanium, manganese, and fluorine.

Figure 8A is a low-magnification backscattered-electron image of a polished slab of a CM rock sample. In the lower part of the figure, a patchwork iron sulfide (pyrite?) vein crosses a largely albitic (dark gray) matrix. Within this vein, many of the grains are rimmed by or composed entirely of iron oxide (or hydroxide or carbonate, all anions that cannot be readily distinguished in our SEM work). Oxidation of pyrite is a probable cause for the rust stains on this rock. The fine vein (v2) toward the top of the figure is also composed of iron oxide or carbonate. Figure 8B, a closeup of the central portion of this vein, shows a molybdenite stringer (white) cutting both the al-

bite and vein v2. This molybdenite is as pure as that at HM except that all of the analyzed CM molybdenites have a small trace of iron in their spectra. Figure 8A shows molybdenite slivers occurring with v2 on the right side of the photograph, but forming a discontinuous vein above v2 on the left side of the photograph. The largest patch of molybdenite (toward the left) occurs in association with potassium feldspar like the association in HM rock sample CDP-92-29 (fig. 7). Immediately above the molybdenite grains is a patchy (light gray) vein of quite pure potassium feldspar; this vein suggests that the rock may have undergone some potassic metasomatism.

Molybdenite also occurs in CM rock sample 92DB-05C, on a natural fracture surface. This surface was examined in its natural state and it may be more likely than a polished surface to contain weathering products. Under the SEM, the molybdenite appears to occur, typically, on an iron-silicate coated substrate of albitic composition. The

albitic areas in this sample are quite interesting. Two smooth albitic areas (fab) shown in the upper left and lower right of figure 9A appear to have been in close contact with molybdenite. Figure 9A shows molybdenite draping over the right side of the upper smooth area; the lower smooth area laps up on molybdenite on the left side and shows central molds that were almost certainly caused by molybdenite plates. The smooth areas are composed largely of aluminum silicate, but both also contain iron. Based on three analyses each, these albitic areas appear to be fairly uniform in composition (and hence probably not mixtures), but they differ from each other in that the upper area (fig. 10 spectrum) is a little richer in iron than the lower area. Compared with the EDS spectrum typical of albite, the spectra of both smooth areas show reduction of aluminum intensity, and even more so of sodium intensity, relative to silica intensity, and we attribute this to absorption by the iron component. Although not quantitative, the

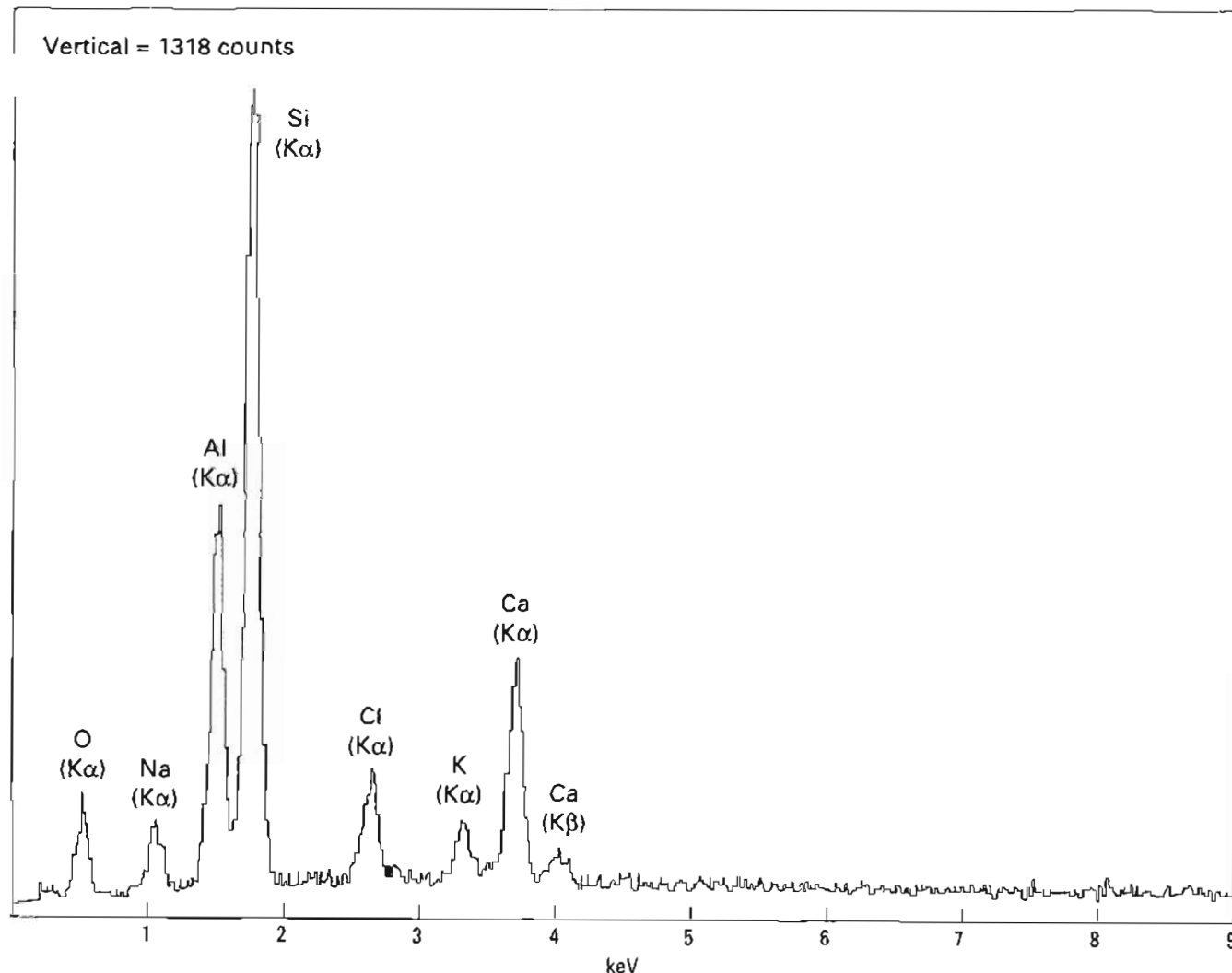


Figure 5. X-ray spectrum of relative intensity versus energy for scapolite in HM rock sample CDP-92-29. Significant peaks are labeled in terms of major contributing X-ray lines.



estimated several percent of iron indicated for this phase would be most unusual for albite, especially a presumed low-temperature albite, inasmuch as pegmatitic albites typically have less than 0.01 percent iron (Smith, 1983). Possibly the phase is a quenched iron-bearing glass, but then its lack of potassium might seem puzzling.

In fact, a potassic mineral is present on the smooth areas on the natural fracture surface of CM rock sample 92DB-05C where it occurs as (light gray) hexagonal plates (fig. 9A). It is even more apparent in the gray area at the lower left of figure 9A. The area, shown enlarged in the upper right of figure 9B, can be seen to consist of two phases. The darker areas showing between the hexagons in figure 9B are of (iron-free) albite composition (ab). The lighter phase (kim) contains abundant potassium (fig. 11). Over a range of a factor of five in potassium peak intensity, Fe/K is acceptably invariant (3 to 3.6) for 9 of 12 analyses. Similarly, eight analyses gave Mo/K peak intensities from 2.1 to 3.1. In contrast, Si/K intensities ranged from 1 to 27 and Si/Al intensities are close to those for albite. We conclude that the spectrum shown in figure 11 likely represents a mixture of albite and a non-silicate mineral containing potassium, iron, and molybdenum. Because the readily observed X-ray peaks for molybdenum and sulfur have overlapping energies that cannot be easily distinguished, the mineral could be a sulfide. It also could be an oxide or hydroxide among other possibilities.

Ferrimolybdate is a known weathering product, and there are several potassic molybdates. This raises the question of the origin of this hexagonal phase. Because we are analyzing a natural, unpolished surface, the phase almost certainly represents some kind of surficial deposit or reaction. The hexagons appear to be oriented parallel to the surface and nucleation appears to have dominated crystal growth kinetics (that is, there are numerous small crystals). If they are weathering products, a source of potassium would be required, and this could be the potassium feldspar contained in the bulk rock. Another possibility is that this potassium-iron-molybdenum phase may have crystallized (perhaps subsolidus) as part of a system quenched in a manner similar to that ascribed above to the conjectured iron-albite glass.

## DISCUSSION

The Dora Bay molybdenite occurrences are only showings, but molybdenite occurs here in similar settings at two localities that are 3 km apart; readily visible molybdenite occurs over a width of about 5 m in the HM pit face; and analyses of two bulk HM samples yielded 0.5 and 1.2 percent molybdenum, respectively. These discoveries offer at least some prospect of a molybdenite deposit in the vicinity. At our current level of understanding, the



Figure 6. Scanning electron microscope backscattered-electron image of HM rock sample CDP-92-29. A grain of scapolite (sc) is veined by calcite (ca) and potassium feldspar (or). Molybdenite (mo) occurs within a calcite vein in the upper left corner of the scapolite grain. Accessory minerals include sphene (sph), apatite (ap), and zircon (zt). Field of view is approximately 2 mm.

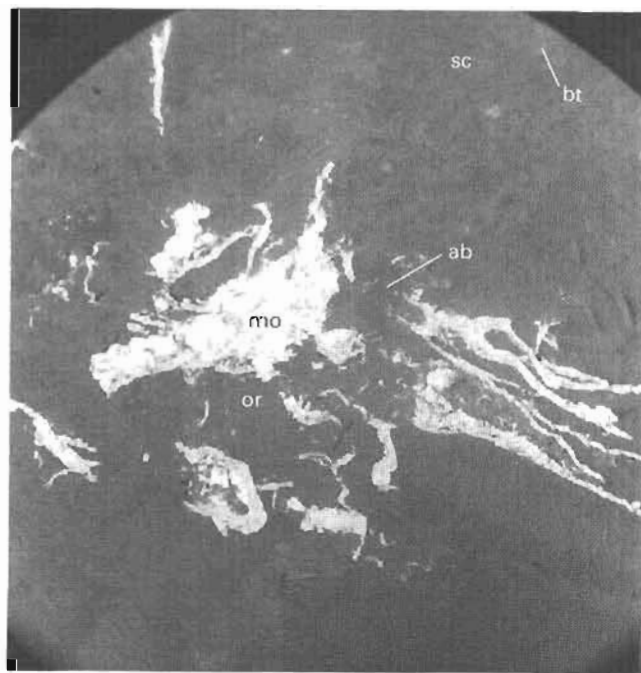
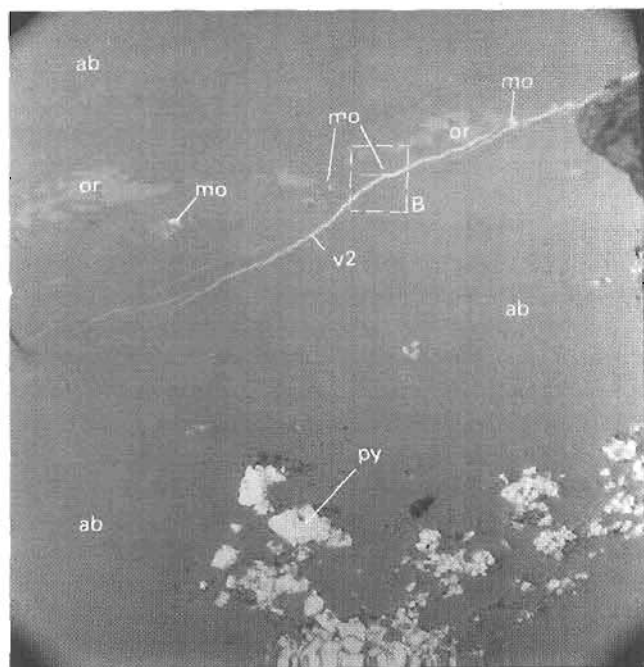
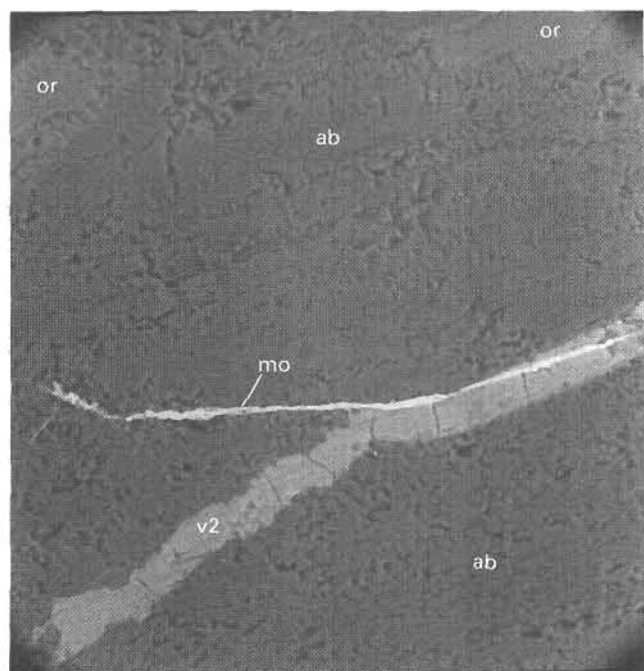


Figure 7. Scanning electron microscope backscattered-electron image of HM rock sample CDP-92-29. Molybdenite (mo) lenses and veins occur in potassium feldspar (or) and albite (ab). Mottled mineral at the top of the photograph is scapolite (sc), which is adjacent to a grain of biotite (bt). Field of view is approximately 8 mm.



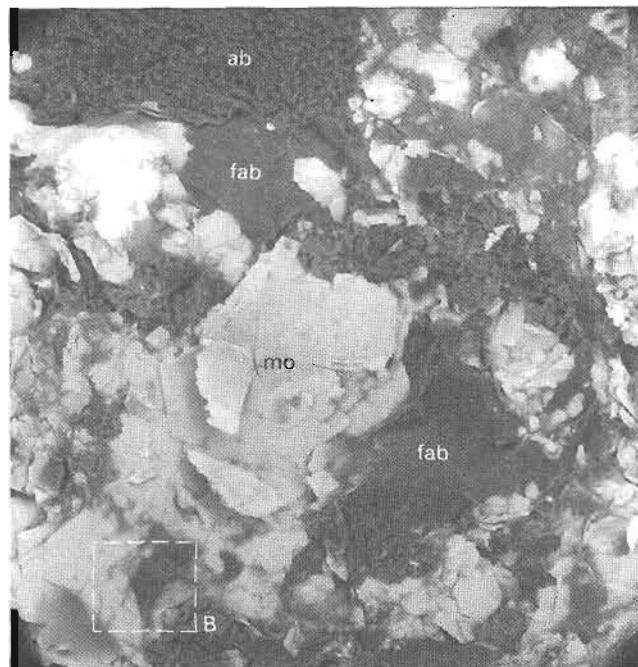


A

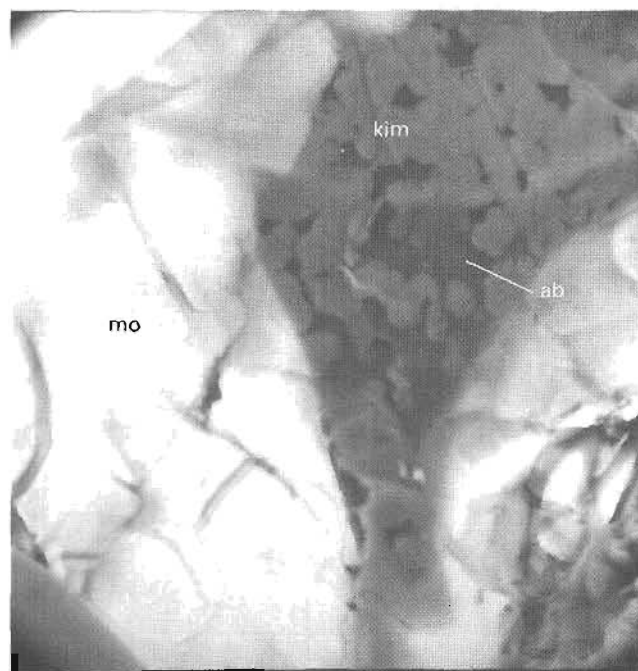


B

Figure 8. Scanning electron microscope backscattered-electron images of CM rock sample 92DB-05C. A, Albite (ab) is the dominant mineral. Grains at bottom of image are partially oxidized pyrite (py). At the top of the image a discontinuous vein of potassium feldspar (or) lies above a discontinuous vein of scattered molybdenite (mo) which intersects a vein of iron oxide or carbonate (v2). Field of view is approximately 4 mm. B, Enlargement of outlined area of A. Molybdenite vein (mo) cuts both the albite matrix and vein v2. Field of view is approximately 0.4 mm.



A



B

Figure 9. Scanning electron microscope backscattered-electron images of a natural fracture surface of the CM rock sample 92DB-05C. A, Smooth albitic patches (fab) occur in the upper left and the lower right of the image adjacent to pitted albitic areas (ab) and plates of molybdenite (mo). Field of view is approximately 1 mm. B, Enlargement of outlined area in A. Molybdenite plates (mo) surround an area in which a phase of albitic composition (ab) alternates with a mineral (kim) containing potassium, iron, and molybdenum. Some grains of the latter mineral have hexagonal form. Field of view is approximately 0.1 mm.

Dora Bay occurrences as yet show no clear genetic affinity with any of the major molybdenite deposit types (White and others, 1981; Cox and Singer, 1986). Nevertheless, HM does contain fluorine-bearing mica and late-stage vein fluorite, and both HM and CM display the potassic metasomatism that is a characteristic of molybdenite ores.

There are a number of interesting aspects concerning the iron phases in our molybdenite-bearing samples. One of these is the crude alignment of iron sulfide in scapolite grains in HM rock sample CDP-92-29 (fig. 4). The orientation appears to be controlled by the crystal structure of the scapolite, although a small-scale localized stockwork of parallel fractures might be another possibility. Other minerals might be similarly aligned, but not as abundant or as readily visible as the sulfide. The sulfate ion can be a component of scapolite, and it is conceivable that the pyrrhotite represents reduction and reaction of such sulfate with iron; however, sulfur was not detected in our scapolite analyses (fig. 5). The pyrrhotite does not occur in the

molybdenite-calcite-biotite veins that formed late in the evolution of this rock.

In the CM rock sample, the crosscutting relation shown in figure 8B indicates that the molybdenum mineralization also postdates at least some of the veining by iron-bearing minerals in this rock. This relation may also be manifested in the natural fracture sample, where we interpret some of the molybdenite as forming on top of iron silicate. Because CM and HM are in a generally similar structural setting at the margin of the same intrusion, it is tempting to attribute the similar features in both rock samples to the same earlier introduction of iron and later molybdenite mineralization.

Problems to be considered in working toward an explanation of the origin of the Dora Bay occurrences include accounting for the enrichment of molybdenum relative to its low levels in local igneous rocks and relative to low observed base-metal abundances. Preliminary examination of chemical analyses of the low-grade rock samples indicates

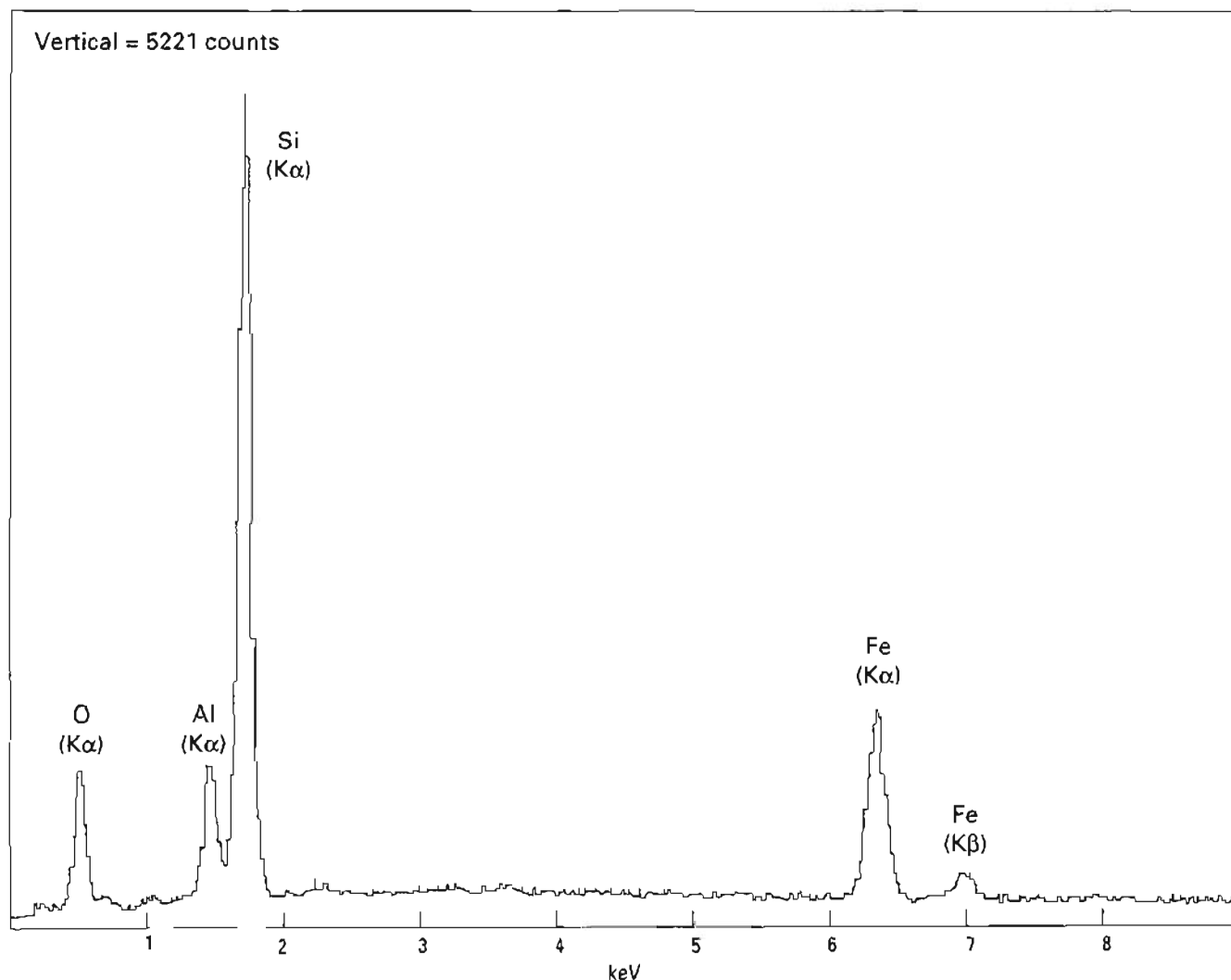


Figure 10. X-ray spectrum of the upper smooth area (fab) shown in figure 9A. Iron is a significant component. The Si/Al peak ratio is higher than that typical of pure albite.

that there are positive correlations of molybdenum with niobium and tungsten abundances. These correlations would be consistent with enrichment of these elements by igneous fractionation; further igneous fractionation, therefore, offers at least a partial possible explanation for the molybdenum enrichment. Molybdenum tends to be an incompatible element in igneous differentiation and does not appear to be strongly fractionated into normal aqueous fluids (Candella and Holland, 1986). For this reason igneous differentiation can play an important role in the enrichment of molybdenum. The experimental study of Isuk (1976) (although lacking aluminum) indicated that (1)  $\text{MoS}_2$  is abundantly soluble in low-temperature aqueous peralkaline melts, particularly potassic melts, and their coexisting vapor, and (2) introduction of chloride or carbonate ions dramatically decreased  $\text{MoS}_2$  solubility. The presence of scapolite at HM and of eudialyte at CM give ample evidence of chlorine-rich fluids. Perhaps a chlorine-rich aqueous phase separated prior to molybdenum enrichment in the magma. The

relative timing of chlorine metasomatism and molybdenite mineralization is known at HM and would be consistent with such a scenario. Based on Isuk's (1976) study, there is a possibility that reaction of a fluid with chlorine- or carbonate-bearing minerals could cause molybdenite precipitation. Both anions occur in the HM high-grade rock and, indeed, both may occur within the mineral scapolite. In this connection, the presence of carbonate and the flatness of the planes in the carbonate on which the molybdenite occurs in HM rock sample CDP-92-29 (fig. 3) indicate that the molybdenite was carried by fluids of neutral or alkaline pH. An alternative to a chloride- or carbonate-induced precipitation scenario might involve molybdenum remaining dissolved in a fluid of low sulfur content until sulfur fugacity was increased via reaction with pyrrhotite- or pyrite-rich rocks such as found at HM and CM. Finally, there is the possibility of molybdenite deposition owing to falling temperature or release of pressure rather than to chemical reaction.

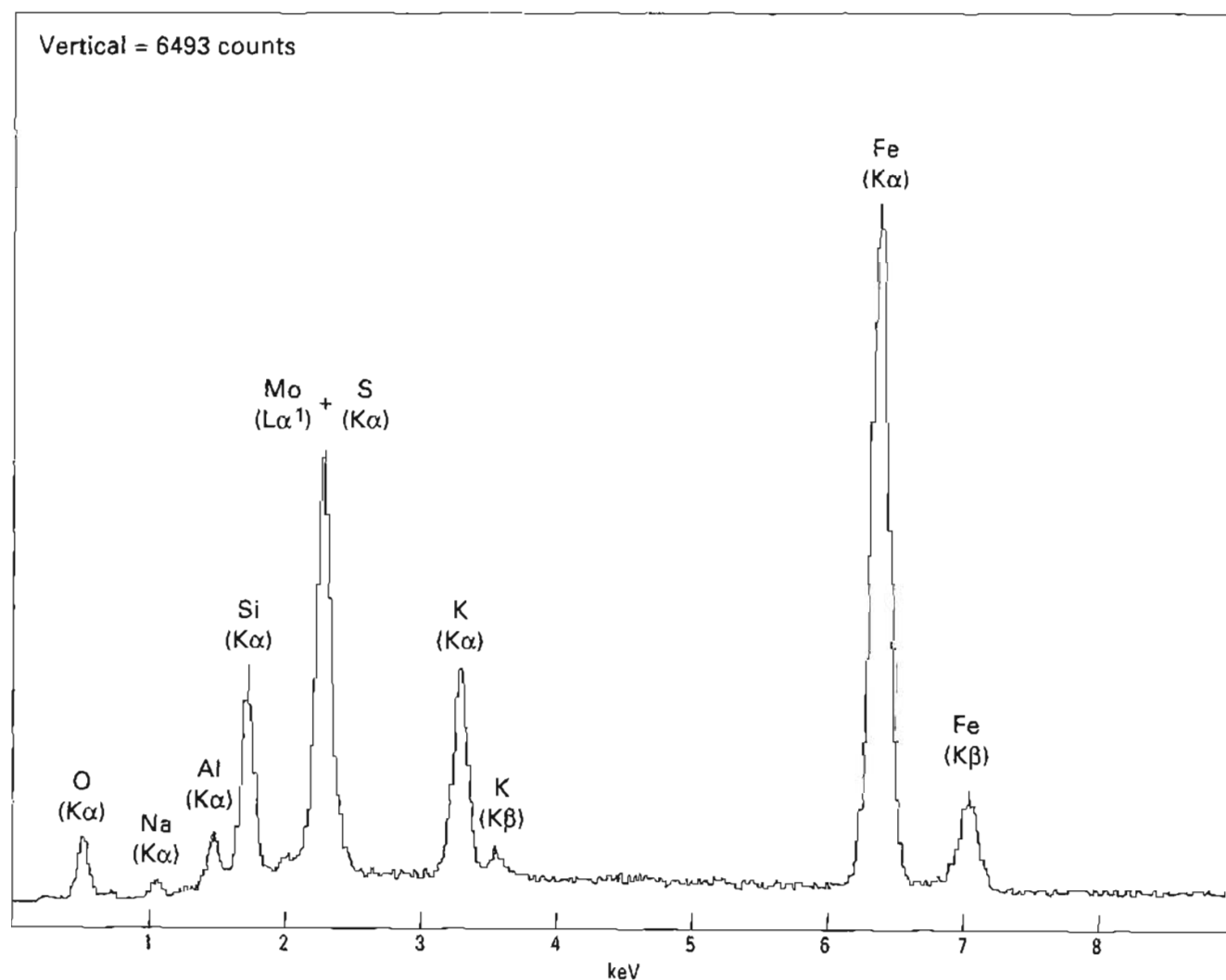


Figure 11. X-ray spectrum of the hexagonal mineral (kim) in the two-phase region shown in figure 9B.

There is also the question of the potassic metasomatism that has affected both HM and CM rock samples and which is characteristic of molybdenite deposits in general. The fact that potassic fluids can carry considerable molybdenum is likely a part of the explanation. Additional factors seem to be required to explain the general co-location of the metasomatism and the molybdenite. These factors may relate to the total volume available of enriched fluid or to rapid crystallization owing to the steepness of gradients in intensive or extensive variables within a constrained structural setting. Crystallization of any extensive portion of a fluid as molybdenite or as other minerals might itself be a factor owing to a consequent increase in volatile content in the remaining fluid. The SEM results that were reported above for the potassic phase occurring on the natural fracture surface permit the additional speculation that molybdenum might be transported as a potassic complex (for example, a K-Fe-Mo complex). If this were the case, then deposition of molybdenite would also free potassium; such released potassium might be responsible for the potassic metasomatism in the immediate depositional environment of the molybdenite.

**Acknowledgments.**—Jim Barker (Interior Development, Fairbanks) provided field guidance in 1991 to rare-earth localities in the Dora Bay area. Dave Taylor provided field assistance in 1992 as a U.S. Geological Survey volunteer. Gary McWilliams captained the research vessel *HYAK* and also made mineralogic contributions to the investigation. The X-ray diffraction confirmation of scapolite was made by Daniel Webster. Short order chemical analyses were provided by M.W. Doughten, P.H. Briggs, D.L. Fey, J.S. Mee, and D.F. Siems.

## REFERENCES CITED

- Barker, J.C., and Mardock, Cheryl, 1990, Rare-earth element- and yttrium-bearing pegmatite dikes near Dora Bay, southern Prince of Wales Island: U.S. Bureau of Mines Open-File Report 19-90, 41 p.
- Brew, D.A., Drew, L.J., Schmidt, J.M., Root, D.H., and Huber, D.F., 1991, Undiscovered locatable mineral resources of the Tongass National Forest and adjacent lands, southeastern Alaska: U.S. Geological Survey Open-File Report 91-10, 370 p., 26 maps.
- Candella, P.A., and Holland, H.D., 1986, A mass transfer model for copper and molybdenum in magmatic hydrothermal systems: the origin of porphyry-type ore deposits: *Economic Geology*, v. 81, p. 1-18.
- Cox, D.P., and Singer, D.A., 1986, Mineral deposit models: U.S. Geological Survey Bulletin 1693, 379 p.
- Eberlein, G.D., Churkin, Michael, Jr., Carter, Claire, Berg, H.C., and Owenshine, A.T., 1983, *Geology of the Craig quadrangle, Alaska*: U.S. Geological Survey Open-File Report 83-91, 30 p., scale 1:250,000.
- Gehrels, G.E., and Berg, H.C., 1984, *Geologic map of southeastern Alaska*: U.S. Geological Survey Open-File Report 84-886, 28 p., scale 1:600,000.
- Herreid, Gordon, Bundtzen, T.K., and Turner, D.L., 1978, *Geology and geochemistry of the Craig A-2 quadrangle and vicinity, Prince of Wales Island, southeastern Alaska*: Alaska Department of Natural Resources, Division of Geological and Geophysical Surveys, *Geologic Report* 48, 49 p., 2 maps, scale 1:40,000.
- Isuk, E.E., 1976, Solubility of molybdenite in the system  $\text{Na}_2\text{O}-\text{K}_2\text{O}-\text{SiO}_2-\text{MoS}_2-\text{H}_2\text{O}-\text{CO}_2$  with geologic application: Ames, University of Iowa, Ph.D. thesis, 101 p.
- Smith, J.V., 1983, Some chemical properties of feldspars, in Ribbe, P.H., ed., *Feldspar mineralogy*: Mineralogical Society of America, p. 281-296.
- U.S. Department of Agriculture, Forest Service, 1991, *Tongass National Forest Land Management Plan Map*, scale 1:760,320.
- White, W.H., Bookstrom, A.A., Kamilli, R.J., Ganster, M.W., Smith, R.P., Ranta, D.E., and Steininger, R.C., 1981, Character and origin of Climax-type molybdenum deposits: *Economic Geology*, 75th Anniversary Volume, p. 270-316.
- Reviewers: Bruce R. Doe, Karen D. Kelley, and Holly J. Stein.

# GEOCHEMICAL CHARACTER OF UPPER PALEOZOIC AND TRIASSIC GREENSTONE AND RELATED METAVOLCANIC ROCKS OF THE WRANGELLIA TERRANE IN NORTHERN SOUTHEASTERN ALASKA

By Arthur B. Ford and David A. Brew

## ABSTRACT

Greenstone and other mafic metavolcanic rocks of late Paleozoic and early Mesozoic age are widespread in northern southeastern Alaska. Major- and trace-element similarities between Upper Triassic greenstone of the Wrangellia terrane (Wrangellia) of the Chilkat Peninsula and greenstone of the Upper Triassic upper part of the Gastineau Volcanics near Juneau indicate that Wrangellia extends southward as a long narrow belt along the west margin of the Coast Mountains. Amphibolite near Juneau has major- and trace-element characteristics similar to those of Upper Triassic metabasalt, which suggests that parts of Wrangellia were involved in amphibolite-facies-grade metamorphism of the western metamorphic belt of the metamorphic and plutonic complex of the Coast Mountains. Greenschist and greenstone of northern Admiralty Island (Barlow Cove) are of unknown age but probably correlative with the Triassic Hyd Group. They have many major- and trace-element signatures of metabasalt of Wrangellia, which suggests that Wrangellia is an integral part of the Alexander terrane of insular areas of southeastern Alaska. The recognition of Wrangellian mafic volcanism in these areas greatly increases the known extent of this basaltic province, which is among the world's largest of this type.

All of the greenstones of the Gastineau Volcanics near Juneau are tholeiitic in composition, but the Permian(?) and Triassic(?) lower part of the formation has trace-element signatures different from those of the Upper Triassic higher part. The lower part of the Gastineau shows an enrichment in large-ion-lithophile elements and has other characteristics of ocean-island basalt, which contrast with the enriched-MORB or back- or inter-arc-basin basalt character of the Upper Triassic metabasalts. Subduction-zone components (Ta and Nb depletions, in particular) are not found in any of the volcanic rocks of Wrangellia in the Juneau area. The metabasalts record different settings of volcanism within a long-lived oceanic volcanic system, the late Paleozoic and Triassic(?) activity of which was related

to ocean-island volcanism and the later activity to Late Triassic rifting or superplume events. Accretion of the volcanic terrane, which either originated or became combined with the Alexander terrane, to North America, may have been associated with Late Cretaceous volcanism of the Douglas Island Volcanics and with Barrovian regional metamorphism at the end of the Cretaceous.

## INTRODUCTION

Linear belts of mafic metavolcanic rocks of late Paleozoic, Triassic, and Triassic(?) age, among others, have long been recognized in northern southeastern Alaska (Knopf, 1911; Martin, 1926; Buddington and Chapin, 1929). This report focuses on one of these belts, termed the Wrangellia terrane (Jones and others, 1977; 1987), of late Paleozoic and Triassic age. This belt was recently identified on the Chilkat Peninsula (Plafker and others, 1989) (fig. 1). For brevity, the terrane is herein also termed Wrangellia, following general usage (Jones and others, 1986; MacIntyre, 1986; Barker and others, 1989; Samson and others, 1990). Faunal evidence and paleomagnetic data support a non-North American origin of Wrangellia (Jones and others, 1986).

Metavolcanic rocks of Triassic and Triassic(?) age extend from the Chilkat Peninsula south to Juneau (Brew and Ford, 1985) and beyond to other parts of mainland southeastern Alaska. Metavolcanic rocks of similar age and type occur on Admiralty Island and elsewhere, as discussed below. Triassic mafic volcanic rocks also occur widely in British Columbia (Souther, 1971; Mortimer, 1987; Henderson and others, 1992). The Triassic and older metavolcanic rocks of southeastern Alaska are variously assigned to different tectonostratigraphic terranes (Brew and Ford, 1984, 1993; Monger and Berg, 1987; Plafker and others, 1989; Silberling and others, 1992; Gehrels and others, 1992). Originally defined as Triassic only (Jones and others, 1977), a definition still followed by some (Lassiter and DePaolo, 1992), Wrangellia is now generally

considered to include Permian volcanic rocks of postulated arc origin below the characteristic Middle and Upper Triassic tholeiitic flows and pillow basalt (Jones and others, 1986, 1987; Howell, 1985). Wheeler and McFeely (1991) also included Devonian rocks in their concept of Wrangellia. The Triassic basalts of Wrangellia form one of

the world's largest flood basalt provinces and were extruded during a short time interval of about 5 m.y. or less (Panuska, 1990). Richards and others (1991) suggested that such an event may be related to the development of a large mantle plume beneath the oceanic lithosphere of an old island-arc complex.

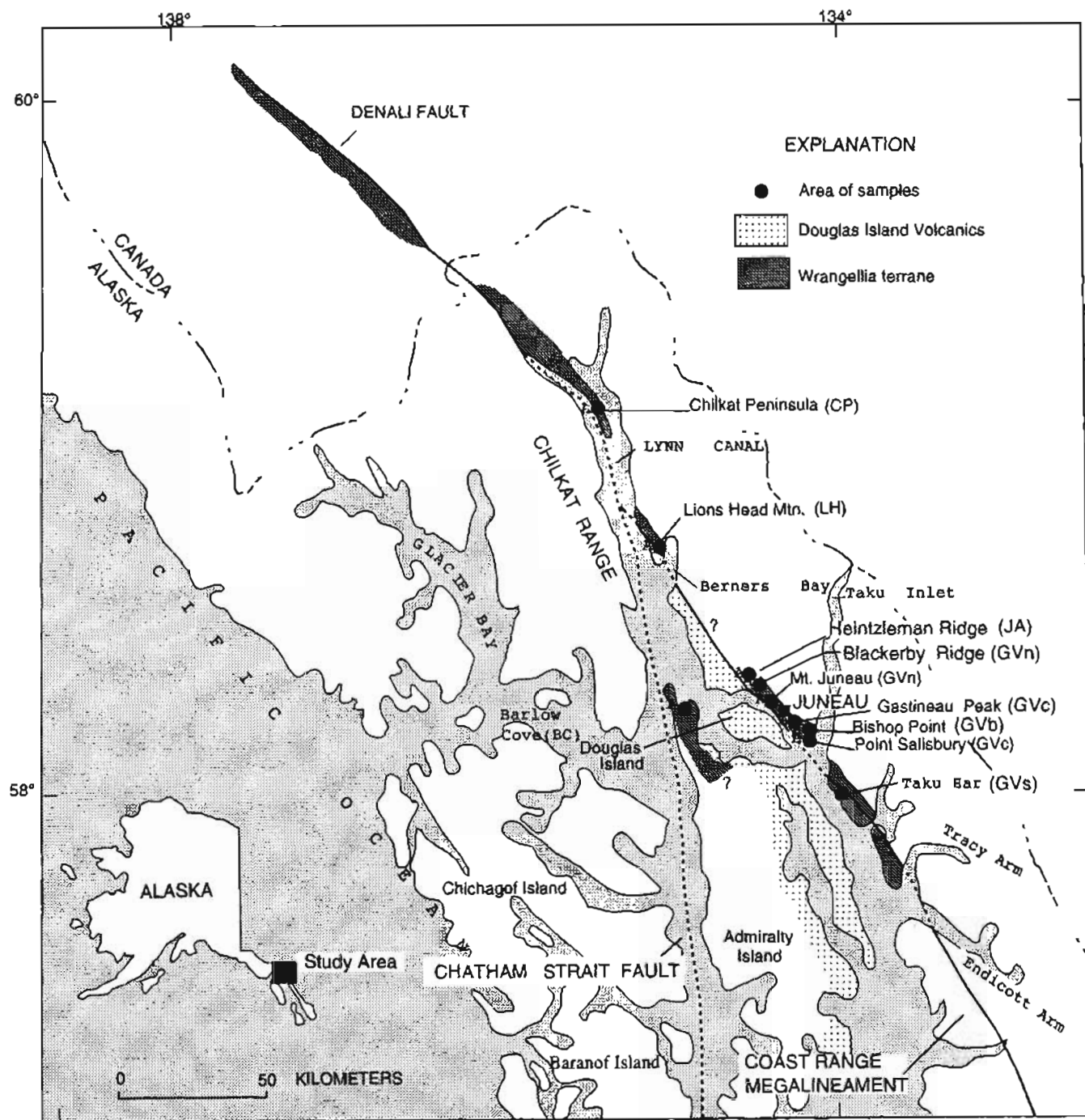


**Figure 1.** Index map of northern southeastern Alaska, showing areas of Permian(?), Triassic, and Triassic(?) metabasalt of the Wrangellia terrane of this study. Other areas of the terrane (Brew, Karl, and others, 1991) not shown. Black dots show areas of samples of this study; letter symbols in parenthesis identified in tables 1 and 2.

The variably metamorphosed mafic volcanic rocks of different ages in northern southeastern Alaska are commonly difficult to distinguish in the field due to general similarity in appearance and scarcity of fossils in associated metasedimentary rocks. Conspicuous major-element differences distinguish greenstone and greenschist of Jurassic and Cretaceous age (Douglas Island Volcanics) from those of Triassic or older age of the region: the former are more alkalic than the tholeiitic compositions of older units (Ford and Brew, 1988). Major-element chemistry alone, however, does not effectively distinguish the various Triassic and older metavolcanic units (Ford and Brew, 1988). The distinction of volcanogenic units of different origin and age is crucial not only to understand the regional tectonic setting and history of this area but also to aid mineral-resource investigations: mafic volcanic rocks of Triassic age, in particular, host volcanogenic metal deposits (Souther, 1971; Berg, 1981; MacIntyre, 1986; Forbes and others, 1989; Nokleberg and others, 1989; Brew, Drew and others, 1991; Brew and Ford, 1993).

This report presents preliminary major- and trace-element data for mafic metavolcanic rocks of Permian(?), Triassic, and Triassic(?) age in northern southeastern Alaska collected during 1964–1991 fieldwork. Published trace-element data are lacking for most metabasalt units of northern southeastern Alaska. New major-element data for some units are incorporated with earlier data of Ford and Brew (1988). Analytical work on some samples of this metavolcanic suite is still incomplete. Objectives of the study are to identify and evaluate geochemical signatures, emphasizing trace elements, of the Triassic and older metavolcanic rocks in order to (1) distinguish different metavolcanic units, (2) interpret tectonic settings of volcanism, and (3) clarify concepts of terranes of this region (compare Brew and Ford, 1984; Monger and Berg, 1987; Plafker and others, 1989; Gehrels and others, 1992; Silberling and others, 1992; Brew and Ford, 1993).

Samples for the present study are from (1) the Chilkat Peninsula, (2) a mainland belt from the Chilkat Peninsula to south of Taku Inlet, and (3) Barlow Cove, Admiralty Island (fig. 1; tables 1, 2). With the exception of amphibolite from near Juneau, all samples are of greenschist-facies metamorphic grade and contain extensively recrystallized assemblages of principally albite, chlorite, epidote, and actinolite. The occurrence of relict pillows in many areas sampled indicates a submarine origin of many of the protoliths, in which chemical interaction with seawater was likely. Problems of element mobility by metamorphism, as well as by seafloor alteration (Winchester and Floyd, 1976; Mottl, 1983), limit utility of many elements for petrogenetic interpretation. Badger's (1993) study found  $K_2O$ ,  $Na_2O$ , Rb, Ba, and Sr to be the most easily mobilized components, and  $TiO_2$ ,  $P_2O_5$ , and  $Al_2O_3$  the least affected by greenschist-facies metamorphism. Seafloor greenschist-facies alteration can also result in uptake of

Mg and loss of Ca, Si, and Mn (Mottl, 1983). This investigation makes particular use of elements considered to be the least mobile during alteration, such as P, Ti, Zr, Y, Nb, Th, Hf, and rare-earth elements (Floyd and Winchester, 1975; Winchester and Floyd, 1976; Mortimer, 1987; Wood and others, 1980). Vanadium is also relatively immobile (Shervais, 1982), and such elements have been used for interpreting metamorphosed mafic volcanic rocks of grade as high as amphibolite facies (Winchester and Floyd, 1976) and even granulite facies (Lawrie, 1992). Anomalous patterns in some of the element-variation diagrams show possible indications of selective element mobility, particularly for Ba, as described below.

## REGIONAL SETTING

The lithotectonic terrane map of Silberling and others (1992) shows the Taku terrane as a long, narrow belt of upper Paleozoic and Triassic rocks extending from the Chilkat Peninsula southward the length of southeastern Alaska along the west margin of the Coast Mountains. Brew, Karl and others (1991) proposed instead that much of this belt as well as island areas to the west consists of the (composite) Wrangellia–Alexander terrane. Upper Triassic metabasalt of the Chilkat Peninsula is similar in age, lithology, and geochemistry to the Nikolai Greenstone of southern Alaska's Wrangellia terrane (Plafker and Hudson, 1980; Davis and Plafker, 1985). Plafker and others (1989) reinterpreted the earlier Taku terrane assignment of Chilkat Peninsula metabasalts and suggested that they form a tectonic sliver of Wrangellia with dextral offset along the Denali fault (fig. 1). We generally follow terrane usage given by Brew and Ford (1984) and Brew, Karl and others (1991), but others have differing definitions and interpretation (for example, Gardner and others, 1988; Plafker and others, 1989; Samson and others, 1990; Silberling and others, 1992; Gehrels and others, 1992; Lassiter and DePaolo, 1992; Rubin and Saleeby, 1992).

The mafic metavolcanic units of the mainland belt of our study (fig. 1) consist of Triassic, Triassic(?), and Permian(?) metavolcanic rocks and associated metasedimentary rocks (Brew and Ford, 1985). The belt includes the metabasalts of the Chilkat Peninsula, Lions Head Mountain near Berners Bay, and the here-revised Gastineau Volcanics, which is reduced to formation status owing to the fact that mappable formations have not been demonstrated for the previously termed Gastineau Volcanic Group of Martin (1926) in the geological mapping of this area (Ford and Brew, 1973, 1977; Brew and Ford, 1977, 1985). We thus disagree with Gehrels and others (1992) assignment of the Gastineau to group status. The metavolcanic rock belt extends more than 50 km farther southeast beyond the area of the present study (Brew and Grybeck, 1984; Gehrels and others, 1992).



**Table 1.** Average major-element composition (weight percent) of Permian(?), Triassic(?), and Triassic metabasalt units of northern southeastern Alaska

[FeO\*, total Fe as FeO; Mg#, molecular ratio, Mg/(Mg + Fe<sup>2+</sup>). Samples were analyzed in laboratories of the U.S. Geological Survey by methods described in Baedeker (1987). Analysts: J. Ardith, L. Aris, A. Bartel, B. Brandt, H.N. Elsheimer, L. Espos, T.L. Fries, R.V. Mendes, S. Neil, S.T. Pribble, D.F. Siems, J.E. Taggart, and D. Vivit]

Unit-----	Chilkat Peninsula	Lions Head Mountain	Gastineau Volcanics <sup>1</sup>	Gastineau Volcanics <sup>2</sup>	Gastineau Volcanics <sup>3</sup>	Gastineau Volcanics <sup>4</sup>	Barlow Cove	Juneau area amphibolite
No. samples---	15	7	6	14	13	5	5	4
Plot symbol---	CP	LH	GVb	GVc	GVn	GVs	BC	JA
SiO <sub>2</sub> -----	49.9	47.3	46.3	46.1	45.9	46.2	47.3	46.8
Al <sub>2</sub> O <sub>3</sub> -----	14.1	14.1	15.6	15.6	15.5	14.2	14.6	16.5
Fe <sub>2</sub> O <sub>3</sub> -----	4.38	4.52	1.97	2.99	2.80	2.69	4.48	2.35
FeO-----	8.16	8.35	8.18	8.93	8.31	8.25	6.17	8.19
MgO-----	6.61	7.21	7.56	6.80	6.49	8.32	8.89	8.24
CaO-----	9.24	8.21	10.90	9.50	10.16	9.92	10.8	11.3
Na <sub>2</sub> O-----	2.74	3.82	2.47	2.56	2.92	2.84	2.30	2.15
K <sub>2</sub> O-----	.43	.29	.36	.86	.70	.75	.55	.52
H <sub>2</sub> O <sup>+</sup> -----	2.25	3.20	2.79	2.89	2.29	2.53	2.94	1.67
H <sub>2</sub> O <sup>-</sup> -----	.15	.17	.06	.06	.06	.04	.05	.04
TiO <sub>2</sub> -----	1.53	2.30	1.51	1.81	2.01	2.47	1.30	1.36
P <sub>2</sub> O <sub>5</sub> -----	.21	.19	.15	.56	.37	.41	.15	.16
MnO-----	.20	.22	.14	.18	.18	.17	.16	.18
CO <sub>2</sub> -----	.13	.32	1.46	.61	1.59	.77	.41	.09
Ratios								
FeO*-----	12.09	12.41	9.95	11.62	10.83	10.67	10.20	10.30
FeO*/MgO-----	1.98	1.75	1.35	1.79	1.68	1.35	1.20	1.25
Mg#-----	58.7	60.9	61.8	57.0	59.2	63.6	71.7	64.4

<sup>1</sup> Eastern area of unit, at Bishop Point, Taku Inlet (fig. 1).

<sup>2</sup> Central (type) area of unit, on Gastineau Peak and vicinity, near Juneau.

<sup>3</sup> Northern area of unit, on Mount Juneau and western Blackberry Ridge.

<sup>4</sup> Southern area of unit, south of Taku Inlet and east of Taku Harbor.

Major- and trace-element geochemistry of the tholeiitic Triassic metabasalts of the Chilkat Peninsula was interpreted by Davis and Plafker (1985) to indicate an intraplate or back- or fore-arc extensional origin, and the associated sedimentary units to suggest deposition farther offshore than parts of the Nikolai Greenstone of the Wrangell Mountains. The apparent continuity of the Chilkat Peninsula rocks with metamorphosed mafic volcanic rocks to the southeast, near Lions Head Mountain (Plafker and Hudson, 1980), and to the vicinity of Juneau and Taku Inlet (Brew and Ford, 1985; Brew, Karl and others, 1991) and beyond (Brew and Grybeck, 1984) suggests that Wrangellia may extend much farther southeastward in Alaska than shown by Gehrels and others (1992) and Silberling and others (1992), who considered the rocks to

be part of the Taku terrane. Nd and Sr isotopic characteristics suggest that at least part of what has heretofore been called the Taku terrane forms a crustal fragment of less-juvenile nature than the Alexander and Wrangellia terranes (Samson and others, 1991) and belongs with the much older Nisling terrane (Wheeler and McFeely, 1991).

Metabasaltic units of late Paleozoic and Triassic age also occur in insular areas of southeastern Alaska, on Chichagof, Baranof, Admiralty, and Kupreanof Islands (Buddington and Chapin, 1929; Loney, 1964; Muffler, 1967; Loney and others, 1975; Brew and others, 1984), in areas considered to be the Alexander terrane that contains a diverse assemblage of variably altered sedimentary, volcanic, and plutonic rocks of pre-Ordovician to Triassic age (Silberling and others, 1992). Triassic(?) metabasalt

**Table 2.** Average trace-element content (parts per million) and ratios for Permian(?), Triassic(?), and Triassic metabasalt units of northern southeastern Alaska

[Samples were analyzed in laboratories of the U.S. Geological Survey by methods described in Baedeker (1987): nd, not determined. Analysts: J.R. Budahn, J.G. Crock, J.R. Evans, B.P. Fabbri, T.P. Frost, Judith Kent, B.W. King, R.J. Knight, P.J. Lamothe, R. Lerner, R.E. Mays, D.M. McKown, S.T. Pribble, R.B. Vaughn, and D. Vivit. Locations of the Gastineau Volcanics subareas given in table 1]

Unit-----	Chilkat Peninsula	Lions Head Mountain	Gastineau Volcanics	Gastineau Volcanics	Gastineau Volcanics	Gastineau Volcanics	Barlow Cove	Juncos area amphibolite
No. samples--	15	7	6	14	13	5	5	4
Plot symbol--	CP	LH	GVb	GVc	GVn	GVs	BC	JA
<b>K-group elements</b>								
Ba <sup>#</sup> -----	106	99	960	317	282	251	208	622
Cs <sup>Δ</sup> -----	.35	.21	.48	.68	1.26	.55	.48	.86
Rb <sup>Δ</sup> -----	11.8	6.8	12.7	13.3	16.4	17.6	15.6	9.8
Sr <sup>#</sup> -----	137	86	210	386	520	291	220	413
<b>REE group elements</b>								
La <sup>Δ</sup> -----	6.4	7.8	7.6	19.1	16.7	15.3	6.2	8.5
Ce <sup>Δ</sup> -----	16.1	21.0	17.2	43.2	40.0	37.0	15.6	21.1
Nd <sup>Δ</sup> -----	11.2	15.7	12.7	22.3	22.1	21.9	10.9	12.9
Sm <sup>Δ</sup> -----	3.57	4.75	3.86	5.41	5.46	5.72	3.24	3.50
Eu <sup>Δ</sup> -----	1.26	1.59	1.45	1.85	1.79	1.70	1.09	1.17
Gd <sup>Δ</sup> -----	3.56	5.48	nd	6.29	5.66	nd	nd	3.67
Tb <sup>Δ</sup> -----	.843	.960	.816	1.12	.838	.794	.579	.575
Tm <sup>Δ</sup> -----	.465	.502	nd	.449	.418	nd	nd	.306
Yb <sup>Δ</sup> -----	3.39	3.18	2.49	2.76	2.47	2.21	1.97	1.94
Lu <sup>Δ</sup> -----	.498	.464	.355	.405	.360	.317	.290	.278
Sum REE---	44.37	59.21	46.11	85.92	87.99	84.67	39.48	53.69
Y <sup>#</sup> -----	25	32	16	23	23	22	14	22
<b>Th group</b>								
Th <sup>Δ</sup> -----	.673	.607	.643	1.50	1.32	1.49	.564	1.08
U <sup>Δ</sup> -----	.388	.203	.43	.59	.56	1.77	.286	.358
<b>Ti group</b>								
Zr <sup>#</sup> -----	91	128	81	161	150	160	78	76
Hf <sup>Δ</sup> -----	2.53	3.48	2.53	3.34	3.62	3.90	1.91	1.85
Nb <sup>#</sup> -----	8.3	15	10	24	21	32	10	12
Ta <sup>Δ</sup> -----	.452	.651	.587	1.34	1.40	1.66	.393	.513
<b>Compatible group</b>								
Co <sup>Δ</sup> -----	43.7	45.9	41.6	40.3	39.3	51.4	43.3	47.7
Cr <sup>Δ</sup> -----	125	261	275	149	143	478	355	307
Ni <sup>Δ</sup> -----	86.5	91.6	nd	92.4	70.7	151	111	107
Sc <sup>Δ</sup> -----	42.6	40.9	44.7	38.2	34.0	41.6	38.7	39.9
V <sup>@</sup> -----	353	400	400	295	336	332	293	nd
<b>Chalcophile group</b>								
Cu <sup>#</sup> -----	140	114	155	116	119	nd	58	83
Zn <sup>Δ</sup> -----	101	117	125	116	88	154	110	88
<b>Ratios</b>								
K/Rb	388	356	340	356	293	384	279	457
Rb/Sr	.09	.08	.06	.03	.03	.06	.07	.02
(Eu/Er*) <sub>N</sub>	1.50	1.19	1.99	1.40	.99	1.67	1.78	1.00

<sup>#</sup> By energy-dispersive XRF analysis.

<sup>Δ</sup> By neutron activation analysis.

<sup>@</sup> By direct-current arc emission spectrographic analysis.

included in the Alexander terrane of the Barlow Cove area, northern Admiralty Island, has tholeiitic major-element characteristics indistinguishable from Triassic metabasalt of the mainland part of Wrangellia (Ford and Brew, 1988). The Barlow Cove rocks probably correlate with the Triassic metabasaltic Hyd Group as defined by Loney (1964) of southern parts of Admiralty Island, a unit that extends at least 25 km farther south to islands near Petersburg (Muffler, 1967; Muffler and others, 1969; Brew and others, 1984). The next-nearest well-documented occurrence of Wrangellia basalt farther south is the Middle to Upper Triassic Karmutsen Formation of the Queen Charlotte Islands (Barker and others, 1989). The Karmutsen, which correlates with the Nikolai Greenstone of the Wrangell Mountains (Barker and others, 1989), may represent back-arc eruptive rocks close behind an arc axis such as in the Wallowa terrane of Oregon and Idaho (Vallier, 1986).

In northern southeastern Alaska, Triassic and older greenstones of the Chilkat Peninsula, Lions Head Mountain, and elsewhere are distinctly different from Jurassic and Cretaceous greenstone of the Douglas Island Volcanics in major-element chemistry, and show conflicting tectonic settings as indicated by different geochemical discriminant diagrams (Ford and Brew, 1988). The Triassic and older metavolcanic rocks have closely similar tholeiitic composition in terms of total alkalis,  $\text{FeO}^*$  (total iron as  $\text{FeO}$ ), and  $\text{MgO}$  in contrast to the calc-alkaline character of the Douglas Island Volcanics (Ford and Brew, 1988). In terms of  $\text{TiO}_2$ - $\text{FeO}^*/\text{MgO}$  variation, the Triassic and older metabasalts show mid-ocean-ridge (MORB) and back-arc-basin basalt (BABB) affinities, and the Douglas Island Volcanics plot in the island-arc tholeiite field (Ford and Brew, 1988). In Mullen's (1983)  $\text{MnO}$ - $\text{TiO}_2$ - $\text{P}_2\text{O}_5$  diagram, the Douglas Island Volcanics show calc-alkaline basalt character, in contrast to an island-arc-tholeiite character of the Gastineau Volcanics and a MORB character for the Triassic units (Ford and Brew, 1988).

## METABASALT UNITS

Samples of metabasalt for our study are from eight areas of northern southeastern Alaska (fig. 1): (1), the Chilkat Peninsula area of Wrangellia (Plafker and Hudson, 1980) (CP; tables 1 and 2, and most figures); (2), the Lions Head Mountain and vicinity area (LH); (3), the Bishop Point area of the Gastineau Volcanics, on Taku Inlet (GVb); (4), the central, type area of the Gastineau Volcanics of Gastineau Peak and vicinity, near Juneau (GVc); (5), a northern area of the Gastineau Volcanics of Mount Juneau and western Blackerby Ridge, near Juneau (GVn); (6), a southern area south of Taku

Inlet and east of Taku Harbor (GVs); (7), the Barlow Cove area, northern Admiralty Island (BC); and (8), an area of amphibolites of western Heintzleman Ridge, near Juneau (JA). Age assignment of some units is uncertain due to the lack of age-diagnostic fossils in associated metasedimentary rocks. Correlations in this report are based primarily on detailed (Ford and Brew, 1973, 1977; Brew and Ford, 1977) and reconnaissance (Brew and Ford, 1985) mapping of the Juneau quadrangle and vicinity, and secondly on lithologic similarities and apparent stratigraphic positions.

## METABASALTS OF THE CHILKAT PENINSULA AND LIONS HEAD MOUNTAIN

The Upper Triassic metabasalts of the Chilkat Peninsula (Plafker and others, 1979), interpreted by Plafker and others (1989) as a displaced fragment of Wrangellia, forms a narrow belt that extends southward to the vicinity of Lions Head Mountain (Plafker and Hudson, 1980; Brew and Ford, 1985; Brew, Karl and others, 1991), as shown in figure 1. Gehrels and Berg (1992), however, interpreted the metabasalt of Lions Head Mountain to be a unit different from the Chilkat Peninsula rocks. Knopf (1911) mapped a 2- to 4-km-wide belt of the amygdaloidal metabasalt of Lions Head Mountain for about 15 km from Lynn Canal to Berners Bay. He considered the metabasalt to be Jurassic or Early Cretaceous in age and correlated it with the Douglas Island Volcanics, although he noted significant petrographic differences. However, major-element chemical and lithologic characteristics clearly show that the Lions Head Mountain rocks are tholeiitic and differ significantly from the calc-alkaline Douglas Island Volcanics (Ford and Brew, 1988). Metasedimentary rocks exposed near the metabasalt of Lions Head Mountain are unfossiliferous, though assigned a Triassic age by Plafker and Hudson (1980). Projection of the rocks along strike to those south of Berners Bay (Brew and Ford, 1985) suggests instead a Jurassic and Cretaceous age for these metasedimentary rocks. The metabasalt of Lions Head Mountain is truncated southward by granitic plutons and higher grade metamorphic rocks of the informally named (Brew and Ford, 1984) Coast plutonic-metamorphic complex (Knopf, 1911; Brew and Ford, 1985), and thus there is no direct continuation of rocks of this belt of Wrangellia with metabasaltic units to the south (fig. 1).

## GASTINEAU VOLCANICS

Greenstone and greenschist of the herein-revised Gastineau Volcanics, near Juneau, lie on strike with the metabasalt of Lions Head Mountain. We interpret the

metabasalt of Lions Head Mountain to correlate with Triassic rocks of the upper part of the Gastineau Volcanics on the basis of petrographic and chemical similarities. The Gastineau was originally assigned a Late Triassic age based on fossils from several localities (Martin, 1926). Additional Late Triassic fossils have been found in metasedimentary rocks adjoining greenstone at Bishop Point, Taku Inlet (Ford and Brew, 1977; Gehrels and others, 1992). On the basis of those occurrences and of poorly preserved late Paleozoic fossils that occur as clasts in interlayers of metasedimentary rocks near Point Salisbury, Ford and Brew (1977) considered metavolcanic rocks that they regarded as "probably partly correlative" with the Gastineau to be Carboniferous or Permian and Late Triassic in age. Gehrels and others (1992), however, considered the Gastineau to be restricted to the Permian, though they provided no new supporting evidence. They excluded from it the greenstone associated with Late Triassic fossils near Bishop Point, and considered the greenstone to be part of what Martin (1926) called the Perseverance Slate, a mostly pelitic unit of slate, phyllite, and mica schist. Gehrels and others (1992) gave the name "Perseverance Group" to this mainly pelitic unit, including the greenstone of Bishop Point, even though formations have not been mapped within it (Ford and Brew, 1977; Brew and Ford, 1985) as required for group status (North American Commission on Stratigraphic Nomenclature, 1983).

Paleontologic ages and our detailed geologic mapping (Ford and Brew, 1973, 1977; Brew and Ford, 1977) do not, in our view, support the restricted Permian-only age assignment for the Gastineau Volcanics (Gehrels and others, 1992). Detailed mapping of the area (Ford and Brew, 1977) shows that the Late Triassic fossils west of Bishop Point (Gehrels and others, 1992) are from a thin metapelite layer or lens within a thick greenstone unit. As noted previously, fossils from the thin metasedimentary units in greenschist mixed with pillow-bearing greenstone to the west, near Point Salisbury, consist of crinoid columnals that are dated only as of "...probable late Paleozoic and possibly Carboniferous or Permian..." in age, and a crinoid columnal in a carbonate cobble of a metaconglomerate that "...indicates a late Paleozoic or younger age of the cobble" (J.T. Dutro, written commun., 1973). Fossils from apparently correlative units to the south (Brew and Grybeck, 1984; Gehrels and others, 1992) are clearly Permian in age. The contact shown by Gehrels and others (1992) between their Gastineau Group and Perseverance Group is, from our mapping (Ford and Brew, 1977), only a contact separating a dominantly greenstone unit of the metavolcanic rocks to the southwest from a mixture of greenstone and metapelite layers to the northeast (Brew and Ford, 1977; Ford and Brew, 1977).

Geochemical data are compiled separately for greenstone of the Bishop Point area of the Gastineau Volcanics (GVb, tables 1 and 2) in order to determine whether geochemical differences exist between the metavolcanic rocks of this area that are known to be Triassic in age and the other parts of the unit that are of uncertain late Paleozoic and Triassic ages. Rocks of both the Triassic (Bishop Point area) and the Permian(?) and Triassic(?) western parts of the Gastineau Volcanics consist of assemblages of granoblastic albite, epidote, chlorite, and actinolite indicative of greenschist-facies metamorphism, and they commonly contain euhedral, small phenocrysts of relict plagioclase. The rocks range from massive to well-foliated greenstone and in places to greenschist. Relict pillows are locally abundant in the Bishop Point area of the Gastineau.

### OTHER PRE-JURASSIC METABASALT UNITS

Numerous layers of amphibolite in pelitic schist of western Heintzleman Ridge, near Juneau (fig. 1), are part of the Barrovian western metamorphic belt of the Coast plutonic-metamorphic complex in which fossils indicate a protolith age of at least Permian to early Late Cretaceous (Brew and others, 1989; Himmelberg and others, 1991). The amphibolite occurs in an area intermediate between the northernmost exposures of the Gastineau Volcanics and southernmost exposures of the metabasalt of Lions Head Mountain. Mineral assemblages consist mainly of plagioclase, epidote, chlorite, and green hornblende, and the rocks show no obvious evidence of non-isochemical metamorphism. Chemical comparisons, discussed below, and geographic relations suggest that the amphibolites represent higher-grade metamorphic equivalents of the greenschist-facies Triassic metabasalts of the Gastineau Volcanics and the Lions Head Mountain and Chilkat Peninsula areas.

Greenschist near Barlow Cove, northern Admiralty Island, was mapped by Barker (1957) as the Barlow Cove Formation and correlated with the Douglas Island Volcanics, but we agree with Lathram and others' (1960, 1965) protolith age of Permian and Triassic(?) assigned to these rocks based on regional mapping. Major-element compositions of this greenschist differ distinctly from those of the Douglas Island Volcanics and are similar to compositions of Triassic and Triassic(?) metavolcanic rocks of other parts of northern southeastern Alaska (Ford and Brew, 1988). We believe that the Barlow Cove Formation (greenschist) is probably correlative with the Triassic Hyd Group of Loney (1964) of southern parts of Admiralty Island. The chemical composition of the Hyd Group of Admiralty Island is poorly known and has been investigated only in areas to the south (Muffler, 1967; Muffler and others, 1969; Douglass and others, 1989).

# CHEMICAL CHARACTERISTICS OF THE METABASALTS

## MAJOR ELEMENTS

Average major-element compositions of the units of this study are given in table 1. Additional analyses for rocks of the Chilkat Peninsula are given in Davis and Plafker (1985). The metabasalt units have only a small range in average  $\text{SiO}_2$  content (46–48 percent), except for the metabasalt of the Chilkat Peninsula that has an unusually high  $\text{SiO}_2$  content of 49.9 percent, which is about the same as reported by Davis and Plafker (1985). The metabasalt of the Chilkat Peninsula is quartz-normative in average composition and all other units contain normative hypersthene and olivine (data not shown). The range in  $\text{FeO}^*/\text{MgO}$  values is small (1.2–2.0) and the rocks are clearly tholeiitic in terms of  $\text{SiO}_2$  and  $\text{FeO}^*/\text{MgO}$  variation (fig. 2).

The three western subareas of the Gastineau Volcanics (GVc, GVn, GVv; tables 1, 2, fig. 1) form a group with higher  $\text{K}_2\text{O}$ , on average, compared with other metabasalts of this study (fig. 3). They also form a group having higher average  $\text{P}_2\text{O}_5$ , but with average  $\text{MgO}$  range overlapping that of other units (fig. 4). The range of average Mg numbers of the Gastineau Volcanics (Mg# 57–64, table 1) overlaps that of most other metabasalts (CP, 59; LH, 61; JA, 64). Mg numbers of the Gastineau Volcanics and the metabasalts of the Chilkat Peninsula and Lions Head Mountain are somewhat lower than those of ocean-island basalt (OIB) reported by Flower (1991, Mg# 64–

80). Except for the greenschist of the Barlow Cove Formation (Mg# 72), average Mg numbers are generally well below those of probable primary mantle melts ( $> 73$ , Gill, 1981) suggesting either melt derivation from other than a primitive source or fractionation prior to eruption.

Major-element compositions (table 1) suggest magmatic settings of units somewhat different from those shown by trace elements that are described later. In terms of  $\text{TiO}_2$  and  $\text{FeO}^*/\text{MgO}$  variation, all units show MORB and back-arc-basin basalt compositions, and the three western subareas of the Gastineau Volcanics and the

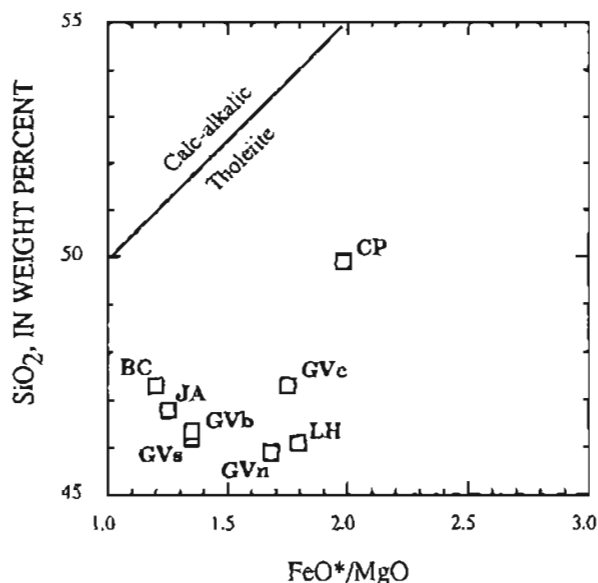


Figure 2. Variation between average  $\text{SiO}_2$  content and  $\text{FeO}^*/\text{MgO}$  of metabasalt units, showing dividing line of calc-alkalic and tholeiitic compositions of Miyashiro (1974). Letter symbols, table 1.

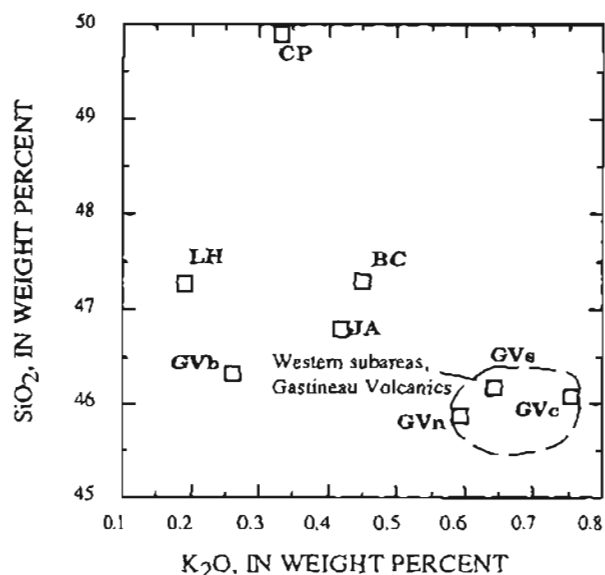


Figure 3. Variation between average  $\text{SiO}_2$  and  $\text{K}_2\text{O}$  content of metabasalt units. Letter symbols, table 1.

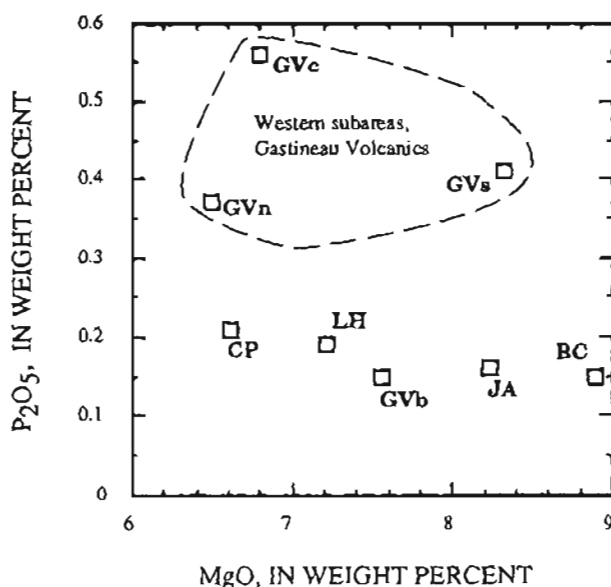


Figure 4. Variation between average  $\text{P}_2\text{O}_5$  and  $\text{MgO}$  content of metabasalt units. Letter symbols, table 1.

metabasalt of Lions Head Mountain have higher  $\text{TiO}_2$  contents than other units (fig. 5). An abyssal tholeiite composition (=MORB?) of all units is suggested by average  $\text{FeO}^*$  versus  $\text{FeO}^*/\text{MgO}$ , according to Miyashiro and Shido's (1975) criteria (fig. 6). The MORB characteristics suggested by such major-element variations are not shown by many trace-element variations discussed below.

### TRACE ELEMENTS

Average trace-element compositions of the units of this study are shown in table 2. Additional trace-element data for the metabasalt of the Chilkat Peninsula and for its correlative Nikolai Greenstone are given in Davis and Plafker (1985). Geochemically, the metabasalts of this study can be divided into two groups on the basis of large-ion-lithophile element (LILE) content. These elements include K, Rb, Sr, Ba, Zr, Th, Ta, and light rare-earth

elements (LREE). *LILE-group 1*, of generally lower LILE content, includes the metabasalts of the Chilkat Peninsula, Lions Head Mountain, and Barlow Cove, the Gastineau Volcanics of the Bishop Point area, and amphibolites of the Juneau area. *LILE-group 2*, with generally higher LILE content, comprises the three western subareas of the Gastineau Volcanics (table 3). LILE groups 1 and 2 are somewhat analogous, respectively, to E-type (enriched) MORB and alkaline OIB of Walker (1991) and Floyd (1991).

The metabasalts of the three western subareas of the Gastineau Volcanics (GVc, GVn, GVs; tables 1–3, fig. 1) differ from other metabasalt units in having generally higher average Sr and Rb contents and lower Rb/Sr (table 2, figs. 7, 8). The metabasalts of the Bishop Point area of the Gastineau Volcanics (GVb), Chilkat Peninsula (CP), Lions Head Mountain (LH), and Barlow Cove (BC) generally group distinctly apart from other units in average  $\text{K}_2\text{O}$  and  $\text{SiO}_2$  variation with Rb/Sr (fig. 8). Variations shown in figure 8A clearly discriminate the Bishop Point area Upper Triassic part of the Gastineau Volcanics from the Permian(?) and Triassic(?) lower part of the Gastineau. The Bishop Point area of the Gastineau Volcanics and the metabasalts of Lions Head Mountain and the Chilkat Peninsula (and other units) have much lower average  $\text{K}_2\text{O}$  than the three western subareas of the Gastineau Volcanics (fig. 8A) and higher average  $\text{SiO}_2$  content (table 1, fig. 8B). Average Rb/Sr of the metabasalts of the Chilkat Peninsula (0.12, Davis and Plafker, 1985; 0.09, table 2) and Lions Head Mountain (0.08, table 2) are higher than those of metabasalts of the Gastineau Volcanics (0.03–0.06, table 2).

Zr-Rb variations show especially well marked discrimination of the three western subareas of the Gastineau Volcanics, with higher Zr content, from other units (fig. 9).

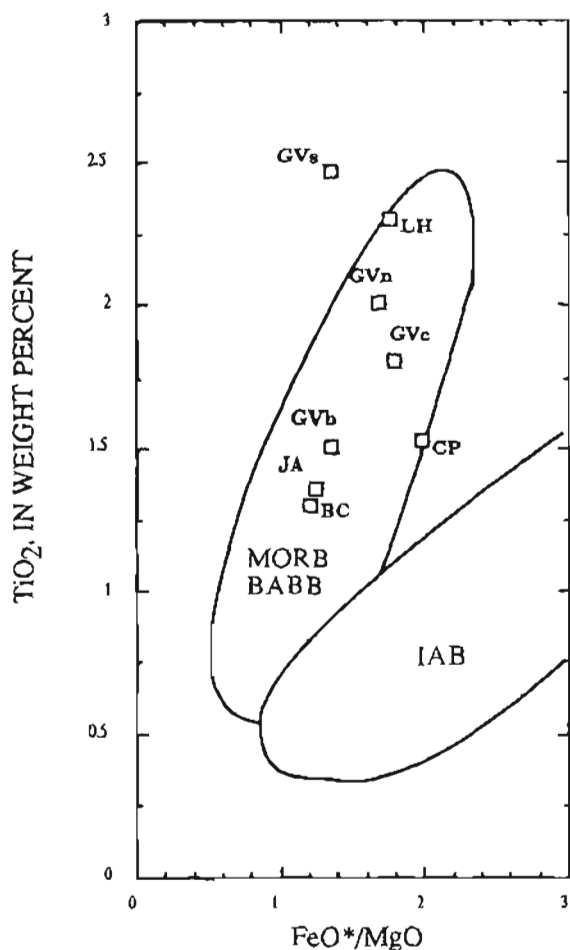


Figure 5. Variation between average  $\text{TiO}_2$  content and  $\text{FeO}^*/\text{MgO}$  of metabasalt units, showing fields of midocean ridge and back-arc basin basalts (MORB, BABB) and island-arc basalt (IAB) of Hawkins and others (1985). Letter symbols, table 1.

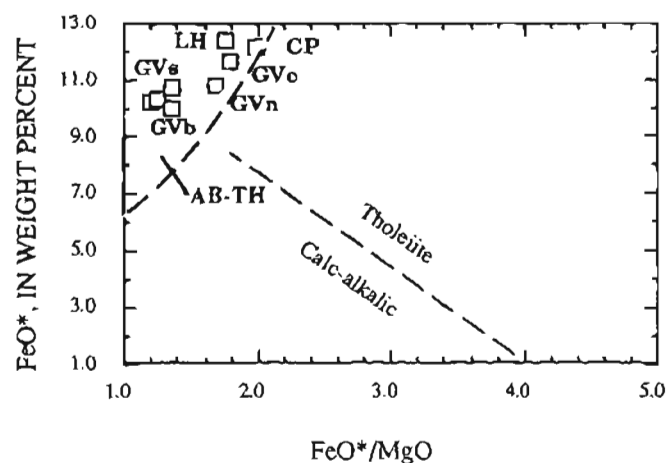


Figure 6. Variation between average  $\text{FeO}^*$  content and  $\text{FeO}^*/\text{MgO}$  of metabasalt units. Tholeiite/calc-alkalic divider from Miyashiro (1974). AB-TH, field of abyssal tholeiite (Miyashiro and Shido, 1975). Letter symbols, table 1.

**Table 3.** Summary of geochemical signatures of metavolcanic units of northern southeastern Alaska

[MORB, midocean-ridge basalt; BABB, back-arc basin basalt; WPB, within-plate basalt; LKT, Low-K tholeiite; OIB, ocean-island basalt; OFB, ocean-floor basalt; CAB, calc-alkalic basalt]

Chemical characteristic	Reference	Geochemical signature					
		Chilkat Peninsula	Lions Head Mountain	Gastineau Volc., Bishop Point area	Gastineau Volcs., western subareas <sup>1</sup>	Barlow Cove	Juneau amphibolites
LILE-group	Text	Lower LILE	Lower LILE	Lower LILE	Higher LILE	Lower LILE	Lower LILE
SiO <sub>2</sub> -FeO*/MgO	Fig. 2	Tholeiite	Tholeiite	Tholeiite	Tholeiite	Tholeiite	Tholeiite
SiO <sub>2</sub> -K <sub>2</sub> O	Fig. 3	High SiO <sub>2</sub> ; low K <sub>2</sub> O	Medium SiO <sub>2</sub> ; low K <sub>2</sub> O	Low SiO <sub>2</sub> ; low K <sub>2</sub> O	Low SiO <sub>2</sub> ; high K <sub>2</sub> O	Medium SiO <sub>2</sub> ; low K <sub>2</sub> O	Low SiO <sub>2</sub> ; low K <sub>2</sub> O
P <sub>2</sub> O <sub>5</sub> -MgO	Fig. 4	Low P <sub>2</sub> O <sub>5</sub>	Low P <sub>2</sub> O <sub>5</sub>	Low P <sub>2</sub> O <sub>5</sub>	High P <sub>2</sub> O <sub>5</sub>	Low P <sub>2</sub> O <sub>5</sub>	Low P <sub>2</sub> O <sub>5</sub>
TiO <sub>2</sub> -FeO*/MgO	Fig. 5	MORB, BABB; low TiO <sub>2</sub>	MORB, BABB; higher TiO <sub>2</sub>	MORB, BABB; lower TiO <sub>2</sub>	MORB, BABB; higher TiO <sub>2</sub>	MORB, BABB; lower TiO <sub>2</sub>	MORB, BABB; lower TiO <sub>2</sub>
K <sub>2</sub> O-Rb/Sr	Fig. 8A	Low K <sub>2</sub> O; high Rb/Sr	Low K <sub>2</sub> O; high Rb/Sr	Low K <sub>2</sub> O; high Rb/Sr	High K <sub>2</sub> O; low Rb/Sr	Low K <sub>2</sub> O; middle Rb/Sr	Low K <sub>2</sub> O; lowest Rb/Sr
Zr-Rb	Fig. 9	Low Zr	Middle Zr	Low Zr	High Zr	Low Zr	Low Zr
REE/chondrite	Fig. 10	Low LREE	Low LREE	Low LREE	High LREE	Low LREE	Low LREE
La-Ba	Fig. 14	Low La, low Ba	Low La, low Ba	Low La, high Ba	High La, low Ba	Low La, low Ba	Low La, high Ba
La-Th	Fig. 15	Low La; low Th	Low La; low Th	Low La; low Th	High La; high Th	Low La; low Th	Low La; low Th
Hf-Th	Fig. 16	Low Hf, low Th	High Hf, low Th	Low Hf, low Th	High Hf, high Th	Low Hf, low Th	Low Hf, low Th
Th/Yb-Ta/Yb	Fig. 17	Nonsubduction; tholeiitic	Nonsubduction; tholeiitic	Nonsubduction; tholeiitic	Nonsubduction; calc-alkaline	Nonsubduction; tholeiitic	Nonsubduction; tholeiitic
Ba-Zr	Fig. 18	MORB, BABB; low Ba, low Zr	MORB, BABB; low Ba, med. Zr	Island-arc <sup>2</sup> ?; high Ba, low Zr	MORB, BABB; low Ba, high Zr	Island arc <sup>2</sup> ?; low Ba, low Zr	Island arc <sup>2</sup> ?; high Ba, low Zr
Ti-Zr-Y variation	Fig. 19	LKT, OFB, CAB	WPB	WPB	WPB	WPB	LKT, OFB, CAB
TiO <sub>2</sub> -Zr	Fig. 20	OFB	OFB	OFB	OFB	OFB	OFB
MORB-normalized elements	Fig. 21	Lower Ta-Nb group	Lower Ta-Nb group	Lower Ta-Nb group; high Ba	Higher Ta-Nb group	Lower Ta-Nb group	Lower Ta-Nb group; high Ba
Hf-Th-Ta	Fig. 22	Nonsubduction; lower Ta group	Nonsubduction; lower Ta group	Nonsubduction; lower Ta group	Nonsubduction; higher Ta group	Nonsubduction; lower Ta group	Nonsubduction; lower Ta group

<sup>1</sup>Includes GVC, GVN, and GVS of tables 1 and 2<sup>2</sup>See text



K/Rb values, however, do not distinguish the metabasalt units (table 2). K/Rb averages for the metabasalt units of this study (279–457, table 2) are in the range for calc-alkaline orogenic basalt and andesite (250–500, Ewart, 1982) and less than values for low-K volcanic suites (>600, Ewart, 1982; ~500, Taylor and others, 1969). Average K/Rb values for all units are lower than those of back-arc tholeiites of Hawkesworth and others (1977, 547–657) and much less than that of MORB varieties (~1000, Viereck and others, 1989).

Differences in total rare-earth-element abundances ( $\Sigma$ REE) of the metabasalts are clearly separable into the same two groups as defined by LILE contents: the three western subareas of the Gastineau Volcanics (LILE-group 2) have distinctly higher  $\Sigma$ REE (85–88 ppm, table 2) than metabasalts of LILE-group 1 units (40–60 ppm). The units show the typical  $\Sigma$ REE increase with increasing  $K_2O$  content (tables 1, 2), but lack showing the general tendency for  $\Sigma$ REE to increase with increasing  $SiO_2$  (Peccerillo and Taylor, 1976).

The two ( $\Sigma$ REE, LILE) groups show small but distinct differences in chondrite-normalized REE patterns (fig. 10). Heavy rare-earth-element (HREE) patterns of the groups overlap in the range 8–15 times chondrite. The metabasalts of the Chilkat Peninsula and Lions Head Mountain, the Bishop Point area of the Gastineau Volcanics, greenschist of the Barlow Cove Formation, and amphibolite (LILE-group 1), however, form a lower LREE group with flat patterns approximately 20 times chondrite and distinct from the more LREE-enriched character of the western subareas of the Gastineau Volcanics (LILE-group 2; La,

Ce ~50 times chondrite). LILE-group 1 metabasalts show more enriched LREE patterns than typical of N-type (normal) MORB (La, 7–10 times chondrite), and lie within Thompson and others' (1989) E-type MORB range. REE patterns show a calc-alkaline character for LILE-group 2 metabasalts and a tholeiitic one for LILE-group 1 metabasalts, according to data of Nicholls and others (1980). LILE-group 1 metabasalts show smaller LREE enrichment than volcanic rocks of nonsubduction-related oceanic islands and seamounts, whereas LILE-group 2 metabasalts show greater LREE enrichment (fig. 10) and patterns that lie within the range for alkaline OIB reported by Floyd (1991, La and Ce ~30–70 times chondrite).

Even relatively immobile elements may decrease or increase in absolute concentrations due to processes such as dilution by hydration, crystallization of secondary minerals, or leaching of more mobile elements, as in the

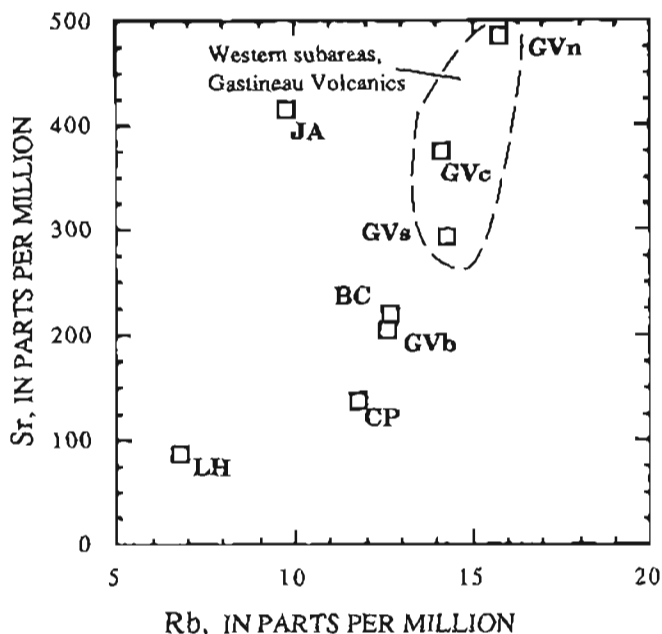


Figure 7. Variation between average Sr and Rb content of metabasalt units. Letter symbols, table 1.

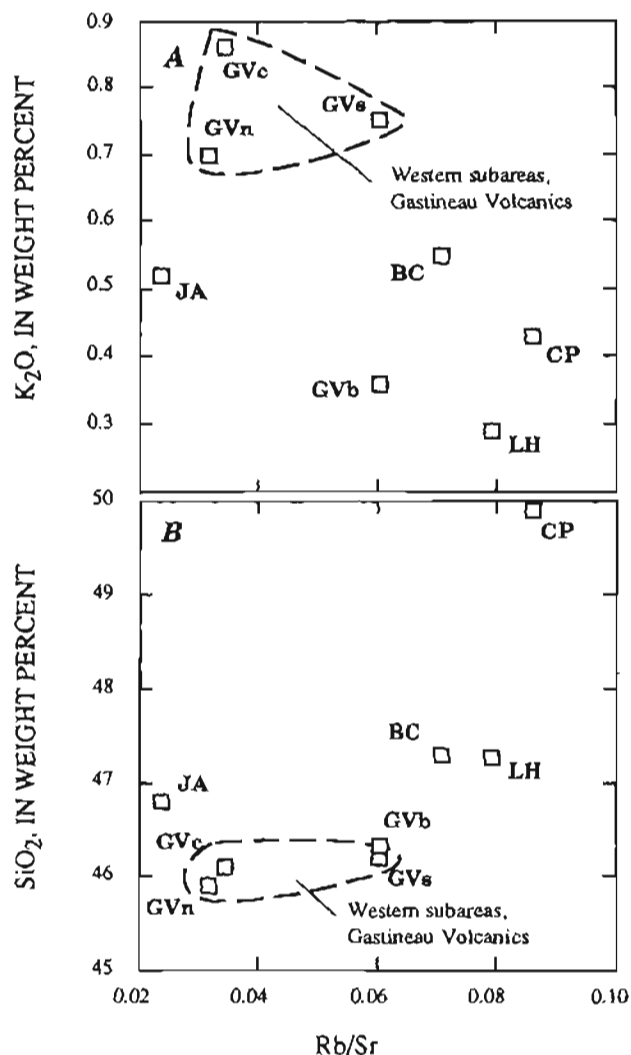


Figure 8. Variation between average (A)  $K_2O$  content and Rb/Sr, and (B)  $SiO_2$  content and Rb/Sr of metabasalt units. Letter symbols, table 1.

alteration of mafic flows and pillows that can significantly change Ti and V contents though Ti/V ratios in altered versus fresh rock remain about the same (Shervais, 1982). Metabasalts of all investigated units have characteristic MORB and back-arc-basin V/Ti values (20:1–50:1) rather than of island-arc and OIB, using Shervais' (1982) diagram (fig. 11). V and Ti variations also show MORB characteristics by Ikeda and Yuasa's (1989) criteria (not shown). V versus FeO\*/MgO variations show tholeiitic character of the metabasalts but higher FeO\*/MgO than typical for MORB, except for the greenschist of the

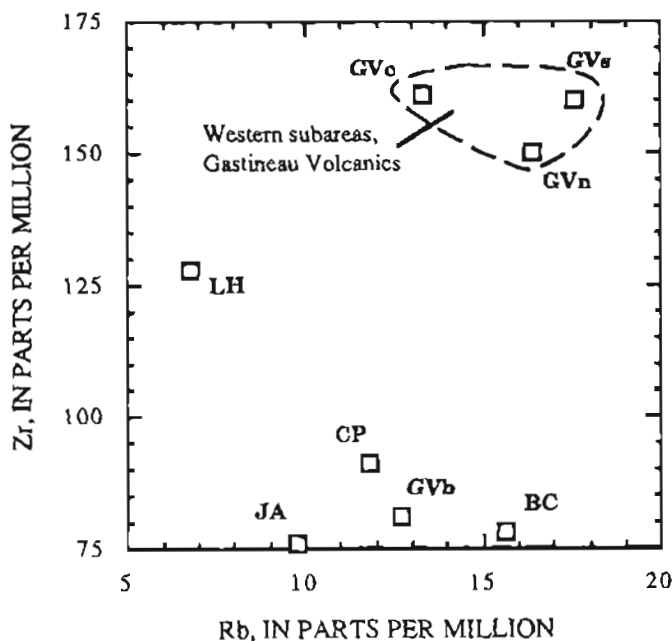


Figure 9. Variation between average Zr and Rb content of metabasalt units. Letter symbols, table 1.

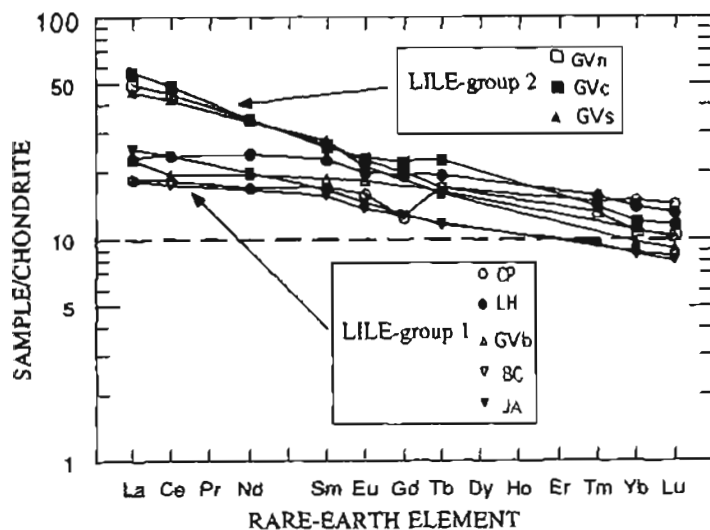


Figure 10. Average chondrite-normalized rare-earth element patterns of metabasalt units. Chondrite-normalization values of Wheatley and Rock (1988). Letter symbols, table 1.

Barlow Cove Formation (fig. 12). All units show V versus Cr variations typical of MORB (fig. 13). Low V/Ni values (2–4, table 2) are similar to tholeiitic values and much lower than calc-alkaline ones (>10; Taylor and others, 1969). The MORB characteristics shown by the V variation diagrams, however, are not found for other trace elements, as discussed below.

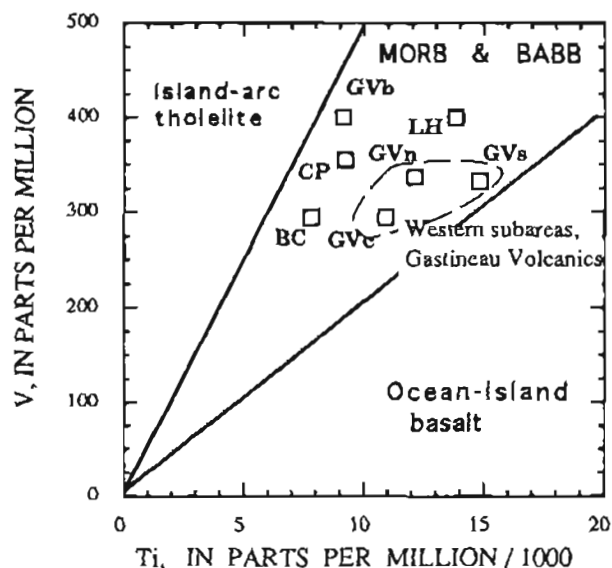


Figure 11. Variation between average V and Ti/1,000 content of metabasalt units, showing field of midocean-ridge basalt and back-arc basin basalt (MORB, BABB), island-arc tholeiite, and ocean-island tholeiite of Shervais (1982). Letter symbols, table 1.

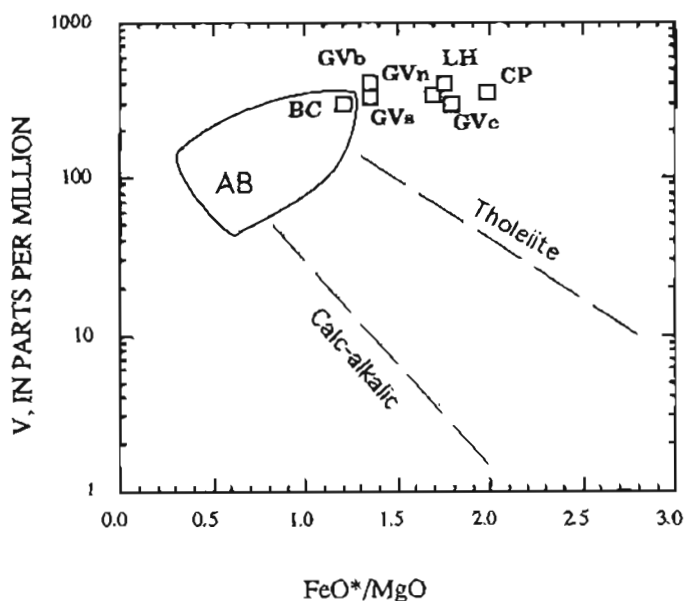


Figure 12. Variation between average log V content and FeO\*/MgO of metabasalt units, showing field of abyssal tholeiite (AB) and tholeiite and calc-alkalic basalt limits of Miyashiro and Shido (1975). Field AB, MORB of Haydoutov (1989). Letter symbols, table 1.

The trace-element ratios La/Ba, La/Th, and Hf/Th are considered the most sensitive discriminators between subduction-zone volcanic series and MORB (Wood and others, 1980). The metabasalt units have Ba/La values ( $\leq 20:1$ ) typical of ocean-floor basalt, except for unusually high "calc-alkaline" ratios for metabasalt of the Bishop Point area and amphibolite (fig. 14) that probably reflect Ba

mobility (Saunders and Tarney, 1991). The western subareas of the Gastineau Volcanics have Ba/La ratios similar to those of metabasalts of the Chilkat Peninsula and Lions Head Mountain, but they form a distinctly higher group in La content (fig. 14). La versus Th variations of metabasalts of the western subareas of the Gastineau Volcanics show arc-basalt characteristics as a group distinct from other units that show inter- and back-arc-basin basalt compositions (fig. 15). Western subareas of the Gastineau also form a distinct group generally similar to Icelandic basalt in Hf and Th contents (fig. 16). Except for the metabasalt of Lions Head Mountain, the characteristics of MORB shown by other elements (figs. 5, 6, 12 and 13) are not shown by the La, Hf, and Th variations (figs 15 and 16).

Yb-normalized ratios of the incompatible elements Th and Ta have been found to be valuable for discrimination between MORB, within-plate basalts, and tholeiitic and alkaline volcanic-arc basalts (Pearce, 1982; 1983). The Yb-normalizing factor effectively eliminates most variations due to partial melting and fractional crystallization, and Yb-normalized Th and Ta values can be used to evaluate components of subduction and crustal contamination (Pearce, 1983). Yb-normalized ratios of Th and Ta show that the three western subareas of the Gastineau Volcanics have calc-alkaline composition, whereas other metabasalt units are tholeiitic (fig. 17). In Wilson's (1989, fig. 7.26) Th/Yb versus Ta/Yb diagram, metabasalts of the western subareas of the Gastineau Volcanics are seen to be OIB derived from an enriched-mantle source. Th/Yb versus Ta/Yb values of all metabasalt units of this study lie within Pearce's (1983) field of basalts formed in nonsubduction settings,

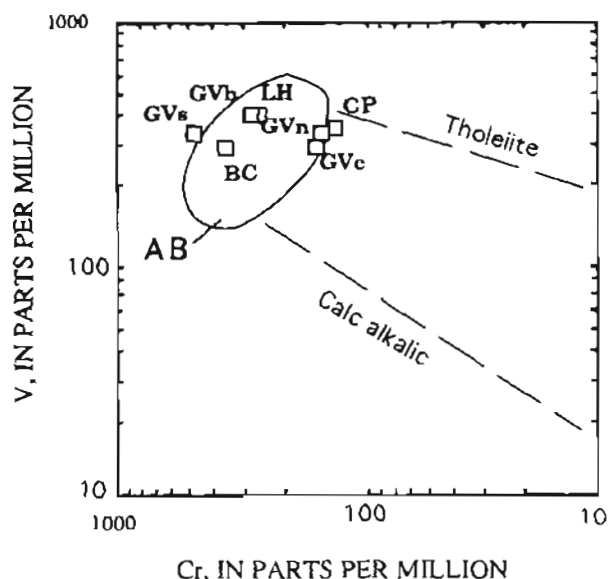


Figure 13. Variation between average log V and log Cr content of metabasalt units, showing field of abyssal tholeiite (AB) and tholeiite and calc-alkalic basalt limits of Miyashiro and Shido (1975). Field AB, MORB of Haydoutov (1989). Letter symbols, table 1.

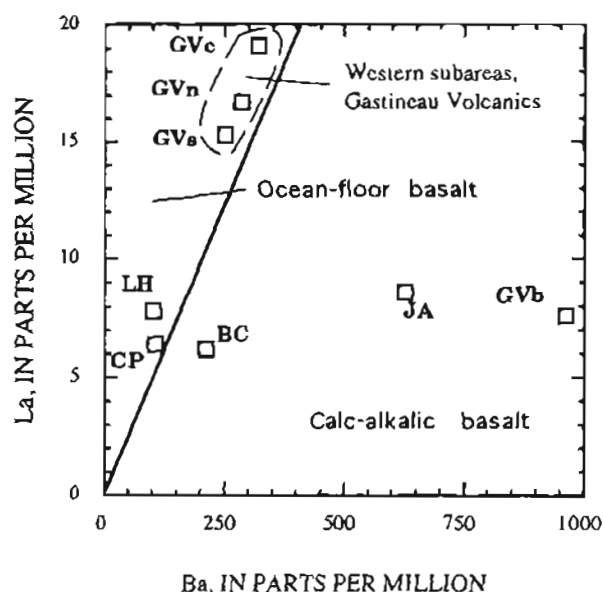


Figure 14. Variation between average La and Ba content of metabasalt units, showing general fields (not outlined) of North Atlantic ocean-floor basalt and calc-alkalic basalt of Wood and others (1980). Unit symbols, table 1.

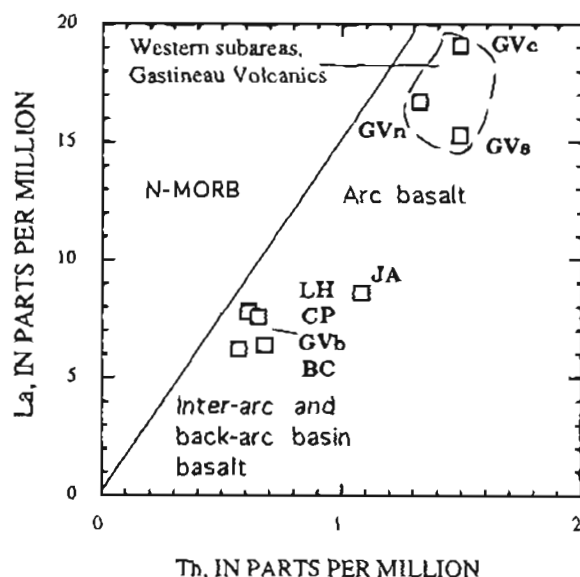


Figure 15. Variation between average La and Th content of metabasalt units. General areas of N-MORB (normal MORB) and of arc basalt and inter-arc- and back-arc-basin basalt (not outlined) from Wood and others (1980). Letter symbols, table 1.

but distinctly different from N-MORB (fig. 17). All units except the high-Ba metabasalt of the Bishop Point area and amphibolite show Ba/Zr values of back-arc-basin basalt, and the western subareas of the Gastineau Volcanics form

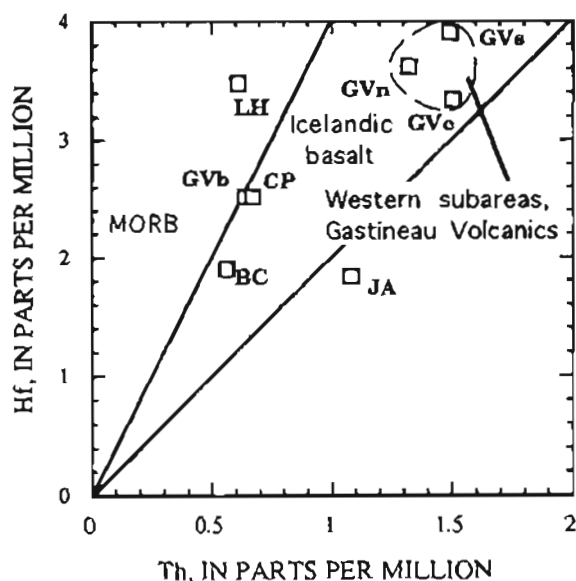


Figure 16. Variation between average Hf and Th content of metabasalt units, showing MORB (normal and transitional) and Icelandic basalt fields of Wood and others (1980). Letter symbols, table 1.

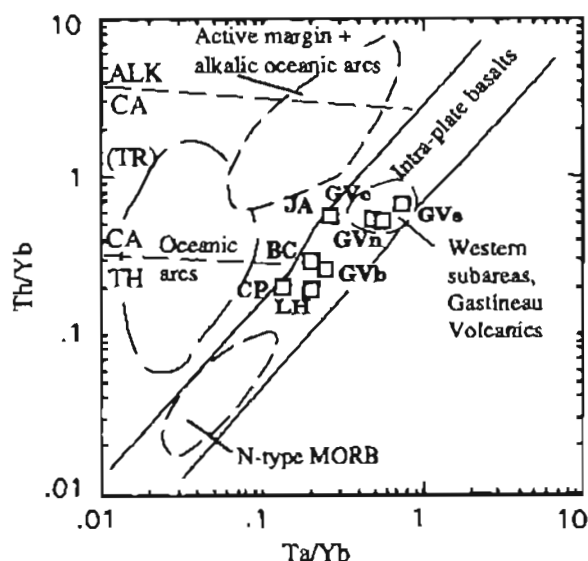


Figure 17. Variation between Yb-normalized average log Th and Ta content of metabasalt units, showing fields of volcanic-arc basalts, N-MORB, and intraplate basalt; and tholeiitic (TH), alkaline (ALK), and calc-alkaline (CA) [transitional (TR)] compositional fields of Pearce (1982, 1983). Band between solid lines shows field of basalt from nonsubduction settings of Pearce (1983). Western subareas of the Gastineau Volcanics (GVs, GVn, and GVc) are in field of enriched mantle source of Wilson (1989). Letter symbols, table 1.

a distinct Ba and Zr group (fig. 18). Because other chemical indicators clearly show tholeiitic composition for the metabasalt of the Bishop Point area and amphibolite, the calc-alkaline island-arc character of these units apparent in figures 14 and 18 is inferred to reflect Ba mobility.

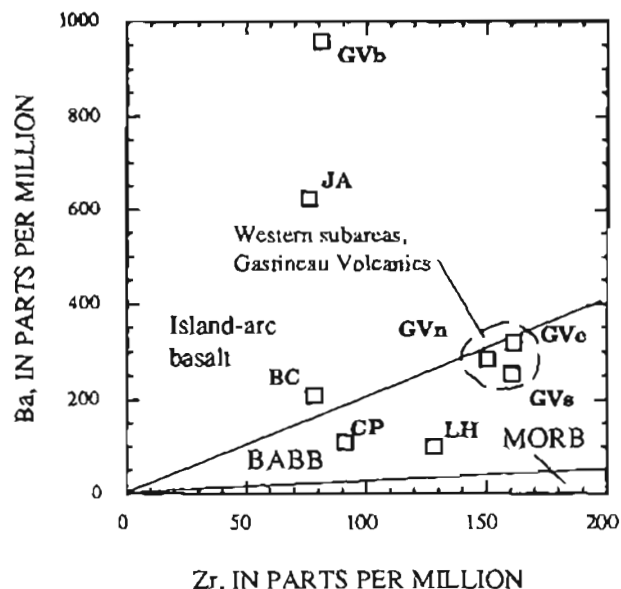


Figure 18. Variation between average Ba and Zr content of metabasalt units, showing fields of island-arc basalt, back-arc-basin basalt (BABB), and MORB of Saunders and Tarney (1991). Letter symbols, table 1.

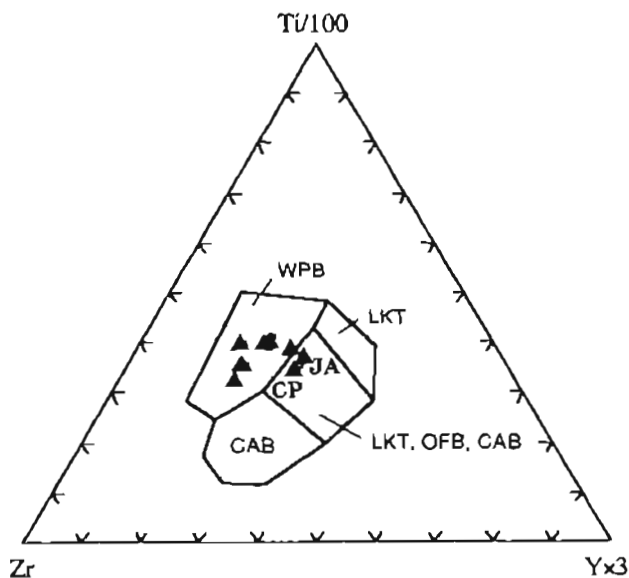
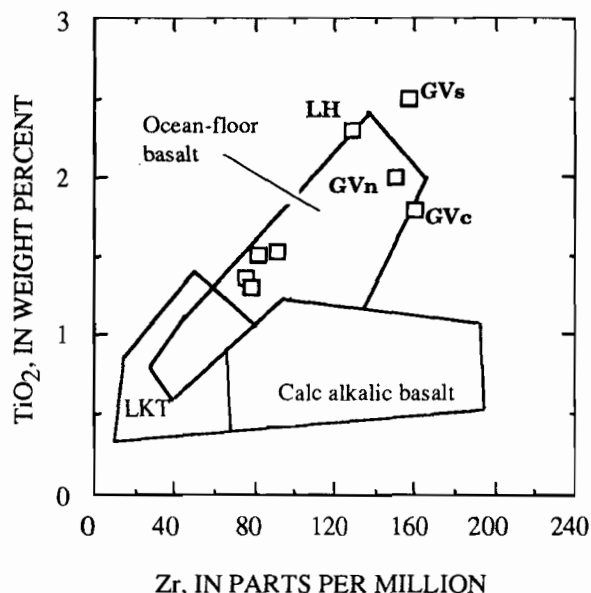


Figure 19. Variation between Ti/100, Zr, and Y times 3 of metabasalt units, showing field of within-plate basalt (WPB) and overlapping fields of low-K tholeiite (LKT), ocean-floor basalt (OFB), and calc-alkaline basalt (CAB) of Pearce and Cann (1973). Field of LKT-OFB-CAB limited to ocean-floor basalt (= back arc) by Hawkins and others (1985). Letter symbols, table 1.

All of the metabasalts of this study have compositions within or near the field of within-plate-basalt in terms of Ti-Zr-Y variation (fig. 19). In terms of  $\text{TiO}_2$  and Zr, all samples plot within or near the field of ocean-floor-basalt



**Figure 20.** Variation between average  $\text{TiO}_2$  and Zr content of metabasalt units, showing fields of ocean-floor basalt, low-K tholeiite (LKT), and calc-alkalic basalt of Pearce and Cann (1973). [In Pearce's (1980)  $\text{TiO}_2$ -Zr diagram all units plot in his MORB field.] Letter symbols, table 1; others grouped closely not identified.

(fig. 20). The three western subareas of the Gastineau Volcanics and the metabasalt of Lions Head Mountain form a scattered, high- $\text{TiO}_2$  and high-Zr group compared with the other metabasalt units that are closely grouped (fig. 20).

Trace-element abundances of all units approximate MORB's for elements between Zr and Ni, and units showing marked positive and negative Cr anomalies do not correspond with the two LILE groups having different patterns between Th and P in the Pearce (1983) diagram of figure 21. The western subareas of the Gastineau Volcanics have MORB-normalized trace-element abundance patterns distinctly more enriched in incompatible elements than those of metabasalts of other areas (LILE-group 1, fig. 21). Those areas of the Gastineau also form a high-Ta group in Wood's (1980) Hf-Th-Ta diagram (fig. 22). The marked Ba enrichment of metabasalts of the Bishop Point area and western Heintzleman Ridge (GVb and JA, fig. 21) may reflect alteration (see also, figs. 14, 18). Alteration may also have produced high-Sr content of some units, as suggested by the albitization of plagioclase (Desmons and others, 1980).

## GEOCHEMICAL DISCRIMINATION OF METABASALT UNITS

Geochemical signatures discriminate rather clearly the Permian(?) and Triassic(?) older part of the Gastineau Volcanics (LILE-group 2) from the Upper Triassic part of

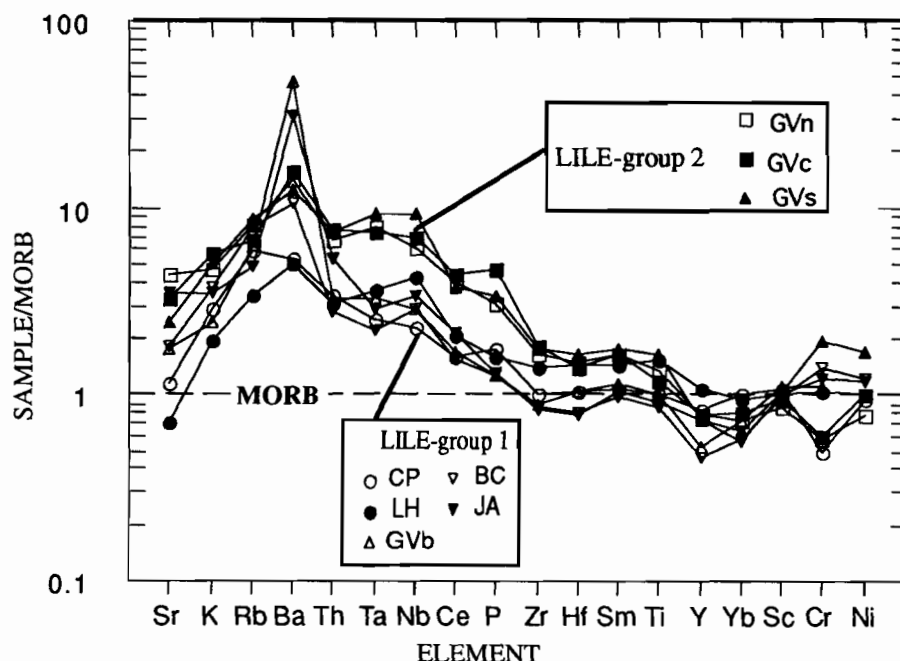


**Figure 21.** MORB-normalized trace-element abundances of metabasalt units, showing different variations for LILE-groups 1 and 2 (see text; table 3). MORB-normalizing values of Pearce (1983). Letter symbols, table 1.

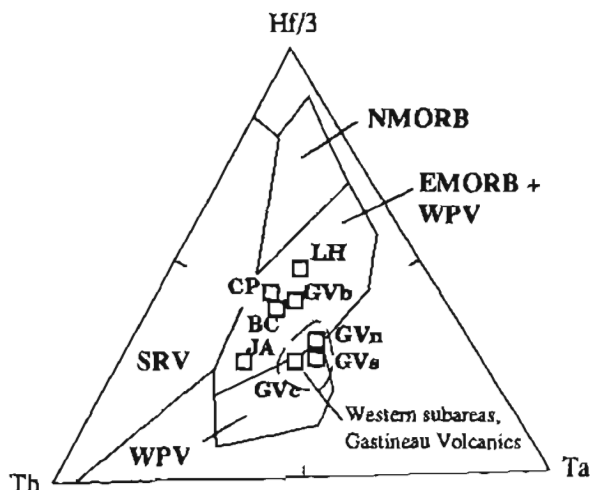


**Figure 22.** Th-Hf-Ta diagram showing fields of major volcanic settings of Wood (1980). SRV, subduction-related volcanics; WPV, within-plate volcanics; NMORB and EMORB, normal and enriched ocean-ridge basalt. Letter symbols, table 1.

the Gastineau at Bishop Point and other metabasalt units of the area (LILE-group 1). Table 3 summarizes the chemical comparisons of the metabasalt units. Signatures particularly apparent for identifying the older parts of the Gastineau Volcanics are (1) higher  $K_2O$  content (fig. 3); (2) higher  $P_2O_5$  content (fig. 4); (3) generally higher  $TiO_2$  content (figs. 5, 20); (4) generally higher Sr and Rb (figs. 7, 9); (5) generally lower Rb/Sr (fig. 8A, B); (6) higher Zr (figs. 9, 18, 20); (7) more enriched chondrite-normalized LREE patterns (fig. 10); (8) distinctly higher La (figs. 14, 15); (9) higher Th (figs. 15, 16); (10) generally higher Hf (fig. 16); (11) generally higher Th/Yb and Ta/Yb (fig. 17); (12) distinctly enriched MORB-normalized abundances of elements between Th and P (fig. 21); and (13) distinctly more abundant Nb and Ta (figs. 21, 22). Major- and trace-element geochemical signatures such as these and as shown in table 3 can aid geologic mapping of the abundant greenstone and greenschist units of this region that are generally difficult to distinguish by field and petrographic characteristics alone.

## INTERPRETATIONS AND CONCLUSIONS

Metabasalts of this study are closely comparable to those of Wrangellia in other southeastern Alaskan and nearby areas. The Wrangellia identification of the metabasalt of the Chilkat Peninsula (Plafker and others, 1989) and chemical comparisons of this study clearly indicate that at least the Triassic upper part of Wrangellia extends much farther to the south (fig. 1) than previously documented. The discontinuity of the Wrangellia greenstone belt between Lions Head Mountain and Blackerby Ridge

near Juneau (fig. 1) is due to plutonic intrusions in intervening areas (Knopf, 1911; Brew and Ford, 1985) and as indicated in this study also to the involvement of Late Cretaceous to early Tertiary amphibolite-facies Barrovian regional metamorphism (Brew and others, 1989; Himmelberg and others, 1991). The amphibolites of western Heintzleman Ridge show many geochemical similarities with greenschist-facies metabasalts of the Chilkat Peninsula and Lions Head Mountain, and the metabasalt of the Bishop Point area of the Gastineau Volcanics (tables 1-3; figs. 2, 5, 9-13, 19-22). The amphibolites have a tholeiitic composition similar to that of Triassic greenschist-facies metavolcanic rocks of the area (figs. 2-6, 9-10, 17, 19-22). Like the greenschist-facies rocks, they show back-arc-basin, within-plate, or ocean-floor basalt composition (figs. 5, 20, 22). Their unusually high Ba content suggestive of calc-alkaline nature (figs. 14, 18) may be an effect of alteration. The amphibolites of the Juneau area lack the island-arc character reported (Stowell and Hooper, 1991; Stowell and others, 1992) for other amphibolites of the west margin of the metamorphic and plutonic belt of the Coast Mountains (JA, figs. 15, 17, 20-22). MORB-normalized geochemical patterns (fig. 21) are those of oceanic within-plate basalt (OIB) that lack the Ta and Nb depletion relative to Th and Hf typical of island-arc basalt (Pearce, 1983; Condie, 1989). An absence of metamorphic equivalents of the voluminous andesites or other more differentiated volcanic rocks typically associated with island-arc suites (Gill, 1981)—and lacking from MORB and intraplate oceanic-basalt associations (Perfit and others, 1980)—is a strong argument against an evolved island-arc origin not only for the amphibolite but for all metabasalts of this study.

The two groups of REE patterns for the metabasalts of this study (fig. 10) lie entirely within the spread of REE patterns reported by Davis and Plafker (1985) for Triassic-age Wrangellia samples from the Chilkat Peninsula and the Nikolai Greenstone. HREE patterns of all units of this study and LREE patterns of the Upper Triassic part of the Gastineau Volcanics approximate those of basalt of the Karmutsen Formation given in Barker and others (1989). The Permian(?) and Triassic(?) lower part of the Gastineau Volcanics, however (fig. 10, GVN, GVC, GVS), differs lack evidence of subduction origin (fig. 22). The many chemical differences between the Permian(?) and Triassic(?) western, older part of the Gastineau Volcanics and the Upper Triassic Bishop Point area of the Gastineau (figs. 3-5, 7-10, 15-17, 20-22) suggest variations in tectonic setting during the formation of this volcanic sequence.

The Wrangellia terrane of mainland southeastern Alaska is found in our study to extend from the Chilkat Peninsula at least as far south as the vicinity of Taku Inlet (fig. 1), and constitutes much of the Taku terrane shown by others in studies described earlier. We believe that the Wrangellia terrane extends even farther south, at least to the vicinity of Tracy Arm, where little-studied Permian

and Triassic metabasalts are reported (Brew and Grybeck, 1984; Gehrels and others, 1992).

Wrangellia is also represented in insular areas of southeastern Alaska. Major- and trace-element composition of the greenschist of the Barlow Cove Formation indicates that rocks of this terrane occur on northern Admiralty Island, an area inferred to be the Alexander terrane by some workers (Silberling and others, 1992; Rubin and Saleeby, 1992; Monger and Berg, 1987) but considered to be a composite of the Alexander and Wrangellia terranes by Brew and Ford (1993). The probable correlation of the Barlow Cove rocks with the Upper Triassic Hyd Group of Loney (1964) suggests that this part of Wrangellia extends southward most of the length of Admiralty Island (Lathram and others, 1960; 1965) and probably farther south to other islands of southeastern Alaska, where correlative rocks occur (Douglass and others, 1989; Muffler, 1967; Muffler and others, 1969).

The Triassic volcanism of Wrangellia has generally been ascribed to varied rift-related tectonic settings. According to Davis and Plafker (1985), volcanism of the metabasalt of the Chilkat Peninsula and the Nikolai Greenstone of the Wrangell Mountains occurred in an extensional intraplate or back- or fore-arc setting. Barker and others (1989) proposed an arc-related rift-basin origin also for the Triassic tholeiite of the Karmutsen Formation of the Queen Charlotte and Vancouver Islands. A back-arc origin close behind an arc axis such as in the Wallowa terrane of Oregon and Idaho is suggested by Vallier (1986, in press) for the setting of Karmutsen volcanism. On the other hand, trace-element and Nd isotopic data of the Triassic flood basalts of Wrangellia show affinity with OIB, and are more likely related to mantle-plume activity than arc-related processes of a back-arc or rifted-arc environment (Lassiter and DePaolo, 1992). We interpret the geochemical characteristics of rocks of our study to be supportive of very large, oceanic mantle plume (super-plume) activity as hypothesized by Richards and others (1991), even though basalts of such origin are not specifically identified based on chemistry in the lack of available discriminant diagrams for that tectonic setting.

The metabasalts of the lower-LILE group of this study show relatively flat REE patterns 10–20 times chondrite (LILE-group 1, fig. 10) that lack La and Ce depletion but otherwise approximate those of basalts of midocean ridge and back-arc (marginal) basin settings (Wood and others, 1980; Brouxel and Lapiere, 1988) and are also similar to basalts of rift-related type (Fodor and Vetter, 1984). Metabasalts of the higher-LREE group, of the western (older) subareas of the Gastineau Volcanics, on the other hand, show similarity with island-arc suites (Peccerillo and Taylor, 1976). Both groups of REE patterns for the metavolcanic rocks of this study (fig. 10) show tholeiitic rather than calc-alkaline signatures (Wilson, 1989). However, Wood and others (1980) reported that both LREE-

enriched and LREE-depleted patterns can occur in either subduction-zone or mid-ocean ridge environments and thus those elements may not uniquely discriminate a tectonic setting.

Many of the major- and trace-element data reported here for the Triassic and Triassic(?) metabasalts of the Chilkat Peninsula, Lions Head Mountain, Barlow Cove, and Bishop Point area of the Gastineau Volcanics, as well as for amphibolite of the Juneau area, are similar to data of Davis and Plafker (1985) used by them to suggest an intraplate or back- or fore-arc extensional setting of the volcanism. The many chemical differences between the Permian(?) and Triassic(?) lower part of the Gastineau Volcanics and its Triassic upper part (tables 1–3 and most figures) are believed to reflect differences in origin. All rock units of this study have ratios of high-field-strength elements versus LILE (represented by Nb/La, 1.3–2.1) that are typical of basalts of Wrangellia (Lassiter and DePaolo, 1992). Many back-arc-basin basalts have compositions transitional between MORB and island-arc tholeiite, showing enrichment in Ba, Rb, K, and LREE relative to MORB (Saunders and Tarney, 1991; Ikeda and Yuasa, 1989), as is shown by the lower part of the Gastineau Volcanics (LILE-group 2). Rb/Sr values do not distinguish back-arc from island-arc settings for the metabasalts of this study but do exclude MORB, according to data of Hawkesworth and others (1977). Th/U ratios (1.6–3.0) of the metabasalt samples are about those of the typically low range found in island-arc volcanic rocks and lower than occur in MORB (Taylor and McLennan, 1985). The Permian(?) and Triassic(?) lower part of the Gastineau Volcanics does not show the E-type MORB characteristics (Floyd, 1991) of the Triassic Bishop Point area of the Gastineau and the Triassic(?) Lions Head Mountain, Barlow Cove, and amphibolite units. All units of this study lack the Nb and Ta depletions (figs. 21, 22) characteristic of island-arc tholeiite and related volcanic rocks formed by subduction processes (Pearce, 1983). On the other hand, the Nb and Th contents of all the metabasalts of this study (table 2) show variations reported by Hofmann (1986) for OIB, with Nb, Ta, and Th contents higher by a factor of two in the metabasalts of the western subareas of the Gastineau Volcanics compared with other units.

The chemical variations in the northern southeastern Alaskan metabasalts of this study reflect long-lived late Paleozoic and Triassic volcanism of diverse tectonic setting that differs in some respects from that reported for other Wrangellia areas of southern Alaska, British Columbia, and Idaho (Jones and others, 1986; Barker and others, 1989; and Vallier, in press). An intra-oceanic, juvenile magmatic environment, with little crustal involvement, is indicated by Nd and Sr isotopic data for the formation of Wrangellia before its accretion to North America (Samson and others, 1990). Samson and others (1990), however, did not distinguish earlier (Permian?) and later (Late Triassic)



Wrangellia environments, as encompassed in the age range of the Gastineau Volcanics. Moreover, their inclusion of samples with a 420–90 Ma age range in their “Wrangellia,” and with lithologies of mudstone to granodiorite (Samson and others, 1990, p. 751, 755), makes interpretation of their data in terms of tectonic setting for the Juneau-area rocks uncertain. The magmatic environment that they inferred, however, is one that seems to be supported by much of our data. In particular, the lack of a subduction-zone component for all units of this study is indicated by Ta abundance in the Hf–Th–Ta diagram of figure 22. The typical depletion of the high-field-strength elements Ta and Nb relative to Th of subduction-related volcanic rocks (Pearce, 1983) is similarly not evident in MORB-normalized element variations (fig. 21). Even tholeiites of arcs of a primitive stage of development show strongly negative Nb anomalies (Arculus, 1987).

The tectonic settings suggested by different chemical signatures of the different metabasalt units of this part of Wrangellia are conflicting, as seen by comparing many of the diagrams of this report. However, we follow Wood (1980), Pearce (1983), Arculus (1987), and others in considering that the relatively immobile HFSE such as Th, Hf, Nb, and Ta afford the best available indicators of tectonic setting. Thus, an arc-derived origin as reported for upper Paleozoic volcanic rocks of Wrangellia elsewhere, such as by Jones and others (1986, 1987) and Monger and Berg (1987), is not indicated for the older part of the Gastineau Volcanics of the terrane near Juneau, nor for the Triassic basalts of the terrane as implied by interpretations of a back- or fore-arc setting of that volcanism in other areas (Davis and Plafker, 1985; Vallier, 1986; Barker and others, 1989). The basaltic volcanism of Wrangellia near Juneau, lacking evidence of a subduction component (fig. 22), is inferred to be instead largely of oceanic within-plate (OIB) type and possibly related to oceanic mantle-plume processes. Such activity might account for the immense scale of Wrangellian volcanism (Richards and others, 1991).

Wrangellia was amalgamated with the Alexander terrane by Carboniferous time (Gardner and others, 1988), if not having originated within that terrane and always a part of it. However combined, the composite Alexander plus Wrangellia terrane (Brew and Ford, 1993) subsequently accreted to the western edge of North America by the time of the Cretaceous to early Tertiary plutonism in the Coast Mountains (DeBiche and others, 1987), in an event that was possibly associated with the regional Barrovian metamorphism described by Himmelberg and others (1991) or with volcanism of the Douglas Island Volcanics.

In summary, geochemical data of our study show that basaltic rocks of the Wrangellia terrane are much more widespread in northern southeastern Alaska than previously recognized, and are represented in the Juneau area by the Gastineau Volcanics and metabasalts of Lions Head Mountain, rather than the Taku terrane as interpreted by

others. The rocks show little geochemical influence of subduction processes. Distinct chemical differences between the Permian(?) and Triassic(?) lower and the Upper Triassic upper parts of the Gastineau Volcanics reflect differences in tectonic settings of the Juneau-area Wrangellia volcanism. Rocks of the lower part of the formation show LILE-enriched abundances and other trace-element characteristics of ocean-island basalt, whereas Upper Triassic rocks of the unit and correlative metabasalts show enriched MORB and other features that may be related to an extensional-rift setting, as suggested for correlative Triassic units of other Wrangellia areas, or to oceanic mantle-plume activity. The metabasalts of the Juneau area record volcanism of diverse tectonic settings and stages of development within a long-lived ocean-island volcanic environment, with earlier activity related to ocean-island volcanism and later events to rifting activity possibly associated with ancestral events preceding amalgamation with the Alexander terrane. Accretion of the combined Alexander plus Wrangellia terrane to North America may have been associated with major Barrovian regional metamorphism near the end of Cretaceous time or with Cretaceous subduction-related volcanism of the Douglas Island Volcanics.

## REFERENCES CITED

- Arculus, R.J., 1987, The significance of source versus process in the tectonic controls of magma genesis: *Journal of Volcanology and Geothermal Research*, v. 32, p. 1–12.
- Badger, R.L., 1993, Fluid interaction and geochemical mobility in metabasalts: An example from the central Appalachians: *Journal of Geology*, v. 101, p. 85–95.
- Baedecker, P.A., ed., 1987, Methods for geochemical analysis: U.S. Geological Survey Bulletin 1770, p. A1–K5.
- Barker, Fred, 1957, Geology of the Juneau (B-3) quadrangle, Alaska: U.S. Geological Survey Geologic Quadrangle Map GQ-100, scale 1:63,360.
- Barker, Fred, Sutherland Brown, A., Budahn, J.R., and Plafker, George, 1989, Back-arc with frontal-arc component origin of Triassic Karmutsen basalt, British Columbia, Canada: *Chemical Geology*, v. 75, p. 81–102.
- Berg, H.C., 1981, Upper Triassic volcanogenic massive-sulfide metallogenic province identified in southeastern Alaska, in Albert, N.R.D., and Hudson, Travis, eds., *The United States Geological Survey in Alaska: Accomplishments during 1979*: U.S. Geological Survey Circular 823-B, p. B104–B108.
- Brew, D.A., Drew, L.J., Schmidt, J.M., Root, D.H., and Huber, D.F., 1991, Undiscovered locatable mineral resources of the Tongass National Forest and adjacent lands, southeastern Alaska: U.S. Geological Survey Open-File Report 91–10, 370 p.
- Brew, D.A., and Ford, A.B., 1977, Preliminary geologic and metamorphic isograd map, Juneau B-1 quadrangle, Alaska: Geological Survey Miscellaneous Field Studies Map MF-846, scale 1:31,680.
- , 1984, Tectonostratigraphic terranes in the Coast plutonic-metamorphic complex, southeastern Alaska, in Bartsch-Winkler, Susan, and Reed, K.M., eds., *The U.S. Geological*

- Survey in Alaska: Accomplishments during 1982: U.S. Geological Survey Circular 939, p. 90-93.
- 1985, Preliminary reconnaissance geologic map of the Juneau, Taku River, Atlin, and part of the Skagway 1:250,000 quadrangles, southeastern Alaska: U.S. Geological Survey Open-File Report 85-395, 23 p.
- 1993, Regional distribution and geologic context of volcanic-rock-hosted massive-sulfide deposits in southeastern Alaska and adjacent parts of British Columbia [abs.]: Abstracts of Professional Papers, Alaska Miner's Association Conference Juneau 1993, Juneau, Alaska, April 21-23, 1993, p. 33-34.
- Brew, D.A., Ford, A.B., and Himmelberg, G.R., 1989, Evolution of the western part of the Coast plutonic-metamorphic complex, south-eastern Alaska, USA, in Daly, J.S., Cliff, R.A., and Yardley, B.W.D., eds., *Evolution of metamorphic belts: Geological Society Special Publication* 43, p. 447-452.
- Brew, D.A., and Grybeck, Donald, 1984, Geology of the Tracy Arm-Fords Terror Wilderness study area and vicinity, Alaska: U.S. Geological Survey Bulletin 1525, p. 23-52.
- Brew, D.A., Karl, S.M., Barnes, D.F., Jachens, R.C., Ford, A.B., and Homer, Robert, 1991, A northern Cordilleran ocean-continent transect: Sitka Sound, Alaska, to Atlin Lake, British Columbia: *Canadian Journal of Earth Sciences*, v. 28, p. 840-853.
- Brew, D.A., Ovenshine, A.T., Karl, S.M., and Hunt, S.J., 1984, Preliminary reconnaissance geologic map of the Petersburg and parts of the Port Alexander and Sumdum 1:250,000 quadrangles, southeastern Alaska: U.S. Geological Survey Open-File Report 84-405, 2 sheets, with 43 p. pamphlet.
- Brouxel, Marc, and Lapierre, Henriette, 1988, Geochemical study of an early Paleozoic island-arc-back-arc basin system. Part 1: The Trinity Ophiolite (northern California): *Geological Society of America Bulletin*, v. 100, p. 1111-1119.
- Buddington, A.F., and Chapin, Theodore, 1929, Geology and mineral deposits of southeastern Alaska: U.S. Geological Survey Bulletin 800, 398 p.
- Condie, K.C., 1989, Plate tectonics and crustal evolution: New York, Pergamon, 476 p.
- Davis, Alicé, and Plafker, George, 1985, Comparative geochemistry and petrology of Triassic basaltic rocks from the Taku terrane on the Chilkat Peninsula and Wrangellia: *Canadian Journal of Earth Sciences*, v. 22, p. 183-194.
- DeBiche, M.G., Cox, Allan, and Engebretson, D.C., 1987, The motion of allochthonous terranes across the north Pacific basin: *Geological Society of America, Special Paper* 207, 49 p.
- Desmons, J., Delaloye, M., Desmet, A., Gagny, C.I., Rocci, G., and Voldet, P., 1980, Trace and rare earth element abundances in Troodos lavas and sheeted dikes, Cyprus: *Ophiolites*, v. 5, p. 35-56.
- Douglass, S.L., Webster, J.H., Burrell, P.D., Lanphere, M.L., and Brew, D.A., 1989, Major element chemistry, radiometric values, and locations of samples from the Petersburg and parts of the Port Alexander and Sumdum quadrangles, southeastern Alaska: U.S. Geological Survey Open-File Report 89-527, 66 p., map scale 1:250,000.
- Ewart, A., 1982, The mineralogy and petrology of Tertiary-Recent orogenic volcanic rocks: with special reference to the andesite-basaltic compositional range, in Thorpe, R.S., ed., *Andesites*: New York, John Wiley & Sons, p. 25-95.
- Flower, Martin, 1991, Magmatic processes in oceanic ridge and intraplate settings, in Floyd, P.A., ed., *Oceanic basalts*: New York, Van Nostrand Reinhold, p. 116-147.
- Floyd, P.A., 1991, Oceanic islands and seamounts, in Floyd, P.A., ed., *Oceanic basalts*: New York, Van Nostrand Reinhold, p. 174-218.
- Floyd, P.A., and Winchester, J.A., 1975, Magma type and tectonic setting discrimination using immobile elements: *Earth and Planetary Science Letters*, v. 27, p. 211-218.
- Fodor, R.V., and Vetter, S.K., 1984, Rift-zone magmatism: petrology of basaltic rocks transitional from CFB to MORB, southeastern Brazil margin: *Contributions to Mineralogy and Petrology*, v. 88, p. 307-321.
- Forbes, R.B., Gilbert, Wyatt, and Redman, Earl, 1989, Geologic setting and petrology of the metavolcanic rocks in the northwestern part of the Skagway B-4 quadrangle, southeastern Alaska: Alaska Division of Geological and Geophysical Surveys, Public-data File 89-14, 43 p.
- Ford, A.B., and Brew, D.A., 1973, Preliminary geologic and metamorphic-isograd map of the Juneau B-2 quadrangle, Alaska: U.S. Geological Survey Miscellaneous Field Studies Map MF-527, scale 1:31,680.
- 1977, Preliminary geologic and metamorphic-isograd map of parts of the Juneau A-1 and A-2 quadrangles, Alaska: U.S. Geological Survey Miscellaneous Field Studies Map MF-847, scale 1:31,680.
- 1988, Major-element geochemistry of metabasalts of the Juneau-Haines region, southeastern Alaska, in Galloway, J.P., and Hamilton, T.D., eds., *Geologic studies in Alaska by the U.S. Geological Survey during 1987: U.S. Geological Survey Circular* 1016, p. 150-155.
- Gardner, M.C., Bergman, S.C., Cushing, G.W., MacKevett, E.M., Jr., Plafker, George, Campbell, R.B., Dodds, C.J., McClelland, W.C., and Mueller, P.A., 1988, Pennsylvanian pluton stitching of Wrangellia and the Alexander terrane, Wrangell Mountains, Alaska: *Geology*, v. 16, p. 967-971.
- Gehrels, G.E., and Berg, H.C., 1992, Geologic map of southeastern Alaska: U.S. Geological Survey Miscellaneous Investigations Series, Map I-1867, scale: 1:600,000.
- Gehrels, G.E., McClelland, W.C., Samson, S.D., Patchett, P.J., and Orchard, M.J., 1992, Geology of the western flank of the Coast Mountains between Cape Fanshaw and Taku Inlet, southeastern Alaska: *Tectonics*, v. 11, p. 567-585.
- Gill, J.B., 1981, Orogenic andesites and plate tectonics: New York, Springer-Verlag, 390 p.
- Hawkesworth, C.J., O'Nions, R.K., Pankhurst, R.J., Hamilton, P.J., and Evensen, N.M., 1977, A geochemical study of island-arc and back-arc tholeiites from the Scotia Sea: *Earth and Planetary Science Letters*, v. 36, p. 253-262.
- Hawkins, J.W., Moore, G.F., Villamor, R., Evans, C., Wright, E., 1985, Geology of the composite terranes of East and Central Mindanao, in Howell, D.G., ed., *Tectono-stratigraphic terranes of the circum-Pacific region: Circum-Pacific Council for Energy and Mineral Resources, Earth Science Series*, number 1, p. 437-462.
- Haydoutov, Ivan, 1989, Precambrian ophiolites, Cambrian island arc, and Variscan suture in the South Carpathian-Balkan region: *Geology*, v. 17, p. 905-908.
- Henderson, J.R., Kirkham, R.V., Henderson, M.N., Payne, J.G., Wright, T.O., and Wright, R.L., 1992, Stratigraphy and structure of the Sulphurets area, British Columbia: *Geological Survey of Canada Paper* 92-1A, p. 323-332.
- Himmelberg, G.R., Brew, D.A., and Ford, A.B., 1991, Develop-

- ment of inverted metamorphic isograds in the western metamorphic belt, Juneau, Alaska: *Journal of Metamorphic Geology*, v. 9, p. 165–180.
- Hofmann, A.W., 1986, Nb in Hawaiian magmas: Constraints on source composition and evolution: *Chemical Geology*, v. 57, p. 17–30.
- Howell, D.G., ed., 1985, Tectonostratigraphic terranes of the Circum-Pacific region: Circum-Pacific Council for Energy and Mineral Resources, Earth Science Series, number 1, 581 p.
- Ikeda, Yasuo, and Yuasa, Makoto, 1989, Volcanism in nascent back-arc basins behind the Shichito Ridge and adjacent areas in the Izu–Ogasawara arc, northwest Pacific: Evidence for mixing between E-type MORB and island arc magmas at the initiation of back-arc rifting: *Contributions to Mineralogy and Petrology*, v. 101, p. 377–393.
- Jones, D.L., Silberling, N.J., and Coney, 1986, Collision tectonics in the Cordillera of western N America: Examples from Alaska, in Coward, M.P., and Ries, A.C., eds., *Collision tectonics: Geological Society Special Publication no. 19*, p. 367–387.
- Jones, D.L., Silberling, N.J., Coney, P.J., and Plafker, G.P., 1987, Lithotectonic terrane map of Alaska (west of the 141st meridian): U.S. Geological Survey Miscellaneous Field Studies Map MF-1874-A, scale 1:2,500,000.
- Jones, D.L., Silberling, N.J., and Hillhouse, John, 1977, Wrangellia—A displaced terrane in northwestern North America: *Canadian Journal of Earth Sciences*, v. 14, p. 2565–2577.
- Knopf, Adolph, 1911, Geology of the Berners Bay region, Alaska: U.S. Geological Survey Bulletin 446, 58 p.
- Lassiter, J.C., and DePaolo, D.J., 1992, Geochemical and isotopic features of oceanic flood basalts: a case study of the Wrangellia terrane [abs.]: *Eos, American Geophysical Union Transactions*, v. 73, p. 533.
- Latham, E.H., Loney, R.A., Berg, H.C., and Pomeroy, J.S., 1960, Progress map of the geology of Admiralty Island, Alaska: U.S. Geological Survey Miscellaneous Investigations Map, I-323, scale 1:250,000.
- Latham, E.H., Pomeroy, J.S., Berg, H.C., and Loney, R.A., 1965, Reconnaissance geology of Admiralty Island, Alaska: U.S. Geological Survey Bulletin 1180-R, 48 p.
- Lawrie, K.C., 1992, Geochemical characterisation of a polyphase deformed, altered, and high grade metamorphosed volcanic terrane: implications for the tectonic setting of the Svecofennides, south-central Finland: *Precambrian Research*, v. 59, p. 171–205.
- Loney, R.A., 1964, Stratigraphy and petrography of the Pybus–Gambier area, Admiralty Island, Alaska: U.S. Geological Survey Bulletin 1178, 103 p.
- Loney, R.A., Brew, D.A., Muffler, L.J.P., and Pomeroy, J.S., 1975, Reconnaissance geology of Chichagof, Baranof, and Kruzof islands, southeastern Alaska: U.S. Geological Survey Professional Paper 792, 105 p.
- MacIntyre, D.G., 1986, The geochemistry of basalts hosting massive sulphide deposits, Alexander terrane, northwest British Columbia, in *Geological fieldwork 1985: British Columbia Ministry of Energy, Mines and Petroleum Resources, Paper 1986 – 1*, p. 197–210.
- Martin, G.C., 1926, The Mesozoic stratigraphy of Alaska: U.S. Geological Survey Bulletin 776, 493 p.
- Miyashiro, Akiho, 1974, Volcanic rock series in island arcs and active continental margins: *American Journal of Science*, v. 274, p. 321–355.
- Miyashiro, Akiho, and Shido, Fumiko, 1975, Tholeiitic and calc-alkalic series in relation to the behaviors of titanium, vanadium, chromium, and nickel: *American Journal of Science*, v. 275, p. 265–277.
- Monger, J.W.H., and Berg, H.C., 1987, Lithotectonic terrane map of western Canada and southeastern Alaska: U.S. Geological Survey Miscellaneous Field Studies Map MF-1874-B, scale 1:2,500,000.
- Mortimer, N., 1987, The Nicola Group: Late Triassic and Early Jurassic subduction-related volcanism in British Columbia: *Canadian Journal of Earth Sciences*, v. 24, p. 2521–2536.
- Mottl, M.J., 1983, Metabasalts, axial hot springs, and the structure of hydrothermal systems at mid-ocean ridges: *Geological Society of America Bulletin*, v. 94, p. 161–180.
- Muffler, L.J.P., 1967, Stratigraphy of the Keku Islets and neighboring parts of Kuiu and Kupreanof Islands, southeastern Alaska: U.S. Geological Survey Bulletin 1241-C, p. C1–C52.
- Muffler, L.J.P., Short, J.M., Keith, T.B.C., and Smith, V.C., 1969, Chemistry of fresh and altered basaltic glass from the Upper Triassic Hound Island Volcanics, southeastern Alaska: *American Journal of Science*, v. 267, p. 196–209.
- Mullen, E.D., 1983, MnO/TiO<sub>2</sub>/P<sub>2</sub>O<sub>5</sub>: A minor element discriminant for basaltic rocks of oceanic environments and its implications for petrogenesis: *Earth and Planetary Science Letters*, v. 62, p. 53–62.
- Nicholls, I.A., Whitford, D.J., Harris, K.L., and Taylor, S.R., 1980, Variation in the geochemistry of mantle sources for tholeiitic and calc-alkaline mafic magmas, western Sunda volcanic arc, Indonesia: *Chemical Geology*, v. 30, p. 177–199.
- Nokleberg, W.J., Bundtzen, T.K., Berg, H.C., Brew, D.A., Grybeck, Donald, Robinson, M.S., and Smith, T.E., 1989, Metallogenic map of significant volcanogenic massive-sulfide and related lode deposits in Alaska: U.S. Geological Survey Miscellaneous Field Studies Map MF-1853-C, scale 1:5,000,000.
- North American Commission on Stratigraphic Nomenclature, 1983, North American Stratigraphic Code: *American Association of Petroleum Geologists Bulletin*, v. 67, p. 841–875.
- Panaska, B.C., 1990, An overlooked, world class Triassic flood basalt event [abs.]: *Geological Society of America, Abstracts with Programs*, v. 22, no. 7, p. A168.
- Pearce, J.A., 1980, Geochemical evidence for the genesis and eruptive setting of lavas from Tethyan ophiolites, in Panayiotou, A., ed., *Ophiolites: Proceedings, International Ophiolite Symposium: Nicosia, Cyprus Geological Survey*, p. 261–272.
- , 1982, Trace element characteristics of lavas from destructive plate boundaries, in Thorpe, R.S., ed., *Andesites: New York, John Wiley & Sons*, p. 525–548.
- , 1983, Role of the sub-continental lithosphere in magma genesis at active continental margins, in Hawkesworth, C.J., and Norry, M.J., eds., *Continental basalts and mantle xenoliths: Nantwich, Shiva*, p. 230–249.
- Pearce, J.A., and Cann, J.R., 1973, Tectonic setting of basic volcanic rocks determined using trace element analyses: *Earth and Planetary Science Letters*, v. 19, p. 290–300.
- Peccherillo, Angelo, and Taylor, S.R., 1976, Geochemistry of Eocene calc-alkaline volcanic rocks from the Kastamonu area, northern Turkey: *Contributions to Mineralogy and Petrology*, v. 58, p. 63–81.

- Perfit, M.R., Gust, D.A., Bence, A.E., Arculus, R.J., and S.R. Taylor, 1980, Chemical characteristics of island-arc basalts: implications for mantle sources: *Chemical Geology*, v. 30, 227-256.
- Plafker, George, Blome, C.D., and Silberling, N.J., 1989, Reinterpretation of lower Mesozoic rocks on the Chilkat Peninsula, Alaska, as a displaced fragment of Wrangellia: *Geology*, v. 17, p. 3-6.
- Plafker, George, and Hudson, Travis, 1980, Regional implications of Upper Triassic metavolcanic and metasedimentary rocks on the Chilkat Peninsula, southeastern Alaska: *Canadian Journal of Earth Sciences*, v. 17, p. 681-689.
- Plafker, George, Hudson, Travis, and Silberling, N.J., 1979, Late Triassic fossils from a sequence of volcanic and sedimentary rocks on the Chilkat Peninsula, southeastern Alaska, in Johnson, K.M., and Williams, J.R., eds., *The United States Geological Survey in Alaska: Accomplishments during 1978: U.S. Geological Survey Circular 804-B*, p. B107-B110.
- Richards, M.A., Jones, D.L., Duncan, R.A., and DePaolo, D.J., 1991, A mantle plume initiation model for the Wrangellia flood basalt and other oceanic plateaus: *Science*, v. 254, p. 263-267.
- Rubin, C.M., and Saleeby, J.B., 1992, Tectonic history of the eastern edge of the Alexander terrane, southeast Alaska: *Tectonics*, v. 11, p. 586-602.
- Samson, S.D., Patchett, P.J., Gehrels, G.E., and Anderson, R.G., 1990, Nd and Sr isotopic characterization of the Wrangellia terrane and implications for crustal growth of the Canadian Cordillera: *Journal of Geology*, v. 98, p. 749-762.
- Samson, S.D., Patchett, P.J., McClelland, W.C., and Gehrels, George, 1991, Nd isotopic characterization of metamorphic rocks in the Coast Mountains, Alaskan and Canadian Cordillera: ancient crust bounded by juvenile terranes: *Tectonics*, v. 10, p. 770-780.
- Saunders, Andrew, and Tarney, John, 1991, Back-arc basins, in Floyd, P.A., ed., *Oceanic basalts: New York, Van Nostrand Reinhold*, p. 219-263.
- Shervais, J.W., 1982, Ti-V plots and the petrogenesis of modern and ophiolitic lavas: *Earth and Planetary Science Letters*, v. 59, p. 101-118.
- Silberling, N.J., Jones, D.L., Monger, J.W.H., and Coney, P.J., 1992, Lithotectonic terrane map of the North American Cordillera: U.S. Geological Survey Miscellaneous Investigations Map I-2176, scale 1:5,000,000.
- Souther, J.G., 1971, *Geology and mineral deposits of Tulsequah Map-area, British Columbia: Geological Survey of Canada Memoir 362*, 84 p.
- Stowell, H.H., and Hooper, R.J., 1991, Character and geochemistry of metabasalts, western metamorphic belt, northern Coast Ranges, SE Alaska [abs.]: *Geological Society of America, Abstracts with Programs*, v. 23, no. 2, p. 101.
- Stowell, H.H., Green, N.L., and Hooper, R.J., 1992, Geochemistry & tectonic setting of Permian? - Cretaceous basaltic volcanism, northern Coast Ranges, SE AK [abs.]: *Geological Society of America, Abstracts with Programs*, v. 24, no. 7, p. 66.
- Taylor, S.R., Kaye, Maureen, White, A.J.R., Duncan, A.R., and Ewart, A., 1969, Genetic significance of Co, Cr, Ni, Sc and V content of andesites: *Geochimica et Cosmochimica Acta*, v. 33, p. 275-286.
- Taylor, S.R., and McLennan, 1985, *The continental crust: Its composition and evolution: Boston, Blackwell*, 312 p.
- Thompson, G., Bryan, W.B., and Humphris, S.E., 1989, Axial volcanism on the East Pacific Rise, 10-12°N, in Saunders, A.D., and Norry, M.J., eds., *Magmatism in the ocean basins: Geological Society Special Publication 42*, p. 181-200.
- Vallier, T.L., 1986, Tectonic implications of arc-axis (Wallowa terrane) and back-arc (Vancouver Island) volcanism in Triassic rocks of Wrangellia [abs.]: *Eos, American Geophysical Union Transactions*, v. 67, p. 1233.
- Vallier, T.L., in press, Petrology of pre-Tertiary igneous rocks in the Blue Mountains region of Oregon, Idaho, and Washington: Implications for the geologic evolution of a complex island arc, in Vallier, T.L., and Brooks, H.C., eds., *The geology of the Blue Mountains region of Oregon, Idaho, and Washington: Petrology and tectonic evolution of pre-Tertiary rocks: U.S. Geological Survey Professional Paper 1438*.
- Viereck, L.G., Flower, M.F.J., Hertogen, J., Schmincke, H.-U., and Jenner, G.A., 1989, The genesis and significance of N-MORB sub-types: *Contributions to Mineralogy and Petrology*, v. 102, p. 112-126.
- Walker, Cherry, 1991, North Atlantic ocean crust and Iceland, in Floyd, P.A., ed., *Oceanic basalts: New York, Van Nostrand Reinhold*, p. 310-352.
- Wheatley, Michael, and Rock, N.M.S., 1988, SPIDER: A Macintosh program to generate normalized multi-element "spidergrams": *American Mineralogist*, v. 73, p. 919-921.
- Wheeler, J.O., and McFeely, P., 1991, Tectonic assemblage map of the Canadian Cordillera and parts of the United States of America: *Geological Survey of Canada Map 1712A*, scale 1:2,000,000.
- Wilson, Marjorie, 1989, *Igneous petrogenesis: Boston, Unwin Hyman*, 466 p.
- Winchester, J.A., and Floyd, P.A., 1976, Geochemical magma type discrimination: application to altered and metamorphosed basic igneous rocks: *Earth and Planetary Science Letters*, v. 28, p. 459-469.
- Wood, D.A., 1980, The application of a Th-Hf-Ta diagram to problems of tectonomagmatic classification and to establishing the nature of crustal contamination of basaltic lavas of the British Tertiary volcanic province: *Earth and Planetary Science Letters*, v. 50, p. 11-30.
- Wood, D.A., Joron, J.-L., Marsh, N.G., Tarney, J., and Treuil, M., 1980, Major- and trace-element variations in basalts from the North Philippine Sea drilled during Deep Sea Drilling Project Leg 58: a comparative study of back-arc-basin basalts with lava series from Japan and mid-ocean ridges: *Initial Reports of the Deep Sea Drilling Project*, v. 58, p. 873-894.

Reviewers: Mary M. Donato and Tracy L. Vallier

# RECONNAISSANCE GEOCHEMISTRY OF PERMIAN AND TRIASSIC BASALTS OF THE TAKU AND WRANGELLIA TERRANES, SOUTHEASTERN ALASKA

By George E. Gehrels and Fred Barker

## ABSTRACT

Major and minor element geochemical data are presented for Permian and Triassic basalts that belong to the Taku terrane, and for Triassic basalts of the Wrangellia terrane. These data indicate that the Permian and Upper Triassic volcanic rocks of the Taku terrane differ significantly in their chemical signatures. The Permian rocks are high-magnesian alkaline basalts, whereas the Upper Triassic rocks are similar to midocean ridge or within-plate tholeiites. The data also indicate that the Triassic rocks of the Taku and Wrangellia terranes are very similar chemically, which supports previous stratigraphic correlations between these two sequences. The Wrangellia and Taku terranes either evolved in close proximity to each other during Late Triassic time, or the Taku terrane of the Juneau-Port Houghton area actually is a facies of the Wrangellia terrane.

## INTRODUCTION

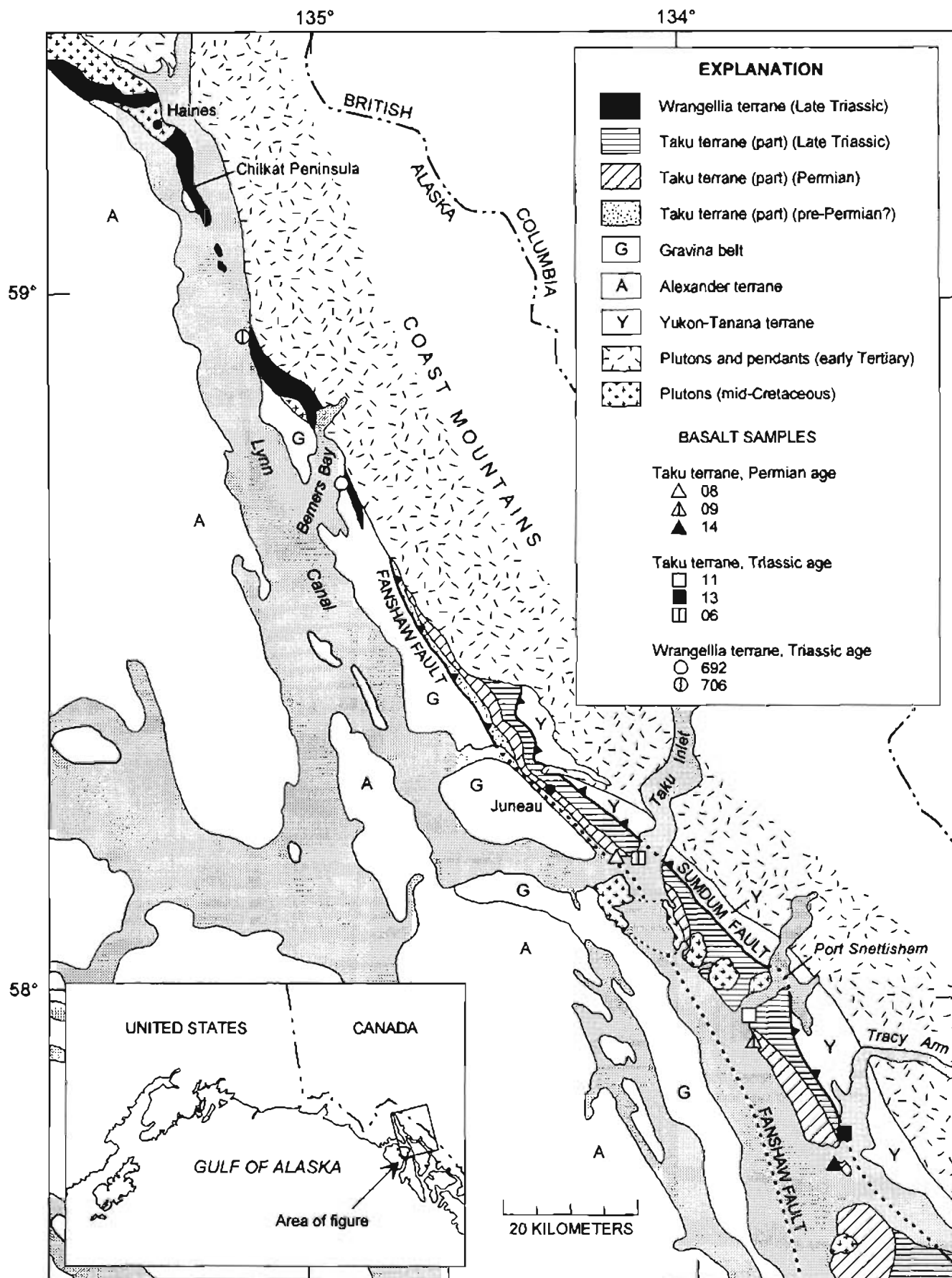
The Taku terrane comprises pre-Permian(?), Permian, and Triassic metavolcanic and metasedimentary rocks that occur in a narrow belt along the west flank of the Coast Mountains (Monger and Berg, 1987) (fig. 1). In central southeastern Alaska, where rocks of the terrane are moderately well preserved, protoliths consist of: (1) unnamed pre-Permian(?) black shale, volcanoclastic graywacke, basalt flows and breccia, and minor felsic tuff; (2) the Permian Gastineau Group of Gehrels and others (1992), which includes basalt flows and breccia interlayered with massive to thick-bedded limestone and thin-bedded gray chert; and (3) the Triassic Perseverance Group of Gehrels and others (1992), which includes Ladinian to Carnian massive and pillowed basalt interlayered with thin-bedded grey chert, limestone, and black shale overlain by Carnian and possibly Norian black shale.

One of the long-standing controversies in southeastern Alaska concerns the primary relations between strata of the Taku terrane and coeval rocks of the nearby Wrangellia, Alexander, and Stikinia terranes. On the basis of differences in stratigraphy, Monger and Berg (1987) and Gehrels and others (1992) have concluded that the Taku terrane is a disparate tectonic fragment. In contrast, Brew and Ford (1984) interpret the Taku terrane to be equivalent to the upper part of the Alexander terrane; Plafker and Hudson (1980), Davis and Plafker (1985), Rubin and Saleeby (1988), and Plafker and others (1989) suggest that the northern part of the Taku terrane, as defined by Monger and Berg (1987), is a sliver of the Wrangellia terrane that is offset by the Denali fault; and Rubin and Saleeby (1991) favor correlations with rocks of the Stikinia terrane.

Uncertainties in these correlations exist primarily because protolith characteristics of the Taku terrane are obscured by regional deformation and greenschist- to amphibolite-facies metamorphism, and because the terrane is juxtaposed against other terranes or overlap assemblages along major mid-Cretaceous or younger faults. In central southeastern Alaska, as shown on the geologic map of Gehrels and others (1992) and on figure 1, the terrane is bound on the west by the Fanshaw fault, which juxtaposes Taku strata over Jurassic and Cretaceous strata of the



Figure 1. Sketch map of geologic units and terranes of Juneau area and locations of samples. Geology is adapted from Brew and Grybeck (1984), Brew and Ford (1985), and Gehrels and others (1992) near and south of Juneau, from Redman (1984) near Berners Bay, and from Plafker and Hudson (1980), Redman and others (1984), Barker and others (1986), and Gehrels (in review) near Haines. Symbols shown for each sample are used in all following figures. Fanshaw and Sumdum faults are denoted by teeth marks on upthrust side where on land and by heavy dots where under water.





Gravina belt. To the east, the terrane is structurally overlain along the Sumdum fault by pre-Triassic metamorphic rocks that are interpreted to be correlative with the Yukon-Tanana terrane (Gehrels and others, 1992). North of Juneau, Taku strata are progressively truncated by the early Tertiary plutons that underlie the higher parts of the Coast Mountains. The structural and stratigraphic framework of the terrane in southern southeastern Alaska is described by Rubin and Saleeby (1991).

This study is an attempt to shed light on the origin and regional correlation of Permian and Triassic strata of the Taku terrane. We present new major- and minor-element data for three samples of Permian basalt from the Taku terrane, three samples of Triassic basalt from the Taku terrane, and two samples of nearby Triassic basalt from the Wrangellia terrane collected 10 to 30 km north of the northernmost exposures of the Taku terrane (fig. 1). These results are also compared with a larger set of geochemical data from Triassic basalts of the Chilkat Peninsula, which have been correlated with Wrangellia terrane stratigraphy by Plafker and Hudson (1980), Davis and Plafker (1985), and Plafker and others (1989). In addition, Ford and Brew (1988) presented averages of major-element analyses of basalts from the Juneau-Berners Bay area. Their basalts include Taku terrane samples of Permian and (or) Triassic age from southeast of Juneau, and Triassic basalt of Wrangellia terrane affinity from the Berners Bay area.

All of the samples analyzed have been metamorphosed to greenschist facies and consist largely of fine-grained to microcrystalline chlorite, plagioclase, and epidote. The Permian samples are generally aphyric and range from faintly foliated (sample 14) to strongly foliated (samples 08 and 09). The Triassic samples from both the Taku and Wrangellia terranes are similar, showing as much as 10 percent plagioclase phenocrysts in most samples and ~10 percent pyroxene phenocrysts in sample 706. Samples 706 and 692 are amygdaloidal, and sample 06 has a pervasive overprint of secondary calcite. The only Triassic sample with a strong foliation is 692.

## GEOCHEMISTRY

Major- and minor-element abundances of three samples of Permian basalt from the Taku terrane, three samples of Triassic basalt from the Taku terrane, and two samples of Triassic basalt from the Wrangellia terrane are given in table 1. Many of these abundances may be used to characterize these three groups of basalts. Please note, however, that sample 06 of the Taku terrane contains 6.2 percent  $\text{CO}_2$  and hence cannot be used for plots of major elements. Its rare-earth elements and some other minor elements, however, apparently remained unaffected by this metasomatism. We first plot 16 of these elements against

MgO in the magnesia-variation plots of figure 2A-D. These plots are more suitable for basaltic rocks than the more common  $\text{SiO}_2$ -variation diagram because fractionating basalts—especially tholeiitic types—tend to show marked changes in concentrations of many elements over small changes of  $\text{SiO}_2$ . The petrogenetic usefulness of these MgO plots is predicated on MgO being immobile during all postmagmatic processes, such as reaction during extrusion into seawater, metamorphism during accretion, percolation of fluids, and so on. We have no absolute method to test immobility of MgO, but linear (or nearly linear) arrays of MgO versus those elements that typically show little or no postmagmatic mobility or metasomatism—such as Co, Zr, Nb, Ta, and Th—are taken as evidence that MgO is immobile. Also, the relatively small proportions of phenocrysts (generally <10 percent) in these rocks indicate that abundances of immobile elements approach, or are identical to, those of the parental magmas.

In figure 2A-D the Permian basalt shows lower  $\text{SiO}_2$  and generally higher  $\text{TiO}_2$ ,  $\text{P}_2\text{O}_5$ , Cr, Ni, Zr, Nb, Ta, and Th than the Triassic basalts. Abundances of  $\text{Al}_2\text{O}_3$ , CaO,  $\text{FeO}^*$  (total iron as  $\text{FeO}$ , or  $\text{FeO}+0.9\text{Fe}_2\text{O}_3$ ), and Co are similar in the two age groups. The  $\text{Na}_2\text{O}$  of the Permian basalt decreases regularly with MgO, whereas its  $\text{K}_2\text{O}$  values are irregular (fig. 2B).  $\text{Na}_2\text{O}$  percentages of the Triassic basalt, on the other hand, range over a factor of two, whereas the  $\text{K}_2\text{O}$  values are consistent at about 0.2 percent. The Rb abundances (23–51 ppm for the Permian and 1–21 ppm for the Triassic samples), Sr abundances (551–690 ppm for the Permian and 77–332 ppm for the Triassic samples), and Ba abundances (402–1,230 ppm for the Permian and 20–235 ppm for the Triassic samples) probably represent a range of near-original to markedly disturbed, or metasomatized, values. However, abundances of all three of these elements tend to be higher in the Permian rocks. We conclude from figure 2 that the Permian basalt is of magnesian (that is,  $\text{MgO}>8$  percent) alkaline type and the Triassic basalts chemically are like enriched midocean-ridge basalt (E-MORB).

The rare-earth elements (REE's) of these basalts are plotted, normalized to REE abundances of chondritic meteorites, in figure 3. Rare-earth elements tend to be resistant to metasomatism, and the regularity of these eight REE patterns is compatible with little or no movement of these elements. The REE patterns of the Permian basalts show the enrichment of light REE's—LaN (La as normalized to the chondritic value) is about 80 to 120—that is typical of alkali basalt. The Triassic basalts, in contrast, show only slight enrichment of light REE's, LaN being 18–23 times chondrites. All REE patterns show heavy REE's grouped near 10 times chondrites, which is typical of most basalts.

Figure 4 shows  $\text{FeO}^*/\text{MgO}$  plotted against  $\text{SiO}_2$ , with Miyashiro's (1974) boundary for tholeiitic and calcalkaline basalts. The Triassic basalts lie in the tholeiitic field. This diagram, however, is not pertinent to alkali basalt, so the



**Table 1.** Elemental abundances and sample locations of Permian and Upper Triassic basalts of the Taku and Wrangellia terranes, southeastern Alaska

[Analyses by XRF (major and some minor elements) and INAA (REE's, Co, Hf, Ta, Th, and U) methods. Analysis: J.E. Taggart, A.J. Bartel, D.F. Siems, K.J. Curry, P.W. Tippitt, J.R. Evans, J.R. Budahn, and R.J. Knight. Data shown for basalts of Chikot Peninsula (designated as C.P. below) are averages (for major elements) and ranges (for minor elements) of seven samples reported by Davis and Plafker (1985). nd, not determined]

	TAKU TERRANE						WRANGELLIA TERRANE		
	PERMIAN			TRIASSIC			TRIASSIC		
	08	09	14	11	13	06	692	706	C.P.
SiO <sub>2</sub> -----	45.91	48.35	44.52	49.25	51.00	44.10	50.47	49.35	49.66
TiO <sub>2</sub> -----	2.47	2.15	2.52	1.38	1.62	2.09	1.91	2.07	2.10
Al <sub>2</sub> O <sub>3</sub> -----	17.04	14.92	15.61	14.99	17.92	15.10	16.11	15.34	13.94
Fe <sub>2</sub> O <sub>3</sub> -----	2.48	3.37	4.34	2.02	3.19	0.69	3.41	5.84	3.89
FeO -----	8.14	6.77	6.93	8.65	5.89	10.00	7.54	7.81	8.80
MnO -----	0.20	0.15	0.18	0.18	0.13	0.18	0.17	0.16	0.19
MgO -----	9.30	11.74	11.21	7.84	4.27	4.52	6.30	6.91	6.47
CaO -----	9.19	7.32	11.00	13.26	13.01	8.56	9.51	7.90	10.70
Na <sub>2</sub> O -----	1.79	2.53	2.00	2.13	2.56	3.33	4.22	4.22	2.21
K <sub>2</sub> O -----	2.83	2.14	.91	.17	.24	.87	.18	.22	.59
H <sub>2</sub> O <sup>+</sup> -----	nd	nd	nd	nd	nd	3.84	nd	nd	nd
H <sub>2</sub> O <sup>-</sup> -----	nd	nd	nd	nd	nd	nd	nd	nd	nd
CO <sub>2</sub> -----	.09	.49	.09	.03	<.01	6.2	.06	.01	nd
P <sub>2</sub> O <sub>5</sub> -----	.65	.56	.79	.13	.17	.22	.17	.19	.20
Total -----	100.09	100.49	100.10	100.03	100.00	99.70	100.05	100.02	98.75
Sc -----	31	31	32	41	27	32	35	41	44-58
Cr -----	356	669	650	428	129	73	285	156	130-220
Co -----	43	49	52	44	24	32	41	43	nd
Ni -----	168	309	375	122	54	61	99	64	96-150
Cu -----	50	1.0	41	134	171	165	67	58	nd
Rb -----	51	38	23	1.0	14	21	1.0	2.0	<5-30
Sr -----	690	560	551	193	332	373	108	77	134-238
Y -----	24	19	28	19	25	29	26	29	25-38
Zr -----	215	190	223	77	99	123	104	115	91-168
Nb -----	32	29	47	5	15	16	10	13	8-20
Ba -----	685	1,230	402	102	235	3,000	27	20	28-122
La -----	31.4	25.5	38.5	5.8	7.6	10.3	6.5	7.3	6-13
Ce -----	70.8	54.5	81.5	16.1	19.5	26.7	18.6	20.6	15-30
Nd -----	32.5	25.5	36.1	11.1	12.6	17.3	13.1	14.3	nd
Sm -----	7.3	6.0	7.6	3.3	3.6	4.9	4.0	4.4	3.6-5.9
Eu -----	2.2	1.8	2.2	1.1	1.2	1.5	1.4	1.4	1.1-1.7
Gd -----	6.5	5.9	6.6	3.8	4.1	5.5	4.7	5.4	nd
Tb -----	.86	.76	.88	.58	.60	.81	.76	.84	.7-1.1
Tm -----	nd	.33	.36	.31	.31	.42	.40	.45	nd
Yb -----	2.3	2.0	2.2	1.9	2.0	2.7	2.5	2.8	2.7-3.8
Lu -----	.33	.29	.33	.28	.29	.40	.37	.42	.44-.56
Hf -----	4.6	3.9	4.5	2.0	2.4	3.1	2.7	2.9	2.3-4.2
Ta -----	2.5	2.0	2.7	.51	.63	.85	.55	.64	.5-1.1
Th -----	2.6	2.1	3.2	.52	.63	.85	.47	.52	.4-1.1
U -----	.96	.79	1.1	.20	.23	.30	.15	.21	nd

Sample locations: 08, north shore of Taku Inlet: 58°12'20" N., 134°12'35" W.  
 09, south shore of Port Snettisham: 57°56'26" N., 133°50'54" W.  
 14, northwest tip of Harbor Island in Tracy Arm: 57°46'01" N., 133°38'49" W.  
 11, south shore of Port Snettisham: 57°57'33" N., 133°50'13" W.  
 13, north shore of Tracy Arm: 57°48'28" N., 133°37'32" W.  
 06, north shore of Taku Inlet: 58°12'28" N., 134°10'0" W.  
 692, southeast shore of Berners Bay: 58°45'11" N., 134°55'42" W.  
 706, east shore of Lynn Canal: 58°57'27" N., 135°10'04" W.

positions of points of the Permian basalts should be disregarded. The commonly used Alk-F-M diagram, of Na<sub>2</sub>O+K<sub>2</sub>O-FeO\*-MgO, is not a reliable indicator of chemical character for these samples because of the disturbance of alkalis (causing points to be radially disposed

either toward or away from the Alk corner of the diagram). The Alk-F-M plot (not shown), however, does place three of the Triassic samples in the tholeiitic field of Irvine and Baragar (1971) and the fourth sample just into the calc-alkaline field.

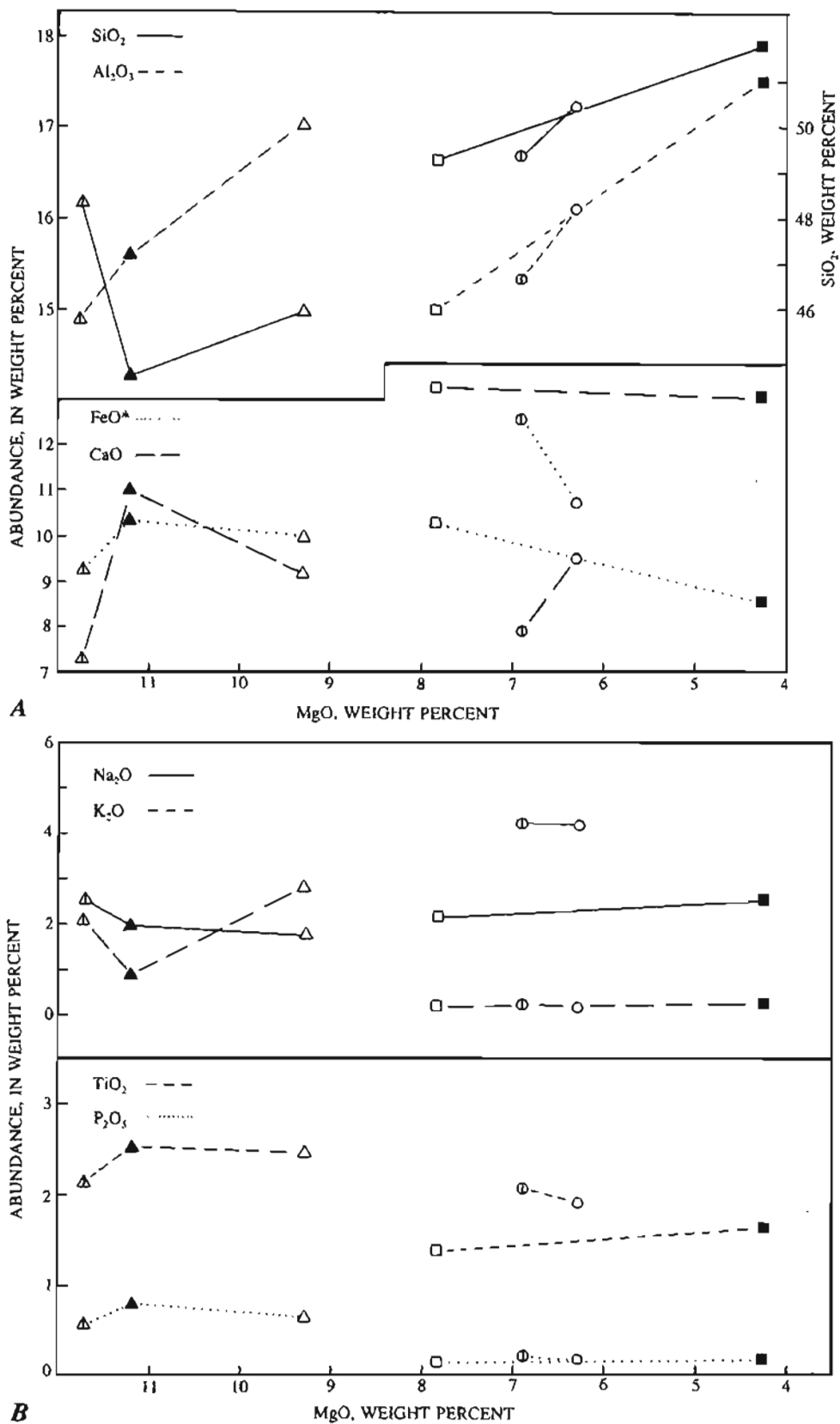


**Figure 2.** MgO-variation diagrams showing weight percent of MgO versus abundances of (A) SiO<sub>2</sub>, Al<sub>2</sub>O<sub>3</sub>, FeO\*, and CaO; (B) Na<sub>2</sub>O, K<sub>2</sub>O, TiO<sub>2</sub>, and P<sub>2</sub>O<sub>5</sub>; (C) Cr, Ni, Co, and Cu; and (D) Zr, Nb, Th, and Ta. Symbols explained in figure 1.

A spider diagram (that is, a chondrite-normalized plot of elements), modified by omission of mobile elements Ba, Rb, and K, is shown in figure 5. The contrast in abundances of 13 elements of the Permian basalt of the Taku terrane and the Triassic basalts of both the Taku

and Wrangellia terranes is prominent. The high-field-strength elements—Ti, Zr, Nb, Hf, and Ta—and Th, P, and light REE's of the Permian alkali basalt show markedly greater abundances than those of the Triassic samples.

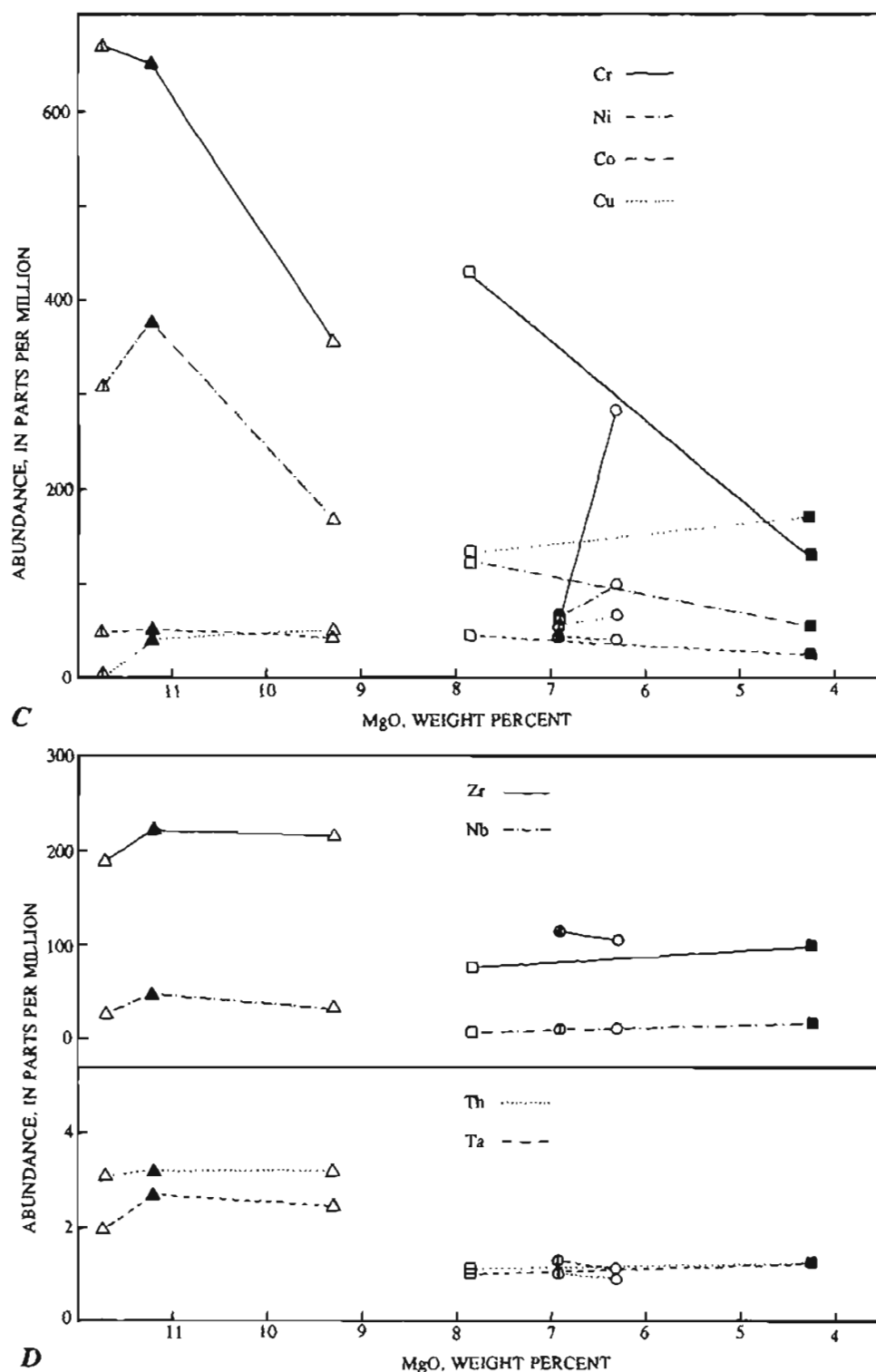


Figure 2. Continued.

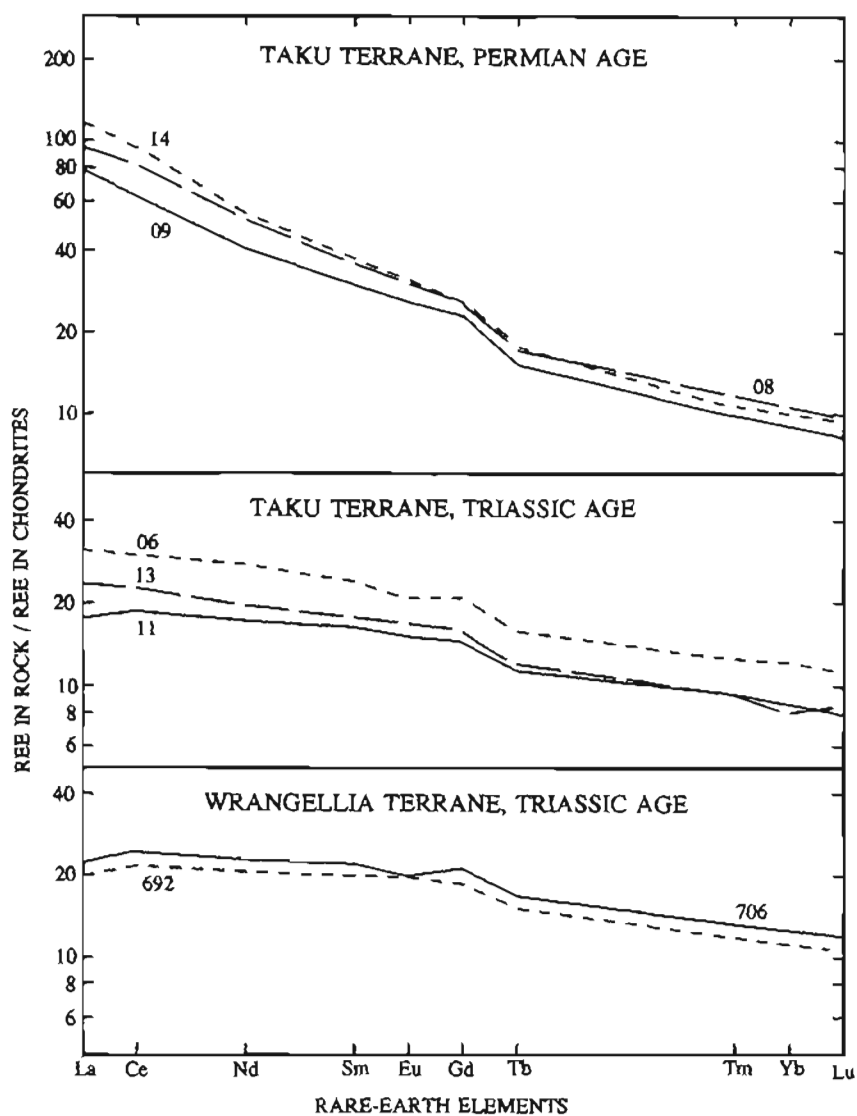


Figure 3. Chondrite-normalized rare-earth element plots.

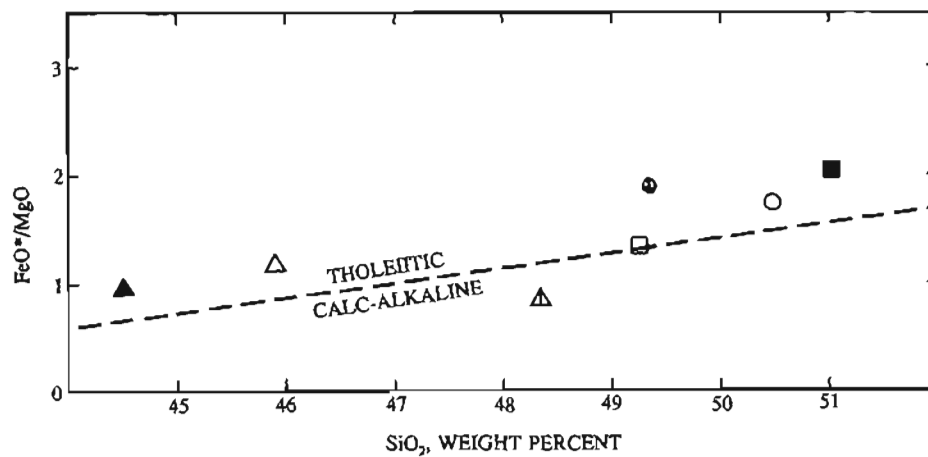


Figure 4.  $\text{FeO}^*/\text{MgO}$ - $\text{SiO}_2$  plot. Boundary between tholeiitic and calc-alkaline basalts is from Miyashiro (1974). Symbols and numbers explained in figure 1.

Discriminant plots also may be used to characterize these basalts. For instance, the  $\text{MnO-TiO}_2\text{-P}_2\text{O}_5$  plot of Mullen (1983) (fig. 6) shows the Permian basalts as ocean-island alkalic type (OIA) and the Triassic ones as either MORB or ocean-island tholeiite. The Th-Hf-Ta plot of Wood (1980) (fig. 7) also shows the Permian samples as OIA type, but it groups the Triassic ones as E-MORB or within-plate tholeiitic (WIP) basalt. The use of several other of the various discriminant plots found in the litera-

ture on tholeiites, however, generally tends to give contradictory results (see, for instance, Barker and others' (1989) discussion of the Karmutsen Formation's basalts of the Wrangellia terrane).

The average major elements of 23 basalt samples, not individually dated, from the Juneau area given by Ford and Brew (1988) generally are like those of the Taku terrane. However, their average values of 0.39 percent for  $\text{P}_2\text{O}_5$  and 1.74 percent for  $\text{TiO}_2$  are intermediate to our Permian and Triassic samples (table 1), which suggests that their 23 samples include both ages of basalt.

### COMPARISON WITH TRIASSIC BASALTS OF CHILKAT PENINSULA

Triassic basalts underlie much of Chilkat Peninsula and extend northwestward into southwestern Yukon (fig. 1). These basalts and related metasedimentary rocks were considered by Monger and Berg (1987) to be part of the Taku terrane. On the basis of similarities in stratigraphy, age, faunal affinities, and geochemistry, Plafker and Hudson (1980), Davis and Plafker (1985), and Plafker and others (1989) correlate these basalts with the widespread Triassic basalts that characterize the Wrangellia terrane in southern Alaska (Nikolai Greenstone) and coastal British Columbia (Karmutsen Formation). Our studies of the rocks as found at Berners Bay and Lynn Canal (see figure 1 and table 1) support this correlation, and are also consistent with Plafker and Hudson's (1980) and Ford and

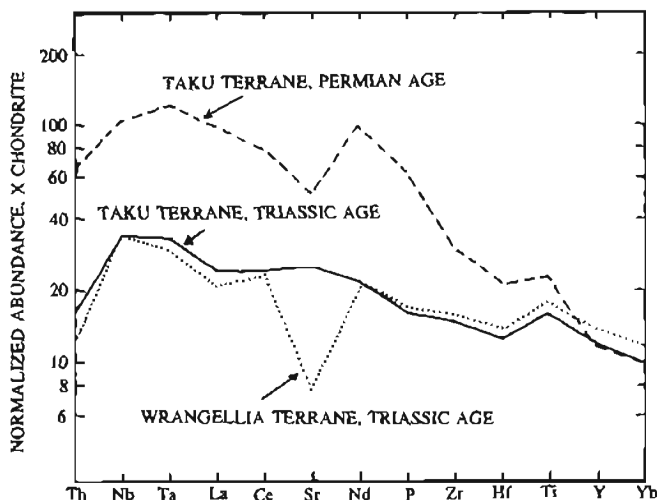


Figure 5. Modified spider diagram of average compositions of Permian and Triassic basalts of the Taku terrane and of Triassic basalt of the Wrangellia terrane. Chondritic normalizing values from Thompson (1985). Note that Ba, Rb, and K are omitted.

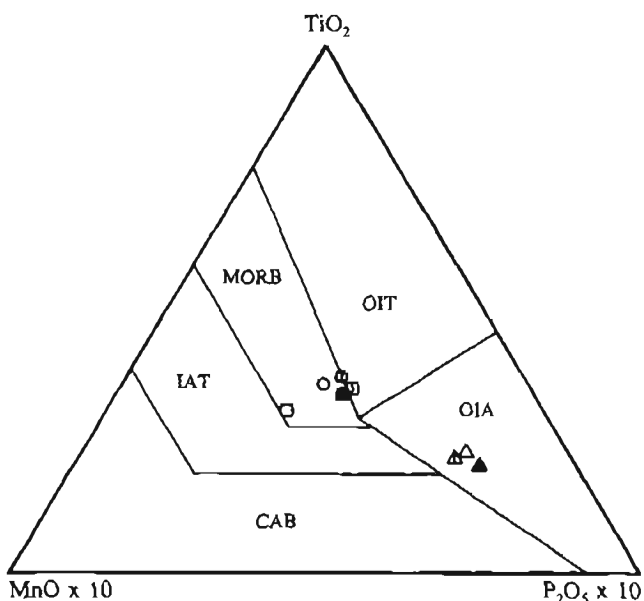


Figure 6.  $\text{MnO-TiO}_2\text{-P}_2\text{O}_5$  discriminant plot of Mullen (1983). CAB, calc-alkaline basalt; IAT, island-arc tholeiite; MORB, midocean-ridge basalt; OIA, ocean-island alkali basalt; OIT, ocean-island tholeiite. Symbols explained in figure 1.

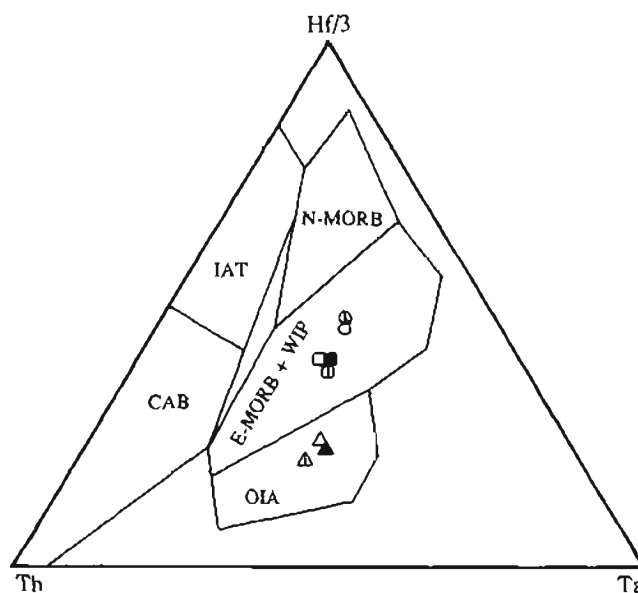


Figure 7. Th-Hf-Ta discriminant plot of Wood (1980). Abbreviations as in figure 6, and E-MORB, enriched MORB; N-MORB, normal MORB; WIP, within-plate basalt. Symbols explained in figure 1.

Brew's (1988) suggestion that these basalts trace south-eastward across Lynn Canal and into Berners Bay (fig. 1).

Davis and Plafker (1985) present major- and minor-element abundances of seven samples of Upper Triassic basalt from Chilkat Peninsula. Their average major elements and ranges of minor elements are shown beside our corresponding values for Upper Triassic basalts in table 1. Comparison of the data for basalts of the Taku terrane and the two sets of basalts of the Wrangellia terrane shows all three units to be very similar in both major- and minor-element abundances. The Chilkat Peninsula rocks do contain higher  $\text{TiO}_2$  and Sc, and lower  $\text{Al}_2\text{O}_3$  and (mobile)  $\text{Na}_2\text{O}$ , but the remaining 25 elements show similar values or ranges. Thus, as discussed below, the geochemical data are consistent with lithic correlation of all three sequences. Major element contents of two analyses of basalt northeast of Berners Bay given by Ford and Brew (1988) are like those of Davis and Plafker (1985) and our values shown in table 1.

In regard to the correlation of Triassic strata of the Taku and Wrangellia terranes in southeastern Alaska with strata of the Wrangellia terrane elsewhere, it should be noted that Barker and others (1989; in press) have divided basalts of the Wrangellia terrane into island-arc type tholeiite and back-arc basin basalts. The Triassic sequences in southeastern Alaska are chemically similar to the back-arc basin components of the Karmutsen Formation and the Nikolai Greenstone.

## CONCLUSIONS

The geochemical signatures of Permian and Triassic basalts along the west flank of the Coast Mountains offer important insights into the tectonic setting in which they formed and their regional correlation. Several first-order conclusions can be reached from this study:

First, the Permian basalts of the Taku terrane have a different chemical signature from Triassic basalts of the Taku and Wrangellia terranes: the Permian rocks show distinctly higher abundances of Ti, P, Zr, Th, Ta, and light rare-earth elements. If confirmed through more detailed studies, this may provide a powerful means of discriminating Permian from Triassic components of Taku rocks in regions where age control is lacking. In terms of their chemical affinities, the Permian volcanic rocks are high-magnesian alkaline basalts, whereas the Triassic basalts of both the Taku and Wrangellia terranes are similar to midocean-ridge or within-plate tholeiite.

Second, the lithologic correlation of basalts along the east shore of Lynn Canal and in Berners Bay with the Chilkat Peninsula section (Plafker and Hudson, 1980), and therefore with the Wrangellia terrane, is supported by the similar geochemical signatures reported by Ford and Brew (1988) and herein for these two sequences.

Third, Triassic basalts of the Taku terrane in central southeastern Alaska are geochemically indistinguishable from those of the Wrangellia terrane that lie along strike to the northwest. In addition, as Gehrels and others (1992) pointed out, the pre-Permian(?), Permian, and Triassic strata of the Taku terrane show *general* lithologic similarities to rocks of the Wrangellian terrane—even though individual sequences cannot be correlated. Hence, it appears likely that rocks of the Taku terrane in the Juneau–Port Houghton area may be a part of the Wrangellia terrane. Such a correlation necessitates a facies change in the region southeast of Berners Bay, presumably where the Fanshaw fault was obliterated by intrusive rocks of the Coast batholith (see figure 1). The facies change would involve gradation of thick, subaerial to shallow-marine Upper Triassic basalt flows of the Chilkat Peninsula into a basinal sequence of basaltic pillow flows and breccia, black carbonaceous shale and limestone, and gray chert—as now exposed near Juneau and to the south. Documentation of such a correlation requires additional studies, especially of the pre-Triassic rocks of the Taku terrane. If future work does not support this correlation, and the Wrangellia and Taku terranes remain distinct entities, their boundary is at least locally the Fanshaw fault.

## REFERENCES CITED

- Barker, Fred, Arth, J.G., and Stern, T.W., 1986, Evolution of the Coast Batholith along the Skagway traverse, Alaska and British Columbia: *American Mineralogist*, v. 71, p. 632-643.
- Barker, Fred, Nokleberg, W.J., Plafker, George, and Leeman, W.P., in press, Wrangellia terrane, in Barker, Fred, ed., Some accreted volcanic rocks of Alaska and their elemental abundances, in Plafker, George, and Berg, H.C., eds., *Geology of Alaska: Geological Society of America, The Geology of North America*.
- Barker, Fred, Sutherland Brown, A., Budahn, J.R., and Plafker, George, 1989, Back-arc with frontal-arc component origin of Triassic Karmutsen basalt, British Columbia, Canada: *Chemical Geology*, v. 75, p. 81-102.
- Brew, D.A., and Ford, A.B., 1984, Tectonostratigraphic terranes in the Coast plutonic-metamorphic complex, southeastern Alaska, in Bartsch-Winkler, S., and Reed, K.M., *The U.S. Geological Survey in Alaska: Accomplishments during 1982: U.S. Geological Survey Circular 939*, p. 90-93.
- Brew, D.A., and Ford, A.B., 1985, Preliminary reconnaissance geologic map of the Juneau, Taku River, Atlin, and part of the Skagway 1:250,000 quadrangles, southeastern Alaska: *U.S. Geological Survey Open-File Report 85-395*.
- Brew, D.A., and Grybeck, Donald, 1984, *Geology of the Tracy Arm-Fords Terror Wilderness study area and vicinity, Alaska: U.S. Geological Survey Bulletin 1525-A*, p. 21-52.
- Davis, Alicé, and Plafker, George, 1985, Comparative geochemistry of Triassic basaltic rocks from the Taku terrane on the Chilkat Peninsula and Wrangellia: *Canadian Journal of Earth Sciences*, v. 22, p. 183-194.

- Ford, A.B., and Brew, D.A., 1988, Major-element geochemistry of metabasalts of the Juneau-Haines region, southeastern Alaska, in Galloway, J.P., and Hamilton, T.D., eds., *Geologic studies in Alaska by the U.S. Geological Survey during 1987*: U.S. Geological Survey Circular 1016, p. 150-155.
- Gehrels, G.E., in review, Geology and U-Pb geochronology of the western flank of the Coast Mountains between Juneau and Skagway, in McClelland, W.C., ed., *Tectonics of the Coast Mountains in southeast Alaska and coastal British Columbia*: Geological Society of America Special Paper.
- Gehrels, G.E., McClelland, W.C., Samson, S.D., and Patchett, P.J., and Orchard, M.J., 1992, Geology of the western flank of the Coast Mountains between Cape Fanshaw and Taku Inlet, southeastern Alaska: *Tectonics*, v. 11, p. 567-585.
- Irvine, T.N., and Baragar, W.R.A., 1971, A guide to the chemical classification of the common volcanic rocks: *Canadian Journal of Earth Sciences*, v. 8, p. 523-548.
- McClelland, W.C., Gehrels, G.E., Samson, S.D., and Patchett, P.J., 1992, Protolith relations of the Gravina belt and Yukon-Tanana terrane in central southeastern Alaska: *Journal of Geology*, v. 100, p. 107-123.
- Miyashiro, A., 1974, Volcanic rock series in volcanic arcs and active continental margins: *American Journal of Science*, v. 274, p. 321-355.
- Monger, J.W.H., and Berg, H.C., 1987, Lithotectonic terrane map of western Canada and southeastern Alaska: U.S. Geological Survey Miscellaneous Field Studies Map MF-1874-B.
- Mullen, E.D., 1983, MnO-TiO<sub>2</sub>-P<sub>2</sub>O<sub>5</sub>: a minor element discriminant for basaltic rocks of oceanic environments and its implications for petrogenesis: *Earth and Planetary Science Letters*, v. 62, p. 53-62.
- Plafker, George, Blome, C.D., and Silberling, N.J., 1989, Reinterpretation of lower Mesozoic rocks on the Chilkat Peninsula, Alaska, as a displaced fragment of Wrangellia: *Geology*, v. 17, p. 3-6.
- Plafker, George, and Hudson, Travis, 1980, Regional implications of Upper Triassic metavolcanic and metasedimentary rocks on the Chilkat Peninsula, southeastern Alaska: *Canadian Journal of Earth Sciences*, v. 17, p. 681-689.
- Redman, Earl, 1984, An unconformity associated with conglomeratic sediments in the Berners Bay area of southeastern Alaska: Alaska Division of Geological and Geophysical Surveys Professional Report 86, p. 1-4.
- Redman, Earl, Retherford, R.M., and Hickock, B.D., 1984, Geology and Geochemistry of the Skagway B-2 quadrangle, southeastern Alaska: Alaska Division of Geological and Geophysical Surveys Report of Investigations 84-31, 34 p.
- Rubin, C.M., and Saleeby, J.B., 1988, A new perspective on what is the Taku terrane in southern SE Alaska: *Geological Society of America Abstracts with Programs*, v. 20, p. 226.
- , 1991, Tectonic framework of the upper Paleozoic and lower Mesozoic Alava sequence: a revised view of the polygenetic Taku terrane in southern southeastern Alaska: *Canadian Journal of Earth Sciences*, v. 28, p. 881-893.
- Thompson, R.N., 1985, Asthenospheric source of Ugandan ultrapotassic magma?: *Journal of Geology*, v. 93, p. 603-608.
- Wood, D.A., 1980, The application of a Th-Hf-Ta diagram to problems of tectonomagmatic classification and to establishing the nature of crystal contamination of basaltic lavas of the British Tertiary volcanic province: *Earth and Planetary Science Letters*, v. 50, p. 11-30.

Reviewers: Richard J. Goldfarb and George Plafker



# OSTRACODE ASSEMBLAGES FROM MODERN BOTTOM SEDIMENTS OF VITUS LAKE, BERING PIEDMONT GLACIER, SOUTHEAST ALASKA

By Elisabeth M. Brouwers and Richard M. Forester

## INTRODUCTION

Bering Glacier, in southeastern Alaska, is the second largest glacier in North America, extending about 200 km from its source in the Bagley Ice Field of the Chugach-St. Elias Mountains to its terminus near the Gulf of Alaska (Post, 1972). A broad sand beach, believed to be underlain by a submarine terminal moraine, separates Bering Glacier from the northeast Pacific Ocean (Molnia and others, 1990). Bering Glacier is retreating rapidly at present, a process significantly accelerated because the southern ice margin is in a large proglacial lake, Vitus Lake. Vitus Lake is 25 km long, 10 km wide, and up to 150 m deep and is drained by the southwest-flowing Seal River for a distance of about 6 km to the Gulf of Alaska (fig. 1). The Seal River is a low-gradient, high-discharge, tidally influenced stream (Molnia and others, 1990). Only small icebergs less than 20 m long can traverse the Seal River; large icebergs ground on shallows on the lake and along the Seal River and drop most of their sediment load as they melt in the lake. The surface of Vitus Lake is approximately 2 m above sea level; tidal action is affecting the entire length of the Seal River. During the last decade, Bering Glacier has retreated sufficiently so that nearly full tidal exchange now exists between Vitus Lake and the ocean. The lake has therefore evolved from a freshwater to a marine system.

The purpose of this study was to collect a series of bottom samples to monitor the response of the lake biota to the shift in salinity during the last few years and to observe the degree of exchange of organisms between the Gulf of Alaska and Vitus Lake. The lake is now essentially an extension of the Pacific Ocean, having nearly normal salinity throughout and with only a thin surficial freshwater layer from ice melt.

## SAMPLE ACQUISITION AND PROCESSING

Twenty-nine samples were taken over three days and three separate traverses during July 1992. Sampling was

by means of a Soutek Van Veen grab sampler deployed from a small Zodiac craft. No winch was available, so the sampler assembly was pulled up by hand. Because of the difficulty of this sample retrieval, the possibility of losing a sample during a haul from great depths, and the danger of being in a small boat in deep, near-freezing water, sampling was conducted within sight of coastlines in shallower water (generally less than 20 m water depth).

Two samples each were taken at the majority of sites, one for paleontological analysis and one for grain-size analysis. Samples generally consisted of medium-gray glacial mud, commonly with scattered sand and gravel suspended in the mud matrix. No organic material was observed. A few samples consisted of fine sand, and these did not contain any fossils. Paleontological samples were further subsampled for palynological analysis, although to date, the modern samples have been examined only for calcareous microfossils. Seven samples contain ostracodes, and fourteen samples contain benthic foraminifers (table 1). Sample processing was qualitative because sample volume depended upon the success of the grab sampler. Initial volumes ranged from a few tens of grams to several hundred kilograms wet weight.

## MARINE OSTRACODES

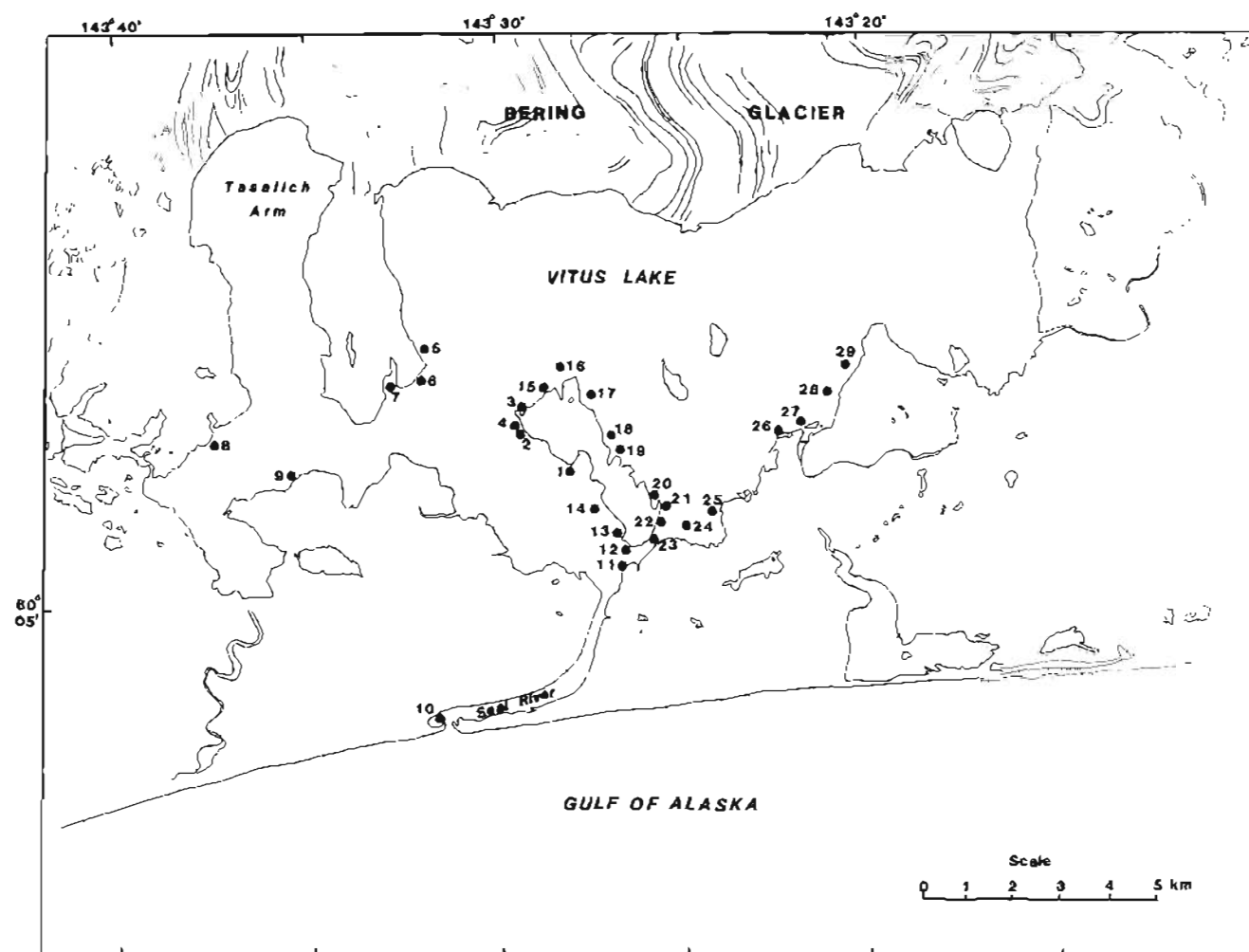
Nine species of marine ostracodes were recovered from 6 of the 29 samples collected (M1, M3, M10, M11, M14, M18; table 1; fig. 3). The seven taxa identifiable to species have been previously described (Brouwers, 1990, 1993, in press). The ostracode-bearing samples were all collected around the periphery of a small island just north of the head of the Seal River in Vitus Lake (fig. 1).

The marine species that now populate Vitus Lake are common elements of the continental shelf in the Gulf of Alaska. The total depth range of the seven known species in the Gulf of Alaska is 20 to 230 m; the taxa are most abundant in a depth range of 20–30 m to 60–80 m (fig. 2). In the Gulf of Alaska, none of the seven species has been found shallower than 20 m, an absence probably related to substrate, as inner sublittoral substrates are predominantly

**Table 1.** Presence-absence table of calcareous fossils recovered from the modern samples, Vitus Lake

[X, present; —, absent]

Sample number .....	M1	M2	M3	M5	M10	M11	M12	M14	M16	M18	M19	M20	M22	M26	M28
<i>Candona caudata</i> .....	X	X	—	—	X	—	—	—	—	—	—	—	—	—	—
<i>Celtia blizhnii</i> .....	—	—	—	—	X	—	—	—	—	—	—	—	—	—	—
<i>Celtia</i> sp. ....	X	—	—	—	—	—	—	—	—	—	—	—	—	—	—
<i>Cythere alveolivalva</i> .....	—	—	—	—	—	—	—	—	—	X	—	—	—	—	—
<i>Cytherideid</i> sp. ....	X	—	—	—	—	—	—	—	—	—	—	—	—	—	—
<i>Cytheromorpha molniai</i> .....	X	—	X	—	—	—	—	—	—	—	—	—	—	—	—
<i>Cytheropteron drybayensis</i> .....	—	—	—	—	—	—	—	—	—	X	—	—	—	—	—
<i>Cytheropteron nodosoalatum</i> ....	—	—	—	—	X	—	—	X	—	—	—	—	—	—	—
<i>Limnocythere ceriotuberosa</i> .....	X	X	—	—	—	—	—	—	—	—	—	—	—	—	—
<i>Palmococoncha russellensis</i> .....	—	—	—	—	—	X	—	—	—	—	—	—	—	—	—
<i>Pectocythere parkerae</i> .....	—	—	—	—	—	X	—	—	—	—	—	—	—	—	—
Benthic foraminifers .....	—	X	X	X	X	X	X	X	X	X	X	X	X	X	X
Cyclostome bryozoan .....	—	—	—	—	—	X	—	—	—	—	—	—	—	—	—
Pelecypod .....	—	—	—	—	X	—	—	—	—	—	—	—	—	—	—
Gastropod .....	—	—	—	—	X	X	—	—	—	—	—	—	—	—	—

**Figure 1.** Map showing locations of bottom grab samples in Vitus Lake.

made up of wave- and current-transported sand. The inferred depth range of 20–80 m corresponds to inner sublittoral and shallow middle sublittoral ostracode Assemblages I and II of the Gulf of Alaska (Brouwers, 1988), which have annual ranges in temperature of 2–15°C and salinity of 30–32.5 parts per thousand.

The rarity and low species diversity of marine ostracodes in the lake samples may imply that these organisms are in the initial stage of colonization. The sparse assemblage more probably is a function of high sediment accumulation and consequent dilution of ostracode productivity. Samples M1 and M10 have a mixture of nonmarine and marine species, implying input either from runoff of the adjacent islands or from erosion of outcrops from the mainland that have been transported by ice into the marine system. The sedimentation rate in Vitus Lake is relatively great because of the high input from iceberg melt. We observed some icebergs which were so dirty that no ice was visible, and they appeared to be floating islands. Sedimentation rate is on the order of meters per year.

## CONTINENTAL OSTRACODES

Two species of continental ostracodes, *Candona caudata* and *Limnocythere ceriotuberosa*, were recovered from 3 of the 29 samples (M1, M2, M10; table 1; fig. 4). Two samples were collected from the northern part of an island just inside of proglacial Vitus Lake and one sample was collected from a shallow lagoon at the mouth of the Seal River (fig. 1). Sample M10 contains a large amount of plant debris from the adjacent coastal plain.

Salinity, expressed as total dissolved solids, major dissolved ion composition, water temperature, general hydrological setting (lake, pond, stream, or aquifer), and the annual variation of physical and chemical water properties determine the biogeography and local occurrences of continental ostracodes (Forester, 1987, 1991a). A large proglacial lake, for example, is usually sustained by meltwater. Meltwater lakes generally remain cold during the

year and are filled with dilute water that has a major ion composition dominated by calcium bicarbonate. Those properties, but especially temperature, limit the occurrence of ostracodes. *Candona subtriangulata* is an example of a species that can survive under such conditions.

Continental ostracodes recovered from the above samples are remarkable because they have no known relationship of any kind with ostracodes from either proglacial lakes or marginal to fully marine environments. *Limnocythere ceriotuberosa* is a euryhaline ostracode that commonly occurs in inland saline to seasonally saline lakes that have a major dissolved ion composition enriched in carbonate (Forester, 1986). Lakes existing under semi-arid to arid climates in regions with volcanic rocks are often inhabited by this species. Ocean water, by contrast, is depleted in carbonate and enriched in calcium. *Candona caudata* lives in freshwater to slightly saline lakes and streams having a major ion chemistry dominated by calcium bicarbonate, but is tolerant of either calcium or carbonate enrichment (Forester, 1991b). Stream-supported, seasonally saline, carbonate-enriched lakes in the Great Basin often contain both of these ostracode species.

Juveniles compose most of the material. Preservation ranges from pristine to highly frosted, partially dissolved valves. Some of the valves are carbonate coated, which is common for ostracode valves found in slightly to fully saline lakes. None of the material contains soft parts. Juvenile-dominated assemblages are often transported, as are assemblages composed of taxa that are ecologically incompatible with their surroundings. Thus, unless evidence to the contrary emerges, these shells must be assumed to have been transported from some as yet unknown sediment in the drainage basin of this lake. Oxygen or strontium isotopes would likely demonstrate that these ostracodes did not calcify their valves in either a proglacial lake or in ocean water.

**Acknowledgments.**—We thank the U.S. Geological Survey Volunteer in Science program for funding Rina Coury, who provided field support. Leonard Wilson and Florian Maldonado assisted in the sample collection.

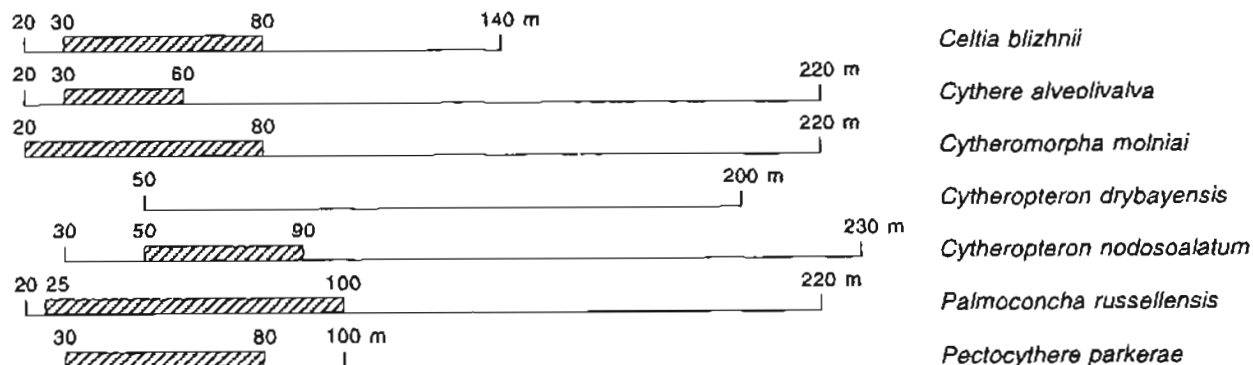


Figure 2. Preferred (hachured) and total depth range in the Gulf of Alaska of six marine and one marginal marine ostracode species recovered from Vitus Lake.

## REFERENCES CITED

- Brouwers, E.M., 1988, Palaeobathymetry on the continental shelf based on examples using ostracods from the Gulf of Alaska, in De Deckker, P., Colin, J.-P., and Peypouquet, J.-P., eds., *Ostracoda in the earth sciences*: Amsterdam, Elsevier, p. 55-76.
- 1990, Systematic paleontology of Quaternary ostracode assemblages from the Gulf of Alaska, Part 1: Families Cytherellidae, Bairdiidae, Eucytheridae, Krithidae, Cushmaniidae: U.S. Geological Survey Professional Paper 1510, 43 p., 39 figs., 13 pls.
- 1993, Systematic paleontology of Quaternary ostracode assemblages from the Gulf of Alaska, Part 2: Families Trachyleberididae, Hemicytheridae, Loxoconchidae, Paracytheridae: U.S. Geological Survey Professional Paper 1531, 40 figs., 11 pls.
- in press, Systematic paleontology of Quaternary ostracode assemblages from the Gulf of Alaska, Part 3: Family Cytheruridae: U.S. Geological Survey Professional Paper, 42 figs., 23 pls.
- Forester, R.M., 1986, Determination of the dissolved anion composition of ancient lakes from fossil ostracodes: *Geology*, v. 14, p. 796-798.
- 1987, Late Quaternary paleoclimate records from lacustrine ostracodes, in Ruddiman, W.F., and Wright, H.E., Jr., eds., *North American and adjacent oceans during the last deglaciation*: Geological Society of America, *Geology of North America*, v. K-3, p. 261-276.
- 1991a, Ostracode assemblages from springs in the western United States: Implications for paleohydrology, in Williams, D.D., and Danks, H.V., eds., *Arthropods of springs, with particular reference to Canada*: Memoirs of the Entomological Society.
- 1991b, Pliocene-climate history of the western United States derived from lacustrine ostracodes: *Quaternary Science Reviews*, v. 10, p. 133-146.
- Molnia, B.F., Trabant, D.C., Post, Austin, and Frank-Molnia, D.G., 1990, Bering Glacier, Alaska: Factors influencing the potential for an irreversible calving retreat: *Eos*, v. 71, no. 43, p. 1314.
- Post, Austin, 1972, Periodic surge origin of folded medial moraines on Bering piedmont glacier, Alaska: *Journal of Glaciology*, v. 11, no. 62, p. 219-226.

Reviewers: Thomas M. Bown and Louie N. Marinovich

**Figure 3.** Marine ostracodes recovered from bottom grab samples in Vitus Lake. Scale bars equal 100 micrometers.

1. *Cytheropteron nodosoalatum* Neale and Howe, 1973, left valve exterior, adult, sample 92-EB-M10.
2. *Celtia blizhnii* Brouwers, 1993, right valve exterior, juvenile, sample 92-EB-M10.
3. *Pectocythere parkerae* Swain and Gilby, 1974, left valve exterior, juvenile, sample 92-EB-M11.
4. *Cytheromorpha molniai* Brouwers, 1990, left valve exterior, adult, sample 92-EB-M1.
5. *Celtia* sp., left valve exterior, juvenile, sample 92-EB-M1.
6. *Palmoconcha russellensis* Brouwers, 1993, right valve exterior, juvenile, sample 92-EB-M11.
7. Pelecypod, sample 92-EB-M10.
8. Benthic foraminifer, sample 92-EB-M10.

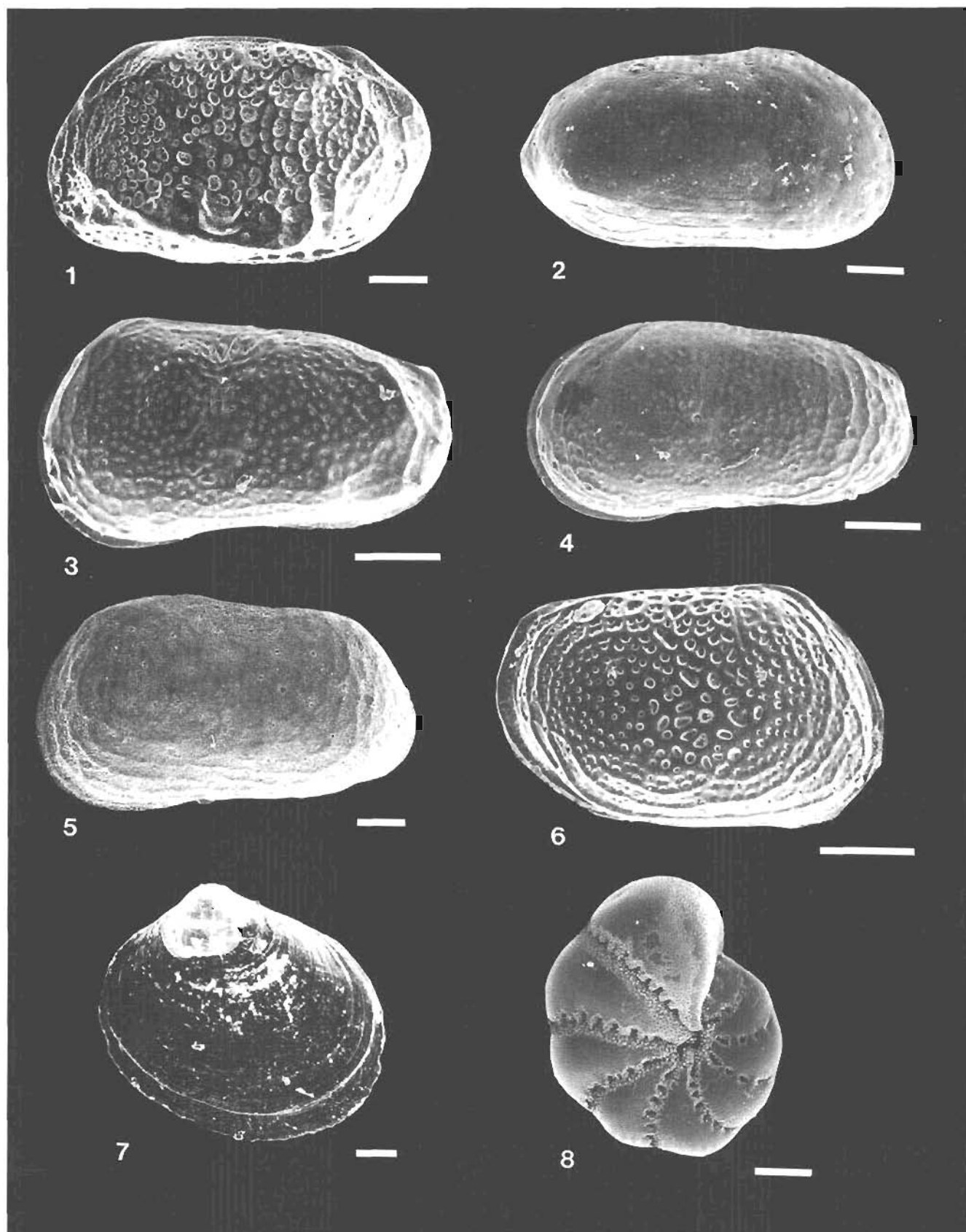
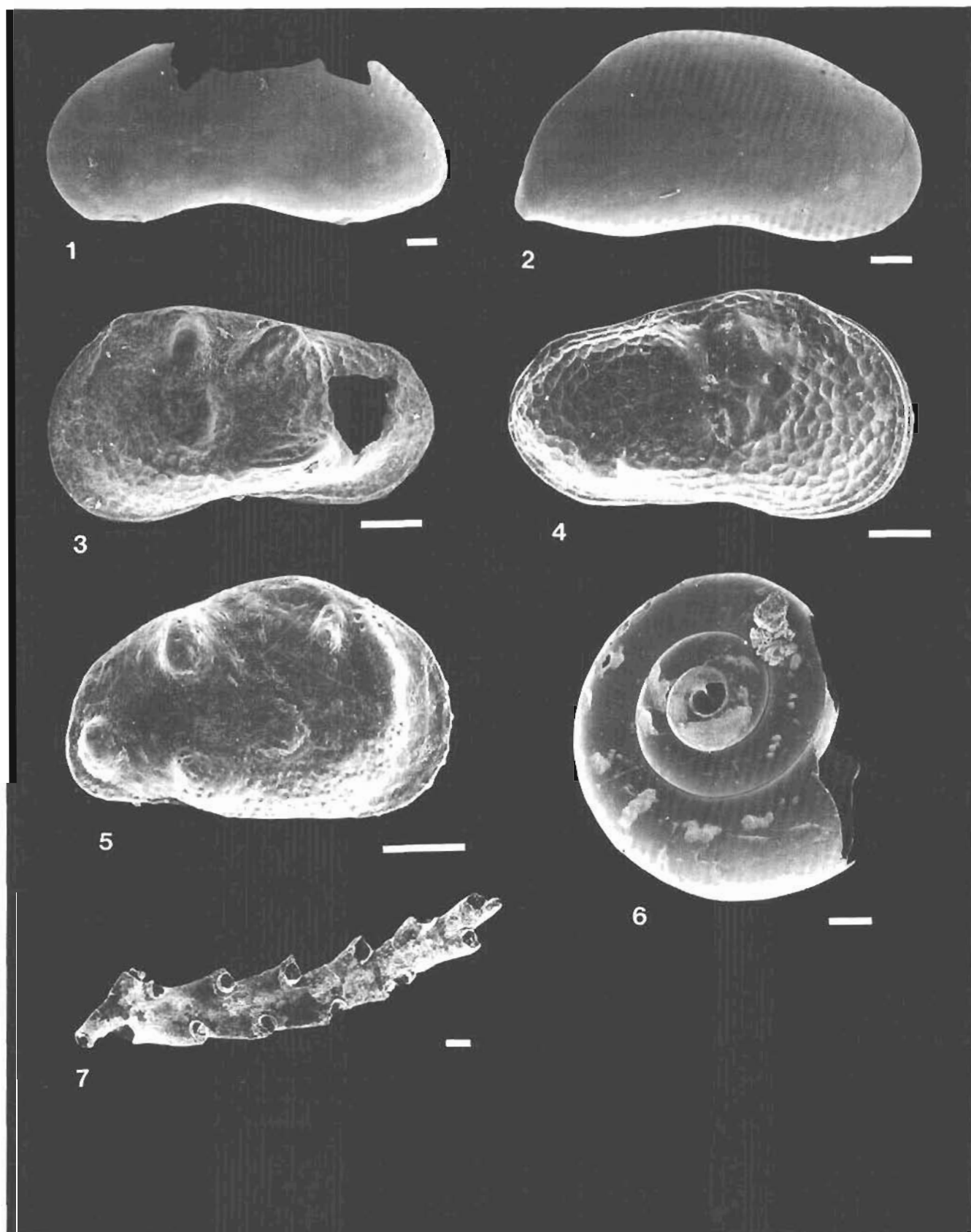


**Figure 4.** Continental ostracodes recovered from bottom grab samples in Vitus Lake. Scale bars equal 100 micrometers.

1. *Candona caudata*, male left valve exterior, adult, sample 92-EB-M1.
2. *Candona caudata*, female right valve exterior, adult, sample 92-EB-M1.
3. *Limnocythere ceriotuberosa* Delorme, left valve exterior, juvenile, sample 92-EB-M1.
4. *Limnocythere ceriotuberosa* Delorme, right valve exterior, adult female, sample 92-EB-M1.
5. Cytherideid, right valve exterior, juvenile, sample 92-EB-M1.
6. Gastropod, sample 92-EB-M10.
7. Cyclostome bryozoan, sample 92-EB-M10.





# RUBIDIUM-STRONTIUM ISOTOPIC SYSTEMATICS OF VEIN MINERALS IN THE JUNEAU GOLD BELT, ALASKA

By Ronald W. Kistler, Rainer J. Newberry, and David A. Brew

## INTRODUCTION

Potassium-argon and rubidium-strontium techniques have been used to determine the ages of Early Cretaceous gold-bearing quartz veins in the Mother Lode (Kistler and others, 1983) and in the northern Sierra Nevada foothills metamorphic belt (Böhlke and Kistler, 1986) in California. The ages of individual veins determined by the two techniques were the same, but the Rb-Sr isochrons yielded additional information about sources of the ore-bearing fluids by virtue of the initial  $^{87}\text{Sr}/^{86}\text{Sr}$  value of the vein minerals that was calculated in the age determination. In fact, vein carbonate, albite, chlorite, or quartz generally have such low Rb abundances that their measured  $^{87}\text{Sr}/^{86}\text{Sr}$  values are close approximations of the initial  $^{87}\text{Sr}/^{86}\text{Sr}$  value of mineralizing fluids.

The Juneau gold belt extends for about 200 km within 5 km of the Coast Range megalineament of Brew and Ford (1978) in southeastern Alaska (fig. 1). Oxygen and hydrogen isotope compositions of vein minerals along the belt indicate that the ore fluids had a deep crustal source, most likely of metamorphic origin, whereas values of  $\delta^{34}\text{S}$  have a provinciality that suggests that sulfur in the vein minerals was derived mostly from rocks near the sites of ore deposition (Goldfarb and others, 1991a). A K-Ar age of hydrothermal muscovite from the Alaska-Juneau deposit is  $55.3 \pm 2.1$  Ma (Goldfarb and others, 1988) and a Rb-Sr isochron on vein alteration minerals indicated an age of  $56.7 \pm 3.7$  Ma for the same deposit (Newberry and Brew, 1988).

This report documents Rb-Sr abundances and isochron ages of quartz, carbonate, albite, phlogopite, chlorite, and white mica from gold-bearing veins from three mines along the northern half of the gold belt (fig. 1): the Alaska-Juneau deposit in the Wrangellia terrane (reported by Newberry and Brew, 1988), the Treadwell deposit in the Gravina overlap assemblage, and the Kensington deposit in the Wrangellia terrane adjacent to Gravina overlap assemblage rocks. Oxygen, hydrogen, and carbon isotope data also are reported for the minerals from the vein at the Alaska-Juneau mine.

## ANALYTICAL TECHNIQUES

Veins were crushed and essentially pure mineral species were separated by standard heavy liquid and magnetic techniques. Pure mica from the Kensington specimens could not be separated from included carbonate by the standard techniques. These micas were treated by attempting to remove the carbonate in 1N HCl. This exercise was successful in cleaning only one of the two mica specimens to a sufficient purity to be geochronologically useful.

Rb and Sr concentrations were determined by standard isotope dilution techniques. Sr was loaded in a double rhenium filament mode and its isotopic composition was determined by multiple collection in a  $90^\circ$  sector mass spectrometer. Oxygen was liberated by reaction of minerals with  $\text{ClF}_3$  in nickel bombs at  $550^\circ\text{C}$  with the technique of Borthwick and Harmon (1982). Hydrogen isotopic composition of phlogopite was determined using the method of Godfrey (1962). Analytical results are given in table 1.

All strontium isotope ratios are normalized to  $^{86}\text{Sr}/^{88}\text{Sr}=0.1194$ . The decay constant for  $^{87}\text{Rb}=1.42 \times 10^{-11} \text{ yr}^{-1}$ . The  $\delta$  values for oxygen and hydrogen are given in per mil relative to SMOW (standard mean ocean water), and the value for carbon is given in per mil relative to the PDB (Pee Dee belemnite) standard.

## AGE AND STRONTIUM ISOTOPE RESULTS

The rubidium-strontium ages for the Alaska-Juneau, Treadwell, and Kensington vein minerals are  $56.7 \pm 3.7$  Ma,  $56.1 \pm 3.1$  Ma, and  $47.6 \pm 1.6$  Ma, respectively. The data are plotted on a strontium evolution diagram in figure 2. The Treadwell and Kensington deposits have similar initial  $^{87}\text{Sr}/^{86}\text{Sr}$  values of  $0.70357 \pm 13$  and  $0.70327 \pm 8$ , respectively. The Alaska-Juneau vein has a much more radiogenic initial  $^{87}\text{Sr}/^{86}\text{Sr}$  value of  $0.70822 \pm 30$ . Figure 3, an expanded view of the Treadwell and Alaska-Juneau data, emphasizes that the quartz and chlorite from the Treadwell

locality are not in isotopic equilibrium with the coexisting ankerite, albite, and white mica.

## DISCUSSION

The Rb-Sr mineral-isochron ages of the Alaska-Juneau and Treadwell deposits are the same within experimental error, and they are also the same as the vein muscovite K-Ar age from the Alaska Juneau mine (Newberry and Brew, 1988) and the  $^{40}\text{Ar}/^{39}\text{Ar}$  mica ages (Goldfarb and others, 1991b) for both of these deposits. However, the rubidium-strontium data yield a significantly younger age (47 Ma) for our Kensington sample, which is not in agreement with a 55-Ma age of mica from the Kensington deposit by the  $^{40}\text{Ar}/^{39}\text{Ar}$  technique (Goldfarb and others, 1991b). Our Kensington sample (90RN102, table 1) is from a musco-

vite-rich vein about 15 m away from the ore zone, and on structural grounds is thought to have formed during the same event as the ore sample. However, on existing time scales (for example, Palmer, 1983) it formed in the middle Eocene rather than in the early Eocene, the common date obtained from all the other specimens dated in the Juneau gold belt.

Goldfarb and others (1991a) noted a strong provinciality in sulfur isotope values of sulfide minerals from the mines along the Juneau gold belt. They interpreted this to be due to a regional metamorphic mineralizing fluid with a uniform sulfur isotope composition that acquired much of its sulfur from rocks near the sites of ore deposition. The strontium isotope values reported here have a provinciality that correlates positively with that observed for sulfur isotopes from the same three mines. The lightest (most

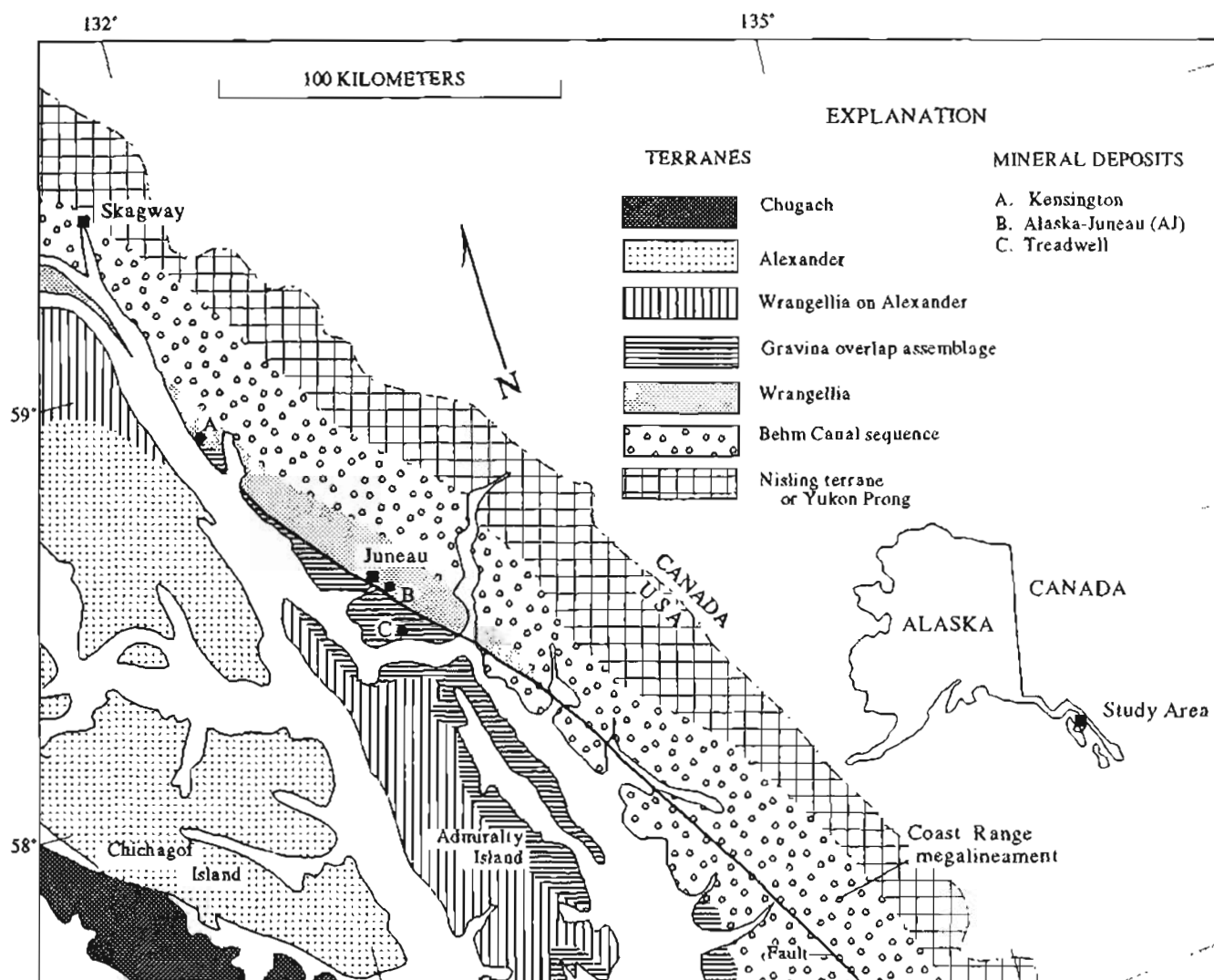


Figure 1. Mineral occurrences within Juneau gold belt that were sampled for Rb-Sr mineral isochron studies. Terrane boundaries and designations from Brew and others (1991).

**Table 1.** Analytical data for vein minerals from mines in the Juneau gold belt

[qz-a is -60 +100 mesh; qz-b is -100 +140 mesh. Minerals: qz, quartz; carb, carbonate; ank, ankerite; alb, albite; phlog, phlogopite; mic, white mica; chl, chlorite; dolo, dolomite; calc, calcite. Kensington mine "mic-a" specimens were treated with 1N HCl for 10 minutes to remove intergrown carbonate. For the A-J mine, hydrogen ( $\delta D$ ) and carbon ( $\delta^{13}C$ ) fractionation values are given in the last column along with oxygen values. nd, not determined]

Sample	Rb(ppm)	Sr(ppm)	Rb/Sr	$^{87}Rb/^{86}Sr$	$^{87}Sr/^{86}Sr$	$\delta^{18}O$
<b>A-J mine, lat 58°18'26" N., long 134°20'47" W.</b>						
86RN16 phlog	427.5	9.98	42.8	125.15	0.80914±7	+13.1
						$\delta D=-96$
016Aqz-a	1.55	3.28	.473	1.368	.70904±9	+18.0
016Aqz-b	.138	3.62	.038	.110	.70829±9	+17.7
016Acarb	.245	983	.0002	.001	.70822±1	+15.9
						$\delta^{13}C=-10.6$
<b>Treadwell mine, lat 58°16'00" N., long 134°22'40" W.</b>						
87RN276B ank	0.2	4844	0.0001	0.0003	0.70362±2	nd
87RN283A alb	1.0	441	.002	.006	.70352±2	nd
87RN280A qz	.02	1.13	.015	.1419	.70443±9	nd
87RN276B mic	349.4	220.5	1.585	4.584	.70722±2	nd
87RN281A chl	21.4	114.3	.187	.542	.70345±2	nd
<b>Kensington mine, lat 58°52'11" N., long 135°06'10" W.</b>						
90RN101A mic	62.3	802.4	0.078	0.225	0.70347±2	nd
90RN101A mic-a	117.5	3400	.035	.1	.70344±2	nd
90RN101B qz	.045	2.6	.017	.05	.70384±2	nd
90RN101C dolo	.866	566	.002	.004	.70336±2	nd
90RN102A mic	88	226	.389	1.126	.70404±2	nd
90RN102A mic-a	110.5	26.5	4.17	12.07	.71143±2	nd
90RN102B calc	1.07	803	.001	.004	.70326±2	nd

negative, -6.2 to -17.8 per mil) and heaviest (most positive, -3.8 to 1.2 per mil)  $\delta^{34}S$  reported by Goldfarb and others (1991a) are from the Alaska-Juneau, and from the Treadwell and Kensington mines, respectively. Even though much of the veining at Alaska-Juneau is hosted by metagabbro sills, this area is largely underlain by black phyllite. The extremely negative sulfur isotope values observed suggest that the sulfur in the vein sulfide minerals was derived from the local, reduced sedimentary rock source (Goldfarb and others, 1991a). The radiogenic strontium isotope composition (0.7081) of the Alaska-Juneau vein minerals is also compatible with having a source in local sedimentary wallrocks. In contrast, the heavier sulfur isotope values from ore veins at the Treadwell and Kensington deposits, hosted in monzonitic-monzodioritic plutonic rocks, are compatible with sulfur derivation from sulfide minerals with  $\delta^{34}S$  close to 0 per mil from earlier sulfide-bearing veins in the plutons (Goldfarb and others, 1991a). This sulfur isotopic composition is typical of many magmatic sulfides, and it correlates positively with the unradiogenic strontium (0.7033-0.7036) that also probably had its source in the local granitoid rock hosts at these mines.

The strontium isotope data indicate that the quartz and carbonate from the Alaska-Juneau vein precipitated in isotopic equilibrium at the same time. If the carbonate were

pure calcite, the about 2 per mil oxygen isotope fractionation between quartz and carbonate (table 1) would indicate their temperature of formation to be about 400°C (Friedman and O'Neil, 1977, fig. 24). Although this is not the case and the carbonate is ferroan dolomite, this temperature is probably not too far out of line given that geothermometry based on arsenopyrite ( $\pm$  pyrite-pyrrhotite or pyrite-sphalerite) indicates temperatures of vein formation in the neighborhood of 300-400°C in the Juneau gold belt (R.J. Newberry, unpublished data). Using a conservative estimate of 350°C for vein formation at the Alaska-Juneau mine, an oxygen-isotope fractionation between quartz and water of about +6 per mil is indicated. Therefore, the vein-forming fluid had a  $\delta^{18}O$  of +11.9 per mil, well within the range of oxygen isotope compositions of metamorphic water and also the compositions of other Juneau gold belt ore fluids reported by Goldfarb and others (1991a). Using the measured  $\delta D$  of -96 from the phlogopite (table 1), the calculated  $\delta D$  for the ore fluid at 350°C is -66 per mil from water-theoretical phlogopite fractionation (Suzuoki and Epstein, 1976). This calculated hydrogen isotopic composition is like that measured from fluid inclusions in quartz rather than that calculated for Juneau gold belt ore fluids by Goldfarb and others (1991a). This suggests that our Alaska-Juneau vein had a minor post-depositional interaction with meteoric water. The carbonate

$\delta^{13}\text{C}$  of  $-10.6$  per mil (table 1) is similar to carbon isotopic compositions of  $\text{CO}_2$  measured in hot springs at Steamboat Springs, Colorado, and at The Geysers and Lassen Peak, California.

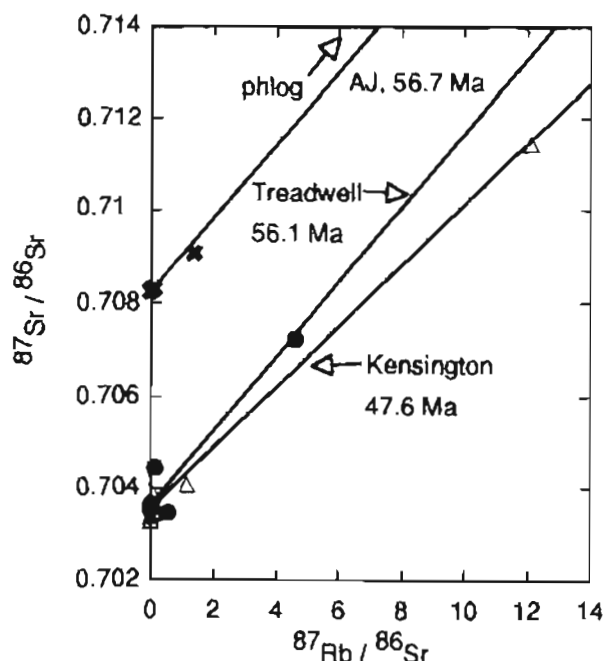


Figure 2. Strontium evolution diagram showing isochrons defined by minerals from Alaska-Juneau, Treadwell, and Kensington deposits in Juneau gold belt. phlog, phlogopite.

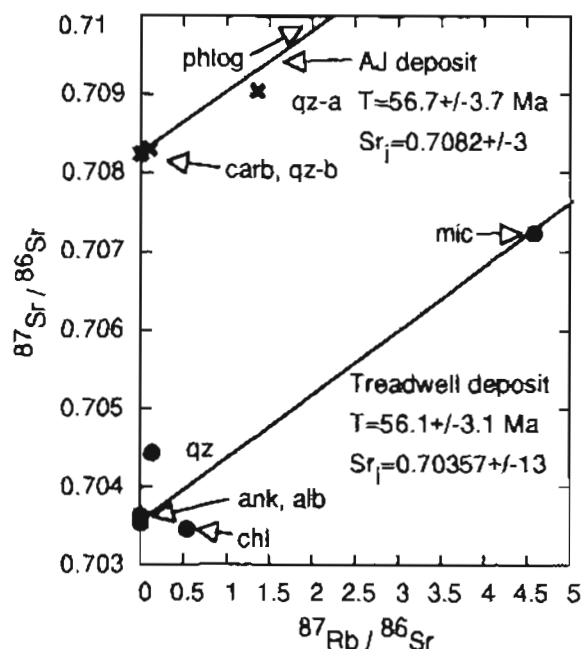


Figure 3. Expanded view of Treadwell and Alaska-Juneau data. Note that quartz and chlorite from Treadwell locality are not in isotopic equilibrium with ankerite, albite, and white mica from there. Mineral abbreviations as in table 1.

## CONCLUSIONS

The Alaska-Juneau, Treadwell, and Kensington deposits in the Juneau gold belt are Eocene in age. The strontium in the vein minerals of the Alaska-Juneau deposit in the Wrangellia terrane was apparently scavenged from sedimentary host rocks, whereas vein minerals of the Treadwell and Kensington deposits have strontium derived from their plutonic rock hosts. The Kensington deposits are hosted by the 106-Ma Jualin pluton (G.R. Tilton, written comm. to D.A. Brew, 1985) in the Wrangellia terrane close to Gravina overlap assemblage rocks. We note here that Goldfarb and others (1991a) reported an erroneous 113-Ma age for the Jualin pluton. Its strontium isotopic characteristics are similar to those of the Treadwell deposits that are localized within a zone of monzonite sills within a sequence of slate in the Gravina overlap assemblage rocks. The mineralizing fluids responsible for the gold belt veins have oxygen isotope characteristics of evolved metamorphic waters.

## REFERENCES CITED

- Böhlke, J.K., and Kistler, R.W., 1986, Rb-Sr, K-Ar, and stable isotope evidence for the ages and sources of fluid components of gold-bearing quartz veins in the northern Sierra Nevada foothills metamorphic belt, California: *Economic Geology*, v. 81, p. 296-322.
- Borthwick, J., and Harmon, R.S., 1982, A note regarding  $\text{ClF}_3$  as an alternative to  $\text{BrF}_5$  for oxygen isotope analysis: *Geochimica et Cosmochimica Acta*, v. 46, p. 1665-1668.
- Brew, D.A., and Ford, A.B., 1978, Megaléonement in southeastern Alaska marks southwest edge of Coast batholithic complex: *Canadian Journal of Earth Sciences*, v. 15, p. 1763-1772.
- Brew, D.A., Karl, S.M., Barnes, D.F., Jachens, R.C., Ford, A.B., and Horner, R., 1991, A northern Cordilleran ocean-continent transect: Sitka Sound to Atlin Lake, British Columbia: *Canadian Journal of Earth Sciences*, v. 28, p. 840-853.
- Friedman, Irving, and O'Neil, J.R., 1977, Compilation of stable isotope fractionation factors of geochemical interest: U.S. Geological Survey Professional Paper 440-KK, 12 p.
- Godfrey, J.D., 1962, The deuterium content of hydrous minerals from the east-central Sierra Nevada and Yosemite National Park: *Geochimica et Cosmochimica Acta*, v. 26, p. 1215-1245.
- Goldfarb, R.J., Leach, D.L., Pickthorn, W.J., and Paterson, C.J., 1988, Origin of lode-gold deposits of the Juneau gold belt, southeastern Alaska: *Geology*, v. 16, p. 440-443.
- Goldfarb, R.J., Newberry, R.J., Pickthorn, W.J., and Gent, C.A., 1991a, Oxygen, hydrogen, and sulfur isotope studies in the Juneau gold belt, southeastern Alaska: Constraints on the origin of hydrothermal fluids: *Economic Geology*, v. 86, p. 66-80.
- Goldfarb, R.J., Snee, L.W., Miller, L.D., and Newberry, R.J., 1991b, Rapid dewatering of the crust deduced from ages of mesothermal gold deposits: *Nature*, v. 354, p. 296-298.

- Kister, R.W., Dodge, F.C.W., and Silberman, M.L., 1983, Isotopic studies of mariposite-bearing rocks from the south-central Mother Lode, California: *California Geology*, v. 36, p. 201–203.
- Newberry, R.J., and Brew, D.A., 1988, Alteration zoning and origin of the Alaska-Juneau gold deposit: U.S. Geological Survey Circular 1016, p. 174–178.
- Palmer, A.R., 1983, Geologic time scale, decade of North American geology: Boulder, Geological Society of America.
- Suzuoki, T., and Epstein, S., 1976, Hydrogen isotope fractionation between OH-bearing minerals and water: *Geochimica et Cosmochimica Acta*, v. 40, p. 1229–1240.

Reviewers: Arthur B. Ford and Marvin A. Lanphere

# U.S. GEOLOGICAL SURVEY REPORTS ON ALASKA RELEASED IN 1992\*

*Compiled by Ellen R. White*

\*[Some reports dated 1991 did not become available until 1992: they are included in this listing.]

## ABBREVIATIONS

- B2041 Bradley, D.C., and Dusel-Bacon, Cynthia, eds., 1992, *Geologic studies in Alaska by the U.S. Geological Survey, 1991: U.S. Geological Survey Bulletin 2041*, 256 p.
- C1074 Carter, L.M.H., 1992, *USGS research on energy resources, 1992, V.E. McKelvey Forum on Mineral and Energy Resources, 8th, Houston, Tex., 1992, Program and abstracts: U.S. Geological Survey Circular 1074*, 89 p.
- OF92-258 Jacobson, M.L., compiler, 1992, *National Earthquake Hazards Reduction Program; Summaries of technical reports, v. XXXIII: U.S. Geological Survey Open-File Report 92-258*, 2 v.

- Abers, G.A., 1992, Seismic monitoring of the Shumagin seismic gap, Alaska: OF92-258, v. 1, p. 121-125.
- Abers, G.A., and Jacob, K.H., 1992, Analysis of seismic data from the Shumagin seismic gap: OF92-258, v. 1, p. 1-5.
- Affolter, R.H., Stricker, G.D., Roberts, S.B., and Brownfield, M.E., 1992, Geochemical variation of arctic margin low-sulfur Cretaceous and Tertiary coals, North Slope, Alaska [abs.], in Barker, C.E., and Coury, A.B., *Abstracts of the U.S. Geological Survey, Central Region, 1992 poster review; collected abstracts of selected poster papers presented at scientific meetings: U.S. Geological Survey Open-File Report 92-391*, p. 8.
- Apodaca, L.E., 1992, Fluid-inclusion study of the Rock Creek area, Nome mining district, Seward Peninsula, Alaska: B2041, p. 3-12.
- Arbogast, B.F., Lee, G.K., and Light, T.D., 1991, Analytical results and sample locality map of stream-sediment and heavy-mineral-concentrate samples from the Livengood 1° × 3° quadrangle, Alaska: U.S. Geological Survey Open-File Report 91-23-A, 121 p., 1 sheet, scale 1:250,000 (paper version), and 91-23-B, data from report, but not map, are on 1.2-MB, 5.25-inch diskette.
- Barker, Fred, Farmer, G.L., Plafker, George, and Ayuso, R.A., 1992, The accretionary prism and magmatism of the Gulf of Alaska [abs.]: U.S. Geological Survey Circular 1089, p. 3-4.
- Barnes, P.W., Reimnitz, Erk, and Rollyson, B.P., 1992, Map showing Beaufort Sea coastal erosion and accretion between Flaxman Island and the Canadian border, northeastern Alaska; Thirty-year coastline comparison, sediment volumes released, and physiographic character: U.S. Geological Survey Miscellaneous Investigations Series Map I-1182-H, 2 sheets.
- Barron, J.A., 1992, Diatoms from ice-rafted sediment collected from the Beaufort Sea, Arctic Alaska: U.S. Geological Survey Open-File Report 92-439, 16 p.
- Beavan, John, 1992, Crustal deformation measurements in the Shumagin seismic gap, Alaska: OF92-258, v. 1, p. 145-150.
- Bird, K.J., and Collett, T.S., 1992, Sagavanirktok Formation—A new look with seismic data in the Prudhoe Bay-Kuparuk River region, Alaskan North Slope [abs.]: C1074, p. 7.
- Bird, K.J., Howell, D.G., Johnsson, M.J., and Magoon, L.B., 1992, Alaskan North Slope geothermics, geodynamics, and hydrology—implications for oil and gas [abs.]: C1074, p. 8.
- Bird, K.J., Johnsson, M.J., Howell, D.G., and Magoon, L.B., 1992, Thermal maturity mapping in Alaska, in U.S. Geological Survey Yearbook, Fiscal year 1991: U.S. Geological Survey, p. 55-57.
- Bliss, J.D., 1992, Grade and tonnage model of Chugach-type low-sulfide Au-quartz veins: U.S. Geological Survey Bulletin 2004, p. 44-46.
- Blodgett, R.B., and Gilbert, W.G., 1992, Upper Devonian shallow-marine siliciclastic strata and associated fauna and flora, Lime Hills D-4 quadrangle, southwest Alaska: B2041, p. 106-115.
- Bohn, Diedra, and Schneider, J.L., eds., 1992 [released 1993], 1992 annual report on Alaska's mineral resources; A summary of mineral resource activities in Alaska during 1991: U.S. Geological Survey Circular 1091, 65 p.
- Borden, J.C., Goldfarb, R.J., Gent, C.A., Burruss, R.C., and Roushey, B.H., 1992, Geochemistry of lode-gold deposits, Nuka Bay district, southern Kenai Peninsula: B2041, p. 13-22.
- Boyd, T.M., 1992, Analysis of the 1957 Andreanof Islands earthquake, Alaska: OF92-258, v. 1, p. 11-15.
- Brabets, T.P., 1992, Hydrologic data for the lower Copper River, Alaska, May to September 1991: U.S. Geological Survey Open-File Report 92-89, 15 p.
- Bradley, D.C., and Dusel-Bacon, Cynthia, 1992, *Geologic studies in Alaska by the U.S. Geological Survey, 1991, Introduction: B2041*, p. 1-2.
- Briggs, P.H., Motooka, J.M., Bailey, E.A., Cieutat, B.A., Burner, S.A., Kelley, K.D., and Ficklin, W.H., 1992, Analytical results of soil, stream sediment, panned concentrate, and water



- samples from the Lik deposit, northwestern Brooks Range, Alaska: U.S. Geological Survey Open-File Report 92-15-A, 53 p. (paper version); 92-15-B (diskette version).
- Brocculieri, Thomas, Underwood, M.B., and Howell, D.G., 1992, Petrography and provenance of sandstones from the Nation River Formation (Devonian) and the Step Conglomerate (Permian), Kandik region, east-central Alaska: B2041, p. 116-124.
- Brouwers, E.M., 1992, Pliocene paleoecologic reconstructions based on ostracode assemblages from the Sagavanirktok and Gubik Formations, Alaskan North Slope: U.S. Geological Survey Open-File Report 92-321, 48 p.
- Brunett, J.O., Solin, G.L., Carr, M.R., Glass, R.L., Nelson, G.L., and Buchmiller, R.C., 1992, Water-quality and soil assessment at 28 exploratory wellsites in the National Petroleum Reserve in Alaska, 1989-90: U.S. Geological Survey Open-File Report 91-458, 118 p., 107 pls., thirteen 5.25-inch diskettes.
- Bruns, T.R., Stevenson, A.J., and Dobson, M.R., 1992, GLORIA investigation of the Exclusive Economic Zone in the Gulf of Alaska and off southeast Alaska; M/V Farnella Cruise F7-89-GA, June 14-July 13, 1989: U.S. Geological Survey Open-File Report 92-317, 16 p.
- Burns, L.E., 1992, Ophiolitic complexes and associated rocks near the Border Ranges fault zone, south central Alaska: U.S. Geological Survey Open-File Report 92-20-E, 8 p., 1 pl.
- Carver, Gary, and Gilpin, L.M., 1992, Paleoseismicity of Kodiak Island, Alaska: OF92-258, v. 1, p. 192-194.
- Cathrall, J.B., VanTrump, George, Jr., Antweiler, J.C., and Mosier, E.L., 1992, Magnetic media file of analytical results and geochemical signatures of lode gold, placer gold, and heavy-mineral concentrates from mining districts in central, western, and northern Alaska: U.S. Geological Survey Open-File Report 92-573, 17 p.
- Church, S.E., Riehle, J.R., Magoon, L.B., and Campbell, D.L., 1992, Mineral and energy resource assessment maps of the Mount Kaunai, Naknek, and western Afognak quadrangles, Alaska: U.S. Geological Survey Miscellaneous Field Studies Map MF-2021-F, 22 p., 2 sheets, scale 1:250,000.
- Cieutat, B.A., Goldfarb, R.J., Bradley, D.C., and Roushey, B.H., 1992, Placer gold of the Kenai lowland: B2041, p. 23-29.
- Collett, T.S., 1992, Natural gas hydrates—a proven resource [abs.]: C1074, p. 714-15.
- Combellick, R.A., and Reger, R.D., 1992, Investigation of peat stratigraphy in estuarine flats near Anchorage, Alaska, as a means for determining recurrence intervals of major earthquakes: OF92-258, v. 1, p. 219-220.
- Conrad, J.E., McKee, E.H., and Turrin, B.D., 1992, Age of tephra beds at the Ocean Point dinosaur locality, North Slope, Alaska, based on K-Ar and  $^{40}\text{Ar}/^{39}\text{Ar}$  analyses: U.S. Geological Survey Bulletin 1990-C, 12 p.
- Crock, J.G., Gough, L.P., Mangis, D.R., Curry, K.L., Fey, D.L., Hageman, P.L., and Welsch, E.P., 1992, Element concentrations and trends for moss, lichen, and surface soils in and near Denali National Park and Preserve, Alaska: U.S. Geological Survey Open-File Report 92-323, 149 p.
- Crysdale, B.L., Schenk, C.J., and Meyer, R.F., 1992, Tar sands and heavy oils—resources, recovery, and realism [abs.]: C1074, p. 15-16.
- Csejtei, Béla, Jr., Mullen, M.W., Cox, D.P., and Stricker, G.D., 1992, Geology and geochronology of the Healy quadrangle, south-central Alaska: U.S. Geological Survey Miscellaneous Investigations Series Map I-1961, 63 p., 2 sheets, scale 1:250,000.
- Detra, D.E., Motooka, J.M., and Cathrall, J.B., 1992, Supplemental analytical results and sample locality map of stream-sediment and heavy-mineral-concentrate samples from the Craig Study Area; Craig, Dixon Entrance, Ketchikan, and Prince Rupert quadrangles, Alaska: U.S. Geological Survey Open-File Report 92-552-A, 16 p., 1 sheet, scale 1:250,000, and tables 1-4 in digital format on 5.25-inch floppy disk in pocket.
- Dolton, G.L., Mast, R.F., and Crovelli, R.A., 1992, Undiscovered oil and gas resources of Federal lands and waters [abs.]: C1074, p. 21-22.
- Dover, J.H., 1992, Geologic map and fold- and thrust-belt interpretation of the southeastern part of the Charley River quadrangle, east-central Alaska: U.S. Geological Survey Miscellaneous Investigations Map I-1942, scale 1:100,000.
- Drinkwater, J.L., Ford, A.B., and Brew, D.A., 1992, Magnetic susceptibilities and iron content of plutonic rocks across the Coast plutonic-metamorphic complex near Juneau, Alaska: B2041, p. 125-139.
- , 1992, Magnetic susceptibility measurements and sample locations of granitic rocks from along a transect of the Coast Mountains near Juneau, Alaska: U.S. Geological Survey Open-File Report 92-724, 22 p.
- Dumoulin, J.A., and Harris, A.G., 1992, Devonian-Mississippian carbonate sequence in the Maiyumerak Mountains, western Brooks Range, Alaska: U.S. Geological Survey Open-File Report 92-3, 83 p.
- Dusel-Bacon, Cynthia, and Hansen, V.L., 1992, High-pressure amphibolite-facies metamorphism and deformation within the Yukon-Tanana and Taylor Mountain terranes, eastern Alaska: B2041, p. 140-159.
- Fitzpatrick, J.J., Hinkley, T.K., Landis, G.P., Rye, R.O., and Holdsworth, G., 1992, High-resolution paleoclimate reconstruction from Alaskan ice-core records [abs.]: C1074, p. 29.
- Flores, R.M., and Stricker, G.D., 1992, Some facies aspects of the upper part of the Kenai Group, southern Kenai Peninsula, Alaska: B2041, p. 160-170.
- Foley, J.Y., 1992, Ophiolitic and other mafic-ultramafic metallogenic provinces in Alaska (west of the 141st meridian): U.S. Geological Survey Open-File Report 92-20-B, 55 p., 1 sheet, scale 1:2,500,000.
- Folger, P.F., Goldfarb, R.J., and Cieutat, B.A., 1992, Geochemical survey of the Baird Mountains  $1^\circ \times 3^\circ$  quadrangle: U.S. Geological Survey Bulletin 2003, 77 p., 1 sheet, scale 1:250,000.
- Foster, H.L., 1992, Geologic map of the eastern Yukon-Tanana region, Alaska: U.S. Geological Survey Open-File Report 92-313, 27 p., scale 1:500,000.
- Friskien, J.G., 1992, Interpretation of reconnaissance geochemical data from the Port Moller, Stepovak Bay and Simeonof Island quadrangles, Alaska Peninsula, Alaska: U.S. Geological Survey Bulletin 1968, 47 p., 3 sheets, scale 1:250,000.
- Friskien, J.G., and Arbogast, B.F., 1992, Map showing the distribution of anomalous concentrations of selected elements determined in stream sediments from the Port Moller, Stepovak Bay, and Simeonof Island quadrangles, Alaska Peninsula, Alaska: U.S. Geological Survey Miscellaneous

- Field Studies Map MF-2155-B, 1 sheet, scale 1:250,000.
- 1992, Maps showing the distribution of anomalous concentrations of selected elements and minerals determined in nonmagnetic heavy-mineral concentrates from the Port Moller, Stepovak Bay, and Simeonof Island quadrangles, Alaska Peninsula, Alaska: U.S. Geological Survey Miscellaneous Field Studies Map MF-2155-C, 3 sheets, scale 1:250,000.
- Friskken, J.G., and Kelly, D.L., 1992, Maps showing the distribution of gold determined in various sample media collected from the Port Moller, Stepovak Bay, and Simeonof Island quadrangles, Alaska Peninsula, Alaska: U.S. Geological Survey Miscellaneous Field Studies Map MF-2155-D, 2 sheets, scale 1:250,000.
- Frost, T.P., 1992, Analytical results in digital format of rock samples from the Bethel and part of the Russian Mission 1 degree by 3 degree quadrangles, Alaska: U.S. Geological Survey Open-File Report 92-582, 6 p.
- Frost, T.P., Bailey, E.A., Bradley, Leon, O'Leary, Richard, and Motooka, Jerry, 1992, Analytical results of non-magnetic heavy-mineral-concentrate sample data from the Bethel and southern part of the Russian Mission 1° × 3° quadrangles, southwest Alaska: U.S. Geological Survey Open-File Report 92-380-A (paper copy, 98 p.) and Open-File Report 92-380-B (3.5-inch floppy disk, 1.44 MB).
- 1992, Analytical results of stream-sediment sample data from the Bethel and southern part of the Russian Mission 1° × 3° quadrangles, southwest Alaska: U.S. Geological Survey Open-File Report 92-379-A (paper copy, 119 p.) and Open-File Report 92-379-B (3.5-inch floppy disk, 1.44 MB).
- Frost, T.P., Box, S.E., and Moll-Stalcup, E.J., 1992, Summary of results of the mineral resource assessment of the Bethel and southeastern part of the Russian Mission 1° by 3° quadrangles, Alaska: B2041, p. 30-48.
- Frost, T.P., Bradley, L.A., O'Leary, Richard, and Motooka, Jerry, 1992, Analytical results, sample locality map, and descriptions of rock samples from the Bethel and southern part of the Russian Mission 1° × 3° quadrangles, southwest Alaska: U.S. Geological Survey Open-File Report 92-315, 229 p., 1 sheet, scale 1:250,000.
- Gault, H.R., and Wahrhaftig, Clyde, 1992, The Salt Chuck copper-palladium mine, Prince of Wales Island, southeastern Alaska, with preface by R.A. Loney: U.S. Geological Survey Open-File Report 92-293, 10 p. [This report was written as a War Minerals Report in 1943 and was classified as "confidential." Here reproduced with only a slight change in format and no change in the original words or data. Open-File Report 46-19 by Gault on the same subject, released in 1946, did not include all the information reproduced in OF 92-293.]
- Gehrels, G.E., 1992, Geologic map of the southern Prince of Wales Island, southeastern Alaska: U.S. Geological Survey Miscellaneous Investigations Series Map I-2169, 23 p., 1 sheet (color), scale 1:63,360. [This map supersedes OF 86-275.]
- Gehrels, G.E., and Berg, H.C., 1992, Geologic map of southeastern Alaska: U.S. Geological Survey Miscellaneous Investigations Map I-1867, scale 1:600,000. [This map supersedes USGS Open-File Report 84-886.]
- Goldfarb, R.J., Case, J.E., Plafker, George, and Winkler, G.R., 1992, Maps showing areas of potential for mineral resources in the Cordova and northern Middleton Island 1° × 3° quadrangles, southern Alaska: U.S. Geological Survey Miscellaneous Field Studies Map MF-2190, scale 1:250,000.
- Goldman, M.R., Fuis, G.S., Luetgert, J.H., and Geddes, D.J., 1992, Data report for the TACT 1987 refraction survey: Fairbanks North and Olnes deployments: U.S. Geological Survey Open-File Report 92-196, 98 p.
- Grantz, Arthur, and Mullen, M.W., 1992, Bathymetric map of the Chukchi and Beaufort Seas and adjacent Arctic Ocean: U.S. Geological Survey Miscellaneous Investigations Series Map I-1182-I, scale 1:1,000,000.
- Gray, J.E., Adrian, B.M., Hageman, P.L., and Kilburn, J.E., 1992, Analytical results and sample locality maps of rock samples from the eastern Goodnews Bay quadrangle, southwest Alaska: U.S. Geological Survey Open-File Report 92-8-A (paper copy, 21 p.), and Open-File Report 92-8-B (5.25-inch diskette).
- Gray, J.E., Hageman, P.L., and Ryder, J.L., 1992, Comparison of the effectiveness of stream-sediment, heavy-mineral-concentrate, aquatic-moss, and stream-water geochemical sample media for the Mineral Assessment Study of the Iditarod quadrangle, Alaska: B2041, p. 49-59.
- Howe, D.L., Sireveler, G.P., and Brew, D.A., 1992 [1993], Bibliography of research and exploration in the Glacier Bay region, southeastern Alaska, 1798-1992: U.S. Geological Survey Open-File Report 92-596, 70 p.
- Johnsson, M.J., Pawlewicz, M.J., Harris, A.G., and Valin, Z.C., 1992, Vitrinite reflectance and conodont color alteration index data from Alaska; data to accompany the thermal maturity map of Alaska: U.S. Geological Survey Open-File Report 92-409, three 3.5-inch diskettes (Macintosh-formatted, high density: 1.44MB).
- Jones, J.L., and Kilburn, J.E., 1992, Geochemical map showing the distribution of selected elements in heavy-mineral concentrate samples from the Goodnews Bay, Hagemaster Island, and Nushagak Bay quadrangles, Alaska: U.S. Geological Survey Miscellaneous Field Studies Map MF-2186, 2 sheets, scale 1:250,000.
- Karl, S.M., and Giffen, C.F., 1992, Sedimentology of the Bay of Pillars and Point Augusta Formations, Alexander archipelago, Alaska: B2041, p. 171-185.
- Kelley, J.S., Wrucke, C.T., and Armstrong, A.K., 1992, Fracturing and reservoir development in the Katakaturuk Dolomite, Arctic National Wildlife Refuge, Alaska [abs.]: C1074, p. 42-43.
- Kelley, K.D., Borden, J.C., Bailey, E.A., Fey, D.L., Motooka, J.M., and Roushey, B.H., 1992, Geochemically anomalous areas in the west-central part of the Howard Pass quadrangle, National Petroleum Reserve, Alaska: Evidence for sediment-hosted Zn-Pb-Ag-Ba mineralization: B2041, p. 60-69.
- Kilburn, J.E., and Jones, J.L., 1992, Geochemical map showing the distribution of selected elements in stream sediments from the Goodnews Bay, Hagemaster Island, and Nushagak Bay quadrangles, Alaska: U.S. Geological Survey Miscellaneous Field Studies Map MF-2355, 2 sheets, scale 1:250,000.
- Kisslinger, Carl, and Kindel, Bruce, 1992, Central Aleutian Islands seismic network: OF92-258, v. 1, p. 369-372.
- Kunk, M.J., and Cortesini, Henry, Jr., 1992, <sup>40</sup>Ar/<sup>39</sup>Ar age-spectrum data for whole rock basalts, and plagioclase and biotite from tephra: A traverse down the Porcupine River,

- east-central Alaska: U.S. Geological Survey Open-File Report 92-701, 81 p.
- Lahr, J.C., Stephens, C.D., Page, R.A., and Fogleman, K.A., 1992, Alaska seismic studies: OF92-258, v. 1, p. 373-380.
- Lockwood, Millington, Elms, J.D., Lockridge, P.A., Smith, R.H., Moore, G.W., Nishenko, S.P., Rinehart, W.A., Simkin, Tom, Siebert, Lee, and Newhall, C.G., 1990 (1992), Natural hazards map of the Circum-Pacific Region, Pacific basin sheet: U.S. Geological Survey Circum-Pacific Map Series CP-0035, 31 p., 1 sheet, scale 1:17,000,000. [Revision and reprint]
- March, G.D., and Murray, T.L., 1992, A PC-based program for viewing Cook Inlet volcano-seismic data: U.S. Geological Survey Open-File Report 92-560-A, 18 p. (paper version), and OFR 92-560-B (one 5.25-inch diskette).
- Mayo, L.R., March, R.S., and Trabant, D.C., 1992, Air temperature and precipitation data, 1967-88, Wolverine Glacier basin, Alaska: U.S. Geological Survey Open-File Report 91-246, 80 p.
- Measures, E.A., Rohr, D.M., and Blodgett, R.B., 1992, Depositional environments and some aspects of the fauna of Middle Ordovician rocks of the Tetsitna Formation, northern Kuskokwim Mountains, Alaska: B2041, p. 186-201.
- Moll-Stalcup, E.J., and Frost, T.P., 1992, The nature of the crust in western Alaska as inferred from the chemical and isotopic composition of Late Cretaceous to early Tertiary magmatic rocks in western Alaska: U.S. Geological Survey Open-File Report 92-525, p. 149-152.
- Moll-Stalcup, E.J., and Patton, W.W., Jr., 1992, Geologic map of the Blackburn Hills volcanic field, western Alaska: U.S. Geological Survey Miscellaneous Field Studies Map MF-2199, scale 1:63,360.
- Moore, G.W., Bogdanov, N.A., Drummond, K.J., Golovchenko, Xenia, Larson, R.L., Pittman, W.C., III, Rinehart, W.A., Siebert, Lee, Simkin, Tom, Tilman, S.M., and Uyeda, Seiya, 1992, Plate-tectonic map of the Circum-Pacific Region, Arctic sheet: U.S. Geological Survey Circum-Pacific Map Series CP-41, scale 1:10,000,000.
- Moore, T.E., 1992, The Arctic Alaska superterrane: B2041, p. 238-244.
- Moore, T.E., Wallace, W.K., Bird, K.J., Karl, S.M., and Mull, C.G., 1992, Development of the Ellesmerian continental margin and the Brookian orogeny, Alaska—a DNAG perspective [abs.]: C1074, p. 51-52.
- Moore, T.E., Wallace, W.K., Bird, K.J., Karl, S.M., Mull, C.G., and Dillon, J.T., 1992, Stratigraphy, structure, and geologic synthesis of northern Alaska: U.S. Geological Survey Open-File Report 92-330, 189 p., scale 1:500,000.
- Nelson, S.W., 1992, Ophiolitic complexes of the Gulf of Alaska: U.S. Geological Survey Open-File Report 92-20-C, 9 p., 1 pl.
- Nokleberg, W.J., Aleinikoff, J.N., Duro, J.T., Jr., Lanphere, M.A., Silberling, N.J., Silva, S.R., Smith, T.E., and Turner, D.L., 1992, Map, tables, and summary of fossil and isotopic age data, Mt. Hayes quadrangle, eastern Alaska Range, Alaska: U.S. Geological Survey Miscellaneous Field Studies Map MF-1996-D, 43 p., scale 1:250,000.
- Nokleberg, W.J., Aleinikoff, J.N., Lange, I.M., Silva, S.R., Miyakawa, R.T., Schwab, C.E., and Zehner, R.E., 1992 [released in 1993], Preliminary geologic map of the Mount Hayes quadrangle, eastern Alaska Range, Alaska: U.S. Geological Survey Open-File Report 92-594, 39 p., 1 sheet, scale 1:250,000.
- Okal, E.A., and Stein, Seth, 1992, Constraints on tectonic deformation in the southern Alaska subduction zone from historical seismicity: OF92-258, v. 1, p. 89-91.
- Patton, W.W., Jr., 1992, Ophiolitic terrane bordering the Yukon-Koyukuk basin, Alaska: U.S. Geological Survey Open-File Report 92-20-F, 7 p., 1 pl.
- , 1992, Ophiolitic terrane of western Brooks Range, Alaska: U.S. Geological Survey Open-File Report 92-20-D, 7 p., 1 pl.
- Patton, W.W., Jr., and Box, S.E., 1992, Ophiolitic terranes of east-central and southwestern Alaska: U.S. Geological Survey Open-File Report 92-20-G, 13 p., 2 pls.
- Patton, W.W., Jr., Murphy, J.M., Burns, L.E., Nelson, S.W., and Box, S.E., 1992, Geologic map of ophiolitic and associated volcanic arc and metamorphic terranes of Alaska (west of the 141st meridian): U.S. Geological Survey Open-File Report 92-20-A, scale 1:2,500,000.
- Phillips, R.L., Grantz, Arthur, Mullen, M.W., Rieck, H.J., McLaughlin, M.W., and Selkirk, T.L., 1992, Summary of lithostratigraphy and stratigraphic correlations in piston cores from Northwind Ridge, Arctic Ocean, from USCGC *Polar Star*, 1988: U.S. Geological Survey Open-File Report 92-426, 110 p., 4 pls.
- Philpotts, John, and Evans, J.R., 1992, Rare earth minerals in "thunder eggs" from Zarembo Island, southeast Alaska: B2041, p. 98-105.
- Plafker, George, 1992, Alaska geologic earthquake hazards: OF92-258, v. 2, p. 542-548.
- Plafker, George, Lull, J.S., Nokleberg, W.J., Pessel, G.A., Wallace, W.K., and Winkler, G.R., 1992, Geologic map of the Valdez A-4, B-3, B-4, C-3, C-4, and D-4 quadrangles, northern Chugach Mountains and southern Copper River basin, Alaska: U.S. Geological Survey Miscellaneous Investigations Series Map I-2164, 1 sheet, scale 1:125,000.
- Plafker, George, Naeser, C.W., Zimmermann, R.A., Lull, J.S., and Hudson, Travis, 1992, Cenozoic uplift history of the Mount McKinley area in the central Alaska Range based on fission-track dating: B2041, p. 202-212.
- Repenning, C.A., and Brouwers, E.M., 1992, Late Pliocene—early Pleistocene ecological changes in the Arctic Ocean borderland: U.S. Geological Survey Bulletin 2036, 37 p.
- Robinson, J.W., and McCabe, P.J., 1992, Reservoir heterogeneities in the Morrison Formation in southern Utah—a Prudhoe Bay analog [abs.]: C1074, p. 67-68.
- Saltus, R.W., 1992, Principal facts for 63 gravity stations in the vicinity of Katmai National Park, Alaska: U.S. Geological Survey Open-File Report 92-310, 13 p.
- Sass, J.H., Lachenbruch, A.H., and Williams, C.F., 1992, Heat flow and tectonic studies: OF92-258, v. 2, p. 892-902. [p. 897-898: North Slope of Alaska and North Slope Basin]
- Schmoll, H.R., and Yehle, L.A., 1992, Geologic map of the lower Beluga-Chuitna area, Tyonek A-3 and A-4 quadrangles, south-central Alaska: U.S. Geological Survey Open-File Report 92-346, 27 p.
- Shelton, K.L., Underwood, M.B., Bergfeld, Deborah, and Howell, D.G., 1992, Isotopic variations in calcite veins from the Kandik region of east-central Alaska: B2041, p. 213-221.
- Shew, Nora, and Lanphere, M.A., 1992, Map showing potassium-argon ages from the Mount Katmai and adjacent parts

- of the Naknek and Afognak quadrangles, Alaska Peninsula, Alaska: U.S. Geological Survey Miscellaneous Field Studies Map MF-2021-E, 1 sheet, scale 1:250,000.
- Silberling, N.J., Jones, D.L., Monger, J.W.H., and Coney, P.J., 1992, Lithotectonic terrane map of the North American Cordillera: U.S. Geological Survey Miscellaneous Investigations Series Map I-2176, scale 1:5,000,000. [This report supersedes Open-File Report 84-523.]
- Snyder, E.F., 1992, Activities of the Alaska district Water Resources Division, U.S. Geological Survey, 1992: U.S. Geological Survey Open-File Report 92-479, 21 p.
- , 1992, The U.S. Geological Survey stream-gaging program in Alaska: water fact sheet: U.S. Geological Survey Open-File Report 92-106, 2 p.
- Stricker, G.D., 1992, Cretaceous coals in Alaska's arctic margin (North Slope)—geology and resources [abs.], in Barker, C.E., and Coury, A.B., Abstracts of the U.S. Geological Survey, Central Region, 1992 poster review; collected abstracts of selected poster papers presented at scientific meetings: U.S. Geological Survey Open-File Report 92-391, p. 13.
- Stricker, G.D., Tripp, R.B., McHugh, J.B., Affolter, R.H., and Cathrall, J.B., 1992, Gold in the Usibelli Group coals, Nenana coal field: B2041, p. 93-97.
- Taylor, C.D., Cieutat, B.A., and Miller, L.D., 1992, A followup geochemical survey of base-metal anomalies in the Ward Creek/Windfall Harbor and Gambier Bay areas, Admiralty Island, southeast Alaska: B2041, p. 70-85.
- Theodorakos, P.M., Borden, J.C., Bullock, J.H., Jr., Gray, J.E., and Hageman, P.L., 1992, Analytical data and sample locality map of stream-sediment and heavy-mineral-concentrate samples collected from the Horn Mountains area, Sleetmute quadrangle, southwest Alaska: U.S. Geological Survey Open-File Report 92-708-A (paper copy, 36 p.), and Open-File Report 92-708-B (5.25-inch diskette), [see p. 8 of paper version for details on computer requirements].
- Townshend, J.B., and others, 1991 (1992), Preliminary geomagnetic data, College Observatory, Fairbanks, Alaska: U.S. Geological Survey Open-File Report 91-300-A-L. [Each monthly report has its own letter designation; authorship and number of pages vary.]
- Townshend, J.B., and others, 1992, Preliminary geomagnetic data, College Observatory, Fairbanks, Alaska: U.S. Geological Survey Open-File Report 92-300-A-D. [Each monthly report has its own letter designation; authorship and number of pages vary. Reports E through L are expected in 1993.]
- U.S. Geological Survey, 1992, Water resources data, Alaska, water year 1991: U.S. Geological Survey Water-Data Report AK-91-1, 415 p.
- Underwood, M.B., Brocculieri, Thomas, Bergfeld, Deborah, Howell, D.G., and Pawlewicz, Mark, 1992, Statistical comparison between illite crystallinity and vitrinite reflectance, Kandik region of east-central Alaska: B2041, p. 222-237.
- Valin, Z.C., and Collett, T.S., 1992, Molecular and isotopic analyses of the hydrocarbon gases within gas hydrate-bearing rock units of the Prudhoe Bay-Kuparuk River area in northern Alaska: U.S. Geological Survey Open-File Report 92-299, 90 p.
- Weber, F.R., Wheeler, K.L., Rinehart, C.D., Chapman, R.M., and Blodgett, R.B., 1992, Geologic map of the Livengood quadrangle, Alaska: U.S. Geological Survey Open-File Report 92-562, 20 p., 1 sheet, scale 1:250,000.
- White, E.R., compiler, 1992, Reports about Alaska in non-USGS publications released in 1991 that include USGS authors: B2041, p. 250-256.
- , 1992, U.S. Geological Survey reports on Alaska released in 1991: B2041, p. 245-249.
- Wilson, F.H., Miller, T.P., and Detterman, R.L., 1992, Preliminary geologic map of the Cold Bay and False Pass quadrangles, Alaska Peninsula: U.S. Geological Survey Open-File Report 92-545, 10 p., scale 1:250,000, color.
- Wilson, F.H., and Shew, Nora, 1992, Map and tables showing geochronology and whole-rock geochemistry of selected samples, Ugashik and part of Karluk quadrangles, Alaska: U.S. Geological Survey Miscellaneous Field Studies Map MF-1539-E, 34 p., 2 sheets, scale 1:250,000.
- Winkler, G.R., 1992, Geologic map and summary geochronology of the Anchorage 1° × 3° quadrangle, southern Alaska: U.S. Geological Survey Miscellaneous Investigations Map I-2283, scale 1:250,000. [This map supersedes USGS Open-File Report 90-83.]
- Winkler, G.R., Goldfarb, R.J., Pickthorn, W.J., and Plafker, George, 1992, The Alaska Mineral Resource Assessment Program—Background information to accompany geologic and mineral-resource maps of the Valdez quadrangle, south-central Alaska: U.S. Geological Survey Circular 1087, 25 p.
- Winkler, G.R., Plafker, George, Goldfarb, R.J., and Case, J.E., 1992, The Alaska Mineral Resource Assessment Program: Background information to accompany geologic and mineral-resource maps of the Cordova and Middleton Island quadrangles, southern Alaska: U.S. Geological Survey Circular 1076, 20 p.
- Woods, P.F., 1992, Limnology of Big Lake, south-central Alaska, 1983-84: U.S. Geological Survey Water-Supply Paper 2382, 108 p.
- Yamaguchi, D.K., 1992, Collaborative research (USGS and Univ. of Colorado): Killed-forest record of the great 1964 earthquake in Alaska: OF92-258, v. 2, p. 1006-1007.
- Yeend, Warren, 1992, Experimental abrasion of detrital gold in a tumbler: B2041, p. 86-92.
- Yehle, L.A., Schmoll, H.R., and Dobrovolsky, Ernest, 1992, Surficial geologic map of the Anchorage A-8-SE quadrangle, Alaska: U.S. Geological Survey Open-File Report 92-350, 33 p., 2 sheets, scale 1:25,000.

# REPORTS ABOUT ALASKA IN NON-USGS PUBLICATIONS RELEASED IN 1992 THAT INCLUDE USGS AUTHORS

Compiled by Ellen R. White

[Some reports dated 1991 did not become available until 1992; they are included in this listing. USGS authors are marked with asterisks (\*)]

## ABBREVIATIONS

- AAAS      AAAS [American Association for the Advancement of Science], Environmental Change: Natural and Man-Made, Arctic Science Conference, 43rd, Valdez, Alaska, 1992, Program and Proceedings: Fairbanks, Alaska, University of Alaska Fairbanks, Geophysical Institute, 186 p.
- GSA5      Geological Society of America Abstracts with Programs, v. 24, no. 5.

- Adams, D.D., Freeman, C.J., \*Goldfarb, R.J., \*Gent, C.A., and \*Snee, L.W., 1992, Age and geochemical constraints on mesothermal gold mineralization, Valdez Creek district, Alaska [abs.]: GSA5, p. 2.
- \*Ager, T.A., and White, James, 1992, Palynological evidence for climate and vegetation changes during middle to late Miocene time in northeastern Alaska [abs.]: GSA5, p. 2.
- Babcock, L.E., and \*Blodgett, R.B., 1992, Biogeographic and paleogeographic significance of Middle Cambrian trilobites of Siberian aspect from southwestern Alaska [abs.]: GSA5, p. 4.
- \*Barker, Fred, Farmer, G.L., \*Ayuso, R.A., \*Plafker, George, and \*Lull, J.S., 1992, The 50 Ma granodiorite of the eastern Gulf of Alaska: Melting in an accretionary prism in the forearc: *Journal of Geophysical Research*, v. 97, no. B5, p. 6757-6778.
- \*Bartsch-Winkler, Susan, and \*Schmoll, H.R., 1992, Utility of radiocarbon-dated stratigraphy in determining late Holocene earthquake recurrence intervals, upper Cook Inlet region, Alaska: *Geological Society of America Bulletin*, v. 104, no. 6, p. 684-694.
- Beaudoin, B.C., \*Fuis, G.S., \*Luter, W.J., \*Mooney, W.D., and \*Moore, T.E., 1992, Crustal velocity structure across terranes between the Yukon-Tanana and Ruby terranes, east-central Alaska: Results from TACT refraction/wide-angle reflection data [abs.]: *Eos (American Geophysical Union Transactions)*, v. 73, no. 43, p. 370-371.
- Beaudoin, B.C., \*Fuis, G.S., \*Mooney, W.D., \*Nokleberg, W.J., and Christensen, N.I., 1992, Thin, low-velocity crust beneath the southern Yukon-Tanana terrane, east-central Alaska: Results from Trans-Alaska Crustal Transect refraction/wide-angle reflection data: *Journal of Geophysical Research*, v. 97, no. B2, p. 1921-1942.
- \*Bird, K.J., and \*Molenaar, C.M., 1992, The North Slope foreland basin, Alaska, in MacQueen, R.W., and Leckie, D.A., *Foreland basins and fold belts*: Tulsa, Okla., American Association of Petroleum Geologists Memoir 55, p. 363-393.
- \*Blodgett, R.B., 1992, Taxonomy and paleobiogeographic affinities of an early Middle Devonian (Eifelian) gastropod faunule from the Livengood quadrangle, east-central Alaska: *Palaeontographica, Abt. A*, v. 221, no. 4-6, p. 125-168, 13 pls.
- \*Blodgett, R.B., and \*Dutro, J.T., Jr., 1992, *Stringocephalus* (Brachiopoda) from Middle Devonian (Givetian) rocks of the Baird Group, western Brooks Range, Alaska: *Oklahoma Geological Survey Bulletin* 145, p. 91-111.
- \*Blodgett, R.B., and Gilbert, W.G., 1992, Paleogeographic relations of lower and middle Paleozoic strata of southwest and west-central Alaska [abs.]: GSA5, p. 8.
- Bol, A.J., Coe, R.S., \*Grommé, C.S., and \*Hillhouse, J.W., 1992, Paleomagnetism of the Resurrection Peninsula, Alaska: Implications for the tectonics of southern Alaska and the Kula-Farallon Ridge: *Journal of Geophysical Research*, v. 97, no. 12, p. 17,213-17,232.
- Bol, A.J., and \*Gibbons, Helen, 1992, Tectonic implications of out-of-sequence faults in an accretionary prism, Prince William Sound, Alaska: *Tectonics*, v. 11, no. 6, p. 1288-1300.
- \*Box, S.E., 1992, Evidence for basin-margin right-slip faulting during Kuskokwim Group deposition, southwestern Alaska [abs.]: GSA5, p. 8-9.
- \*Brew, D.A., 1992, Mesozoic and Cenozoic intrusions and batholiths of the Circum-Pacific region as analogs of pre-Phanerozoic batholiths—A summary, in Bartholomew, M.J., Hyndman, D.W., Mogk, D.W., and Mason, R., eds., *Characterization and comparison of ancient (Precambrian-Mesozoic) continental margins*, International Conference on Basement Tectonics, 8th, Butte, Mont., 1988, Proceedings: Dordrecht, Netherlands, Kluwer, p. 169-177.
- , 1992, Origin and distribution of granitic and related rocks in the Coast plutonic-metamorphic complex, N. American Cordillera, southeastern Alaska, U.S.A. [abs.], in Brown, P.E., and Chappell, B.W., eds., *The second Hutton Symposium on the Origin of Granites and Related Rocks*:

- Boulder, Colo., Geological Society of America, Special Paper 272, p. 486.
- 1992, Origin and distribution of granitic rocks in the Coast plutonic-metamorphic complex, N. American Cordillera, south-eastern Alaska, U.S.A., [abs.]: Royal Society of Edinburgh, Transactions, Earth Sciences, v. 83, parts 1 and 2, p. 486.
- \*Brew, D.A., \*Drew, L.J., \*Schmidt, J.M., \*Root, D.H., \*Huber, D.F., and \*Drinkwater, J.L., 1992, Firsthand USGS-Alaskan Branch experience with probabilistic assessment of undiscovered mineral resources: The Tongass National Forest and adjacent areas, southeastern Alaska [abs.], in British Columbia Ministry of Energy, Mines and Petroleum Resources, Mineral Potential Map Methodology Workshop, Victoria, British Columbia, Canada, 1992 [Program and Abstracts], p. 3-4. [Enquiries to: Ward Kilby, Project Leader, Mineral Potential Mapping Project, B.C. Geological Survey Branch, Tel. (604) 356-2276, FAX (604) 356-8153.]
- \*Brew, D.A., \*Himmelberg, G.R., \*Loney, R.A., and \*Ford, A.B., 1992, Distribution and characteristics of metamorphic belts in the south-eastern Alaska part of the North American Cordillera: *Journal of Metamorphic Geology*, v. 10, no. 3, p. 465-482.
- \*Brew, D.A., \*Karl, S.M., \*Loney, R.A., \*Ford, A.B., \*Himmelberg, G.R., and \*Hammarstrom, J.M., 1992, Jurassic and Cretaceous batholiths of southeastern Alaska: How many arcs? [abs.]: *GSA5*, p. 9.
- Brigham-Grette, J., and \*Carter, L.D., 1992, Pliocene marine transgressions of northern Alaska: Circumarctic correlations and paleoclimatic interpretations: *Arctic (Journal of the Arctic Institute of North America)*, v. 45, no. 1, p. 74-89.
- Bundtzen, T.K., and \*Miller, M.L., 1992, Petrology and metallogeny of Late Cretaceous-early Tertiary igneous rocks, Kuskokwim Mountains, southwest Alaska [abs.]: *GSA5*, p. 11.
- \*Carlson, P.R., \*Karl, H.A., and \*Edwards, B.D., 1991, Mass sediment failure and transport features revealed by acoustic techniques, Beringian margin, Bering Sea, Alaska: *Marine Geotechnology*, v. 10, no. 1/2, p. 33-51.
- \*Carlson, P.R., and \*Kvenvolden, K.A., 1992, Sediment of Prince William Sound: the aftermath of the Exxon Valdez oil spill [abs.], in AAAS, p. 128.
- \*Carlson, P.R., Powell, R.D., and Phillips, A.C., 1992, Submarine sedimentary features on a fjord delta front, Queen Inlet, Glacier Bay, Alaska: *Canadian Journal of Earth Sciences*, v. 29, no. 3, p. 565-573.
- \*Carter, L.D., 1991, Eolian sediments in Arctic Alaska as sources of paleoenvironmental data [abs.], in Weller, Gunter, Wilson, C.L., and Severin, B.A.B., eds., International Conference on the Role of the Polar Regions in Global Change, Fairbanks, Alaska, 1990, Proceedings: Fairbanks, University of Alaska, v. 2, p. 593.
- \*Carter, L.D., and \*Whelan, J.F., 1992, Restricted Arctic sea ice during deposition of the late Pleistocene Flaxman Member of the Gubik Formation, Alaska [abs.]: *Eos (American Geophysical Union Transactions)*, v. 73, no. 14 suppl., p. 287-288.
- Clough, J.G., and \*Blodgett, R.B., 1992, A southwest Alaska Late Silurian-Early Devonian algal reef-rimmed carbonate ramp: Depositional cycles and regional significance [abs.]: *GSA5*, p. 16.
- \*Clow, G.D., 1992, Twentieth century warming in the Alaskan Arctic revealed from borehole temperature measurements [abs.], in AAAS, p. 45.
- \*Clow, G.D., \*Lachenbruch, A.H., and McKay, C.P., 1991, Inversion of borehole temperature data for recent climatic changes: Examples from the Alaskan Arctic and Antarctica [abs.], in Weller, Gunter, Wilson, C.L., and Severin, B.A.B., eds., International Conference on the Role of the Polar Regions in Global Change, Fairbanks, Alaska, 1990, Proceedings: Fairbanks, University of Alaska, v. 2, p. 533.
- \*Cooper, A.K., \*Marlow, M.S., \*Scholl, D.W., and \*Stevenson, A.J., 1992, Evidence for Cenozoic crustal extension in the Bering Sea region: *Tectonics*, v. 11, no. 4, p. 719-731.
- Cowan, E.A., Powell, R.D., Lawson, D.E., and \*Carlson, P.R., 1992, Direct measurements by submersible of surge-type turbidity currents in a fjord channel, southeast Alaska [abs.]: *Geological Society of America, Abstracts with Programs*, v. 24, no. 7, p. 84.
- \*Crock, J.G., \*Severson, R.C., and \*Gough, L.P., 1992, Geochemical and biogeochemical baselines for three national parks and preserves, Alaska [abs.], in AAAS, p. 116. [Kenai National Wildlife Refuge, Denali National Park and Preserve, Wrangell-Saint Elias Park and Preserve.]
- Crowe, D.E., \*Nelson, S.W., Brown, P.E., \*Shanks, W.C., III, and Valley, J.W., 1992, Geology and geochemistry of volcanogenic massive sulfide deposits and related igneous rocks, Prince William Sound, south-central Alaska: *Economic Geology*, v. 87, no. 7, p. 1722-1746.
- \*Dawson, P.B., \*Chouet, B.A., \*Page, R.A., and \*Lahr, J.C., 1992, A post-eruptive seismic survey of Redoubt Volcano, Alaska [abs.]: *Seismological Research Letters*, v. 63, no. 1, p. 67.
- \*Deming, David, \*Sass, J.H., \*Lachenbruch, A.H., and \*De Rito, R.F., 1992, Heat flow and subsurface temperature as evidence for basin-scale ground-water flow, North Slope of Alaska: *Geological Society of America Bulletin*, v. 104, no. 6, p. 528-542.
- Dobson, M.R., \*Scholl, D.W., and \*Stevenson, A.J., 1991, Interplay between arc tectonics and sea-level changes as revealed by sedimentation patterns in the Aleutians, in Macdonald, D.I.M., ed., Sedimentation, tectonics and eustasy: sea-level changes at active margins: Boston, Mass., Blackwell Scientific Publications for the International Association of Sedimentologists, Special Publication 12, p. 151-163.
- \*Drew, L.J., \*Brew, D.A., and \*Menzie, W.D., 1992, A metric for estimating mineral deposit occurrence probabilities—A progress report [abs.], in International Geological Congress, 29th, Kyoto, Japan, 1992, Abstracts, v. 1, p. 83. [Examples from Alaska.]
- \*Dusel-Bacon, Cynthia, and Hansen, V.L., 1992, High-P, moderate-T metamorphism and ductile deformation during early Mesozoic subduction and accretion, east-central Alaska [abs.]: *GSA5*, p. 21.
- \*Elder, W.P., 1992, Paleobiogeographic implications of Middle and Late Cretaceous molluscan assemblages from Alaska [abs.]: *American Association of Petroleum Geologists Bulletin*, v. 76, no. 3, p. 417-418.
- Elias, S.A., Short, S.K., and \*Phillips, R.L., 1992, Paleoecology of late-glacial peats from the Bering Land Bridge, Chukchi Sea shelf region, northwestern Alaska: *Quaternary Research*, v. 38, no. 3, p. 371-378.



- \*Evans, J.R., \*Philpotts, J.A., and \*Taylor, C.D., 1992, Rare earth minerals in a "thunder egg" from Zarembo Island, southeast Alaska: A scanning electron microscopy study [abs.]: *Eos (American Geophysical Union Transactions)*, v. 73, no. 14 suppl., p. 352.
- \*Fisher, W.A., 1992, Photogeologic studies of Arctic Alaska and other areas, in Foster, N.H., and Beaumont, E.A., compilers, *Photogeology and photogeomorphology*: Tulsa, Okla., American Association of Petroleum Geologists, Treatise of Petroleum Geology, Reprint Series no. 18, p. 175-182. [Reprinted from: *Selected papers on photogeology and photo interpretation*: Washington, D.C., Committee on Geophysics and Geography, Research and Development Board, 1953, p. 207-214.]
- \*Ford, A.B., and \*Brew, D.A., 1992, Sitkoh Bay long-duration alkalic plutonism, Chichagof Island, SE Alaska [abs.]: *GSA5*, p. 24.
- \*Frost, T.P., \*Moll-Stalcup, E.J., and \*Box, S.E., 1992, Early Cretaceous and Late Cretaceous-Paleocene plutonism in the Bethel region, southwestern Alaska: Products of two magmatic arcs [abs.]: *GSA5*, p. 25.
- \*Geist, E.L., and \*Scholl, D.W., 1992, Application of continuum models to deformation of the Aleutian Island Arc: *Journal of Geophysical Research*, v. 97, no. B4, p. 4953-4967.
- \*Gerlach, T.M., Westrich, H.R., and \*Casadevall, T.J., 1990 [1992], High sulfur and chlorine magma during the 1989-90 eruption of Redoubt Volcano, Alaska [abs.]: *Fluid Inclusion Research*, v. 23, p. 55. (From: *Eos*, v. 71, p. 1702.)
- Getaahun, Abera, Reed, M.H., and \*Symonds, R.B., 1992, Augustine volcano fumarole wall rock alteration: Mineralogy, zoning and numerical models of its formation process, in Kharaka, Y.K., and Maest, A.S., eds., *Water-Rock Interactions, International Symposium on Water-Rock Interactions*, 7th, Park City, Utah, 1992, Proceedings: Rotterdam, Netherlands, Balkema, v. 2, p. 1411-1414.
- Gilbert, S.A., Casey, J.F., \*Bradley, Dwight, and Kusky, Timothy, 1992, Geochemistry of siliclastic rocks in the Peninsular, Chugach, and Prince William terranes: Implications for the tectonic evolution of south central Alaska [abs.]: *Geological Society of America, Abstracts with Programs*, v. 24, no. 7, p. 305.
- \*Grantz, Arthur, and \*May, S.D., 1992, The Alaska aulacogen of the Arctic Mid-Ocean Ridge system [abs.]: *Eos (American Geophysical Union Transactions)*, v. 73, no. 14 suppl., p. 287.
- \*Grantz, Arthur, \*Mullen, M.W., \*Phillips, R.L., and \*Hart, P.E., 1992, Significance of extension, convergence, and transform faulting in the Chukchi borderland for the Cenozoic tectonic development of the Arctic Basin [abs.]: *Geological Association of Canada, Mineralogical Association of Canada, Joint Annual Meeting*, Wolfville, Nova Scotia, Canada, 1992, Abstracts Volume 17: *Geoscience Canada and Canadian Mineralogist Suppl.*, p. A42.
- \*Gray, J.E., \*Goldfarb, R.J., \*Snee, L.W., and \*Gent, C.A., 1992, Geochemical and temporal conditions for the formation of mercury-antimony deposits, southwestern Alaska [abs.]: *GSA5*, p. 28.
- \*Haeussler, P.J., 1992, Structural evolution of an arc-basin: The Gravina belt in central southeastern Alaska: *Tectonics*, v. 11, no. 6, p. 1245-1265.
- \*Hammarstrom, J.M., 1992, Mineral chemistry of Cretaceous plutons: Hornblende geobarometry in southern California and southeastern Alaska [abs.]: *GSA5*, p. 30.
- \*Heinrichs, T.A., \*Mayo, L.R., Echelmeyer, K.E., and Harrison, W.D., 1992, Black Rapids Glacier, Alaska—Near the Trans-Alaska Pipeline—Unexpected behavior for a surge-type glacier [abs.], in *AAAS*, p. 38.
- Himmelberg, G.R., \*Brew, D.A., and \*Ford, A.B., 1992, Low-grade metamorphism of the Douglas Island Volcanics: Earliest recognized metamorphic event in the western metamorphic belt near Juneau, Alaska [abs.], in Schiffman, Peter, Day, H.W., and Beiersdorf, R.E., convenors, *The transition from basalt to metabasalt: environments, processes and petrogenesis: International Geological Correlation Project 294: Very Low Grade Metamorphism meeting*, Davis, Calif., 1992, Abstracts and Program, n.p.
- Huggett, Q.J., \*Cooper, A.K., Somers, M.L., and Stubbs, A.R., 1992, Interference fringes on GLORIA side-scan sonar images from the Bering Sea and their implications: *Marine Geophysical Research*, v. 14, no. 1, p. 47-63.
- \*Jones, J.E., and \*Molnia, B.F., 1991, Radar mapping of Malaspina Glacier, Alaska, with applications for global change investigations [abs.] in Weller, Gunter, Wilson, C.L., and Severin, B.A.B., eds., *International Conference on the Role of the Polar Regions in Global Change*, Fairbanks, Alaska, 1990, Proceedings: Fairbanks, University of Alaska, v. 2, p. 524.
- Juday, G.P., and \*Trabant, D., 1992, Photographing changes in Columbia Glacier: 1899-1992 [abs.], in *AAAS*, p. 175.
- Kamata, Hiroki, \*Johnston, D.A., and \*Waitt, R.B., 1992, Mode of emplacement and hazards of an ash-cloud surge erupted in the early stage of the 1976 eruption of Augustine volcano, Alaska [abs.], in *International Geological Congress*, 29th, Kyoto, Japan, 1992, Abstracts, v. 2, p. 488.
- \*Kayen, R.E., and \*Lee, H.J., 1991, Pleistocene slope instability of gas hydrate-laden sediment on the Beaufort Sea margin: *Marine Geotechnology*, v. 10, no. 1/2, p. 125-141.
- \*Keith, T.E.C., \*Thompson, J.M., Hutchinson, R.A., and \*White, L.D., 1992, Geochemistry of waters in the Valley of Ten Thousand Smokes region, Alaska: *Journal of Volcanology and Geothermal Research*, v. 49, no. 3/4, p. 209-231.
- \*Kelley, K.D., and Kelley, D.L., 1992, Reconnaissance exploration geochemistry in the central Brooks Range, northern Alaska: Implications for exploration of sediment-hosted zinc-lead-silver deposits: *Journal of Geochemical Exploration*, v. 42, no. 2/3, p. 273-300.
- \*Kirschner, C.E., \*Grantz, Arthur, and \*Mullen, M.W., 1992, Impact origin of the Avak structure, arctic Alaska, and genesis of the Barrow gas fields: *American Association of Petroleum Geologists Bulletin*, v. 76, no. 5, p. 651-679.
- \*Krimmel, R.M., 1992, The retreat of Columbia Glacier, Alaska [abs.], in *AAAS*, p. 143.
- \*Krimmel, R.M., and \*Trabant, D.C., 1992, The terminus of Hubbard Glacier, Alaska: *Annals of Glaciology*, v. 16, p. 151-157. (Symposium on Mountain Glaciology relating to Human Activity, Lanzhou, Gansu Province, China, 1991, Proceedings.)
- \*Kvenvolden, K.A., and \*Carlson, P.R., 1992, Non-Exxon Valdez-related tar on the shores of Prince William Sound, Alaska [abs.], in *AAAS*, p. 130.
- \*Kvenvolden, K.A., \*Lorenson, T.D., and Reeburgh, W.S., 1992, Methane in permafrost—Preliminary studies at the



- CRREL permafrost tunnel near Fox, Alaska [abs.]: *Eos* (American Geophysical Union Transactions), v. 73, no. 14 suppl., p. 119.
- Langseth, M.G., and \*Lachenbruch, A.H., 1992, Review of thermal constraints on the age and evolution of the Amerasian Basin [abs.]: *Eos* (American Geophysical Union Transactions), v. 73, no. 14 suppl., p. 286.
- \*Loney, R.A., and \*Himmelberg, G.R., 1992, The Pd-rich intrusion at Salt Chuck, Prince of Wales Island: An early Paleozoic Alaskan-type ultramafic body [abs.]: *GSA5*, p. 65.
- 1992, Petrogenesis of the Pd-rich intrusion at Salt Chuck, Prince of Wales Island: An early Paleozoic Alaskan-type ultramafic body: *Canadian Mineralogist*, v. 30, no. 4, p. 1005–1022.
- Mangus, M.D., 1991, \*Robert L. Detterman (1919–1990): Arctic (Journal of the Arctic Institute of North America), v. 44, no. 2, p. 174.
- 1992, [Memorials] \*Robert L. Detterman (1919–1990): American Association of Petroleum Geologists Bulletin, v. 76, no. 2, p. 286–287. [Reprinted from *Arctic*, but uses different photo.]
- \*Marincovich, Louie, Jr., 1992, Late Cenozoic evolution and development of the North Pacific molluscan fauna [abs.], in Western Society of Malacologists, 1992, Annual report, v. 24, p. 20. (Combined Annual Meetings, Western Society of Malacologists and American Malacological Union, Berkeley, Calif., 1991, abstracts and proceedings.)
- Measures, E.A., \*Blodgett, R.B., and Rohr, D.M., 1992, Depositional setting and fauna of Middle Ordovician rocks of the Tetsitna Formation, northern Kuskokwim Mountains, Alaska [abs.]: *GSA5*, p. 70.
- Miller, L.D., \*Barton, C.C., Fredericksen, R.S., and Bressler, J.R., 1992, Structural evolution of the Alaska Juneau lode gold deposit, southeastern Alaska: *Canadian Journal of Earth Sciences*, v. 29, no. 5, p. 865–878.
- \*Miller, M.L., and Bundtzen, T.K., 1992, Geologic history of the post-accretionary rocks, Iditarod quadrangle, west-central Alaska [abs.]: *GSA5*, p. 71.
- \*Moll-Stalcup, E.J., \*Box, S.E., and \*Lanphere, M.A., 1992, Eocene transition from arc to intraplate magmatism in southwestern Alaska [abs.]: *GSA5*, p. 71.
- \*Molnia, B.F., 1992, Latest neoglacial history of Bering Glacier, Alaska [abs.], in International Geological Congress, 29th, Kyoto, Japan, 1992, Abstracts, v. 2, p. 370.
- \*Molnia, B.F., and Frank-Molnia, D.G., 1992, Analysis of Alaskan glacial features using side-looking airborne radar data from CD-ROM [abs.]: *Eos* (American Geophysical Union Transactions), v. 73, no. 14 suppl., p. 87.
- \*Murchey, B.L., and Jones, D.L., 1992, A mid-Permian chert event: Widespread deposition of biogenic siliceous sediments in coastal, island arc and oceanic basins: *Palaeogeography, Palaeoclimatology, Palaeoecology*, v. 96, no. 1/2, p. 161–174.
- \*Nokleberg, W.J., \*Grantz, Arthur, \*Patton, W.P., Jr., \*Plafker, George, \*Scholl, D.W., \*Tabor, R.W., \*Vallier, T.L., Fujita, Kazuya, Natal'in, B.A., Parfenov, L.M., Khanchuk, A.I., Sokolov, S.D., Tsukanov, N.V., Natapov, L.M., Monger, J.W.H., Gordey, S.P., and Feeney, T.D., 1992, Circum-North Pacific tectono-stratigraphic terrane map [abs.], in International Geological Congress, 29th, Kyoto, Japan, 1992, Abstracts, v. 2, p. 256.
- Patrick, B.E., and \*Till, A.B., 1992, Cordilleran high pressure metamorphism in northern Alaska: a consequence of island arc-continent collision [abs.], in International Geological Congress, 29th, Kyoto, Japan, 1992, Abstracts, v. 1, p. 63.
- \*Phillips, J.D., and \*Morin, R.L., 1992, New aeromagnetic and gravity maps and interpretations for the Bethel 1° × 3° quadrangle, southwestern Alaska [abs.]: *GSA5*, p. 75.
- \*Pohn, H.A., and \*Molnia, B.F., 1992, Structural analysis of side-looking airborne radar data for the western Brooks Range, AK [abs.]: *Eos* (American Geophysical Union Transactions), v. 73, no. 14 suppl., p. 288.
- \*Poore, R.Z., \*Phillips, R.L., \*Rieck, H.J., and McNeil, Dave, 1992, Quaternary paleoclimate record of the Northwind Ridge, western Arctic Ocean [abs.]: *Eos* (American Geophysical Union Transactions), v. 73, no. 14 suppl., p. 287.
- Potter, A.W., and \*Blodgett, R.B., 1992, Paleobiogeographic relations of Ordovician brachiopods from the Nixon Fork terrane, west-central Alaska [abs.]: *GSA5*, p. 76.
- \*Powell, C.L., II, 1992, Preliminary review of Holocene and Pleistocene northeastern Pacific *Glycymeris* [abs.], in Western Society of Malacologists, 1992, Annual report, v. 24, p. 8–9. (Combined Annual Meetings, Western Society of Malacologists and American Malacological Union, Berkeley, Calif., 1991, abstracts and proceedings.)
- \*Riehle, J.R., \*Champion, D.E., \*Brew, D.A., and \*Lanphere, M.A., 1992, Pyroclastic deposits of the Mount Edgecumbe volcanic field, southeast Alaska: Eruptions of a stratified magma chamber: *Journal of Volcanology and Geothermal Research*, v. 53, no. 1/4, p. 117–143.
- \*Riehle, J.R., Mann, D.H., Peteet, D.M., Engstrom, D.R., \*Brew, D.A., and \*Meyer, C.E., 1992, The Mount Edgecumbe tephra deposits, a marker horizon in southeastern Alaska near the Pleistocene–Holocene boundary: *Quaternary Research*, v. 37, no. 2, p. 183–202.
- Roeske, S.M., and \*Box, S.L., 1992, Metamorphism and deformation of oceanic lithologies in a Cretaceous subduction/collision setting, southwestern Alaska [abs.]: *GSA5*, p. 79.
- Roeske, S.M., \*Bradshaw, J.Y., and \*Snee, L.W., 1992, High/low metamorphism of oceanic and continental crust in the Ruby anticline, north-central Alaska [abs.]: *GSA5*, p. 79.
- Sheppard, D.S., Janik, C.J., and \*Keith, T.E.C., 1992, A comparison of gas geochemistry of fumaroles in the 1912 ash-flow sheet and on active stratovolcanoes, Katmai National Park, Alaska: *Journal of Volcanology and Geothermal Research*, v. 53, no. 1/4, p. 185–197.
- \*Till, A.B., 1992, Blueschists developed during collision, not subduction, in the internal zone of the Brooks Range fold and thrust belt [abs.]: *GSA5*, p. 86.
- 1992, Detrital blueschist-facies metamorphic mineral assemblages in Early Cretaceous sediments of the foreland basin of the Brooks Range, Alaska, and implications for orogenic evolution: *Tectonics*, v. 11, no. 6, p. 1207–1223.
- \*Trabant, D.C., and \*Meyer, D.F., 1992, Flood generation and destruction of "Drift" Glacier by the 1989–90 eruption of Redoubt Volcano, Alaska: *Annals of Glaciology*, v. 16, p. 33–38. (Symposium on Mountain Glaciology relating to Human Activity, Lanzhou, Gansu Province, China, 1991, Proceedings.)
- \*Vallier, T.L., \*Karl, H.A., \*Frueher, L.M., and Masson, D.G., 1992, Deformation in the western Aleutian fore-arc region

- caused by impingement of Stalenate ridge on the trench inner wall [abs.]: GSA5, p. 87.
- Waller, T.R., and \*Marincovich, Louie, Jr., 1992, New species of *Camptochlamys* and *Chlamys* (Mollusca: Bivalvia: Pectinidae) from near the Cretaceous/Tertiary boundary at Ocean Point, North Slope, Alaska: *Journal of Paleontology*, v. 66, no. 2, p. 215–227.
- \*Watterson, J.R., 1992, Preliminary evidence for the involvement of budding bacteria in the origin of Alaskan placer gold: *Geology*, v. 20, no. 4, p. 315–318.
- \*Wilson, F.H., 1992, New geologic map and digital database of the Alaska Peninsula, southwestern Alaska [abs.]: GSA5, p. 91.
- 1992, Tectonic history of the Alaska Peninsula terrane, southwestern Alaska [abs.]: GSA5, p. 90.